Saravanan Rajendran
Mu. Naushad
D. Durgalakshmi
Eric Lichtfouse   *Editors*

Metal, Metal Oxides and Metal Sulphides for Biomedical Applications

Springer

Environmental Chemistry for a Sustainable World

Volume 58

Series Editors

Eric Lichtfouse ⓘ, Aix-Marseille University, CNRS, IRD, INRAE, Coll France, CEREGE, Aix-en-Provence, France

Jan Schwarzbauer, RWTH Aachen University, Aachen, Germany

Didier Robert, CNRS, European Laboratory for Catalysis and Surface Sciences, Saint-Avold, France

Other Publications by the Editors

Books
Environmental Chemistry
http://www.springer.com/978-3-540-22860-8

Organic Contaminants in Riverine and Groundwater Systems
http://www.springer.com/978-3-540-31169-0

Sustainable Agriculture
Volume 1: http://www.springer.com/978-90-481-2665-1
Volume 2: http://www.springer.com/978-94-007-0393-3

Book series
Environmental Chemistry for a Sustainable World
http://www.springer.com/series/11480

Sustainable Agriculture Reviews
http://www.springer.com/series/8380

Journals
Environmental Chemistry Letters
http://www.springer.com/10311

Saravanan Rajendran • Mu. Naushad
D. Durgalakshmi • Eric Lichtfouse
Editors

Metal, Metal Oxides and Metal Sulphides for Biomedical Applications

Springer

Editors
Saravanan Rajendran
Department of Mechanical Engineering
University of Tarapacá
Arica, Chile

Mu. Naushad
Yonsei frontier lab
Yonsei University
Seoul, Korea (Republic of)

D. Durgalakshmi
Department of Medical Physics
Anna University
Chennai, Tamil Nadu, India

Eric Lichtfouse
CNRS, IRD, INRAE, Coll France, CEREGE
Aix-Marseille University
Aix-en-Provence, France

Preface

In the history of science, we often find that the study of some natural phenomenon has been the starting point in the development of a new branch of knowledge

Sir. C. V. Raman

The design of new materials for improved healthcare has always been at the core of medicinal research. The recent discovery of nanomaterials of unprecedented properties due to their nanosize opened a new vista for inventing new approaches for bioengineering, diagnosis, and therapy of many diseases. This book reviews the synthesis, toxicity, biosensing, and therapeutic use of metals, metal oxides, and metal sulphides. The chapters detail four main areas: functional nanoparticles for therapies, nanomaterials for bioimaging, biosensors for monitoring diseases, and green synthesis of advanced materials.

Chapter 1 by Joicy and Thangadurai reviews the applications of sulfide nanomaterials for bioimaging and biosensing, with focus on fluorescence, magnetic resonance, and acoustics. Here, sulfide-based chalcogenide materials appear non-toxic and highly performing in terms of optical properties. Biomedical applications of Ti alloys, for example, in dentistry, are presented by Rokaya et al. in Chap. 2, with emphasis on surface, mechanical, corrosion, and biological properties. Medicinal applications of metal complexes are discussed in Chap. 3 by Prasad et al. Chapter 4 by Parsanathan and Jagadeeshan explains the links between various metals, for example, Zn, Cr, Cu, Mn, Mg, and Fe, and the metabolic syndrome causing diabetes, obesity, and cardiovascular diseases. Antimicrobials based on metal and metal oxide–based nanomaterials are reviewed in Chap. 5 by Nas et al.

Application of CuO nanoparticles in the fields of medicine and biology (Chap. 9)

Cancer diagnosis and treatment benefits from new nanoparticles made of metals, metal oxides, and metal sulphides are reviewed by Pachaiappan* and Kovendhan Manavalan in Chap. 6. Chapter 7 by Kalambate and Huang discusses the use of electrochemical biosensors for the quantification of disease biomarkers and drug molecules by voltammetry, impedimetry, and potentiometry. Therapy and bioimaging have recently improved with the design of novel inorganic nanoparticles, as presented by Prabha et al. in Chap. 8. The eco-friendly applications of metals and metal oxides in drug delivery and bio-imaging are reviewed by Prasad et al. in Chap. 9. Chapter 10 by Jagadeeshan and Parsanathan describes the use of nanomaterials made of metal oxides to treat cancer. Varier et al. and Jayamurali

et al. discuss the neurotoxicity, cardiotoxicity, hepatotoxicity, and developmental and reproductive toxicity of metals such as Hg, Pb, Al, Fe, Cd, and As in Chaps. 11 and 12. We thank very much the contributing authors for their valuable contributions.

Arica, Chile   Saravanan Rajendran
Riyadh, Saudi Arabia   Mu. Naushad
Chennai, Tamil Nadu, India   D. Durgalakshmi
Aix-en-Provence, France   Eric Lichtfouse

Acknowledgments

Contents

About the Editors

Saravanan Rajendran received his Ph.D. in Physics–Material Science in 2013 from the Department of Nuclear Physics at the University of Madras, Chennai, India. He was awarded the University Research Fellowship (URF) during the years 2009–2011 by the University of Madras. After working as an Assistant Professor at Dhanalakshmi College of Engineering, Chennai, India, during the years 2013–2014, he was awarded SERC and CONICYT-FONDECYT Postdoctoral Fellowship, University of Chile, Santiago, in the years of 2014–2017. Dr. Rajendran has worked (2017–2018) in the research group of Professor John Irvine, School of Chemistry, University of St Andrews, UK, as a Postdoctoral Research Fellow within the framework of a EPSRC-Global Challenges Research Fund for the removal of Blue-Green Algae and their toxins. He is currently working as a Research Scientist in the Faculty of Engineering, Department of Mechanical Engineering, University of Tarapacá, Arica, Chile. Addition to this, he is also working as a Research Associate in SERC, Santiago, Chile. Dr. Rajendran is the Associate Editor for *International Journal of Environmental Science and Technology* (Springer). His research interests focus in the area of nanostructured functional materials, photophysics, surface chemistry, and nanocatalysts for renewable energy and wastewater purification. Dr. Rajendran has published in several international peer-reviewed journals, eight book chapters, and seven books published by renowned international publishers.

Mu. Naushad is presently working as an Associate Professor in the Department of Chemistry, College of Science, King Saud University (KSU), Riyadh, Kingdom of Saudi Arabia. He obtained his M.Sc. and Ph.D. degrees in Analytical Chemistry from Aligarh Muslim University, Aligarh, India, in 2002 and 2007, respectively. Dr. Naushad has a vast research experience in the multidisciplinary fields of Analytical Chemistry, Materials Chemistry, and Environmental Science. He holds several US patents, over 290 publications in the international journals of repute, 20 book chapters, and several books published by renowned international publishers. Dr. Naushad has >11000 citations with a Google Scholar H-Index of >60. He has

been included in the list of Highly Cited Researchers 2019. He has successfully run several research projects funded by National Plan for Science and Technology (NPST) and King Abdulaziz City for Science and Technology (KACST), Kingdom of Saudi Arabia. Dr. Naushad is the Editor/Editorial Member of several reputed journals. Dr. Naushad has been awarded the Scientist of the Year Award 2015 by the National Environmental Science Academy, Delhi, India; Almarai Award 2017, Saudi Arabia; and Best Research Quality Award 2019, King Saud University, Saudi Arabia.

D. Durgalakshmi is presently working as a DST-INSPIRE Faculty in Department of Medical Physics, Anna University, Chennai, India. Her core research area is nanostructured materials for biomedical applications including biomaterials, biophotonics, and biosensors. She is also having vast research experience in the field of sustainable materials for energy and environmental remediation. Dr. Durgalaksmi's doctoral work was funded by Lady Tata Memorial Scholarship for researchers working in advanced life sciences. Her doctoral work was awarded Best Ph.D. Thesis in Materials Science in 2016 by Materials Research Society of India (MRSI), Indian Institute of Sciences, India. Dr. Durgalakshmi has published several research articles in international journals and seven book chapters. She received seven best paper awards in the national/international conferences.

Eric Lichtfouse is Geochemist and Professor of Scientific Writing at Aix-Marseille University, France, and Visiting Professor at Xi'an Jiaotong University, China. He has discovered temporal pools of molecular substances in soils, invented carbon-13 dating, and published the book *Scientific Writing for Impact factor Journals*. Dr. Lichtfouse is Chief Editor and founder of the journal *Environmental Chemistry Letters* and the book series Sustainable Agriculture Reviews and Environmental Chemistry for a Sustainable World. He has awards in analytical chemistry and scientific editing. He is World XTerra Vice-Champion.

Contributors

P. Aruna Department of Medical Physics, Anna University, Chennai, Tamil Nadu, India

Tamizhanban Ayyapillai Department of Chemistry, School of Chemical and Biotechnology, SASTRA Deemed University, Thanjavur, Tamil Nadu, India

Yaacov Ben-David Department of Biology and Chemistry, The Key Laboratory of Chemistry for Natural Products of Guizhou Province and Chinese Academy of Sciences, Guiyang, Guizhou Province, China
State Key Laboratory of Functions and Applications of Medicinal Plants, Guizhou Medical University, Guiyang, Guizhou Province, China

Muskan Bhatnagar Department of Chemistry, National Institute of Technology Warangal (Institute of National Importance), Warangal, Telangana, India

Hakan Burhan Sen Research Group, Department of Biochemistry, Faculty of Arts and Science, Dumlupınar University, Kütahya, Turkey

Mehmet Harbi Calimli Sen Research Group, Department of Biochemistry, Faculty of Arts and Science, Dumlupınar University, Kütahya, Turkey
Tuzluca Vocational High School, Igdir University, Igdir, Turkey

Arulvasu Chinnasamy Department of Zoology, University of Madras, Chennai, Tamil Nadu, India

Jugun Prakash Chinta Department of Chemistry, National Institute of Technology Warangal (Institute of National Importance), Warangal, Telangana, India

Aenugu Sravya Chowdary Department of Chemistry, National Institute of Technology Warangal (Institute of National Importance), Warangal, Telangana, India

D. Durgalakshmi Department of Medical Physics, Anna University, Chennai, Tamil Nadu, India

Babu Gajendran Department of Biology and Chemistry, The Key Laboratory of Chemistry for Natural Products of Guizhou Province and Chinese Academy of Sciences, Guiyang, Guizhou Province, China
State Key Laboratory of Functions and Applications of Medicinal Plants, Guizhou Medical University, Guiyang, Guizhou Province, China

S. Ganesan Department of Medical Physics, Anna University, Chennai, Tamil Nadu, India

Yunhui Huang State Key Laboratory of Materials Processing and Die & Mould Technology, School of Materials Science and Engineering, Huazhong University of Science and Technology, Wuhan, Hubei, P. R. China

Sankar Jagadeeshan The Shraga Segal Department of Microbiology, Immunology, and Genetics, Faculty of Health Sciences, Ben-Gurion University of the Negev, Beer-Sheva, Israel

Dheepthi Jayamurali Department of Physiology, Dr. ALM PGIBMS, University of Madras, Chennai, Tamil Nadu, India

S. Joicy Centre for Nanoscience and Technology, Pondicherry University, Kalapet, Puducherry, India

Pramod K. Kalambate State Key Laboratory of Materials Processing and Die & Mould Technology, School of Materials Science and Engineering, Huazhong University of Science and Technology, Wuhan, Hubei, P. R. China

Lalitha Krishnamoorthy Department of Chemistry, School of Chemical and Biotechnology, SASTRA Deemed University, Thanjavur, Tamil Nadu, India

Yanmei Li Department of Biology and Chemistry, The Key Laboratory of Chemistry for Natural Products of Guizhou Province and Chinese Academy of Sciences, Guiyang, Guizhou Province, China
State Key Laboratory of Functions and Applications of Medicinal Plants, Guizhou Medical University, Guiyang, Guizhou Province, China

Wuling Liu Department of Biology and Chemistry, The Key Laboratory of Chemistry for Natural Products of Guizhou Province and Chinese Academy of Sciences, Guiyang, Guizhou Province, China
State Key Laboratory of Functions and Applications of Medicinal Plants, Guizhou Medical University, Guiyang, Guizhou Province, China

Kovendhan Manavalan Department of Environmental Engineering, Inha University, Incheon, South Korea

Mehmet Salih Nas Sen Research Group, Department of Biochemistry, Faculty of Arts and Science, Dumlupınar University, Kütahya, Turkey
Department of Environmental Engineering, Faculty of Engineering, Igdir University, Igdir, Turkey

Rekha Pachaiappan Adhiyaman Arts and Science College for Women, Uthangarai, Tamil Nadu, India

Rajesh Parsanathan Department of Pediatrics and Centre for Cardiovascular Diseases and Sciences, Louisiana State University Health Sciences Center, Shreveport, LA, USA

S. Prabha Department of Medical Physics, Anna University, Chennai, Tamil Nadu, India

Siva Prasad Y. Department of Chemistry, School of Chemical and Biotechnology, SASTRA Deemed University, Thanjavur, Tamil Nadu, India

Jiaqian Qin Metallurgy and Materials Science Research Institute (MMRI), Chulalongkorn University, Bangkok, Thailand

Jegadeesh Raman Mushroom Research Division, National Institute of Horticultural and Herbal Science, Rural Development Administration, Eumsung, Republic of Korea

Dinesh Rokaya Department of Clinical Dentistry, Walailak University International College of Dentistry, Walailak University, Bangkok, Thailand

Arpita Salkade Living Systems Institute, College of Medicine and Health, University of Exeter, Exeter, UK

Fatih Sen Sen Research Group, Department of Biochemistry, Faculty of Arts and Science, Dumlupınar University, Kütahya, Turkey

Atul Sharma Department of Chemistry, National Institute of Technology Warangal (Institute of National Importance), Warangal, Telangana, India

Xiangchun Shen Department of Biology and Chemistry, The Key Laboratory of Chemistry for Natural Products of Guizhou Province and Chinese Academy of Sciences, Guiyang, Guizhou Province, China
State Key Laboratory of Functions and Applications of Medicinal Plants, Guizhou Medical University, Guiyang, Guizhou Province, China

Viritpon Srimaneepong Department of Prosthodontics, Faculty of Dentistry, Chulalongkorn University, Bangkok, Thailand

Nagarajan Subbiah Department of Chemistry, School of Chemical and Biotechnology, SASTRA Deemed University, Thanjavur, Tamil Nadu, India
Department of Chemistry, National Institute of Technology Warangal (Institute of National Importance), Warangal, Telangana, India

P. Thangadurai Centre for Nanoscience and Technology, Pondicherry University, Kalapet, Puducherry, India

Sumathi Thangarajan Department of Medical Biochemistry, Dr. ALM PGIBMS, University of Madras, Chennai, Tamil Nadu, India

Krishnapriya Madhu Varier Department of Medical Biochemistry, Dr. ALM PGIBMS, University of Madras, Chennai, Tamil Nadu, India

Yang Xiaosheng Department of Biology and Chemistry, The Key Laboratory of Chemistry for Natural Products of Guizhou Province and Chinese Academy of Sciences, Guiyang, Guizhou Province, China
State Key Laboratory of Functions and Applications of Medicinal Plants, Guizhou Medical University, Guiyang, Guizhou Province, China

Chapter 1
Metal Sulfide Nanostructures
for Bioimaging and Biosensing Applications

S. Joicy and P. Thangadurai

Contents

Abstract   Medical field has been growing enormously in the recent years in terms of diagnosis as well as treatment. People are interested to do diagnosis quickly and more importantly with high precision. In this aspect, many researches have been carried out to develop and improve diagnostic tools. In particular, imaging and sensing are the two major tools that are highly useful for medical diagnostics. There are two aspects in developing these tools. One is the technology aspect, and the second is the development of materials that are used in these tools. More precisely, the imaging as well as sensing devices work on the type of materials, and their performance is highly depending on the quality of the materials. These materials are mostly used as probes, based on their active property. The probe can be optical, electric, magnetic and electronic depending on the requirement. Thus, the importance of the materials in medical diagnostics has been improving, especially with the development of nanomaterials. Materials are highly researched for their

S. Joicy · P. Thangadurai (✉)
Centre for Nanoscience and Technology, Pondicherry University, Kalapet, Puducherry, India
e-mail: thangaduraip.nst@pondiuni.edu.in

applications in bioimaging and biosensing. In this aspect, the present chapter has been written on the application of sulfide nanomaterials for bioimaging and biosensing. Out of many types of materials, the sulfide-based chalcogenide materials are nontoxic and highly performing especially in terms of their optical properties and can be exploited for these applications. Many imaging techniques based on fluorescence, magnetic resonance and acoustic are discussed in this chapter. As far as the biosensing is concerned, fluorescent sensors, calorimetric sensor and electrochemical sensors are discussed.

Keywords Metal sulfides · Bioimaging · Image-guided therapy · Biosensing

Abbreviations

CDT	Chemodynamic therapy
CT	X-ray computed tomography
DNA	Deoxyribonucleic acid
FLI	Fluorescence imaging
FRET	Fluorescence (or Förster) resonance energy transfer
GCE	Glassy carbon electrode
IRT	Infrared thermal
MOST	Multispectral optical tomography
MRI	Magnetic resonance imaging
PAI	Photoacoustic imaging
PAT	Photoacoustic tomography
PDT	Photodynamic therapy
PET	Positron emission tomography
PTT	Photothermal therapy
RT	Radio therapy
ssDNA	Single-stranded deoxyribonucleic acid
TRT	Thermoradiotherapy

1.1   Introduction

Currently, biomedical research is one of the vast-growing research areas with advanced technologies due to its direct impact on human health. Bioimaging and biosensing are two different significant aspects of biomedical research. The main focus of those fields lies in the development of probes for selective detection and specific treatment of infectious diseases. These two directions of biomedical research field are individually classified based on their functionality. Bioimaging is an important method that visualizes and monitors the physical and molecular events in living cells. Bioimaging utilizes photons, X-rays, magnetic resonance, ultrasounds and positrons as imaging sources. By utilizing those imaging sources, wide range of

imaging techniques such as optical imaging, magnetic resonance imaging, photoacoustic imaging and positron emission tomography have been developed for understanding basic molecular aspects of living organisms and earlier detection of diseases. Bioimaging studies are typically achieved in two kinds of environments, which are, in vitro and in vivo, in which the efficiency of the developed imaging agents could be determined. On the other hand, biosensing mainly deals with the quantitative and qualitative detection of biological analytes by characterizing absorption, emission and electrocatalytic behavior of the sensor system. The biological analytes include nucleic acids, proteins, vitamins, virus and glucose. On the basis of signal transduction, biosensors can be classified as optical, electrochemical and thermal biosensors.

Nanotechnology plays a major role in scientific development of biomedical research. Unique physical and chemical features of nanomaterials differ from their bulk counterparts due to their quantum size effect. Nanomaterials are materials with morphological features whose sizes are smaller than 100 nm, at least in one dimension. With the development of nanotechnologies, various nanomaterials with unique properties are being introduced into bioimaging and biosensing applications. Those nanomaterials include metal oxides (Andreescu et al. 2012), metal sulfides (Martynenko et al. 2017; Yadav et al. 2019), carbon materials (Wen et al. 2015; Hong et al. 2015) and graphene (Shen et al. 2012; Hai et al. 2018). Nanomaterials offer more advantages such as biomedical agents due to their smaller size, large surface-to-volume ratio and ease of surface modification. Among the most fascinating nanomaterials, metal cations with sulfide-based nanomaterials have been employed intensively to serve as bioimaging and biosensing nanoagents for various biological applications because of their unique optical, magnetic, electronic and catalytic properties. These unique properties of metal sulfides can be tunable by altering size, shapes, composition and doping, which facilitate opportunities to enhance the bio-performance (Yong et al. 2010; Geszke-Moritz et al. 2013a; Gao et al. 2015; Zhao et al. 2017; Yu et al. 2017). Metal sulfides made in various nanostructured forms such as quantum dots, nanoparticles, nanorods, nanotubes, nanosheets and nanocubes have been prepared and used for biomedical applications.

The performance of bioimaging and biosensing nanoagents based on metal sulfides depends significantly on their size, dimension, morphology and surface activity. For instance, hollow and porous nanostructures are more favorable for high drug loading capacity because those nanostructures provide more space to load drugs (Li et al. 2016; Wang et al. 2016; Zhang et al. 2019). Next, biosensor based on one-dimensional nanostructures such as nanorods and nanotubes is attractive for detection of biological analytes due to their confined electron transportation along the one-dimensional direction (Zhang et al. 2008; Guan et al. 2015). On the other hand, high density of active surface sites over a large area of two-dimensional metal sulfides makes them ideal for biosensing application (Vilian et al. 2019).

The current chapter focuses on bioimaging and biosensing applications of most widely used metal sulfides and their nanocomposites. Various imaging techniques where metal sulfides employed as imaging agent have been deliberated in the first part of the chapter. Also, imaging-guided therapy system based on the metal sulfide

nanostructures was also explained with various examples. The second part of the chapter has focused on the biosensing applications based on the metal sulfide nanostructures.

1.2 Metal Sulfide Nanostructures for Bioimaging and Therapy

In medical field, imaging method has become a crucial tool in clinical trials, medical practice and cancer research. At present, numerous technologies such as imaging and therapeutic technologies have been developed and applied for medical imaging and therapy to appropriately diagnose and treat the diseased tissues. Those technologies include photoluminescence imaging (PLI), magnetic resonance imaging (MRI), photoacoustic imaging (PAI), photothermal therapy (PTT), photodynamic therapy (PDT) and chemotherapy. Nanomaterials with transition metal sulfide nanostructures have attracted great attention in the field of biomedical therapy and imaging due to their optical (such as near-infrared absorption and photoluminescence) and magnetic properties. These properties made them potential probes in biomedical field such PLI, PAI, MRI, PDT and PTT. This section presents very successful results of functionalized/conjugated transition metal sulfide nanostructures applied for imaging and imaging-guided therapy.

1.2.1 Fluorescence Imaging

Optical imaging using luminescent probes has greatly attracted fast-growing research interest due to its high specificity and sensitivity and has potential to offer high-resolution images. To date, there have been a number of studies on using transition metal sulfide nanomaterials as optical probes for photoluminescence imaging of cells and tissues, from in vitro and in vivo imaging to specific tissue targeted imaging.

Metal sulfides based on group II–VI semiconductors (ZnS, CdS and HgS) have been attracted and used for fluorescence imaging due to their attractive photophysical properties, improved processability and good host material for luminescent activators (i.e., dopants). Of them, narrow bandgap semiconductor CdS quantum dots have been extensively studied due to its size-tunable absorption and emission properties (Fig. 1.1a) and have been implemented in biomedical applications (Shen et al. 2010; Huang et al. 2013; Shivaji et al. 2018). Conjugated CdS quantum dots were used as fluorescent probes for targeted imaging of various cancerous cell lines. For example, human transferrin protein- conjugated CdS quantum dots with quantum yield of 74% were used for targeted fluorescence imaging of human breast adenocarcinoma cell (MCF-7 cells) (Pedram et al. 2016).
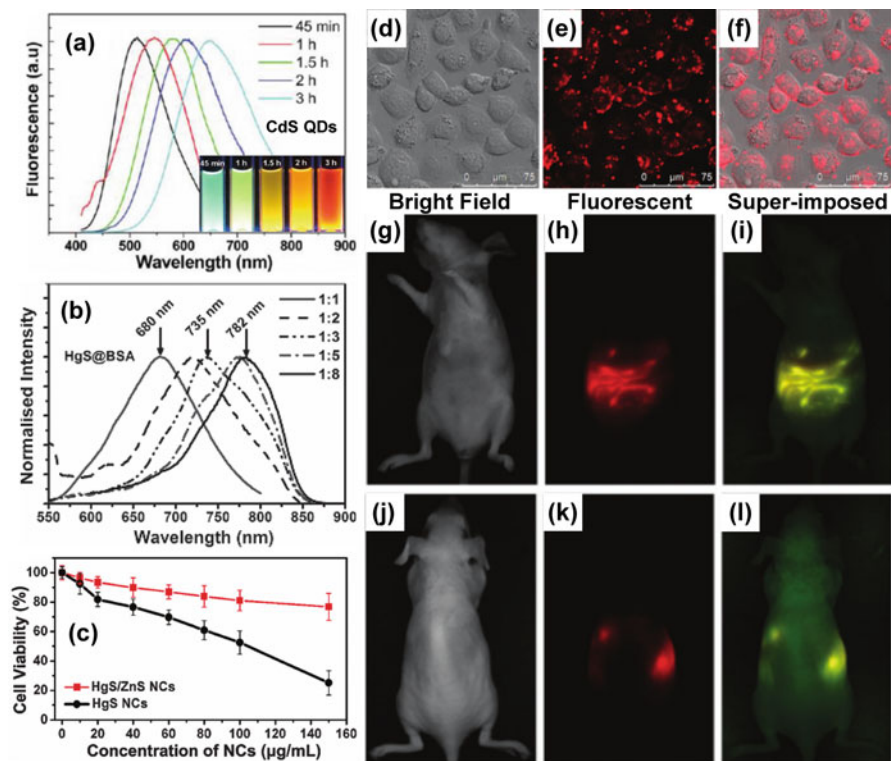
Fig. 1.1 (**a**) Tunable photoluminescence of CdS quantum dots (QDs) by varying size based on the reaction time. (Modified after Aboulaich et al. (2012). Copyright 2012 American Chemical Society). (**b**) Normalized luminescence spectra of HgS@BSA (*BSA – bovine serum albumin*) quantum dots with different Hg/S molar ratios. (Reprinted with permission from Goswami et al. (2012). Copyright 2012 John Wiley and Sons). (**c**) MTT (3-(4,5-dimethylthiazol-2-yl)-2,5-diphenyltetrazolium bromide) calorimetric assay on Hela cells exposed to HgS–ZnS nanocrystals (NCs) and bare HgS core nanocrystals at different concentrations from 0 to $150\mu g\ mL^{-1}$ for 24 h, respectively. Bright-field (**d**) and confocal fluorescence (**e**) images of Hela cells incubated with HgS–ZnS nanocrystals emitting at 785 nm for 3 h at a concentration of $100\mu g\ mL^{-1}$, and overlay images of (**d**) and (**e**) are (**f**). The images were obtained by excitation at 633 nm. (**g** to **l**) In vivo NIR fluorescence imaging of a nude mouse with HgS–ZnS nanocrystals emitting at 785 nm. (**g** and **j**) Bright-field images of the nude mouse on the abdominal side and on the backside; (**h** and **k**) unmixed images of the HgS–ZnS nanocrystals fluorescence signal from the abdominal cavity and the backside of the nude mouse with HgS–ZnS nanocrystals injected into the abdominal cavity; (**i** and **l**) superimposed images of autofluorescence of nude mouse and fluorescence of the nanocrystals. (Reprinted with permission from Yang et al. (2015a). Copyright 2015 Royal Society of Chemistry)

In another work, mouse liver cancer cells (CBRH-7919) were imaged by the fluorescent CdS-MAA-PEI quantum dots conjugated with folic acid as targeting ligand through receptor (folate receptor)-mediated endocytosis (Wei et al. 2012).

Mercury sulfide (HgS) is another type of II-VI narrow bandgap semiconductor whose emission wavelength can also be tailored in NIR-I window by varying their size (Fig. 1.1b) (Yang et al. 2012; Goswami et al. 2012). The NIR photons with longer wavelength in biomedical application provide less tissue scattering and absorption, which leads to deep tissue penetration and minimized background autofluorescence. However, apart from the consideration of optical bioimaging window, toxicity of heavy metals Cd^{2+} and Hg^{2+} is another major blockade in the practical use of Cd and Hg-sulfides, especially for in vivo imaging applications (Tchounwou et al. 2012; L'Azou et al. 2014). Therefore, approaches to nontoxic semiconductor quantum dots have been focused on the preparation of core–shell architectures with an exterior layer of nontoxic material (i.e., ZnS as shell). Also, core–shell structures based on CdS and HgS greatly increase their stability and quantum yields.

Liu et al. (Liu et al. 2014) reported that the CdS–ZnS core–shell quantum dots with QY of 42% can be used as an efficient photoluminescent probe for bioimaging application. After stabilized with pluronic block copolymer micelles, CdS–ZnS quantum dots exhibited a bright emission with QY of ~ 65% and high colloidal photostability. Subsequently, these quantum dots were used for in vitro and in vivo optical imaging studies. Zhang and group (Zhang et al. 2013) have fabricated folic acid-assembled PEI-coated CdS–ZnS quantum dots as a turn-on fluorescent probe for targeted imaging of folate receptor overexpressed cancer cells (HeLa, HepG2 and A549). In another report (Yang et al. 2015a), the biocompatible HgS–ZnS core–shell quantum dots with tunable emission in wide NIR window (785–1060 nm) and higher QY of 43.8% were obtained by aqueous route using glutathione (GSH) as stabilizing agent and used for imaging study. The results of this study showed that the GSH-stabilized HgS–ZnS core–shell quantum dots exhibited significantly lower cytotoxicity (above 80% viability) compared to the GSH-HgS core nanocrystals (Fig. 1.1c). This implies that the ZnS shell proficiently inhibited the release of free-Hg^{2+} ions from the HgS core material and thus reduced cytotoxicity. Then, the resultant low-toxic GSH-stabilized HgS–ZnS core–shell nanocrystals have been proved as an effective NIR fluorescent label in both in vitro (Fig. 1.1d–f) and in vivo (Fig. 1.1g–l) imaging. The penetration depth of NIR emitting HgS–ZnS core–shell nanocrystals in nude mouse reached to 2 cm with a distinct separation of fluorescence of nanocrystals from the background autofluorescence.

On the other hand, a non-toxic zinc sulfide (ZnS) semiconductor is one of the most important versatile and fluorescent materials with a wide bandgap of ~3.6 eV. Particularly, transition metal ions-doped ZnS luminescent probe have received much attention recently as a class of luminescent material, where dopant ions act as a recombination centers for the electron–hole pairs which results in strong and characteristic radiative emission. The potential of various metal ions-doped ZnS nanocrystals (single or co-doped form) in biomedical application has been reported by different research groups (Xu et al. 2011; Bhowal et al. 2018; Selvaraj et al. 2019). In particular, manganese ion (Mn^{2+})-doped ZnS phosphors have been extensively studied for their longer excited state life time and larger Stokes shift. The large Stokes shift is a crucial benefit for bioimaging application in terms of minimalizing

self-reabsorption and distinguishing the photon emission from background autofluorescence. Labeling of cancer cells by folic acid-conjugated Mn:ZnS quantum dots as fluorescent probes was studied by various researchers (Geszke et al. 2011; Geszke-Moritz et al. 2013b; Mohammad et al. 2016) and proved this quantum dots are very specific towards their targets. Another research group (Yu et al. 2013) had developed three photon-excited photoluminescence characteristics of Mn^{2+}-doped ZnS quantum dots for high resolution in vitro and in vivo tumor targeted imaging.

Another interesting longer wavelength (NIR-II, 1000–1400 nm) photon-emitting metal sulfide is silver sulfide, Ag_2S that belongs to I-VI group semiconductor. As NIR-II emitting substance without any heavy metals, the Ag_2S is an ideal candidate for the study of multicolor in vivo imaging and multiple nanodiagnostics with high spatial and temporal resolution with high signal-to-background ratio. Both in vitro and in vivo NIR-II imaging studies by Ag_2S quantum dots have been reported by various research groups. For example, PEGylated Ag_2S quantum dots (particle size ~5.4 nm) with NIR-II emission at 1200 nm (Fig. 1.2a) have been developed as imaging contrast agent for in vivo NIR fluorescence imaging of xenograft 4T1 tumors-bearing mouse (Hong et al. 2012). The experimental results showed that PEG-Ag_2S quantum dots were able to detect the xenograft tumors with high tumor-to-background signal contrast through passive targeting based on enhanced permeability and retention (EPR) effect (Fig. 1.2b, c). Another group (Tang et al. 2015) had synthesized water-dispersible 3-Mercaptopropionic acid (MPA)-capped Ag_2S quantum dots with distinct tunable emission from 500 to 820 nm. In their subsequent work, a cyclic peptide, arginine-glycine-aspartic acid-(D)phenylalanine-lysine (cRGDfk) was conjugated to MPA-Ag_2S quantum dots using EDC-NHS chemistry for fluorescence imaging of different mouse models of cancer. The results of in vivo imaging study (Fig. 1.2d) showed that cRGDfk- conjugated Ag_2S quantum dots were mainly accumulated in the tumor sites with minimal background fluorescence at 24 h postinjection of quantum dot-cRGDfk conjugates through tail vein of bilateral tumor-bearing mouse. The observed result has been further supported with ex vivo biodistribution (Fig. 1.2e) and relative fluorescence intensity analysis of different organs and tissues.

Recently, research community have concentrated on multinary I-III-VI_2 and I_2-II-IV-VI_4 group alloyed semiconductor nanomaterials of Cu/Ag-based metal sulfides, such as $CuInS_2$, $AgInS_2$, Cu_2ZnInS_4 and Ag_2ZnInS_4. Because these nanomaterials contain no highly toxic elements and exhibit composition tunable optical and electronic properties, high photoluminescence quantum yield (PLQY) and resistance to photobleaching. Multinary I-III-VI_2 and I_2-II-IV-VI_4 quantum dots with these exclusive features can be applied to bioimaging application. Peng group (Xie et al. 2009) had proposed a greener method to synthesize ZnS coated CuInS quantum dots with high QY of ~30% in non-coordinating solvent. Figure 1.2f shows the emission wavelength of CuInS–ZnS core–shell quantum dots which covers a broad emission window from 500 (visible) to 950 (NIR-I) nm. The CuInS–ZnS quantum dots exhibit good optical characteristics, and are highly hopeful for NIR fluorescent imaging and multicolor imaging. In one of the earlier studies, oil
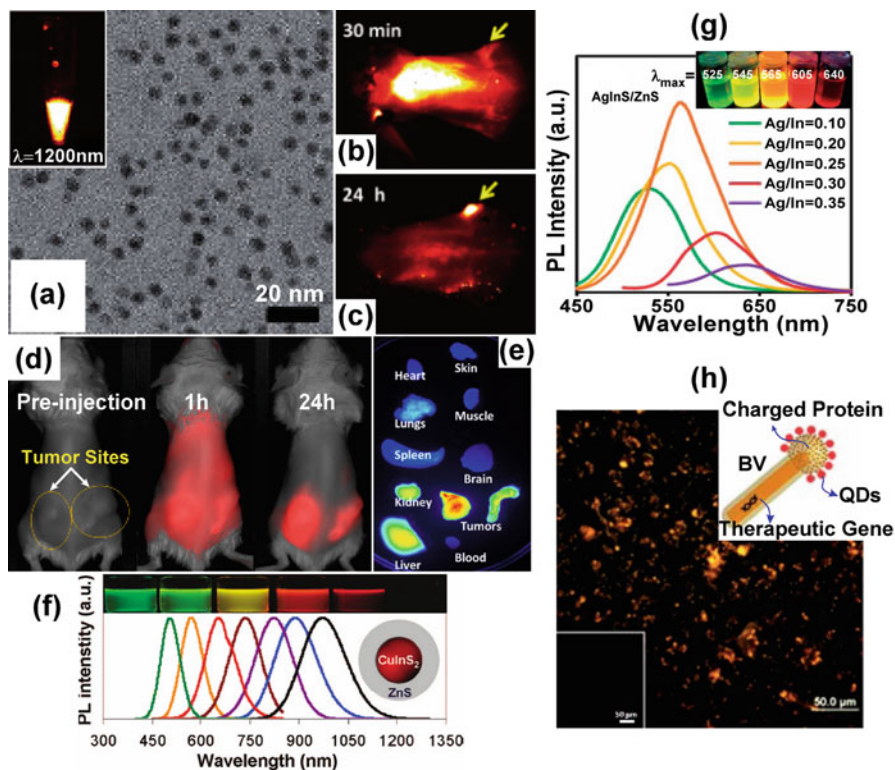
Fig. 1.2 (**a**) A TEM image of 6PEG-Ag$_2$S quantum dots. Insert image denotes the photoluminescence image of 6PEG-Ag$_2$S quantum dots suspended in PBS at a concentration of 1.34 mg mL^{-1}. (**b** and **c**) NIR-II fluorescence imaging of a xenograft 4T1 tumor with high uptake of 6PEG-Ag$_2$S quantum dots. (Modified after Hong et al. (2012). Copyright 2012 John Wiley and Sons). (**d**) Representative in vivo fluorescence imaging of cRGDfK-Ag$_2$S in 4T1luc tumor-bearing Balb/c mouse at different time points after intravenous administration. (**e**) Representative ex vivo fluorescence image of organ tissues from 4T1luc bilateral tumor bearing mice 24 h postinjection. (Reprinted with permission from Tang et al. (2015). Copyright 2015 American Chemical Society). (**f**) Photoluminescence properties of the CuInS$_2$–ZnS core–shell nanocrystals. (Reprinted with permission from Xie et al. (2009). Copyright 2009 American Chemical Society). (**g**) Photoluminescence spectra of water dispersible AgInS–ZnS quantum dots with varying Ag:In ratios. (Insert: the photograph was taken under ultraviolet light). (**h**) Fluorescence image of HeLa cells incubated overnight with baculoviral vectors (BVs) that are labeled with orange-emitting polyacrylic acid and mercaptoacetic acid ligand-capped AgInS–ZnS (PM-AgInS–ZnS) quantum dots. Insert image (left bottom) shows the fluorescence image of HeLa cells incubated solely with PM-AgInS–ZnS quantum dots. Insert graphical representation denotes the BV labeled with negatively charged PM-AgInS–ZnS quantum dots. (Modified after Regulacio et al. (2013). Copyright 2013 Royal Society of Chemistry)

dispersible CuInS$_2$–ZnS core–shell quantum dots (Yong et al. 2010) were encapsulated within functionalized PEGylated phospholipid micelles, and further conjugated with folic acid for in vivo tumor targeting and imaging. Strong fluorescence signal

was observed from the tumor area of mouse treated with folic acid- conjugated $CuInS_2$–ZnS quantum dots, whereas weak signal was attained from the tumor sites for unconjugated quantum dots. In addition to this, in vivo multiplex luminescence imaging was achieved by administering two different color-emitting $CuInS_2$–ZnS quantum dot micelles (quantum dot 640 and quantum dot 710) subcutaneously. As shown in Fig. 12 of work done by Yong et al. (Yong et al. 2010), the fluorescence signals from two different quantum dots are well distinguished. The results confirm that the efficiency of $CuInS_2$–ZnS core–shell quantum dots bioconjugates as an optical contrast agent for targeted and multiplexed optical bioimaging. In another study, a bright and stable $CuInS_2$–ZnS quantum dots embedded in silica nanobeads were fabricated and further conjugated with holo-Transferrin (TF) protein for targeted cancer cell imaging (Foda et al. 2014). And, in vitro bioimaging study had suggested that the quantum dots@SiO_2@TF conjugates were capable of targeting cancer cells. Yang et al. employed alpha-fetoprotein (AFP) antibody as a tumor targeting ligand (Yang et al. 2016a). Intense fluorescent signal was observed in the cytoplasm of HepG2 cells treated with CuInS–ZnS-AFP probe, while no signal was observed from the control one, bare CuInS–ZnS quantum dots.

On other hand, there are a few research papers demonstrating $AgInS_2$ ternary and $AgZnInS_2$ quaternary quantum dots in the form of bare or core–shell architecture efficiently used for optical in vitro and in vivo imaging (Chang et al. 2012; Shamirian et al. 2015; Tan et al. 2015b; Song et al. 2016a; Mansur et al. 2017). For example, Regulacio and co-workers had demonstrated that $AgInS_2$–ZnS quantum dots coated on baculoviral vectors act as efficient vectors for co-delivery of therapeutic genes and quantum dot luminescent probe to the cells (Regulacio et al. 2013). In this study, air stable $AgInS_2$–ZnS quantum dots with tunable emission from 525 to 640 nm (Fig. 1.2g) and the PLQYs of up to 20% were synthesized by varying Ag:In ratios in aqueous phase in the presence of polycarboxylate (polyacrylic acid, PAA) and thiol-containing ligand (mercaptoacetic acid, MAA). PM-coated $AgInS_2$–ZnS quantum dots display very low cytotoxicity (9.5% for 200μg mL^{-1}, 48 h of incubation) and colloidal stability in the physiological pH range. The negatively charged PM-$AgInS_2$–ZnS-565 nm quantum dots were electrostatically bind with positively charged end of baculoviral vectors (insert graphical representation of Fig. 1.2h). In vitro study on HeLa cells (Fig. 1.2h) suggests that baculoviral vectors attached with PM-$AgInS_2$–ZnS quantum dots can efficiently enter and label the cells. In another study on multinary Ag chalcogenides, Song et al. demonstrated a method for synthesizing ternary $AgInS_2$, quaternary AgZnInS, $AgInS_2$–ZnS and AgZnInS–ZnS quantum dots based on cation exchange and diffusion process (Song et al. 2016b). L-glutathione (GSH) was used to make water-dispersible alloyed core–shell quantum dots, and alpha-fetoprotein antibodies (AFP, a specific indicator in diagnosing hepatocellular carcinoma) were used to conjugate with GSHcapped quantum dots for targeted fluorescent labeling. For in vitro imaging, Hep-G2 cells were treated with GSH-quantum dots@AFP antibody conjugates. Optical images showed that GSH-quantum dots@AFP conjugates bound to the antigen receptors in the cytoplasm of Hep-G2 cells via antigen–antibody reaction. On the contrary, quantum dots without conjugating AFP could

not label the cytoplasm of Hep-G2 cells. According to the above studies, targeted labeling efficiency of multinary Ag-based metal sulfides has been realized.

1.2.2 Magnetic Resonance Imaging

Magnetic resonance imaging (MRI) is a broadly used diagnostic imaging tool in the clinical procedures and is based on the magnetization properties of atomic nuclei. As an effective imaging technique, MR contrast imaging has advantages such as high spatial resolution (~1 mm), deep tissue penetration and three-dimensional anatomical information. Moreover, MR contrast agents are often used to further improve their imaging sensitivity by interacting with water molecule protons in surrounding tissues, leading to shorten the longitudinal (spin-lattice) and transverse (spin–spin) relaxation times, thereby enhancing image contrast. Paramagnetic and superparamagnetic metal ions are used as contrast agents for MRI. Paramagnetic materials boost the longitudinal relaxation processes (known as T_1 relaxation processes), making brighter MR signal, whereas superparamagnetic and ferromagnetic materials accelerate the transverse relaxation processes (known as T_2 relaxation processes), which has resulted in hypointense MR signal.

Lanthanide metal ion gadolinium (III) has been confirmed to exhibit superior paramagnetic contrast efficiency due to its unique magnetic characteristics. Therefore, incorporation of Gd(III) ions into the host nanomaterials is one of the ways to achieve enhanced MRI signal intensity by serving as paramagnetic module. Metal sulfide nanomaterials embedded with Gd^{3+} dopant or decorated with Gd chelates have been developed as efficient positive (T_1) contrast agents for MR imaging. For instance, Chang et al. synthesized Gd^{3+} ion-doped $CuInS_2$–ZnS core–shell quantum dots in the presence of dual stabilizers glutathione and citric acid trisodium salt by microwave irradiation technique as shown in Fig. 1.3a (Chang et al. 2016). This T_1 contrast agent exhibits a significantly high longitudinal relaxivity ($r_1 = 55.90$ mM^{-1} s^{-1}) and low r_2/r_1 ratio of 1.42 (Fig. 1.3b, c). In a work by Anbazhagan et al., paramagnetic MoS_2-Gd chelate core–shell nanoparticle was synthesized by a multistep process as shown in Fig. 1.3d (Anbazhagan et al. 2016). In this MoS_2-Gd chelate core–shell structured nanoparticles, a conjugated gadolinium-chelate shell significantly improves the magnetic property and longitudinal relaxation rate (9.4 mM^{-1} s^{-1}) to the MoS_2 core. In vivo MR imaging was also performed, which displayed hyperintense signal in the kidney, heart and bladder (Fig. 1.3e, f). Transition element manganese(II)-doped nanomaterials are the another category of efficient MRI contrast agents. The potential of 1.5–2 nm-sized Mn^{2+}-doped ZnS quantum dots with different dopant concentrations as MRI-positive contrast agents has been studied by evaluating their relaxivities (Jahanbin et al. 2015). According to MRI studies, Mn^{2+}:ZnS quantum dots generate strong T_1 contrast enhancement. And Mn:ZnS quantum dots exhibit high longitudinal (r_1) relaxivity varying between 20.34 and 75.5 mM^{-1} s^{-1} with concentration of Mn^{2+} increasing from 10% to 30%.
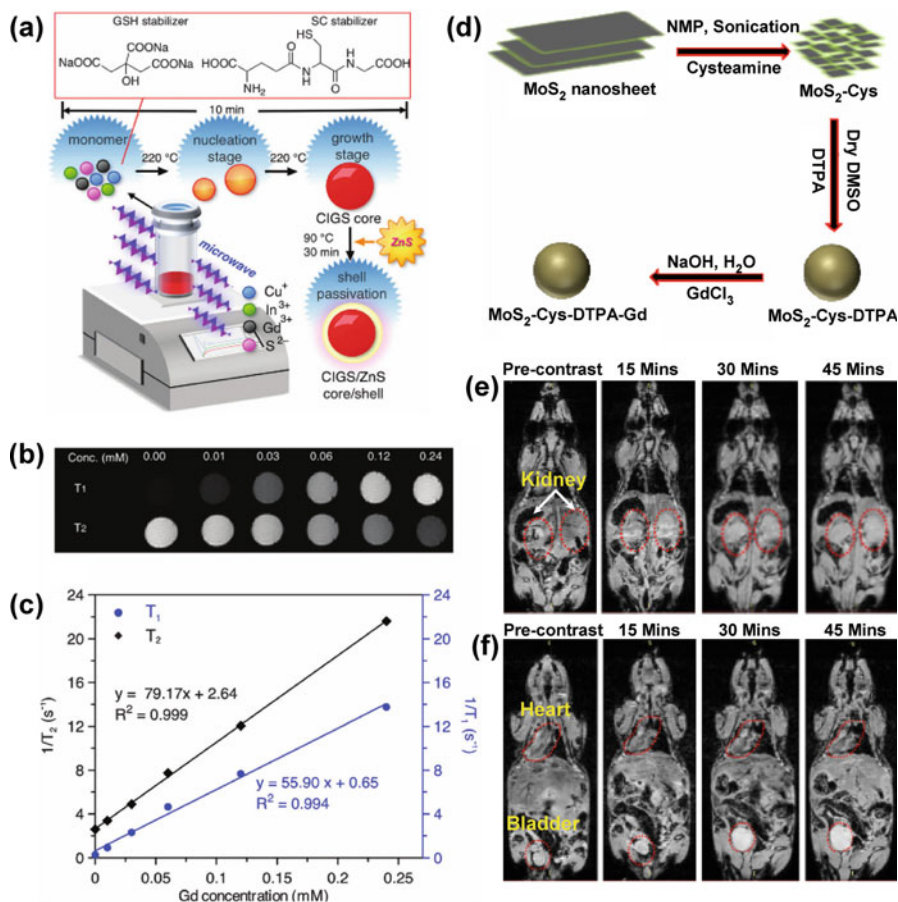
Fig. 1.3 (**a**) Formation of the Gd:CuInS$_2$ core and Gd:CuInS$_2$–ZnS core–shell quantum dots under microwave irradiation. (**b**) T_1- and T_2-weighted images of phantoms containing various Gd concentrations. (**c**) Plots of inverse relaxation times ($1/T_1$ and $1/T_2$) versus Gd concentration of the as-synthesized Gd:CuInS$_2$–ZnS quantum dots. (Reprinted with permission from Chang et al. (2016). Copyright 2016 Royal Society of Chemistry). (**d**) Synthetic approach used to prepare the core–shell gadolinium (Gd)-chelate functionalized MoS$_2$ nanomaterials. (**e**) The T_1-weighted MR images of the mice injected with MoS$_2$-Cys-DTPA-Gd at image layer with the kidney. (**f**) T_1-weighted MR images of the mice injected with MoS$_2$-Cys-DTPA-Gd at image layer with the heart and bladder. (Reprinted with permission from Anbazhagan et al. (2016). Copyright 2016 American Chemical Society)

1.2.3 Photoacoustic Imaging

The photoacoustic imaging (PAI) is otherwise termed as optoacoustic imaging. The PAI has been emerged as promising deep tissue imaging modality that is capable of mapping the optical absorption coefficient of biological tissues via photoacoustic

effect. In PAI, the nanosecond laser pulses absorbed by the biomolecules (endogenous photo-absorbers) undergo time-varying thermal expansion–relaxation process which results in generation of acoustic waves in the tissue. Finally, images are formed by reconstructing the generated photoacoustic signals acquired at different positions around the tissue surface. Detection sensitivity and specific tissue target abilities of PAI modality can be potentially extended by employing exogenous contrast agent. The agents that strongly absorb NIR radiation are highly suitable for high-contrast PAI with enhanced detection sensitivity at depths.

Nanomaterial-based exogenous contrast agents play a crucial role in PAI with high signal-to-noise ratio. Nanostructures with NIR-absorbing metal sulfides such as Ag_2S, MoS_2 and CuS have shown remarkable potential as PAI contrast agents. Due to NIR absorption ability and low toxicity, Ag_2S nanoparticles are promising nanoprobes for PAI. Zhang and co-workers have developed an anti-EGFR affibody (ZEGFR:1907) conjugated Ag_2S quantum dots with average size of 14 nm and exhibited surface plasmon resonance absorption at ~800 nm (Zhang et al. 2018b). Ex vivo and in vivo studies showed good biosafety and excellent efficiency in the NIR-I PAI of tumor cells when illuminated by 808 nm laser (NIR-I window, 100 mW cm^{-2}). In another case, contrast agent of folic acid-modified PF127@Ag_2S quantum dots have been used for photoacoustic imaging of tumor cell targeting (Zhang et al. 2018a). On the other hand, CuS has also received a great attention due to its localized surface plasmonic absorption in NIR window, making CuS as a suitable candidate for PAI. In 2013, Feng et al. had designed and synthesized a smart "off–on" PAI contrast agent of CuS based on the significant change in the NIR absorption that originates from the amorphous–crystalline phase transition in response to the body temperature (Feng et al. 2018). In vivo study proved that the PAI ability of amorphous CuS can be efficiently activated by body temperature. In another study, CuS nanoparticles with absorption tuned to 990 nm as an excellent contrast agent suitable for deep tissue PA tomography (PAT) imaging. Lie's group was first demonstrated in NIR-II PAT using CuS nanoparticles (~11±3 nm) with 1064 nm Nd:YAG laser (Ku et al. 2012). This PA contrast agent allowed visualization of mouse brain after intracranial injection (Fig. 1.4a1) and rat lymph nodes 12 mm below the skin after interstitial injection (Fig. 1.4a2). In addition, agarose gel containing CuS contrast agent embedded in chicken breast muscle could be mapped at a depth of ~5 cm. Recently, nanoprobe of hybrid protein–CuS (CuS@BSA-RGD) nanoparticles possessing high optical absorption at 1064 nm have been fabricated and applied for PAI of orthotopic hepatocellular carcinoma with high signal-to-noise ratio (Yan et al. 2019). Also, the experimental results revealed that this nanoprobe has excellent photoacoustic properties at 1064 nm pulse laser excitation.

As a NIR absorbing material, molybdenum sulfide (MoS_2) nanostructures have also been exploited as contrast agents for enhanced PAI. The MoS_2 is a known material to have layered structure and comparable to graphene for many characteristics. For instance, single-layer MoS_2 nanosheets were employed as efficient probe for highly sensitive PAI of orthotopic brain tumors (Chen et al. 2016). In this study, the MoS_2 nanosheets with different layered nanostructures were prepared by
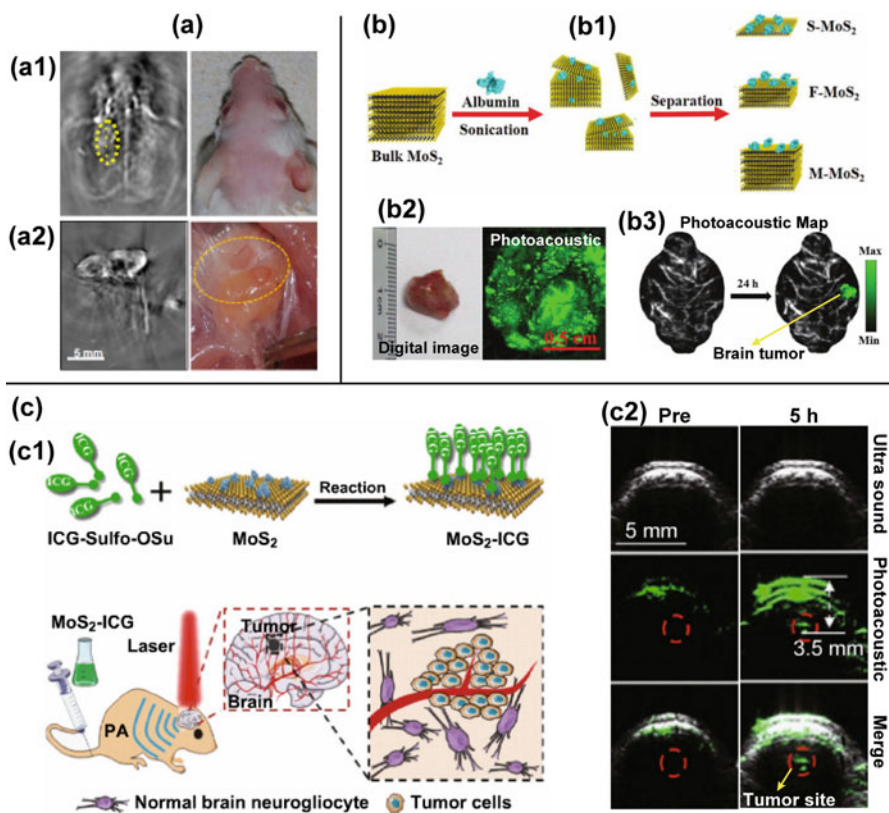
Fig. 1.4 (**a**) Copper sulfide nanoparticles for deep tissue imaging, (a1) representative in vivo PAT images of a mouse brain at 1064 nm 24 h after intracranial injection of 15μL of CuS nanoparticle solution and photograph of the head of the mouse, (a2) PAT image of auxiliary and brachial lymph nodes acquired on the right side of a rat 24 h after interstitial injection of 200μL of CuS nanoparticle solution into the right front paw pad and corresponding photograph of exposed rat under arm after imaging experiment. Yellow circle indicates lymph nodes. (Reprinted with permission from Ku et al. (2012). Copyright 2012 American Chemical Society). (**b**) Single-layer MoS_2 nanosheets with amplified photoacoustic effect for highly sensitive PAI of orthotopic brain tumors, (b1) synthesis procedure of MoS_2 nanosheets with various layered nanostructures, (b2) digital photograph and photoacoustic maximum amplitude projection image of exfoliated tumor at 24 h post i.v. injection of S-MoS_2, (b3) photoacoustic maximum amplitude projection image of brain tumor region before and after 24 h post i.v. injection of S-MoS_2 showing blood vessels (gray) and brain tumor (green color). (Reprinted with permission from Chen et al. (2016). Copyright 2016 John Wiley and Sons). (**c**) Molybdenum disulfide and indocyanine green (MoS_2-ICG) hybrid for in vivo photoacoustic imaging, (c1)MoS_2–ICG hybrid synthesis and its application in photoacoustic imaging of orthotopic brain glioma, (c2) cross-sectional ultrasound, photoacoustic, and their merged images of the brain tumor region before and after 5 h intravenous injection of MoS_2–ICG. (Reprinted with permission from Liu et al. (2018). Copyright 2018 Springer)
S-MoS₂ Single layer MoS_2, *F-MoS₂* few layer MoS_2, *M-MoS₂ multilayer MoS₂*, and *ICG* indocyanine green

albumin-assisted layer-by-layer exfoliation method as described in Fig. 1.4b1. It was found out that, decreasing the number of nanosheet layers of MoS_2 from multilayer (M-MoS_2) to single layer (S-MoS_2) can remarkably improve the NIR absorption and enhanced the elastic properties of the nanoprobe, thus resulted in a greatly amplified photoacoustic effect. As shown in Fig. 1.4b2, b3, in vivo PAI with S-MoS_2 nanosheets was achieved in subcutaneous (Fig. 1.4b2) and orthotopic brain tumor models (Fig. 1.4b3), revealing their high sensitivity and effective imaging depth. The maximum imaging depth of tumor site was measured to be approximately 1.5 mm below the scalp. In another case, albumin-capped single-layered MoS_2 nanosheets were covalently conjugated with NIR dye indocyanine green for in vivo PAI of orthotropic glioma at deep site (Fig. 1.4c1, c2) (Liu et al. 2018). The imaging depth of as large as ~3.5 mm below the skull has been reached. Over all, these reports proved the efficiency of NIR-absorbing transition metal sulfides in PAI.

1.2.4   Multimodality Imaging

Recently, multimodality imaging strategy has received extensive attention because this methodology integrates the strengths of each imaging modality and simultaneously eliminates one or more negatives of single modality. This effective approach expands the accuracy of diagnosis and offer wide-range of biomedical information. There are a number of studies where it was demonstrated that highly versatile metal sulfide nanoprobes can be utilized as multimodality imaging probes (Table 1.1).

As a promising imaging tool, the nanoprobe combined fluorescence with MRI modality has attracted much attention owing to the capability of integrating the high sensitivity FLI to the high resolution and deep tissue penetration of MRI. Incorporation of magnetic ions with florescent metal sulfides makes them efficient in FLI as well as in MRI dual-modality diagnosis nanoprobes. For example, MnS shell overcoated Mn^{2+}-doped ZnS nanorods were applied for FL imaging in vitro and MR imaging in vivo imaging (Zhao et al. 2016). This one-dimensional contrast agent has exhibited a distinct orange luminescence at 587 nm with a high longitudinal relaxivity of 9.1 mM^{-1} s^{-1}. Further, in vivo studies showed the prepared ZnS: Mn–MnS nanorods were indeed effective MRI T_1 contrast agent for the gallbladder and pancreas in mice. Moreover, some of other studies have demonstrated that paramagnetic Gd^{3+}-doped Cu-based ternary and quaternary nanomaterials were efficient FLI–MRI dual-modal nanoprobes (Table 1.1). As shown in Fig. 1.5a, a bimodal nanoprobe of chelate-free hydrophobic Gd^{3+}-doped $CuInS_2$–ZnS quantum dots was developed and subsequently surface engineered into aqueous phase with PEGylated dextran-stearyl acid polymeric lipid vesicles (PEG-DS PLVs) (Yang et al. 2015b). The PEGylated bimodal nanoprobe had exhibited a distinct fluorescence at 670 nm with PLQY of ~50% and high longitudinal relaxivity r_1 of 9.45 mM^{-1} s^{-1} in water phase with good colloidal stability. The succeeding tumor-bearing animal experiments further demonstrated that remarkable tumor-targeted contrast enhancement could be observed by both FL and MR

Table 1.1 Examples of various metal sulfide nanostructures used as bimodal nanoprobe

Imaging agent	Nanostructure	Particle size (nm)	Imaging modality	$\lambda_{Em}/\lambda_{Abs}$ (nm)	Relaxivity (mM^{-1} s^{-1})	Reference
ZnS:Mn–MnS	Rod	Dia. 8–10 Length 20–50	FLI and MRI	λ_{Em} = 587	9.30	Zhao et al. (2016)
Ag,Mn co-doped In$_2$S$_3$–ZnS	Spherical	6.5–7.5	FLI and MRI	λ_{Em} = 535–755	6.84	Lai et al. (2017)
Gd-doped ZnCuInS–ZnS	Spherical	~4.0	FLI and MRI	λ_{Em} = 550–725	11.5–15.8	Guo et al. (2014)
Gd doped CuInS$_2$–ZnS	Spherical	~6.0	FLI and MRI	λ_{Em} = 580		Gedda et al. (2017)
Gd-doped CuInS$_2$–ZnS	Spherical	~3.0	FLI and MRI	λ_{Em} = 591	20.4	Yu et al. (2017)
CuInS$_2$–ZnS@ DTDTPA-Gd	Spherical	~24.7	FLI and MRI	λ_{Em} = 710	9.91	Yang et al. (2017b)
Ag$_2$S@Gd-DOTA	Spherical		NIR-FLI and MRI	λ_{Em} = 1200	4.9	Li et al. (2015)
Ag$_2$S-iodinate oil hybrid	Spherical	~139.6	NIR-FLI and CT	λ_{Em} = 1170		Qin et al. (2015)
Ni-doped CuS	Spherical	~7.0	PAI and MRI	λ_{Abs} = 1060	2.3	Gao et al. (2015)
CuS@ DTPA-Gd	Triangle	~14	PAI and MRI	λ_{Abs} = 1100	6.94	Gao et al. (2017a)

FLI Fluorescence imaging, *NIR-FLI* near-infrared fluorescence imaging, *MRI* magnetic resonance imaging, *PAI* photoacoustic imaging, and *CT* X-ray computed tomography
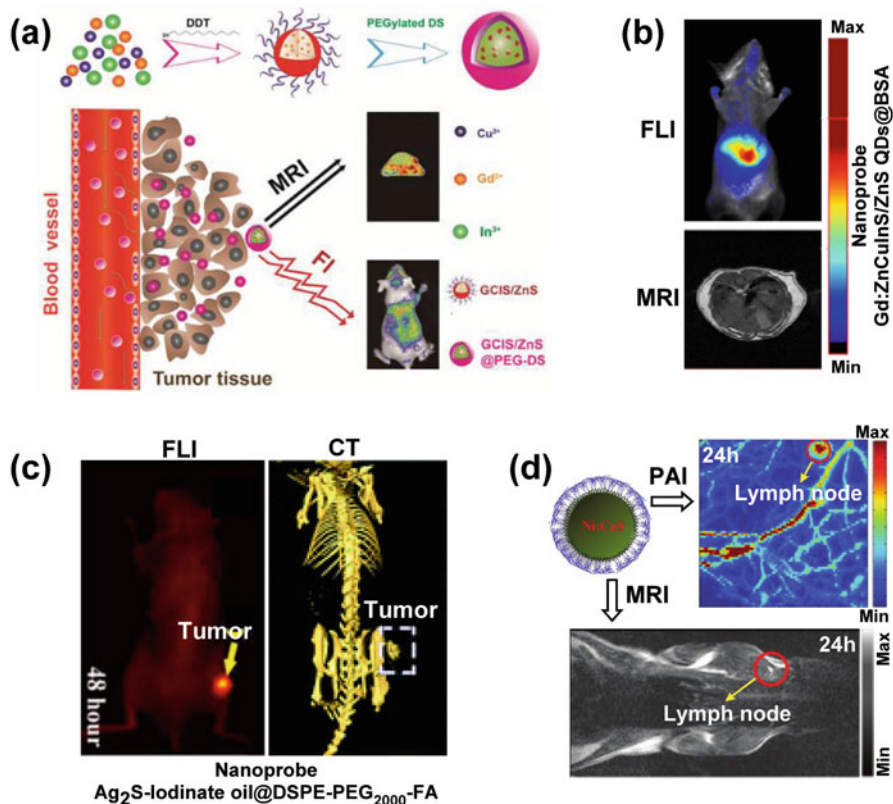
Fig. 1.5 (**a**) Synthesis and surface modification of Gd-doped CuInS–ZnS quantum dots and used for dual-modal fluorescence and magnetic resonance imaging. (Reprinted with permission from Yang et al. (2015b). Copyright 2015 American Chemical Society). (**b**) The fluorescence in vivo images and T_1-weighted transverse magnetic resonance images of the liver of BALB/c mice acquired at 4 h postinjection of Gd:ZnCuInS–ZnS core–shell quantum dots at a dose of 0.05 mmol Gd/kg mouse body weight. (Reprinted with permission from Guo et al. (2014). Copyright 2014 Springer Nature). (**c**) Fluorescence and X-ray computed tomography of HeLa xenograft nude mice acquired after 48 h postinjection of Ag$_2$S-I@DSPE-PEG$_{2000}$-FA nanoprobe. (Modified after Qin et al. (2015). Copyright 2015 Royal Society of Chemistry). (**d**) In vivo photoacoustic and T_1-weighted magnetic resonance imaging of a mouse after injected with 0.05 mL (0.4 mg mL^{-1}) PMAH-PEG capped Ni-doped CuS nanoparticles. Red circle indicates the lymph node. (Modified after Gao et al. (2015). Copyright 2015 Royal Soceity of Chemistry) *FLI* Fluorescence imaging, *MRI* magnetic resonance imaging, *PAI* photoacoustic imaging, and *CT* X-ray computed tomography

imaging (Fig. 1.5a). This signifies the great potential of Gd:CuInS$_2$–ZnS@PLVs quantum dots for tumor-targeted bimodal in vivo imaging by fluorescence and magnetic resonance. In another case, Gd^{3+} doped in ZnCuInS quaternary quantum dots coated with ZnS shell has been introduced as an effective FLI–MRI dual-modality nanoprobe (Fig. 1.5b) (Guo et al. 2014). The obtained nanoprobe has

shown good quantum yield (up to 40%), high longitudinal relaxivity (15.78 mM^{-1} s^{-1}) and robust colloidal stability. Besides, for the first time, Li et al. have demonstrated a novel Gd-Ag$_2$S bimodal nanoprobe with NIR-FL and MR imaging for simultaneous preoperative diagnosis and intraoperative brain tumor resection (Li et al. 2015).

The combination of fluorescence and X-ray computed tomography (CT) imaging approach is another kind of ideal bimodal molecular imaging, which unifies molecular functional imaging and anatomical imaging perfectly. Zhao's group has made the hybrid of Ag$_2$S quantum dots and iodinate oil to form a new kind of multifunctional single Ag$_2$S-I bimodal nanoprobe, which integrated the significant NIR-II luminescence of Ag$_2$S (1170 nm) and CT ability of iodinate oil (Qin et al. 2015). Phospholipid-polyethylene-glycol-folate (DSPE-PEG$_{2000}$-FA) and other amphiphilic molecules were used to wrap the hydrophobic Ag$_2$S-I nanoprobe and formed a complex Ag$_2$S-I@DSPE-PEG$_{2000}$-FA nanoparticles. As shown in Fig. 1.5c, intensive fluorescence and X-ray CT enhancement signals were found in tumor site when the Ag$_2$S-I@DSPE-PEG$_{2000}$-FA nanoparticles were injected into the HeLa xenograft nude mice by tail vein. Therefore, the results revealed that this new multifunctional nanoprobe has good tumor targeting capabilities, and it has great potential in FLI–CT bimodal in vivo imaging.

Gao et al. had fabricated an exogenous bimodal PAI–MRI nanoprobe of diethylenetriaminepentaacetic acid (DTPA)-Gd^{3+}functionalized bovine serum albumin (BSA) protein-modified CuS nanotriangles (Gao et al. 2017a). Hydrophilic protein BSA-modified CuS nanotriangles were prepared in the presence of halides, and it exhibited strong absorption in the NIR-II region (1100 nm), good stability in a wide pH range (4–10) and good thermal stability up to 75 °C. Moreover, gadolinium ion chelated diethylenetriaminepentaacetic acid (DTPA-Gd^{3+}) was conjugated on BSA-CuS nanotriangles to perform as a bimodal PAI–MRI agent. The T_1 relaxivity of DTPA-Gd^{3+}functionalized BSA-modified CuS nanotriangles was found to be 6.94 mM^{-1} s^{-1}. in vivo PAI and MRI studies using DTPA-Gd^{3+}functionalized BSA-modified CuS nanotriangles were performed in nude mice bearing the U87 tumor. Both photoacoustic and T_1-weighted magnetic resonance in vivo results (Fig. 5 of work done by (Gao et al. 2017a)) showed that the contrast in U87 tumor site was increased with increasing time from 0 to 24 h. Overall the findings revealed that the multifunctional nanotriangle has significant value in PA–MR dual-modal imaging in targeting tumor with enhanced resolution and contrast. In another report (Gao et al. 2015), CuS as a NIR absorbing material and nickel ion as a MR contrast agent were chosen to prepare the multifunctional Ni^{2+}-doped CuS nanoparticles for PA–MR in vivo mapping of lymph nodes (Fig. 1.5d). The PMAH-PEG capped Ni-doped CuS nanoparticles with size around 7 nm displayed a wide tunable NIR absorption between 740 nm and 1400 nm and specific relaxivity of about 2.3 mM^{-1} s^{-1}. The PA imaging in Fig. 1.5d indicates that the multifunctional nanoprobe had traveled through lymphatic vessels and concentrated into the lymph nodes. Similarly, the increment of T_1-weighted magnetic resonance signals was observed in lymph nodes after 24 h of postinjection (Fig. 1.5d).

1.2.5   Image-Guided Therapy

Imaging-guided synergistic cancer therapy by integrating imaging and therapeutic agent in a single nanoplatform is recently attracted great attention for accurate tumor diagnosis and higher treatment proficiency. The emergence of nanomaterials has provided substantial progress that can be concurrently used for cancer diagnosis and therapy. Table 1.2 summarizes some examples of metal sulfide nanostructures that have been used as cancer theranostic probes. Several research groups have proved the potential of CuS-based nanomaterials as theranostic agents. Zhang et al. have developed a template method to construct uniform and porous three-dimensional CuS hollow nanoflowers comprising of two-dimensional nanoplates for multifunctional application in MRI-guided thermochemotherapy of cancer (Fig. 1.6a) (Zhang et al. 2019). It has high photothermal conversion efficiency of 30%. At the same time, the hollow structure in them makes CuS a perfect nanoplatform for drug loading with laser-activated drug release. As shown in Table 1.2, the studies on magnetic ions such as Fe, Gd, Mn and Ga doped in CuS nanoparticles have shown good capability in multimodal imaging along with targeted photothermal therapy of tumors. Besides, ternary compounds based on copper with different nanostructures (Cu_3BiS_3 nanorods, Cu_5FeS_4 nanocubes and CuInS quantum dots) have been reported to be promising theranostic agents for cancer diagnosis and therapy (Table 1.2). In an innovative imaging-guided therapy system, Wang et al. have proposed a biomimetic synthesis for loading radioisotopes inside the ferritin nanocage for cancer theranostics (Wang et al. 2016). As shown in Fig. 1.6b1, Cu^{2+} and radioactive $^{64}Cu^{2+}$ ions were initially encapsulated into the 12 nm of ferritin cages. Then, stable CuS nanoparticles inside the ferritin cages were attained by inclusion of Na_2S solution. This uniform CuS-Ferritin nanocages exhibited a strong NIR absorbance in the range of 700–1100 nm, strong photoacoustic contrast and high photothermal conversion efficiency. in vitro (Fig. 1.6b2) and in vivo (Fig. 1.6b3–b5) studies showed that CuS-Ferritin nanoagent achieved greater tumor therapeutic efficiency.

As shown in Fig. 1.7, triple-modal imaging (PAI, CT and IRT)-guided thermo-chemotherapy by a single urchin-like PEGylated Bi_2S_3@DOX nanoagent was achieved (Li et al. 2016). More importantly, highly porous nanostructure of PEGylated Bi_2S_3@DOX nanoagent have showed enhanced chemotherapeutic drug-loading capacity ($\sim 37.9\%$ for DOX). Under NIR laser irradiation at 808nm, in vivo evaluation revealed that PEG-Bi_2S_3@DOX nano-urchins can perform efficient tumor growth inhibition as a result of synergetic effect of thermo-chemotherapy (Fig. 1.7e–g). Another kind of nanostructured metal sulfide, as cancer theranostic agent, is the two-dimensional transition metal chalcogenides such as MoS_2 and WS_2. More importantly, nanomaterials or nanocomposites based on two-dimensional transition metal chalcogenides such as MoS_2 sheet, MoS_2@BSA-Gd nanoflakes, Bi_2S_3 nanoparticles decorated MoS_2 nanosheet and WS_2 quantum dots (Table 1.2) have been used in the combined treatment (PTT combined with RT or PDT) for tumors. For example, as shown in Fig. 1.8a, Liang Cheng et al. have

Table 1.2 Examples of various metal sulfide nanostructures used as cancer theranostic nanoagents

Theranostics agent	Nanostructure	Particle size (nm) from TEM or DLS	Imaging modality	Therapy	Reference
CuS	Flower	Dia. ~30–120 Thickness ~ 5.0	MRI	PTT and chemotherapy	Zhang et al. (2019)
Gd^{3+} doped CuS	Spherical	~9.0	PAI and MRI	PTT	Yang et al. (2016b)
Fe^{3+} doped CuS	Spherical	~5.6	MRI	PTT	Wang et al. (2019a)
Mn^{2+} and $^{68}Ga^{3+}$ doped CuS	Spherical	~3.0–4.0	PAI, MRI and PET	PTT	Zhou et al. (2018)
CuS-ferritin	Cage	~ 8.0 (CuS) ~12.0 (Ferritin cavity)	PAI and PET	PTT	Wang et al. (2016)
Cu_3BiS_3	Rod	Dia. ~8 Length ~ 25	PAI and CT	TRT	Li et al. (2017)
Cu_5FeS_4	Cube	~5	MRI	PTT	Wang et al. (2018)
CuInS–ZnS	Spherical	–	FLI and MOST	PTT and PDT	Lv et al. (2016)
Ag_2S	Spherical	~ 4–10	FLI and PAI	PTT	Yang et al. (2017a)
Ag_2S@polypeptide hybrid nanogel	Spherical	~ 4 (Ag_2S)	NIR-FLI and PAI	PTT	Zhao et al. (2018)
Cu-Ag_2S	Spherical	~8.6	PAI and PTI	PTT	Dong et al. (2018)

(continued)

Table 1.2 (continued)

Theranostics agent	Nanostructure	Particle size (nm) from TEM or DLS	Imaging modality	Therapy	Reference
FeS_2	Spherical	~7	FLI and PAI and MRI	PTT and PDT	Jin et al. (2018)
Fe_3S_4	Sheet	Length – ~120 thickness ~ 15–25	MRI and IRT	PTT and CDT	Guan et al. (2018)
CoS	Sheet	~179 (lateral size of sheet)	PAI and IRT and MRI	PTT	Li et al. (2018)
Bi_2S_3	Urchin	–	PAI and IRT and CT	PTT and chemotherapy	Li et al. (2016)
MoS_2	Sheet	~ 454	FLI and PAI	PTT and PDT	Song et al. (2017)
Bi_2S_3 nanoparticles decorated MoS_2 nanosheet	Spherical and sheet	~10 (nanoparticle) ~300 (lateral size of sheet)	PAI and CT	PTT and RT	Wang et al. (2015)
MoS_2@BSA-Gd complex	Flakes	~297	PAI and MRI	PTT	Chen et al. (2017)
Gd-doped WS_2	Flakes	~80	PAI, MRI and CT	PTT and RT	Cheng et al. (2015)
WS_2	Spherical	~3	PAI and CT	PTT and RT	Yong et al. (2015)

TEM Transmission electron microscope, *DLS* dynamic light scattering, *BSA* bovine serum albumin, *FLI* fluorescence imaging, *NIR* near infrared, *MRI* magnetic resonance imaging, *PAI* photoacoustic imaging, *IRT* infrared thermal, *PET* positron emission tomography, *MOST* multispectral optical tomography, *CT* X-ray computed tomography, *PTT* photothermal therapy, *TRT* thermoradio therapy, *PDT* photodynamic therapy, *CDT* chemodynamic therapy, and *RT* radio therapy
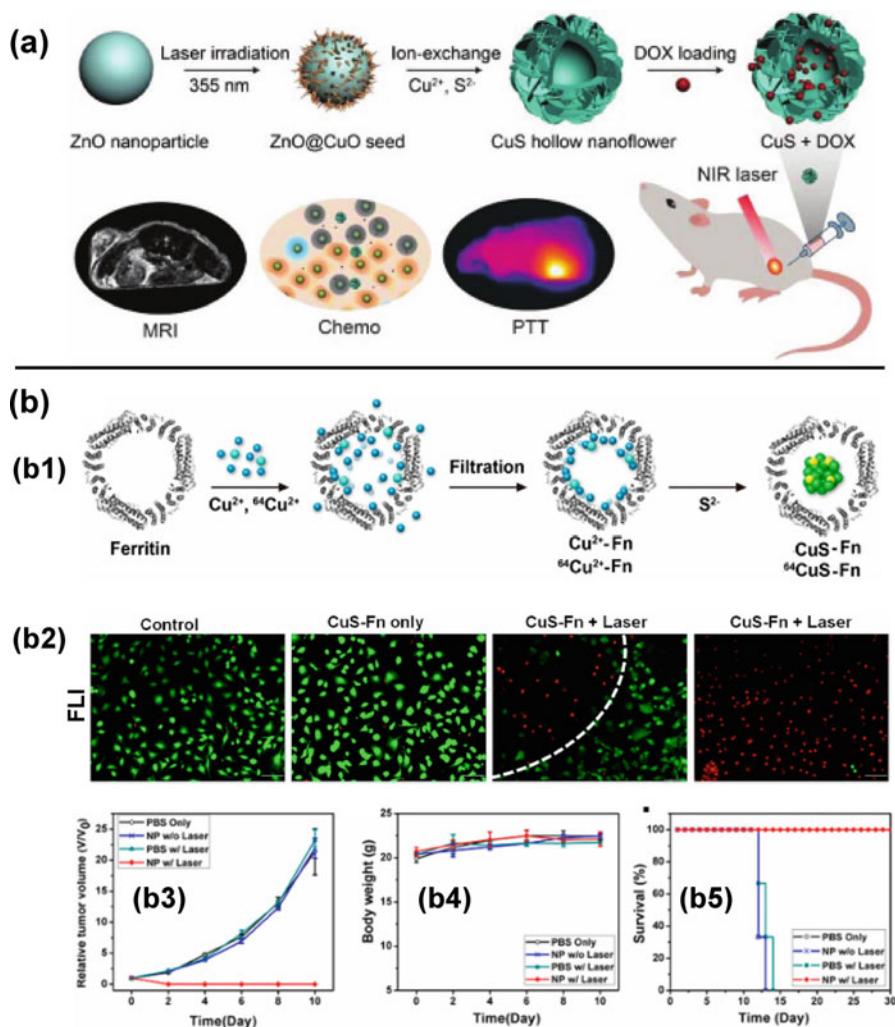
Fig. 1.6 (**a**) Synthetic processes of CuS hollow nanoflowers and magnetic resonance imaging-guided synergistic therapy by combining photothermal therapy and chemotherapy. (Reprinted with permission from Zhang et al. (2019). Copyright 2019 Royal Soceity of Chemistry). (**b**) CuS-Ferritin (CuS-Fn) nanocages as clinically translatable cancer theranostics for positron emission tomography and photoacoustic dual-modal imaging-guided photothermal therapy. (b1) The synthetic procedure of CuS-Fn nanocages. (b2) Fluorescence images of calcein AM/PI stained U87 MG cells after 4 h incubation with fresh medium, CuS-Fn, and CuS-Fn exposed to 808 nm laser. A clear laser spot can be seen in the irradiated CuS-Fn group. Scale bar is 100μm. Tumor volume (b3), body weight (b4), and mice survival rate (b5) curves of different groups of tumor-bearing mice after photothermal therapy treatment. (Reprinted with permission from Wang et al. (2016). Copyright 2016 American Chemical Society)

MRI Magnetic resonance imaging, *PTT* photothermal therapy, *PET* positron emission tomography, *FLI fluorescence imaging*, *PAI* photoacoustic imaging
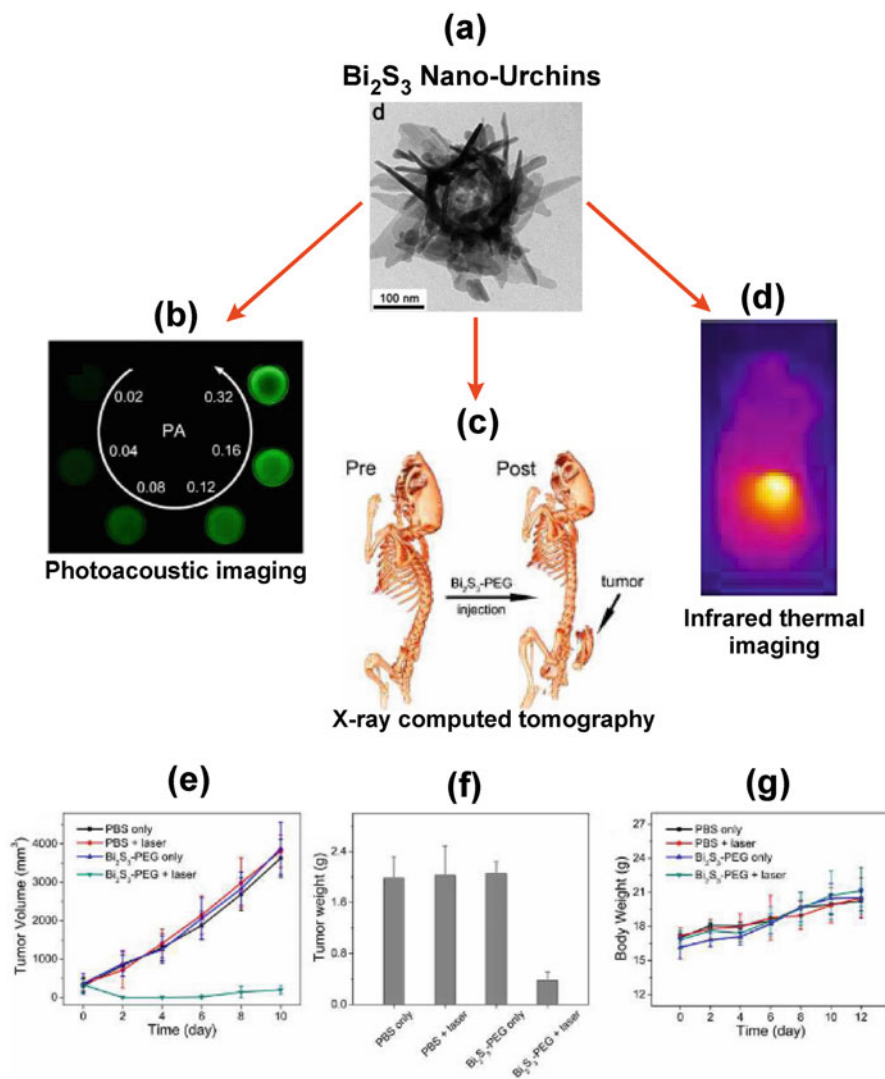
Fig. 1.7 Multifunction of bismuth sulfide-polyethylene glycol (Bi_2S_3-PEG) nano-urchins. (**a**) TEM image of the Bi_2S_3 nano-urchins. (**b**) Photoacoustic images of the Bi_2S_3-PEG nano-urchin aqueous dispersions at different concentrations (unit: mg mL^{-1}). (**c**) 3D in vivo X-ray computed tomography images of mice before (pre) and after (post) injection with the Bi_2S_3-PEG Nus (10 mg mL^{-1}, 200μL). The computed tomography contrast was obviously enhanced in the tumor after the injection. (**d**) Infrared thermal images of tumor-bearing mice i.v. injected with Bi_2S_3-PEG nano-urchin plus 10-min laser irradiation. (**e**) Tumor growth curves after various treatments. (**f**) Average weight of tumors collected from the mice. (**g**) Body weight of mice after various treatments. (Reprinted with permission from Li et al. (2016). Copyright 2016 Royal Society of Chemistry)
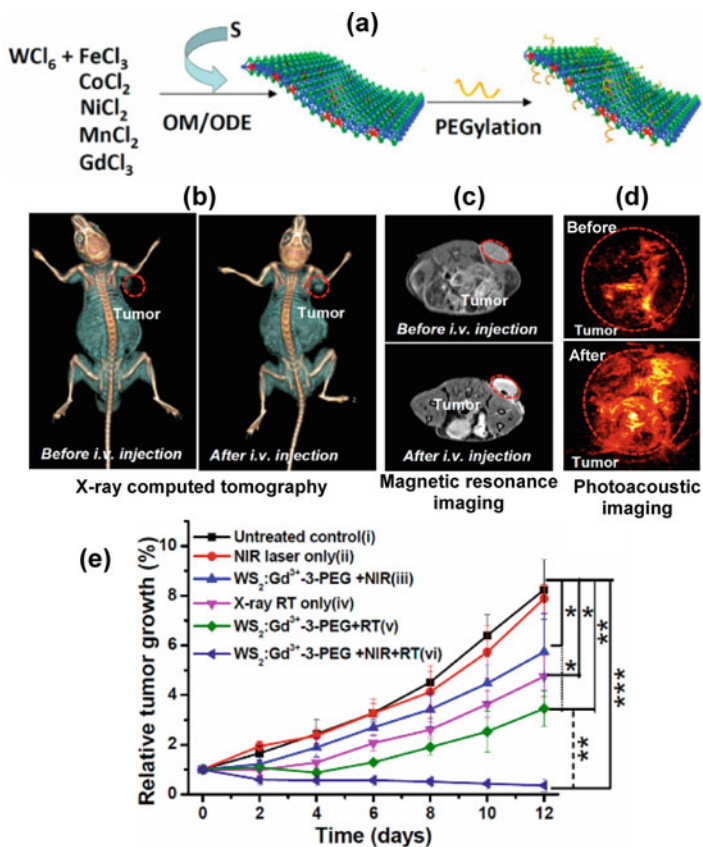
Fig. 1.8 (**a**) Synthesis and composition analysis of $WS_2:M^{n+}$ (M = Fe^{3+}, Co^{2+}, Ni^{2+}, Mn^{2+} and Gd^{3+}) nanoflakes prepared by a bottom-up method. In vivo triple-model imaging in 4T1 tumor-bearing mice. (**b**) In vivo X-ray computed tomography images of mice before and 24 h after i.v. injection with $WS_2:Gd^{3+}$-3-poly ethylene glycol (5 mg mL^{-1}, 200μL). (**c**) The T_1-weighted magnetic resonance images of mice before and 24 h after i.v. injection with $WS_2:Gd^{3+}$-3-PEG (2 mg mL^{-1}, 200μL). (**d**) In vivo photoacoustic images of tumors on mice before and 24 h after i.v. injection with $WS_2:Gd^{3+}$-3-PEG (2 mg mL^{-1}, 200μL). (**e**) Tumor volume growth curves of mice after various treatments (5 mice for each group). (Reprinted with permission from Cheng et al. (2015). Copyright 2015 American Chemical Society)

proposed a general method to dope various types of metal ions into WS_2 nanoflakes with PEG modification (Cheng et al. 2015). The PEGylated Gd^{3+}-doped WS_2 nanoflakes were preferred as a multifunctional nanoprobe for imaging-guided combination cancer treatment. In vivo PA, MR and CT multimodal imaging ability with the use of PEGylated $Gd^{3+}:WS_2$ nanoflakes (Fig. 1.8b–d) was realized by a strong NIR absorption of WS_2, the paramagnetic property contributed from Gd^{3+} dopant and the X-attenuation ability of W and Gd elements. As shown in Fig. 1.8e, as compared to PTT or RT alone, combination of $Gd^{3+}:WS_2$ nanoflakes-improved RT

with PTT proficiently inhibited the tumor growth, which proved the synergistic effect of combined PTT with RT.

1.3 Metal Sulfide Nanostructures for Biosensing

Nanomaterials with unique properties have sparked extensive attention in their use in the research field of biosensing. Metal sulfides with various nanostructures have been employed in the construction of various biosensors with high sensitivity and selectivity. Tables 1.3, 1.4 and 1.5 provide a list of metal sulfide nanostructure-based biosensors and their sensing performance such as the limit of detection (LOD). The performance of biosensors based on metal sulfide nanostructures depends on their morphology, dimension and surface activity. Based on the various reports (refer Tables 1.3, 1.4 and 1.5), metal sulfide-based biosensors can be categorized according to the signal transduction modes such as fluorescent biosensors, colorimetric biosensors and electrochemical biosensors. The following sections highlight the application of metal sulfides for biosensing based on the above said various detection approaches.

1.3.1 Optical Sensor

Optical sensing assays have gained intensive attention in biomedical field due to their rapid response and high sensitivity, and have been extensively studied for the detection of biological molecules. Optical biosensing is achieved by exploiting the effective interaction of optical fields with biorecognition elements. Optical sensors based on different metal sulfide nanostructures and their composites for the detection of various biological molecules have been widely studied. And some examples are listed in Tables 1.3 and 1.4.

Fluorescent Sensor

Fluorescence probe-based homogeneous assays have attracted much attention in the development of biosensing application because of their flexibility, selectivity and high sensitivity. Fluorescence sensing highly relies on the phenomenon of physical and chemical interactions occur on the surface of nanomaterials, which results in a change of radiative transition efficiency (either enhancement or quenching). Fluorescence (or Förster) resonance energy transfer (FRET) strategy has been extensively used for the development of homogeneous fluorescent sensors with high sensitivity. FRET is a radiationless and distance-dependent process, wherein non-radiative energy transfers from excited donor fluorophore to nearby suitable acceptor/ quencher through a long-range of dipole–dipole interaction. Many fluorescent

Table 1.3 Sensing performance of various metal sulfide nanostructure-based fluorescence resonance energy transfer sensors

Target analyte	Sensing system		Limit of detection (LOD)	Reference
	Donor	Acceptor		
Ascorbic acid	CdS quantum dots	Diphenylcarbadiazone	2 nM	Ganiga and Cyriac (2016)
Anthrax lethal factor DNA	CuInS$_2$ quantum dots	Graphene oxide nanosheet	0.013 nmol L^{-1}	Liu and Su (2016)
HER2 aptamer	MnCuInS–ZnS quantum dots	Urchin-like au nanoparticles	1 ng mL^{-1}	Xing et al. (2018)
Antibiotic kanamycin	Carbon dots	MoS$_2$ nanosheet	1.1μM	Wang et al. (2017)
Cardiac troponin T	Carbon dots	MoS$_2$ nanosheet	0.12 ng mL^{-1}	Gogoi and Khan (2018)
Prostate-specific antigen	Dye-labeled aptamer	MoS$_2$ nanosheet	0.2 ng mL^{-1}	Kong et al. (2015)
DNA	Dye-labeleddssDNA probe	MoS$_2$ nanosheet	500 pM	Zhu et al. (2013a)
Adenosine	FAM-tagged anti-adenosine aptamer		5μM	
Epithelial cell adhesion molecule (EpCAM) protein	Graphene quantum dots	MoS$_2$ nanosheet	450 pM	Shi et al. (2017)
Malarial biomarker *Plasmodium* lactate dehydrogenase (pLDH)	6-carboxyfluorescein	MoS$_2$ nanosheet	550 pM	Geldert et al. (2017)
Pathogens	A fluorescein-tagged aptamer	MoS$_2$ nanosheet	10 CFU·mL^{-1}	Singh et al. (2016)
DNA	Dye-labeleddssDNA probe	Layered nanosheets MoS$_2$	0.1 nM	Zhang et al. (2015)
		TiS$_2$	0.2 nM	
		TaS$_2$	0.05 nM	

Table 1.3 (continued)

Target analyte	Sensing system		Limit of detection (LOD)	Reference
	Donor	Acceptor		
Interferon-gamma (IFN-γ)	Carboxyfluorescein dye-labeled IFN-γ single stranded DNA	Nanosheets ReS$_2$ and	57.6 pM	Dhenadhayalan et al. (2018)
		TiS$_2$	82.7 pM	
DNA	The dye-labeled ssDNA	Ta$_2$NiS$_5$ Nanosheet	50 pM	Tan et al. (2015a)
Collagen peptide	Peptide FAM-PRG	WS$_2$ and MoS$_2$	41 and 21 nM in human urine and human saliva samples respectively	Sun et al. (2017)
Nucleic acid	Tetramethylrhodamine dye-labeled ssDNA	WS$_2$ nanosheet	60 PM	Yuan et al. (2014)
Protein	Tetramethylrhodamine dye-labeled CEA aptamer		---	

DNA Deoxyribonucleic acid, *ssDNA* single-stranded deoxyribonucleic acid, *HER2* human epidermal growth factor receptor 2, and *CEA* carcinoembryonic antigen

Table 1.4 Sensing performance of various metal sulfide nanostructure-based colorimetric sensors

Sensing system	Target analyte	Linear range	Limit of detection (LOD)	Reference
Ag–Ag$_2$S nanoparticles	Glucose	0–1.25 mM	176.21μM	Díez-Buitrago et al. (2019)
CoS nanoparticles decorated CoFe$_2$O$_4$ nanotubes	Dopamine	0–50μM	0.58μM	Yang et al. (2018)
Fe-doped ZnS quantum dots	H$_2$O$_2$	4.1–98μg L^{-1}	3.06μg L^{-1}	Abbasifar and Samadi-Maybodi (2017)
Hierarchical CuS decorated reduced graphene oxide nanosheets	Dopamine	2–100μM	0.48μM	Dutta et al. (2015)
Hollow copper sulfide nanocubes	Dopamine	2–150μM	1.67μM	Zhu et al. (2019)
CuS nanorods	H$_2$O$_2$	1.0×10^{-6} to 1.0×10^{-3} Mol L^{-1}	1.1×10^{-7} Mol L^{-1}	Guan et al. (2015)
CuS nanoparticles	Glucose	25–600μM	4.9μM	Niu et al. (2018)
MXene-Ti$_3$C$_2$–CuS nanocomposites	Cholesterol	10–100μM	1.9μM	Li et al. (2019b)
Hollow and porous nickel sulfide nanocubes	H$_2$O$_2$	4–40μM	1.72μM	Liu et al. (2019)
MoS$_2$ nanosheets	Choline	–	0.4μM	Nirala et al. (2018)
MoS$_2$ nanosheets	Uric acid	0.5–100μM	0.3μM	Wang et al. (2019b)
Au nanoparticles@MoS$_2$-quantum dots composite	Glucose	20–400μM	0.068μM	Vinita et al. (2018)
MoS$_2$-FePt nanocomposites	H$_2$O$_2$	8–300μM	2.24μM	Hu et al. (2019)
WS$_2$ nanosheets	Glucose	5–300μM	2.9μM	Lin et al. (2014)
WS$_2$ nanosheets	Glutathione	100 pM–10 nM	61 pM	Li et al. (2019a)

Table 1.5 Various reports utilizing metal sulfides and its nanocomposite-based biosensors for the detection of various enzymatic or nonenzymatic biomolecules

Sensing type	Sensing system	Target analyte	Linear range	Limit of detection (LOD)	Reference
Nonenzymatic	Tremella-like CoS	H_2O_2	0.005–14.82 mM	1.5	Wu et al. (2017)
		Glucose	0.005–1.10 mM and 1.20–10.20 mM	1.5	
	ZnS quantum dots @PANI nanocomposite	Clenbuterol hydrochloride	0.01–10 ng · mL-1	5.5 pg mL^{-1}	Zhang et al. (2016)
	Bi_2S_3 nanorod	Ascorbic acid	1.0×10^{-6} to 1.0×10^{-3} Mol L^{-1}	8.3×10^{-7} Mol L^{-1}	Dong et al. (2012)
	Polyaniline capped Bi_2S_3 nanorod	DNA	1.0×10^{-15} to 1.0×10^{-11} M	4.37×10^{-16} M	Zhu et al. (2015)
	Bi_2S_3–titanate nanofiber nanocomposite	Ascorbic acid	1–10 mM	–	Cabrita et al. (2014)
	Hierarchical cauliflower-like Ni_3S_2	Glucose	0.0005–3 mM	0.82μM	Kim et al. (2016)
	3D flower-like Ni_7S_6	H_2O_2	0.005–20.5 mM	0.15μM	Wu et al. (2016)
		Glucose	0.005 mM–3.7 mM	0.15μM	
	3D Ni_3S_2 nanosheet arrays supported on Ni foam	Glucose	0.005–3.0 mM	1.2μM	Huo et al. (2014)
	Nickel cobalt sulfide nanosheet film	Glucose	0.001–3 mM	0.12μM	Cao et al. (2016)
	3D flowerlike $NiCo_2S_4$	Glucose	0.5μM–6 mM	50 nM	Babu et al. (2018)
	Mesoporous ZnS–NiS nanocomposite	Glucose	–	0.125μM	Wei et al. (2015)
	VS_2 nanoparticle	H_2O_2	0.5μM–2.5 mM	0.224μM	Sarkar et al. (2018)
		Glucose	0.5μM–3 mM	0.211μM	

CuS nanotube	Glucose	0.05–5µM	–	Zhang et al. (2008)
CuS nanotube	Glucose	0.5–7.5µmol L^{-1}	0.25µmol L^{-1}	Liu and Xue (2011)
Hollow CuS nanocubes	Glucose	0.1–10 mM	–	Zhu et al. (2019)
CuS nanoflower	H$_2$O$_2$	1×10^{-6}–1×10^{-4} M	3×10^{-7} M	Yang et al. (2014)
	Glucose	1×10^{-5}–1×10^{-2} M	1×10^{-5} M	(2014)
CuS nanoflakes–RGO nanocomposite	Glucose	1–2000µM	0.19µM.	Yan et al. (2018)
CuS-MoS$_2$ hybrid	Glucose	$1.0 \times 10^{-6} \sim 1.0 \times 10^{-4}$ Mol L^{-1}	3.0×10^{-7} Mol L^{-1}	Gao et al. (2017b)
Gold nanoparticle-decorated MoS$_2$ nanosheet	Ascorbic acid	50–100,000 mM	100µM	Sun et al. (2014)
	Dopamine	0.05–30 mM	0.05µM	
	Uric acid	50–40,000 mM	10µM	
Ni nanoparticle-MoS$_2$ nanosheet hybrid	Glucose	0–4 mM	0.31µM	Huang et al. (2014)
MoS$_2$-prussian blue nanocubesnanohybrid	H$_2$O$_2$	0.01–300µM	4.1 nM	Su et al. (2017)
	Carcinoembryonic antigen	0.005–10 ng mL^{-1}	0.54 pg mL^{-1}	
CoS$_2$-MoS$_2$ nanocomposite	Ascorbic acid	9.9–6582µM	3.0µM	Zhang et al. (2017b)
	Dopamine	0.99–261.7µM	0.25µM	
	Nitrite	0.5–5160µM	0.20µM	
ZnS–graphene oxide nanocomposite	Ascorbic acid	50.0–1000µM	30µM	Yang (2015)
	Dopamine	1.0–500µM	0.5µM	
	Uric acid	1.0–500µM	0.4µM	
CdS nanorods–reduced graphene oxide nanocomposites	H$_2$O$_2$	5×10^{-6} M to 1.5×10^{-2} M	1.67µM	An et al. (2013)

(continued)

Table 1.5 (continued)

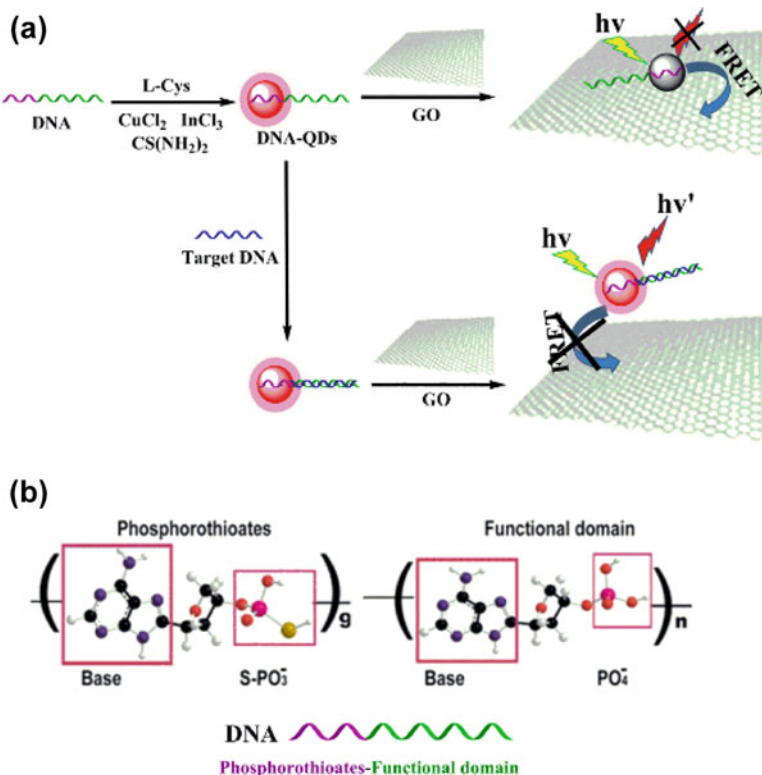| Sensing type	Sensing system	Target analyte	Linear range	Limit of detection (LOD)	Reference
Enzymatic	Cu$_2$S nanoplates	H$_2$O$_2$	10μM–3.75 mM	1.1μM	Maji et al. (2013)
		Glucose	10μM–3.1 mM	1.3μM	
	ZnS nanoparticles	Uric acid	0.01–1.5 mM	1.79μM	Zhao et al. (2017)
	ZnS nanoflakes		0.01–2.0 mM	1.51μM	
	ZnS urchin-like nanostructure		0.01–1.7 mM	0.7μM	
	MoS$_2$ nanosheets	Chikungunya virusDNA	0.1 nM–100μM	3.4 nM	Singhal et al. (2018)
	ZnS nanoparticles decorated graphene nanoplatelets	Glucose	–	–	Suganthi et al. (2016)
	CdS–graphene composite	Glucose	2.0–16 mM	0.7 mM	Wang et al. (2011)

Fig. 1.9 (**a**) Preparation of DNA-CuInS$_2$ quantum dots by a one-step synthesis method and its use for *anthrax lethal factor* DNA detection and (**b**) chemical structure of the phosphorothioates and functional domain. (Reprinted with permission from Liu and Su (2016). Copyright 2016 Elsevier) *DNA* Deoxyribonucleic acid, *L-cys* L-cysteine, *QDs quantum dots*, *GO* graphene oxide, and *FRET* fluorescence resonance energy transfer

metal sulfide quantum dots have been used as energy donors in FRET-based fluorescent sensing systems for the detection of various biological molecules (Table 1.3).

As presented in Fig. 1.9, a FRET biosensor with CuInS$_2$ quantum dots as the energy transfer donor and graphene oxide nanosheets as the nano-quencher was established for the detection of *anthrax lethal factor* DNA (Liu and Su 2016). In this study, L-cysteine and a specific-sequence DNA (Fig. 1.9b) were used as co-ligands to stabilize the fluorescent CuInS$_2$ quantum dots with emission at 652 nm. As shown in Fig. 1.9a, single-stranded DNA (ssDNA) labeled with CuInS$_2$ quantum dots are adsorbed on the surface of graphene oxide sheets through π-π stacking and hydrogen–bonding interactions between hydroxyl/amine groups of ssDNA and hydroxyl/carboxyl groups of graphene oxide. Subsequently, energy transfer from CuInS$_2$ quantum dots donor to the graphene oxide acceptor would occur that resulted in fluorescence quenching. Upon addition of target DNA (*anthrax lethal*

factor DNA), ssDNA-CuInS$_2$ quantum dots probe preferentially hybridized with its complementary target DNA to form a double-stranded DNA (dsDNA)-CuInS$_2$ quantum dots complex, and then detached from the surface of the quencher. DNA hybridization was detected by measuring the fluorescence recovery. The detection limit of DNA-CuInS$_2$-graphene oxide FRET system is 0.013 nmol L^{-1} for the *anthrax lethal factor* DNA detection in serum samples. For the sensitive detection of vitamin C, Manjunatha Ganiga et al. have developed a FRET sensor using CdS quantum dots and diphenylcarbadiazone (DPCD) as donor and aceptor, repsectively (Ganiga and Cyriac 2016). In this sensor, DPCD was reduced to diphenylcarbazide (DPC) by the addition of ascorbic acid, resulting in FRET turn−off. The present probe showed a detection limit of 2 nM for ascorbic acid. In another case, Hong Xing et al. have fabricated an enhanced FRET biosensing system by implementing a novel donor–acceptor pair for the sensitive detection of biomarker-HER2 protein (Xing et al. 2018). In this system, NIR-emitting MnCuInS–ZnS quantum dots encapsulated in bovine serum albumin (BSA) were used as the energy donor, and urchin-like Au nanoparticles were served as the energy acceptor. Subsequently, the energy donors were conjugated with HER2 aptamers, and acceptors were modified with ssDNA that is partially complementary to the HER2 aptamer. Then, the FRET process has occurred by the binding between MnCuInS–ZnS@BSA-Aptamer and urchin-like Au nanoparticles-ssDNA that resulted in a fluorescence quenching. Whereas in the presence of target HER2 protein, the FRET effect was broken, which leads to a recovery of fluorescence signal. By measuring the change in the fluorescence signal, HER2 protein in human serum samples could be detected with a wide detection range from 2 to 100 ng mL^{-1}. A low detection limit was achieved with 1 ng mL^{-1}.

On the other side, transition metal dichalcogenides have been demonstrated as effective fluorescence quenchers, that is, acceptors in FRET-based sensing platform (see Table 1.3 for the list). As one of them, the two-dimensional MoS$_2$ nanosheets have attracted significant attention in biosensing because of their outstanding structural and electronic properties. With high fluorescence quenching ability, the layered MoS$_2$ nanosheets have been employed to develop FRET sensing nanoplatform for sensitive detection of various biomolecules. For instance, Zhu et al. have developed an electrochemical lithium intercalation method to exfoliate bulk MoS$_2$ into single-layer nanosheets as effective fluorescence quenchers for homogeneous detection of DNA and small molecules (Zhu et al. 2013b). As shown in Fig. 1.10a, a fluorescence immunosensor based on FRET between anti- cardiac troponin T-labeled carbon quantum dots and MoS$_2$ nanosheet sensing platform was also fabricated and used for selective detection of cardiac troponin T (cTnT) protein (Gogoi and Khan 2018). When exfoliated MoS$_2$ nanosheets grasp the NIR-active fluorescent anti-cTnT-functionalized carbon dots over their surface, FRET takes place from dots to MoS$_2$ acceptor, thereby quenching the fluorescence signal. In the presence of target cTnT, anti-cTnT-functionalized carbon dots bind them strongly to form an antibody–antigen (cTnT/anti-cTnT) complex. This interaction causes effective detachment of carbon dots from the surface of MoS$_2$ nanosheets with subsequent restoration of upconversion fluorescence intensity. The fluorescence immunosensor based on
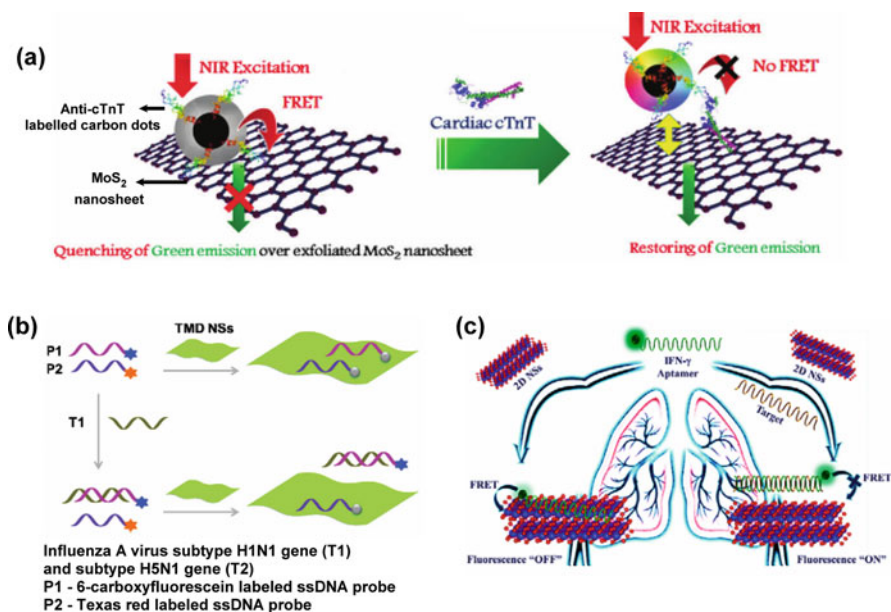
Fig. 1.10 (**a**) Detection of cardiac troponin T (cTnT) protein based on FRET dynamics between anti-cTnT-functionalized carbon dots and MoS_2 nanosheets. (Reprinted with permission from Gogoi and Khan (2018). Copyright 2018 Royal Society of Chemistry). (**b**) Single-layer transition metal dichalcogenide nanosheet-based multiplexed fluorescent DNA detection. (Reprinted with permission from Zhang et al. (2015). Copyright 2015 John Wiley and Sons). (**c**) Fluorescence sensing mechanism of interferon-gamma (IFN-γ) aptamer with two-dimensional transition metal dichalcogenides (TMD) as sensing platform (Reprinted with permission from Dhenadhayalan et al. (2018). Copyright 2018 Elsevier)

NIR Near infrared, *FRET* fluorescence resonance energy transfer, and *NSs* nanosheets

carbon dot/MoS_2 nano-couple showed very high sensitivity to cTnT protein with a detection limit of 0.12 ng mL^{-1}.

Besides layered MoS_2 nanosheets, other transition metal dichalcogenides such as TaS_2, ReS_2, TiS_2 and WS_2 have also been applied as effective nano-quenchers in FRET-based fluorescent sensing platform (Table 1.3). For example, Zhang et al. have synthesized three different single-layered transition metal dichalcogenides such as MoS_2, TiS_2 and TaS_2 as fluorescent nano-quenchers based on the lithium-intercalation method (Zhang et al. 2015). The prepared nanosheets possessed robust fluorescence quenching ability and different affinities towards the ssDNA and dsDNA. Among them, the TaS_2 nanosheet-based FRET sensors have exhibited the best performance. Interestingly, the TaS_2 nanosheets have been successfully applied for multiplexed fluorescent detection of DNA as shown in Fig. 1.10b. In another case, fluorogenic aptamer sensing of interferon gamma (IFN-γ) using layered transition metal dichalcogenides (ReS_2 and TiS_2) have been reported (Dhenadhayalan et al. 2018). As shown in Fig. 1.10c, the fluorogenic aptamer sensor was performed based on the fluorescence turn-off and turn-on mechanism by the involvement of

ReS_2/TiS_2 nanosheets and target with IFN-γ aptamer. The results have concluded that the ReS_2 and TiS_2 nanosheets-based FRET sensors exhibited high specific selectivity in the detection of IFN-γ aptamer with low detection limit of 57.6 and 82.7 pM, respectively.

Colorimetric Sensor

As a simplest optical mode of detection, visible colorimetric assays have been extensively explored in detecting various analytes for providing simple naked-eye readout signals. Enzyme-mimetic inorganic nanomaterials termed as nanozymes have been emerged as significant tool for colorimetric detection. ecause the large surface-to-volume-ratio of nanomaterials is beneficial for accomplishing very efficient catalytic activity. Various metal sulfide nanomaterials have also been proven as efficient biomimetic catalysts for the detection of various analytes. This section highlights a few of the reports on metal sulfide-based colorimetric sensors. The properties and the performances of colorimetric sensing based on various metal sulfides and its composites are summarized in Table 1.4.

Niu and co-workers found peroxidase-like capability of surface engineered CuS nanoparticles with aspartic acid (Asp) to catalytically oxidize the colorless 3,3′,5,5′-tetramethylbenzidine (TMB) into its blue color oxidized product by H_2O_2 (Niu et al. 2018). This surface-modified $CuS-Asp_{0.05}$ nanozymes exhibited good activity in a wide pH range varying from 3 to 7. Then, direct detection of H_2O_2 in neutral pH was realized with the TMB color reaction catalyzed by $CuS-Asp_{0.05}$ nanozymes. Since H_2O_2 is the key product of glucose oxidase (GO_x)-catalyzed reaction, authors performed colorimetric detection of glucose by coupling peroxidase-mimicking $CuS-Asp_{0.05}$ nanozyme with GO_x. In another study, peroxidase-like catalytic activity of CuS nanorods was studied by using o-phenylenediamine (OPD) as the substrate in the presence of H_2O_2 (Guan et al. 2015). As shown in Fig. 1.11a, CuS nanorods were acted as an efficient catalyst in the oxidation of OPD to 2,3–diaminophenazine (DAP) using H_2O_2 as oxidant. Dutta et al. have developed a highly efficient colorimetric sensor for detecting dopamine based on the peroxidase-like catalytic activity of hierarchical CuS decorated reduced graphene oxide (rGO) nanocomposites, as shown in Fig. 1.11b (Dutta et al. 2015). The experimental results implied that strong covalent interaction between the hierarchical CuS and rGO nanosheets synergistically improved the catalytic activity of CuS-rGO nanocomposites in comparison with its individual counterparts.

Similar to graphene oxide, transition metal chalcogenide nanosheets also possess an intrinsic peroxidase-mimicking catalytic activity. For example, WS_2 nanosheets were used as peroxidase mimics for colorimetric detection of glucose (Lin et al. 2014) and glutathione (Li et al. 2019a). Figure 1.11c shows the principle of glutathione detection by using WS_2 nanosheet-TMB colorimetric system (Li et al. 2019a). In the absence of target, WS_2 nanosheets could catalyze the oxidation of TMB

Glucose (Glu), Ascorbic acid (AA), Phenylalanine (Phe), Tryptophan (Tryp), Tyrosine (Tyro), Uric acid (UA), Dopamine (DA), L-DOPA
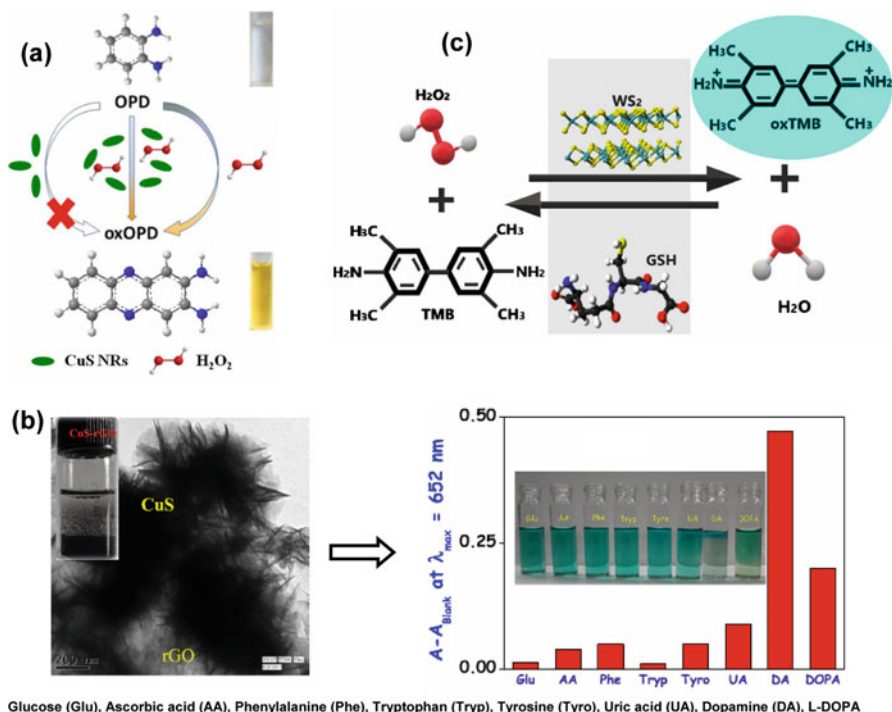
Fig. 1.11 (**a**) The colorimetric detection of hydrogen peroxide (H_2O_2)-based copper sulfide nanorods (CuS NRs) as peroxidase mimetics. (Reprinted with permission from Guan et al. (2015). Copyright 2015 Royal Society of Chemistry). (**b**) Colorimetric detection of dopamine using hierarchical CuS decorated reduced graphene oxide nanosheets. (Modified after Dutta et al. (2015). Copyright 2015 American Chemical Society). (**c**) Detection of glutathione (GSH) through WS_2-TMB-H_2O_2 colorimetric system. (Reprinted with permission from Li et al. (2019a). Copyright 2019 Springer Nature. Abbreviations are added at the bottom for better clarity)

substrate in the presence of H_2O_2, causing distinct color change (colorless to blue) in the solution. However, when target glutathione was added in this system, glutathione causes the reduction of oxidized TMB, which leads to lower the absorbance signal with substantial blue color fading of oxidized TMB. By this strategy, colorimetric detection of glutathione has been achieved with a detection limit of 61 pM. In another research, a nanocomposite of Au nanoparticles decorated over MoS_2 quantum dots (Au nanoparticles@MoS_2-quantum dots) were obtained by a one-step synthesis (Vinita et al. 2018). This nanozyme showed excellent peroxidase-like activity through catalytic oxidation of TMB by H_2O_2. Au nanoparticles@MoS_2-quantum dot composite system has been further applied for sensitive and selective detection of glucose in human biological fluids such as serum, tears and saliva (Fig. 1.12).
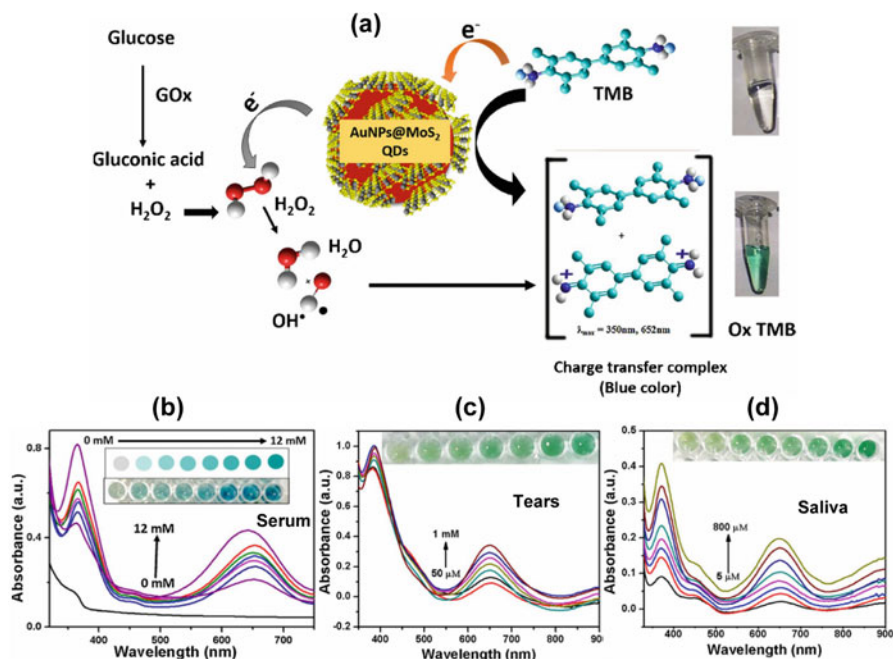
Fig. 1.12 (**a**) The catalytic mechanism of 3,3′,5,5′-tetramethylbenzidine (TMB) oxidation in the presence H_2O_2 catalyzed by Au nanoparticles@MoS_2-quantum dot composite. (**b**) UV–vis spectra test of glucose level in serum by portable test kit (based on Au nanoparticles@MoS_2-quantum dot composite), and the inset change the color of wells hydrogel with the presence glucose level, with typical colorimetric chart with the level of glucose (in order of 0, 2, 4, 5, 8, 10, 11, 12 mM). (**c**) Absorption spectra of test of glucose level in tear by portable test kit, and the inset change the color of wells hydrogel with the presence glucose level (50 M, 100, 250, 400, 600, 800, and 1 mM) in tear. (**d**) Absorption spectra of test of glucose level in saliva by portable test kit, and inset shows change in the color of wells hydrogel with the presence glucose level (5 M, 150, 250, 350, 450, 550, 700, and 800 M) in saliva. (Reprinted with permission from Vinita et al. (2018). Copyright 2018 Elsevier)

1.3.2 Electrochemical Sensor

Electrochemical technique is one of the preferred approaches for the development of biosensing because it facilitates better analytical characteristics in terms of fast response, high sensitivity, ease of operation and reliability. The electrochemical detection assay involves redox reaction of target analytes at the interface of electrode and electrolyte, which produces analyte concentration-dependent redox current. In electrochemical sensors, nanomaterials have been employed as electrode surface modifiers to increase the amount of immobilized bioreceptors. Electrochemical

biosensors based on nanomaterials have been operated through various detection approaches, such as voltammetry, amperometry and impedimetric, depending on the kind of analytes and nanomaterials used. As evidenced from Table 1.5, different microstructures of metal sulfide nanomaterials and its nanocomposites have also been extensively used as electrode modifiers for electrochemical sensing in both nonenzymatic and enzymatic manner. Some explanatory examples for metal sulfide-based electrochemical biosensing are discussed in this section.

As a significant metal chalcogenide semiconductor, copper sulfide nanostructures with various morphologies have been recognized as efficient electrode modifiers for the development of nonenzymatic and enzymatic electrochemical biosensor. For example, the CuS nanotube-modified glassy carbon electrode (GCE) has been used for enzyme-free electrochemical detection of glucose (Zhang et al. 2008; Liu and Xue 2011). A flower-like CuS semiconductor synthesized by hydrothermal method showed a detection limit of 3×10^{-7} M and 1×10^{-5} M towards nonenzymatic sensing of H_2O_2 and glucose, respectively (Yang et al. 2014). Zhu et al. reported that hollow CuS nanocubes can be acted as a modified electrode for enzyme-free detection of glucose in alkaline condition, which showed good linearity from 0.1 to 10 mM (Zhu et al. 2019). Very recently, a sensitive nonenzymatic glucose sensor hybridizing Au nanoparticles on the surface of Cu_xS nanosheets supported three-dimensional framework have developed (Mai et al. 2019). Firstly, the two-dimensional Cu_xS nanosheet arrays on three-dimensional copper foam (3DCF) was formed by anodization of Cu foam with thermal treatment, and then Au nanoparticles were electrodeposited on the surface of Cu_xS–3DCF. This Au-Cu_xS–3DCF nonenzymatic sensor exhibited high conductivity and large electroactive surface area, which support to detect glucose with a sensitivity of 0.059 mAµM^{-1} cm^{-2}, large linear detection range of 1.98–976.56µM and detection limit of 7.62µM.

Nickel sulfide (Ni_xS_y) nanostructures with various morphologies including nanoflower, nanosheet and hierarchical structure has also been employed as electrode modifiers for the nonenzymatic electrochemical detection of glucose (Table 1.5). For instance, as shown in Fig. 1.13a, Kim et al. have designed nano-crystalline Ni_3S_2 with different morphologies such as nanoflakes, hierarchical cauliflower-like and dendrite nanostructures on Ni foam by altering the solvent composition (Kim et al. 2016). Among various Ni_3S_2 nanostructures synthesized, the hierarchical cauliflower-like Ni_3S_2 on Ni foam with large electroactive surface area and low electron transfer resistance was applied to detect glucose in human blood serum, exhibiting very high sensitivity of 16,640µA mM^{-1} cm^{-2} and low detection limit of 0.82µM with excellent selectivity. In another study, a self-standing electrode based on three-dimensional flower-like $NiCo_2S_4$ electrochemically deposited over the Ni-modified cellulose filter paper (CFP) has been used for nonenzymatic electrochemical detection of glucose in alkaline media (Babu et al. 2018). In the $NiCo_2S_4$–Ni–CFP self-standing electrode, Ni–CFP and ternary $NiCo_2S_4$ nanostructures were served as current collector and active material,
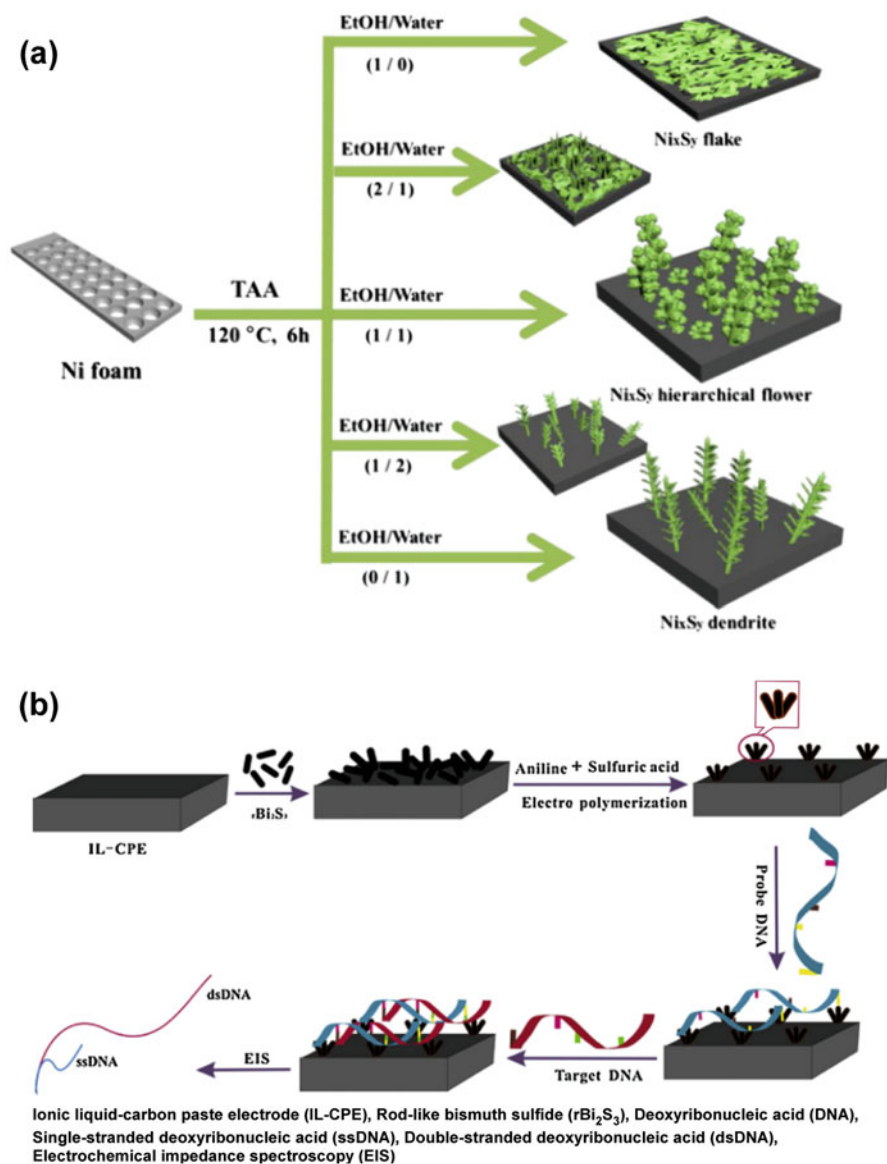
Fig. 1.13 (**a**) Schematic representation of preparation of nickel sulfide on Ni foam as a reactive substance according to the volume ratio between ethanol (EtOH) and water. (Reprinted with permission from Kim et al. (2016). Copyright 2016 Elsevier). (**b**) The electrochemical preparation of polyaniline capped rBi$_2$S$_3$ nanocomposite on IL-CPE and its application in impedimetric DNA biosensor. (Reprinted with permission from Zhu et al. (2015). Copyright 2015 Elsevier. Abbreviations are added at the bottom for better clarity

respectively. The developed $NiCo_2S_4$–Ni–CFP electrode possessed an excellent electrocatalytic activity towards glucose oxidation with low detection limit of 50 nM. On the other hand, Bi_2S_3 nanorods have also been employed in the enzyme-free electrochemical sensing of ascorbic acid (Dong et al. 2012) and DNA (Zhu et al. 2015). Figure 1.13b shows an impedimetric DNA biosensor based on polyaniline capped rod-like Bi_2S_3 film-modified ionic liquid–carbon paste electrode (IL-CPE). In this enzyme-free sensing system, polyaniline capped Bi_2S_3 nanorods were used as immobilization matrix for oligonucleotides probe to achieve impedimetric detection of DNA hybridization. The hybridization experiments showed that the target DNA could be quantified in a large dynamic detection range from 1.0×10^{-15} to 1.0×10^{-11} M along with a detection limit of 4.37×10^{-16} M.

Carbon-based material-supported metal sulfide nanohybrid frameworks have gained very significant attention in electrochemical biosensing due to its synergistic effect property that leads to the enhancement in electrical conductivity, stability and improvement of electrocatalytic activity. For instance, Yan et al. have demonstrated the fabrication of enzyme-free glucose sensor by using CuS nanoflakes–rGO nanocomposite-modified GCE (Fig. 1.14a) (Yan et al. 2018). Due to the synergetic effect between CuS nanoflakes and rGO, the fabricated electrode showed significant electrocatalytic activity towards the glucose oxidation with a fast response time of <6 s, a high sensitivity of 53.5μM $(cm^2\ mM)^{-1}$, a wide linear range from 1 to 2000μM, and a low detection limit of 0.19μM. In addition, a selective detection of glucose in human blood serum and urine samples was successfully realized. As presented in Fig. 1.14b, Xu et al. have reported a nonenzymatic DNA sensor based on CuS–graphene–Au nanoparticle-modified electrode (Xu et al. 2014). An enzymatic glucose biosensor has also been achieved by drop-casting solution of graphene–CdS nanocomposite on the surface of GCE, followed by the deposition of glucose oxidase enzyme over graphene–CdS–GCE (Wang et al. 2011). Due to the synergy effect of graphene sheet and CdS quantum dots, graphene–CdS nanocomposite showed excellent electron transfer characteristics for glucose oxidase with the rate constant of $5.9\ s^{-1}$. Similarly, an enzymatic glucose sensor utilizing graphene-ZnS nanoparticles composite as an immobilization matrix for glucose oxidase enzyme was reported (Suganthi et al. 2016). Thermally exfoliated graphene nanosheets served as an excellent supporting platform for deposition of ZnS nanoparticles. The nanocomposite enhances the electron transfer property of the enzymatic glucose biosensor. Besides graphene, the two-dimensional MoS_2 nanosheet hybrid has also been recognized as an excellent candidate for development of electrochemical biosensor (Table 1.5). For example, nitrogen-doped lignocellulose–CoS_2–MoS_2 nanocomposite has been used as an effective electrode modifier for the simultaneous determination of ascorbic acid, dopamine and nitrite (Zhang et al. 2017a).
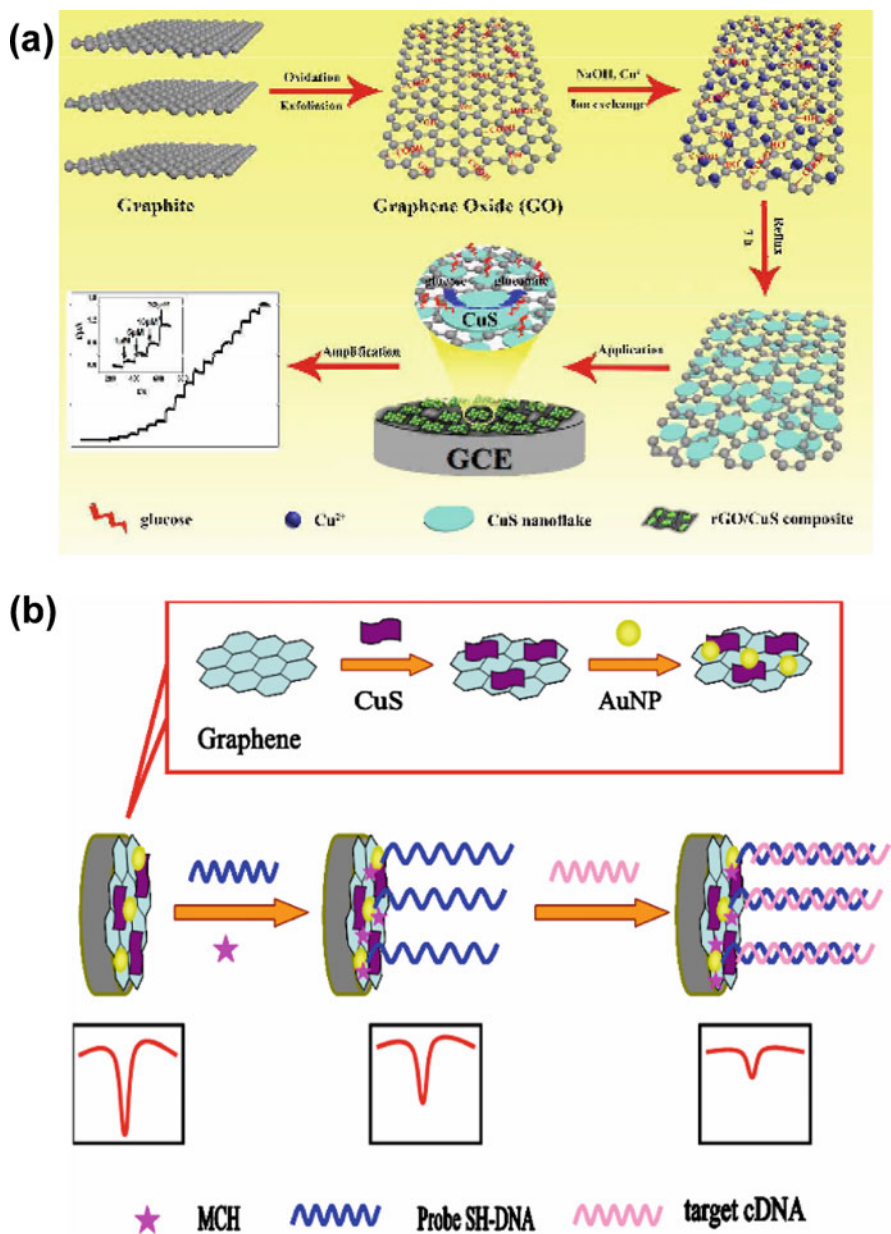
Fig. 1.14 (**a**) rGO–CuS nanoflake composite formation and their application in nonenzymatic glucose sensing. (Reprinted with permission from Yan et al. (2018). Copyright 2018 Royal Society of Chemistry). (**b**) The electrochemical DNA biosensor. (Reprinted with permission from Xu et al. (2014). Copyright 2014 Springer Nature)

rGO Reduced graphene oxide, *GCE* glassy carbon electrode, *cDNA* complementary deoxyribonucleic acid, *MCH* 6-mercapto-1-hexane

1.4 Conclusions

This chapter has been written to contain mainly two concepts based on the application of metal sulfides for bioimaging and biosensing. The first part has explained all the imaging techniques where metal sulfides played a crucial role. Imaging techniques have become unavoidable in medical diagnosis in order to treat many diseases in these days. Right from X-ray imaging, so many techniques have been developed and successfully implemented in medical diagnosis. Many powerful methods such as PLI, PAI, MRI, PDT and PTT were explained thoroughly in this section. In order to use these techniques for practical applications, the probe materials are very much essential. Out of many materials available, sulfide-based materials are much useful mainly because of its non-toxicity while interacting with a biological structure. Thus, the use of sulfides prepared in nanostructured form was discussed for these applications in real models. The second part of this chapter has focused on the application of metal sulfide nanostructures on biosensing. Different types of biosensors have been classified based on the signal that is transduced in them. Based on that, biosensors can be classified as fluorescent, colorimetric and electrochemical. The working principle of every type was thoroughly discussed, and the application of metal sulfides in each type of sensors has been explained well with examples. Many literature works have been cited to support their application. In summary, the importance of nanostructured metal sulfide materials, especially with high fluorescence emission has been discussed for the application of bioimaging and biosensing.

References

Abbasifar J, Samadi-Maybodi A (2017) Application of enzyme-like activity of Fe-doped ZnS QDs for colorimetric determination of hydrogen peroxide. Int J Environ Anal Chem 97:563–572. https://doi.org/10.1080/03067319.2017.1329425

Aboulaich A, Billaud D, Abyan M et al (2012) One-pot noninjection route to CdS quantum dots via hydrothermal synthesis. ACS Appl Mater Interfaces 4:2561–2569. https://doi.org/10.1021/am300232z

An X, Yu X, Yu JC, Zhang G (2013) CdS nanorods/reduced graphene oxide nanocomposites for photocatalysis and electrochemical sensing. J Mater Chem A 1:5158. https://doi.org/10.1039/c3ta00029j

Anbazhagan R, Su Y-A, Tsai H-C, Jeng R-J (2016) MoS$_2$ –Gd chelate magnetic nanomaterials with Core–Shell structure used as contrast agents in in vivo magnetic resonance imaging. ACS Appl Mater Interfaces 8:1827–1835. https://doi.org/10.1021/acsami.5b09722

Andreescu S, Ornatska M, Erlichman JS et al (2012) Biomedical applications of metal oxide nanoparticles. In: Matijević E (ed) Fine particles in medicine and pharmacy. Springer, Boston, pp 57–100

Babu KJ, Kumar RT, Yoo DJ et al (2018) Electrodeposited nickel cobalt sulfide flowerlike architectures on disposable cellulose filter paper for enzyme-free glucose sensor applications. ACS Sustain Chem Eng 6:16982–16989. https://doi.org/10.1021/acssuschemeng.8b04340

Bhowal S, Ghosh A, Chowdhuri SP et al (2018) A novel metallogel based approach to synthesize (Mn, Cu) doped ZnS quantum dots and labeling of MCF-7 cancer cells. Dalt Trans 47:6557–6569. https://doi.org/10.1039/C7DT03864J

Cabrita JF, Ferreira VC, Monteiro OC (2014) Titanate nanofibers sensitized with nanocrystalline Bi_2S_3 as new electrocatalytic materials for ascorbic acid sensor applications. Electrochim Acta 135:121–127. https://doi.org/10.1016/j.electacta.2014.04.135

Cao X, Wang K, Du G et al (2016) One-step electrodeposition of a nickel cobalt sulfide nanosheet film as a highly sensitive nonenzymatic glucose sensor. J Mater Chem B 4:7540–7544. https://doi.org/10.1039/c6tb01736c

Chang J-Y, Wang G-Q, Cheng C-Y et al (2012) Strategies for photoluminescence enhancement of $AgInS_2$ quantum dots and their application as bioimaging probes. J Mater Chem 22:10609. https://doi.org/10.1039/c2jm30679d

Chang J-Y, Chen G-R, Li J-D (2016) Synthesis of magnetofluorescence Gd-doped $CuInS_2/ZnS$ quantum dots with enhanced longitudinal relaxivity. Phys Chem Chem Phys 18:7132–7140. https://doi.org/10.1039/C5CP07063E

Chen J, Liu C, Hu D et al (2016) Single-layer MoS_2 Nanosheets with amplified photoacoustic effect for highly sensitive photoacoustic imaging of orthotopic brain tumors. Adv Funct Mater 26:8715–8725. https://doi.org/10.1002/adfm.201603758

Chen L, Zhou X, Nie W et al (2017) Marriage of albumin–gadolinium complexes and MoS_2 nanoflakes as cancer theranostics for dual-modality magnetic resonance/photoacoustic imaging and photothermal therapy. ACS Appl Mater Interfaces 9:17786–17798. https://doi.org/10.1021/acsami.7b04488

Cheng L, Yuan C, Shen S et al (2015) Bottom-up synthesis of metal-ion-doped WS_2 nanoflakes for cancer theranostics. ACS Nano 9:11090–11101. https://doi.org/10.1021/acsnano.5b04606

Dhenadhayalan N, Sriram MI, Lin K-C (2018) Aptamer-based fluorogenic sensing of interferon-gamma probed with ReS_2 and TiS_2 nanosheets. Sensors Actuators B Chem 258:929–936. https://doi.org/10.1016/j.snb.2017.11.178

Díez-Buitrago B, Barroso J, Saa L et al (2019) Facile synthesis and characterization of Ag/Ag_2S nanoparticles enzymatically grown in situ and their application to the colorimetric detection of glucose oxidase. ChemistrySelect 4:8212–8219. https://doi.org/10.1002/slct.201901673

Dong YP, Huang L, Zhang J et al (2012) Electro-oxidation of ascorbic acid at bismuth sulfide nanorod modified glassy carbon electrode. Electrochim Acta 74:189–193. https://doi.org/10.1016/j.electacta.2012.04.063

Dong L, Ji G, Liu Y et al (2018) Multifunctional $Cu–Ag_2S$ nanoparticles with high photothermal conversion efficiency for photoacoustic imaging-guided photothermal therapy in vivo. Nanoscale 10:825–831. https://doi.org/10.1039/C7NR07263E

Dutta S, Ray C, Mallick S et al (2015) A gel-based approach to design hierarchical CuS decorated reduced graphene oxide nanosheets for enhanced peroxidase-like activity leading to colorimetric detection of dopamine. J Phys Chem C 119:23790–23800. https://doi.org/10.1021/acs.jpcc.5b08421

Feng Q, Xu Y, Hu B et al (2018) A smart off–on copper sulfide photoacoustic imaging agent based on amorphous–crystalline transition for cancer imaging. Chem Commun 54:10962–10965. https://doi.org/10.1039/C8CC06736H

Foda MF, Huang L, Shao F, Han H (2014) Biocompatible and highly luminescent near-infrared $CuInS_2/ZnS$ quantum dots embedded silica beads for cancer cell imaging. ACS Appl Mater Interfaces 6:2011–2017. https://doi.org/10.1021/am4050772

Ganiga M, Cyriac J (2016) An ascorbic acid sensor based on cadmium sulphide quantum dots. Anal Bioanal Chem 408:3699–3706. https://doi.org/10.1007/s00216-016-9454-7

Gao D, Zhang P, Liu C et al (2015) Compact chelator-free Ni-integrated CuS nanoparticles with tunable near-infrared absorption and enhanced relaxivity for in vivo dual-modal photoacoustic/MR imaging. Nanoscale 7:17631–17636. https://doi.org/10.1039/C5NR05237H

Gao D, Sheng Z, Liu Y et al (2017a) Protein-modified CuS nanotriangles: a potential multimodal nanoplatform for in vivo tumor photoacoustic/magnetic resonance dual-modal imaging. Adv Healthc Mater 6:1601094. https://doi.org/10.1002/adhm.201601094

Gao Z, Lin Y, He Y, Tang D (2017b) Enzyme-free amperometric glucose sensor using a glassy carbon electrode modified with poly(vinyl butyral) incorporating a hybrid nanostructure composed of molybdenum disulfide and copper sulfide. Microchim Acta 184:807–814. https://doi.org/10.1007/s00604-016-2061-7

Gedda G, Chen G-R, Yao Y-Y et al (2017) Aqueous synthesis of dual-targeting Gd-doped CuInS$_2$/ZnS quantum dots for cancer-specific bi-modal imaging. New J Chem 41:14161–14170. https://doi.org/10.1039/C7NJ02252B

Geldert A, Kenry K, Zhang X et al (2017) Enhancing the sensing specificity of a MoS$_2$ nanosheet-based FRET aptasensor using a surface blocking strategy. Analyst 142:2570–2577. https://doi.org/10.1039/C7AN00640C

Geszke M, Murias M, Balan L et al (2011) Folic acid-conjugated core/shell ZnS:Mn/ZnS quantum dots as targeted probes for two photon fluorescence imaging of cancer cells. Acta Biomater 7:1327–1338. https://doi.org/10.1016/j.actbio.2010.10.012

Geszke-Moritz M, Piotrowska H, Murias M et al (2013a) Thioglycerol-capped Mn-doped ZnS quantum dot bioconjugates as efficient two-photon fluorescent nano-probes for bioimaging. J Mater Chem B 1:698–706. https://doi.org/10.1039/c2tb00247g

Geszke-Moritz M, Piotrowska H, Murias M et al (2013b) Thioglycerol-capped Mn-doped ZnS quantum dotbioconjugates as efficient two-photon fluorescent nano-probes for bioimaging. J Mater Chem B 1:698–706. https://doi.org/10.1039/C2TB00247G

Gogoi S, Khan R (2018) Fluorescence immunosensor for cardiac troponin T based on Förster resonance energy transfer (FRET) between carbon dot and MoS$_2$ nano-couple. Phys Chem Chem Phys 20:16501–16509. https://doi.org/10.1039/c8cp02433b

Goswami N, Giri A, Kar S et al (2012) Protein-directed synthesis of NIR-emitting, tunable HgS quantum dots and their applications in metal-ion sensing. Small 8:3175–3184. https://doi.org/10.1002/smll.201200760

Guan J, Peng J, Jin X (2015) Synthesis of copper sulfide nanorods as peroxidase mimics for the colorimetric detection of hydrogen peroxide. Anal Methods 7:5454–5461. https://doi.org/10.1039/C5AY00895F

Guan G, Wang X, Li B et al (2018) "Transformed" Fe$_3$S$_4$ tetragonal nanosheets: a high-efficiency and body-clearable agent for magnetic resonance imaging guided photothermal and chemodynamic synergistic therapy. Nanoscale 10:17902–17911. https://doi.org/10.1039/C8NR06507A

Guo W, Yang W, Wang Y et al (2014) Color-tunable Gd-Zn-Cu-In-S/ZnS quantum dots for dual modality magnetic resonance and fluorescence imaging. Nano Res 7:1581–1591. https://doi.org/10.1007/s12274-014-0518-8

Hai X, Feng J, Chen X, Wang J (2018) Tuning the optical properties of graphene quantum dots for biosensing and bioimaging:3219–3234. https://doi.org/10.1039/c8tb00428e

Hong G, Robinson JT, Zhang Y et al (2012) In vivo fluorescence imaging with Ag$_2$S quantum dots in the second near-infrared region. Angew Chemie Int Ed 51:9818–9821. https://doi.org/10.1002/anie.201206059

Hong G, Diao S, Antaris AL, Dai H (2015) Carbon nanomaterials for biological imaging and nanomedicinal therapy. Chem Rev 115:10816–10906. https://doi.org/10.1021/acs.chemrev.5b00008

Hu Z, Dai Z, Hu X et al (2019) A facile preparation of FePt-loaded few-layer MoS$_2$ nanosheets nanocomposites (F-MoS$_2$-FePt NCs) and their application for colorimetric detection of H$_2$O$_2$ in living cells. J Nanobiotechnol 17:38. https://doi.org/10.1186/s12951-019-0465-3

Huang P, Jiang Q, Yu P et al (2013) Alkaline post-treatment of Cd(II)–glutathione coordination polymers: toward green synthesis of water-soluble and cytocompatible CdS quantum dots with tunable optical properties. ACS Appl Mater Interfaces 5:5239–5246. https://doi.org/10.1021/am401082n

Huang J, He Y, Jin J et al (2014) A novel glucose sensor based on MoS_2 nanosheet functionalized with Ni nanoparticles. Electrochim Acta 136:41–46. https://doi.org/10.1016/j.electacta.2014.05.070

Huo H, Zhao Y, Xu C (2014) 3D Ni_3S_2 nanosheet arrays supported on Ni foam for high-performance supercapacitor and non-enzymatic glucose detection. J Mater Chem A 2:15111. https://doi.org/10.1039/C4TA02857K

Jahanbin T, Gaceur M, Gros-Dagnac H et al (2015) High potential of Mn-doped ZnS nanoparticles with different dopant concentrations as novel MRI contrast agents: synthesis and in vitro relaxivity studies. J Nanopart Res 17:258. https://doi.org/10.1007/s11051-015-3038-x

Jin Q, Liu J, Zhu W et al (2018) Albumin-assisted synthesis of ultrasmall FeS_2 nanodots for imaging-guided photothermal enhanced photodynamic therapy. ACS Appl Mater Interfaces 10:332–340. https://doi.org/10.1021/acsami.7b16890

Kim S, Lee SH, Cho M, Lee Y (2016) Solvent-assisted morphology confinement of a nickel sulfide nanostructure and its application for non-enzymatic glucose sensor. Biosens Bioelectron 85:587–595. https://doi.org/10.1016/j.bios.2016.05.062

Kong R-M, Ding L, Wang Z et al (2015) A novel aptamer-functionalized MoS_2 nanosheet fluorescent biosensor for sensitive detection of prostate specific antigen. Anal Bioanal Chem 407:369–377. https://doi.org/10.1007/s00216-014-8267-9

Ku G, Zhou M, Song S et al (2012) Copper sulfide nanoparticles as a new class of photoacoustic contrast agent for deep tissue imaging at 1064 nm. ACS Nano 6:7489–7496. https://doi.org/10.1021/nn302782y

L'Azou B, Passagne I, Mounicou S et al (2014) Comparative cytotoxicity of cadmium forms ($CdCl_2$, CdO, CdS micro-and nanoparticles) in renal cells. Toxicol Res 3:32–41. https://doi.org/10.1039/C3TX50063B

Lai P-Y, Huang C-C, Chou T-H et al (2017) Aqueous synthesis of Ag and Mn co-doped In_2S_3/ZnS quantum dots with tunable emission for dual-modal targeted imaging. Acta Biomater 50:522–533. https://doi.org/10.1016/j.actbio.2016.12.028

Li C, Cao L, Zhang Y et al (2015) Preoperative detection and intraoperative visualization of brain tumors for more precise surgery: a new dual-modality MRI and NIR nanoprobe. Small 11:4517–4525. https://doi.org/10.1002/smll.201500997

Li Z, Hu Y, Chang M et al (2016) Highly porous PEGylated Bi_2S_3 nano-urchins as a versatile platform for in vivo triple-modal imaging, photothermal therapy and drug delivery. Nanoscale 8:16005–16016. https://doi.org/10.1039/C6NR03398A

Li A, Li X, Yu X et al (2017) Synergistic thermoradiotherapy based on PEGylated Cu_3BiS_3 ternary semiconductor nanorods with strong absorption in the second near-infrared window. Biomaterials 112:164–175. https://doi.org/10.1016/j.biomaterials.2016.10.024

Li Z, Li Z, Chen L et al (2018) Polyethylene glycol-modified cobalt sulfide nanosheets for high-performance photothermal conversion and photoacoustic/magnetic resonance imaging. Nano Res 11:2436–2449. https://doi.org/10.1007/s12274-017-1865-z

Li L, Wang Q, Chen Z (2019a) Colorimetric detection of glutathione based on its inhibitory effect on the peroxidase-mimicking properties of WS_2 nanosheets. Microchim Acta 186:257. https://doi.org/10.1007/s00604-019-3365-1

Li Y, Kang Z, Kong L et al (2019b) MXene-Ti_3C_2/CuS nanocomposites: enhanced peroxidase-like activity and sensitive colorimetric cholesterol detection. Mater Sci Eng C 104:110000. https://doi.org/10.1016/j.msec.2019.110000

Lin T, Zhong L, Song Z et al (2014) Visual detection of blood glucose based on peroxidase-like activity of WS_2 nanosheets. Biosens Bioelectron 62:302–307. https://doi.org/10.1016/j.bios.2014.07.001

Liu Z, Su X (2016) One-pot synthesis of strongly fluorescent DNA-CuInS$_2$ quantum dots for label-free and ultrasensitive detection of anthrax lethal factor DNA. Anal Chim Acta 942:86–95. https://doi.org/10.1016/j.aca.2016.09.004

Liu J, Xue D (2011) Rapid and scalable route to CuS biosensors: a microwave-assisted Cu-complex transformation into CuS nanotubes for ultrasensitive nonenzymatic glucose sensor. J Mater Chem 21:223–228. https://doi.org/10.1039/C0JM01714K

Liu LW, Hu SY, Pan Y et al (2014) Optimizing the synthesis of CdS/ZnS core/shell semiconductor nanocrystals for bioimaging applications. Beilstein J Nanotechnol 5:919–926. https://doi.org/10.3762/bjnano.5.105

Liu C, Chen J, Zhu Y et al (2018) Highly sensitive MoS$_2$–indocyanine green hybrid for photoacoustic imaging of orthotopic brain glioma at deep site. Nano Micro Lett 10:48. https://doi.org/10.1007/s40820-018-0202-8

Liu H, Ma H, Xu H et al (2019) Hollow and porous nickel sulfide nanocubes prepared from a metal-organic framework as an efficient enzyme mimic for colorimetric detection of hydrogen peroxide. Anal Bioanal Chem 411:129–137. https://doi.org/10.1007/s00216-018-1423-x

Lv G, Guo W, Zhang W et al (2016) Near-infrared emission CuInS/ZnS quantum dots: all-in-one theranostic nanomedicines with intrinsic fluorescence/photoacoustic imaging for tumor photo-therapy. ACS Nano 10:9637–9645. https://doi.org/10.1021/acsnano.6b05419

Mai LNT, Tran TH, Bui QB, Nhac-Vu H-T (2019) A novel nanohybrid of gold nanoparticles anchored copper sulfide nanosheets as sensitive sensor for nonenzymatic glucose detection. Colloid Surf A Physicochem Eng Asp:123936. https://doi.org/10.1016/j.colsurfa.2019.123936

Maji SK, Dutta AK, Bhadu GR et al (2013) A novel amperometric biosensor for hydrogen peroxide and glucose based on cuprous sulfide nanoplates. J Mater Chem B 1:4127. https://doi.org/10.1039/c3tb20846j

Mansur AAP, Mansur HS, Carvalho SM, Caires AJ (2017) One-pot aqueous synthesis of fluorescent Ag-In-Zn-S quantum dot/polymer bioconjugates for multiplex optical bioimaging of glioblastoma cells. Contrast Media Mol Imaging 2017:1–15. https://doi.org/10.1155/2017/3896107

Martynenko IV, Litvin AP, Purcell-Milton F et al (2017) Application of semiconductor quantum dots in bioimaging and biosensing. J Mater Chem B 5:6701–6727. https://doi.org/10.1039/C7TB01425B

Mohammad F, Bwatanglang IB, Yusof NA et al (2016) Folic acid targeted Mn:ZnS quantum dots for theranostic applications of cancer cell imaging and therapy. Int J Nanomedicine 11:413. https://doi.org/10.2147/IJN.S90198

Nirala NR, Vinita, Prakash R (2018) Quick colorimetric determination of choline in milk and serum based on the use of MoS$_2$ nanosheets as a highly active enzyme mimetic. Microchim Acta 185:224. https://doi.org/10.1007/s00604-018-2753-2

Niu X, Xu X, Li X et al (2018) Surface charge engineering of nanosized CuS via acidic amino acid modification enables high peroxidase-mimicking activity at neutral pH for one-pot detection of glucose. Chem Commun 54:13443–13446. https://doi.org/10.1039/C8CC07800A

Pedram P, Mahani M, Torkzadeh-Mahani M et al (2016) Cadmium sulfide quantum dots modified with the human transferrin protein siderophiline for targeted imaging of breast cancer cells. Microchim Acta 183:67–71. https://doi.org/10.1007/s00604-015-1593-6

Qin M-Y, Yang X-Q, Wang K et al (2015) In vivo cancer targeting and fluorescence-CT dual-mode imaging with nanoprobes based on silver sulfide quantum dots and iodinated oil. Nanoscale 7:19484–19492. https://doi.org/10.1039/C5NR05620A

Regulacio MD, Win KY, Lo SL et al (2013) Aqueous synthesis of highly luminescent AgInS$_2$–ZnS quantum dots and their biological applications. Nanoscale 5:2322. https://doi.org/10.1039/c3nr34159c

Sarkar A, Ghosh AB, Saha N et al (2018) Newly designed amperometric biosensor for hydrogen peroxide and glucose based on vanadium sulfide nanoparticles. ACS Appl Nano Mater. https://doi.org/10.1021/acsanm.8b00076

Selvaraj J, Mahesh A, Baskaralingam V et al (2019) Organic-to-water dispersible Mn:ZnS–ZnS doped core–shell quantum dots: synthesis, characterization and their application towards optical bioimaging and a turn-off fluorosensor. New J Chem 43:11912–11925. https://doi.org/10.1039/C9NJ02222H

Shamirian A, Appelbe O, Zhang Q et al (2015) A toolkit for bioimaging using near-infrared AgInS$_2$/ZnS quantum dots. J Mater Chem B 3:8188–8196. https://doi.org/10.1039/C5TB00247H

Shen R, Shen X, Zhang Z et al (2010) Multifunctional conjugates to prepare nucleolar-targeting CdS quantum dots. J Am Chem Soc 132:8627–8634. https://doi.org/10.1021/ja1002668

Shen H, Zhang L, Liu M, Zhang Z (2012) Biomed Appl Graphene:2. https://doi.org/10.7150/thno.3642

Shi J, Lyu J, Tian F, Yang M (2017) A fluorescence turn-on biosensor based on graphene quantum dots (GQDs) and molybdenum disulfide (MoS$_2$) nanosheets for epithelial cell adhesion molecule (EpCAM) detection. Biosens Bioelectron 93:182–188. https://doi.org/10.1016/j.bios.2016.09.012

Shivaji K, Mani S, Ponmurugan P et al (2018) Green-synthesis-derived CdS quantum dots using tea leaf extract: antimicrobial, bioimaging, and therapeutic applications in lung cancer cells. ACS Appl Nano Mater 1:1683–1693. https://doi.org/10.1021/acsanm.8b00147

Singh P, Gupta R, Sinha M et al (2016) MoS$_2$ based digital response platform for aptamer based fluorescent detection of pathogens. Microchim Acta 183:1501–1506. https://doi.org/10.1007/s00604-016-1762-2

Singhal C, Khanuja M, Chaudhary N et al (2018) Detection of chikungunya virus DNA using two-dimensional MoS$_2$ nanosheets based disposable biosensor. Sci Rep 8:1–11. https://doi.org/10.1038/s41598-018-25824-8

Song J, Ma C, Zhang W et al (2016a) Tumor cell-targeted Zn$_3$In$_2$S$_6$ and Ag–Zn–In–S quantum dots for color adjustable luminophores. J Mater Chem B 4:7909–7918. https://doi.org/10.1039/C6TB02297A

Song J, Ma C, Zhang W et al (2016b) Bandgap and structure engineering via cation exchange: from binary Ag$_2$S to ternary AgInS$_2$, quaternary AgZnInS alloy and AgZnInS/ZnS core/shell fluorescent nanocrystals for bioimaging. ACS Appl Mater Interfaces 8:24826–24836. https://doi.org/10.1021/acsami.6b07768

Song C, Yang C, Wang F et al (2017) MoS$_2$-based multipurpose theranostic nanoplatform: realizing dual-imaging-guided combination phototherapy to eliminate solid tumor via a liquefaction necrosis process. J Mater Chem B 5:9015–9024. https://doi.org/10.1039/C7TB02648J

Su S, Han X, Lu Z et al (2017) Facile synthesis of a MoS$_2$-Prussian blue nanocube nanohybrid-based electrochemical sensing platform for hydrogen peroxide and carcinoembryonic antigen detection. ACS Appl Mater Interfaces 9:12773–12781. https://doi.org/10.1021/acsami.7b01141

Suganthi G, Arockiadoss T, Uma TS (2016) ZnS nanoparticles decorated graphene nanoplatelets as immobilisation matrix for glucose biosensor. Nanosyst Phys Chem Math 7:637–642. https://doi.org/10.17586/2220-8054-2016-7-4-637-642

Sun H, Chao J, Zuo X et al (2014) Gold nanoparticle-decorated MoS$_2$ nanosheets for simultaneous detection of ascorbic acid, dopamine and uric acid. RSC Adv 4:27625. https://doi.org/10.1039/c4ra04046e

Sun X, Fan J, Fu C et al (2017) WS$_2$ and MoS$_2$ biosensing platforms using peptides as probe biomolecules. Sci Rep 7:10290. https://doi.org/10.1038/s41598-017-10221-4

Tan C, Yu P, Hu Y et al (2015a) High-yield exfoliation of ultrathin two-dimensional ternary chalcogenide nanosheets for highly sensitive and selective fluorescence DNA sensors. J Am Chem Soc 137:10430–10436. https://doi.org/10.1021/jacs.5b06982

Tan L, Liu S, Li X et al (2015b) A new strategy for synthesizing AgInS$_2$ quantum dots emitting brightly in near-infrared window for in vivo imaging. Colloid Surf B Biointerface 125:222–229. https://doi.org/10.1016/j.colsurfb.2014.11.041

Tang R, Xue J, Xu B et al (2015) Tunable ultrasmall visible-to-extended near-infrared emitting silver sulfide quantum dots for integrin-targeted cancer imaging. ACS Nano 9:220–230. https://doi.org/10.1021/nn5071183

Tchounwou PB, Yedjou CG, Patlolla AK, Sutton DJ (2012) Heavy metal toxicity and the environment. In: Luch A (ed) Nih. Birkhäuser Basel, Basel, pp 133–164

Vilian ATE, Dinesh B, Kang SM et al (2019) Recent advances in molybdenum disulfide-based electrode materials for electroanalytical applications. Microchim Acta 186:22212. https://doi.org/10.1007/s00604-019-3287-y

Vinita, Nirala NR, Prakash R (2018) One step synthesis of AuNPs@MoS$_2$-QDs composite as a robust peroxidase- mimetic for instant unaided eye detection of glucose in serum, saliva and tear. Sensors Actuators B Chem 263:109–119. https://doi.org/10.1016/j.snb.2018.02.085

Wang K, Liu Q, Guan Q-M et al (2011) Enhanced direct electrochemistry of glucose oxidase and biosensing for glucose via synergy effect of graphene and CdS nanocrystals. Biosens Bioelectron 26:2252–2257. https://doi.org/10.1016/j.bios.2010.09.043

Wang S, Li X, Chen Y et al (2015) A facile one-pot synthesis of a two-dimensional MoS$_2$/Bi$_2$S$_3$ composite theranostic nanosystem for multi-modality tumor imaging and therapy. Adv Mater 27:2775–2782. https://doi.org/10.1002/adma.201500870

Wang Z, Huang P, Jacobson O et al (2016) Biomineralization-inspired synthesis of copper sulfide–ferritin nanocages as cancer theranostics. ACS Nano 10:3453–3460. https://doi.org/10.1021/acsnano.5b07521

Wang Y, Ma T, Ma S et al (2017) Fluorometric determination of the antibiotic kanamycin by aptamer-induced FRET quenching and recovery between MoS$_2$ nanosheets and carbon dots. Microchim Acta 184:203–210. https://doi.org/10.1007/s00604-016-2011-4

Wang D, Zhang Y, Guo Q (2018) Sub-10 nm Cu$_5$FeS$_4$ cube for magnetic resonance imaging-guided photothermal therapy of cancer. Int J Nanomed 13:7987–7996. https://doi.org/10.2147/IJN.S181056

Wang L, Xu X, Mu X et al (2019a) Fe-doped copper sulfide nanoparticles for in vivo magnetic resonance imaging and simultaneous photothermal therapy. Nanotechnology 30:415101. https://doi.org/10.1088/1361-6528/ab2c13

Wang X, Yao Q, Tang X et al (2019b) A highly selective and sensitive colorimetric detection of uric acid in human serum based on MoS$_2$-catalyzed oxidation TMB. Anal Bioanal Chem 411:943–952. https://doi.org/10.1007/s00216-018-1524-6

Wei G, Yan M, Ma L, Zhang H (2012) The synthesis of highly water-dispersible and targeted CdS quantum dots and it is used for bioimaging by confocal microscopy. Spectrochim Acta Part A Mol Biomol Spectrosc 85:288–292. https://doi.org/10.1016/j.saa.2011.10.011

Wei C, Cheng C, Zhao J et al (2015) Mesoporous ZnS-NiS nanocomposites for nonenzymatic electrochemical glucose sensors. ChemistryOpen 4:32–38. https://doi.org/10.1002/open.201402044

Wen J, Xu Y, Li H et al (2015) Recent applications of carbon nanomaterials in fluorescence biosensing and bioimaging. Chem Commun 51:11346–11358. https://doi.org/10.1039/C5CC02887F

Wu W, Li Y, Jin J et al (2016) A novel nonenzymatic electrochemical sensor based on 3D flower-like Ni7S6 for hydrogen peroxide and glucose. Sensors Actuators B Chem 232:633–641. https://doi.org/10.1016/j.snb.2016.04.006

Wu W, Yu B, Wu H et al (2017) Synthesis of tremella-like CoS and its application in sensing of hydrogen peroxide and glucose. Mater Sci Eng C 70:430–437. https://doi.org/10.1016/j.msec.2016.08.084

Xie R, Rutherford M, Peng X (2009) Formation of high-quality I−III−VI semiconductor nanocrystals by tuning relative reactivity of cationic precursors. J Am Chem Soc 131:5691–5697. https://doi.org/10.1021/ja9005767

Xing H, Wei T, Lin X, Dai Z (2018) Near-infrared MnCuInS/ZnS@BSA and urchin-like au nanoparticle as a novel donor-acceptor pair for enhanced FRET biosensing. Anal Chim Acta 1042:71–78. https://doi.org/10.1016/j.aca.2018.05.048

Xu Z, Li B, Tang W et al (2011) Glycopolypeptide-encapsulated Mn-doped ZnS quantum dots for drug delivery: fabrication, characterization, and in vitro assessment. Colloid Surf B Biointerface 88:51–57. https://doi.org/10.1016/j.colsurfb.2011.05.055

Xu CX, Zhai QG, Liu YJ et al (2014) A novel electrochemical DNA biosensor construction based on layered CuS-graphene composite and Au nanoparticles. Anal bioanal Chem:6943–6951. https://doi.org/10.1007/s00216-014-7904-7

Yadav V, Roy S, Singh P et al (2019) 2D MoS$_2$-based nanomaterials for therapeutic, bioimaging, and biosensing applications. Small 15:1803706. https://doi.org/10.1002/smll.201803706

Yan X, Gu Y, Li C et al (2018) A non-enzymatic glucose sensor based on the CuS nanoflakes–reduced graphene oxide nanocomposite. Anal Methods 10:381–388. https://doi.org/10.1039/C7AY02290E

Yan H, Chen J, Li Y et al (2019) Ultrasmall hybrid protein–copper sulfide nanoparticles for targeted photoacoustic imaging of orthotopic hepatocellular carcinoma with a high signal-to-noise ratio. Biomater Sci 7:92–103. https://doi.org/10.1039/C8BM00767E

Yang YJ (2015) One-pot synthesis of reduced graphene oxide/zinc sulfide nanocomposite at room temperature for simultaneous determination of ascorbic acid, dopamine and uric acid. Sensors Actuators B Chem 221:750–759. https://doi.org/10.1016/j.snb.2015.06.150

Yang J, Zhang W-H, Hu Y-P, Yu J-S (2012) Aqueous synthesis and characterization of glutathione-stabilized β-HgS nanocrystals with near-infrared photoluminescence. J Colloid Interface Sci 379:8–13. https://doi.org/10.1016/j.jcis.2012.04.057

Yang YJ, Zi J, Li W (2014) Enzyme-free sensing of hydrogen peroxide and glucose at a CuS nanoflowers modified glassy carbon electrode. Electrochim Acta 115:126–130. https://doi.org/10.1016/j.electacta.2013.10.168

Yang J, Hu Y, Tan J et al (2015a) Ultra-bright near-infrared-emitting HgS/ZnS core/shell nanocrystals for in vitro and in vivo imaging. J Mater Chem B 3:6928–6938. https://doi.org/10.1039/c5tb01034a

Yang W, Guo W, Gong X et al (2015b) Facile synthesis of Gd–Cu–In–S/ZnS bimodal quantum dots with optimized properties for tumor targeted fluorescence/MR in vivo imaging. ACS Appl Mater Interfaces 7:18759–18768. https://doi.org/10.1021/acsami.5b05372

Yang M-Y, Hong J, Zhang Y et al (2016a) Bio-compatibility and cytotoxicity studies of water-soluble CuInS$_2$-ZnS-AFP fluorescence probe in liver cancer cells. Hepatobiliary Pancreat Dis Int 15:406–411. https://doi.org/10.1016/S1499-3872(16)60112-1

Yang W, Guo W, Le W et al (2016b) Albumin-bioinspired Gd:CuS Nanotheranostic agent for in vivo photoacoustic/magnetic resonance imaging-guided tumor-targeted photothermal therapy. ACS Nano 10:10245–10257. https://doi.org/10.1021/acsnano.6b05760

Yang T, Tang Y, Liu L et al (2017a) Size-dependent Ag$_2$S nanodots for second near-infrared fluorescence/photoacoustics imaging and simultaneous photothermal therapy. ACS Nano 11:1848–1857. https://doi.org/10.1021/acsnano.6b07866

Yang Y, Lin L, Jing L et al (2017b) CuInS$_2$/ZnS quantum dots conjugating Gd(III) chelates for near-infrared fluorescence and magnetic resonance bimodal imaging. ACS Appl Mater Interfaces 9:23450–23457. https://doi.org/10.1021/acsami.7b05867

Yang Z, Zhu Y, Chi M et al (2018) Fabrication of cobalt ferrite/cobalt sulfide hybrid nanotubes with enhanced peroxidase-like activity for colorimetric detection of dopamine. J Colloid Interface Sci 511:383–391. https://doi.org/10.1016/j.jcis.2017.09.097

Yong K-T, Roy I, Hu R et al (2010) Synthesis of ternary CuInS$_2$/ZnS quantum dot bioconjugates and their applications for targeted cancer bioimaging. Integr Biol 2:121. https://doi.org/10.1039/b916663g

Yong Y, Cheng X, Bao T et al (2015) Tungsten sulfide quantum dots as multifunctional nanotheranostics for in vivo dual-modal image-guided photothermal/radiotherapy synergistic therapy. ACS Nano 9:12451–12463. https://doi.org/10.1021/acsnano.5b05825

Yu JH, Kwon S-H, Petrášek Z et al (2013) High-resolution three-photon biomedical imaging using doped ZnS nanocrystals. Nat Mater 12:359–366. https://doi.org/10.1038/nmat3565

Yu C, Xuan T, Lou S et al (2017) Gd^{3+}doped CuInS$_2$/ZnS nanocrystals with high quantum yield for bimodal fluorescence/magnetic resonance imaging. J Rare Earths 35:382–388. https://doi.org/10.1016/S1002-0721(17)60923-2

Yuan Y, Li R, Liu Z (2014) Establishing water-soluble layered WS_2 nanosheet as a platform for biosensing. Anal Chem 86:3610–3615. https://doi.org/10.1021/ac5002096

Zhang X, Wang G, Gu A et al (2008) CuS nanotubes for ultrasensitive nonenzymatic glucose sensors. Chem Commun 5945. https://doi.org/10.1039/b814725f

Zhang Y, Liu J-M, Yan X-P (2013) Self-assembly of folate onto polyethyleneimine-coated CdS/ZnS quantum dots for targeted turn-on fluorescence imaging of folate receptor overexpressed cancer cells. Anal Chem 85:228–234. https://doi.org/10.1021/ac3025653

Zhang Y, Zheng B, Zhu C et al (2015) Single-layer transition metal dichalcogenide nanosheet-based nanosensors for rapid, sensitive, and multiplexed detection of DNA. Adv Mater 27:935–939. https://doi.org/10.1002/adma.201404568

Zhang Z, Duan F, He L et al (2016) Electrochemical clenbuterol immunosensor based on a gold electrode modified with zinc sulfide quantum dots and polyaniline. Microchim Acta 183:1089–1097. https://doi.org/10.1007/s00604-015-1730-2

Zhang Y, Wen F, Huang Z et al (2017a) Nitrogen doped lignocellulose/binary metal sulfide modified electrode: preparation and application for non-enzymatic ascorbic acid, dopamine and nitrite sensing. J Electroanal Chem 806:150–157. https://doi.org/10.1016/j.jelechem.2017.10.066

Zhang Y, Wen F, Huang Z et al (2017b) Nitrogen doped lignocellulose/binary metal sulfide modified electrode: preparation and application for non-enzymatic ascorbic acid, dopamine and nitrite sensing. J Electroanal Chem 806:150–157. https://doi.org/10.1016/j.jelechem.2017.10.066

Zhang R-Y, Wang Z-Y, Yang X-Q et al (2018a) Folic acid modified Pluronic F127 coating Ag_2S quantum dot for photoacoustic imaging of tumor cell-targeting. Nanotechnology 29:055101. https://doi.org/10.1088/1361-6528/aa9acc

Zhang Y, Zhao N, Qin Y et al (2018b) Affibody-functionalized Ag_2S quantum dots for photoacoustic imaging of epidermal growth factor receptor overexpressed tumors. Nanoscale 10:16581–16590. https://doi.org/10.1039/C8NR02556H

Zhang H, Chen Y, Cai Y et al (2019) Paramagnetic CuS hollow nanoflowers for T2-FLAIR magnetic resonance imaging-guided thermochemotherapy of cancer. Biomater Sci 7:409–418. https://doi.org/10.1039/C8BM01412D

Zhao Y, Meng J, Sheng X, Tian Y (2016) Synthesis of ultrathin MnS Shell on ZnS:Mn nanorods by one-step coating and doping for MRI and fluorescent imaging. Adv Opt Mater 4:1115–1123. https://doi.org/10.1002/adom.201600154

Zhao Y, Wei X, Peng N et al (2017) Study of ZnS nanostructures based electrochemical and photoelectrochemical biosensors for uric acid detection. Sensors (Switzerland):17. https://doi.org/10.3390/s17061235

Zhao D-H, Yang J, Xia R-X et al (2018) High quantum yield Ag_2S quantum dot@polypeptide-engineered hybrid nanogels for targeted second near-infrared fluorescence/photoacoustic imaging and photothermal therapy. Chem Commun 54:527–530. https://doi.org/10.1039/C7CC09266K

Zhou B, Zhao J, Qiao Y et al (2018) Simultaneous multimodal imaging and photothermal therapy via renal-clearable manganese-doped copper sulfide nanodots. Appl Mater Today 13:285–297. https://doi.org/10.1016/j.apmt.2018.09.011

Zhu C, Zeng Z, Li H et al (2013a) Single-layer MoS_2-based nanoprobes for homogeneous detection of biomolecules. J Am Chem Soc 135:5998–6001. https://doi.org/10.1021/ja4019572

Zhu C, Zeng Z, Li H et al (2013b) Single-layer MoS_2-based nanoprobes for homogeneous detection of biomolecules. J Am Chem Soc 135:5998–6001. https://doi.org/10.1021/ja4019572

Zhu Q, Gao F, Yang Y et al (2015) Electrochemical preparation of polyaniline capped Bi_2S_3 nanocomposite and its application in impedimetric DNA biosensor. Sensors Actuators B Chem:819–826. https://doi.org/10.1016/j.snb.2014.10.120

Zhu J, Peng X, Nie W et al (2019) Hollow copper sulfide nanocubes as multifunctional nanozymes for colorimetric detection of dopamine and electrochemical detection of glucose. Biosens Bioelectron 141:111450. https://doi.org/10.1016/j.bios.2019.111450

Chapter 2
Modification of Titanium Alloys for Dental Applications

Dinesh Rokaya, Viritpon Srimaneepong, and Jiaqian Qin

Contents

Abstract Titanium alloys have wide biomedical applications, and the alloys can be modified according to the requirements. In addition, various surface modifications for titanium alloys have been tried for the better functionality and biocompatibility. This chapter gives an overview of titanium alloys for biomedical applications and

D. Rokaya
Department of Clinical Dentistry, Walailak University International College of Dentistry, Walailak University, Bangkok, Thailand

V. Srimaneepong (✉)
Department of Prosthodontics, Faculty of Dentistry, Chulalongkorn University, Bangkok, Thailand
e-mail: viritpon.s@chula.ac.th

J. Qin
Metallurgy and Materials Science Research Institute (MMRI), Chulalongkorn University, Bangkok, Thailand

presents recent and popular surface modifications focusing on its application, surface, mechanical, corrosion, and biological properties. Common titanium and its alloys include titanium–aluminum–vanadium (Ti–Al–V), titanium–aluminum–niobium (Ti–Al–Nb), titanium–aluminum–iron (Ti–Al–Fe), titanium–zirconium (Ti–Zr), titanium–zirconium–niobium–tantalum–palladium (Ti–Zr–Nb–Ta–Pd), titanium–niobium–tantalum–zirconium (Ti–Nb–Ta–Zr), and nickel–titanium alloy (Ni–Ti). Surface modifications can be grouped as thermal treatment and plasma surface modification, various nanocomposites, and carbon-related coatings.

Keywords Titanium alloy · Nickel–titanium alloy · Surface modifications · Surface coatings · Thermal treatment · Graphene

Abbreviations

(Si, O, N)/(Ti, O, N)/Ti	Silicon–oxygen–nitrogen–titanium
PIII	Plasma immersion ion implantation
PIIID	Plasma immersion ion implantation and deposition
PSA	Plasma surface alloying
Ti–Al–Fe	Titanium–aluminum–iron
Ti–Al–Nb	Titanium–aluminum–niobium
Ti–Al–V	Titanium–aluminum–vanadium
Ti–Nb–Ta–Zr	Titanium–niobium–tantalum–zirconium
Ti–Zr–Nb–Ta–Pd	Titanium–zirconium–niobium–tantalum–palladium
Zn–HA/Ti$_2$	Zinc–hydroxyapatite–titania

2.1 Introduction

Titanium and its alloys are of an increasing importance since 1960 in various fields, such as automotive, chemical, and biomedical industries including medicine and dentistry, because of improved mechanical, corrosion, and biological properties (Revankar et al. 2017). Titanium alloy has wide applications.

Generally used titanium alloy applications in medicine and dentistry include titanium–aluminum–vanadium (Ti–Al–V) alloy, titanium–aluminum–niobium (Ti–Al–Nb) alloy, and nickel–titanium (Ni–Ti, Nitinol) alloy. The titanium is favored by low density (4.5 g/cm^3), better biocompatibility, and modulus of elasticity than cobalt-chrome and stainless steel (Bolzoni et al. 2013).

Various biomedical applications of titanium alloys include fabrication of various prostheses, in orthodontics, endodontics, implant dentistry, and maxillofacial surgery (Figs. 2.1 and 2.2) (Caldas et al. 2014). Ti–6Al–4 V alloy is useful for the fixation of bone fractures and joint replacement as Ti–6Al–4 V alloys have good mechanical and corrosion properties. Other advantages include shorter healing at the bone-implant interface with good implant stability with longevity (Liu et al. 2004).
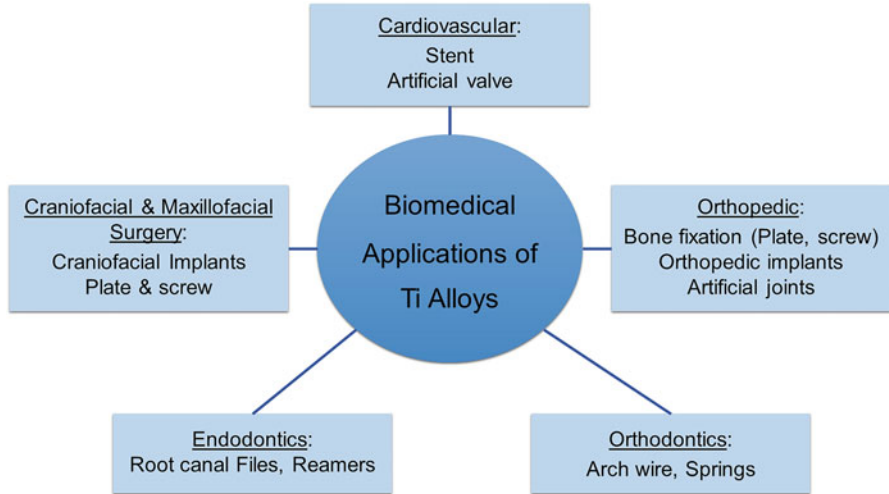
Fig. 2.1 Biomedical applications of titanium alloys; cardiovascular, orthopedic, orthodontics, endodontics, and maxillofacial surgery
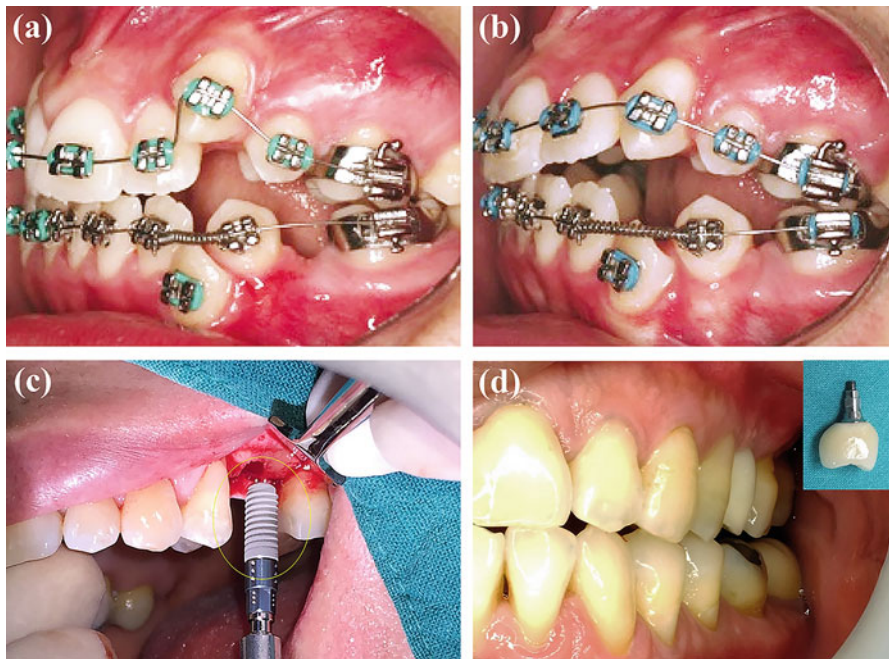

Fig. 2.2 Titanium alloys for dental applications; in orthodontics for teeth alignment (**a**, **b**) and dental implant applications (**c**, **d**). Small picture showing the implant prosthetic crown. (Figure 2.2a, b reprinted with permission of Dental Press Journal of Orthodontics under the Creative Commons Attribution Non-Commercial License from Caldas et al. 2014)

To eliminate the cytotoxicity and neurologic disorders related to vanadium and aluminum elements in the human body, other alloys such as Ti–6Al–7Nb, tin–titanium, and titanium–zirconium based were developed (Choubey et al. 2004; Okazaki et al. 1995). Similarly, NiTi alloy is also invented which has as wide biomedical applications because of the shape memory effect and superelastic properties (Duerig et al. 1999).

2.2 Titanium and Titanium Alloys for Biomedical Applications

The titanium and its alloys can be of various types according to different compositions for various biomedical applications, such as commercially pure titanium, Ti–Al–V alloy, Ti–Al–Nb alloy, titanium–aluminum–iron (Ti–Al–Fe), titanium–niobium–tantalum–zirconium (Ti–Nb–Ta–Zr), titanium–zirconium–niobium–tantalum–palladium (Ti–Zr–Nb–Ta–Pd), and Ni–Ti alloy (Fig. 2.3).

Generally, titanium alloys may be α, α–β, or β type according to the structure. Consequently, major elements for alloying titanium of each type include α–stabilizers (carbon, oxygen, nitrogen, aluminum), β–stabilizers (hydrogen, iron, chromium, nickel, silicon, cobalt, manganese, vanadium, niobium, tantalum, molybdenum, tungsten, and neutrals (tin and zirconium) (Guo et al. 2013; Liu et al. 2017). The α alloys have high corrosion behavior but show low strength. The α + β alloys display higher strength because α + β alloys have α and β phases. The β alloys show superior corrosion behavior with low elastic modulus, but α + β alloys have low rigidity for promoting bone remodeling (Liu et al. 2017). The α + β titanium alloys have greater rigidity than the cortical bone but less than cobalt-chrome and stainless steel. Some important mechanical properties of various alloys are shown in Table 2.1. It shows that the alloys have suitable mechanical properties for biomedical applications.

Fig. 2.3 Classifications of titanium and titanium alloys for biomedical applications; commercially pure titanium, titanium–aluminum–vanadium, titanium–aluminum–niobium, titanium–aluminum–iron, titanium–zirconium, and nickel–titanium
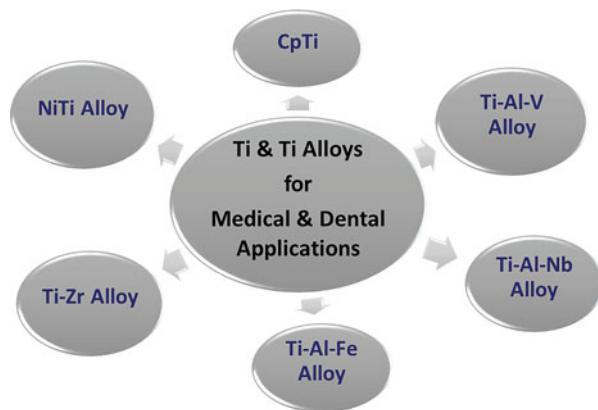
Table 2.1 Physical and mechanical properties of titanium alloys

Titanium and titanium alloys	Ultimate tensile strength (MPa)	Yield strength (MPa)	Elastic modulus (GPa)	Elongation %	Density (g/cm^3)	Alloy type %
Commercially pure titanium	579	483	97.4	11.6	4.5	α
Ti–6Al–4V	860	795	110	9	4.4	α + β
Ti–6Al–7Nb	943	860	106.3	5.8	4.4	α + β
Ti–5Al–2.5Fe	1020	895	112	15	4.4	α + β
Ti–15Zr–4Nb–2Ta–0.2Pd	715–919	693–806	94–99	18–28	4.4	α + β
Ti–29Nb–13Ta–4.6Zr	911	864	80	13.2	4.4	β
Ni–Ti	70–110$^\alpha$ 21–69$^\beta$	379	100–800$^\alpha$ 50–300$^\beta$	13–40%	6.45	β

Berner et al. (2009), Fernandes et al. (2015), Koizumi et al. (2018), Lemons (1990), Osman and Swain (2015), and Thompson (2000)

α austenitic, *β* martensitic, *Ti–6Al–V* titanium–aluminum–vanadium, *Ti–6Al–Nb* titanium–aluminum–niobium, *Ti–5Al–1.5Fe* titanium–aluminum–iron, *Ti–15Zr–4Nb–2Ta–0.2Pd* titanium–zirconium–niobium–tantalum–palladium, *Ti–29Nb–13Ta–4.6Zr* titanium–niobium–tantalum–zirconium, *Zn–HA/Ti$_2$* zinc–hydroxyapatite–titanium, *Ni-Ti* Nickel–titanium

2.2.1 Commercially Pure Titanium

Commercially pure titanium has been used in dentistry for more than a decade for dental implant, crowns and bridges, and metal-ceramic restorations due to improved mechanical properties and biocompatibility (Bolzoni et al. 2013; Özcan and Hämmerle 2012; Raman et al. 2005). They can be classified into four grades (I–IV) by the American Society for Testing and Materials according to the presence of oxygen nitrogen, hydrogen, iron, and carbon, and each type shows different physical and mechanical properties (*American Society for Testing and Materials – ASTM. ASTM F67–13: standard specifications for unalloyed titanium, for surgical implant applications* 2013). Grade I is the purest with the least oxygen content (approx. 0.18%) and highest corrosion resistance and formability. However, it has low mechanical strength (Liu et al. 2017). Still, grades I and grade II are generally used in dentistry for porcelain fused to metal restorations and implant materials.

Abey et al. (2014) did corrosion tests of commercially pure titanium in artificial saliva and its relation to the pH and found that the commercially pure titanium showed less corrosion behavior at the neutral pH. But commercially pure titanium has certain disadvantages which include low strength, poor wear resistance, and polishing difficulty hence inappropriate for applications in high stress areas, such as long span prosthesis (López et al. 2003). Similarly, another study showed that the commercially pure titanium exhibits poor corrosion resistance compared to Ti–6Al–7Nb (Poon et al. 2005). Hence, these have resulted in the development of other

alloys with higher mechanical strength, wear resistance, and better surface properties.

2.2.2 Titanium–Aluminum–Vanadium Alloy

Ti–6Al–4V alloy is the most common alloy of Ti–Al–V group and originally developed for the aeronautical purpose, but this alloy has potential biomedical uses and is considered better than commercially pure titanium because it shows better mechanical and corrosion properties. This alloy has lower weight compared to commercially pure titanium and has less allergic response but has good mechanical properties, such as good strength, high modulus, good corrosion resistance, low density, and creep resistance (Almanzaa et al. 2017; Guitar et al. 2009; Lee et al. 2005).

Figure 2.4 shows the surface structure of Ti–6Al–4V alloy under scanning electron microscope which show fine grained with α and β phases with majority containing α phase (Choubey et al. 2004). Hence, these two phases, with complexe structures and components determine the microstructure and mechanical properties of Ti–6Al–4V alloy.

During manufacturing of Ti–6Al–4V alloy, the freezing rate is enhanced to obtain good castings with high density with good surface structure and reduced porosities as this alloy is susceptible to porosity due to high chemical reactivity and less flow (Almanzaa et al. 2017). Another limitation is the cytotoxicity related to the vanadium and aluminum. Hence, vanadium and aluminum alternatives were considered (Bolzoni et al. 2013; Choubey et al. 2004).
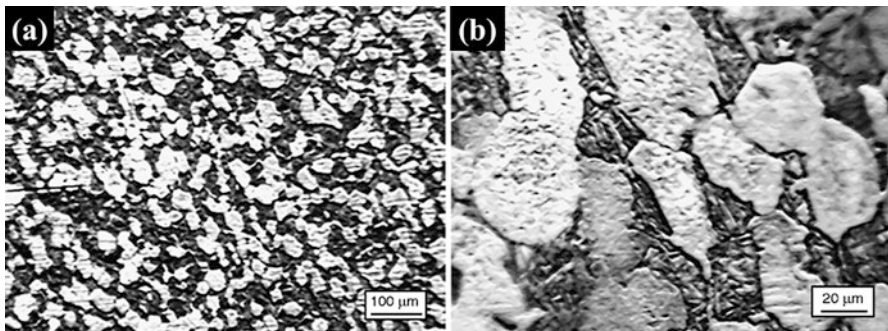

Fig. 2.4 Surface structure of titanium–aluminum–vanadium (Ti–6Al–4V) alloy under scanning electron microscope in low magnification (**a**) and high magnification (**b**). Images show fine grained with α and β phases with majority containing α phase. (Reprinted with permission of Elsevier from Choubey et al. 2004)

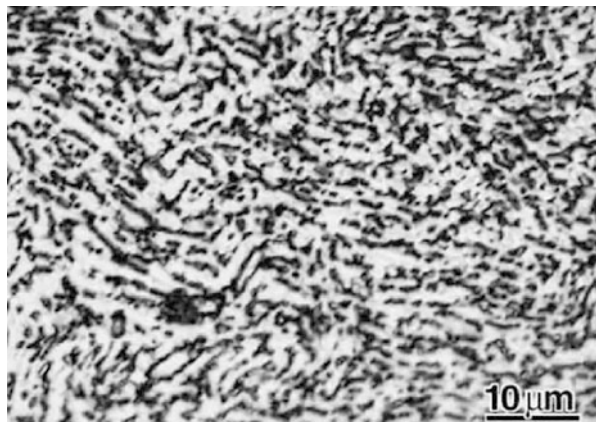## 2.2.3   Titanium–Aluminum–Niobium Alloy

The Ti–6Al–7Nb is common alloy of Ti–Al–Nb group which was specially developed to eliminate the cytotoxicity of vanadium to the human body with improved mechanical, corrosion, and biological properties (Bolzoni et al. 2013; Choubey et al. 2004; Srimaneepong et al. 2004, 2008). Various dental prostheses can be fabricated from Ti–6Al–7Nb as this alloy has suitable mechanical properties (Koizumi et al. 2019; Srimaneepong et al. 2004, 2005). This alloy can be fabricated by ingot metallurgy (powder metallurgy) with specific properties. Various manufacturing techniques for the Ti–6Al–7Nb components include hot pressing, cold uniaxial pressing and sintering, and uniaxial inductive hot pressing with a sintering at >1100 °C to result homogeneous distribution of alloying (Bolzoni et al. 2013). Changing the fabrication conditions, such as the sintering temperature, may vary the porosity level.

Niobium has a similar stabilizing action as vanadium in the titanium–niobium binary system which results in favorable surface structure of Ti–6Al–7Nb alloy as seen in scanning electron microscope (Fig. 2.5) (Miura et al. 2007). This alloy is generally used for orthopedics application for total hip prostheses.

2.2.4   Titanium–Aluminum–Iron Alloy

Ti–5Al–2.5Fe alloy is a common type of Ti–Al–Fe alloy which is also another alternative to eliminate the cytotoxicity of vanadium with improved mechanical properties. This alloy can be produced from various methods, such as vacuum sintering, cold compaction, forging, and heat treatment (Tang et al. 2018). Figure 2.6 shows the surface structure of Ti–5Al–2.5Fe alloy fabricated by two steps rolling at

Fig. 2.5 Surface structure of titanium–aluminum–niobium (Ti–6Al–7Nb) alloy under the scanning electron microscope. Niobium has a similar stabilizing action as vanadium in the titanium–niobium binary system which results in favorable surface structure of Ti–6Al–7Nb alloy. (Reprinted with permission of The Japan Institute of Metals and Materials from Miura et al. 2007)
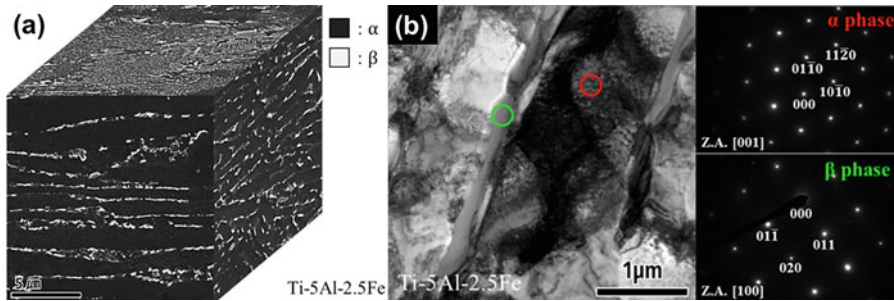
Fig. 2.6 Surface structure of the titanium–aluminum–iron (Ti–5Al–2.5Fe) alloy; 3D microstructure (**a**) and transmission electron microscope images (**b**). It shows less precipitates of titanium and aluminum than iron. (Reprinted with permission of Elsevier from Bak et al. 2018)

1100 °C and 880 °C (Bak et al. 2018). It shows less precipitates of titanium and aluminum than iron which shows about 51 wt.%.

Yamanoglu et al. did modification of Ti–5Al2.5Fe alloy for biomedical applications by adding Cu and studied the mechanical and antibacterial properties with biocompatibility (Yamanoglu et al. 2017). The alloys showed improved mechanical properties (from hardness and bending tests) and surface properties. The alloy's antibacterial properties were greatly improved for the *S. aureus* and *E. coli* strains. Finally, all samples showed very good cell biocompatibility.

2.2.5 Titanium–Zirconium Alloy

Zirconium is a biocompatible element and can be coupled with titanium as it has similar allotropic transformation and phase transition temperature. With titanium, in both α and β phases, it helps hardening, slows the process of phase transformation, increases mechanical properties (such as hardness, tensile, and flexural strength), and also improves corrosion properties (Correa et al. 2014). Titanium–zirconium exhibits a shape memory stain of 1.4% and good plasticity which are useful for biomedical applications (Li et al. 2011). Moreover, these alloys are able to avoid the adverse tissue reactions in human and help replacing the lost or diseased organs by restoring the structure and function (Mantshiu et al. 2018).

Cordeiro et al. (2017) developed binary and ternary titanium alloys containing zirconium and niobium and the alloys showed better microstructure of both alloys and better mechanical properties of binary alloys (increase hardness) and ternary alloys (decrease the elastic modulus). The results showed that zirconium improved the mechanical and surface properties of titanium–zirconium alloys compared to commercially pure titanium and Ti–Al–V alloy (Fig. 2.7). The double acid etching treatment of titanium–zirconium alloys was beneficial in terms of mechanical behavior, surface properties, and cell adhesion and proliferation, as well as for the corrosion resistance.
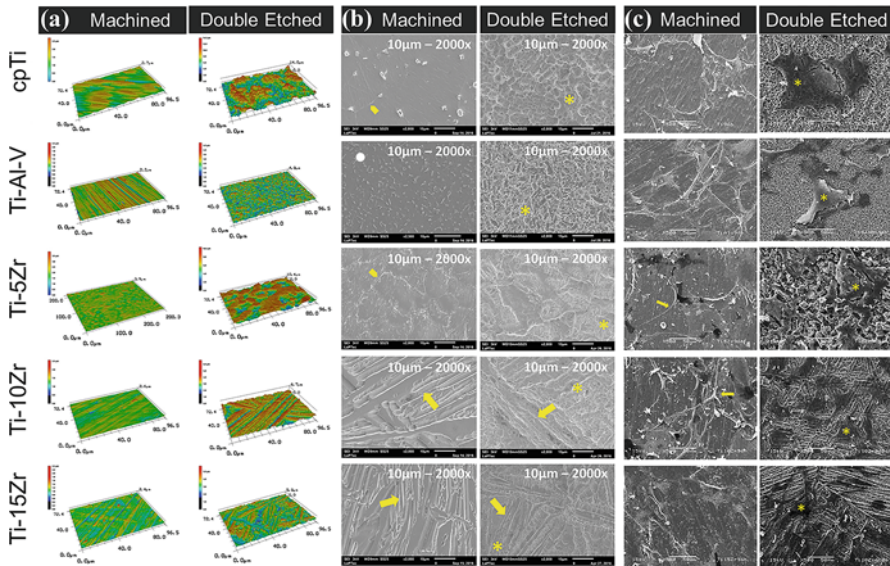
Fig. 2.7 Surface structure of machined and double-etched commercially pure titanium, Ti–Al–V, and titanium–zirconium alloys under laser scanning confocal microscopy (**a**), scanning electron microscopy images of surface structure (**b**) (arrows indicate the lamellae and fine needle-like structure), and scanning electron microscopy images of MC3T3 cultured surface (**c**) (arrows indicate elongated cells, whereas asterisks show spread-shaped ones). (Reprinted with permission of Elsevier from Cordeiro et al. 2018)

Modifications of titanium–zirconium alloys include the addition of elements such as niobium, tantalum, and palladium. Two such important modified alloys include Ti–1Zr–4Nb–2Ta–0.2Pd and Ti–29Nb–13Ta–4.6Zr alloys. Cordeiro et al. (2017) developed binary and ternary titanium alloys containing zirconium and niobium and the alloys showed better microstructure of both alloys and better mechanical properties of binary alloys (increase hardness) and ternary alloys (decrease the elastic modulus). Titanium–zirconium alloys displayed greater corrosion resistance with higher polarization resistance and lower capacitance. In addition, the alloys were not harmful to albumin adsorption.

Ti–15Zr–4Nb–2Ta–0.2Pd alloy has advantage of good mechanical and biological properties with biocompatible elements, such as zirconium, niobium, tantalum, and palladium. This alloy can be produced from spark plasma sintering (Mantshiu et al. 2018). The microstructure of the alloy shows fine acicular structures containing both α and β phases as shown in Fig. 2.8 (Ito et al. 1995).

Another study produced Ti–15Zr–4Nb–2Ta–0.2Pd alloy and studied cytocompatibility, mechanical properties, and corrosion resistance (Ito et al. 1995). It has high-level cytocompatibility, corrosion resistance and favorable tensile strength (725 MPa), elongation (23.6%), and reduction of area (54.9%). It was suggested that addition of zirconium >15% deteriorated the tensile properties.

Fig. 2.8 Surface structure of Ti–29Nb–13Ta–4.6Zr alloy showing honeycomb pattern under the scanning electron microscope. [Reprinted with permission of Elsevier from Niinomi (2003)]

Fig. 2.9 Surface structure of Ti–29Nb–13Ta–4.6Zr alloy showing honeycomb pattern under the scanning electron microscope. (Reprinted with permission of Elsevier from Niinomi 2003)
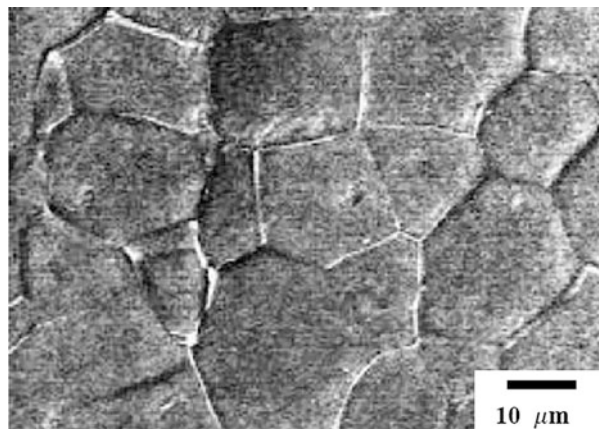
Ti–29Nb–13Ta–4.6Zr alloy is the most common alloy of titanium–zirconium group. This alloy contains more biocompatible alloying elements, such as zirconium, niobium, and tantalum with no palladium. The surface structure under scanning electron microscope shows honeycomb pattern (Fig. 2.9).

Yttrium or cerium is added in the alloy for better mechanical properties by dispersion strengthening without raising the elastic modulus by the formation of metal oxides (Hieda et al. 2013). Although Ti–29Nb–13Ta–4.6Zr has less cytotoxicity than Ti–6Al–4 V, the cytotoxicity of Ti–29Nb–13Ta–4.6Zr is similar to commercially pure titanium due to diffusion of metal ion from the alloy.

2.2.6 Nickel–Titanium Alloy

Nickel–titanium alloys have two unique and important characteristics: shape memory effect (Y. Wang et al.) and super elasticity (Jani et al. 2014; Wang et al. 1972). These are of relevance for biomedical applications, such as in vascular stents, bone fracture fixtures, catheter guide wire, and staples for bone fracture healing, orthodontic wires, and endodontic reamers and files (Hanawa 2004; Petrini and Migliavacca 2011; Thompson 2000). In addition, Ni–Ti alloys fully recover from 8% deformation strain compared to stainless steel, magnesium, and zinc which is due to the two-phase transformation phenomenon, austenite-martensitic as shown in Fig. 2.10 (Thompson 2000). Ni–Ti shows hexagonally close-packed structure (α type) till 882 °C and behaves as body-centered cubic structure (β type) higher than that temperature.

Other useful properties include good tensile strength, flexibility, machinability, formability, and apparent biocompatibility (Hanawa 2004; Petrini and Migliavacca 2011; Thompson 2000; Williams 2008).

The microstructure of Ni–Ti alloy shows rough structure with some manufacturing defects under the scanning electron microscope (Fig. 2.11). Titanium is very reactive, and some amount of oxygen is invariably present in the alloy, and generally it contains thin oxide layer on its surface.

Most often, the Ni–Ti alloys contain approximately 56% nickel and 44% titanium by weight. At low temperatures, the homogenous range of Ni–Ti alloy contains
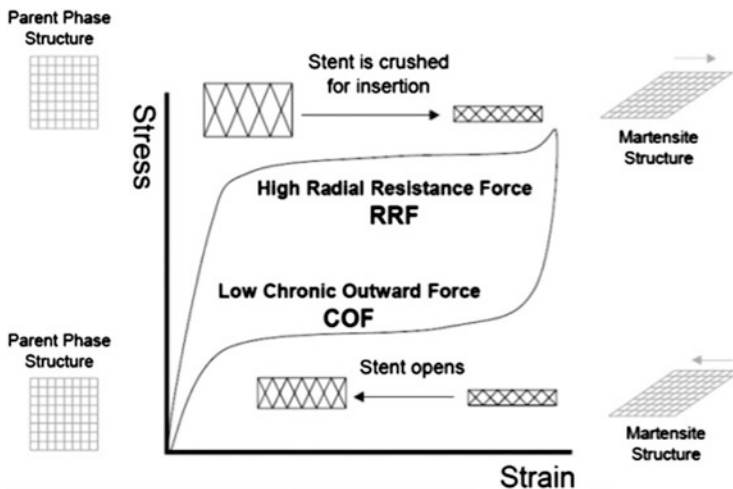

Fig. 2.10 Austenite to martensite transformation, shape memory effect, and superelastic hysteresis of nickel–titanium alloy application in stent. It shows hexagonally close-packed structure (α type) till 882 °C and behaves as body-centered cubic structure (β type) higher than that temperature. (Reprinted with permission of Elsevier from Jani et al. (2014) at the end of the caption)
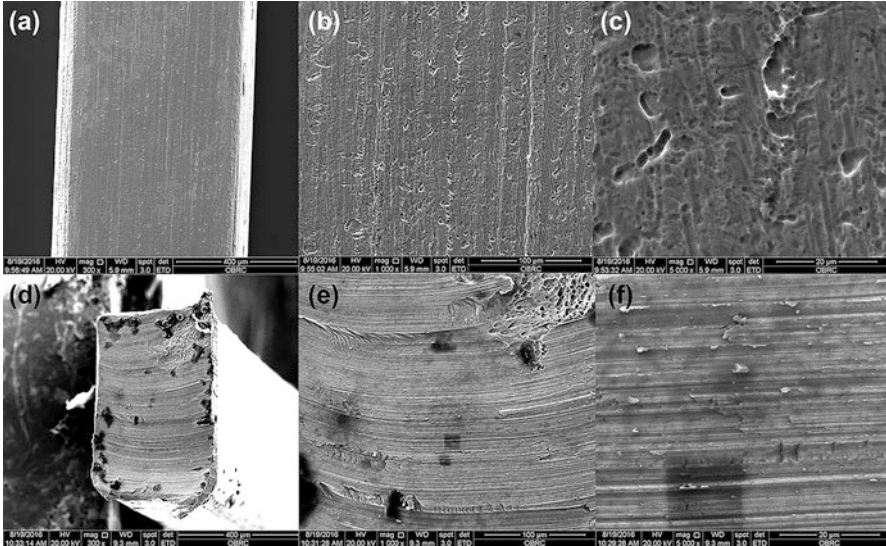
Fig. 2.11 Surface and internal structure of nickel–titanium archwire showing rough structure with manufacturing defects under the scanning electron microscope. Surface image (**a**, **b**, **c**) and cross-sectional image (**d**, **e**, **f**)

precipitates of a second intermetallic phase, either Ni_3Ti (at nickel rich side) or Ti_2Ni (at titanium rich side) (Fuentes et al. 2002).

2.3 Biological Concerns of Titanium Alloy

The vanadium and aluminum elementals released from Ti–6Al–4V alloy are cytotoxic (Exley 2016; Gomes et al. 2011). It has shown that those ions may cause nucleus and deoxyribonucleic acid (DNA) damage (Gomes et al. 2011). In addition, another study found that although Ti–6Al–4V alloy components could result in apoptosis, necrosis, and cellular proliferation interference, the extract were nontoxic to ovary cells (Gomes et al. 2011). Similarly, aluminum toxicity has also shown correlations with the systemic diseases like breast cancer, Alzheimer's disease, and autism (Exley 2016).

Although the titanium oxide on the Ni–Ti alloy can be rapidly re-passivated with its local loss from mechanical wear, the surface oxide layer over the titanium alloy is very thin (<1 μm) and is non-elastic and tends to degrade or erode (Ong and Lucas 1998; Tengvall and Lundström 1992). The bare Ni–Ti has rough surface and has high friction, and the alloy releases nickel and titanium ions (Rokaya et al. 2019). Generally, the alloy shows pitting-type corrosion compared to stainless steel, cobalt-chrome, and β-titanium (Sarkar et al. 1983). The nickel released from the nickel–titanium, such as orthodontic wires, may causes various oral signs and symptoms,

such as stomatitis, burning sensation, gingival hyperplasia, perioral rash, and loss of taste (Hussain et al. 2016; Petoumenou et al. 2009; Rokaya et al. 2018a, b).

In addition, a study done on the mechanical and tribological behavior of NiTi showed that high friction exists between wires and brackets which results in loss of forces for tooth movement prolonging the orthodontic treatment duration (Kumar et al. 2016). Similarly, inside the human body, friction and wear of Ni–Ti biomaterials can result in hemolysis and thrombus formation in blood vessels or failure of a biomaterial (Xie et al. 2015).

Hence, the surface modification of titanium alloys is a viable strategy to improve the surface, mechanical, tribological, and corrosion properties. In addition, surface modification of titanium alloys improves the implant osseointegration and accelerates healing.

2.4   Modifications of Nickel–Titanium and Titanium Alloys

Wide studies have been done on the modification and improvement of Ni–Ti alloys for various biomedical applications. Figure 2.12 shows the various surface modifications of titanium alloys for biomedical applications. Some of the advantages of the surface improvement of Ni–Ti alloys are as follows (Adya et al. 2005; Torabi and Sadrnezhaad 2011; Yoon et al. 2010):

- Improved strength, fatigue resistance, ductility, and elastic modulus
- Low friction and wear and corrosion resistance
- Dimensional stability
- Improved biocompatibility
- Better osseointegration (bone ingrowth)

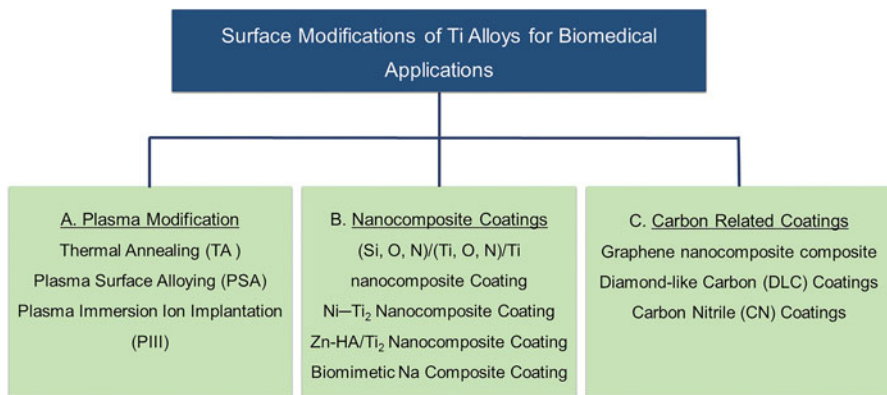Following presents various newer surface modifications of nickel–titanium alloys.

Fig. 2.12 Various surface modifications of titanium alloys for biomedical applications

2.4.1 Heat Treatment and Plasma Surface Modification

Thermal Annealing

Titanium is chemically reactive at high temperatures and reacts readily with oxygen, nitrogen, carbon, and hydrogen. Hence, titanium is heat treated under clean conditions keeping the workpiece separated from all foreign substances, such as organics, iron oxides, and refractory debris. In addition, the oxidation and heating times are kept short.

Thermal annealing is a useful technique for the treatment of Ni–Ti alloy especially for the porous type (Firstov et al. 2002; Wu et al. 2007). Porous nickel–titanium alloys are suitable biomaterials for implants because of porous structure in addition to super elastic and shape memory effects, but it is difficult to modify the surfaces using conventional surface techniques. Wu et al. (2007) modified the surfaces of porous single-phase Ni–Ti using the oxidation in air for 1 h with combination with heat treatment. At 550–800 °C temperature, nickel leakage increases by 12–25 times than the untreated Ni–Ti which contains a thick nickel-rich layer beneath the titanium dioxide or titania surfaces. Hence, they recommended to use annealing at lesser temperatures (300–450 °C) to reduce nickel leakage twice than the untreated Ni–Ti. Although titanium have shown antibacterial actions against *S. typhimurium* histidine-auxotrophic strains, heat treatment (>1250 °C) of titanium is possible to make bacteria-free surface (Ranjan and Ramalingam 2016).

In addition, Firstov et al. (2002) did heat treatment of $Ni_{50}Ti_{50}$ alloy at 300–800 °C temperature in air. They found that a nickel-free zone was seen within the oxide layer at 500 °C and 600 °C temperature. At 500 °C, a nickel-free oxide layer, which is smooth and protective, can be produced with less nickel at the air and oxide border. Furthermore, they mentioned that Ni–Ti alloy shows diverse oxidation behavior at temperatures above and below 500 °C which might be due to the breakdown of titanium oxide at the oxide/alloy interface by the metallic titanium. This breakdown takes place during oxidation of titanium >350 °C and creates vacancies permitting quick diffusion of O_2 (Duc et al. 1980). Hence, a temperature of between 300 and 500 °C is suitable for the thermal annealing and oxidation of Ni–Ti alloy to produce a protective nickel-free oxide layer for biocompatibility.

Tang et al. (2018) studied the role of solution with aging treatment and heat treatments on the properties of forged Ti–5Al–2Fe and found that after heating at the temperature of 1250 °C, the residual pores were removed completely. The ductility was greatly improved by both solutions with aging treatment and mill annealing without no changing in ultimate tensile strength.

Plasma Surface Alloying

The $Ti_{49}Ni_{51}$ alloy can be modified using plasma surface alloying (PSA), and hydrogen (H_2) can be added to smoothen the plasma process (Duerig et al. 1999). The process can be done in a glow discharge plasma unit of 40 kW using two techniques: (a) at 500 °C in a gas composition of air/H_2: 2% for 4 h, 9 h, and 16 h and (b) at 400 °C in a gas composition of air/H_2: 2% for 4 h, 9 h, and 16 h. The plasma surface alloys show two layers: TiO_2 layer (outer) and $TiNi_3$-rich layer (inner). The PSA with air helped in the reduction of Ni at the surface of the Ni–Ti alloy and improved the surface hardness (PSA: 11–23 GPa and untreated alloy: 2.5 GPa), wear properties, and corrosion resistance (reduced corrosion current and increased corrosion potential) of the alloy.

The biocompatibility of the low-temperature plasma-coated Ni–Ti alloy intravascular stents was studied by Wang et al. (2007) in terms of adhesion of endothelial cells. In addition, they studied anticoagulation, hemocytolysis, hydrophilicity, and cytotoxicity. The surface roughness of the plasma-coated alloy was found as 1–5 μm. The plasma-coated Ni–Ti stents had improved anticoagulation property with increased surface hydrophilicity compared to the untreated alloy.

Plasma Immersion Ion Implantation

Plasma immersion ion implantation (PIII) is a type of plasma-based surface modification and it is an useful and economical technique that alters the functionality of biomaterials to produce a long-term corrosion resistance with improved mechanical properties (especially hardness and strength), and cytocompatible surface that can be used for the orthodontic and orthopedic applications (Chu et al. 2002; Gan and Berndt 2015). PIII can be done with nitrogen (N−PIII), carbon (C−PIII), and oxygen (O−PIII) on NiTi alloy. Shanaghi and Chu (2019) did C-PIII of the $Ni_{50.8}Ti_{49.2}$ (at.%) alloy for 2 h and studied the properties. They obtained a uniform, defect-free surface layer of 50 nm thickness. In addition, it showed reduced roughness (from 17.4 nm to 6.1 nm), and increases hardness (from 64.31 GPa to 4.77 GPa) and increased elastic modulus (from 2.74 GPa to 4.77 GPa) for the C-PIII of pristine NiTi alloy sample (Fig. 2.13). In addition, corrosion property was tested using electrochemical impedance spectroscopy and showed that C-PIII improved the pitting or local corrosion resistance of the Ni–Ti alloy by 85% and the passive layer was stable at the immersion time point of 96 h.

Zhao et al. (2013) conducted nitrogen and carbon plasma immersion ion implantation (N-PIII and C-PIII) to modify Ti-6Al-4V to produce a graded surface layer composed of TiN and TiC, respectively (Fig. 2.14). In both PIII, the corrosion
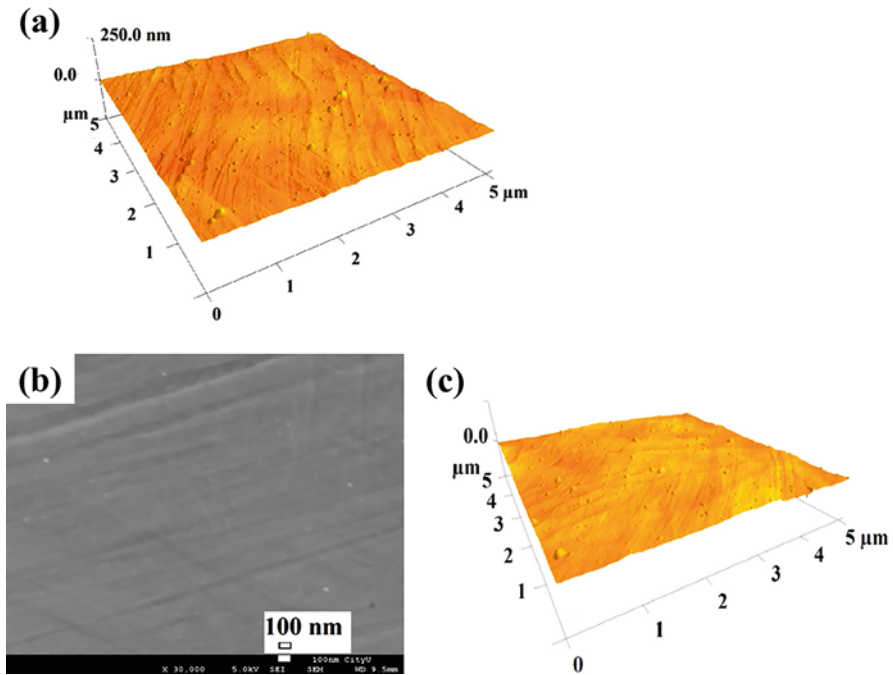
Fig. 2.13 Atomic force microscopy (AFM) image of the nickel–titanium alloy (**a**), field-emission scanning electron microscopy image, and AFM image of the C-PIII sample (**b**) and (**c**). (Reprinted with permission of Elsevier from Shanaghi and Chu 2019)

resistance and surface roughness were increased without altering the surface hydrophilicity significantly. The unimplanted sample showed relatively smooth topography, but nano-holes were seen from the surfaces of C−PIII and N−PIII. Following the PIII, the proliferation and cell adhesion of preosteoblasts and fibroblasts were improved. Micro-CT done at 1–12 weeks after the surgery showed less bone resorption and larger bone volumes on the N−PIII and C−PIII compared to the unimplanted sample at every time point. Titanium nitride and titanium carbide stimulated the preosteoblasts and fibroblasts and induced bone formation. Therefore, both titanium nitride and titanium carbide showed corrosion property and good cytocompatibility, and compared to the two PIII processes, N−PIII showed better results (Zhao et al. 2013).

Yang et al. (2011) studied the corrosion properties and cell adhesion of Ti dental implant surface modified by plasma ion implantation using oxygen (O−PIII). They also studied the adhesion and distribution of human bone marrow mesenchymal stem cells. It was found that O−PIII treatment had no effect on the surface structure of titanium specimens (Fig. 2.15). The thickness of oxide layer, especially titania, increased with the oxygen dose implanted on the titanium samples. Higher elastic modulus and surface hardness were found in O−PIII-treated specimens compared to the untreated specimens. They also showed lower corrosion rate than the untreated
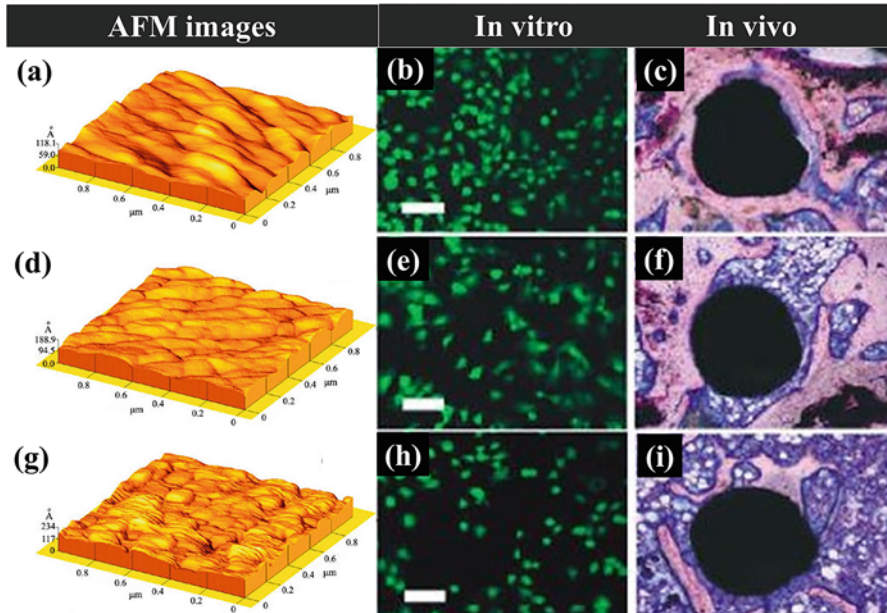
Fig. 2.14 Atomic force microscopy images of dental implants, fluorescence microscope of bone marrow showing fibroblasts adhesion (after incubation for 4 h), and Giemsa and eEosin stained bone around the implant of in vivo hard tissue after 12 weeks following nitrogen plasma immersion ion implantation (N−PIII) titanium alloy (**a**, **b**, **c**), carbon plasma immersion ion implantation (C−PIII) titanium alloy (**d**, **e**, **f**), and unimplanted titanium alloy (**g**, **h**, **i**). (Reprinted with permission of American Chemical Society from Zhao et al. 2013)

surface from the potentiodynamic polarization tests. In addition, the O−PIII treatment improved the adhesion and spreading of stem cells because of increase in the surface thickness of titanium oxides (mainly TiO_2) on titanium. Hence, O−PIII treatment can be useful for producing corrosion resistance coatings and cell adhesion properties on titanium surface for dental implant applications.

2.4.2   Nanocomposite Composite Coating

Silicon–Oxygen–Nitrogen–Titanium Composite Coating

Silicon–oxygen–nitrogen–titanium (Si, O, N)/(Ti, O, N)/Ti composite coating has been tried as potential protective coatings (Sun et al. 2011). Suna et al. (2015) developed a multifunctional composite coatings of (Si, O, N)/(Ti, O, N)/Ti on a Ni–Ti shape memory alloy via plasma immersion ion implantation and deposition (PIIID) with magnetron sputtering for promoting bioactivity and biocompatibility of nickel–titanium shape memory alloys which show similar surface structure as
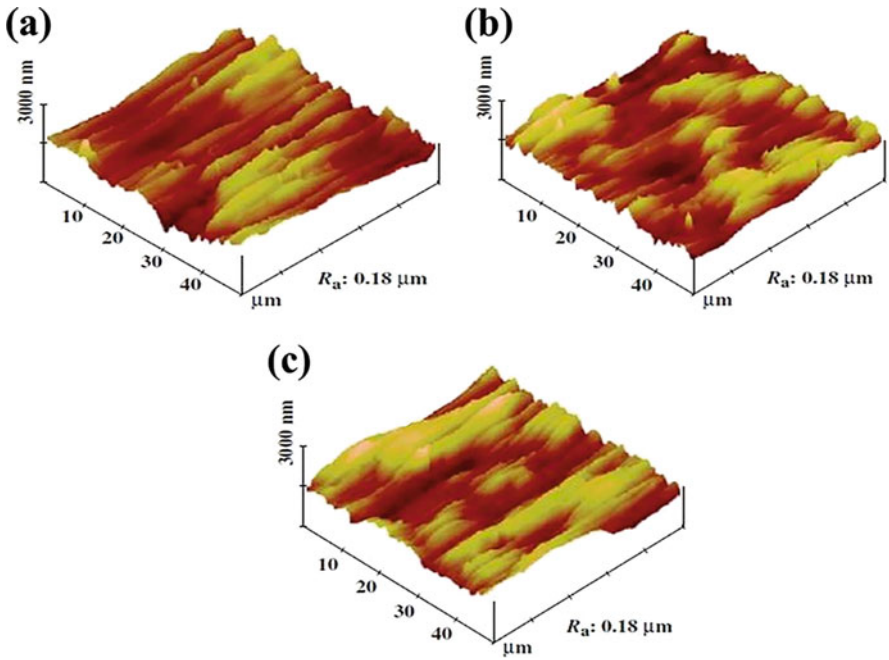
Fig. 2.15 Atomic force microscopy image of titanium samples: (**a**) untreated TC; (**b**) oxygen plasma immersion ion implantation (O−PIII)-treated TL (low dose: 1×10^{16}ions/cm^2); and (**c**) OPIII-treated TH (high dose: 4×10^{16} ions/cm^2) showing similar surface structure. (Reprinted with permission of John Wiley and Sons from Yang et al. 2011)
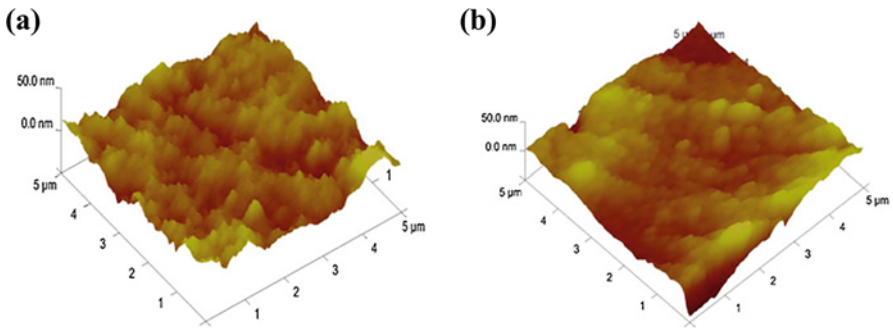

Fig. 2.16 Atomic force microscopy images of titanium–oxygen–nitrogen [(Ti, O, N)/Ti]-coated nickel–titanium surface (**a**) and silicon–oxygen–nitrogen–titanium [(Si, O, N)/(Ti, O, N)/Ti]-coated nickel–titanium surface (**b**) showing similar surface structure. (Reprinted with permission of Elsevier from Sun et al. 2015)

titanium–oxygen–nitrogen [(Ti, O, N)/Ti]-coated Ni–Ti surface (Fig. 2.16). The nanocoating thickness was 0.84 μm, and nickel was reduced on the coated surface which was confirmed from energy dispersive spectroscopy and X-ray photoelectron

spectroscopy analyses, and silicon was incorporated into the composite coating. In addition, the nanocomposite-coated samples showed enhanced wear, corrosion properties, and apatite formation rendering Ni–Ti bioactivity.

Nickel–Titanium Nanocomposite Coating

Nickel-based coatings either in one phase (nickel and nickel alloys) or nickel nanocomposites have improved mechanical properties, corrosion, and wear behavior. Hence, nickel-based coatings can be used for several applications including for medical devices (Miguel et al. 2015). Nickel titania nanocomposite coatings can be fabricated by electrodeposition containing various sizes of titania nanoparticles (Birlik et al. 2016). Figure 2.17 shows the surface structure of nickel coatings (Fig. 2.17a) and nickel titania nanocomposite coatings which were crack-free and homogeneous prepared with nanoparticles of size 80 nm and 50 nm (Fig. 2.17b, c). Alternately, nickel composites containing titania nanoparticles can be fabricated by electrodeposition using sulfamate or Watts plating baths (Spanou et al. 2009).
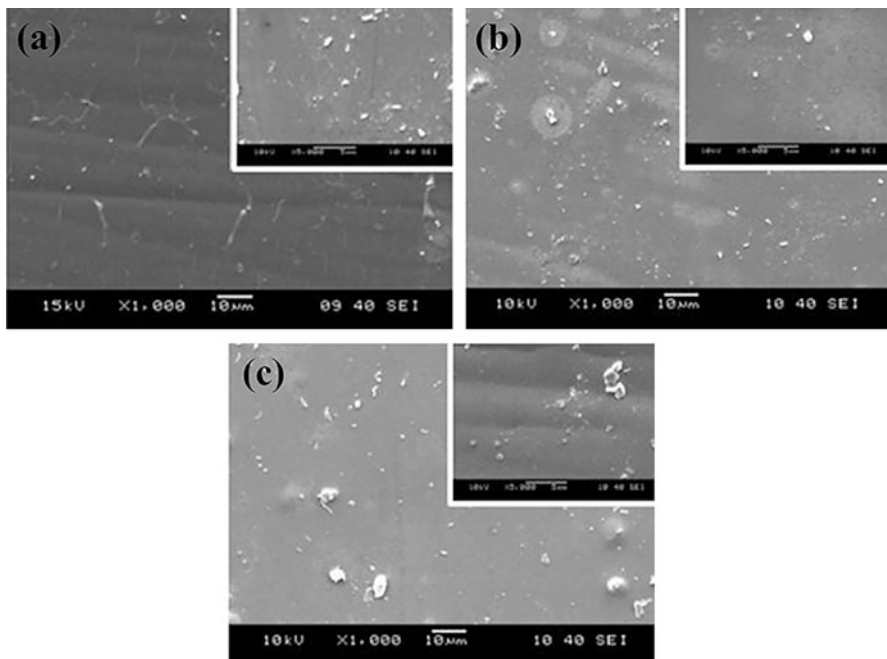

Fig. 2.17 Surface morphologies of nickel coatings (**a**) and nickel titania nanocomposite coatings prepared with nanoparticles of size 80 nm (**b**) and 50 nm (**c**). (Reprinted with permission of Frontiers Media S.A. under Creative Commons Attribution License (CC BY 4.0) from Birlik et al. 2016)

The disadvantage of nickel-based coatings is the nickel allergy; hence, they should be used cautiously. When applied for any specific purpose, its biocompatibility should be assessed. Still, they are used for the coating of medical devices.

Zinc–Hydroxyapatite–Titania Nanocomposite Coating

Hydroxyapatite $[Ca_{10}(PO_4)_6(OH)_2]$ is one of the popular biocompatible coatings due to the close similarity to the natural bone tissue (Mirak et al. 2016; Mohan et al. 2012). Hydroxyapatite is used for coating dental and orthopedic implants because they can result in quick osseointegration (Suchanek and Yoshimura 1998). But the pure hydroxyapatite has low bonding strength and results in detachment after implantation (Nelea et al. 2000). Hence, hydroxyapatite nanocomposite by incorporating some elements, such as zinc or titanium, helps in producing successful coating using proper coating technique. Use of zinc from the matrix in the composite coating helps in proper bonding between the substrate and the hydroxyapatite coating (Xu et al. 2006). Mirak et al. prepared a biocompatible zinc–hydroxyapatite–titanium $(Zn–HA/Ti_2)$ nanocomposite coatings prepared on nickel–titanium shape memory alloy by the process of electrodeposition (Mirak et al. 2016). The surface morphologies of Zinc-Hydroxyapatite-Titania $(Zn-HA/TiO_2)$ coating in scanning electron microscope showed that porous structure with various size of plate-like regions that can facilitate bone growth as shown in Fig. 2.18. They also found that addition of titania particles causes the reduction in the crystallite size of coating. The $Zn–HA/TiO_2$ nanocomposite coatings showed strong coating with better hardness than the zinc–hydroxyapatite coatings and showed the better corrosion properties compared to zinc–hydroxyapatite and bare Ni–Ti.

Another study done by Lee (2012) studied the structure, mechanical, and corrosion properties of the electroplated HA/nano-TiO$_2$ coatings on Ti–6Al–4V alloy. They did anodize at room temperature at 10 volts for different times of 40–180 min to enhance the adhesion of the composite coatings on alloy. It showed that increasing anodizing duration of alloy, the wear and corrosion resistance of the HA/nano-TiO$_2$ composite coatings were improved. In addition, the hardness of alloy increased after anodizing and increased the adhesion of HA/nano-TiO$_2$ composite coatings. The nano-titania particles co-deposited on the alloys reinforced the hydroxyapatite coating to increase the hardness and the surface structure.

Biomimetic Sodium Composite Coating

Biomimetic surface has become a popular method to improve host tissue-implant integration. Biomimetic surfaces can be produced by thermochemical treatments and have ability to produce coating complex shapes with tunable chemical composition of the coating (Gu et al. 2005; Mediaswanti et al. 2013). Kokubo et al. (1996) produced bonelike apatite on commercially pure titanium chemically induced by an alkali, and heat treatment process improved the implant integration.
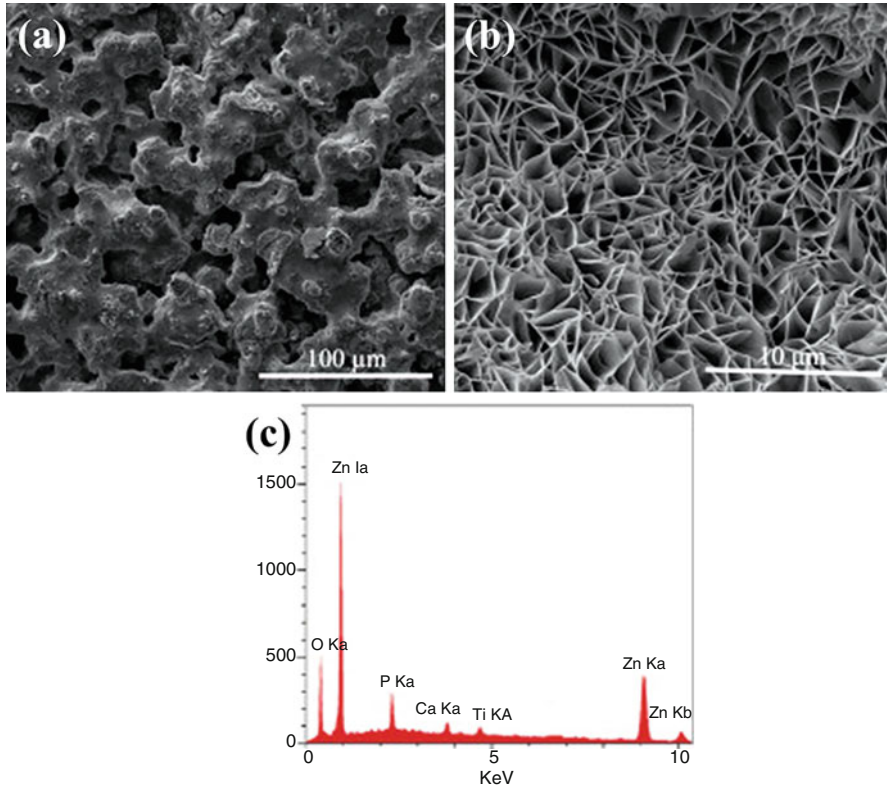
Fig. 2.18 Surface morphologies under scanning electron microscope of zinc–hydroxyapatite–titania (Zn–HA–TiO$_2$) coatings on nickel–titanium alloy: low magnification (**a**), high magnification (**b**), and elemental analysis (**c**). The scanning electron microscopy images show porous structure with various sizes of platelike regions. (Reprinted with permission of Elsevier from Mirak et al. 2016)

Rupérez et al. (2016) developed sodium biomimetic surface on Ni–Ti alloy. At first, they produced a rutile/anastase protective layer with nickel free on the nickel–titanium alloy surface (Fig. 2.19a). After that, a sodium alkaline titanate hydrogel was formed from oxidized surface, which can induce apatite formation. The tissue-implant integration and the bioactivity of Ni–Ti alloys were improved by reducing the Ni ions. The glazing incidence X-ray diffraction shows similar structure of both austenitic and martensitic type of Ni–Ti alloy showing peaks matching to metallic Ni–Ti, rutile, and various sodium–titanate ratios (Na$_2$Ti$_3$O$_7$, Na$_2$Ti$_6$O$_{13}$, and NaTiO$_2$) (Fig. 2.19b).

Similarly, another study produced biomimetic apatite coatings on Ni–Ti by treating the alloy with HNO$_3$ and then NaOH aqueous solution in stimulated buffer fluid. The osteoblasts were actively proliferated on this hydroxyapatite-coated surface at 6 weeks after the implantation (Chen et al. 2004). The advantage of the apatite
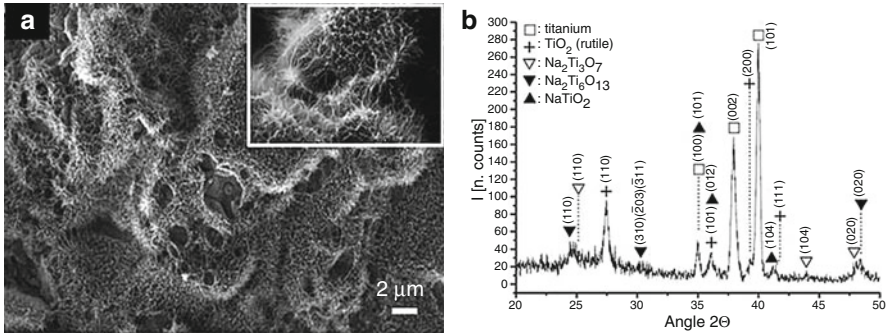
Fig. 2.19 The microporous layer made up of a sodium titanate on the nickel–titanium surface (**a**). The glazing incidence X-ray diffraction patterns of both austenitic and martensitic type of nickel–titanium alloys showing similar peaks corresponding to metallic nickel–titanium, rutile, and different sodium titanate ratios (**b**). (Reprinted with permission of MDPI AG under the Creative Commons Attribution License (CC BY 4.0) from Rupérez et al. 2016)

layer thus produced by plasma spray technique is this does not delaminate or decompose at high temperature (Mediaswanti et al. 2013).

2.4.3   Carbon-Related Coatings

Graphene Composite Coating

Graphene-based materials have various biomedical applications (Chamundeeswari et al. 2019; Xie et al. 2017; Yang et al. 2013). It is also used to modify various titanium alloys to improve surface, mechanical, frictional, and biocompatibility (Jankovic et al. 2015; Rokaya et al. 2018a). Rokaya et al. (2018a, b) developed the graphene oxide/silver nanoparticles coatings of thickness ranging from 0.46 μm to 1.34 μm on the medical grade Ni–Ti alloy using the electrophoretic deposition. The graphene oxide/silver nanoparticles nanocomposite-coated alloy demonstrated improved mechanical strength and a reduced friction coefficient favorable for the biomedical applications. Similarly, another study evaluated the surface adhesion and cytotoxicity of the graphene oxide coatings and graphene oxide/silver nanoparticle nanocomposite coatings, and they found that the nanocomposite coatings showed favorable surface adhesion, mechanical properties, and good high cell viability of the human gingival fibroblasts (Rokaya et al. 2019). Figure 2.20 shows the surface microstructure of the bare Ni–Ti alloy and the coated Ni–Ti alloys (with graphene oxide and graphene oxide/silver nanoparticles) under the surface profilometer, scanning electron microscope, and atomic force microscopy. Bare Ni–Ti alloys showed rough with some voids and defects but the coated alloys (with graphene oxide and graphene oxide/silver nanoparticles) showed homogenous pattern. In addition, the graphene oxide-coated and graphene oxide/silver-coated Ni–Ti alloys
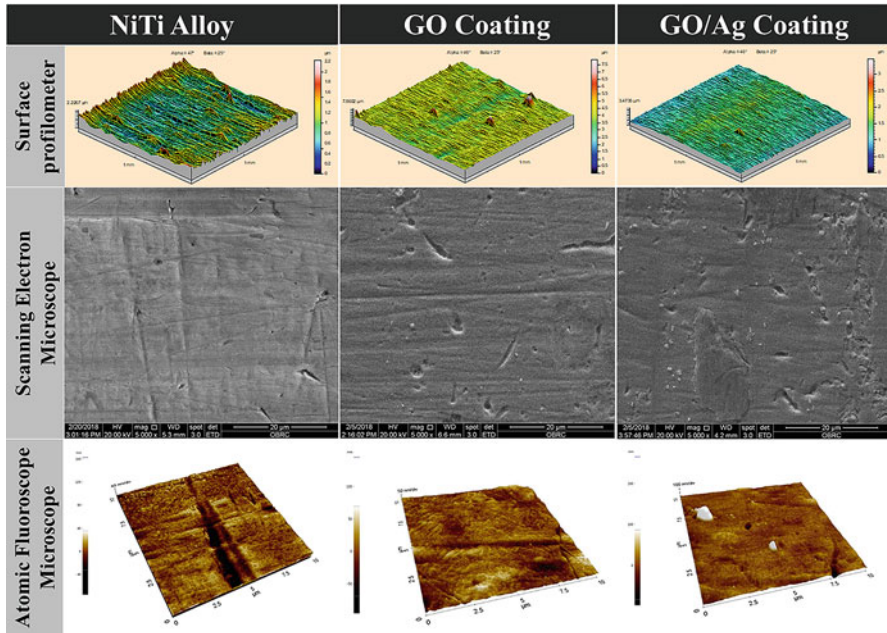
Fig. 2.20 Figure 2.20 shows the surface microstructure of the bare nickel–titanium alloy and the coated nickel–titanium alloys (with graphene oxide and graphene oxide/silver nanoparticles) under the surface profilometer, scanning electron microscope, and atomic force microscopy. Bare nickel–titanium alloys showed rough with some voids and defects but the coated alloys (with graphene oxide and graphene oxide/silver nanoparticles) showed homogenous pattern.

showed superior corrosion properties (better corrosion resistance, a lower rate of corrosion, and higher protection efficiency) than the bare Ni–Ti alloy (Srimaneepong et al. 2020). The coated Ni–Ti alloys were biocompatible to human pulp fibroblasts and showed upregulation of interleukin-6 and interleukin-8 levels.

Additionally, Podila et al. (2013) coated Ni–Ti alloy with graphene using chemical vapor deposition, and they found that the graphene coatings do not exhibit any significant in vitro toxicity for smooth muscle cells and aortic endothelial cells, confirming their biocompatibility. Further, graphene coatings were found to be chemically inert, durable, and impermeable in an environment that is more severe than the flowing blood environment. All these characteristics make graphene superior to other coatings for biomedical implants and devices. Hence, graphene-coated Ni–Ti showed excellent biocompatible leading to better cell proliferation.

Another study fabricated graphene oxide–hydroxyapatite composite coating on titanium substrate fabricated by electrochemical deposition technique and studied the microstructure, phase constituents, bonding strength, and in vitro cellular responses of the coatings. It showed that addition of graphene oxide has enhanced the bonding strength of the coatings and the crystallinity of deposited apatite particles. Moreover, the coatings showed better biocompatibility of composite

coatings compared to titanium substrate and the hydroxyapatite coating as shown from the cell culture results. Hence, graphene oxide–hydroxyapatite composite coatings might be a promising candidate in the field of biomaterials, especially for implant coatings.

Jankovik et al. (2015) developed silver/hydroxyapatite/graphene composite coatings produced by electrophoretic deposition on titanium substrate. It showed the coatings had reduced surface cracks, better mechanical resistance (hardness and elastic modulus increased by 10%), and enhanced thermal stability. The composite coatings were biocompatible and non-cytotoxic against the healthy peripheral blood mononuclear cells as shown by the formation of apatite layer in simulated body fluid with enhanced corrosion stability. But the coatings showed antibacterial activity against S. aureus and E. coli. This indicates that the composite coatings have high potential for the biomedical applications.

Diamond-Like Carbon Coating

The diamond-like carbon (DLC) has promising properties such as high hardness, low friction, and smooth surfaces which make them favorable for wear protection (Cui and Lia 2000; Sui and Cai 2006). The DLC films are gaining popularity for biomedical application because of low friction, inertness, and high corrosion resistance (Grill 1999; Huang et al. 2013; Ohgoe et al. 2006). DLC coatings are also used in the reduction of the wire-bracket friction in orthodontic therapy due to its high slip capacity, making higher efficiency in tooth movement (Grill 1999). In recent studies, DLC films are greatly used as a nickel-free new biocompatible coating on Ni–Ti alloy archwires (Ohgoe et al. 2006).

Huang et al. (2013) used DLC films coatings on Ni–Ti archwires and they found that the film provided fluoride-induced corrosion resistance with improved friction. In addition, the results showed the DLC coating had better properties, with less surface roughness following dipping in a high fluoride ion solution (Fig. 2.21). DLC coating reduced the wear and friction significantly. Thus, DLC coatings on Ni–Ti alloys can reduce corrosion and friction and these can be applied in clinical orthodontics.

Kang et al. (2015) assessed the effects of DLC films on wear at archwire-bracket interfaces and also studied the coating thickness, surface roughness, and bonding structure. The DLC-coated wires resulted low friction and wear from the microscopic analysis than the uncoated wires. Hence, the DLC coating can decrease the orthodontic fretting friction and wear on archwires. Furthermore, Kobayashi et al. (2007) studied the DLC-coated Ni–Ti archwires to prevent nickel release. They immersed the orthodontic wire in physiological saline at 37 °C for 6 months. The nickel ions concentration in the solutions was reduced 1/6th by DLC films than the non-coated wire. This showed that DLC films have protective effect and non-cytotoxic to squamous cells.
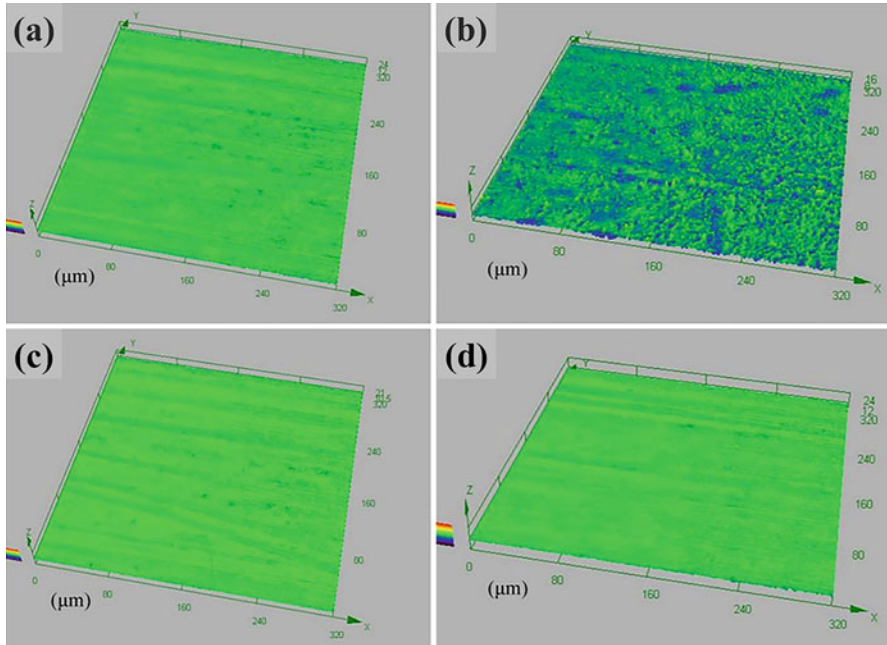
Fig. 2.21 Surface analysis of nickel–titanium archwire using 3D laser microscope: uncoated wire before dipping in fluoride (**a**), uncoated wire after dipping in fluoride (**b**), diamond-like carbon wire before dipping in fluoride (**c**), and diamond-like carbon wire after dipping in fluoride (**d**). The diamond-like carbon coating had better properties, with less surface roughness following dipping in a high fluoride ion solution. (Reprinted with permission of Springer Nature from Huang et al. 2013)

Carbon Nitride Coating

The carbon nitride film and titanium nitride are chemically inert and also show good hardness, electrical and optical properties, and biocompatibility. Hence, they can have potential applications in medicine and biomedical science (Cheng and Zheng 2006; Cui and Lia 2000). Wang et al. (Wang and Jiang 2009) studied the carbon nitride, DLC, and titanium nitride film on Ni–Ti substrates using direct current magnetron sputtering. They found that the blood compatibilities were improved by the hard films. Compared to titanium nitride and DLC film, carbon nitride film showed the best surface characteristics showing minimum hemolysis ratio and the best anticoagulation property.

2.5   Conclusion

Following conclusions can be drawn from this chapter:

- Various types of titanium alloys can be fabricated and modified for biomedical applications according to the need, such as commercially pure titanium, titanium–aluminum–vanadium (Ti–Al–V) alloy, titanium–aluminum–niobium (Ti–Al–Nb) alloy, titanium–aluminum–iron (Ti–Al–Fe) alloy, titanium–zirconium alloy, titanium–zirconium–niobium–tantalum–palladium (Ti–Zr–Nb–Ta–Pd) alloy, titanium–niobium–tantalum–zirconium (Ti–Nb–Ta–Zr), and nickel–titanium (Ni–Ti) alloy.
- Different surface modifications can improve the functionality and biocompatibility, and modification techniques can be grouped as heat treatment and plasma surface modification (thermal alloying, plasma surface alloying, plasma immersion ion implantation); nanocomposite coatings (silicon–oxygen–nitrogen–titanium composite coating, Ni–Ti nanocomposite coating, and zinc–hydroxyapatite–titania nanocomposite coating); and carbon–related coatings (graphene composite, diamond-like carbon coatings, carbon nitrile coatings).
- Various surface modifications produce different surface structure and varying mechanical properties, corrosion, and biocompatibility.
- Various surface coatings are suitable in improving the surface, mechanical, and biological properties for various biomedical applications. In addition, these coatings may be potential for clinical applications, but further research in clinical applications is required before using these coating and possible modifications for further medical and dental applications.

References

Abey S, Mathew MT, Lee DJ, Knoernschild KL, Wimmer MA, Sukotjo C (2014) Electrochemical behavior of titanium in artificial saliva: influence of pH. J Oral Implantol 40(1):3–10. https://doi.org/10.1563/AAID-JOI-D-1511-00054

Adya M, Alam M, Ravindranath T, Mubeen A, Saluja B (2005) Corrosion in titanium dental implants: literature review. J Indian Prosthodont Soc 53:126–131. https://doi.org/10.4103/0972-4052.17104

Almanzaa E, Péreza MJ, Rodrígueza NA, Murrb LE (2017) Corrosion resistance of Ti-6Al-4V and ASTM F75 alloys processed by electron beam melting. J Mater Res Technol 6(3):251–257. https://doi.org/10.1016/j.jmrt.2017.1005.1003

American Society for Testing and Materials – ASTM. ASTM F67-13: standard specifications for unalloyed titanium, for surgical implant applications. (2013) West Conshohocken: ASTM

Bak GR, Jeong DW, Hyun YT, Park HS (2018) Effect of Mn addition on microstructural changes and mechanical properties of Ti–5Al–2.5Fe alloys. Met Mater Int. https://doi.org/10.1007/s12540-12018-10115-12546

Berner S, Dard M, Gottlow J, Molenberg A, Wieland M (2009) Titanium-zirconium: a novel material for dental implants. Eur Cell Mater 17:16

Birlik I, Azem NFA, Toparli M, Celik E, Delice TK, Yildirim S et al (2016) Preparation and characterization of Ni–TiO2 nanocomposite coatings produced by electrodeposition technique. Front Mater 3:1–7. https://doi.org/10.3389/fmats.2016.00046

Bolzoni L, Babu NH, Ruiz-Navas EM, Gordo E (2013) Comparison of microstructure and properties of Ti-6Al-7Nb alloy processed by different powder metallurgy routes. Key Eng Mater 551:161–179. https://doi.org/10.4028/www.scientific.net/KEM.551.161

Caldas SGFR, Ribeiro AA, Simplício H, Machado AW (2014) Segmented arch or continuous arch technique? A rational approach. Dental Press J Orthod 19(2):126–141. https://doi.org/10.1590/2176-9451.1519.1592.1126-1141.sar

Chamundeeswari M, Jeslin J, Verma ML (2019) Nanocarriers for drug delivery applications. Environ Chem Lett 17(2):849–865. https://doi.org/10.1007/s10311-018-00841-1

Chen MF, Yang XJ, Hu RX, Cui ZD, Man HC (2004) Bioactive NiTi shape memory alloy used as bone bonding implants. Mater Sci Eng 24:497–502. https://doi.org/10.1016/j.msec.2003.1011.1001

Cheng Y, Zheng YF (2006) Formation of TiN films on biomedical NiTi shape memory alloy by PIIID. Mater Sci Eng A 434(1–2):99–104. https://doi.org/10.1016/j.msea.2006.1007.1027

Choubey A, Balasubramaniam R, Basu B (2004) Effect of replacement of V by Nb and Fe on the electrochemical and corrosion behavior of Ti–6Al–4V in simulated physiological environment. J Alloys Compd 381(1–2):288–294. https://doi.org/10.1016/j.jallcom.2004.1003.1096

Chu PK, Chen JY, Wang LP, Huang N (2002) Plasma-surface modification of biomaterials. Mater Sci Eng R Rep 36(5–6):143–206. https://doi.org/10.1016/S0927-1796X(1002)00004-00009

Cordeiro JM, Beline T, Ribeiro ALR, Rangel EC, da Cruz NC, Landers R et al (2017) Development of binary and ternary titanium alloys for dental implants. Dent Mater 33(11):1244–1257. https://doi.org/10.1016/j.dental.2017.1207.1013

Cordeiro JM, Faverani LP, Grandini CR, Rangel EC, da Cruz NC, Nociti Junior FH et al (2018) Characterization of chemically treated Ti-Zr system alloys for dental implant application. Mater Sci Eng C Mater Biol Appl 92:849–861. https://doi.org/10.1016/j.msec.2018.07.046

Correa DR, Vicente FB, Donato TA, Arana-Chavez VE, Buzalaf MA, Grandini CR (2014) The effect of the solute on the structure, selected mechanical properties, and biocompatibility of Ti-Zr system alloys for dental applications. Mater Sci Eng C Mater Biol Appl 34:354–359. https://doi.org/10.1016/j.msec.2013.1009.1032

Cui FZ, Lia DJ (2000) A review of investigations on biocompatibility of diamond-like carbon and carbon nitride films. Surf Coat Technol 131(1–3):481–487. https://doi.org/10.1016/S0257-8972(1000)00809-00804

Duc BM, Jardin C, Gauthier JP, Thollet G, Michel P (1980) Oxidation mechanism, oxide decomposition and phase transition in industrial titanium studied by high resolution low energy electron spectrometry. In: Kimura H, Izumi O (eds) Titanium'80: proceedings of the fourth international conference on titanium, Kyoto, vol 4. The Metallurgical Society of AIME, Warrendale, pp 2821–2827

Duerig T, Pelton A, Stockel D (1999) An overview of nitinol medical applications. Mater Sci Eng 149:273–275. https://doi.org/10.1016/S0921-5093(1099)00294-00294

Exley C (2016) The toxicity of aluminium in humans. Morphologie 100(329):51–55. https://doi.org/10.1016/j.morpho.2015.1012.1003

Fernandes DJ, Elias CN, Valiev RZ (2015) Properties and performance of ultrafine grained titanium for biomedical applications. Mater Res 18(6):1163–1175. https://doi.org/10.1590/1516-1439.005615

Firstov GS, Vitchev VR, Kumar H, Blanpain B, Van Humbeeck J (2002) Surface oxidation of NiTi shape memory alloy. Biomaterials 23(24):4863–4871. https://doi.org/10.1016/S0142-9612(4802)00244-00242

Fuentes JMG, Gümpel P, Strittmatter J (2002) Phase change behavior of nitinol shape memory alloys. Adv Eng Mater 4(7):437–452. https://doi.org/10.1002/1527-2648(20020717)20020714:20020717<20020437::AID-ADEM20020437>20020713.20020710.CO;20020712-20020718

Gan JA, Berndt CC (2015) Plasma surface modification of metallic biomaterials. In: Wen C (ed) Surface coating and modification of metallic biomaterials. Woodhead Publishing, Philadelphia, pp 103–157. https://doi.org/10.1016/B978-1-011-78242-78303-78244.00004-78241

Gomes CC, Moreira LM, Santos VJSV, Ramos AS, Lyon JP, Soares CP, Santos FV (2011) Assessment of the genetic risks of a metallic alloy used in medical implants. Genet Mol Biol 34(1):116–121. https://doi.org/10.1590/S1415-47572010005000118

Grill A (1999) Diamond-like carbon: state of the art. Diam Relat Mater 8:428–434. https://doi.org/10.1016/S0925-9635(1998)00262-00263

Gu YW, Tay BY, Lim CS, Yong MS (2005) Biomimetic deposition of apatite coating on surface-modified NiTi alloy. Biomaterials 26(34):6916–6923. https://doi.org/10.1016/j.biomaterials.2005.6904.6051

Guitar A, Vegan G, Luppo MI (2009) Microstructure and tensile properties after thermo hydrogen processing of Ti-6Al-4V. J Mech Behav Biomed Mater 2(2):156–163. https://doi.org/10.1016/j.jmbbm.2008.1006.1002

Guo S, Meng Q, Liao G, Hu L, Zhao X (2013) Microstructural evolution and mechanical behavior of metastable β-type Ti–25Nb–2Mo–4Sn alloy with high strength and low modulus microstructural evolution and mechanical behavior of metastable β-type Ti–25Nb–2Mo–4Sn alloy with high strength and low modulus retain. Prog Nat Sci-Mater 23(2):174–182. https://doi.org/10.1016/j.pnsc.2013.1003.1008

Hanawa T (2004) Surface modification of metallic biomaterials. In: Teoh SH (ed) Engineering materials for biomedical applications. World Scientific Publishing, Singapore, pp 1–36

Hieda J, Niinomi M, Nakai M, Cho K (2013) Mechanical properties of biomedical β-type titanium alloy with rare-earth metal oxide particles formed by rare-earth metal addition. Mater Trans 54 (8):1361–1367. https://doi.org/10.2320/matertrans.MF201308

Huang SY, Huang JJ, Kang T, Diao DF, Duan YZ (2013) Coating NiTi archwires with diamond-like carbon films: reducing fluoride-induced corrosion and improving frictional properties. J Mater Sci Mater Med 24(10):2287–2292. https://doi.org/10.1007/s10856-10013-14988-10850

Hussain HD, Ajith SD, Goel P (2016) Nickel release from stainless steel and nickel titanium archwires – an in vitro study. J Oral Biol Craniofac Res 6(3):213–218. https://doi.org/10.1016/j.jobcr.2016.1006.1001

Ito A, Okazaki Y, Tateishi T, Ito Y (1995) In vitro biocompatibility, mechanical properties, and corrosion resistance of Ti-Zr-Nb-Ta-Pd and Ti-Sn-Nb-Ta-Pd alloys. J Biomed Mater Res 29 (7):893–899. https://doi.org/10.1002/jbm.820290715

Jani JM, Leary M, Subic A, Gibson MA (2014) A review of shape memory alloy research, applications and opportunities. Mater Des 56:1078–1113. https://doi.org/10.1016/j.matdes.2013.1011.1084

Jankovic A, Erakovic S, Vukasinovic-Sekulic M, Miskovic-Stankovic V, Park SJ, Rhee KY (2015) Graphene-based antibacterial composite coatings electrodeposited on titanium for biomedical applications. Prog Org Coat 83:1–10. https://doi.org/10.1016/j.porgcoat.2015.1001.1019

Kang T, Huang SY, Huang JJ, Li QH, Diao DF, Duan YZ (2015) The effects of diamond-like carbon films on fretting wear behavior of orthodontic archwire-bracket contacts. J Nanosci Nanotechnol 15(6):4641–4647. https://doi.org/10.2319/090715-090602.090711

Kobayashi S, Ohgoe Y, Ozeki K, Hirakuri K, Aoki H (2007) Dissolution effect and cytotoxicity of diamond-like carbon coatings on orthodontic archwires. J Mater Sci Mater Med 18 (2):2263–2268. https://doi.org/10.1007/s10856-10007-13118-10852

Koizumi H, Ishii T, Okazaki T, Kaketani M, Matsumura H, Yoneyama T (2018) Castability and mechanical properties of Ti-15Mo-5Zr-3Al alloy in dental casting. J Oral Sci 60(2):285–292. https://doi.org/10.2334/josnusd.2317-0280

Koizumi H, Takeuchi Y, Imai H, Kawai T, Yoneyama T (2019) Application of titanium and titanium alloys to fixed dental prostheses. J Prosthodont Res 63(3):266–270. https://doi.org/10.1016/j.jpor.2019.04.011

Kokubo T, Mijyaji F, Kim HM (1996) Spontaneous formation of bonelike apatite layer on chemically treated titanium metals. J Am Ceram Soc 79:1127–1129. https://doi.org/10.1111/j.1151-2916.1996.tb08561.x

Kumar A, Khanam A, Ghafoor H (2016) Effects of intraoral aging of arch-wires on frictional forces: an ex vivo study. J Orthod Sci 5(4):109–116. https://doi.org/10.4103/2278-0203.192112

Lee C-K (2012) Fabrication, characterization and wear corrosion testing of bioactive hydroxyapatite/nano-TiO2 composite coatings on anodic Ti–6Al–4V substrate for biomedical applications. Mater Sci Eng B 177(11):810–818. https://doi.org/10.1016/j.mseb.2012.1003.1034

Lee DG, Lee YH, Lee CSS, Lee S (2005) Effects of volume fraction of tempered martensite on dynamic deformation properties of a Ti-6Al-4V alloy having a bimodal microstructure. Metall Mater Trans A 36A:741–748. https://doi.org/10.1007/s11661-11005-10189-x

Lemons LE (1990) Dental implants biomaterials. J Am Dent Assoc 121:716–719. https://doi.org/10.14219/jada.archive.11990.10268

Li Y, Cui Y, Zhang F, Xu H (2011) Shape memory behavior in Ti–Zr alloys. Scr Mater 64 (6):584–587. https://doi.org/10.1016/j.scriptamat.2010.1011.1048

Liu X, Chu PK, Ding C (2004) Surface modification of titanium, titanium alloys, and related materials for biomedical applications. Mater Sci Eng R Rep R47(3–4):49–121. https://doi.org/10.1016/j.mser.2004.1011.1001

Liu X, Chen S, Tsoi JKH, Matinlinna JP (2017) Binary titanium alloys as dental implant materials – a review. Regen Biomater 4(5):315–323. https://doi.org/10.1093/rb/rbx1027

López MF, Jiménez JA, Gutiérrez A (2003) Corrosion study of surface-modified vanadium-free titanium alloys. Electrochim Acta 48(10):1395–1401. https://doi.org/10.1016/S0013-4686 (1303)00006-00009

Mantshiu A, Matizamhuka W, Yamamoto A, Shongwe B, Machaka R (2018) Cytocompatibility evaluation of nano-sintered Ti-15Zr-4Nb2Ta-0.2Pd alloy produced by spark plasma sintering technique. Paper presented at the Conference of the South African Advanced Materials Initiative (CoSAAMI-2018)

Mediaswanti K, Wen C, Ivanova EP, Berndt CC, Wang J (2013) Sputtered hydroxyapatite nanocoatings on novel titanium alloys for biomedical applications. In: Sieniawski J, Ziaja W (eds) Titanium alloys-advances in properties control. InTechOpen, Rijeka

Miguel FL, Müller R, Mathur S, Mücklich F (2015) Microstructure and mechanical properties of electrodeposited Ni and Ni-matrix-nanocomposite thin films. Mater Sci Eng A 646:254–262. https://doi.org/10.1016/j.msea.2015.1008.1069

Mirak M, Alizadeh M, Ghaffari M, Ashtiani MN (2016) Characterization, mechanical properties and corrosion resistance of biocompatible Zn-HA/TiO2 nanocomposite coatings. J Mech Behav Biomed Mater 62:282–290. https://doi.org/10.1016/j.jmbbm.2016.1005.1016

Miura E, Kato H, Ogata T, Nishiyama N, Specht ED, Shiraishi T et al (2007) Mechanical property and corrosion resistance evaluations of Ti-6Al-7Nb alloy brazed with bulk metallic glasses. Mater Trans 48(8):2235–2243. https://doi.org/10.2320/matertrans.MER2007612

Mohan L a, Durgalakshmi D, Geetha M, Sankara Narayanan TSN, Asokamani R (2012) Electro-phoretic deposition of nanocomposite (HAp+ TiO2) on titanium alloy for biomedical applica-tions. Ceram Int 38(4):3435–3443. https://doi.org/10.1016/j.ceramint.2011.3412.3056

Nelea V, Ristoscu C, Chiritescu C, Ghica C, Mihailescu IN, Pelletier H et al (2000) Pulsed laser deposition of hydroxyapatite thin films on Ti–5Al–2.5 Fe substrates with and without buffer layers. Appl Surf Sci 168:127–131. https://doi.org/10.1016/S0169-4332(1000)00616-00614

Niinomi M (2003) Fatigue performance and cyto-toxicity of low rigidity titanium alloy, Ti-29Nb-13Ta-4.6Zr. Biomaterials 24(16):2673–2683. https://doi.org/10.1016/S0142-9612(2603) 00069-00063

Ohgoe Y, Kobayashi S, Ozeki K, Aoki H, Nakamori H, Hirakuri KK, Miyashita O (2006) Reduction effect of nickel ion release on a diamond-like carbon film coated onto an orthodontic archwire. Thin Solid Films 497:218–222. https://doi.org/10.1016/j.tsf.2005.1011.1003

Okazaki Y, Ito Y, Tateishi T, AIto T (1995) Effect of heat treatment on microstructure and mechanical properties of new titanium alloys for surgical implantation. J Jpn Inst Metals 59 (1):108–115. https://doi.org/10.2320/jinstmet1952.2359.2321_2108

Ong JL, Lucas LC (1998) Auger electron spectroscopy and its use for the characterization of titanium and hydroxyapatite surfaces. Biomaterials 19(4–5):455–464. https://doi.org/10.1016/S0142-9612(1097)00224-X

Osman RB, Swain MV (2015) A critical review of dental implant materials with an emphasis on titanium versus zirconia. Materials 8:932–958. https://doi.org/10.3390/ma8030932

Özcan M, Hämmerle C (2012) Titanium as a reconstruction and implant material in dentistry: advantages and pitfalls. Materials 5:1528–1545. https://doi.org/10.3390/ma5091528

Petoumenou E, Arndt M, Keilig L, Reimann S, Hoederath H, Eliades T et al (2009) Nickel concentration in the saliva of patients with nickel-titanium orthodontic appliances. Am J Orthod Dentofac Orthop 135(1):59–65. https://doi.org/10.1016/j.ajodo.2006.1012.1018

Petrini L, Migliavacca F (2011) Biomedical applications of shape memory alloys. J Metall 2011:1–15. https://doi.org/10.1155/2011/501483

Podila R, Moore T, Alexisc F, Rao AM (2013) Graphene coatings for enhanced hemo-compatibility of nitinol stents. RSC Adv 3:1660–1665. https://doi.org/10.1039/c1662ra23073a

Poon RWY, Yeung KWK, Liu XY, Chu PK, Chung CY, Lu WW et al (2005) Carbon plasma immersion ion implantation of nickel–titanium shape memory alloys. Biomaterials 26:2265–2272. https://doi.org/10.1016/j.biomaterials.2004.2207.2056

Raman V, Tamilselvi S, Nanjundan S, Rajendran N (2005) Electrochemical behaviour of titanium and titanium alloy in artificial saliva. Trends Biomater Artif Organs 18(2):137–140. https://doi.org/10.1563/AAID-JOI-D-1511-00054

Ranjan S, Ramalingam C (2016) Titanium dioxide nanoparticles induce bacterial membrane rupture by reactive oxygen species generation. Environ Chem Lett 14(4):487–494. https://doi.org/10.1007/s10311-016-0586-y

Revankar GD, Shetty R, Rao SS, Gaitonde VN (2017) Wear resistance enhancement of titanium alloy (Ti–6Al–4V) by ball burnishing process. J Mater Res Technol 6(1):13–32. https://doi.org/10.1016/j.jmrt.2016.1003.1007

Rokaya D, Srimaneepong V, Qin J, Siraleartmukul K, Siriwongrungson V (2018a) Graphene oxide/silver nanoparticles coating produced by electrophoretic deposition improved the mechanical and tribological properties of NiTi alloy for biomedical applications. J Nanosci Nanotechnol 18:1–7. https://doi.org/10.1166/jnn.2019.16327

Rokaya D, Srimaneepong V, Sapkota J, Qin J, Siraleartmukul K, Siriwongrungson V (2018b) Polymeric materials and films in dentistry: an overview. J Adv Res 14:25–34. https://doi.org/10.1016/j.jare.2018.05.001

Rokaya D, Srimaneepong V, Qin J, Thunyakitpisal P, Siraleartmukul K (2019) Surface adhesion properties and cytotoxicity of graphene oxide coatings and graphene oxide/silver nanocomposite coatings on biomedical NiTi alloy. Sci Adv Mater 11:1474–1487. https://doi.org/10.1166/sam.2019.3536

Rupérez E, Manero JM, Bravo-González LA, Espinar E, Gil FJ (2016) Development of biomimetic NiTi alloy: influence of thermo-chemical treatment on the physical. Mech Biol Behav Mater (Basel, Switz) 9(6):402. https://doi.org/10.3390/ma9060402

Sarkar NK, Redmond W, Schwaninger B, Goldberg AJ (1983) The chloride corrosion behaviour of four orthodontic wires. J Oral Rehabil 10(2):121–128. https://doi.org/10.1111/j.1365-2842.1983.tb00106.x

Shanaghi A, Chu PK (2019) Enhancement of mechanical properties and corrosion resistance of NiTi alloy by carbon plasma immersion ion implantation. Surf Coat Technol 365:52–57. https://doi.org/10.1016/j.surfcoat.2018.1004.1027

Spanou S, Pavlatou EA, Spyrellis N (2009) Ni/nano-TiO2 composite electrodeposits: textural and structural modifications. Electrochim Acta 54:2547–2555. https://doi.org/10.1016/j.electacta.2008.2506.2068

Srimaneepong V, Yoneyama T, Wakabayashi N, Kobayashi E, Hanawa T, Doi H (2004) Deformation properties of Ti-6A1-7Nb alloy castings for removable partial denture frameworks. Dent Mater J 23(4):497–503. https://doi.org/10.4012/dmj.23.497

Srimaneepong V, Yoneyama T, Kobayashi E, Doi H, Hanawa T (2005) Mechanical strength and microstructure of laser-welded Ti-6Al-7Nb alloy castings. Dent Mater J 24(4):541–549. https://doi.org/10.4012/dmj.24.541

Srimaneepong V, Yoneyama T, Kobayashi E, Doi H, Hanawa T (2008) Comparative study on torsional strength, ductility and fracture characteristics of laser-welded α+β Ti–6Al–7Nb alloy, CP Titanium and Co–Cr alloy dental castings. Dent Mater 24(6):839–845. https://doi.org/10.1016/j.dental.2007.10.002

Srimaneepong V, Rokaya D, Thunyakitpisal P, Qin J, Saengkiettiyut K (2020) Corrosion resistance of graphene oxide/silver coatings on Ni-Ti alloy and expression of IL-6 and IL-8 in human oral fibroblasts. Sci Rep 10(1):3247–3247. https://doi.org/10.1038/s41598-020-60070-x

Suchanek W, Yoshimura M (1998) Processing and properties of hydroxyapatite-based biomaterials for use as hard tissue replacement implants. J Mater Res 13:94–117. https://doi.org/10.1557/JMR.1998.0015

Sui JH, Cai W (2006) Effect of diamond-like carbon (DLC) on the properties of the NiTi alloys. Diam Relat Mater 15(10):1720–1726. https://doi.org/10.1016/j.diamond.2006.1703.1004

Sun T, Wang LP, Wang M (2011) (Ti, O)/Ti and (Ti, O, N)/Ti composite coatings fabricated via PIIID for the medical application of NiTi shape memory alloy. J Biomed Mater Res 96B (2):249–260. https://doi.org/10.1002/jbm.b.31760

Sun T, Xue N, Liu C, Wang C, Hea J (2015) Bioactive (Si, O, N)/(Ti, O, N)/Ti composite coating on NiTi shape memory alloy for enhanced wear and corrosion performance. Appl Surf Sci 356:599–609. https://doi.org/10.1016/j.apsusc.2015.1007.1185

Tang H, Qian M, Liu Y, Cao P, Chen G (2018) Microstructure and mechanical properties of Ti-5Al-2.5Fe alloy produced by powder forging. Key Eng Mater 770:39–44. https://doi.org/10.4028/www.scientific.net/KEM.4770.4039

Tengvall P, Lundström I (1992) Physico-chemical considerations of titanium as a biomaterial. Clin Mater 9(2):115–134. https://doi.org/10.1016/0267-6605(1092)90056-Y

Thompson SA (2000) An overview of nickel–titanium alloys used in dentistry. Int Endontic J 33 (4):297–310. https://doi.org/10.1046/j.1365-2591.2000.00339.x

Torabi M, Sadrnezhaad SK (2011) Corrosion behavior of polypyrrole/hydroxyapatite nanocomposite thin films electropolymerized on NiTi substrates in simulated body fluid. Mater Corros 62(3):252–257. https://doi.org/10.1002/maco.200905399

Wang J, Jiang N (2009) Blood compatibilities of carbon nitride film deposited on biomedical NiTi alloy. Diam Relat Mater 18(10):1321–1325. https://doi.org/10.1016/j.diamond.2009.1307.1003

Wang FE, Pickart SJ, Alperin HA (1972) Mechanism of the TiNi martensitic transformation and the crystal structures of TiNi-II and TiNi-III phases. J Appl Phys 43:97–112. https://doi.org/10.1063/1061.1660844

Wang G, Shen Y, Cao Y, Yu Q, Guidoin R (2007) Biocompatibility study of plasma-coated nitinol (NiTi alloy) stents. IET Nanobiotechnol 6:102–106. https://doi.org/10.1049/iet-nbt:20070011

Williams D (2008) On the mechanisms of biocompatibility. Biomaterials 29(20):2941–2953. https://doi.org/10.1016/j.biomaterials.2008.2904.2023

Wu S, Liu X, Chan YL, Ho JPY, Chung CY, Chu PK et al (2007) Nickel release behavior, cytocompatibility, and superelasticity of oxidized porous single-phase NiTi. J Biomed Mater Res A 81A:948–955. https://doi.org/10.1002/jbm.a.31115

Xie D, Leng YX, Jing FJ, Huang N (2015) A brief review of bio-tribology in cardiovascular devices. Biosurf Biotribol 1(4):249–262. https://doi.org/10.1016/j.bsbt.2015.1011.1002

Xie H, Cao T, Rodríguez-Lozano FJ, Luong-Van EK, Rosa V (2017) Graphene for the development of the next-generation of biocomposites for dental and medical applications. Dent Mater 33 (7):765–774. https://doi.org/10.1016/j.dental.2017.1004.1008

Xu W, Hu WY, Li MH, Ma QQ, Hodgson PD, Wen CE (2006) Sol-gel derived HA/TiO2 double coatings on Ti scaffolds for orthopaedic applications. Trans Nonferrous Metals Soc 16:209–216. https://doi.org/10.1016/S1003-6326(1006)60177-60175

Yamanoglu R, Efendi E, Daoud I (2017) Production and mechanical properties of Ti-5Al-2.5Fe-xCu alloys for biomedical applications. Int J Chem Mol Nucl Mater Metall Eng 11(5):322–326. https://doi.org/10.5281/zenodo.1129940

Yang CH, Wang YT, Tsai WF, Ai CF, Lin MC, Huang HH (2011) Effect of oxygen plasma immersion ion implantation treatment on corrosion resistance and cell adhesion of titanium surface. Clin Oral Implants Res 22(12):1426–1432. https://doi.org/10.1111/j.1600-0501.2010.02132.x

Yang Y, Asiri AM, Tang Z, Du D, Lin Y (2013) Graphene based materials for biomedical applications. Mater Today 16(10):365–373. https://doi.org/10.1016/j.mattod.2013.1009.1004

Yoon H, King MW, Michielsen S, El-Shafei A, Johnson E (2010) Influence of surface modification on the adhesion between nitinol wire and fluoropolymer films. J Appl Biomater Biomech 8 (1):7–13. https://doi.org/10.1177/228080001000800102

Zhao Y, Wong SM, Wong HM, Wu S, Hu T, Yeung KWK, Chu PK (2013) Effects of carbon and nitrogen plasma immersion ion implantation on in vitro and in vivo biocompatibility of titanium alloy. ACS Appl Mater Interfaces 5(4):1510–1516. https://doi.org/10.1021/am302961h

Chapter 3
Metals and Metal Complexes for Medicinal Applications

**Siva Prasad Y., Lalitha Krishnamoorthy, Aenugu Sravya Chowdary,
Jugun Prakash Chinta, and Nagarajan Subbiah**

Contents

Abstract In recent decades the roles of metals and metal complexes in the medicinal field are increasing due to their clinical and commercial importance. Most of the metal ions act as the essential components in many biological processes. In particular, metals like silver, copper, gold, ruthenium, and platinum possess good antimicrobial activity as well as anticancer property in both micro and nanoscales. Owing to the potential medicinal applications of metal complexes, recently researchers have

Siva Prasad Y. · L. Krishnamoorthy
Department of Chemistry, School of Chemical and Biotechnology, SASTRA Deemed
University, Thanjavur, Tamil Nadu, India

A. S. Chowdary · J. P. Chinta
Department of Chemistry, National Institute of Technology Warangal (Institute of National
Importance), Warangal, Telangana, India

N. Subbiah (✉)
Department of Chemistry, School of Chemical and Biotechnology, SASTRA Deemed
University, Thanjavur, Tamil Nadu, India

Department of Chemistry, National Institute of Technology Warangal (Institute of National
Importance), Warangal, Telangana, India
e-mail: snagarajan@nitw.ac.in

focused their interest on synthesizing metal-based complexes in order to develop potential multi-targeted drugs especially in the case of anticancer applications. In this chapter, we discuss the significance of various metals and metal-based complexes for biomedical applications.

Keywords Transition metals · Metal complexes · Anticancer agent · Antimicrobial agent · Biomedical applications

Abbreviations

(DNA)   Deoxyribonucleic acid
(HeLa)   Epithelioid cervix carcinoma
(MCF-7)   Breast adenocarcinoma
(RAPTA)   Ruthenium–arene–PTA

3.1   Introduction

Generally, the metals like magnesium (Mg), calcium (Ca), manganese (Mn), iron (Fe), cobalt (Co), nickel (Ni) copper (Cu), and zinc (Zn) are found in enzymes and proteins and play a vital role in structural and regulatory functions, electron transfer, cell signaling, oxygen transport, DNA transcription, etc. (Begley and Williams 2008). Inspired by nature, several attempts were made to synthesize metal-based compounds for medical applications. The history of using metals and metal-based compounds as therapeutic potentials began from the ancient period, and the trend has been carried to the modern era. For example, ancient Assyrians, Egyptians, and Chinese used cinnabar (mercury sulfide) to treat trachoma and venereal diseases; arsenic oxide is used for rheumatoid treatment; metal surfaces of silver (Ag), gold (Au), copper (Cu), and platinum (Pt) exhibit antimicrobial property; and palladium alloys (Pd) as temporary implants to prevent cardiovascular infections (Jungwirth et al. 2012; Norn et al. 2008; Umar Ndagi and Ndumiso Mhlongo 2017; Vaidya et al. 2017). The discovery of *cis*-diamminedichloroplatinum(II) by Barnett Rosenberg and its clinical success in cancer treatment have marked the basis for the metal-based anticancer drug treatment (Jungwirth et al. 2012). Despite the success of *cis*-diamminedichloroplatinum(II), in cancer treatment, they produce side effects like nausea, vomiting, and bone marrow suppression. Hence a clear understanding of dose-related biological responses is required to identify the disparity between therapeutic and toxic doses of metal-based compounds and design the target-specific drugs (Turel 2015; Umar Ndagi and Ndumiso Mhlongo 2017).

Transition metals exhibit variable valency and can bind with a number of ligands to form metal complexes of unique geometries based on their oxidation state, coordination site, bond length, bond angle, and the strength of metal–ligand interactions (Turel 2015; Umar Ndagi and Ndumiso Mhlongo 2017). The transition metal

complexes display diverse electronic and magnetic characteristics that vary with the number of electrons in the d- or f- shell (Umar Ndagi and Ndumiso Mhlongo 2017). As the transition metals can form complexes of definite coordination number, geometry, redox activity, and binding interactions, they show unique therapeutic value and play a crucial role in designing and generating drugs for pharmacological applications such as anticancer, anti-inflammatory, antimalarial, antifungal, antipyretic, and antidiabetic drugs, cellular imaging, and sensors. In this chapter, we discuss the metal complexes, metal nanoparticles, and metals for medicinal applications.

3.2   Medical Applications of Metal Complexes

As transition metals provide features to generate bioactive species by utilizing the binding interactions, we discuss applications of some metal complexes in the felid of medicine in this section.

3.2.1   Platinum Complexes

Platinum is a transition metal existing in various oxidation states such as +1 to +4, out of which +2, +4 are the most common oxidation states, whereas +1 and +3 are rare oxidation states. *Cis*-diamminedichloroplatinum(II), a square planar platinum complex, is used to treat neck, head, lung, breast, testis, and ovarian cancer (Miller et al. 2010). It undergoes ligand exchange reaction with H_2O upon cell entry and damages DNA by cross-linking to it by a covalent coordinate bond to nitrogen (N) of guanidine and adenine (Fig. 3.1) (Lazarević et al. 2017; Silconi et al. 2016) which results in apoptosis, cell death. A positively charged metabolite generated by the hydrolysis of cisplatin gets accumulated in negatively charged mitochondria. As the kidney has a large number of mitochondria, nephrotoxicity occurs (Lazarević et al. 2017; Miller et al. 2010). Other side effects caused due to cisplatin administration are neurotoxicity, ototoxicity, hematological toxicity, gastrointestinal disorders, respiratory disorders, and dermatological disorders (Astolfi et al. 2013). Intravenous administration of platinum drugs causes the interaction of the drug with the sulfur donors (cysteine thiols, thioether side chains of methionine residues) present in the human serum albumin in bloodstream. This platinum–sulfur interaction is responsible for the side effects produced during the anticancer treatment (Lazarević et al. 2017; Miller et al. 2010).

In order to surmount the drawbacks of *cis*-diamminedichloroplatinum(II), several platinum(II) complexes like carboplatin, nedaplatin, oxaliplatin, heptaplatin, and lobaplatin were developed to treat cancer (Fig. 3.2) (Lazarević et al. 2017). Compared to *cis*-diamminedichloroplatinum(II), carboplatin displays negligible nephrotoxicity, oxaliplatin produces no significant nephrotoxicity and ototoxicity, and
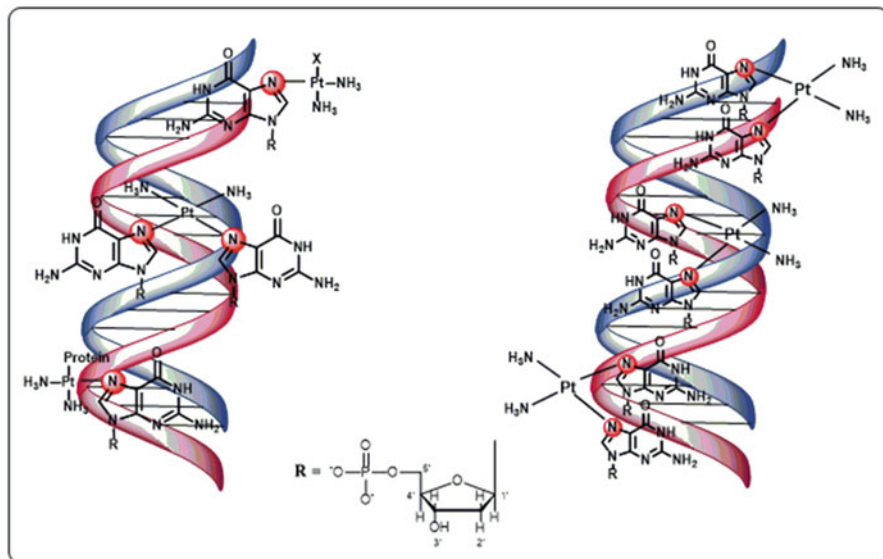
Fig. 3.1 The different possibilities of the attachment of cis-diamminedichloroplatinum(II) to DNA. (Modified after Lazarević et al. 2017)
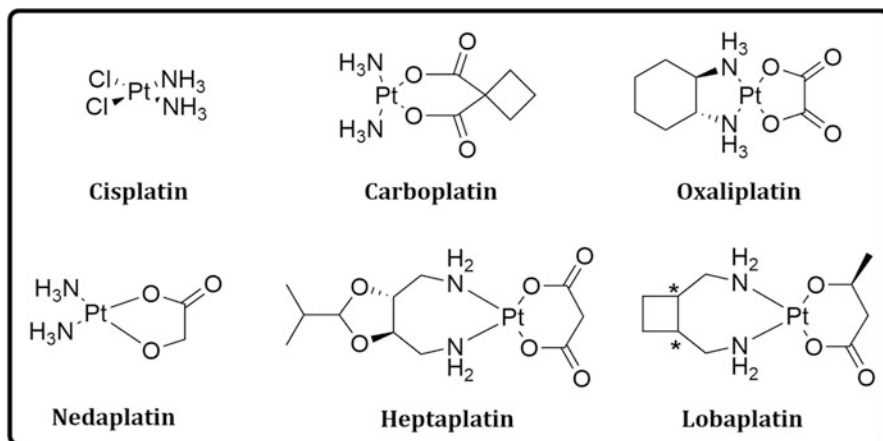

Fig. 3.2 Representative examples of clinically approved and marketed platinum-based anticancer drugs (Lazarević et al. 2017)

nedaplatin shows less nephrotoxicity and gastrointestinal toxicity. All these platinum (II) drugs are clinically approved as anticancer agents (Lazarević et al. 2017).

Cummings have reviewed the reactivity, redox, and photophysical properties of platinum(II) terpy complexes, $[Pt(Ytrepy)X]^{n+}$ (terpy = 2,2′:6′,6″-terpyridine; Y = substituent on the terpy ligand; X = ligands occupying the fourth coordination
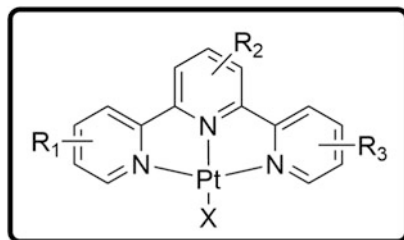
Fig. 3.3 Structure of platinum (II) terpy complexes where (terpy = 2,2′:6′,6″-terpyridine; Y = substituent on the terpy ligand; X = ligands occupying the fourth coordination site) (Cummings 2009)
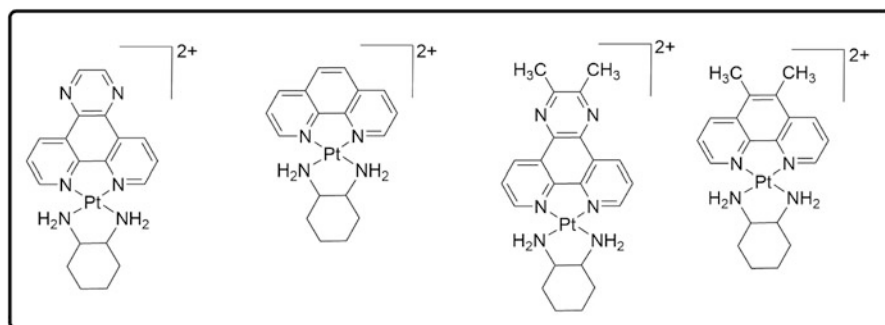
Fig. 3.4 Representative examples for platinum (II) complexes exhibiting non-covalent interactions with DNA (Lazarević et al. 2017)
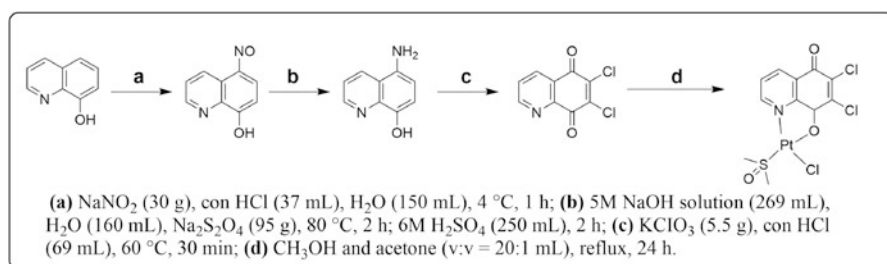
site) (Fig. 3.3) and their biological activity due to binding interaction (covalent/non-covalent) with biomolecules such as nucleic acids, proteins, peptides, etc. (Cummings 2009).

Platinum(II) complexes bind with DNA via non-covalent interactions such as electrostatic interaction between the positively charged metal complex and the negatively charged phosphate groups of DNA, van der Waals interactions, hydrogen bonding, and stacking interactions. The platinum complexes that cause intercalation in DNA can act as an anticancer agent. Few representative examples for platinum complexes interacting with DNA in non-covalent manner are given in Fig. 3.4 (Lazarević et al. 2017).

Owing to the therapeutic value of the natural building blocks, curcumin (curc), and caffeine, Censi et al. used them as ligands to synthesize three platinum (II) complexes, namely, [Pt(curcumin)(triphenylphosphines)₂]Cl, [PtCl(curcumin)(dimethylsulfoxide)], and *trans*-[Pt(caffeine)Cl₂(dimethylsulfoxide)], with antiproliferative activity (Scheme 3.1) (Censi et al. 2019). The curcuminate complex was found to induce cell degradation by interacting with DNA through intercalation between nucleobase pair in the case of [Pt(curcumin)(triphenylphosphines)₂]Cl and through groove binding in the case of [PtCl(curcumin)(dimethylsulfoxide)], while the caffeine complex was inactive (Censi et al. 2019). Cytotoxicity studies with five
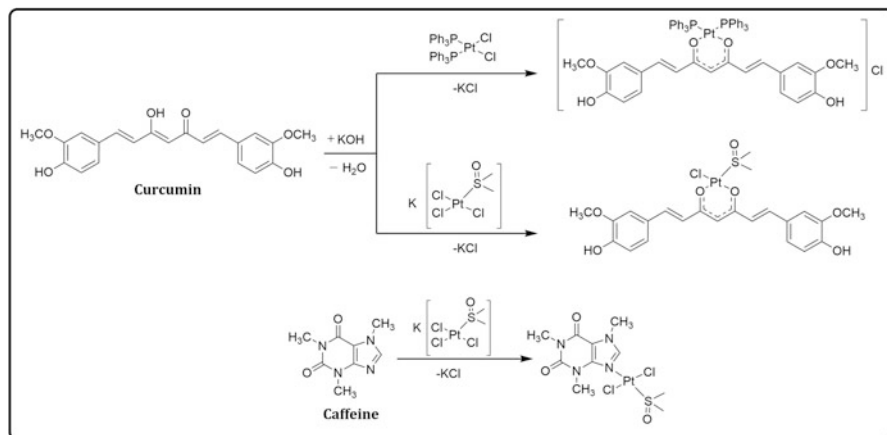
Scheme 3.1 Synthesis of platinum (II) complexes using natural ligand, curcumin, and caffeine (Censi et al. 2019)

(a) NaNO$_2$ (30 g), con HCl (37 mL), H$_2$O (150 mL), 4 °C, 1 h; (b) 5M NaOH solution (269 mL), H$_2$O (160 mL), Na$_2$S$_2$O$_4$ (95 g), 80 °C, 2 h; 6M H$_2$SO$_4$ (250 mL), 2 h; (c) KClO$_3$ (5.5 g), con HCl (69 mL), 60 °C, 30 min; (d) CH$_3$OH and acetone (v:v = 20:1 mL), reflux, 24 h.

Scheme 3.2 Synthesis of the ligand,6,7-dichloro-5,8-quinolinedione and the corresponding platinum (II) complex (Li et al. 2019b)

cancer cell lines, namely, A549, A375, MCF-7, SKOV3, and SW620, and normal breast cell line(MCF-10A) revealed that the therapeutic potential of curcuminate complex [PtCl(curcumin)(dimethylsulfoxide)] is greater with IC$_{50}$ = 2.5 μm, which improved selectivity to cancer cells than the parent drug cisplatin and the activity increased by irradiating with ultraviolet light (Censi et al. 2019).

In order to treat testicular seminoma, Li et al. synthesized platinum(II) complex using 6,7-dichloro-5,8-quinolinedione ligand and investigated the suitability of using the complex to treat testicular seminoma (Li et al. 2019b). As phosphoinositide-3 kinase/protein kinase B, the important signaling pathway towards the formation of seminoma, the usage of this platinum complex to treat tumor was performed, and the results displayed that the complex exhibited anticancer activity by inducing apoptosis via phosphoinositide-3 kinase/protein kinase B signaling pathway and mitochondria-mediated apoptotic pathway (Li et al. 2019b) (Scheme 3.2).

Here, we have discussed the binding interaction of platinum-based metal complexes and their potential anticancer activity. The adverse side effects exerted with the usage of platinum drugs have initiated the search for suitable transition metal such as gold, silver, copper, iron, and ruthenium to replace platinum.

3.2.2 Gold Complexes

Gold complexes have been used for the medicinal preparations from the early civilizations in countries like India, China, and Egypt (Fernández-Moreira et al. 2019). Since 2500 BC, Chinese used the compounds of gold to treat furuncles and smallpox and as a remedy to attain long life (Fernández-Moreira et al. 2019). Japanese used thin gold foils in tea and food in order to acquire good health. Though there exists historical evidence for the gold usage in treating plenty of disorders, the actual usage of gold in medicine began with the testing the activity of $K[Au(CN)_2]$ clinically towards mycobacteria treatment (Fernández-Moreira et al. 2019). Gold (I) complexes consisting of thiolate ligands such as aurothiomalate and aurothioglucose are initially used for treating rheumatoid arthritis. The observation of toxic side effects such as nephrotoxicity due to the accumulation of gold in the kidney has prompted the search for less toxic gold complex and led to discovery and usage of oral drugs, like auranofin, to treat rheumatoid arthritis treatment (Fig. 3.5) (Milacic and Dou 2009). This was found to be less effective than aurothiomalate and aurothioglucose.

Later, several gold compounds were reported as drugs. High stability of gold complexes in +1 and +3 oxidation states under physiological conditions has kindled the attention and checked their suitability as potent anticancer agents (Fernández-Moreira et al. 2019). Usually the ligands such as thiolates, dithiocarbamates, phosphines, phosphole, N-heterocyclic carbenes, thiourea, alkynyl, and cyclometallated are chosen to design gold complex-based drugs (Fernández-Moreira et al. 2019). Some of the examples of gold compounds exhibiting antitumor activity are given in Fig. 3.6 (Fernández-Moreira et al. 2019; Milacic and Dou 2009).

Even though the gold complex can be used as an anticancer agent like platinum complex, their biological targets are different. Anticancer activity of *cis*-diamminedichloroplatinum(II) occurs via the interaction with DNA, whereas the
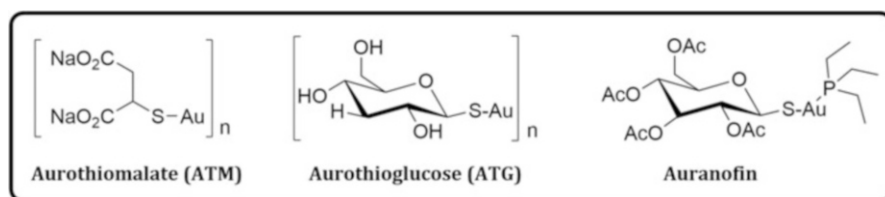

Fig. 3.5 Chemical structures of gold (I) complexes which are used to treat rheumatoid arthritis (Milacic and Dou 2009)
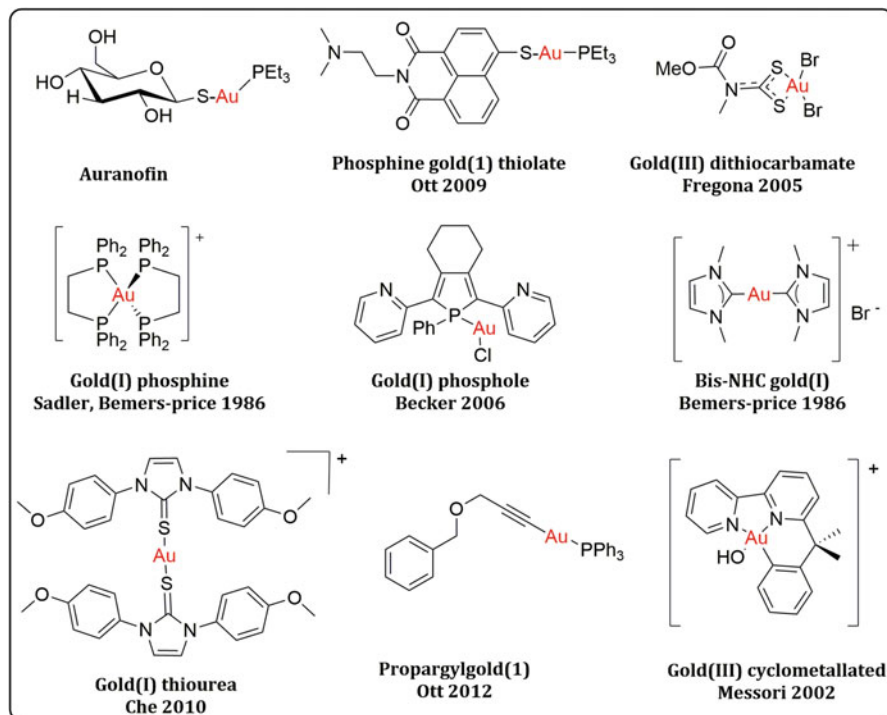
Fig. 3.6 Representative examples of gold complexes exhibiting antitumor activity (Fernández-Moreira et al. 2019)

gold complexes exhibit the antiproliferative activity by disturbing the functionality of mitochondria (Visbal et al. 2016).

In 2016, Visbal et al. synthesized a series of N-heterocyclic gold (I) and silver (I) carbene complexes. As these N-heterocyclic gold (I) and silver (I) carbene complexes exhibited emissive properties in solution due to intra-ligand transitions, the suitability of N-heterocyclic gold (I) and silver(I) carbene complexes as a cell imaging agent and the antiproliferative activity of N-heterocyclic gold (I) and silver (I) carbene complexes against various tumor cell lines was studied (Visbal et al. 2016). In particular, gold (I) complex displayed enhanced antiproliferative activity towards lung and pancreatic cells than silver (I) complex (Visbal et al. 2016). The biodistribution pattern and the lysosomal localization of complexes were identified using fluorescence cell microscopy. Electrophoresis analysis showed that the DNA interaction was due to metal fragment (Visbal et al. 2016) (Scheme 3.3).

Williams et al. synthesized a series of cationic mixed cyclometallated gold (III) dithiocarbamate $[(C^\wedge N)Au^{III}(S_2CNR_2)]^+$ of varying alkyl chain length in good yields (Williams et al. 2018). Comparison of in vitro cytotoxicity of these complexes towards various human cancer cell lines such as breast adenocarcinoma (MCF-7 and MDA-MB-231), adenocarcinoma cells (A549), human colon cancer (HCT-116),
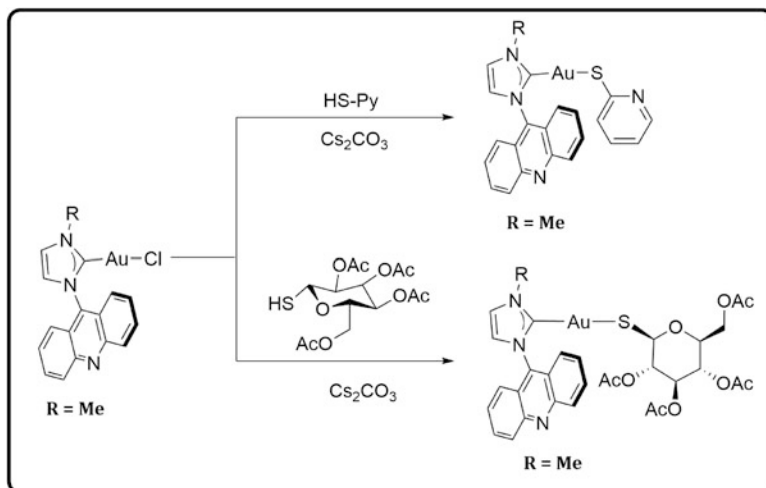
Scheme 3.3 Synthesis of thiolate gold (I)-N-heterocyclic carbene derivatives (Visbal et al. 2016)
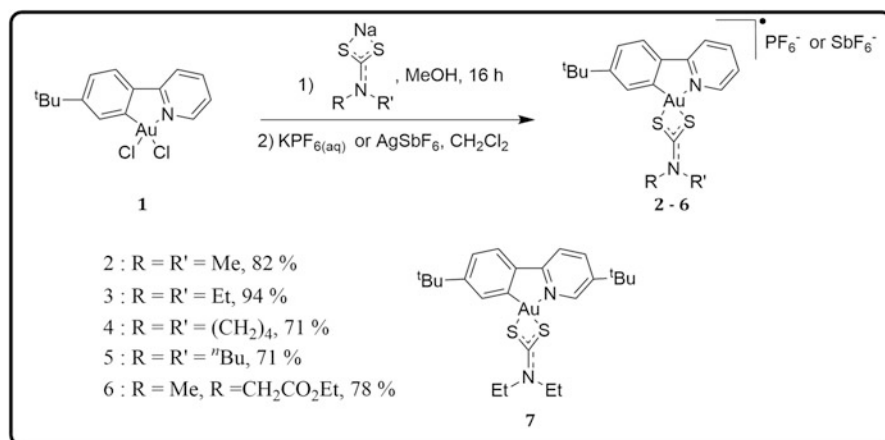
Scheme 3.4 Synthesis of cyclometallated gold (III)complexes of varying alkyl chain length (Williams et al. 2018)

and promyelocytic leukemia (HL60) with human umbilical vein endothelial cells (HUVEC) displayed cellular uptake and higher cytotoxicity with IC_{50} values dropping to submicromolar levels (Williams et al. 2018). The cellular uptake can be ascribed to the antiproliferative property of these complexes. The interaction study of these gold (III) with DNA structures and thioredoxin reductase inhibiting tendency demonstrated the selective stabilization of noncanonical DNA-G-quadruplex and ruled out the possibility of reactive oxygen species involvement (Williams et al. 2018) (Scheme 3.4).
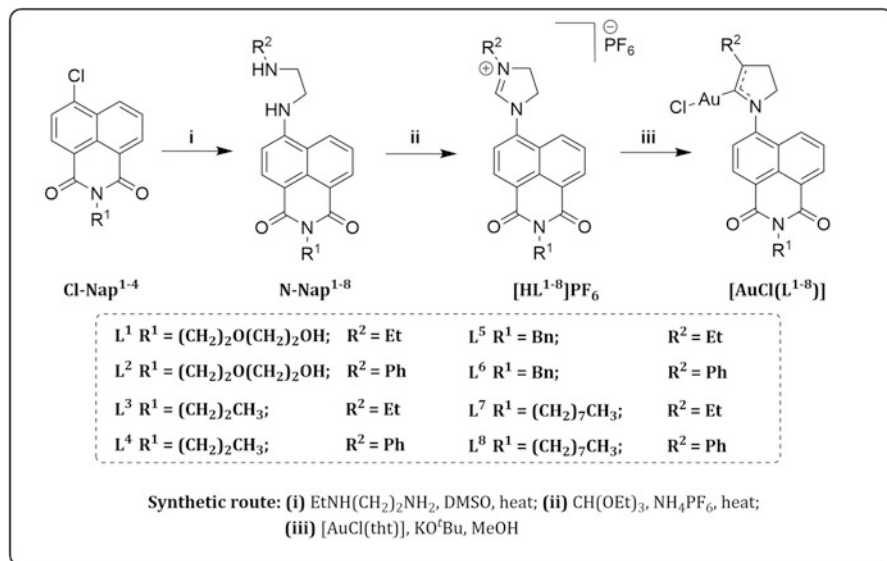
Scheme 3.5 Synthesis of N-heterocyclic carbene-based gold (I) complex (Groves et al. 2019)

A series of cationic proligands, hexafluorophosphate salts of dihydroimidazolinium-functionalized 1,8-naphthalimide fluorophores [HL]PF₆, were used to synthesize N-heterocyclic carbene-based gold (I) complex, [AuCl(L)] from [AuCl(tht)] [where (tht = tetrahydrothiophene)] in presence of base (Groves et al. 2019). Cytotoxicity of cationic proligands was found to be more than the corresponding complexes and the cytotoxicity increases with the added lipophilicity (Groves et al. 2019). Through the co-localization studies, the lysosomal staining pattern was identified to be predominant, and its applicability as probe due to the liberation of gold from the complex into the cell was established using lifetime imaging studies (Groves et al. 2019) (Scheme 3.5).

The possibility of gold (III) reduction to gold (I) or metallic gold in vivo has restricted the possibility of using them as a drug. Gold (III) complex stability can be increased by employing multidentate ligand with nitrogen atoms as donor groups to synthesize the gold (III) complexes. For example, series of gold (III) complexes with 2-[(dimethylamino)methylphenyl] (damp), N,N-dimethylbenzylamine ligands were reported to have high stability and exert anticancer activity (Milacic and Dou 2009).

Designing traceable anticancer drugs helps to detect and understand the interaction of the drug with the biomolecules within the body (Luengo et al. 2017). There are several gold-based tractable drugs designed by incorporating organic fluorophores such as anthracene, acridine, naphthalimide, coumarins, and boron dipyrromethene into the gold complex to attain further insight in the mechanism of internalization, biodistribution, and their interaction with the biological targets (Fig. 3.7) (Luengo et al. 2017). As their photophysical properties were not suitable for bioimaging applications, luminescent bimetallic species comprising the
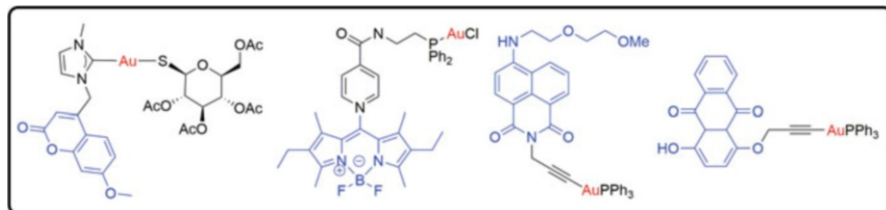
Fig. 3.7 Few examples of gold complexes with the incorporation of luminophore (Luengo et al. 2017)
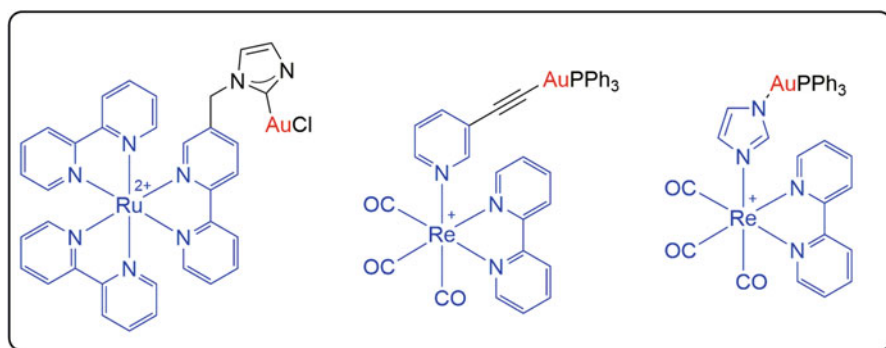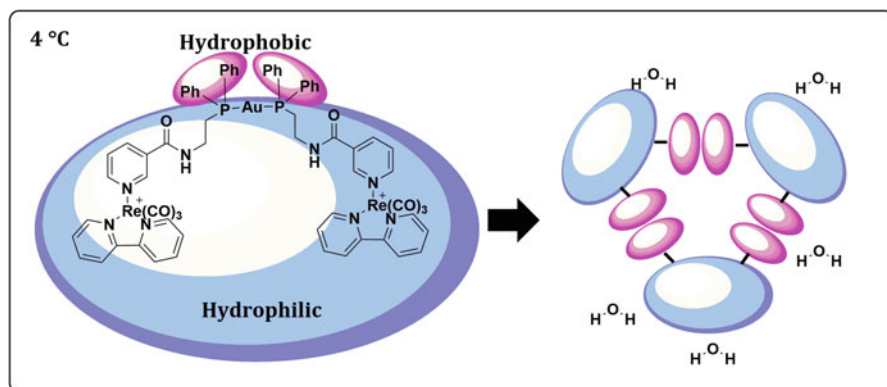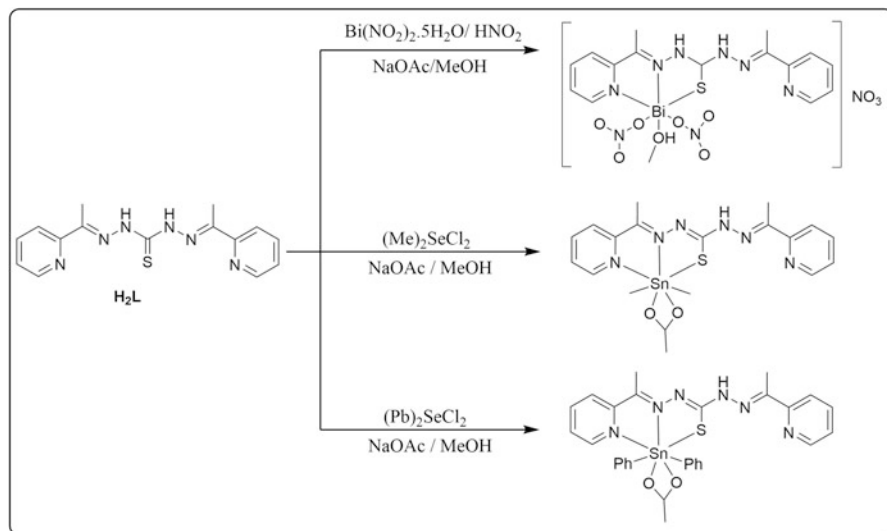

Fig. 3.8 Few examples for bimetallic combination of gold (I) complex with ruthenium (II) or rhenium (I) (Luengo et al. 2017)

combination of gold(I) complex with ruthenium (II) or rhenium(I) were used as cell imaging agents because of their phosphorescence nature (Fig. 3.8) (Luengo et al. 2017).

Gimeno and co-workers have developed the ditopic P, N-donor ligand, N-(diphenylphosphino)ethylamidepyridine derivatives and used them as linker between Re(I) and gold(I) to prepare hetero-metallic rhenium(I)/gold(I) complexes by exploiting the selective metal binding affinity (in this case phosphine can bind to gold(I) and pyridine bind to rhenium (I)) (Scheme 3.6) (Luengo et al. 2017). The suitability of these hetero-metallic rhenium (I)–gold(I) complexes as cell imaging agents were confirmed by the redshift up to 609 nm in dimethylsulfoxide compared to the metal-to-ligand charge-transfer transition, which appears between 550 and 590 nm in dichloromethane. Incubation experiment performed at 4 °C revealed that these complexes cross the cell membrane by passive transport and displayed a bright emissive droplet-shape pattern because of the micelle or an aggregate formation during the protection of hydrophobic groups such as phenyls from the media (Fig. 3.9) (Luengo et al. 2017). In particular, preliminary investigations for antiproliferative activity revealed that the DNA was one of the targets.

Apart from anticancer property, gold complexes are known to exhibit antibacterial property. The bactericidal character of these compounds depends on their ability to traverse the membrane and generate changes that are responsible for

Scheme 3.6 Synthesis of bismuth (III) and diorganotin (IV) complexes of bis(2-acetylpyridine) thiocarbonohydrazone (Fang et al. 2018)

Fig. 3.9 Proposed disposition of rhenium (I)–gold (I) complex in polar solvents at 4 °C modified after (Luengo et al. 2017)

bacterial death. According to the recent reports, gold complexes display antimalarial, antileishmanial, antitrypanosomal, and antischistosomal activities also (Navarro 2009).

3.2.3 Ruthenium Complexes

Recently, as an alternative for platinum complexes, ruthenium-based metal complexes have attracted researchers to investigate their role as anticancer metallotherapeutic drugs. Ruthenium-based complexes act as a potential anticancer drug because of the formation of diverse structural dimensions favoring the target-specific designing of compounds, their interaction with DNA and activating DNA damage mechanisms, and selective inhibition of the enzyme activity. Some of the beneficial properties of ruthenium are multivalency, low cytotoxicity and genotoxicity, activity against cisplatin-resistant cell lines, high cancer cells selectivity compared to the normal cells, ligand exchange kinetics, and the biomolecule binding tendency mimicking the iron (Thangavel et al. 2017; Thota et al. 2018). The unique properties of ruthenium that are responsible for their potent chemotherapeutic activity are: (Leijen et al. 2015; Thangavel et al. 2017)

- Selective uptake and increased accumulation of Ru-based complexes in cancer cells
- Antimetastatic effect
- Unique DNA binding patterns
- Slow ligand exchange kinetics which contributes to their general inertness and prevention of rapid equilibration process
- Activation by reduction of ruthenium (III) to ruthenium (II) under hypoxia, acid tumor microenvironment in the tissue resulting in the accumulation of ruthenium (II) (Leijen et al. 2015; Thangavel et al. 2017)

On comparing the ruthenium complexes with the other metal complexes, ruthenium compounds play a key role in signal transduction pathways as they mimic iron in binding and modify the cell adhesion and migration (Thangavel et al. 2017). Table 3.1 provides the relationship between the biological functions of ruthenium complexes with their composition.

The instability of the +4 state of ruthenium among its three possible oxidation states limits the application and development of ruthenium (IV) compounds. Excellent stability of ruthenium (III) complexes enables them to act as a prodrug under physiological conditions such as acidic pH, hypoxia, and high glutathione level and exhibits antitumor effect by their in vivo reduction to the corresponding ruthenium (II) analogs (Lin et al. 2018). The properties such as photothermal stability, enormous stokes shift, and long luminescence lifetime of ruthenium (II) complexes suggest their suitability as catalysts, photosensitizers, imaging agent for phototherapy, and excellent probes and tracers for subcellular structure localization (Lin et al. 2018).

Some of the ruthenium complexes like imidazolium *trans*-[tetrachloro(dimethyl sulfoxide)imidazoleruthenium(III)]; NAMI-A (novel antitumor metastasis inhibitor A) (Leijen et al. 2015); indazolium *trans*-[tetrachlorobis(1*H*-indazole)-ruthenate (III)]; KP1019 (Hartinger et al. 2008); Na-*trans*-[RuCl$_4$(1*H*-indazole)$_2$]; NKP-1339, the sodium salt analogue of KP1019 (Kuhn et al. 2015); and the first

Table 3.1 Composition of various ruthenium complexes and their biological functions (Thangavel et al. 2017)

S. no	Composition of ruthenium complexes	Functions
1	Lewis bases with lone pairs surrounding ruthenium	Possess some ligands that favor the approach towards cancerous cells as the ligands can be hydrolyzed
2	Ruthenium organometallics	Exhibit significant anticancer activity because of their high water and air stability
3	Ruthenium platinum mixed metal compounds	Display high selectivity towards both neoplastic tumors and metastatic cancers
4	Ruthenium cluster complexes	Show biological activity due to the supramolecular interactions with arenes and other functions
5	Ruthenium DNA intercalators	Display high cytotoxicity due to the two *cis* chloride ligands, which might be exchanged for biological targets as DNA
6	Ruthenium linked with an organic directing molecule	Facilitate the direct ruthenium binding with the cellular target resulting in an extraordinary increase of therapeutic value

ruthenium (II)-based photosensitizer, TLD-1433 $[Ru(dmb)_2(LL')]^{2+}$, where dmb = 4,4′-dimethyl-2,2′-bipyridine and LL′ = 2-([2,2′:5′,2″-terthiophene]-5-yl)-1H-imidazo[4,5-f][1,10]phenanthroline, are already under clinical trials (ClinicalTrials.gov Identifier: NCT03053635) (Fig. 3.10) (Kuhn et al. 2015). Analogous to antitumor platinum(II) drugs, many ruthenium complexes were designed to target DNA through the formation of ruthenium-DNA coordinate bonds (Brabec and Nováková 2006).

In order to target cancer cells resistant to *cis*-diamminedichloroplatinum(II), RM175, "piano stool"-shaped pseudo octahedral organoruthenium complex, in which the arene ligand represents piano while the amine ligands, chloride leaving group, represent the stool leg, was designed. The hydrophobic properties of the complex due to arene coordinated to the ruthenium facilitate the antitumor activity by DNA damage via the hydrophobic interaction of the arene ligand with DNA resulting in arene intercalation and groove binding in addition to coordination with guanine (Bergamo et al. 2012). RAPTA compounds are the arene complexes of ruthenium having the ligand, 1,3,5-triaza-7-phosphatricyclo-[3.3.1.1]decane. RAPTA-type complexes incorporate the ligand 1,3,5-triaza-7-phosphaadamantane and provide greater clinical benefit as these complexes can be modified to display required physical, chemical, and biological properties and provide an efficient clinical cancer therapy by targeting selectively the cancer cells. RAPTA-C, RAPTA-B, and RAPTA-T are few examples of (η6-arene)ruthenium-(II) complexes (Fig. 3.11). RAPTA-C damages DNA at the pH corresponding to tumor cells in hypoxic condition, whereas no DNA damage is observed at the pH of healthy cells. Bergamo et al. investigated the metastatic development of breast cancer through in vitro and in vivo models using RAPTA-T and confirmed their target selective anticancer activity (Bergamo et al. 2008).
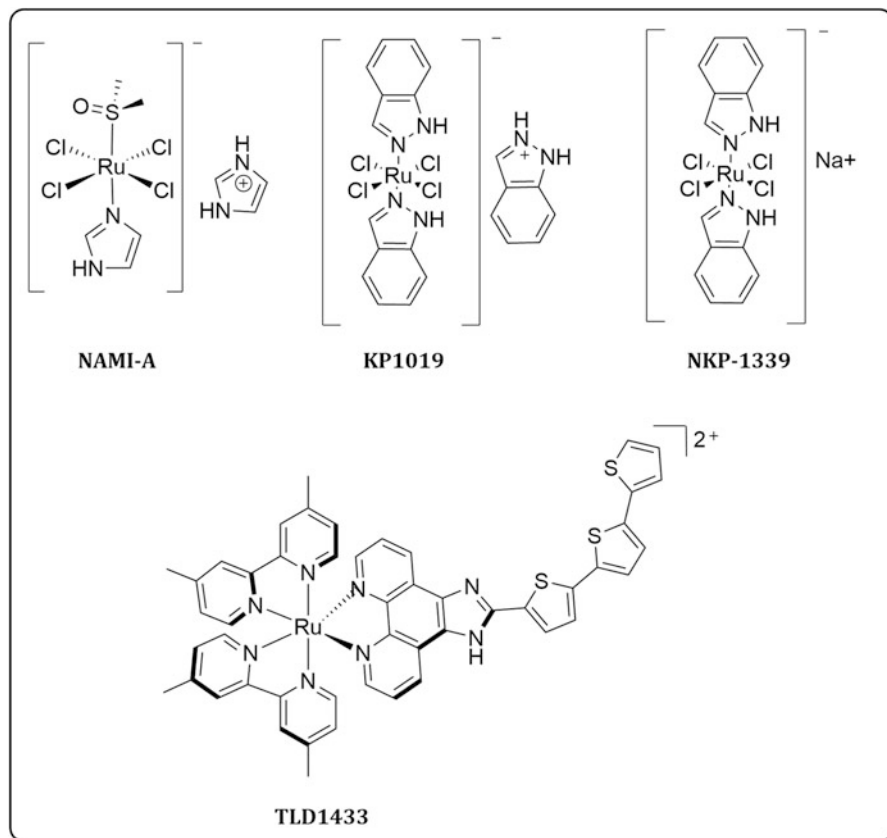
Fig. 3.10 Representative examples of ruthenium complexes tested in clinical trials like imidazolium *trans*-[tetrachloro(dimethyl sulfoxide)imidazoleruthenium(III)], NAMI-A (novel antitumor metastasis inhibitor A) (Leijen et al. 2015); indazolium *trans*-[tetrachlorobis(1*H*-indazole)-ruthenate(III)]; KP1019 (Hartinger et al. 2008); Na-*trans*-[RuCl$_4$(1*H*-indazole)$_2$]; NKP-1339, the sodium salt analogue of KP1019 (Kuhn et al. 2015); and TLD-1433 [Ru (dmb)$_2$(LL′)]$^{2+}$, where dmb = 4,4′-dimethyl-2,2′-bipyridine and LL′ = 2-([2,2′:5′,2″-terthiophene]-5-yl)-1*H*-imidazo[4,5-*f*][1,10]phenanthroline (Kuhn et al. 2015)

Mukhopadhyay et al. reported the ruthenium(II)–arene complex synthesis using various nonsteroidal anti-inflammatory drugs like diclofenac, naproxen, ibuprofen, and aspirin as chelating ligands that target the cyclooxygenase and lipoxygenase which are upregulated in many tumor cells for effective cancer treatment. They also explored the significance of using the nonsteroidal anti-inflammatory drug ligands to produce ruthenium(II)–arene complex in enhancing the target selective antiproliferative activities of these complexes by using various cancer cell lines (Fig. 3.12) (Mandal et al. 2018). All these complexes inhibited cyclooxygenase and lipoxygenase more effectively when compared with their non-complexed non-steroidal anti-inflammatory drug counterparts.
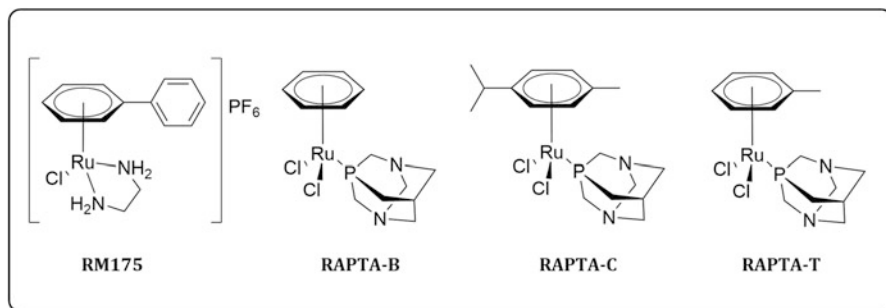
Fig. 3.11 Chemical structures of an organoruthenium(II) complex bearing an ethylenediamine ligand (RM175) and organoruthenium complexes bearing a 1,3,5-triaza-7-phosphaadamantane ligand (RAPTA-B, RAPTA-C, and RAPTA-T)
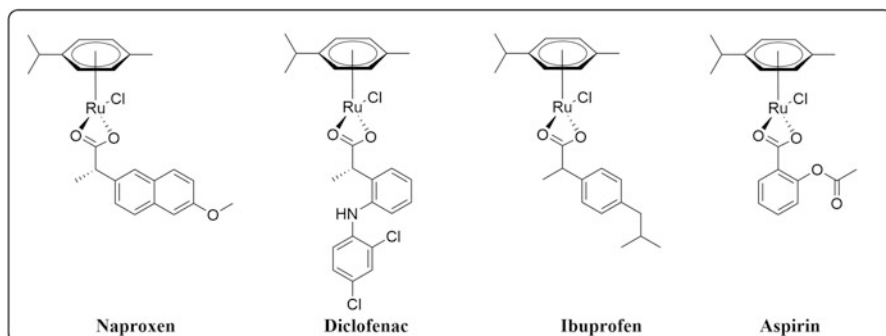

Fig. 3.12 Chemical structures of ruthenium(II)–arene complexes bearing nonsteroidal anti-inflammatory drugs like naproxen, diclofenac, ibuprofen, and aspirin as chelating ligands (Mandal et al. 2018)

Recent research revealed that ruthenium(II)–arene complexes can target several enzymes such as glutathione-S-transferase, thioredoxin reductase, poly(ADP-ribose) polymerase, cytochrome P450, topoisomerase IIα, cyclin-dependent kinase, peptidase, carbonic anhydrase, aldo-ketoreductase, aromatase, and urease besides cyclooxygenase, lipoxygenase inhibition and exhibit anticancer activity (Kenny and Marmion 2019). De Oliveira Silva et al. generated various multivalent dinuclear ruthenium(II, III) complexes with carboxylate ligands derived from drug molecules including nonsteroidal anti-inflammatory drug and γ-linolenic acid (de Oliveira Silva 2012). The in vitro and in vivo investigation studies of axially modified metallodrug chloridotetrakis(ibrufenato)diruthenium(II, III) ([Ru$_2$(Ibp)$_4$Cl] or RuIbpCl where Ibp = carboxylate anion derived from the nonsteroidal anti-inflammatory drug ibuprofen) (Fig. 3.13) displayed apoptosis and inhibited both cell migration and cell proliferation/mitosis (Hanif-Ur-Rehman et al. 2016). A brief note on various nanomaterials functionalized ruthenium complexes for target-specific drug delivery is given in Table 3.2.
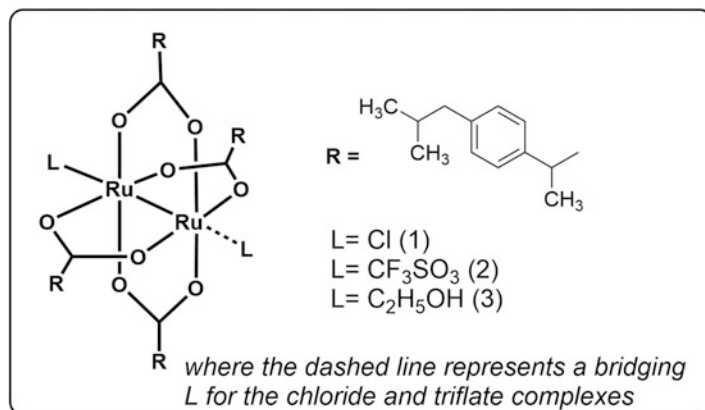
Fig. 3.13 Chemical structures of diruthenium–ibrufenato complexes (Hanif-Ur-Rehman et al. 2016)

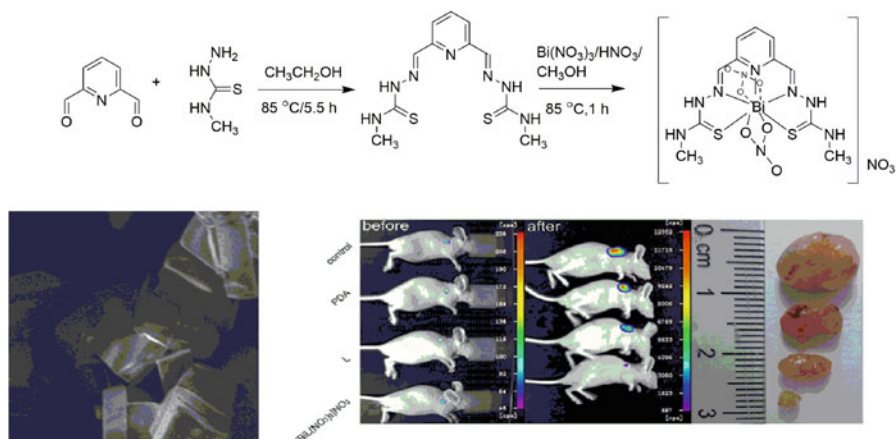### 3.2.4 Other Metal Complexes

Bismuth Complexes

Low toxicity and eco-friendliness of bismuth compounds account for their suitability as an anticancer agent and an antimicrobial agent in treating various microbial infections like gastritis, diarrhea, syphilis and colitis, etc. Xie and co-workers have synthesized a dodecahedral bismuth complex $[Bi(HL)(NO_3)_3]$ (HL = 2-acetylpyridine N(4)-pyridylthiosemicarbazone) (Li et al. 2012) and used for biological studies. An antibacterial assay using gram-positive bacteria like *Bacillus subtilis*, *Bacillus cereus*, *Staphylococcus aureus*, and *Sarcina lutea* and gram-negative bacteria such as *Agrobacterium tumefaciens*, *Escherichia coli*, *Pseudomonas aeruginosa*, and *Salmonella typhimurium* displayed appreciable antibacterial activity (Li et al. 2012). Moreover, as compared with the bismuth salt, a higher activity against *Bacillus cereus* and decreased activity against *E. coli* were observed. A cytotoxic assay using the human cancer cells such as leukemia K562, colorectal cancer HCT-116, cervical carcinoma HeLa cells, and hepatocellular carcinoma HepG2 cells displayed the anticancer activity (Li et al. 2012). Zhang and co-workers synthesized bismuth(III) and diorganotin(IV) complexes of bis (2-acetylpyridine) thiocarbonohydrazone that exhibited greater human hepatocellular carcinoma and HepG2 cell inhibition and displayed less toxicity towards normal hepatocyte QSG7701 cells (Scheme 3.6) (Fang et al. 2018). The dose-dependent inhibition of cell growth by the bismuth complex was confirmed in the cytotoxicity experiments involving mitochondria (Fang et al. 2018). Further, capase-3 cascade activation by bismuth complex mediated through the inhibition of Bcl-2 expression and promotion of Bax expression was revealed in the protein analysis (Fang et al. 2018).

Table 3.2 List of nanostructured materials functionalized with ruthenium complexes for targeted drug delivery

No	Nanostructured material	Ruthenium complex	Target
1	Tetrahedral nanostructure of DNA (height 2.0 nm; size 33.5 nm)	Ruthenium polypyridyl complex	Reactive oxygen species-mediated cell apoptosis (human liver carcinoma cells) (Chen et al. 2016)
2	The core/shell structured nanocapsule (size 103.1 ± 11.3 nm)	Ruthenium complex tris (1,10-phenanthroline) Ru (II) complex (3P-Ru)	Inhibition of cell growth (glioma cells) (Lv et al. 2016)
3	pH-sensitive mesoporous silica nanocarrier (MSN) (size 90 nm)	Ruthenium (II) N-heterocyclic carbene complex coated with chitosan biotin	The selectivity of ruthenium (II) N-heterocyclic carbene complex between cancer and normal cells. The biotin on the surface of the drug-loaded nanoparticles mediated higher accumulation in cancer cells (Shi et al. 2016)
4	Lanthanide-doped up-conversion nanoparticles coated with human serum albumin (size 60–120 nm)	A photo-sensitive ruthenium complex, [Ru (bpy)$_2$(dmbpy)]Cl where bpy = bipyridine and dmpy = 2,6-dimethanolpyridine	Controlled release of active anticancer agents in tumor sites (Rojas et al. 2017)
5	Inorganic mesoporous silicas (size 40 nm)	Anthracene-based half-sandwich organometallic ruthenium (II) compounds	Cytotoxic activity towards leukemia cells (HL-60) via apoptosis (Xue et al. 2017)
6	Self-assembled supramolecular nanoparticles (height 1.5 nm; size 30–50 nm)	β-Cyclodextrin-functionalized ruthenium (II) polypyridyl complex	Controlled drug release and induce cell death in integrin αvβ3-rich tumor cells (Zhang et al. 2015)
7	Single-walled carbon nanotemplates (size ranged from 20 nm)	Ruthenium (II) complexes	Photothermally triggered release (Wang et al. 2015)
8	Functionalized multiwalled carbon nanotubes as carriers (the average diameter is 224.9 nm)	Ruthenium polypyridyl complex	Induction of cell death by activation of downstream signaling pathways, including DNA damage-mediated p53 phosphorylation, activation of p38, and inactivation of AKT and extracellular signal-regulated kinase (Zhang et al. 2016)

Recently, Zhou and co-workers have reported the synthesis and anticancer activity of bismuth(III) complex [BiL(NO$_3$)$_2$]NO$_3$ where L = 2,6-Pyridinedicarboxaldehyde bis([4]N-methylthiosemicarbazone) (Scheme 3.7). This compound exhibited target-specific anticancer activity by reducing the colony formation/migration and enhancing the apoptosis of human lung cancer cells A549 and H460, while the cell viability of healthy cells is not reduced. This was demonstrated

Scheme 3.7 Synthesis of [BiL(NO₃)₂]NO₃ where L = 2,6-Pyridinedicarboxaldehydebis ([4]N-methylthiosemicarbazone). (Reprinted with permission of journal of inorganic biochemistry, Elsevier from Ouyang et al. 2017)

through their in vitro and in vivo studies using the cancer-bearing mice model, and the suppression of A549 xenograft cancer growth without inducing any harmful side effects was established (Ouyang et al. 2017).

Investigation on the biological activity of bismuth(III) complex [Bi (HCQ)$_2$(H$_2$O) Cl$_3$] prepared from clioquinol, (5-chloro-7-iodo-8-hydroxyquinoline, HCQ) and bismuth(III)chloride displayed an enhanced antimicrobial activity against *S. aureus* and *Candida albicans* (*C. albicans*) (Ferraz et al. 2013). Barszcz and co-workers have highlighted the synthesis, characterization, and efficiency of various bismuth complexes in cancer chemo- and radiotherapy (Kowalik et al. 2017).

Silver Complexes

Owing to the antibacterial activity of silver, it has been widely used in wound care products, cosmetics, textiles, etc. From ancient times, many silver compounds were used as an antibacterial agent (Liang et al. 2018). For example, silver nitrate is used to cure various diseases such as venereal diseases, blisters, burns, itchiness, and warts (e.g., silver sulfadiazine cream for treating wounds and burns) and colloidal silver in wound healing as they stimulate the immune system and healing processes and are found to be effective with a broad antibacterial spectrum (Liang et al. 2018). Japanese used ceramic-coated silver zeolites for the disinfection of medical products and to prevent contamination of sanitary materials because of the antibacterial properties. The antibacterial water-based paint suitable for coating the kitchens, bathrooms, and hospital environments was reported to contain the nanostructured silver vanadate (Holtz et al. 2012). Despite these advantages, their clinical usefulness is limited by the high solubility of silver nitrate salts under physiological conditions
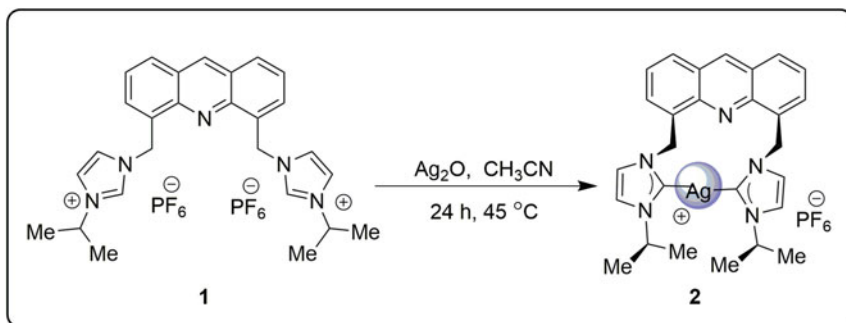
Scheme 3.8 Synthesis of 4,5-bis N-heterocyclic carbene-tethered acridine silver (I) hexafluorophosphate complex (Prabusankar et al. 2019)

leading to dissociation followed by rapid complexation with chloride and low stability of silver ions due to complexation.

Banti and Hadjikakou have reviewed the antiproliferative property of silver (I) complexes with various ligands such as amino acids, carboxylic acids, sulfur, phosphorus, and nitrogen. Generally, N-heterocyclic carbenes are strong ligands that can be used to chelate metals like platinum, gold, silver, etc. to form N-heterocyclic carbene-metal complexes of potential therapeutic value (Garner et al. 2015; Garrison and Youngs 2005; Muskawar et al. 2016). Few examples of these type of complexes are silver xanthine complexes and benzimidazole and imidazolium silver complexes (Garner et al. 2015; Garrison and Youngs 2005; Muskawar et al. 2016). Silver (I)-N-heterocyclic carbenes are stable complexes and can serve as an antibacterial and anticancer agent (Johnson et al. 2017). Youngs and co-workers have reviewed the recent developments of silver-N-heterocyclic carbene complexes and imidazolium salts for medicinal applications (Johnson et al. 2017). The light-sensitive 4,5-bis-N-heterocyclic carbene-tethered acridine silver (I) hexafluorophosphate complex was synthesized in excellent yield as a white solid (Scheme 3.8), and the investigation of photophysical properties revealed the blue emission with increased fluorescence quantum yield from all three excitations (Prabusankar et al. 2019).

Yilmaz and co-workers reported the synthesis of silver (I) 5,5′-diethylbarbiturate complexes [$Ag_2(\mu$-barb$)_2$L], where L = PPh_3 (triphenylphosphines) or PPh_2Cy (diphenylcyclohexylphosphine) or $PPhCy_2$ (phenyldicyclohexylphosphine) or PCy_3 (tricyclohexylphosphine) that exhibited significant antimicrobial activity selectively against gram-positive bacteria and increased anticancer activity selectively against human breast cancer cells by damaging both mitochondria and genomic DNA compared to healthy cells (Yilmaz et al. 2017). As the water solubility can be increased by the complexation of silver salts with polar organic ligands, Jaros et al. have synthesized the light stable, water-soluble polypyridine silver (I) complexes with 1,3,5-triaza-7-phosphaadamantane (PTA) and 1,3,5-triaza-7-phosphaadamantane-7-sulfide (PTA = S) and investigated their antiproliferative activity against human cancer lines like lung carcinoma (A549), breast

adenocarcinoma (MCF-7), and epithelioid cervix carcinoma (HeLa) cell lines (Jaros et al. 2019).

Oxovanadium (IV)-Vitamin-B$_6$ Complex

Oxovanadium (IV) complex of Schiff base derived from vitamin-B$_6$ and (acridinyl)-dipyridophenazine displayed specific localization to the endoplasmic reticulum and induce apoptosis of cancer cells (IC50 < 0.6 μM) significantly in visible light (400–700 nm) by generating stress on endoplasmic reticulum (Banerjee et al. 2014). Moreover, the additional demand for vitamin-B$_6$ by cancer cells than normal cells promotes the uptake of the complex containing VB6 into the cancer cells in preference to healthy cells, through vitamin-B$_6$ transporting carrier membrane diffusion pathway that triggers the endoplasmic reticulum triggered photocytotoxicity when exposed to visible light (Banerjee et al. 2014) (Fig. 3.14).

Iridium (III) Complexes

On comparing common organic fluorophores with the iridium (III) complexes, the complexes displayed unique photophysical properties such as large stokes shifts limiting the self-quenching, long-standing luminescence emission with a long lifetime, which permit their usage even in autofluorescent matrices when compared with the (Ma et al. 2018). Additionally, they displayed low cytotoxicity, high target selectivity and enhanced cellular uptake, a wider array of emission wavelength, and variable emission colors due to the larger ligand field stabilization energy ranging from green to red (Ma et al. 2018). The bioavailability, cytotoxicity, and selectivity of the target molecules and photophysical properties can be achieved by modifying the auxiliary ligands (Ma et al. 2018). This enhances the feasibility of using the iridium (III) complexes as probes for medical diagnosis. A few examples of
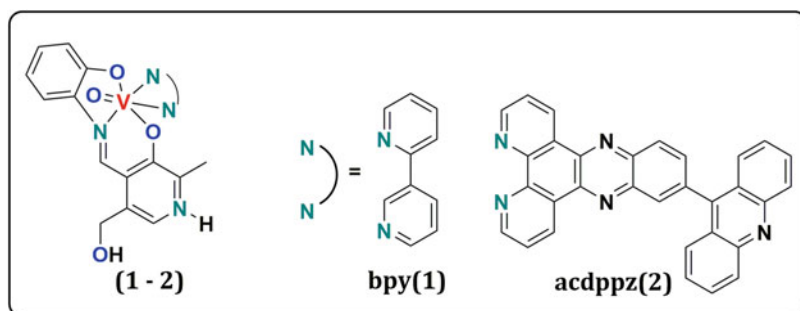

Fig. 3.14 Structure of oxovanadium complexes where bpy = bipyridine and acdppz–(acridinyl)-dipyridophenazine (Banerjee et al. 2014)
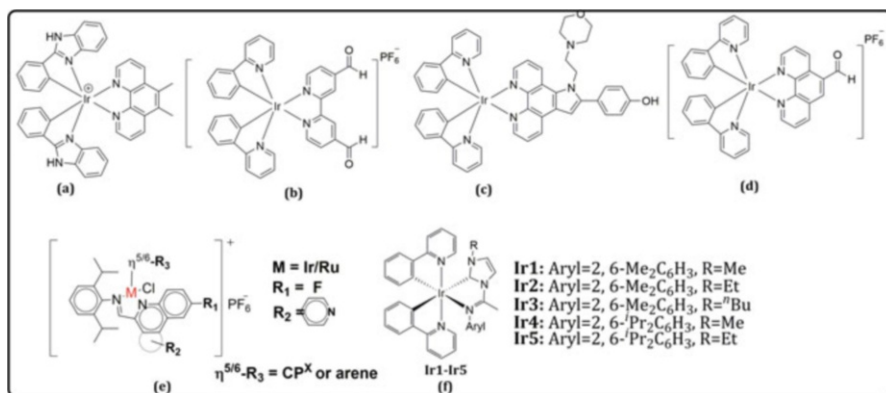
Fig. 3.15 Representative examples for iridium (II) complexes: (**a**) aluminum and fluoride ion sensor; (**b**) bisulfite ion sensor (**c**) lysosome tracker in vivo (**d**) proline sensor in vivo (**e**) half-sandwich iridium[III] and ruthenium[III] complex with antiproliferative activity where CP[x] = cyclopentadienyl ligand (**f**) cyclometalated iridium (III) anticancer complexes (Li et al. 2019a; Ma et al. 2018; Yang et al. 2019)

iridium (III) complex are given in Fig. 3.15 (Li et al. 2019a; Ma et al. 2018; Yang et al. 2019).

Copper Complexes

Copper plays a vital role in the development of anticancer agents as it can selectively seep into the cancer cell membranes and generate less toxicity compared to platinum complexes. It also has antimalarial, antibacterial, and antifungal effects. The cell division can be inhibited by reducing the length of telomere because the tendency of mammalian cells to replicate depends on the telomere length (Yu et al. 2019). In this regard, a series of copper complex was synthesized that can act as artificial nucleases that exhibit strong cleavage reactivity towards G-quadruplex telomeric DNA compared to duplex DNA because of selective DNA binding affinity to G-quadruplex telomeric DNA and cause rapid degradation (Yu et al. 2019). Compared to protein-based nucleases, the cellular uptake for these complexes was significantly increased, and an improved nuclear localization was observed (Yu et al. 2019).

Several terpyridine-based copper (II) complexes were developed as anticancer agents. Among them, anthracenyl terpyridine copper (II) complex showed unique antiproliferative activity in various cancer cell lines, such as cervical (HeLa, SiHa, CaSki), breast (MCF-7), liver (HepG2), and lung (H1299) (Kumar et al. 2011). The complex exhibited higher activity in cells infected with human papilloma virus [viz., CaSki (IC$_{50}$–0.8 ± 0.2 μM), HeLa (0.7 ± 0.1), and SiHa (3.1 ± 0.9)] than nonhuman papilloma virus-infected cell lines [viz., HepG2, (3.6 ± 0.2), MCF (5.4 ± 0.1) and H1299 (6.3 ± 0.8)]. These results suggested that copper complex causes cell death by interaction with human papilloma virus oncoprotein that resulted in remarkable
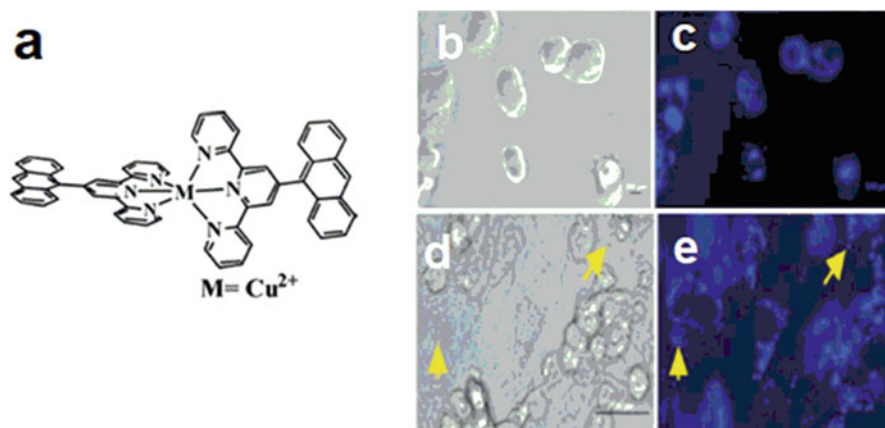
Fig. 3.16 (**a**) Anthracenyl terpyridine copper (II) complex. Phase-contrast and fluorescence microscopy images of MCF-7 cells (**b** and **c**) and human papilloma virus-transfected MCF-7 cells (**d** and **e**). Arrow shows granular structures. (Reprinted with permission of royal society of chemistry (Kumar et al. 2011))

antiproliferative activity. The results were further supported by phase-contrast and fluorescence microscopy; only the incubation of human papilloma virus-infected cells with the copper complex resulted in granular structures and not with others. The mechanism of action was proven by transfecting the MCF-7 cells (originally not containing human papilloma virus) with e6 oncoprotein cDNA. The activity in transfected MCF-7 cells (1.7 ± 0.3 μM) was found to be better compared to the non-transfected ones (5.4 ± 0.1 μM) (Fig. 3.16).

Multinuclear water-soluble complexes such as a trinuclear copper(II) complex, $Cu_3(ppbm)_2(SO_4)_3$, and a binuclear complex, $Co_2(ppbm)_2(NO_3)_4$ (ppbm = 2-(pyridine-2-yl)-1-(pyridine-3-ylmethyl)-1H-benzo[d] imidazole), were synthesized, and their interaction with DNA and cytotoxicity was evaluated (Zhao et al. 2019). Compared to cobalt(II) complex, $Co_2(ppbm)_2(NO_3)_4$, the copper(II) complex, $Cu_3(ppbm)_2(SO_4)_3$, displayed antiproliferative activity with IC_{50} value less than cisplatin (Zhao et al. 2019). As shown in Fig. 3.17, tetrakis(4-carboxyphenyl) porphyrin was used as a probe and therapeutic for nuclear medicine (Kilian et al. 2016).

Currently, the interest in the development of renewable resource-derived functional materials is rising in order to meet the sustainability challenges (Lalitha et al. 2017). In an era of the inevitable evolution of antimicrobial resistance, there is enormous demand for the efficient antimicrobial thin film coating material derived from renewable resources to meet the public bacterial threats and biomedical applications (Lalitha et al. 2017). There are several disadvantages such as leachability, the stability of coated surface, and availability of metal to the environment associated with the usage of commercial metal-blended coating (Lalitha et al. 2017). However, to overcome the existing limitations on the development of an antimicrobial thin film surface, Nagarajan and co-workers have reported the

Fig. 3.17 Chemical structure of tetrakis (4-carboxyphenyl)porphyrin (Kilian et al. 2016)
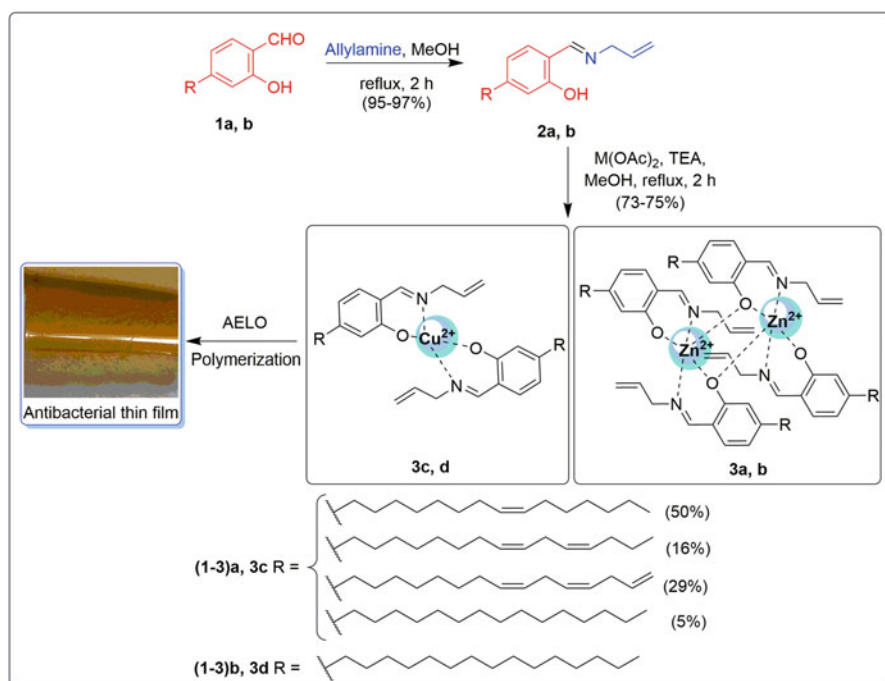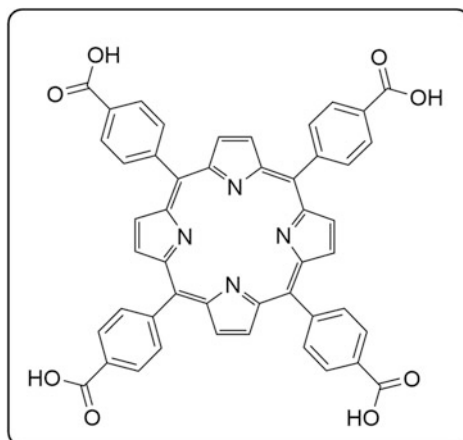
Scheme 3.9 Synthesis of thin film coating material [AELO = acrylate-epoxidized linseed oil, TEA = triethylamine] (Lalitha et al. 2017)

synthesis and assembly of zinc- and copper-based complexes derived from cardanol in acrylate-epoxidized linseed oil (Scheme 3.9) and explored their subsequent utility in developing antimicrobial thin film coating material (Lalitha et al. 2017).

The assembled thin film is formed under atmospheric conditions due to the presence of double bond in the hydrophobic part of metal complexes and acrylate-epoxidized linseed oil, in the absence of any initiators (Lalitha et al. 2017). This thin film coating exhibited non-leaching behavior and thermal stability. Though these compounds displayed antimicrobial activity against both gram-positive and gram-negative bacteria, the bio-based thin film coating material was found to inhibit the formation of uropathogenic *Escherichia coli* bacterial film effectively (Lalitha et al. 2017). Hence, the derived thin film coating material can be potentially used to develop antibacterial urinary catheter tubes with intrinsic hydrophobicity (Lalitha et al. 2017).

Manganese Complexes

Among the two existing antioxidant system, the nonenzymatic system depends on the molecules that quench the reactive oxygen species, whereas the enzymatic system superoxide dismutase modulates the oxidative stress (Bresciani et al. 2015). Miriyala et al. highlighted the effectiveness of mitochondrially targeted redox-active compounds, manganese-porphyrins to treat the injuries in the central nervous system where mitochondria play a vital role (Miriyala et al. 2012). Preparation and characterization of the manganese (III) complex of biliverdin IX dimethyl ester, $\{Mn^{III}BVDME\}_2$, reveal the presence of manganese (III) or manganese (IV) redox couple in aqueous medium that catalyze the dismutation of O_2^- efficiently. The complex shows specificity towards O_2^-, resistant to H_2O_2 and no NO° binding. Thus, it can act as a proficient superoxide dismutase mimic in vivo by causing the growth of superoxide dismutase-deficient *E. coli* aerobically (Spasojević et al. 2001).

Palladium Complexes

Though the coordination chemistry of palladium (II) and platinum (II) compounds is similar, they differ in kinetic liability and solubility. Compared to platinum (II) compounds, palladium (II) compounds possess antitumor activity with fewer side effects (Jia et al. 2017). Hence, a number of palladium complexes were synthesized, and their utility in treating various types of tumors was explored (Jia et al. 2017).

Flubendazole palladium (II) complexes, $[Pd(FLU)_2X_2].yH_2O.zCH_3OH$, where FLU = flubendazole, X = Cl or Br or NO_3 or SCN, y = 0,2, and z = 0,3 were synthesized (Scheme 3.10), and the cytotoxicity investigation against various cancer cell lines such as breast cancer, hepatocarcinoma, and colon carcinoma revealed that these complexes can act as potent anticancer agent (Mansour et al. 2016). Further, the cytotoxicity of these Pd (II) complexes vary with the coordinated ion X (X = Cl, Br, SCN, and NO_3), and the order of inhibition is $NO_3 > Br > SCN > Cl$ for MCF-7 (Mansour et al. 2016).
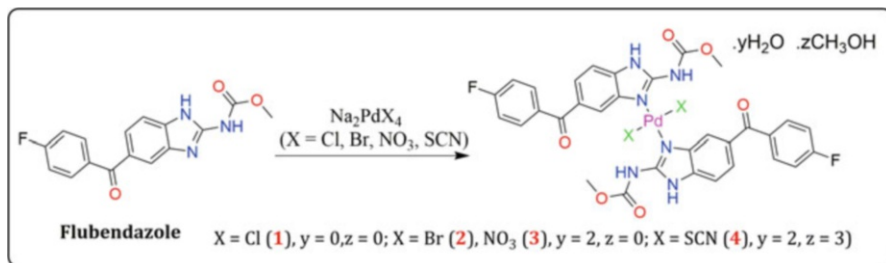
Scheme 3.10 Synthesis of palladium (II)–flubendazole complexes (Mansour et al. 2016)

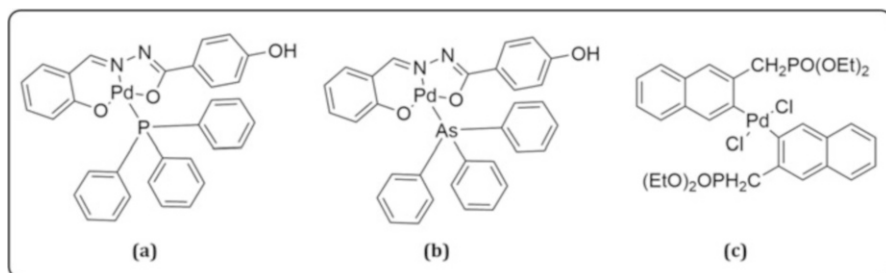**Fig. 3.18** (**a**) [Pd(L)(PPh$_3$)], (**b**) [Pd(L)(AsPh$_3$)] where L = 4-hydroxybenzoic acid (5-chloro-2-hydroxy-benzylidene)-hydrazide and (**c**) trans [PdCl$_2$(diethyl-2-quinolmethylphosphonate)] (Lazarević et al. 2017)

Glyco-conjugated palladium (II) complex, [PdCl$_2$ (L)], and Pt(II) complex, [PdCl$_2$ (L)], where L = 2-deoxy-2-[(2-pyridinylmethylene) amino]-α-D-glucopyranose were synthesized by Tanaka et al. (2013). *Cis*-diamminedichloroplatinum(II)-resistant gastric cancer cell lines formed by exposing the gastric cancer cell lines continuously to *cis*-diamminedichloroplatinum(II) were used for the cytotoxicity assay (Tanaka et al. 2013). Palladium (II) exhibited anti-cancer effect in *cis*-diamminedichloroplatinum(II)-sensitive gastric cancer cell lines by inducing apoptosis (Tanaka et al. 2013). Moreover, palladium (II) complex was able to overcome cross-resistance to *cis*-diamminedichloroplatinum(II) in gastric cancer when compared with the corresponding platinum (II) complex. Drug solubility and tumor selectivity were increased by glucose conjugation (Tanaka et al. 2013). Lazarević et al. have highlighted the examples of palladium complexes (Fig. 3.18) with enhanced anticancer activity (Lazarević et al. 2017).

Metal Complexes of Curcumin and Coumarin

Curcumin, a polyphenolic species exists as an active ingredient of turmeric displayed antiproliferative, anti-inflammatory, and antiseptic properties. The ability of the curcumin-based metal complex to retain its therapeutic potential has led to the
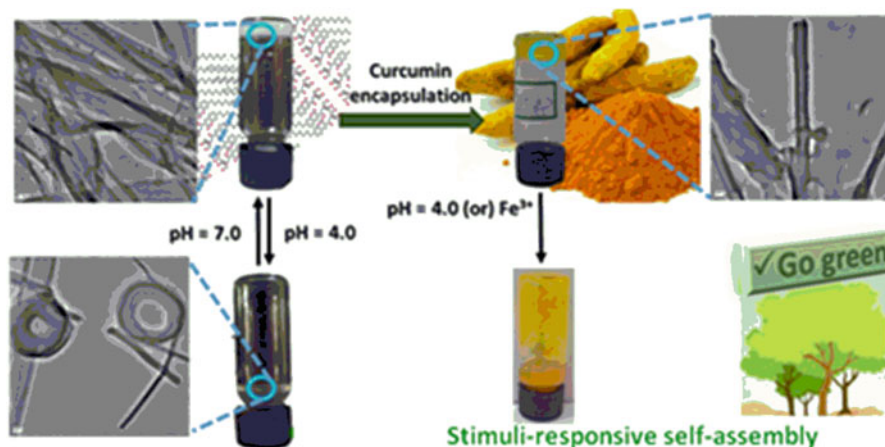
Fig. 3.19 Photograph of the reversible conversion of gel-to-sol under various pH levels, the composite gel degradation under acidic pH/the presence of Fe^{3+} ions and its corresponding HRTEM image reprinted with permission of royal society of chemistry from (Lalitha et al. 2015)

development of curcumin-based metal complexes as anticancer agents (e.g., zinc (II) complexes of curcumin display moderate cytotoxicity against prostate cancer and neuroblastoma cell lines) (Banerjee and Chakravarty 2015)

Nagarajan et al. reported the design and synthesis of renewable resource-derived coumarin-tris derivatives that self-assemble into hydrogels (Lalitha et al. 2015). The reversible morphological transition was observed from nanofibers to vesicles and nanotubes with the pH variation (Lalitha et al. 2015). The existence of π–π stacking and hydrogen bonding interactions as the driving force for gelation process was confirmed with ^{1}H NMR and XRD studies (Lalitha et al. 2015). Rheological investigations revealed the viscoelastic behavior of the hydrogel. The potential usage of this stimuli-responsive gel was demonstrated by encapsulating the chemo-preventive drug, curcumin, into the gel and its subsequent release induced by pH and or Fe^{3+} stimuli (Fig. 3.19) (Lalitha et al. 2015).

3.3 Rare Earth Metals in Medical Applications

Owing to the unique magnetic, catalytic, and optical properties, lanthanides are used as vehicles to deliver the drug/gene, as sensitizers in photodynamic cancer therapy and as contrast agents in magnetic resonance imaging (Palasz and Czekaj 2000). Lanthanides affect the biochemical pathways and alter the physiological processes in human tissues (Palasz and Czekaj 2000). For example, gadolinium and praseodymium protect the liver cells by inhibiting Kupffer cell secretion, reducing the activity of cytochrome P450m in hepatocytes (Palasz and Czekaj 2000). Trivalent lanthanum ions are commonly known as calcium analogs because of their similar ionic radii and

ligand specificities. Lanthanides such as La^{3+} and Gd^{3+} block calcium channels in human and animal cells, Dy^{3+} and La^{3+} block Ca^{2+}/Mg^{2+}-ATPase, and Eu^{3+} and Tb^{3+} inhibit calcineurin (Palasz and Czekaj 2000).

Lanthanum compounds can be used in the treatment and the prevention of bone diseases as they can suppress the osteoporosis effect and influence the bone remodeling cycle (Wieszczycka et al. 2019). Lanthanum's role in bone-building response is due to the osteoblasts stimulation by La^{3+} and reducing the osteoclast formation (Wieszczycka et al. 2019). Wieszczycka et al. have highlighted the significance of lanthanides and their compounds for bone regeneration and to treat orthopedic injuries (Wieszczycka et al. 2019).

3.4 Metal Nanoparticles in Health Applications

Silver nanoparticles are one of the most popular inorganic nanoparticles used in consumer products because of their antimicrobial properties. Silver is used as additives to produce textiles, injection-molded plastic products and coating materials with the antimicrobial activity. The rapid and significant antimicrobial activity of silver nanoparticles is due to the antibacterial action of silver nanoparticles on plasma membrane mediated via the shed of Ag^+ ions (Bondarenko et al. 2018). Silver nanoparticles can fragment the cell by inducing pits and gaps in the bacterial membrane (Zhang et al. 2016). As silver nanoparticles are potent antimicrobial agents, Qing et al. have discussed various methods of implant modifications, the enhancement of biocompatibility, and the cellular effects of palladium nanoparticles on osteogenic-related cells (Qing et al. 2018).

Silver nanoparticles coated with zinc(II) complex of lipoic acid-conjugated terpyridine (ZnLATP) were reported as a colorimetric assay for arginine (Velugula and Chinta 2017). These nanoparticles showed high selectivity towards arginine by exhibiting distinctive color change, among all the naturally occurring amino acids. The color change is due to arginine-induced aggregation of the silver nanoparticle ensemble (Fig. 3.20). The nanoparticle assay could be used for the detection arginine as low as 200 nM and has several advantages over the others due to their rapidness, simplicity, and selectivity. The applicability of this method was demonstrated by the quantification of arginine in supplement tablets. The method showed high accuracy and thus can be used for the quantification of arginine in biological samples.

Copper nanoparticles possess unique physical, chemical, biological, and antimicrobial activities. Copper chitosan nanoparticle antimicrobial activities and antifungal activities were evaluated by Usman et al. against several microorganisms including methicillin-resistant *S. aureus*, *B. subtilis*, *P. aeruginosa*, *C. albicans*, etc. and demonstrated their potential to combat pathogenic microorganism (Usman et al. 2013). The silicon nanowires were prepared by etching of crystalline silicon in $HF/AnNO_3$ aqueous solution (Fellahi et al. 2013). The silicon wire can be decorated with silver/copper nanoparticles by immersing in HF aqueous solution containing silver/copper salts (Fellahi et al. 2013). The silver nanoparticle-coated silicon wire
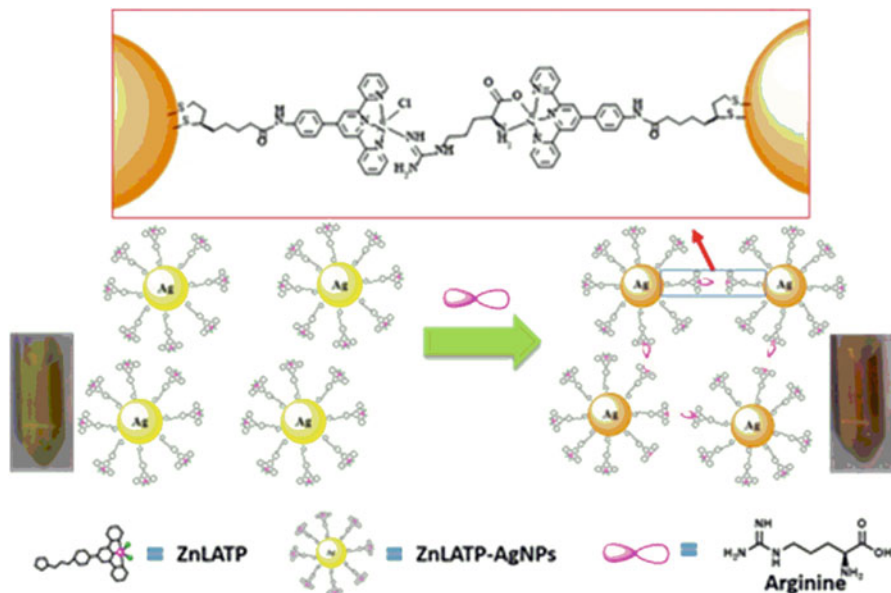
Fig. 3.20 Schematic representation of the principle involved in the colorimetric detection of arginine using zinc(II) complex of lipoic acid-conjugated terpyridine (ZnLATP)-coated silver nanoparticles reprinted with permission of Elsevier from (Velugula and Chinta 2017)

was found to be biocompatible with human lung cancer epithelial cell line, A549, and strong antimicrobial effect towards *E. coli*, whereas copper nanoparticle-coated silicon wire was found to have high cytotoxicity and comparatively low antibacterial activity (Fellahi et al. 2013). Wheate and co-workers have reported the synthesis of gold nanoparticle functionalized with thiolated poly(ethylene glycol) monolayer capped with a carboxylate group and complexed with [Pt(1R, 2R-diaminocyclohexane)(H$_2$O)$_2$]2NO$_3$ to enhance the delivery of anticancer drug oxaliplatin (Brown et al. 2010).

Gold nanoparticles (AuNPs) have emerged as promising agents in cancer nanotechnology, owing to their inherent nontoxicity, inertness, biocompatibility, high surface area to volume ratio, and multivalent surface structure favoring the incorporation of drug and/or biomacromolecules via covalent or non-covalent interactions (Rana et al. 2012). Hence these nanoparticles are extensively used as nanocarriers to deliver drugs, gene, proteins, radiosensitizers, etc. to enhance radiotherapy (Rana et al. 2012). Gold nanoparticles can be used in photothermal therapy due to its biocompatibility, capability to penetrate tumors upon systemic delivery, easy conjugation with the desired molecules, significant light to heat conversion, and easy tuning to absorb IR light (Rana et al. 2012). Riley and Day have explored the prospects and challenges for using gold nanoparticle-mediated photodynamic therapy in cancer treatment (Rana et al. 2012). Klajnert-Maculewicz and co-workers have highlighted the physiochemical properties of nanogold, kinetics of the release

of the drug, complexation/conjugation with nanocarriers, stability in different environmental conditions and their suitability as drug delivery devices, destruction of tumor tissue with the help of heat-activated factors, and as modulators of angiogenesis which may lead to the development of novel cancer treatment methods as an alternative for the most commonly used chemotherapeutics (Sztandera et al. 2019).

Neurological disorders can also be treated with metal complexes. For example, lithium is used in the treatment of various neurological disorders like Huntington's chorea, tardive dyskinesia, spasmodic torticollis, Tourette's syndrome, L-dopa-induced hyperkinesis, Parkinsonism, organic brain disorders, migraine, cluster headache, and periodic epilepsy (Rafique et al. 2010). The resynthesis of polyphosphoinositides involving inositol capture in the scavenging pathway is inhibited by lithium (Rafique et al. 2010). Similarly, zinc(II) is used to regulate the signaling component initiating the neuroprotective pathway (Rafique et al. 2010).

3.5   Conclusion

Besides the limitations, metal and metal complexes are widely used in every walk of life. Recently, owing to technological improvement, the usage of metal complexes for medicinal purposes is gaining importance. Nowadays, the metal complexes are used to replace a number of age-old drugs, in addition to their use as a remedy for a number of deadly diseases. In our day-to-day life, metals play a vital role ranging from home appliances to space crafts. Hence the metals and metal complexes may become an ideal solution for a number of problems in near future.

References

Astolfi L, Ghiselli S, Guaran V, Chicca M, Simoni E, Olivetto E et al (2013) Correlation of adverse effects of cisplatin administration in patients affected by solid tumours: a retrospective evaluation. Oncol Rep 29(4):1285–1292. https://doi.org/10.3892/or.2013.2279

Banerjee S, Chakravarty AR (2015) Metal complexes of curcumin for cellular imaging, targeting, and photoinduced anticancer activity. Acc Chem Res 48(7):2075–2083. https://doi.org/10.1021/acs.accounts.5b00127

Banerjee S, Dixit A, Shridharan RN, Karande AA, Chakravarty AR (2014) Endoplasmic reticulum targeted chemotherapeutics: the remarkable photo-cytotoxicity of an oxovanadium(IV) vitamin-B6 complex in visible light. Chem Commun 50(42):5590–5592. https://doi.org/10.1039/c4cc02093f

Begley TP, Williams RJP (2008) Metallo-enzymes and metallo-proteins. In: Chemistry of. Wiley encyclopedia of chemical biology. Wiley, Hoboken, pp 1–8. https://doi.org/10.1002/9780470048672.wecb327

Bergamo A, Masi A, Dyson PJ, Sava G, Onlus CF, Fleming VA (2008) Modulation of the metastatic progression of breast cancer with an organometallic ruthenium compound. Int J Oncol 33:1281–1289. https://doi.org/10.3892/ijo

Bergamo A, Gaiddon C, Schellens JHM, Beijnen JH, Sava G (2012) Approaching tumour therapy beyond platinum drugs: status of the art and perspectives of ruthenium drug candidates. J Inorg Biochem 106(1):90–99. https://doi.org/10.1016/j.jinorgbio.2011.09.030

Bondarenko OM, Sihtmäe M, Kuzmičiova J, Ragelienė L, Kahru A, Daugelavičius R (2018) Plasma membrane is the target of rapid antibacterial action of silver nanoparticles in escherichia coli and Pseudomonas aeruginosa. Int J Nanomedicine 13:6779–6790. https://doi.org/10.2147/IJN.S177163

Brabec V, Nováková O (2006) DNA binding mode of ruthenium complexes and relationship to tumor cell toxicity. Drug Resist Updat 9(3):111–122. https://doi.org/10.1016/j.drup.2006.05.002

Bresciani G, da Cruz IBM, González-Gallego J (2015) Manganese superoxide dismutase and oxidative stress modulation. Adv Clin Chem 68:87–130. https://doi.org/10.1016/bs.acc.2014.11.001

Brown SD, Nativo P, Smith JA, Stirling D, Edwards PR, Venugopal B et al (2010) Gold nanoparticles for the improved anticancer drug delivery of the active component of oxaliplatin. J Am Chem Soc 132(13):4678–4684. https://doi.org/10.1021/ja908117a

Censi V, Caballero AB, Pérez-Hernández M, Soto-Cerrato V, Korrodi-Gregório L, Pérez-Tomás R et al (2019) DNA-binding and in vitro cytotoxic activity of platinum(II) complexes of curcumin and caffeine. J Inorg Biochem 198(February):110749. https://doi.org/10.1016/j.jinorgbio.2019.110749

Chen L, Fu C, Deng Y, Wu W, Fu A (2016) A pH-sensitive nanocarrier for tumor targeting: delivery of ruthenium complex for tumor theranostic by pH-sensitive nanocapsule. Pharm Res 33(12):2989–2998

Cummings SD (2009) Platinum complexes of terpyridine : interaction and reactivity with biomolecules. Coord Chem Rev 253:1495–1516. https://doi.org/10.1016/j.ccr.2008.12.009

de Oliveira Silva D (2012) Perspectives for novel mixed diruthenium-organic drugs as metallopharmaceuticals in cancer therapy. Anti Cancer Agents Med Chem 10(4):312–323. https://doi.org/10.2174/187152010791162333

Fang Y, Wang YT, Zhao M, Lu YL, Li MX, Zhang YH (2018) Bismuth(III) and diorganotin (IV) complexes of bis(2-acetylpyridine) thiocarbonohydrazone: synthesis, characterization, and apoptosis mechanism of action in vitro. Polyhedron 24(49):495101. https://doi.org/10.1016/j.poly.2018.08.049

Fellahi O, Sarma RK, Das MR, Saikia R, Marcon L, Coffinier Y et al (2013) The antimicrobial effect of silicon nanowires decorated with silver and copper nanoparticles. Nanotechnology 24 (49):495101. https://doi.org/10.1088/0957-4484/24/49/495101

Fernández-Moreira V, Herrera RP, Gimeno MC (2019) Anticancer properties of gold complexes with biologically relevant ligands. Pure Appl Chem 91(2):247–269. https://doi.org/10.1515/pac-2018-0901

Ferraz KSO, Reis DC, Da Silva JG, Souza-Fagundes EM, Baran EJ, Beraldo H (2013) Investigation on the bioactivities of clioquinol and its bismuth(III) and platinum(II, IV) complexes. Polyhedron 63:28–35. https://doi.org/10.1016/j.poly.2013.07.008

Garner ME, Niu W, Chen X, Ghiviriga I, Abboud KA, Tan W, Veige AS (2015) N-heterocyclic carbene gold(i) and silver(i) complexes bearing functional groups for bio-conjugation. Dalton Trans 44(4):1914–1923. https://doi.org/10.1039/c4dt02850c

Garrison JC, Youngs WJ (2005) Ag(I) N-heterocyclic carbene complexes: synthesis, structure, and application. Chem Rev 105(11):3978–4008. https://doi.org/10.1021/cr050004s

Groves LM, Williams CF, Hayes AJ, Ward BD, Isaacs MD, Symonds NO et al (2019) Fluorescent functionalised naphthalimides and their Au(i)-NHC complexes for potential use in cellular bioimaging. Dalton Trans 48(5):1599–1612. https://doi.org/10.1039/c8dt04069a

Hanif-Ur-Rehman, Freitas TE, Gomes RN, Colquhoun A, de Oliveira Silva D (2016) Axially-modified paddlewheel diruthenium(II,III)-ibuprofenato metallodrugs and the influence of the structural modification on U87MG and A172 human glioma cell proliferation, apoptosis, mitosis and migration. J Inorg Biochem 165:181–191. https://doi.org/10.1016/j.jinorgbio.2016.10.003

Hartinger CG, Jakupec MA, Zorbas-Seifried S, Groessl M, Egger A, Berger W et al (2008) KP1019, a new redox-active anticancer agent – preclinical development and results of a clinical phase I study in tumor patients. Chem Biodivers 5(10):2140–2155. https://doi.org/10.1002/cbdv.200890195

Holtz RD, Lima BA, Souza Filho AG, Brocchi M, Alves OL (2012) Nanostructured silver vanadate as a promising antibacterial additive to water-based paints. Nanomedicine 8(6):935–940. https://doi.org/10.1016/j.nano.2011.11.012

Jaros SW, Śliwińska-Hill U, Białońska A, Nesterov DS, Kuropka P, Sokolnicki J et al (2019) Light-stable polypyridine silver(i) complexes of 1,3,5-triaza-7-phosphaadamantane (PTA) and 1,3,5-triaza-7-phosphaadamantane-7-sulfide (PTA=S): significant antiproliferative activity of representative examples in aqueous media. Dalton Trans 48(30):11235–11249. https://doi.org/10.1039/c9dt01646e

Jia P, Ouyang R, Cao P, Tong X, Zhou X, Lei T et al (2017) Review: recent advances and future development of metal complexes as anticancer agents. J Coord Chem 70(13):2175–2201. https://doi.org/10.1080/00958972.2017.1349313

Johnson NA, Southerland MR, Youngs WJ (2017) Recent developments in the medicinal applications of silver-nhc complexes and imidazolium salts. Molecules 22(8):1263. https://doi.org/10.3390/molecules22081263

Jungwirth U, Kowol CR, Keppler BK, Christian G (2012) Europe PMC Funders Group anticancer activity of metal complexes: involvement of redox processes. Antioxid Redox Signal 15 (4):1085–1127. https://doi.org/10.1089/ars.2010.3663.Anticancer

Kenny RG, Marmion CJ (2019) Toward multi-targeted platinum and ruthenium drugs – a new paradigm in cancer drug treatment regimens? Chem Rev. Review-article, American Chemical Society. https://doi.org/10.1021/acs.chemrev.8b00271

Kilian K, Pęgier M, Pyrzyńska K (2016) The fast method of Cu-porphyrin complex synthesis for potential use in positron emission tomography imaging. Spectrochim Acta A Mol Biomol Spectrosc 159:123–127. https://doi.org/10.1016/j.saa.2016.01.045

Kowalik M, Masternak J, Barszcz B (2017) Recent research trends on bismuth compounds in cancer chemo and radiotherapy. Curr Med Chem 26(4):729–759. https://doi.org/10.2174/0929867324666171003113540

Kuhn PS, Pichler V, Roller A, Hejl M, Jakupec MA, Kandioller W, Keppler BK (2015) Improved reaction conditions for the synthesis of new NKP-1339 derivatives and preliminary investigations on their anticancer potential. Dalton Trans 44(2):659–668. https://doi.org/10.1039/c4dt01645a

Kumar A, Prakash Chinta J, Kumar Ajay A, Kumar Bhat M, Rao CP (2011) Synthesis, characterization, plasmid cleavage and cytotoxicity of cancer cells by a copper(ii) complex of anthracenyl-terpyridine. Dalton Trans 40(41):10865–10872. https://doi.org/10.1039/C1DT10201J

Lalitha K, Prasad YS, Maheswari CU, Sridharan V, John G, Nagarajan S (2015) Stimuli responsive hydrogels derived from a renewable resource: synthesis, self-assembly in water and application in drug delivery. J Mater Chem B 3(27):5560–5568. https://doi.org/10.1039/c5tb00864f

Lalitha K, Sandeep M, Prasad YS, Sridharan V, Maheswari CU, Srinandan CS, Nagarajan S (2017) Intrinsic hydrophobic antibacterial thin film from renewable resources: application in the development of anti-biofilm urinary catheters. ACS Sustain Chem Eng 5(1):436–449. https://doi.org/10.1021/acssuschemeng.6b01806

Lazarević T, Rilak A, Bugarčić ŽD (2017) Platinum, palladium, gold and ruthenium complexes as anticancer agents: current clinical uses, cytotoxicity studies and future perspectives. Eur J Med Chem 142:8–31. https://doi.org/10.1016/j.ejmech.2017.04.007

Leijen S, Burgers SA, Baas P, Pluim D, Tibben M, Van Werkhoven E et al (2015) Phase I/II study with ruthenium compound NAMI-A and gemcitabine in patients with non-small cell lung cancer after first line therapy. Investig New Drugs 33(1):201–214. https://doi.org/10.1007/s10637-014-0179-1

Li M, Lu Y, Yang M, Li Y, Zhang L, Xie S (2012) One dodecahedral bismuth(iii) complex derived from 2-acetylpyridine N(4)-pyridylthiosemicarbazone: synthesis, crystal structure and biological evaluation. Dalton Trans 41(41):12882–12887. https://doi.org/10.1039/c2dt31256e

Li JJ, Tian Z, Ge X, Xu Z, Feng Y, Liu Z (2019a) Design, synthesis, and evaluation of fluorine and Naphthyridine–based half-sandwich organoiridium/ruthenium complexes with bioimaging and anticancer activity. Eur J Med Chem 163:830–839. https://doi.org/10.1016/j.ejmech.2018.12.021

Li Z, Zhou J, Gan Y, Yin Y, Zhang W, Yang J et al (2019b) Synthesis of a novel platinum (II) complex with 6,7-dichloro-5,8-quinolinedione and the study of its antitumor mechanism in testicular seminoma. J Inorg Biochem 197(April):110701. https://doi.org/10.1016/j.jinorgbio.2019.110701

Liang X, Luan S, Yin Z, He M, He C, Yin L et al (2018) Recent advances in the medical use of silver complex. Eur J Med Chem 157:62–80. https://doi.org/10.1016/j.ejmech.2018.07.057

Lin K, Zhao ZZ, Bo HB, Hao XJ, Wang JQ (2018) Applications of ruthenium complex in tumor diagnosis and therapy. Front Pharmacol 9(November):1–10. https://doi.org/10.3389/fphar.2018.01323

Luengo A, Fernández-Moreira V, Marzo I, Gimeno MC (2017) Trackable metallodrugs combining luminescent Re(I) and bioactive Au(I) fragments. Inorg Chem 56(24):15159–15170. https://doi.org/10.1021/acs.inorgchem.7b02470

Lv G, Qiu L, Liu G, Wang W, Li K, Zhao X, Lin J (2016) pH sensitive chitosan-mesoporous silica nanoparticles for targeted delivery of a ruthenium complex with enhanced anticancer effects. Dalton Trans 45(45):18147–18155

Ma DL, Ng HP, Wong SY, Vellaisamy K, Wu KJ, Leung CH (2018) Iridium(iii) complexes as reaction based chemosensors for medical diagnostics. Dalton Trans 47(43):15278–15282. https://doi.org/10.1039/C8DT03492C

Mandal P, Kundu BK, Vyas K, Sabu V, Helen A, Dhankhar SS et al (2018) Ruthenium(II) arene NSAID complexes: inhibition of cyclooxygenase and antiproliferative activity against cancer cell lines. Dalton Trans 47(2):517–527. https://doi.org/10.1039/c7dt03637j

Mansour AM, Bakry EME, Abdel-Ghani NT (2016) Flubendazole Pd(II) complexes: structural studies, cytotoxicity, and quantum chemical calculations. J Iran Chem Soc 13(8):1429–1437. https://doi.org/10.1007/s13738-016-0858-2

Milacic V, Dou QP (2009) The tumor proteasome as a novel target for gold(III) complexes: implications for breast cancer therapy. Coord Chem Rev 253(11–12):1649–1660. https://doi.org/10.1016/j.ccr.2009.01.032

Miller RP, Tadagavadi RK, Ramesh G, Reeves WB (2010) Mechanisms of cisplatin nephrotoxicity. Toxins 2(11):2490–2518. https://doi.org/10.3390/toxins2112490

Miriyala S, Spasojevic I, Tovmasyan A, Salvemini D, Vujaskovic Z, St. Clair D, Batinic-Haberle I (2012) Manganese superoxide dismutase, MnSOD and its mimics. Biochim Biophys Acta Mol basis Dis 1822(5):794–814. https://doi.org/10.1016/j.bbadis.2011.12.002

Muskawar PN, Karthikeyan P, Aswar SA, Bhagat PR, Senthil Kumar S (2016) NHC–metal complexes based on benzimidazolium moiety for chemical transformation: 1st cancer update. Arab J Chem 9:S1765–S1778. https://doi.org/10.1016/j.arabjc.2012.04.040

Navarro M (2009) Gold complexes as potential anti-parasitic agents. Coord Chem Rev 253:1619–1626. https://doi.org/10.1016/j.ccr.2008.12.003

Norn S, Permin H, Kruse E, Kruse PR (2008) Mercury – a major agent in the history of medicine and alchemy. [Danish] Kviksolv – et centralt stof i medicinens og alkymiens historie. Dan Medicinhist Arbog

Ouyang R, Yang Y, Feng K, Zong T, Cao P, Xiong F et al (2017) Potent anticancer activity of a new bismuth (III) complex against human lung cancer cells. J Inorg Biochem 168:18–26. https://doi.org/10.1016/j.jinorgbio.2016.12.006

Palasz A, Czekaj P (2000) Toxicological and cytophysiological aspects of lanthanides action. Acta Biochim Pol 47:1107–1114

Prabusankar G, Muthukumaran N, Vaddamanu M, Raju G, Velappan K, Sathyanarayana A et al (2019) Blue-emitting acridine-tagged silver(i)-bis-N-heterocyclic carbene. RSC Adv 9 (13):7543–7550. https://doi.org/10.1039/c9ra00281b

Qing Y, Cheng L, Li R, Liu G, Zhang Y, Tang X et al (2018) Potential antibacterial mechanism of silver nanoparticles and the optimization of orthopedic implants by advanced modification technologies. Int J Nanomedicine 13:3311–3327. https://doi.org/10.2147/IJN.S165125

Rafique S, Idrees M, Nasim A, Akbar H, Athar A (2010) Transition metal complexes as potential therapeutic agents. Biotechnol Mol Biol Rev 5(2):38–45

Rana S, Bajaj A, Mout R, Rotello VM (2012) Monolayer coated gold nanoparticles for delivery applications. Adv Drug Deliv Rev 64(2):200–216. https://doi.org/10.1016/j.addr.2011.08.006

Rojas S, Carmona FJ, Barea E, Maldonado CR (2017) Inorganic mesoporous silicas as vehicles of two novel anthracene-based ruthenium metalloarenes. J Inorg Biochem 166:87–93

Silconi ŽB, Benazic S, Milovanovic J, Arsenijevic A, Stojanovic B, Milovanovic M, Kanjevac T (2016) Platinum complexes and their anti-tumour activity against chronic lymphocytic leukaemia cells. Serbian J Exp Clin Res 16(3):181–186. https://doi.org/10.1515/sjecr-2015-0023

Spasojević I, Batinić-Haberle I, Stevens RD, Hambright P, Thorpe AN, Grodkowski J et al (2001) Manganese(III) biliverdin IX dimethyl ester: a powerful catalytic scavenger of superoxide employing the Mn(III)/Mn(IV) redox couple. Inorg Chem 40:726. https://doi.org/10.1021/ic0004986

Sztandera K, Gorzkiewicz M, Klajnert-Maculewicz B (2019) Gold nanoparticles in cancer treatment. Mol Pharm 16(1):1–23. https://doi.org/10.1021/acs.molpharmaceut.8b00810

Tanaka M, Kataoka H, Yano S, Ohi H, Kawamoto K, Shibahara T et al (2013) Anti-cancer effects of newly developed chemotherapeutic agent, glycoconjugated palladium (II) complex, against cisplatin-resistant gastric cancer cells. BMC Cancer 13(1):1. https://doi.org/10.1186/1471-2407-13-237

Thangavel P, Viswanath B, Kim S (2017) Recent developments in the nanostructured materials functionalized with ruthenium complexes for targeted drug delivery to tumors. Int J Nanomedicine 12:2749. https://doi.org/10.2147/IJN.S131304

Thota S, Rodrigues DA, Crans DC, Barreiro EJ (2018) Ru(II) compounds: next-generation anticancer metallotherapeutics? J Med Chem. Review-article, American Chemical Society. https://doi.org/10.1021/acs.jmedchem.7b01689

Turel I (2015) Special issue: practical applications of metal complexes. Molecules 20 (5):7951–7956. https://doi.org/10.3390/molecules20057951

Umar Ndagi, Ndumiso Mhlongo MES (2017) Metal complexes in cancer therapy an update from drug design perspective. Drug Des Devel Ther 11:599–616. https://doi.org/10.2147/DDDT.S119488

Usman MS, El Zowalaty ME, Shameli K, Zainuddin N, Salama M, Ibrahim NA (2013) Synthesis, characterization, and antimicrobial properties of copper nanoparticles. Int J Nanomedicine 8:4467–4479. https://doi.org/10.2147/IJN.S50837

Vaidya MY, McBain AJ, Butler JA, Banks CE, Whitehead KA (2017) Antimicrobial efficacy and synergy of metal ions against Enterococcus faecium, Klebsiella pneumoniae and Acinetobacter baumannii in planktonic and biofilm phenotypes. Sci Rep 7(1):1–9. https://doi.org/10.1038/s41598-017-05976-9

Velugula K, Chinta JP (2017) Silver nanoparticles ensemble with Zn(II) complex of terpyridine as a highly sensitive colorimetric assay for the detection of Arginine. Biosens Bioelectron 87:271–277. https://doi.org/10.1016/j.bios.2016.08.023

Visbal R, Fernández-Moreira V, Marzo I, Laguna A, Gimeno MC (2016) Cytotoxicity and biodistribution studies of luminescent Au(i) and Ag(i) N-heterocyclic carbenes. Searching for new biological targets. Dalton Trans 45(38):15026–15033. https://doi.org/10.1039/c6dt02878k

Wang N, Feng Y, Zeng L, Zhao Z, Chen T (2015) Functionalized multiwalled carbon nanotubes as carriers of ruthenium complexes to antagonize cancer multidrug resistance and radioresistance. ACS Appl Mater Interfaces 7:14933–14945

Wieszczycka K, Staszak K, Woźniak-Budych MJ, Jurga S (2019) Lanthanides and tissue engineering strategies for bone regeneration. Coord Chem Rev 388:248–267. https://doi.org/10.1016/j.ccr.2019.03.003

Williams MRM, Bertrand B, Hughes DL, Waller ZAE, Schmidt C, Ott I et al (2018) Cyclometallated Au(iii) dithiocarbamate complexes: synthesis, anticancer evaluation and mechanistic studies. Metallomics 10(11):1655–1666. https://doi.org/10.1039/c8mt00225h

Xue SS, Tan CP, Chen MH et al (2017) Tumor-targeted supramolecular nanoparticles self-assembled from a ruthenium-β-cyclodextrin complex and an adamantane-functionalized peptide. Chem Commun (Camb) 53(5):842–845

Yang Y, Guo L, Ge X, Tian Z, Gong Y, Zheng H et al (2019) Novel lysosome-targeted cyclometalated Iridium(III) anticancer complexes containing imine-N-heterocyclic carbene ligands: synthesis, spectroscopic properties and biological activity. Dyes Pigments 161 (iii):119–129. https://doi.org/10.1016/j.dyepig.2018.09.044

Yilmaz VT, Icsel C, Batur J, Aydinlik S, Cengiz M, Buyukgungor O (2017) Synthesis, structures and biomolecular interactions of new silver(i) 5,5-diethylbarbiturate complexes of monophosphines targeting Gram-positive bacteria and breast cancer cells. Dalton Trans 46 (25):8110–8124. https://doi.org/10.1039/c7dt01286a

Yu Z, Fenk KD, Huang D, Sen S, Cowan JA (2019) Rapid telomere reduction in cancer cells induced by G-quadruplex-targeting copper complexes. J Med Chem 62(10):5040–5048. https://doi.org/10.1021/acs.jmedchem.9b00215

Zhang P, Huang H, Huang J, Chen H, Wang J, Qiu K, Zhao D, Ji L, Chao H (2015) Noncovalent ruthenium (II) complexes–single-walled carbon nanotube composites for bimodal photothermal and photodynamic therapy with near-infrared irradiation. ACS Appl Mater Interfaces 7:23278–23290

Zhang XF, Liu ZG, Shen W, Gurunathan S (2016) Silver nanoparticles: synthesis, characterization, properties, applications, and therapeutic approaches. Int J Mol Sci 17(9):1534. https://doi.org/10.3390/ijms17091534

Zhao Z, Zhang J, Zhi S, Song W, Zhao J (2019) Novel binuclear and trinuclear metal (II) complexes: DNA interactions and in vitro anticancer activity through apoptosis. J Inorg Biochem 197(April):110696. https://doi.org/10.1016/j.jinorgbio.2019.110696

Chapter 4
Therapeutic Potential of Metals in Managing the Metabolic Syndrome

Rajesh Parsanathan and Sankar Jagadeeshan

Contents

R. Parsanathan (✉)
Department of Pediatrics and Centre for Cardiovascular Diseases and Sciences, Louisiana State University Health Sciences Center, Shreveport, LA, USA

S. Jagadeeshan
The Shraga Segal Department of Microbiology, Immunology, and Genetics, Faculty of Health Sciences, Ben-Gurion University of the Negev, Beer-Sheva, Israel

Abstract The metabolic syndrome is a major public health issue worldwide with a cluster of risk factors, which predicts future type 2 diabetes and cardiovascular disease-related morbidity and mortality. Oxidative stress may be a prognostic marker for metabolic syndrome. Uncontrolled generation of free radicals leads later to disease. Accumulating evidence suggests a link between the importance of trace elements such as zinc, chromium, copper, magnesium, manganese, and iron and its potential benefits for metabolic syndrome. On the one side, metabolic syndrome affects trace elements homeostasis in a many-faceted fashion. This chapter deals with indispensable essential trace element minerals (metals) both in excess and deficient amounts in the metabolic syndrome conditions such as insulin resistance, diabetes, obesity, and cardiovascular diseases; and its therapeutic potential is also discussed. Understanding the therapeutic usages of metals and the risk factors of excessively using them may yield valuable insights into the pathophysiology and prevention of metabolic syndrome in a high-risk population at an early stage.

Keywords Metals · Metabolic syndrome · Diabetes · Obesity · Cardiovascular diseases · Reactive oxygen species · Nonalcoholic fatty liver disease

List of Abbreviations

CVD   Cardiovascular disease
NAFLD   Nonalcoholic fatty liver disease
ROS   Reactive oxygen species
T2DM   Type 2 diabetes mellitus

4.1   Introduction

Metal ions play crucial roles in the biological system and human health. Their deficiency may lead to several diseases in human, and many enzymes require metals for their catalytic action. They have also been exploited to treat several conditions associated with metabolisms such as diabetes and cancer.

However, a few metal ions can be dangerous due to their toxic effects on a biological system, mostly heavy metal ions, such as lead and mercury. Few essential

Fig. 4.1 *Metals that are essential for normal biological functions in humans* are [1] calcium (Ca), magnesium (Mg), sodium (Na), and potassium (K), that belong to most important group of elements [2], and transition metal group – cadmium (Cd), chromium (Cr), cobalt (Co), copper (Cu), iron (Fe), manganese (Mn), molybdenum (Mo), nickel (Ni), vanadium (V), and zinc (Zn). Notably, among these metals which exist in the form of ions are Fe, Co, Ni, Ca, Cu, Zn, and Cr
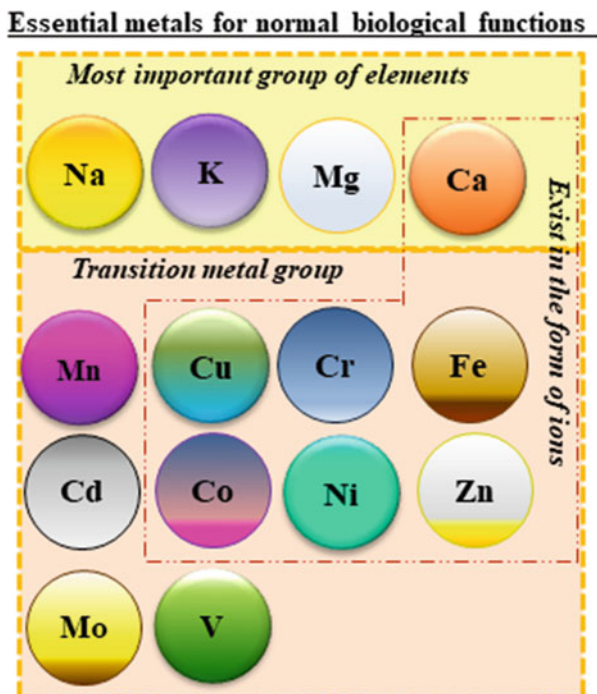
metal ions can also be toxic at excess level, but their presence is necessary for health and survival. Metals that are essential for normal biological functions in humans are [1] calcium (Ca), magnesium (Mg), sodium (Na), and potassium (K), which belong to the most important group of elements [2], and transition metal group – cadmium (Cd), chromium (Cr), cobalt (Co), copper (Cu), iron (Fe), manganese (Mn), molybdenum (Mo), nickel (Ni), vanadium (V), and zinc (Zn). Notably, among these metals which exist in the form of ions are Fe, Co, Ni, Ca, Cu, Zn, and Cr (Fig. 4.1).

Accumulating evidence suggests a link between the importance of trace elements such as Zn, Cu, and Fe and its potential benefits for metabolic syndrome (Aguilar et al. 2007). On the one side, metabolic syndrome affects trace elements homeostasis in a many-faceted fashion. Population-based interventions aimed at halting the increasing prevalence of metabolic syndrome require a thorough understanding of dietary interplays such as nutrients, vitamins, and mineral trace elements (metals). To halting the global incidence of metabolic syndrome and its associated complications, by emerging promising approaches such as metal chelation/depletion/reductive therapies in excess conditions or metal supplementation therapies during deficient status maybe use in the overall management of the screening, diagnosis, and treatment of at-risk subjects/patients.

This chapter has examined indispensable essential trace element minerals (metals) both in excess or deficient amounts in the metabolic syndrome conditions such as insulin resistance, diabetes, obesity, and cardiovascular diseases (CVD); and

its therapeutic potential is also discussed. Understanding the therapeutic usages of bodily metals and the risk factors of excessively using them may yield valuable insights into the pathophysiology and prevention of metabolic syndrome in a high-risk population at an early stage.

4.2 Metabolic Syndrome and Oxidative Stress

Metabolic syndrome is a major public health issue worldwide with a cluster of risk factors, which predicts future type 2 diabetes mellitus (T2DM) and CVD-related morbidity and mortality. Hence, metabolic syndrome is a common and complex disorder combining obesity, dyslipidemia, hypertension, and insulin resistance (Fig. 4.2) as the primary risk factors for the onset or progression of diabetes and CVD (Hutcheson and Rocic 2012; Manna and Jain 2015; Roberts and Sindhu 2009). Diabetes is increasing at an alarming rate (Jayawardena et al. 2012).

Free radicals appear to be essential modulators of metabolic syndrome in all stages of development and progression (Rains and Jain 2011). Physiologically, they are signal transducers in cell communication and homeostasis, including gene expression and cell interactions (Kunsch and Medford 1999). Uncontrolled generation of free radicals leads later to disease. Oxidative stress may be a prognostic marker for metabolic syndrome (Vichova and Motovska 2013). The primary sources

Fig. 4.2 *Role of metals on metabolic syndrome.* Metals at physiological range inhibit redox imbalances (free radical generation/oxidative stress) and prevent metabolic syndrome. Either deficient or excess conditions induce oxidative stress and favor metabolic syndrome and related complications
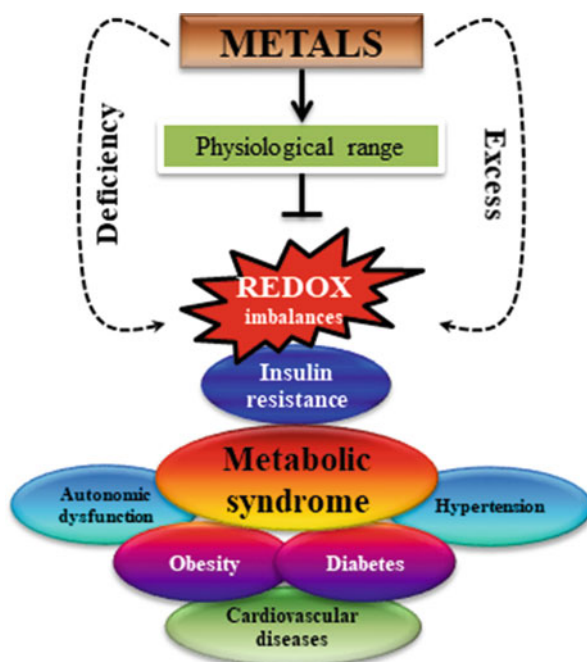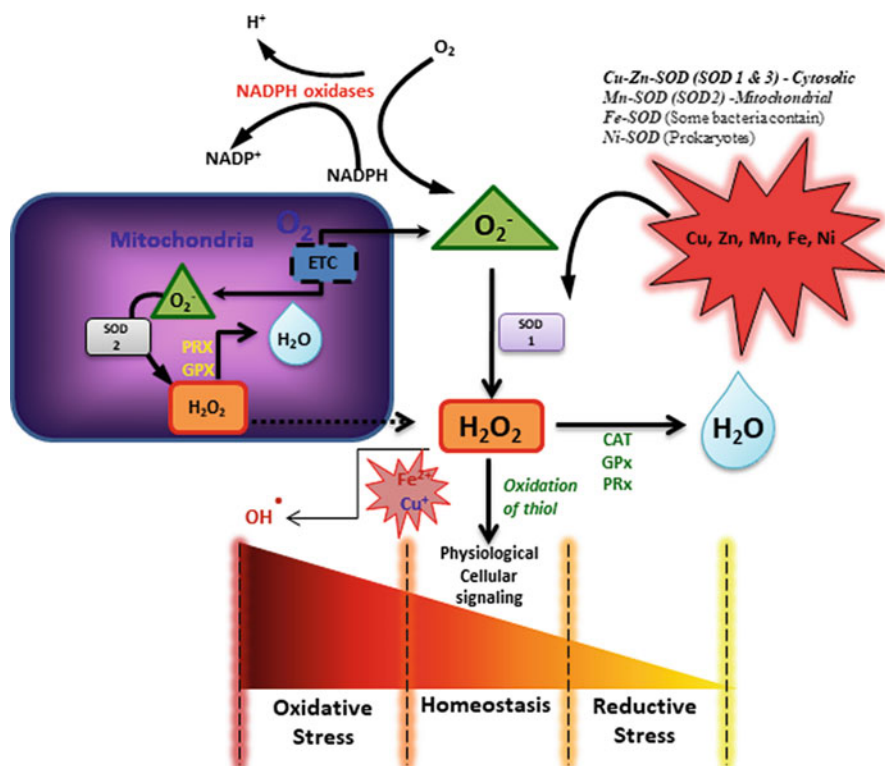
Fig. 4.3 *Role of metals (Cu, Zn, Mn, Fe, Ni) on redox mechanisms*. Mitochondria generate superoxides (O_2^{-}) which are then converted to hydrogen peroxide (H_2O_2) either by mitochondrial–manganese superoxide dismutase (Mn-SOD) or cytosolic Cu/Zn SOD which maintains physiological homeostasis. Further, H_2O_2 is converted to water (H_2O) by catalase (CAT) and other peroxidases (GPx, PRx). Iron and copper (Fe^{2+}, Cu^{+}) are involved in the production of hydroxyl radical (OH·) which induces oxidative stress. Either excess or deficiency of these metals causes oxidative stress which leads to metabolic disorders

of ROS (reactive oxygen species) are mitochondrial NADPH oxidases (NOX) (Cervantes Gracia et al. 2017). It has been shown that increased renin–angiotensin–aldosterone system activity stimulates NADH/NADPH oxidase (Griendling et al. 1994; Rajagopalan et al. 1996).

The critical role of oxidative stress in metabolic syndrome pathophysiology has encouraged quantification of ROS as a promising biomarker reflecting the disease process (Fig. 4.3). However, the transitory nature and short half-life confound in the measurements of ROS by standard approaches such as spin-trapping (Griendling and FitzGerald 2003) method.

4.3   Metals and Metabolic Syndrome

Various studies on animals and humans have shown that supplementation with metals, such as zinc, chromium, magnesium, manganese, vanadium, and cobalt, can have potential benefits to prevent metabolic syndrome (Lee et al. 2013; Panchal et al. 2017; Ranasinghe et al. 2015; Shahbah et al. 2017) (Fig. 4.2). Metal compounds induce hypoglycemia by a wide variety of mechanisms such as antioxidant properties (cobalt, magnesium), activation of insulin receptor signaling (chromium), inhibition of the formation of too many phosphates (vanadium), stimulation of glucose uptake (chromium and cobalt), and stimulation of activities of gluconeogenic enzymes (manganese) (Sakurai et al. 2010; Wiernsperger and Rapin 2010).

A study carried out on diabetic patients showed they had deficient levels of chromium, manganese, and zinc in their blood (Forte et al. 2013). However, some metals can be toxic. Other toxic metals that induce high levels of ROS are arsenic, cadmium, mercury, and lead (Sharma et al. 2014; Tchounwou et al. 2012). Research has shown that some toxic metals, such as As, Cd, Hg, and Pb induce oxidative stress by increasing the concentration of ROS (Sharma et al. 2014; Tchounwou et al. 2012) (Fig. 4.3). This increase in ROS can harm islet β-cells because these cells have a weak antioxidant defense system.

Studies show that the concentration of toxic metals is higher in diabetic patients than in nondiabetic patients (Chen et al. 2009). Some metals appear to affect diabetes through body weight changes. For example, a study showed that ingesting Pb during development caused higher food intake, higher body weight, and body fat (Faulk et al. 2014).

4.4   Metals and Oxidative Stress

Oxidative pentose phosphate pathway (OPPP) plays numerous fundamental roles, such as biosynthesizing precursors for nucleic acids and fatty acids, providing NADPH essential for primary metabolism and oxidizing GSSG to be reduced to GSH (a vital major cellular antioxidant) (Parsanathan and Jain 2018a), and counteracting oxidative stress (Jain et al. 2018; Parsanathan and Jain 2019b). The crucial role in the whole process is played by glucose-6-phosphate dehydrogenase (G6PD), by catalytic conversion of glucose-6-phosphate (G-6-P) to 6-phosphogluconate in the presence of $NADP^+$ (Parsanathan and Jain 2018b, 2019a).

Magnesium (Mg^{++}) has a positive regulatory role in G6PD activity (Sanwal 1970). Further, it was suggested that Mg^{++} could affect the oligomeric state of the enzyme in human placental and dog liver G6PD (Ozer et al. 2001; Ozer et al. 2002).

Metals such as Cu, Cd, Ni, and Zn may be competitively inhibiting G6PD with Mg^{++} and/or $NADP^+$ binding sites and can reduce the G6PD activity (De Lillo et al.
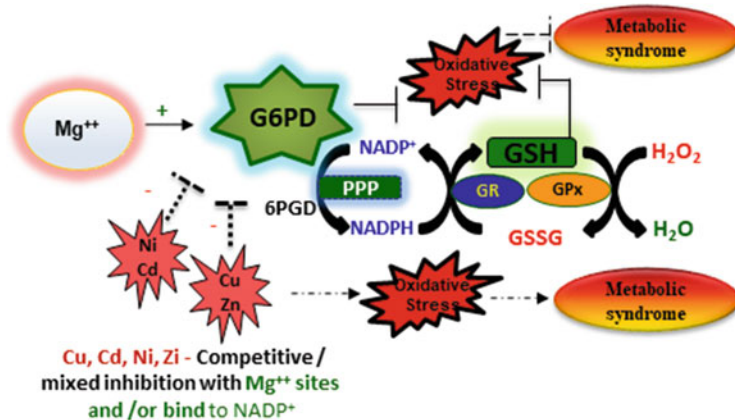
Fig. 4.4 *Role of metals on pentose phosphate pathway (PPP) enzyme glucose-6-phosphate dehydrogenase (G6PD) and oxidative stress*. Oxidative pentose phosphate pathway (OPPP) essentially provides NADPH for oxidizing glutathione/glutathione disulfide (GSSG) to be reduced to glutathione (GSH) (a major cellular antioxidant) and for counteracting oxidative stress. Glutathione reductase (GR) and glutathione peroxidase (GPx) are involved in the recycling process. Metals such as Cu, Cd, Ni, and Zn may be competitively or mixed inhibition with Mg^{++} and/or $NADP^+$ binding sites and reduces the G6PD activity, thus inducing oxidative stress and favoring metabolic syndrome

2018), thus inducing oxidative stress and favoring metabolic syndrome progression or onset (Fig. 4.4).

4.5 Calcium (Ca) Supplementation Prevents Diabetes

Calcium is an essential mineral that helps our bones grow (Zhu and Prince 2012) and muscles contract (Webb 2003). A large study, consisting of 41,186 subjects, found that individuals who had higher levels of calcium intake were at lower risk of developing T2DM compared to individuals who had lower levels of calcium intake (van Dam et al. 2006). An additional study showed that individuals who consumed more than 1200 mg/d of calcium had a 21% reduced risk of developing T2DM than those who consumed less than 600 mg/d (Pittas et al. 2006). It is heavily regarded that a diet rich in calcium can reduce one's risk of developing T2DM (Pittas et al. 2006; van Dam et al. 2006), and those who have diabetes have low calcium levels (Colditz et al. 1992; Pittas et al. 2006; van Dam et al. 2006).

According to a 2016 study, calcium intake is inversely related to fat mass, waist circumference, and obesity markers (Castro Burbano et al. 2016). Obese individuals had lower consumption of calcium in their diet compared to nonobese individuals (Castro Burbano et al. 2016). It is agreeable that high calcium intake can reduce the risk of diabetes and obesity, but according to a study done on Chinese women, how we consume calcium is the most important in regard to reducing risks of obesity. The

study compared the body composition of two groups of Chinese women; one group received 430 mg/d of calcium through food intake, while the other group received the same amount of calcium but through supplement intake. Results showed that the group of women who received calcium from food had greater beneficial effects on maintenance of body composition compared to the other group (Castro Burbano et al. 2016).

4.6   Chromium (Cr)

Chromium is an essential mineral that participates in carbohydrate and lipid metabolism. (San Mauro-Martin et al. 2016). Even though there is presence of several different oxidation states of Cr, biologically relevant form of chromium is the trivalent form Cr^{3+}. Chromium regulates insulin and blood glucose levels by stimulating insulin signaling pathway and metabolism by up-regulating glucose transporter (GLUT4) translocation in muscle cells (Qiao et al. 2009). Chromium deficiency induces an elevation of blood glucose levels, which can cause the onset of diabetes (Wiernsperger and Rapin 2010).

4.6.1   The Beneficial Role of Cr Supplementation in Diabetes

A study in 2016 looked at the effects of chromium supplementation in patients with diabetes. They reported that there were positive effects of chromium supplementation on glycemic control in diabetic patients (San Mauro-Martin et al. 2016). Another study looked at chromium methionine supplementation in mouse models and found that the supplementation had beneficial effects on glucose and lipid metabolism (Tang et al. 2015). Other studies have shown that chromium deficiency could cause diabetes and reversible insulin resistance (Freund et al. 1979; Vincent 2010).

Many minerals, such as chromium, serve as dietary supplements for obese individuals, but there have not been many studies done to prove the effectiveness of chromium as a supplement for overweight individuals. One study in 2013 showed that chromium supplementation could generate reductions in body weight, but the effect was minimal (Onakpoya et al. 2013). Another study looked at the use of chromium picolinate (CrP), a supplement that is supposed to reduce body fat, by obese individuals, and there was no reliable evidence found linking CrP to weight loss (Tian et al. 2013). However, one study suggested that chromium could potentially intensify metabolic syndrome (Rotter et al. 2015). Some research has shown that in people with diabetes, an inverse relationship takes place, that is, increasing chromium can decrease blood glucose levels, but it is dependent on other factors such as micronutrient consumption (Lai et al. 2006).

4.7 Copper (Cu)

Copper (Cu) is a vital trace element for humans and animals. The human body contains ~70–80 mg of copper (Gibson 2005). The highest concentrations of Cu are found in the brain, liver, central nervous system, and heart (Gibson 2005). This metal participates in multiple cellular processes, including energy metabolism, antioxidant activity, and neurotransmitter and tissue synthesis. Cu exists in two forms – the first and second oxidation form, the latter being predominant in the biological system. Copper deficit or surfeit can affect different organ systems, causing diseases such as diabetes, cardiovascular diseases, Alzheimer's disease, angiogenesis, and some forms of cancer.

4.7.1 The Physiological Functions of Cu and Oxidative Stress

Copper is a critical functional component of numerous essential enzymes, known as copper enzymes – cytochrome c oxidase, superoxide dismutase, and others (Uauy et al. 1998). Cytochrome oxidase plays a crucial role in cellular energy, which catalyzes the reduction of molecular oxygen (O_2) to water (H_2O). Copper-dependent enzymes are implicated in the regulation of gene expression. Protein synthesis may be affected by cellular Cu levels by enhancing or inhibiting the transcription of specific genes. Cu and Zn are the components of SOD, which is an antioxidant enzyme. Enzymes which are implicated in the gene expression are copper/zinc superoxide dismutase (Cu/Zn SOD), catalase (another antioxidant enzyme), and some proteins associated with cell storage of copper (Uauy et al. 1998).

Fe and Cu participate in the Fenton reaction in the tissue. The free electrons generated in the reaction increased lipid peroxidation and cell damage. Thus, Fe and Cu contribute to the process of lipid peroxidation. High levels of Fe and Cu indicate increased lipid peroxidation and oxidative stress accordingly (Senapati et al. 1985). Salonen et al. showed that there is increased lipid peroxidation in patients with increased Cu (Salonen et al. 1991). The capability of copper to easily attach and accept electrons explains its importance in redox processes and in removing/disposing free radicals.

4.7.2 The Detrimental Effect of Cu in Metabolic Syndrome

Metabolic complications that appear to be associated with alterations in the level of Cu are associated with metabolic syndrome (Aguilar et al. 2007). Evidence has shown that a disorder in serum copper (Cu) level could have effects on humans. Copper seems to have an antagonist effect on patients with diabetes compared to zinc. The role of copper in glucose homeostasis in diabetic patients has not been

thoroughly determined. Studies have also reported higher levels of copper concentration in streptozotocin-induced diabetic rats (Craft and Failla 1983).

A study on Japanese children showed that high levels of dietary copper were associated with a higher risk of T2DM, while higher levels of dietary zinc were associated with a lower risk of T2DM (Eshak et al. 2018). Like zinc, copper is an essential micronutrient, but too much of it can cause diabetic complications (Zheng et al. 2008). One study showed that the binding of copper with amylin could cause the formation of H_2O_2, a free radical, which can lead to oxidative stress (Seal and Dey 2018). Amylin, a hormone that is secreted from the pancreas with insulin, binds with copper, which can create five different pH-dependent components (Seal and Dey 2018). Two of the components produced, components I and II, can generate H_2O_2 (Seal and Dey 2018). However, overproduction of H_2O_2, an oxygen-derived free radical, can cause oxidative stress, which is associated with T2DM (Seal and Dey 2018).

Another study compared the concentration of free copper in three different groups: the first group was type 2 diabetic, the second was type 1 diabetic, and the third was the control group who had no diabetic patients (Squitti et al. 2017). Results demonstrated that the type 2 diabetic group had significantly higher concentrations of free copper compared to the type 1 diabetic and control group (Squitti et al. 2017). A multinomial logistic model also revealed that a one-unit standard deviation of increase in free copper increased the relative risk of having T2DM by 9.64% concerning the control group (Squitti et al. 2017).

Concentrations of copper in blood serum in T2DM were significantly higher than those in controls. The reduction in plasma copper concentration in patients with poor metabolic control is less strong in women than in men with diabetes (Ruiz et al. 1998). A recent study showed that in non-Hispanic black, the serum Cu concentrations positively associated with fasting blood glucose and with the prevalence of metabolic syndrome (Xiaowei et al. 2018) (Figs. 4.3 and 4.4).

4.7.3   Cu Deficiency in Obesity

Conversely, Cu deficiency is common among obese individuals (Boullata et al. 2017), and studies have shown that Cu concentration is related to fat accumulation (Yang et al. 2019). A recent study showed the effects of a high Zn and Cu diet fed to wild mice vs. mice fed with a diet deficient in zinc and copper. The mice fed with high Zn and Cu diet had reduced adipose tissue (AT) macrophage accumulation and AT inflammation (Perriotte-Olson et al. 2016). The study also showed that high zinc and copper diet was effective in promoting triglyceride metabolism in obesity (Perriotte-Olson et al. 2016).

4.7.4 Cu Associated with Increased Cardiovascular Risk

Cardiovascular diseases are widely spread, and their diagnostics and treatment are essential for human life and health. High serum levels of Cu are associated with increased cardiovascular risk. An increase in copper consumption has been linked to disorders in the structure of arterial walls, stress, infection, and diabetes (Serdar et al. 2009). Studies on atherosclerosis have shown contradictory results. Some studies suggest that elevated levels of copper can increase the risk of atherosclerosis (Fox et al. 2000), and other studies show that copper deficiency rather than copper excess holds an increased risk of CVD (Jones et al. 1997) maybe by increasing oxidative stress (Figs. 4.3 and 4.4).

4.7.5 Cu-Chelating Agent Decreases the Degree of Metabolic Syndrome

As a result of Cu-chelating agent treatment to diabetic mice, serum (Uauy et al. 1998) copper was reduced to levels consistent with those of controls, and further therapy with Cu-chelating agent decreased insulin resistance and improved glucose intolerance and reduced triglyceride in diabetic animals (Tanaka et al. 2009). Cu may be related to the manifestation of diabetes, and Cu chelation can be beneficial for a subject having higher blood Cu levels.

4.8 Iron (Fe)

Iron is similar to copper in that high concentrations of it can lead to the onset of diabetes by forming free radicals that can damage DNA, proteins, and cellular membranes (Emerit et al. 2001). Iron has an essential role in oxygen transport and in enzymes implicated in mitochondrial respiration, biosynthesis of DNA, and the citric acid cycle via the capability to change its redox state. High concentrations of iron have also shown to increase ROS while also reducing exercise performance. An increase in ROS is known to induce oxidative stress, which may lead to severe organ damage and excess obesity, diabetes, and other serious health problems (Reardon and Allen 2009) (Fig. 4.3).

4.8.1 Iron (Fe) Metabolism

Iron gets absorbed in proximal duodenum as Fe^{2+} by the divalent metal transporter 1. Iron exporter ferroportin subsequently transfers through the duodenal basolateral

membrane (McKie et al. 2000). Where oxidation of iron by the membrane-bound copper-containing ferroxidase hephaestin facilitate incorporation into transferrin for further transport in the circulation (Vulpe et al. 1999). Transferrin-bound iron (Fe^{3+}) is taken up by the cells via the transferrin receptor (McKie et al. 2000). Iron is required physiologically for heme biosynthesis and other heme-containing enzymes (cytochromes). Excess iron is stored in the hepatocytes (liver). Hepcidin peptide is secreted from hepatocytes in response to iron overload, inflammation, hypoxia, or anemia (Nicolas et al. 2002). Systemic iron homeostasis is maintained in a negative feedback fashion by hepcidin (Datz et al. 2013).

4.8.2   Ferritin Overload Favors Metabolic Syndrome

Accumulating data suggests a link between body iron excess and insulin metabolism (Fernandez-Real et al. 2002). The association between serum ferritin overload and one or more metabolic syndrome features has been shown (Bozzini et al. 2005; Fernandez-Real et al. 1998; Jehn et al. 2004; Williams et al. 2002). Diabetic individuals with increased iron levels place them at higher risk for CVD compared to healthy individuals (Khan and Awan 2014). Elevated serum ferritin levels, though within the normal range, are significantly associated with both metabolic syndrome and insulin resistance (Padwal et al. 2015).

Hyperferritinemia with healthy or mildly elevated transferrin saturation; dysmetabolic iron overload syndrome (DIOS) is observed in around one-third of subjects with nonalcoholic fatty liver disease (NAFLD) or the metabolic syndrome (Datz et al. 2013). DIOS may facilitate the onset of T2DM by altering beta-cell function and the progression of cardiovascular disease. Oxidant and antioxidant imbalance is another trigger suggested for justifying this relationship, whereas ferritin is an acute phase reactant (Morita et al. 2012).

Iron overload can be a factor in the onset of diabetes, but the mechanism by which this occurs is not entirely understood and remains to be studied further (Khan and Awan 2014). A childhood study, all subjects were under the age of 16, compared blood iron levels of two groups; one group was diabetic, and the other was not. Results showed that iron levels were higher in the diabetic group and that a doubling of iron content increased the odds of developing type 1 diabetes (Kyvsgaard et al. 2017).

Another study showed that pregnant women who had an elevated dietary intake of iron were more prone to developing gestational diabetes mellitus (Zhao et al. 2017). Iron levels can potentially affect T2DM as well. Iron overload is a genetic disorder that occurs when excess levels of iron accumulate within the body, and studies show this may have a role in T2DM (Khan and Awan 2014). In people with diabetes, iron storage decreases insulin from the pancreas, leading to insulin resistance (Jehn et al. 2004), which can induce

4.8.3 Iron Depletion Therapy Benefits Insulin Signaling

Iron depletion restores liver and muscle insulin sensitivity as well as pancreatic insulin secretion (Abraham et al. 2006), as iron is an amplification of oxidative stress. Oxidative stress induces IR and increases T2DM and obesity (Furukawa et al. 2004). In vitro excess, iron decreases insulin receptor activity, whereas intracellular iron chelation enhances insulin receptor signaling. Intracellular iron depletion by desferrioxamine leads to an increase in insulin signaling (Green et al. 2006).

Indeed, iron depletion, most frequently achieved by phlebotomy or frequent blood donation or iron chelation therapy, showed to decrease metabolic alterations and liver enzymes in controlled studies in NAFLD. Future studies are warranted to evaluate the potential of iron reduction therapy on hard clinical outcomes in patients with DIOS (Dongiovanni et al. 2011).

4.8.4 Obesity-Related Iron Deficiency

Many studies had linked iron deficiency to obesity with the first one being in 1961 when lower levels of serum iron were evident in obese subjects compared with nonobese subjects (Wenzel et al. 1962). A study in 2003 looked at iron levels of obese children and compared them to nonobese children, and they found that iron deficiency was prevalent in the obese subjects (Pinhas-Hamiel et al. 2003).

A recent meta-analysis of controlled studies showed that adult obesity is associated with low iron stores (Cheng et al. 2012). Iron deficiency has shown to impair mitochondrial and cellular energy homeostasis and increase inactivity and fatigue of obese subjects (Aigner et al. 2014). Fat accumulation in the liver can potentially harm hepatic iron metabolism (Radmard et al. 2016). Compared to healthy lean controls, a drastic decrease in duodenal iron absorption has been observed in obese subjects.

Although iron excess as indicated by hyperferritinemia, transferrin saturation, and iron deposition in the liver is a characteristic feature of NAFLD and the metabolic syndrome, severe forms of obesity are frequently accompanied by iron deficiency and even anemia. However, there is also a clear association between iron stores and total cholesterol, triglycerides, blood pressure, and glucose, which are factors that are often negatively impacted by diabetes (Khan and Awan 2014).

4.8.5 Copper Modulates Iron Homeostasis

Copper is a chief modulator of iron homeostasis via hephaestin ferroxidase activity, and Cu status is linked to iron perturbations in metabolic syndrome. Cu is essential for ferroxidase ceruloplasmin activity which mobilizes stored iron (De Domenico

et al. 2007). Decreased serum and liver copper levels were found in metabolic syndrome with iron accumulation (Aigner et al. 2008). Low Cu bioavailability impairs iron transport from the liver in subjects with metabolic syndrome (Aigner et al. 2008).

4.9 Magnesium (Mg)

Magnesium is a cofactor for ~300 essential metabolic reactions and abundant intracellular ions. Magnesium appears to play an indispensable role in insulin action and a protective role in the occurrence of metabolic disorders (Rotter et al. 2015). Insulin action facilitates the transport of Mg from the extracellular to the intracellular compartment of a cell, thereby increasing energy production using magnesium-dependent adenosine triphosphate (ATP) (Khan and Awan 2014). Magnesium is a mineral that is important for bone structure, and it has shown to be an effective supplement for T2DM patients (Verma and Garg 2017).

4.9.1 Mg and Diabetes

A study showed that individuals with T2DM had improved fasting plasma glucose and systolic blood pressure after they received Mg supplementation (Verma and Garg 2017). They concluded that Mg supplementation might decrease the risk of T2DM-related cardiovascular diseases (Verma and Garg 2017). Cellular and extra-cellular Mg depletion could cause T2DM (Barbagallo and Dominguez 2007).

Many studies reported hypomagnesemia is being very common in patients with T2DM (Gommers et al. 2016; Vanroelen et al. 1985), and another study showed that increased Mg intake is directly correlated to a decline in the development of T2DM (Colditz et al. 1992). Magnesium deficiency can potentially result in disorders of tyrosine kinase activity on the insulin receptor. This type of magnesium deficiency can lead to insulin resistance and less utilization of cellular glucose (Forouhi et al. 2007).

4.9.2 Mg and Obesity

Mg deficiency, like Mn deficiency, contributes to oxidative stress in obese individuals (Morais et al. 2017). One study reported that abdominally obese individuals had lower Mg levels compared to non-obese individuals, and their insulin resistance, oxidative stress, and inflammatory response showed exaggeration as well (Mostafavi et al. 2015). Another recent study showed that Mg supplementation could help the

cardiovascular health of obese individuals by reducing their arterial stiffness (Joris et al. 2016).

4.9.3   Mg and Other Metabolic Syndrome-Associated Diseases

Reports have shown that low magnesium levels can cause ischemic heart disease in diabetic patients. In patients with type 1 diabetes, serum magnesium levels have been associated with early onset of atherosclerosis (Atabek et al. 2006). Magnesium deficiency is related to vascular complications, ischemic heart disease, and severe retinopathy in patients often associated with diabetes (Barbagallo et al. 1996).

Low levels of magnesium have also shown to have a negative impact on renal function (Lopez-Ridaura et al. 2004). In people with diabetes, magnesium deficiency reduces insulin's ability to uptake glucose into cells (Lopez-Ridaura et al. 2004). Oral supplementation of magnesium improves insulin sensitivity and enhances insulin-mediated glucose uptake (Guerrero-Romero and Rodriguez-Moran 2005; Paolisso and Barbagallo 1997).

Magnesium (Mg^{++}) has a positive regulatory role in the G6PD activity (Sanwal 1970); it was suggested that Mg^{++} could affect the oligomeric state of the enzyme G6PD (Ozer et al. 2001; Ozer et al. 2002) and increase its activity. Metals such as Cu, Cd, Ni, and Zn may be competitively inhibiting G6PD with Mg^{++} and/or $NADP^+$ binding sites and can reduce the G6PD activity (De Lillo et al. 2018), thus inducing oxidative stress and favoring metabolic syndrome progression or onset (Fig. 4.4).

4.10   Manganese (Mn)

Manganese (Mn) is an essential micronutrient that participates in various functions like carbohydrate, lipid, protein metabolism, bone growth, cellular energy, and immune functions (Aschner and Aschner 2005). Mn deficiency is associated with diabetes (Shan et al. 2016).

4.10.1   Manganese Superoxide Dismutase (MnSOD) Prevents Oxidative Stress

Like Cu, manganese is the center of manganese superoxide dismutase (MnSOD) and plays an essential role in the regulation of antioxidant defense functions (Aschner and Aschner 2005). MnSOD is an antioxidant located in the mitochondrial matrix and prevents oxidative stress from occurring (Chen et al. 2005). Whenever Mn is

low, the proper amount of MnSOD is not produced, which leads to oxidative stress (Fig. 4.3). The low levels of Mn in animals caused decreased levels of MnSOD activity (Burlet and Jain 2013; Lee et al. 2013), lower insulin secretion (Baly et al. 1985), and reduced glucose uptake (Baly et al. 1990).

However, too much Mn can be harmful to the central nervous system, which helps in the regulation of glucose homeostasis (Sidoryk-Wegrzynowicz and Aschner 2013). As stated above, Mn deficiency can lead to oxidative stress, which can cause diabetes. Animal and human studies have also related oxidative stress to obesity and its associated risk factors (Savini et al. 2013).

Oxidative stress can trigger obesity by altering food intake and causing the deposition of white adipose tissue to occur (Manna and Jain 2015). Physiological levels of Mn are required for insulin synthesis and secretion (Naga Raju et al. 2006), and its deficiency is associated with poor glucose metabolism.

4.10.2   Mn Supplementations Prevents Metabolic Syndrome

A study in 2015 looked at the effects of Manganese III Tetrakis [5, 10, 15, 20]-Benzoic Acid porphyrin (MnTBAP), an antioxidant, supplementation on obese mice. Results showed that MnTBAP supplementation decreased body weight and reduced adipose tissue in the mice by reducing their caloric intake (Brestoff et al. 2015). A study done on Chinese population showed that higher intake of Mn by men was related to fewer incidents of metabolic syndrome, while higher intake of Mn by women was associated with many incidents of metabolic syndrome (Zhou et al. 2016).

People with metabolic disorders usually have less Mn in their diet compared to individuals that do not have a metabolic disease (Choi and Bae 2013). This can suggest that a diet rich in Mn can help prevent metabolic syndrome. As obesity has increased in the past 20 years, Mn intake, along with several other metals such as zinc, has also decreased (Freeland-Graves et al. 2016).

4.11   Potassium (K) Deficiency Associated with Metabolic Syndrome

Potassium is an essential mineral that is one of the driving forces for the resting membrane potential (Ekmekcioglu et al. 2016). Reports have shown that potassium deficiency leads to an increased risk of insulin resistance or diabetes (Ekmekcioglu et al. 2016; Thornley-Brown et al. 2006). Potassium is essential for blood glucose control because it is involved in the secretion of insulin from the pancreas (Ekmekcioglu et al. 2016). A study done on hypokalemia individuals showed that

they had abnormal glucose metabolism due to decreased insulin secretion (Helderman et al. 1983; Rowe et al. 1980).

An investigation revealed that potassium might also enhance vascular smooth muscle relaxation and an increase in blood flow (Haddy et al. 2006). Potassium supplementation has shown to decrease systolic blood pressure in humans (Liu et al. 2013). An interesting study in 2016 looked at the relationship between dietary potassium consumption and obesity levels. They found that potassium intake was associated with metabolic syndrome and that adequate potassium intake had a protective effect from obesity and metabolic syndrome (Cai et al. 2016).

Potassium supplementation has also shown to improve impaired glucose tolerance and secretion of insulin in obese individuals (Potassium supplementation during fasting for obesity 1970). Another study compared lean marathon runners whose fat content was 15% to obese individuals with a fat content of 55%. Results showed that the obese subjects had a 36% reduction in intracellular potassium compared to the marathon runners (Colt et al. 1981).

However, the low potassium levels in the obese subjects might have been from the lower proportion of muscle they had compared to the marathon runners (Colt et al. 1981). The low levels of potassium in the obese subjects should not be taken directly as potassium deficiency, because it was not sure if that was the cause (Colt et al. 1981).

4.12   Sodium (Na) Excess in Association with Metabolic Syndrome

Sodium is a chemical element that serves as an electrolyte for the body, and it is essential for good health. However, too much sodium has shown to have adverse effects on the body (O'Donnell et al. 2016). A study done on children with type 1 diabetes reported that high dietary sodium intake was typical in these individuals, and the high sodium intake was associated with vascular dysfunction and high blood pressure and can impair glycemic control (Anderson et al. 2018). Another study reported similar findings in Korean Americans with T2DM (Ko et al. 2018). The study showed that 69% of these individuals consumed well over the recommended sodium guideline intake (Ko et al. 2018).

A study done in 2014 concluded that high dietary sodium intake was associated with elevated incidences in CVD in patients with T2DM (Horikawa et al. 2014). Diets restricted in sodium have shown to have benefits on blood pressure levels, and they are highly recommended for individuals with metabolic syndrome (Dickinson et al. 2014).

In regard to reducing obesity, low-sodium diets seem to be better. A study done in 2017 on Korean adults showed that there was a positive correlation between high sodium intake and obese individuals (Nam et al. 2017). Sodium is significantly

associated with components of metabolic syndrome, body fat, and insulin resistance, so a high-sodium diet has a greater risk for a metabolic disorder to occur (Oh et al. 2015).

4.13 Zinc (Zn)

Zinc (Zn) is an indispensable essential trace element that is required for a range of cellular homeostasis. Zn dyshomeostasis leads to disorders such as metabolic syndrome and diabetes and diabetic complications. 2–4 g of zinc is present in the human body, and 12–16 μM can be generally measured in plasma, a free zinc pool that is required for the distribution of zinc (Jansen et al. 2009).

4.13.1 The Physiology Roles of Zn

The associations of Zn with metabolic syndrome or associated complications thus came from the numerous functions of Zn: (I) a constructive component of many vital enzymes or proteins; (II) a requirement for insulin biosynthesis, storage, and secretion; (III) a direct/indirect antioxidant action; and (IV) an insulin-mimetic activity. Further, Zn participates in multiple biochemical pathways such as transcription, translation, and cell division; more than 300 enzymes need zinc to function properly (Khan and Awan 2014). Removal of zinc can cause activity loss of enzymes, which can create numerous disorders such as dermal, gastrointestinal, neurological, and immunological abnormalities (Khan and Awan 2014).

4.13.2 Role of Zn in Pancreatic β-Cells

Zinc is present in pancreatic β-cells at higher concentrations compared with various other cells. Insulin consists of a hexamer of six insulin and two zinc molecules binding to histidine residue (Dunn 2005). Zinc is an essential micronutrient that is primarily involved in the biosynthesis, storage, and secretion of insulin (Song et al. 2005). Zinc transporter (ZnT8) plays a crucial role in the accumulation of zinc within insulin secretory granules (Chimienti et al. 2006).

4.13.3   Evidence of the Role of Zn and Its Supplementation in Redox Metabolism

Zinc deficiency is a higher risk factor for obesity and diabetes (Fukunaka and Fujitani 2018). Oxidative stress, caused by the accumulation of free radicals, is associated with diabetes (Jayawardena et al. 2012). Zn has been found to play a role in redox metabolism. Zinc is an essential part of antioxidant enzymes (Kelly 1998), including Cu/Zn SOD (superoxide dismutase) and catalase (Fig. 4.3). When the concentration of zinc decreases, this impairs the synthesis of antioxidants, which leads to oxidative stress (Kelly 1998), further damaging the pancreatic β-cells.

Zinc supplementation has shown to decrease lipid peroxidation (Faure et al. 1995). Oxidative stress can cause problems due to the formation of free radicals in the body. A strong correlation is seen between people with high levels of oxidative stress and diabetes (Anderson et al. 2001). Zinc has shown to decrease the levels of oxidative stress by acting as an antioxidant (a compound that inhibits oxidation and keeps free radicals from accumulating) (Anderson et al. 2001).

Zinc can also stimulate metallothionein (MT) synthesis, which can be beneficial for diabetic patients (Islam and Loots 2007). MT, an abundant cysteine protein, can reduce oxidative stress that is accompanied with the diabetic condition (Yang and Cherian 1994). Several elements can induce MT synthesis in the body, but zinc has proven to be the most effective (Ohly et al. 1998; Vallee and Falchuk 1993).

In 2008, Oh and Yoon showed that zinc could promote the production of insulin, which was indicated by the increase in C peptide after zinc supplementation (de Carvalho et al. 2017). C-peptide is secreted by the β-cells in the pancreas, along with insulin, and it can act as an antioxidant by working on peripheral targets to reduce oxidative stress (Fig. 4.3).

4.13.4   The Beneficial Role of Zinc in Metabolic Syndrome

Zinc plays a crucial role in the beneficial effect to overcome conditions associated with metabolic syndromes such as insulin resistance, oxidative stress, and inflammation (Hashemipour et al. 2009; Kelishadi et al. 2010). Zinc deficiency is a risk factor for obesity in the rodent model (Li et al. 2017). Zinc supplementation on obese subjects reported an improvement in insulin resistance, and these studies suggest that zinc supplementation can help aid the health of obese individuals (Cruz et al. 2017; Li et al. 2017) and delay the onset of obesity (Luo et al. 2016).

A previous study reported the effect of zinc supplementation to prepubertal obese children on insulin resistance and metabolic syndrome (Hashemipour et al. 2009). Zn supplementation may be a useful and safe additional intervention treatment for preventing metabolic syndrome and diabetes.

In vitro, preclinical (animal), and clinical (human) studies have shown that zinc supplementation can improve the health of diabetic and associated complications

(Faure et al. 1995; Khan et al. 2013; Shidfar et al. 2010; Simon and Taylor 2001). Diabetic patients have low serum zinc level, and zinc supplementation has proven to increase this deficiency while improving the patients' glycemic control (Al-Maroof and Al-Sharbatti 2006). Though the exact mechanism is not established, loss of bone strength and density is seen in diabetic patients (Loureiro et al. 2014; McCabe 2007; Prisby et al. 2008).

A study on induced diabetic rats showed that rats that received zinc supplementation had better biomechanical parameters (stiffness, maximum load, ultimate strain) and increased type 1 collagen content compared to the diabetic rats that did not receive zinc supplementation (Bortolin et al. 2015).

Higher serum zinc levels are also associated with less risk of CVD (Chu et al. 2016). Poor glycemic control is the foremost cause of diabetes; this condition leads to lipid peroxidation, oxidative stress, and more complications (Fatani et al. 2016). Also, zinc supplementation caused a significant reduction of plasma total cholesterol while increasing HDL-c levels in type 2 diabetic patients (Jayawardena et al. 2012).

Zinc supplementation has also shown to decrease systolic blood pressure in type 2 diabetic patients (Farvid et al. 2004, 2005). Zinc supplementation also showed great benefits when combined with vitamin C, vitamin E, and magnesium for patients with T2DM by decreasing fasting serum glucose and malondialdehyde concentrations in obese individuals (Farvid et al. 2005). A prospective cohort study in the USA analyzed 82,000 women and verified that women taking less amounts of Zn have increased risk of developing diabetes (17%) compared with those women taking adequate amounts of Zn (Sun et al. 2009). Also, this study suggested that higher zinc intake might be associated with a slightly lower risk of T2DM in women.

4.13.5   Zn Increases Risk of Metabolic Syndrome

Conversely, loss-of-function mutations on human SNPs showed that ZnT8 mutants protect against T2DM with 65% reduced risk of the disease (Flannick et al. 2014). A study from China has demonstrated a negative correlation between the onset of diabetes and plasma Zn (Shan et al. 2014). Also, they suggested that a decline in ZnT8 function, as well as a decrease in plasma Zn concentrations, may coordinately raise the risk of diabetes. Chronic low intake of Zn was associated with an increased risk of diabetes, and diabetes impairs Zn metabolism (Miao et al. 2013).

Excessive Zn supplementation may have harmful effects (Fig. 4.4), as excessive consumption may cause an adverse increase in HbA1c levels and high blood pressure (Miao et al. 2013). Zn supplementation prevents disruption of glucose homeostasis, mainly in people with Zn deficiency. Future prospective intervention studies may clarify Zn supplementation and prevention of the onset of metabolic syndrome.

4.14   Conclusion

Deficiency or excess of metal ions leads to metabolic syndrome and associated complications, because metals are required by enzymes for their catalytic reactions (Figs. 4.2, 4.3, and 4.4). Population-based interventions aimed at halting the increasing prevalence of metabolic syndrome require a thorough understanding of dietary interplays such as nutrients, vitamins, and mineral trace elements (metals). Emerging promising approaches such as metal chelation/depletion/reductive therapies in excess conditions or metal supplementation therapies during deficient status may be used in the overall management of the screening, diagnosis, and treatment of at-risk subjects/patients. Some metals can be toxic, but the majority of the metals at physiological levels have more significant beneficial effects. Hence, optimum levels of certain metals may be therapeutically useful against metabolic syndrome.

References

Abraham D, Rogers J, Gault P, Kushner JP, McClain DA (2006) Increased insulin secretory capacity but decreased insulin sensitivity after correction of iron overload by phlebotomy in hereditary haemochromatosis. Diabetologia 49:2546–2551. https://doi.org/10.1007/s00125-006-0445-7

Aguilar MV, Saavedra P, Arrieta FJ, Mateos CJ, Gonzalez MJ, Meseguer I, Martinez-Para MC (2007) Plasma mineral content in type-2 diabetic patients and their association with the metabolic syndrome. Ann Nutr Metab 51:402–406. https://doi.org/10.1159/000108108

Aigner E et al (2008) Copper availability contributes to iron perturbations in human nonalcoholic fatty liver disease. Gastroenterology 135:680–688. https://doi.org/10.1053/j.gastro.2008.04.007

Aigner E, Feldman A, Datz C (2014) Obesity as an emerging risk factor for iron deficiency. Nutrients 6:3587–3600. https://doi.org/10.3390/nu6093587

Al-Maroof RA, Al-Sharbatti SS (2006) Serum zinc levels in diabetic patients and effect of zinc supplementation on glycemic control of type 2 diabetics. Saudi Med J 27:344–350

Anderson RA, Roussel AM, Zouari N, Mahjoub S, Matheau JM, Kerkeni A (2001) Potential antioxidant effects of zinc and chromium supplementation in people with type 2 diabetes mellitus. J Am Coll Nutr 20:212–218

Anderson J et al (2018) Dietary sodium intake relates to vascular health in children with type 1 diabetes. Pediatr Diabetes 19:138–142. https://doi.org/10.1111/pedi.12537

Aschner JL, Aschner M (2005) Nutritional aspects of manganese homeostasis. Mol Asp Med 26:353–362. https://doi.org/10.1016/j.mam.2005.07.003

Atabek ME, Kurtoglu S, Pirgon O, Baykara M (2006) Serum magnesium concentrations in type 1 diabetic patients: relation to early atherosclerosis. Diabetes Res Clin Pract 72:42–47. https://doi.org/10.1016/j.diabres.2005.09.002

Baly DL, Curry DL, Keen CL, Hurley LS (1985) Dynamics of insulin and glucagon release in rats: influence of dietary manganese. Endocrinology 116:1734–1740. https://doi.org/10.1210/endo-116-5-1734

Baly DL, Schneiderman JS, Garcia-Welsh AL (1990) Effect of manganese deficiency on insulin binding, glucose transport and metabolism in rat adipocytes. J Nutr 120:1075–1079. https://doi.org/10.1093/jn/120.9.1075

Barbagallo M, Dominguez LJ (2007) Magnesium metabolism in type 2 diabetes mellitus, metabolic syndrome and insulin resistance. Arch Biochem Biophys 458:40–47. https://doi.org/10.1016/j.abb.2006.05.007

Barbagallo M, Gupta RK, Resnick LM (1996) Cellular ions in NIDDM: relation of calcium to hyperglycemia and cardiac mass. Diabetes Care 19:1393–1398. https://doi.org/10.2337/diacare.19.12.1393

Bortolin RH et al (2015) Protection against T1DM-induced bone loss by zinc supplementation: biomechanical, Histomorphometric, and molecular analyses in STZ-induced diabetic rats. PLoS One 10:e0125349. https://doi.org/10.1371/journal.pone.0125349

Boullata J, Muthukumaran G, Piarulli A, Labarre J, Compher C (2017) Oral copper absorption in men with morbid obesity. J Trace Elem Med Biol 44:146–150. https://doi.org/10.1016/j.jtemb.2017.07.005

Bozzini C et al (2005) Prevalence of body iron excess in the metabolic syndrome. Diabetes Care 28:2061–2063. https://doi.org/10.2337/diacare.28.8.2061

Brestoff JR et al (2015) Manganese [III] Tetrakis [5,10,15,20]-benzoic acid porphyrin reduces adiposity and improves insulin action in mice with pre-existing obesity. PLoS One 10:e0137388. https://doi.org/10.1371/journal.pone.0137388

Burlet E, Jain SK (2013) Manganese supplementation reduces high glucose-induced monocyte adhesion to endothelial cells and endothelial dysfunction in Zucker diabetic fatty rats. J Biol Chem 288:6409–6416. https://doi.org/10.1074/jbc.M112.447805

Cai X et al (2016) Potassium and obesity/metabolic syndrome: a systematic review and meta-analysis of the epidemiological evidence. Nutrients 8:183. https://doi.org/10.3390/nu8040183

Castro Burbano J, Fajardo Vanegas P, Robles Rodriguez J, Pazmino Estevez K (2016) Relationship between dietary calcium intake and adiposity in female adolescents. Endocrinol Nutr 63:58–63. https://doi.org/10.1016/j.endonu.2015.10.010

Cervantes Gracia K, Llanas-Cornejo D, Husi H (2017) CVD and oxidative stress. J Clin Med 6. https://doi.org/10.3390/jcm6020022

Chen H, Li X, Epstein PN (2005) MnSOD and catalase transgenes demonstrate that protection of islets from oxidative stress does not alter cytokine toxicity. Diabetes 54:1437–1446. https://doi.org/10.2337/diabetes.54.5.1437

Chen YW, Yang CY, Huang CF, Hung DZ, Leung YM, Liu SH (2009) Heavy metals, islet function and diabetes development. Islets 1:169–176. https://doi.org/10.4161/isl.1.3.9262

Cheng HL, Bryant C, Cook R, O'Connor H, Rooney K, Steinbeck K (2012) The relationship between obesity and hypoferraemia in adults: a systematic review. Obes Rev 13:150–161. https://doi.org/10.1111/j.1467-789X.2011.00938.x

Chimienti F et al (2006) In vivo expression and functional characterization of the zinc transporter ZnT8 in glucose-induced insulin secretion. J Cell Sci 119:4199–4206. https://doi.org/10.1242/jcs.03164

Choi MK, Bae YJ (2013) Relationship between dietary magnesium, manganese, and copper and metabolic syndrome risk in Korean adults: the Korea National Health and nutrition examination survey (2007–2008). Biol Trace Elem Res 156:56–66. https://doi.org/10.1007/s12011-013-9852-z

Chu A, Foster M, Samman S (2016) Zinc status and risk of cardiovascular diseases and type 2 diabetes mellitus-a systematic review of prospective cohort studies. Nutrients 8. https://doi.org/10.3390/nu8110707

Colditz GA, Manson JE, Stampfer MJ, Rosner B, Willett WC, Speizer FE (1992) Diet and risk of clinical diabetes in women. Am J Clin Nutr 55:1018–1023. https://doi.org/10.1093/ajcn/55.5.1018

Colt EW, Wang J, Stallone F, Van Itallie TB, Pierson RN Jr (1981) A possible low intracellular potassium in obesity. Am J Clin Nutr 34:367–372. https://doi.org/10.1093/ajcn/34.3.367

Craft NE, Failla ML (1983) Zinc, iron, and copper absorption in the streptozotocin-diabetic rat. Am J Phys 244:E122–E128. https://doi.org/10.1152/ajpendo.1983.244.2.E122

Cruz KJ, Morais JB, de Oliveira AR, Severo JS, Marreiro DD (2017) The effect of zinc supplementation on insulin resistance in obese subjects: a systematic review. Biol Trace Elem Res 176:239–243. https://doi.org/10.1007/s12011-016-0835-8

Datz C, Felder TK, Niederseer D, Aigner E (2013) Iron homeostasis in the metabolic syndrome. Eur J Clin Investig 43:215–224. https://doi.org/10.1111/eci.12032

de Carvalho GB, Brandao-Lima PN, Maia CS, Barbosa KB, Pires LV (2017) Zinc's role in the glycemic control of patients with type 2 diabetes: a systematic review. Biometals 30:151–162. https://doi.org/10.1007/s10534-017-9996-y

De Domenico I, Ward DM, di Patti MC, Jeong SY, David S, Musci G, Kaplan J (2007) Ferroxidase activity is required for the stability of cell surface ferroportin in cells expressing GPI-ceruloplasmin. EMBO J 26:2823–2831. https://doi.org/10.1038/sj.emboj.7601735

De Lillo A, Cardi M, Landi S, Esposito S (2018) Mechanism(s) of action of heavy metals to investigate the regulation of plastidic glucose-6-phosphate dehydrogenase. Sci Rep 8:13481. https://doi.org/10.1038/s41598-018-31348-y

Dickinson KM, Clifton PM, Burrell LM, Barrett PH, Keogh JB (2014) Postprandial effects of a high salt meal on serum sodium, arterial stiffness, markers of nitric oxide production and markers of endothelial function. Atherosclerosis 232:211–216. https://doi.org/10.1016/j.atherosclerosis.2013.10.032

Dongiovanni P, Fracanzani AL, Fargion S, Valenti L (2011) Iron in fatty liver and in the metabolic syndrome: a promising therapeutic target. J Hepatol 55:920–932. https://doi.org/10.1016/j.jhep.2011.05.008

Dunn MF (2005) Zinc-ligand interactions modulate assembly and stability of the insulin hexamer -- a review. Biometals 18:295–303. https://doi.org/10.1007/s10534-005-3685-y

Ekmekcioglu C, Elmadfa I, Meyer AL, Moeslinger T (2016) The role of dietary potassium in hypertension and diabetes. J Physiol Biochem 72:93–106. https://doi.org/10.1007/s13105-015-0449-1

Emerit J, Beaumont C, Trivin F (2001) Iron metabolism, free radicals, and oxidative injury. Biomed Pharmacother 55:333–339

Eshak ES, Iso H, Maruyama K, Muraki I, Tamakoshi A (2018) Associations between dietary intakes of iron, copper and zinc with risk of type 2 diabetes mellitus: a large population-based prospective cohort study. Clin Nutr 37:667–674. https://doi.org/10.1016/j.clnu.2017.02.010

Farvid MS, Jalali M, Siassi F, Saadat N, Hosseini M (2004) The impact of vitamins and/or mineral supplementation on blood pressure in type 2 diabetes. J Am Coll Nutr 23:272–279

Farvid MS, Jalali M, Siassi F, Hosseini M (2005) Comparison of the effects of vitamins and/or mineral supplementation on glomerular and tubular dysfunction in type 2 diabetes. Diabetes Care 28:2458–2464. https://doi.org/10.2337/diacare.28.10.2458

Fatani SH, Babakr AT, NourEldin EM, Almarzouki AA (2016) Lipid peroxidation is associated with poor control of type-2 diabetes mellitus. Diabetes Metab Syndr 10:S64–S67. https://doi.org/10.1016/j.dsx.2016.01.028

Faulk C, Barks A, Sanchez BN, Zhang Z, Anderson OS, Peterson KE, Dolinoy DC (2014) Perinatal lead (Pb) exposure results in sex-specific effects on food intake, fat, weight, and insulin response across the murine life-course. PLoS One 9:e104273. https://doi.org/10.1371/journal.pone.0104273

Faure P, Benhamou PY, Perard A, Halimi S, Roussel AM (1995) Lipid peroxidation in insulin-dependent diabetic patients with early retina degenerative lesions: effects of an oral zinc supplementation. Eur J Clin Nutr 49:282–288

Fernandez-Real JM et al (1998) Serum ferritin as a component of the insulin resistance syndrome. Diabetes Care 21:62–68. https://doi.org/10.2337/diacare.21.1.62

Fernandez-Real JM, Lopez-Bermejo A, Ricart W (2002) Cross-talk between iron metabolism and diabetes. Diabetes 51:2348–2354. https://doi.org/10.2337/diabetes.51.8.2348

Flannick J et al (2014) Loss-of-function mutations in SLC30A8 protect against type 2 diabetes. Nat Genet 46:357–363. https://doi.org/10.1038/ng.2915

Forouhi NG et al (2007) Elevated serum ferritin levels predict new-onset type 2 diabetes: results from the EPIC-Norfolk prospective study. Diabetologia 50:949–956. https://doi.org/10.1007/s00125-007-0604-5

Forte G et al (2013) Blood metals concentration in type 1 and type 2 diabetics. Biol Trace Elem Res 156:79–90. https://doi.org/10.1007/s12011-013-9858-6

Fox PL, Mazumder B, Ehrenwald E, Mukhopadhyay CK (2000) Ceruloplasmin and cardiovascular disease. Free Radic Biol Med 28:1735–1744. https://doi.org/10.1016/s0891-5849(00)00231-8

Freeland-Graves JH, Mousa TY, Kim S (2016) International variability in diet and requirements of manganese: causes and consequences. J Trace Elem Med Biol 38:24–32. https://doi.org/10.1016/j.jtemb.2016.05.004

Freund H, Atamian S, Fischer JE (1979) Chromium deficiency during total parenteral nutrition. JAMA 241:496–498

Fukunaka A, Fujitani Y (2018) Role of zinc homeostasis in the pathogenesis of diabetes and obesity. Int J Mol Sci 19. https://doi.org/10.3390/ijms19020476

Furukawa S et al (2004) Increased oxidative stress in obesity and its impact on metabolic syndrome. J Clin Invest 114:1752–1761. https://doi.org/10.1172/JCI21625

Gibson RS (2005) Principles of nutritional assessment, 2nd edn. Oxford University, New York, pp 697–711

Gommers LM, Hoenderop JG, Bindels RJ, de Baaij JH (2016) Hypomagnesemia in type 2 diabetes: a vicious circle? Diabetes 65:3–13. https://doi.org/10.2337/db15-1028

Green A, Basile R, Rumberger JM (2006) Transferrin and iron induce insulin resistance of glucose transport in adipocytes. Metabolism 55:1042–1045. https://doi.org/10.1016/j.metabol.2006.03.015

Griendling KK, FitzGerald GA (2003) Oxidative stress and cardiovascular injury: part I: basic mechanisms and in vivo monitoring of ROS. Circulation 108:1912–1916. https://doi.org/10.1161/01.CIR.0000093660.86242.BB

Griendling KK, Minieri CA, Ollerenshaw JD, Alexander RW (1994) Angiotensin II stimulates NADH and NADPH oxidase activity in cultured vascular smooth muscle cells. Circ Res 74:1141–1148

Guerrero-Romero F, Rodriguez-Moran M (2005) Complementary therapies for diabetes: the case for chromium, magnesium, and antioxidants. Arch Med Res 36:250–257. https://doi.org/10.1016/j.arcmed.2005.01.004

Haddy FJ, Vanhoutte PM, Feletou M (2006) Role of potassium in regulating blood flow and blood pressure. Am J Physiol Regul Integr Comp Physiol 290:R546–R552. https://doi.org/10.1152/ajpregu.00491.2005

Hashemipour M et al (2009) Effect of zinc supplementation on insulin resistance and components of the metabolic syndrome in prepubertal obese children. Hormones (Athens) 8:279–285. https://doi.org/10.14310/horm.2002.1244

Helderman JH, Elahi D, Andersen DK, Raizes GS, Tobin JD, Shocken D, Andres R (1983) Prevention of the glucose intolerance of thiazide diuretics by maintenance of body potassium. Diabetes 32:106–111. https://doi.org/10.2337/diab.32.2.106

Horikawa C et al (2014) Dietary sodium intake and incidence of diabetes complications in Japanese patients with type 2 diabetes: analysis of the Japan Diabetes Complications Study (JDCS). J Clin Endocrinol Metab 99:3635–3643. https://doi.org/10.1210/jc.2013-4315

Hutcheson R, Rocic P (2012) The metabolic syndrome, oxidative stress, environment, and cardiovascular disease: the great exploration. Exp Diabetes Res 2012:271028. https://doi.org/10.1155/2012/271028

Islam MS, Loots DT (2007) Diabetes, metallothionein, and zinc interactions: a review. Biofactors 29:203–212

Jain SK, Parsanathan R, Achari AE, Kanikarla-Marie P, Bocchini JA Jr (2018) Glutathione stimulates vitamin D regulatory and glucose-metabolism genes, lowers oxidative stress and

inflammation, and increases 25-Hydroxy-vitamin D levels in blood: a novel approach to treat 25-Hydroxyvitamin D deficiency. Antioxid Redox Signal 29:1792–1807. https://doi.org/10.1089/ars.2017.7462

Jansen J, Karges W, Rink L (2009) Zinc and diabetes--clinical links and molecular mechanisms. J Nutr Biochem 20:399–417. https://doi.org/10.1016/j.jnutbio.2009.01.009

Jayawardena R, Ranasinghe P, Galappatthy P, Malkanthi R, Constantine G, Katulanda P (2012) Effects of zinc supplementation on diabetes mellitus: a systematic review and meta-analysis. Diabetol Metab Syndr 4:13. https://doi.org/10.1186/1758-5996-4-13

Jehn M, Clark JM, Guallar E (2004) Serum ferritin and risk of the metabolic syndrome in U.S. adults. Diabetes Care 27:2422–2428. https://doi.org/10.2337/diacare.27.10.2422

Jones AA, DiSilvestro RA, Coleman M, Wagner TL (1997) Copper supplementation of adult men: effects on blood copper enzyme activities and indicators of cardiovascular disease risk. Metabolism 46:1380–1383. https://doi.org/10.1016/s0026-0495(97)90135-9

Joris PJ, Plat J, Bakker SJ, Mensink RP (2016) Long-term magnesium supplementation improves arterial stiffness in overweight and obese adults: results of a randomized, double-blind, placebo-controlled intervention trial. Am J Clin Nutr 103:1260–1266. https://doi.org/10.3945/ajcn.116.131466

Kelishadi R et al (2010) Effect of zinc supplementation on markers of insulin resistance, oxidative stress, and inflammation among prepubescent children with metabolic syndrome. Metab Syndr Relat Disord 8:505–510. https://doi.org/10.1089/met.2010.0020

Kelly FJ (1998) Use of antioxidants in the prevention and treatment of disease. J Int Fed Clin Chem 10:21–23

Khan AR, Awan FR (2014) Metals in the pathogenesis of type 2 diabetes. J Diabetes Metab Disord 13:16. https://doi.org/10.1186/2251-6581-13-16

Khan MI, Siddique KU, Ashfaq F, Ali W, Reddy HD, Mishra A (2013) Effect of high-dose zinc supplementation with oral hypoglycemic agents on glycemic control and inflammation in type-2 diabetic nephropathy patients. J Nat Sci Biol Med 4:336–340. https://doi.org/10.4103/0976-9668.117002

Ko J, Kim KB, Timmerman GM, Clark AP, Kim M (2018) Factors predicting sodium intake of Korean Americans with type 2 diabetes. J Immigr Minor Health 20:641–650. https://doi.org/10.1007/s10903-017-0602-8

Kunsch C, Medford RM (1999) Oxidative stress as a regulator of gene expression in the vasculature. Circ Res 85:753–766

Kyvsgaard JN et al (2017) High neonatal blood iron content is associated with the risk of childhood type 1 diabetes mellitus. Nutrients 9. https://doi.org/10.3390/nu9111221

Lai MH, Chen YY, Cheng HH (2006) Chromium yeast supplementation improves fasting plasma glucose and LDL-cholesterol in streptozotocin-induced diabetic rats. Int J Vitam Nutr Res 76:391–397. https://doi.org/10.1024/0300-9831.76.6.391

Lee SH, Jouihan HA, Cooksey RC, Jones D, Kim HJ, Winge DR, McClain DA (2013) Manganese supplementation protects against diet-induced diabetes in wild type mice by enhancing insulin secretion. Endocrinology 154:1029–1038. https://doi.org/10.1210/en.2012-1445

Li Y, Li M, Liu X, Wu M, Yang L, Yang L, Yang X (2017) Effects of marginal zinc deficiency on obesity. Wei Sheng Yan Jiu 46:373–377

Liu Z et al (2013) Salt loading and potassium supplementation: effects on ambulatory arterial stiffness index and endothelin-1 levels in normotensive and mild hypertensive patients. J Clin Hypertens (Greenwich) 15:485–496. https://doi.org/10.1111/jch.12109

Lopez-Ridaura R, Willett WC, Rimm EB, Liu S, Stampfer MJ, Manson JE, Hu FB (2004) Magnesium intake and risk of type 2 diabetes in men and women. Diabetes Care 27:134–140. https://doi.org/10.2337/diacare.27.1.134

Loureiro MB et al (2014) Low bone mineral density is associated to poor glycemic control and increased OPG expression in children and adolescents with type 1 diabetes. Diabetes Res Clin Pract 103:452–457. https://doi.org/10.1016/j.diabres.2013.12.018

Luo M et al (2016) Zinc delays the progression of obesity-related glomerulopathy in mice via down-regulating P38 MAPK-mediated inflammation. Obesity (Silver Spring) 24:1244–1256. https://doi.org/10.1002/oby.21463

Manna P, Jain SK (2015) Obesity, oxidative stress, adipose tissue dysfunction, and the associated health risks: causes and therapeutic strategies. Metab Syndr Relat Disord 13:423–444. https://doi.org/10.1089/met.2015.0095

McCabe LR (2007) Understanding the pathology and mechanisms of type I diabetic bone loss. J Cell Biochem 102:1343–1357. https://doi.org/10.1002/jcb.21573

McKie AT et al (2000) A novel duodenal iron-regulated transporter, IREG1, implicated in the basolateral transfer of iron to the circulation. Mol Cell 5:299–309. https://doi.org/10.1016/s1097-2765(00)80425-6

Miao X, Sun W, Fu Y, Miao L, Cai L (2013) Zinc homeostasis in the metabolic syndrome and diabetes. Front Med 7:31–52. https://doi.org/10.1007/s11684-013-0251-9

Morais JB et al (2017) Role of magnesium in oxidative stress in individuals with obesity. Biol Trace Elem Res 176:20–26. https://doi.org/10.1007/s12011-016-0793-1

Morita M et al (2012) Fatty liver induced by free radicals and lipid peroxidation. Free Radic Res 46:758–765. https://doi.org/10.3109/10715762.2012.677840

Mostafavi E et al (2015) Abdominal obesity and gestational diabetes: the interactive role of magnesium. Magnes Res 28:116–125. https://doi.org/10.1684/mrh.2015.0392

Naga Raju GJ et al (2006) Estimation of trace elements in some anti-diabetic medicinal plants using PIXE technique. Appl Radiat Isot 64:893–900. https://doi.org/10.1016/j.apradiso.2006.02.085

Nam GE et al (2017) Association between 24-h urinary sodium excretion and obesity in Korean adults: a multicenter study. Nutrition 41:113–119. https://doi.org/10.1016/j.nut.2017.04.006

Nicolas G et al (2002) The gene encoding the iron regulatory peptide hepcidin is regulated by anemia, hypoxia, and inflammation. J Clin Invest 110:1037–1044. https://doi.org/10.1172/JCI15686

O'Donnell M et al (2016) Dietary sodium and cardiovascular disease risk. N Engl J Med 375:2404–2406. https://doi.org/10.1056/NEJMc1612304

Oh SW, Han KH, Han SY, Koo HS, Kim S, Chin HJ (2015) Association of sodium excretion with metabolic syndrome, insulin resistance, and body fat. Medicine (Baltimore) 94:e1650. https://doi.org/10.1097/MD.0000000000001650

Ohly P, Wang Z, Abel J, Gleichmann H (1998) Zincsulphate induced metallothionein in pancreatic islets and protected against the diabetogenic toxin streptozotocin. Talanta 46:355–359

Onakpoya I, Posadzki P, Ernst E (2013) Chromium supplementation in overweight and obesity: a systematic review and meta-analysis of randomized clinical trials. Obes Rev 14:496–507. https://doi.org/10.1111/obr.12026

Ozer N, Aksoy Y, Ogus IH (2001) Kinetic properties of human placental glucose-6-phosphate dehydrogenase. Int J Biochem Cell Biol 33:221–226. https://doi.org/10.1016/s1357-2725(01)00011-5

Ozer N, Bilgi C, Hamdi Ogus I (2002) Dog liver glucose-6-phosphate dehydrogenase: purification and kinetic properties. Int J Biochem Cell Biol 34:253–262. https://doi.org/10.1016/s1357-2725(01)00125-x

Padwal MK, Murshid M, Nirmale P, Melinkeri RR (2015) Association of serum ferritin levels with metabolic syndrome and insulin resistance. J Clin Diagn Res 9:BC11–BC13. https://doi.org/10.7860/JCDR/2015/13480.6564

Panchal SK, Wanyonyi S, Brown L (2017) Selenium, vanadium, and chromium as micronutrients to improve metabolic syndrome. Curr Hypertens Rep 19:10. https://doi.org/10.1007/s11906-017-0701-x

Paolisso G, Barbagallo M (1997) Hypertension, diabetes mellitus, and insulin resistance: the role of intracellular magnesium. Am J Hypertens 10:346–355. https://doi.org/10.1016/s0895-7061(96)00342-1

Parsanathan R, Jain SK (2018a) Hydrogen sulfide increases glutathione biosynthesis, and glucose uptake and utilisation in C2C12 mouse myotubes. Free Radic Res 52:288–303. https://doi.org/10.1080/10715762.2018.1431626

Parsanathan R, Jain SK (2018b) L-cysteine in vitro can restore cellular glutathione and inhibits the expression of cell adhesion molecules in G6PD-deficient monocytes. Amino Acids 50:909–921. https://doi.org/10.1007/s00726-018-2559-x

Parsanathan R, Jain SK (2019a) Glucose-6-phosphate dehydrogenase deficiency increases cell adhesion molecules and activates human monocyte-endothelial cell adhesion: protective role of l-cysteine. Arch Biochem Biophys 663:11–21. https://doi.org/10.1016/j.abb.2018.12.023

Parsanathan R, Jain SK (2019b) Glutathione deficiency alters the vitamin D-metabolizing enzymes CYP27B1 and CYP24A1 in human renal proximal tubule epithelial cells and kidney of HFD-fed mice. Free Radic Biol Med 131:376–381. https://doi.org/10.1016/j.freeradbiomed.2018.12.017

Perriotte-Olson C et al (2016) Nanoformulated copper/zinc superoxide dismutase reduces adipose inflammation in obesity. Obesity (Silver Spring) 24:148–156. https://doi.org/10.1002/oby.21348

Pinhas-Hamiel O, Newfield RS, Koren I, Agmon A, Lilos P, Phillip M (2003) Greater prevalence of iron deficiency in overweight and obese children and adolescents. Int J Obes Relat Metab Disord 27:416–418. https://doi.org/10.1038/sj.ijo.0802224

Pittas AG, Dawson-Hughes B, Li T, Van Dam RM, Willett WC, Manson JE, Hu FB (2006) Vitamin D and calcium intake in relation to type 2 diabetes in women. Diabetes Care 29:650–656. https://doi.org/10.2337/diacare.29.03.06.dc05-1961

Potassium supplementation during fasting for obesity (1970) Nutr Rev 28:177–178. https://doi.org/10.1111/j.1753-4887.1970.tb06216.x

Prisby RD, Swift JM, Bloomfield SA, Hogan HA, Delp MD (2008) Altered bone mass, geometry and mechanical properties during the development and progression of type 2 diabetes in the Zucker diabetic fatty rat. J Endocrinol 199:379–388. https://doi.org/10.1677/JOE-08-0046

Qiao W, Peng Z, Wang Z, Wei J, Zhou A (2009) Chromium improves glucose uptake and metabolism through upregulating the mRNA levels of IR, GLUT4, GS, and UCP3 in skeletal muscle cells. Biol Trace Elem Res 131:133–142. https://doi.org/10.1007/s12011-009-8357-2

Radmard AR et al (2016) Central obesity and liver iron content: a noninvasive assessment in general population by magnetic resonance imaging. Ann Nutr Metab 69:181–189. https://doi.org/10.1159/000453111

Rains JL, Jain SK (2011) Oxidative stress, insulin signaling, and diabetes. Free Radic Biol Med 50:567–575. https://doi.org/10.1016/j.freeradbiomed.2010.12.006

Rajagopalan S, Kurz S, Munzel T, Tarpey M, Freeman BA, Griendling KK, Harrison DG (1996) Angiotensin II-mediated hypertension in the rat increases vascular superoxide production via membrane NADH/NADPH oxidase activation. Contribution to alterations of vasomotor tone. J Clin Invest 97:1916–1923. https://doi.org/10.1172/JCI118623

Ranasinghe P, Pigera S, Galappatthy P, Katulanda P, Constantine GR (2015) Zinc and diabetes mellitus: understanding molecular mechanisms and clinical implications. Daru 23:44. https://doi.org/10.1186/s40199-015-0127-4

Reardon TF, Allen DG (2009) Iron injections in mice increase skeletal muscle iron content, induce oxidative stress and reduce exercise performance. Exp Physiol 94:720–730. https://doi.org/10.1113/expphysiol.2008.046045

Roberts CK, Sindhu KK (2009) Oxidative stress and metabolic syndrome. Life Sci 84:705–712. https://doi.org/10.1016/j.lfs.2009.02.026

Rotter I, Kosik-Bogacka D, Dolegowska B, Safranow K, Lubkowska A, Laszczynska M (2015) Relationship between the concentrations of heavy metals and bioelements in aging men with metabolic syndrome. Int J Environ Res Public Health 12:3944–3961. https://doi.org/10.3390/ijerph120403944

Rowe JW, Tobin JD, Rosa RM, Andres R (1980) Effect of experimental potassium deficiency on glucose and insulin metabolism. Metabolism 29:498–502

Ruiz C, Alegria A, Barbera R, Farre R, Lagarda J (1998) Selenium, zinc and copper in plasma of patients with type 1 diabetes mellitus in different metabolic control states. J Trace Elem Med Biol 12:91–95

Sakurai H, Katoh A, Kiss T, Jakusch T, Hattori M (2010) Metallo-allixinate complexes with anti-diabetic and anti-metabolic syndrome activities. Metallomics 2:670–682. https://doi.org/10.1039/c0mt00025f

Salonen JT, Salonen R, Korpela H, Suntioinen S, Tuomilehto J (1991) Serum copper and the risk of acute myocardial infarction: a prospective population study in men in eastern Finland. Am J Epidemiol 134:268–276. https://doi.org/10.1093/oxfordjournals.aje.a116080

San Mauro-Martin I, Ruiz-Leon AM, Camina-Martin MA, Garicano-Vilar E, Collado-Yurrita L, Mateo-Silleras B, Redondo Del Rio Mde P (2016) Chromium supplementation in patients with type 2 diabetes and high risk of type 2 diabetes: a meta-analysis of randomized controlled trials. Nutr Hosp 33:27. https://doi.org/10.20960/nh.v33i1.27

Sanwal BD (1970) Regulatory mechanisms involving nicotinamide adenine nucleotides as allosteric effectors. 3. Control of glucose 6-phosphate dehydrogenase. J Biol Chem 245:1626–1631

Savini I, Catani MV, Evangelista D, Gasperi V, Avigliano L (2013) Obesity-associated oxidative stress: strategies finalized to improve redox state. Int J Mol Sci 14:10497–10538. https://doi.org/10.3390/ijms140510497

Seal M, Dey SG (2018) Active-site environment of copper-bound human amylin relevant to type 2 diabetes. Inorg Chem 57:129–138. https://doi.org/10.1021/acs.inorgchem.7b02266

Senapati A, Carlsson LK, Fletcher CD, Browse NL, Thompson RP (1985) Is tissue copper deficiency associated with aortic aneurysms? Br J Surg 72:352–353. https://doi.org/10.1002/bjs.1800720507

Serdar MA et al (2009) Trace and toxic element patterns in nonsmoker patients with noninsulin-dependent diabetes mellitus, impaired glucose tolerance, and fasting glucose. Int J Diabetes Dev Ctries 29:35–40. https://doi.org/10.4103/0973-3930.50713

Shahbah D et al (2017) Oral magnesium supplementation improves glycemic control and lipid profile in children with type 1 diabetes and hypomagnesaemia. Medicine (Baltimore) 96:e6352. https://doi.org/10.1097/MD.0000000000006352

Shan Z et al (2014) Interactions between zinc transporter-8 gene (SLC30A8) and plasma zinc concentrations for impaired glucose regulation and type 2 diabetes. Diabetes 63:1796–1803. https://doi.org/10.2337/db13-0606

Shan Z et al (2016) U-shaped association between plasma manganese levels and type 2 diabetes. Environ Health Perspect 124:1876–1881. https://doi.org/10.1289/EHP176

Sharma B, Singh S, Siddiqi NJ (2014) Biomedical implications of heavy metals induced imbalances in redox systems. Biomed Res Int 2014:640754. https://doi.org/10.1155/2014/640754

Shidfar F, Aghasi M, Vafa M, Heydari I, Hosseini S, Shidfar S (2010) Effects of combination of zinc and vitamin a supplementation on serum fasting blood sugar, insulin, apoprotein B and apoprotein A-I in patients with type I diabetes. Int J Food Sci Nutr 61:182–191. https://doi.org/10.3109/09637480903334171

Sidoryk-Wegrzynowicz M, Aschner M (2013) Manganese toxicity in the central nervous system: the glutamine/glutamate-gamma-aminobutyric acid cycle. J Intern Med 273:466–477. https://doi.org/10.1111/joim.12040

Simon SF, Taylor CG (2001) Dietary zinc supplementation attenuates hyperglycemia in db/db mice. Exp Biol Med (Maywood) 226:43–51. https://doi.org/10.1177/153537020122600107

Song Y, Wang J, Li XK, Cai L (2005) Zinc and the diabetic heart. Biometals 18:325–332. https://doi.org/10.1007/s10534-005-3689-7

Squitti R, Mendez AJ, Simonelli I, Ricordi C (2017) Diabetes and Alzheimer's disease: can elevated free copper predict the risk of the disease? J Alzheimers Dis 56:1055–1064. https://doi.org/10.3233/JAD-161033

Sun Q, van Dam RM, Willett WC, Hu FB (2009) Prospective study of zinc intake and risk of type 2 diabetes in women. Diabetes Care 32:629–634. https://doi.org/10.2337/dc08-1913

Tanaka A et al (2009) Role of copper ion in the pathogenesis of type 2 diabetes. Endocr J 56:699–706. https://doi.org/10.1507/endocrj.k09e-051

Tang HY, Xiao QG, Xu HB, Zhang Y (2015) Hypoglycemic activity and acute oral toxicity of chromium methionine complexes in mice. J Trace Elem Med Biol 29:136–144. https://doi.org/10.1016/j.jtemb.2014.07.001

Tchounwou PB, Yedjou CG, Patlolla AK, Sutton DJ (2012) Heavy metal toxicity and the environment. Exp Suppl 101:133–164. https://doi.org/10.1007/978-3-7643-8340-4_6

Thornley-Brown D et al (2006) Differing effects of antihypertensive drugs on the incidence of diabetes mellitus among patients with hypertensive kidney disease. Arch Intern Med 166:797–805. https://doi.org/10.1001/archinte.166.7.797

Tian H, Guo X, Wang X, He Z, Sun R, Ge S, Zhang Z (2013) Chromium picolinate supplementation for overweight or obese adults. Cochrane Database Syst Rev:CD010063. https://doi.org/10.1002/14651858.CD010063.pub2

Uauy R, Olivares M, Gonzalez M (1998) Essentiality of copper in humans. Am J Clin Nutr 67:952S–959S. https://doi.org/10.1093/ajcn/67.5.952S

Vallee BL, Falchuk KH (1993) The biochemical basis of zinc physiology. Physiol Rev 73:79–118. https://doi.org/10.1152/physrev.1993.73.1.79

van Dam RM, Hu FB, Rosenberg L, Krishnan S, Palmer JR (2006) Dietary calcium and magnesium, major food sources, and risk of type 2 diabetes in U.S. black women. Diabetes Care 29:2238–2243. https://doi.org/10.2337/dc06-1014

Vanroelen WF, Van Gaal LF, Van Rooy PE, De Leeuw IH (1985) Serum and erythrocyte magnesium levels in type I and type II diabetics. Acta Diabetol Lat 22:185–190

Verma H, Garg R (2017) Effect of magnesium supplementation on type 2 diabetes associated cardiovascular risk factors: a systematic review and meta-analysis. J Hum Nutr Diet 30:621–633. https://doi.org/10.1111/jhn.12454

Vichova T, Motovska Z (2013) Oxidative stress: predictive marker for coronary artery disease. Exp Clin Cardiol 18:e88–e91

Vincent JB (2010) Chromium: celebrating 50 years as an essential element? Dalton Trans 39:3787–3794. https://doi.org/10.1039/b920480f

Vulpe CD et al (1999) Hephaestin, a ceruloplasmin homologue implicated in intestinal iron transport, is defective in the sla mouse. Nat Genet 21:195–199. https://doi.org/10.1038/5979

Webb RC (2003) Smooth muscle contraction and relaxation. Adv Physiol Educ 27:201–206. https://doi.org/10.1152/advan.00025.2003

Wenzel BJ, Stults HB, Mayer J (1962) Hypoferraemia in obese adolescents. Lancet 2:327–328. https://doi.org/10.1016/s0140-6736(62)90110-1

Wiernsperger N, Rapin J (2010) Trace elements in glucometabolic disorders: an update. Diabetol Metab Syndr 2:70. https://doi.org/10.1186/1758-5996-2-70

Williams MJ, Poulton R, Williams S (2002) Relationship of serum ferritin with cardiovascular risk factors and inflammation in young men and women. Atherosclerosis 165:179–184. https://doi.org/10.1016/s0021-9150(02)00233-2

Xiaowei HJ, Yun YS, Qinglin LS, Wei Tang S (2018) Copper is associated with metabolic syndrome and fasting blood glucose in non-Hispanic black—Results from National Health and Nutrition Examination Survey. Diabetes 67(Supplement 1). https://doi.org/10.2337/db18-1598-P

Yang J, Cherian MG (1994) Protective effects of metallothionein on streptozotocin-induced diabetes in rats. Life Sci 55:43–51. https://doi.org/10.1016/0024-3205(94)90080-9

Yang H et al (2019) Obesity is associated with copper elevation in serum and tissues. Metallomics 11(8):1363–1371. https://doi.org/10.1039/c9mt00148d

Zhao L et al (2017) Dietary intake of heme iron and body iron status are associated with the risk of gestational diabetes mellitus: a systematic review and meta-analysis. Asia Pac J Clin Nutr 26:1092–1106. https://doi.org/10.6133/apjcn.022017.09

Zheng Y, Li XK, Wang Y, Cai L (2008) The role of zinc, copper and iron in the pathogenesis of diabetes and diabetic complications: therapeutic effects by chelators. Hemoglobin 32:135–145. https://doi.org/10.1080/03630260701727077

Zhou B et al (2016) Dietary intake of manganese and the risk of the metabolic syndrome in a Chinese population. Br J Nutr 116:853–863. https://doi.org/10.1017/S0007114516002580

Zhu K, Prince RL (2012) Calcium and bone. Clin Biochem 45:936–942. https://doi.org/10.1016/j.clinbiochem.2012.05.006

Chapter 5
Antimicrobial Effects of Metal, Metal Oxide Nanomaterials, and Sulfonamide Complexes

Mehmet Salih Nas, Mehmet Harbi Calimli, Hakan Burhan, and Fatih Sen

Contents

Abstract In this chapter, the recent developments and antibacterial properties of metal, metal oxide-based nanomaterials have been discussed in detail. Microorganisms resistant to the effects of antibiotics and drugs administered in humans and

M. S. Nas
Sen Research Group, Department of Biochemistry, Faculty of Arts and Science, Dumlupınar University, Kütahya, Turkey

Department of Environmental Engineering, Faculty of Engineering, Igdir University, Igdir, Turkey

M. H. Calimli
Sen Research Group, Department of Biochemistry, Faculty of Arts and Science, Dumlupınar University, Kütahya, Turkey

Tuzluca Vocational High School, Igdir University, Igdir, Turkey

H. Burhan · F. Sen (✉)
Sen Research Group, Department of Biochemistry, Faculty of Arts and Science, Dumlupınar University, Kütahya, Turkey
e-mail: fatih.sen@dpu.edu.tr

animals may occur. In order to improve the antibacterial effects of the drugs, metal and metal oxide-based nanomaterials are highly effective and have exhibited various positive results. Due to these properties, an expanding field of use of the nanoparticles in the antibacterial field has been formed. The mechanisms of action of nanomaterials that provide antibacterial effects have not been fully elucidated. However, with the use of antibacterial effective and metal-based nanomaterials, reactive oxygen species formation were observed. Besides, some living organisms, such as bacteria and fungi, contain molecular agents that increase resistance to external influences. Disease-forming microorganisms may be resistant to both antibiotics and chromosomal gene mutations and gene transfers. The section also discusses the antimicrobial effects of sulfonamides. Additionally, specifically some effective nanoparticles, including ZnO_2, TiO_2, and SiO_2, Ag, and Al nanoparticles are mentioned in the chapter. Some important information about the properties and characterization methods are also addressed in this report.

Keywords Antimicrobial · Metal · Metal oxide · Nanomaterials

5.1   Introduction

Microorganisms have negative effects on human life. Numerous drugs are used to control infections caused by microorganisms. The resistance of these microorganisms to drugs brings about important health problems. There has been an intensive study recently to develop antimicrobial efficiency and methods. The design and development of antimicrobial agents or substances will be highly effective in eliminating the adverse conditions caused by microorganisms such as bacteria. The design of drugs or different agents that can exert a powerful antimicrobial effect is crucial to prevent microorganisms (Khameneh et al. 2016; Regiel-Futyra et al. 2017). For this purpose, the use of nanometals with antimicrobial properties has been applied very effectively in the field (Malarkodi et al. 2014). Nanomaterials were generally used for many kinds of applications (Çelik et al. 2016; Sert et al. 2016; Gezer et al. 2017; Yildiz et al. 2017; Ayranci et al. 2017a, b; Yıldız et al. 2017; Akocak et al. 2017; Demir et al. 2017; Sen et al. 2017a, b, c, d, 2018a, b, c, d, e, f, g; Bozkurt et al. 2017; Şahin et al. 2017; Eris et al. 2018a, b; Şen et al. 2018a, b, c, d, e; Çalımlı et al. 2018; Lolak et al. 2019). For instance, nanometals such as iron, copper platinum, and the like, which have an antimicrobial effect, have been used for a long time for many applications. However, the mechanisms and role of metals and microorganisms are not fully elucidated, as nanomaterials, metals, metal oxides, or sulfides may interact with molecules such as proteins, RNA, DNA, and lipids etc (Brown and Wright 2016). There are so many studies related to the antimicrobial effects of nanometals (Khezerlou et al. 2018). Studies in the literature suggest various solutions for this mechanism. One of the most accepted of these is the
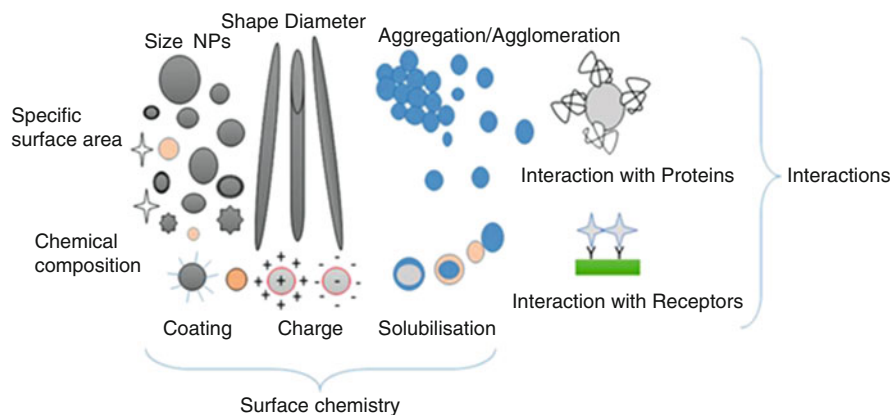
Fig. 5.1 Nanoparticles and its crystal structure, size, and shape. ("Reprinted with permission of [Nanoparticles and their antimicrobial properties against pathogens including bacteria, fungi, parasites and viruses, A. Khezerlou, M. Alizadeh-Sani, M. Azizi-Lalabadi, A. Ehsani, Elsevier]" from (Khezerlou et al. 2018) at the end of the caption)

soluble and antimicrobial effect on the surfaces of nanometals. The other one is the oxidative species that causes reactive oxygen formation on the nanoparticle surface (Fellahi et al. 2013) (Fig. 5.1).

In studies carried out on antimicrobial effects, the morpological properties and chemical effects of nanoparticles were found to be very important. It has been proven that the nanoparticles having smaller particle sizes have exhibited much more effective antibacterial effects. Additionally, the surface properties and nanoparticle shapes are the other important factors in the antimicrobial effect. For example, having positive agents on their surface facilitates the binding of negative bacteria (Khezerlou et al. 2018). Some living things, such as bacteria and fungi, contain molecular agents that increase resistance to external influences. Disease-forming microorganisms may be resistant to both antibiotics and chromosomal gene mutations and gene transfers. Therefore, the resistance of microbes to commonly used antibiotics has developed against all kinds of drugs. According to researches, bacterial resistance occurs within approximately 50 years after the first use of an antibiotic. Microorganisms constitute significant problems in many activities such as sterilization of medical devices and implants, food packaging, and food storage (Huttner et al. 2013; Brooks and Brooks 2014). Due to the resistance of bacteria and other microorganisms to antibiotics, it is necessary to intensify research in more effective and powerful material design studies. For this purpose, thanks to the unique properties of nanomaterials, significant progress has been made in overcoming these obstacles. Thus, significant opportunities have been gained in overcoming existing biological barriers and increasing drug benefits. The ability to adjust the shape and size of nanomaterials can be used for direct or indirect results on the target biological molecule. For this purpose, nanotechnological method could be used as a different method for dynamic treatment in antimicrobial applications. In this chapter, the main

properties of the metal, metal oxide nanoparticles, their antibacterial effects, and antimicrobial phenomena caused by cell/intracellular contact are described. Additionally, the section also discusses the antimicrobial properties of sulfonamide-based metal complexes.

5.2 Metal Oxide and Their Interactions in Antimicrobial Events

Copper oxides and cobalt oxides have been used as effective antibacterial materials having a nanoscale size. With the effects of these metal oxides, the formation of reactive oxygen species can be achieved. Thus, the resulting reactive oxygen species can be used to mitigate the effects of the microorganism having many pathogen plantations. The reactive oxygen species can damage protein and DNA/RNA. The bacteria membranes can be damaged by integration with material composed of reactive oxygen and phospholipid. Silver metals have also been used as disinfectants in sterilization processes. The presence of other mechanism facilitates the antimicrobial activities sourced from nanomaterials (Fones and Preston 2012; Vatansever et al. 2013). In some studies, it has been shown that hydrogen peroxide produced from water by using metal oxide including ZnO could exhibit antimicrobial effects on some microorganisms such as *E. coli* and *S. aureus* (Wyszogrodzka et al. 2016). As a result of the functionalization of metals and metal oxides, proteins in the composition of the cell membrane are disrupted. The events of functionalized metal oxides in intracellular are like those of chemical disinfectants. Unlike disinfectants, metal oxides or metals present in the antimicrobial events are not consumed or clear away. When the functionalized metal oxide or metals are produced as antimicrobial materials, chitosan, polymers, silica, nanotubes, binary/triple size compounds, and colloids are used as supporting precursor chemicals. If the supporting precursor material is an organic chemical, there may be various functional groups in the lattice structure formed. The metal–organic framework functionalized with the support material is formed as a porous structure with various functional groups. Thus, the functional structure of the formed material can be used in many fields such as adsorption, catalyst, sensor, gas storage, and purification (Janiak and Vieth 2010; Akhbari and Morsali 2013; Dechnik et al. 2017a, b). The metal–organic material is a structure containing organic chemicals in the form of binders and knots by clustering the metals or ions they contain. By means of these knot-shaped clusters, the desired structure adjustments can be made in the material formed. However, the changes in pure chemicals cannot be done. The materials containing metal oxide/metal–organic support material have a wide range of usage due to their high surface areas, porous structure, and adjustable properties.

The metal–organic nanomaterials can be used at low doses and long reuse times, and size control can be achieved. The metal–organic lattice material may form a networked spiral around the environment of the causative microorganisms. Due to the three-dimensional helical structure, metal–organic structure material is widely studied in antimicrobial studies. As mentioned earlier, nanomaterials can be more effective at low concentrations and have higher movement speeds than other antimicrobial chemicals. Increased surface area causes interaction with more microorganisms. The interaction event can occur in two ways, the inner and outer structures of the material. The use of the material in low amounts allows for long-term use and high activity coagulation. In addition, by-products of metal oxide nanomaterials do not result in disinfection. The metal oxide nanomaterials obtained may cause oxidation in the germ membranes and thus prevent the synthesis of proteins by depolarization.

5.2.1 Some Features of Metal- and Metal Oxide-Based Nanomaterials

Various methods have been used to prepare metal and metal oxide nanomaterials. The preparation methods are effective in the determining chemical and physical features of metal nanoparticles. The morphological, surface, and chemical properties of the obtained material are very important for the intended purpose. The particle size of the metal oxide or metal-coordinated organic material to be used is very important for the target to which the material obtained will affect. Therefore, having a particle size greater than 200 nm limits the range of motion of the material, and the material cannot move freely. Therefore, the particle size of the material used should be less than 200 nm. Numerous methods such as sonochemistry, hydro- or solvothermal synthesis, microwave, reverse phase microemulsion, and mechanochemistry have been developed to have the desired particle size of the material to be prepared. Advanced analytical methods such as XRD, XPS, Raman spectroscopy, TEM, and HRTEM are used for the morphological and structural analysis of the synthesized materials. These methods are applied according to the structural condition of the material or the condition of the room. Silver-based materials may have antibacterial properties and are well-known for their high stability. Important structural elements that increase the stability of the material are the supporting components containing ligands. Additionally, the shape of nanoparticle-based material is very important and affects the antimicrobial effects and activities. Generally, the metal-based antimicrobial materials used were antiviral agents with ligand shell and core structures.

5.2.2 Antimicrobial Nanoparticles and Antibiotic Effects on the Events Occurring in Microorganisms

External factors that occur in the environment and internal factors such as stress in the organism affect the susceptibility of the organisms to antibiotics, the resistance of microorganisms that reduce antibiotic effects, cell responses, and environmental adaptation. Bacteria are resistant to antibiotics in certain metals, such as copper and zinc, at high concentrations. The most important cause of environmental stress is the low concentration of metal cations. Antibiotics cause to formation of copper chelates such as tetracycline, aminoglycosides, and lactam to increase and decrease the activity of antibiotics (Carter et al. 1989; Si et al. 2008; Zawisza et al. 2016; Zarkan et al. 2016; Poole 2017). As a result of the interaction between cations formed by metal and oxides and antibiotics, antibiotic activity decreases. This reduced activity is limited in susceptibility to microorganisms in metal cations. Thus, the penetration of the membrane changes, resulting in the level of antimicrobial activity. Nanoparticle-size metals and oxides are associated with gram-negative, pathogenic microorganisms such as *P. aeruginosa* and *E. coli*. Recent studies have discovered that copper-based antibiotics act on copper deficiency (Dalecki et al. 2015; Khezerlou et al. 2018). Metal oxide-based nanoparticles have been used very effectively against microorganisms that limit antibiotic activity since they contain many active sites, porous structures, and different functional groups. The shapes of metal-based nanoparticles can be highly effective at the molecular level and these types of nanomaterials can be used very effectively as effective oxygen generator. Some studies have shown that clay structure nanoparticles are effective in membrane degradation in bacteria. Other types of nanoparticles have been shown to give effective results in food and pharmaceutical applications. Nano-sized metal oxides were found to have more antimicrobial effect than micro-dimensional metal oxides. Nanoscale metal oxides are found to be more effective in the formation of active oxygen that adds antimicrobial activity (Rongione et al. 2017; Dasgupta et al. 2017). Inductive oxidative stress caused by nanoparticles has been found to cause the formation of cytotoxicity in the human organism. It causes the formation of intracellular oxidative stress as a result of the clumping of nanoparticles in cell cytoplasm and nucleus. Small-scale nanoparticles also interact with intracellular genetic structures. The presence of a high concentration of nanoparticles (microgram) activates intracellular proliferation. In contrast, low concentration nanoparticles reduce cell proliferation. Nano-dimensionality and material type affect cytotoxicity by intracellular entry and depend on partial trends in nanoscale dimensions. Surface charges and nanomaterial concentration also affect nanoparticle toxicity. This is due to the electrostatic bonding of the intracellular substances with the nanoparticles.

5.3 Entrance of Nanoparticle into Cells and Occurred Toxic Events

The interaction and unit identity of nanoparticles in the human organism are not fully elucidated. Some nanoparticles, such as gold, have been found to accumulate in white blood cells of the human organism by phagocytosis or direct penetration. Since the size of the nanoparticles is very small, it can easily pass through the human body by inhalation or digestion. It is used extensively in health and industry fields. So, it can meet a lot of human bodies. In addition, nanoparticles can enter human nerve cells as a result of transport by the skin from nerve endings. As their concentration increases and their size decreases, their toxic effects increase considerably. In living organisms formed with nanoparticles, cytotoxicity causes oxidative stress and DNA damage.

In addition to the ions formed by nanoparticles, other cellular events also have toxic effects. In other words, toxic induction has not been fully elucidated. However, it is certain that the amount of active oxygen in the cell increases with nanoparticles (Karlsson et al. 2008; Rice et al. 2009; Prabhu et al. 2010). A possible explanation of the entrance of nanoparticle into cells has been explained in a study (Khezerlou et al. 2018) summarized as nanoparticles are taken into cells according to their energy capacity with endosomes, lysosomes, and vascular structures. A lysosome is having an acidic feature combining nanoparticles taken into cells that enhance toxic ions number. The formed ions affect some curtain cell structures and cellular processes like mitochondria, membrane, lysosomes, protein production, etc. by apoptosis, dysfunction, or lysosomal damage. As a result of this process, the level of active oxygen is enhanced, and apoptosis and DNA and membrane damage occur. The nanoparticle entrance into cells is illustrated as in Fig. 5.2.

As again given the study, some nanoparticles, like ZnO and TiO_2, induce some cellular events of necrosis, autophagy, and cell apoptosis, forming active oxygen. These nanoparticles enhance the amount of reactive oxygen in the cytoplasm that forms the thioredoxin oxidation and signals regular kinase apoptosis. The regular forming apoptosis controls the anti- and proapoptotic protein and death ligands. At the end of this event, cell apoptosis AKT kinase occurs that induces proteins of Bcl-Xl and Bcl-2 (Fig. 5.3.) (Khezerlou et al. 2018).

5.3.1 Strategies for Developing Antimicrobial Agents

In order to investigate the antimicrobial activities, various methods have been applied. Novel drugs fabricated with new therapeutic techniques are an effective and promising materials. New drugs are effective with simultaneous actions and mechanisms. The resistance to antimicrobial effective and multifunctional materials leads to the formation of many gene mutations. Recent studies demonstrated that new metal-based antimicrobial precursor is effective agents against antimicrobial
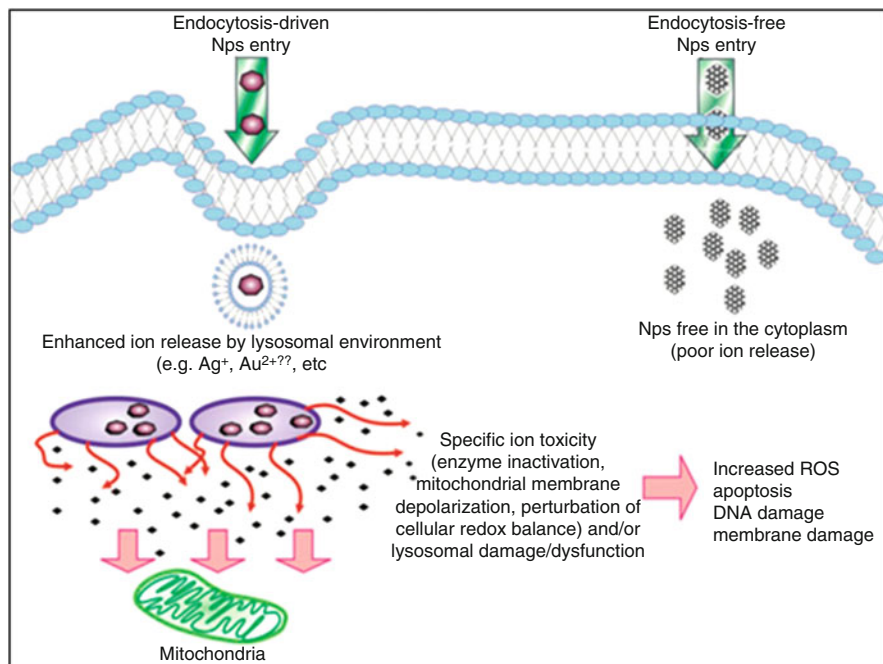
Fig. 5.2 The illustration of nanoparticle entrance into cells and events occurred intake of cells. ("Reprinted with permission of [Nanoparticles and their antimicrobial properties against pathogens including bacteria, fungi, parasites and viruses, A. Khezerlou, M. Alizadeh-Sani, M. Azizi-Lalabadi, A. Ehsani, Elsevier]" from (Khezerlou et al. 2018) at the end of the caption)

effects and may be replaced to conventional drugs. Recent studies demonstrated that new metal-based antimicrobial precursors are effective agents against antimicrobial effects and may replace conventional drugs. In designing new materials, it is required to replace new materials that enhance the antimicrobial activities. Mechanisms composed of multiple effects can be an excellent strategy to prevent microorganism's drug resistance. The literature includes so many studies of metal and metal oxide-based bioorganic materials that have been used as antimicrobial agents (Fellahi et al. 2013). These studies revealed that the antimicrobial agents with positive charge is feasible the combining with negatively charged molecules and components in the structure of cells and this combination improve the antimicrobial activities. Combination of metals with the biological composition led to forming of new agents as drugs with multiple effects and activity that clear the resistance pathways.

Due to the multimodal effects of the modified macromolecule with metal and metal oxide, great importance has been given to multifunctional synthesis materials. To overcome the challenges of microbial resistance, various metal-based biomacromolecules having many mechanisms have been fabricated using multitask strategies. Generally, mentioned macromolecules combined with metal and metal
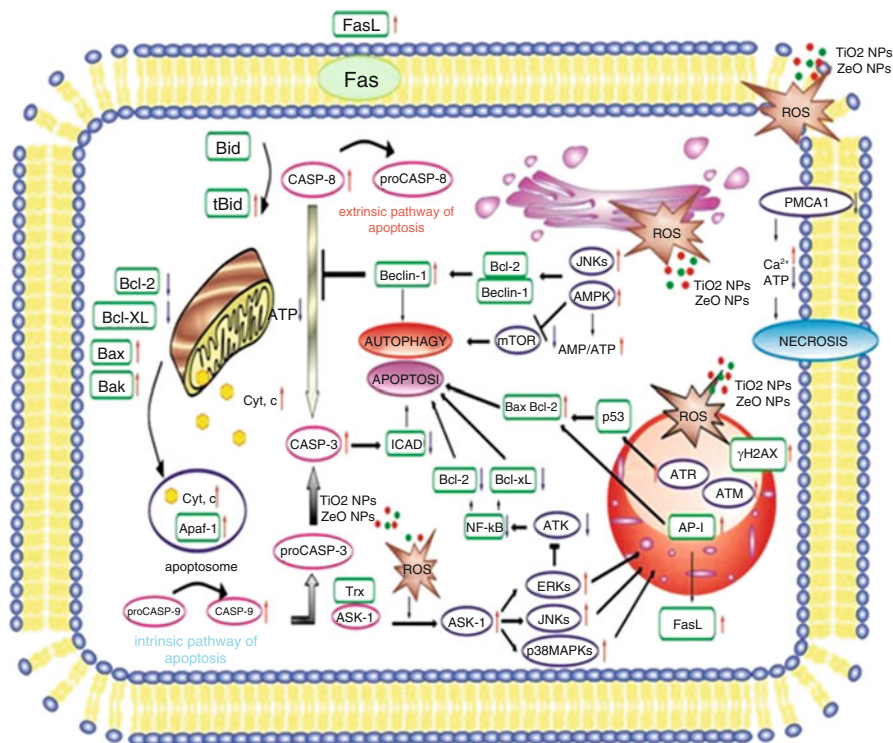
Fig. 5.3 TiO$_2$, ZnO, and molecular mechanisms of ROS-mediated. ("Reprinted with permission of [Nanoparticles and their antimicrobial properties against pathogens including bacteria, fungi, parasites and viruses, A. Khezerlou, M. Alizadeh-Sani, M. Azizi-Lalabadi, A. Ehsani, Elsevier]" from (Khezerlou et al. 2018) at the end of the caption)

oxide are dendrimers, peptides, polymers or their derivatives and proteins. Antimicrobial materials consisting of metal-based and biomacromolecules are used for many processes such as interacting with the cell wall, removing nutrients from pathogens, and reducing microbial drainage. Synthesized materials combined with metal/metal oxide and macromolecular interact with the parts of the composition of cells like proteins or lipids by biochemical events. Some redox metals in the composition materials cause to formation of oxidative chemicals that lead to defense against pathogenic microorganisms. The synthesized metal and metal oxide-based nanomaterials are developed against antimicrobial activities caused by fungi and bacteria. Concurrent mechanisms are being developed to prevent these antimicrobial effects. Cell deaths caused by antimicrobial effects are explained by a mechanism such as a cell wall damage which is the first explanation for antimicrobial effects. Another explanation for the mechanism is cell damage caused by active oxygen generated by nanomaterials.

During the use of nanomaterials, identifying the target sites where infection occurs minimizes microbial resistance and side effects. The presence of a large

number of active substances in the material structure increases the likelihood of the targeted effect. From this point of view, strategies based on different bioinorganic processes should be developed in material design. The preparation of different bactericidal surfaces and antibiotics should be focused on. Nowadays, various developed and commercialized bioorganic nanoproducts including sutures, dentistry cement, and catheters have been developed and approved by authorities to be used in biomedicine (Regiel-Futyra et al. 2017). The development of these materials can affect microorganisms as antimicrobial agents. These materials are effective with various events such as killing pathogenic cells, preventing pathogenic adhesion, and releasing pathogenic agents. Nanoparticles not only affect the mentioned antimicrobial event but also cause to form some different niches. Developments of nanomaterials combining different functions are enabled to prevent pathogenic effects and overcome the microbial resistance.

5.3.2   Sulfonamide-Based Metal Complexes

The activity of the sulfonamides is due to the inhibition of microbial folic acid and nucleic synthesis. They are used as antifungal and bacterial compounds. The resistance formed by sulfonamides is formed by the compound formed as dihydropteroate synthase. The amino groups present in the sulfonamides are targeted binding sites for metal and metal oxide complexes. Materials with different toxicological and pharmacological effects are formed by the coordination of the metals with sulfonamides. Sulfonamides composed of Fe(II), Fe(III), Cd(II), Cu(II), and Zn(II) are called as Schiff bases that exhibit antibacterial and antifungal effects. Experimental results have shown that sulfonamide-based metal complexes are effective agents against antimicrobial activities, which are superior to some antibiotics such as cephalothin, cycloheximide, and chloramphenicol. The mostly used bacteria are *B. subtilis, S. aureus*, gram-negative, *E. coli*, fungi *Aspergillus*, etc. The experimental findings showed that complexes formed with Cd(II) are to be the highest antimicrobial agents against the mentioned bacteria. The other sulfonamide complexes composed of Fe(II), Fe(III), Cu(II), and Zn(II) metal were also found as antimicrobial agents gram-positive microorganisms including *S. aureus*, *E. faecalis*, *B. subtilis*, *B. cereus*, and gram-negative bacteria like *K. pneumoniae*, *E. coli*, and *P. aeruginosa* (Byarugaba 2010; Özbek et al. 2017; Sharaby et al. 2017).

5.3.3   Silver (Ag), Silicium Oxide, and Aluminum Oxide Nanoparticles as Antimicrobial Agents

Silver nanoparticles (Ag) are common nanomaterials used as antimicrobial effective agents. Because of the antimicrobial effects of Ag nanoparticle (Klaus et al. 1999;

Mittal et al. 2014; Kumar et al. 2016; Peng et al. 2016; Bahram 2016; Rai et al. 2017; Francis et al. 2018) additives, it is widely used in the production of several polymeric products, textiles, and coating materials. Ag nanoparticles have been used in numerous biomedical applications due to their antimicrobial effects (Şahin et al. 2017). As a result of the studies, it has been shown that metallic silver exhibited more antimicrobial effect than metallic silver ionic forms. As a result of the studies, it has been found that Ag nanoparticles have a wide antibacterial potential against bacteria. The effects of Ag nanoparticles were found to be effective in the damage to bacterial cell membranes. Studies have shown that Ag nanoparticles can be used effectively in cell membrane lysis. It has been found that the degradation of intracellular metabolic events occurs by the interaction of these materials with disulfide and sulfhydryl group (Allahverdiyev et al. 2011; Zinjarde 2012; Malarkodi et al. 2014). Silicium oxide (SiO$_2$)-based nanoparticles have been found to be effective in increasing the surface area of nanoscale materials. Bacteria have been found to prevent oral film adhesion. Material design has been made in recent years by using silicon with another metal. Silicium nanoparticles have been found to be antimicrobial effective against a large number of microorganisms such as *E. coli* and *C. albicans* (Kim et al. 2006; Cousins et al. 2007; Dhapte et al. 2014). Another important nanoparticle is aluminum oxide. Aluminum oxide (Al$_2$O$_3$) nanoparticles are widely used in personal and industrial applications. It has been shown that the application of these nanoparticles on *E. coli* bacteria prevents bacterial growth and can be used as an effective antibacterial agent. These agents have been found to be effective in cell membrane, wall, and cell. In addition, it has been found that these nanoparticles prevent free radical removal and cell wall degradation (Martínez-Flores et al. 2003; Sadiq et al. 2009).

5.4 Conclusion

The materials containing metal oxide/metal–organic support material have a wide range of usage due to their high surface areas, porous structure, and adjustable properties. The metal–organic nanomaterials can be used at low doses and long reuse times, and size control can be achieved. The metal–organic lattice material may form a networked spiral around the environment of the causative microorganisms. Due to the three-dimensional helical structure, metal–organic structure material is widely studied in antimicrobial studies. The morphological, surface, and chemical properties of the obtained material are very important for the intended purpose. The particle size of the metal oxide or metal-coordinated organic material to be used is very important for the target to which the material obtained will affect. Therefore, having a particle size greater than 200 nm limits the range of motion of the material, and the material cannot move freely. Some nanoparticles, such as gold, have been found to accumulate in white blood cells of the human organism by phagocytosis or direct penetration. Since the size of the nanoparticles is very small, it can easily pass through the human body by inhalation or digestion. It is used

extensively in health and industry fields. In addition, nanoparticles can enter human nerve cells as a result of transport by the skin from nerve endings. As their concentration increases and their size decreases, their toxic effects increase considerably. In living organisms formed with nanoparticles, cytotoxicity causes oxidative stress and DNA damage. Sulfonamide-based metal complexes are effective agents against antimicrobial activities, which are superior to some antibiotics such as cephalothin, cycloheximide, and chloramphenicol. Mostly used bacteria are *B. subtilis*, *S. aureus*, gram-negative, *E. coli*, fungi *Aspergillus*, etc. It can be concluded that complexes formed with Cd (II) are to be one of the highest antimicrobial agents against the mentioned bacteria.

References

Akhbari K, Morsali A (2013) Modulating methane storage in anionic nano-porous MOF materials via post-synthetic cation exchange process. Dalt Trans 42:4786. https://doi.org/10.1039/c3dt32846e

Akocak S, Şen B, Lolak N et al (2017) One-pot three-component synthesis of 2-amino-4H-chromene derivatives by using monodisperse Pd nanomaterials anchored graphene oxide as highly efficient and recyclable catalyst. Nano-Struct Nano-Objects 11:25–31. https://doi.org/10.1016/j.nanoso.2017.06.002

Allahverdiyev AM, Abamor ES, Bagirova M, Rafailovich M (2011) Antimicrobial effects of TiO 2 and Ag 2 O nanoparticles against drug-resistant bacteria and leishmania parasites. Future Microbiol 6:933–940. https://doi.org/10.2217/fmb.11.78

Ayranci R, Baskaya G, Guzel M et al (2017a) Activated carbon furnished monodisperse Pt nanocomposites as a superior adsorbent for methylene blue removal from aqueous solutions. Nano-Struct Nano-Objects 11:13–19. https://doi.org/10.1016/j.nanoso.2017.05.008

Ayranci R, Başkaya G, Güzel M et al (2017b) Carbon based Nanomaterials for high performance Optoelectrochemical systems. ChemistrySelect 2:1548–1555. https://doi.org/10.1002/slct.201601632

Bahram GE (2016) An investigation of the effect of copper oxide and silver nanoparticles on E. Coli genome by rapd molecular markers. Adv Biotechnol Microbiol 1:555559. https://doi.org/10.19080/AIBM.2016.01.555559

Bozkurt S, Tosun B, Sen B et al (2017) A hydrogen peroxide sensor based on TNM functionalized reduced graphene oxide grafted with highly monodisperse Pd nanoparticles. Anal Chim Acta 989:88–94. https://doi.org/10.1016/j.aca.2017.07.051

Brooks BD, Brooks AE (2014) Therapeutic strategies to combat antibiotic resistance. Adv Drug Deliv Rev 78:14–27. https://doi.org/10.1016/j.addr.2014.10.027

Brown ED, Wright GD (2016) Antibacterial drug discovery in the resistance era. Nature 529:336–343. https://doi.org/10.1038/nature17042

Byarugaba DK (2010) Mechanisms of antimicrobial resistance. In: Antimicrobial resistance in developing countries. Springer New York, New York, pp 15–26

Çalımlı MH, Demirbaş Ö, Aygün A et al (2018) Immobilization kinetics and mechanism of bovine serum albumin on diatomite clay from aqueous solutions. Appl Water Sci 8:209. https://doi.org/10.1007/s13201-018-0858-8

Carter MT, Rodriguez M, Bard AJ (1989) Voltammetric studies of the interaction of metal chelates with DNA. 2. Tris-chelated complexes of cobalt(III) and iron(II) with 1,10-phenanthroline and 2,2′-bipyridine. J Am Chem Soc 111:8901–8911. https://doi.org/10.1021/ja00206a020

Çelik B, Kuzu S, Erken E et al (2016) Nearly monodisperse carbon nanotube furnished nanocatalysts as highly efficient and reusable catalyst for dehydrocoupling of DMAB and C1 to C3 alcohol oxidation. Int J Hydrog Energy 41:3093–3101. https://doi.org/10.1016/j.ijhydene.2015.12.138

Cousins B, Allison H, Doherty PJ et al (2007) Effects of a nanoparticulate silica substrate on cell attachment of Candida albicans. J Appl Microbiol 102:757–765. https://doi.org/10.1111/j.1365-2672.2006.03124.x

Dalecki AG, Haeili M, Shah S et al (2015) Disulfiram and copper ions kill Mycobacterium tuberculosis in a synergistic manner. Antimicrob Agents Chemother 59:4835–4844. https://doi.org/10.1128/AAC.00692-15

Dasgupta N, Ranjan S, Ramalingam C (2017) Applications of nanotechnology in agriculture and water quality management. Environ Chem Lett 15:591–605. https://doi.org/10.1007/s10311-017-0648-9

Dechnik J, Gascon J, Doonan CJ et al (2017a) Mixed-matrix membranes. Angew Chemie Int Ed 56:9292–9310. https://doi.org/10.1002/anie.201701109

Dechnik J, Sumby CJ, Janiak C (2017b) Enhancing mixed-matrix membrane performance with metal–organic framework additives. Cryst Growth Des 17:4467–4488. https://doi.org/10.1021/acs.cgd.7b00595

Demir E, Sen B, Sen F (2017) Highly efficient Pt nanoparticles and f-MWCNT nanocomposites based counter electrodes for dye-sensitized solar cells. Nano-Struct Nano-Objects 11:39–45. https://doi.org/10.1016/j.nanoso.2017.06.003

Dhapte V, Kadam S, Pokharkar V et al (2014) Versatile SiO 2 nanoparticles@polymer composites with pragmatic properties. ISRN Inorg Chem 2014:1–8. https://doi.org/10.1155/2014/170919

Eris S, Daşdelen Z, Sen F (2018a) Enhanced electrocatalytic activity and stability of monodisperse Pt nanocomposites for direct methanol fuel cells. J Colloid Interface Sci 513:767–773. https://doi.org/10.1016/j.jcis.2017.11.085

Eris S, Daşdelen Z, Yıldız Y, Sen F (2018b) Nanostructured polyaniline-rGO decorated platinum catalyst with enhanced activity and durability for methanol oxidation. Int J Hydrog Energy 43:1337–1343. https://doi.org/10.1016/j.ijhydene.2017.11.051

Fellahi O, Sarma RK, Das MR et al (2013) The antimicrobial effect of silicon nanowires decorated with silver and copper nanoparticles. Nanotechnology 24:495101. https://doi.org/10.1088/0957-4484/24/49/495101

Fones H, Preston GM (2012) Reactive oxygen and oxidative stress tolerance in plant pathogenic Pseudomonas. FEMS Microbiol Lett 327:1–8. https://doi.org/10.1111/j.1574-6968.2011.02449.x

Francis S, Joseph S, Koshy EP, Mathew B (2018) Microwave assisted green synthesis of silver nanoparticles using leaf extract of elephantopus scaber and its environmental and biological applications. Artif Cells Nanome Biotechnol 46:795–804. https://doi.org/10.1080/21691401.2017.1345921

Gezer B, Sert H, Onal Okyay T et al (2017) Reduced graphene oxide (rGO) as highly effective material for the ultrasound assisted boric acid extraction from ulexite ore. Chem Eng Res Des 117:542–548. https://doi.org/10.1016/j.cherd.2016.11.007

Huttner A, Harbarth S, Carlet J et al (2013) Antimicrobial resistance: a global view from the 2013 World Healthcare-Associated Infections Forum. Antimicrob Resist Infect Control 2:31. https://doi.org/10.1186/2047-2994-2-31

Janiak C, Vieth JK (2010) MOFs, MILs and more: concepts, properties and applications for porous coordination networks (PCNs). New J Chem 34:2366. https://doi.org/10.1039/c0nj00275e

Karlsson HL, Cronholm P, Gustafsson J, Möller L (2008) Copper oxide nanoparticles are highly toxic: a comparison between metal oxide nanoparticles and carbon nanotubes. Chem Res Toxicol 21:1726–1732. https://doi.org/10.1021/tx800064j

Khameneh B, Diab R, Ghazvini K, Fazly Bazzaz BS (2016) Breakthroughs in bacterial resistance mechanisms and the potential ways to combat them. Microb Pathog 95:32–42. https://doi.org/10.1016/j.micpath.2016.02.009

Khezerlou A, Alizadeh-Sani M, Azizi-Lalabadi M, Ehsani A (2018) Nanoparticles and their antimicrobial properties against pathogens including bacteria, fungi, parasites and viruses. Microb Pathog 123:505–526. https://doi.org/10.1016/j.micpath.2018.08.008

Kim YH, Lee DK, Cha HG et al (2006) Preparation and characterization of the antibacterial Cu nanoparticle formed on the surface of SiO 2 nanoparticles. J Phys Chem B 110:24923–24928. https://doi.org/10.1021/jp0656779

Klaus T, Joerger R, Olsson E, Granqvist C-G (1999) Silver-based crystalline nanoparticles, microbially fabricated. Proc Natl Acad Sci 96:13611–13614. https://doi.org/10.1073/PNAS.96.24.13611

Kumar B, Smita K, Cumbal L (2016) Biosynthesis of silver nanoparticles using lavender leaf and their applications for catalytic, sensing, and antioxidant activities. Nanotechnol Rev 5:521–528. https://doi.org/10.1515/ntrev-2016-0041

Lolak N, Kuyuldar E, Burhan H et al (2019) Composites of palladium–nickel alloy nanoparticles and graphene oxide for the Knoevenagel condensation of aldehydes with malononitrile. ACS Omega 4:6848–6853. https://doi.org/10.1021/acsomega.9b00485

Malarkodi C, Rajeshkumar S, Paulkumar K et al (2014) Biosynthesis and antimicrobial activity of semiconductor nanoparticles against oral pathogens. Bioinorg Chem Appl 2014:1–10. https://doi.org/10.1155/2014/347167

Martínez-Flores E, Negrete J, Villasenor GT (2003) Structure and properties of Zn-Al-Cu alloy reinforced with alumina particles. Mater Des 24:281–286. https://doi.org/10.1016/S0261-3069(03)00028-1

Mittal AK, Kumar S, Banerjee UC (2014) Quercetin and gallic acid mediated synthesis of bimetallic (silver and selenium) nanoparticles and their antitumor and antimicrobial potential. J Colloid Interface Sci 431:194–199. https://doi.org/10.1016/j.jcis.2014.06.030

Özbek N, Alyar S, Memmi BK et al (2017) Synthesis, characterization, computational studies, antimicrobial activities and carbonic anhydrase inhibitor effects of 2-hydroxy acetophenone-N-methyl p-toluenesulfonylhydrazone and its Co(II), Pd(II), Pt(II) complexes. J Mol Struct 1127:437–448. https://doi.org/10.1016/j.molstruc.2016.07.122

Peng Z, Jiang Z, Huang X, Li Y (2016) A novel electrochemical sensor of tryptophan based on silver nanoparticles/metal–organic framework composite modified glassy carbon electrode. RSC Adv 6:13742–13748. https://doi.org/10.1039/C5RA25251B

Poole K (2017) At the nexus of antibiotics and metals: the impact of Cu and Zn on antibiotic activity and resistance. Trends Microbiol 25:820–832. https://doi.org/10.1016/j.tim.2017.04.010

Prabhu BM, Ali SF, Murdock RC et al (2010) Copper nanoparticles exert size and concentration dependent toxicity on somatosensory neurons of rat. Nanotoxicology 4:150–160. https://doi.org/10.3109/17435390903337693

Rai T, Sharma A, Panda D (2017) Quantifying the role of silver nanoparticles in the modulation of the thermal energy storage properties of PAM–Ag nanocomposites. New J Chem 41:2029–2036. https://doi.org/10.1039/C6NJ04077B

Regiel-Futyra A, Dąbrowski JM, Mazuryk O et al (2017) Bioinorganic antimicrobial strategies in the resistance era. Coord Chem Rev 351:76–117. https://doi.org/10.1016/J.CCR.2017.05.005

Rice RH, Vidrio EA, Kumfer BM et al (2009) Generation of oxidant response to copper and iron nanoparticles and salts: stimulation by ascorbate. Chem Biol Interact 181:359–365. https://doi.org/10.1016/j.cbi.2009.08.007

Rongione NA, Floerke SA, Celik E (2017) Developments in antibacterial disinfection techniques. In: Materials science and engineering. IGI Global, Hershey, pp 594–612

Sadiq IM, Chowdhury B, Chandrasekaran N, Mukherjee A (2009) Antimicrobial sensitivity of Escherichia coli to alumina nanoparticles. Nanomed Nanotechnol Biol Med 5:282–286. https://doi.org/10.1016/j.nano.2009.01.002

Şahin B, Demir E, Aygün A et al (2017) Investigation of the effect of pomegranate extract and monodisperse silver nanoparticle combination on MCF-7 cell line. J Biotechnol 260:79–83. https://doi.org/10.1016/j.jbiotec.2017.09.012

Sen B, Kuzu S, Demir E et al (2017a) Highly efficient catalytic dehydrogenation of dimethyl ammonia borane via monodisperse palladium–nickel alloy nanoparticles assembled on PEDOT. Int J Hydrog Energy 42:23307–23314. https://doi.org/10.1016/j.ijhydene.2017.05.115

Sen B, Kuzu S, Demir E et al (2017b) Highly monodisperse RuCo nanoparticles decorated on functionalized multiwalled carbon nanotube with the highest observed catalytic activity in the dehydrogenation of dimethylamine−borane. Int J Hydrog Energy 42:23292–23298. https://doi.org/10.1016/j.ijhydene.2017.06.032

Sen B, Kuzu S, Demir E et al (2017c) Hydrogen liberation from the dehydrocoupling of dimethylamine–borane at room temperature by using novel and highly monodispersed RuPtNi nanocatalysts decorated with graphene oxide. Int J Hydrog Energy 42:23299–23306. https://doi.org/10.1016/j.ijhydene.2017.04.213

Sen B, Kuzu S, Demir E et al (2017d) Polymer-graphene hybride decorated Pt nanoparticles as highly efficient and reusable catalyst for the dehydrogenation of dimethylamine–borane at room temperature. Int J Hydrog Energy 42:23284–23291. https://doi.org/10.1016/j.ijhydene.2017.05.112

Şen B, Aygün A, Okyay TO et al (2018a) Monodisperse palladium nanoparticles assembled on graphene oxide with the high catalytic activity and reusability in the dehydrogenation of dimethylamine-borane. Int J Hydrog Energy 43:20176–20182. https://doi.org/10.1016/j.ijhydene.2018.03.175

Sen B, Demirkan B, Şavk A et al (2018b) Trimetallic PdRuNi nanocomposites decorated on graphene oxide: a superior catalyst for the hydrogen evolution reaction. Int J Hydrog Energy 43:17984–17992. https://doi.org/10.1016/j.ijhydene.2018.07.122

Şen B, Aygün A, Şavk A et al (2018c) Bimetallic palladium–iridium alloy nanoparticles as highly efficient and stable catalyst for the hydrogen evolution reaction. Int J Hydrog Energy 43:20183–20191. https://doi.org/10.1016/j.ijhydene.2018.07.081

Sen B, Demirkan B, Şimşek B et al (2018d) Monodisperse palladium nanocatalysts for dehydrocoupling of dimethylamine borane. Nano-Struct Nano-Objects 16:209–214. https://doi.org/10.1016/j.nanoso.2018.07.008

Şen B, Demirkan B, Savk A et al (2018e) High-performance graphite-supported ruthenium nanocatalyst for hydrogen evolution reaction. J Mol Liq 268:807–812. https://doi.org/10.1016/J.MOLLIQ.2018.07.117

Sen B, Kuyuldar E, Demirkan B et al (2018f) Highly efficient polymer supported monodisperse ruthenium-nickel nanocomposites for dehydrocoupling of dimethylamine borane. J Colloid Interface Sci 526:480–486. https://doi.org/10.1016/J.JCIS.2018.05.021

Sen B, Şavk A, Sen F (2018g) Highly efficient monodisperse Pt nanoparticles confined in the carbon black hybrid material for hydrogen liberation. J Colloid Interface Sci 520:112–118. https://doi.org/10.1016/J.JCIS.2018.03.004

Sert H, Yıldız Y, Okyay TO et al (2016) Monodisperse Mw-Pt NPs@VC as highly efficient and reusable adsorbents for methylene blue removal. J Clust Sci 27:1953–1962. https://doi.org/10.1007/s10876-016-1054-3

Sharaby CM, Amine MF, Hamed AA (2017) Synthesis, structure characterization and biological activity of selected metal complexes of sulfonamide Schiff base as a primary ligand and some mixed ligand complexes with glycine as a secondary ligand. J Mol Struct 1134:208–216. https://doi.org/10.1016/j.molstruc.2016.12.070

Si H, Hu J, Liu Z, Zeng Z (2008) Antibacterial effect of oregano essential oil alone and in combination with antibiotics against extended-spectrum β-lactamase-producing Escherichia coli : table 1. FEMS Immunol Med Microbiol 53:190–194. https://doi.org/10.1111/j.1574-695X.2008.00414.x

Vatansever F, de Melo WCMA, Avci P et al (2013) Antimicrobial strategies centered around reactive oxygen species – bactericidal antibiotics, photodynamic therapy, and beyond. FEMS Microbiol Rev 37:955–989. https://doi.org/10.1111/1574-6976.12026

Wyszogrodzka G, Marszałek B, Gil B, Dorożyński P (2016) Metal-organic frameworks: mechanisms of antibacterial action and potential applications. Drug Discov Today 21:1009–1018. https://doi.org/10.1016/j.drudis.2016.04.009

Yildiz Y, Okyay TO, Sen B et al (2017) Highly monodisperse Pt/Rh nanoparticles confined in the graphene oxide for highly efficient and reusable sorbents for methylene blue removal from aqueous solutions. ChemistrySelect 2:697–701. https://doi.org/10.1002/slct.201601608

Yıldız Y, Kuzu S, Sen B et al (2017) Different ligand based monodispersed Pt nanoparticles decorated with rGO as highly active and reusable catalysts for the methanol oxidation. Int J Hydrog Energy 42:13061–13069. https://doi.org/10.1016/j.ijhydene.2017.03.230

Zarkan A, Macklyne H-R, Truman AW et al (2016) The frontline antibiotic vancomycin induces a zinc starvation response in bacteria by binding to Zn(II). Sci Rep 6:19602. https://doi.org/10.1038/srep19602

Zawisza B, Baranik A, Malicka E et al (2016) Preconcentration of Fe(III), Co(II), Ni(II), Cu(II), Zn(II) and Pb(II) with ethylenediamine-modified graphene oxide. Microchim Acta 183:231–240. https://doi.org/10.1007/s00604-015-1629-y

Zinjarde S (2012) Bio-inspired nanomaterials and their applications as antimicrobial agents. Chronicles Young Sci 3:74. https://doi.org/10.4103/2229-5186.94314

Chapter 6
Role of Metals, Metal Oxides, and Metal Sulfides in the Diagnosis and Treatment of Cancer

Rekha Pachaiappan and Kovendhan Manavalan

Contents

Abstract According to the World Health Organization, cancer is the second main reason of demise after cardio-related health problems, and it documented 9.6 million cancer deaths in 2018. So, it is inevitable to detect cancer at an early stage in deciding the suitable therapy to provide successful treatment for patients. In this scenario, extraordinary growth of nanotechnology emerged with the new nanoparticles which find its valid place in the early detection and treatment of cancer. In the field of oncology, nanoparticles are employed in both detecting and treatment process. As nanoparticles are smaller in size, desired shape and surface area to volume ratio are high enabling them to easily combine with biomolecules such as proteins, DNA, RNA, small molecular drugs, etc. Thus, nanoparticles are able to function as effective drug carriers in various cancer therapies such as gene,

R. Pachaiappan (✉)
Adhiyaman Arts and Science College for Women, Uthangarai, Tamilnadu, India

K. Manavalan
Department of Environmental Engineering, Inha University, Incheon, South Korea

photodynamic, thermal therapy, etc. and act as a molecular imaging agent to detect and monitor cancer cell progression. Metals, metal oxides, and metal sulfide nanoparticles were found simultaneously more powerful as a diagnostic tool in the detection of cancer cells and as a therapeutic agent in cancer therapy by offering enhanced targeting, gene silencing, and drug delivery. This chapter briefly addresses the various metals, metal oxides, and metal sulfide nanoparticles in diagnosis and treatment of cancer.

Keywords Gold nanoparticles · Silver nanoparticles · Iron oxide nanoparticles · Zinc oxide nanoparticles · Zinc sulphide nanoparticles · Copper sulphide nanoparticles · Rhenium sulphide nanoparticles · Early cancer diagnosis · Cancer treatment · Photo imaging

Abbreviations

anti-EGFR	anti-epidermal growth factor
AS Tf-HMCuS nanoparticles	artesunate coupled transferrin-hollow mesoporous copper sulfide nanoparticles
Au nanoparticles	gold nanoparticles
BM	*Butea monosperma*
CT	computed tomography
CuS nanoparticles	copper sulfide nanoparticles
CuS FN nanoparticles	copper sulfide ferritin nanoparticles
DMR	diffusion molecular retention
FAD	flavin adenine dinucleotide
IO nanoparticles	iron oxide nanoparticles
M nanoparticles	magnetic nanoparticles
MRI	magnetic resonance imaging
NIR	near-infrared
OCT	optical coherence tomography
PAI	photoacoustic imaging
PDA	polydopamine
PDT	photodynamic therapy
PTT	photothermal therapy
PVP	polyvinylpyrrolidone
PET	positron emission tomography
PSA	prostate-specific antigen
PSMA	prostate-specific membrane antigen
ROS	reactive oxygen species
RGO	reduced graphene oxide
RES	reticular endothelial system
SLN	sentinel lymph nodes
SERS	surface-enhanced RAMAN spectroscopy
Ag nanoparticles	silver nanoparticles

SPIO	superparamagnetic iron oxide
SPR	surface plasmon resonance
THG	third-harmonic generation
USPIO	ultrasmall superparamagnetic iron oxide
WHO	World Health Organization
ZnO nanoparticles	zinc oxide nanoparticles

6.1   Introduction

Standard several diagnostic and treatment methods are available to deal with cancer. However, cancer remains the cause for death after cardio-related health issues and provides economic burden to the society. More than 200 types of cancers were identified based on the origin of the cancer cell and its functions/effects over the normal system. According to a recent report released by the World Health Organization (WHO) in 2018, cancer burden was increased with 18.1 million new cases and 9.6 million cancer-related deaths (https://www.who.int/cancer/PRGlobocanFinal.pdf). The continent Asia had produced 50% of new cancer cases and greater than 50% of cancer deaths, as it comprises 60% of the global population. Cancer-related deaths are due to metastasis which is responsible for ~90% death rate (Mehlen and Puisieux 2006). Globally, five year survival/prevalence rate was provided to be 43.8 million people. Several factors were responsible for the cancer burden which includes growth in population, aging, lifestyles, socioeconomic problems like poverty, infections, lack of awareness about cancer, need of suitable mass screening techniques, etc. Further, tobacco usage is the major cause of global cancer burden, accounting for 20% deaths all over the world.

In the case of cancer diagnosis, tissue biopsy and obtaining the histopathological report remain as a golden standard technique. This technique has several pitfalls like being subjective, causing mental and physical pain to patients, and is time-consuming, and the final result depends on the clinician's view. While considering treatment for cancer – surgery, radiotherapy, chemotherapy, hormone therapy, immunotherapy, and a combination of these techniques were also used. The tumor site, grade, stage of primary tumor, and patient age determine the treatment plan. Cancer treatment was given in such a way to reduce the mental and physical burden caused by it, to improve the survival rate, and to prevent the recurrence of cancer cells. These regular treatment methods have their own limitations/side effects. Surgery of cancer tumor produces side effects like swelling of surgery site, infection, bleeding, fatigue, loss of appetite, etc. Radiotherapy side effects are skin changes, loss of appetite, weakness, fatigue, less immunity, etc. Chemotherapy's common side effects are nausea, fatigue, hair loss, reduction in blood components, mental changes, constipation problems, etc., and in some cases, permanent damage to the organs and nervous system also occurs. Certain medications used in hormone therapy cause regular pattern changes in the human system, e.g., impotence in the

case of prostate cancer. Immunotherapy produces side effects such as cold, fever, swelling, tiredness, etc. Due to lack in early diagnosis of cancer, side effects of conventional treatment methods, and recurrence of cancer cells after treatment made the researchers to explore the new strategies in the diagnosis and therapy of cancer.

In this scenario, the development in nanoscience and technology had improved the diagnostics and treatment/therapeutics methods in the detection and treatment of cancer and many other diseases. The novelty of nanomaterials allow the researchers and scientists to attain their expectations and move towards the clinical setup. Biological environments are not the same, so the nanomaterials interacting with those also vary. The physiochemical properties of nanomaterials are influenced by the size, shape, and composition, i.e., optical properties are tunable for nanomaterials. Hence, the desired nanomaterials/particles (nanoparticles) with multi-functionalities were obtained depending upon the biomedical application, device, etc. Thus, synthesized nanoparticles are biocompatible and enhanced optical properties, rich surface chemistry, and confinement effects at quantum and physical levels. The injection/interaction of nanoparticles to a biosystem has produced significant changes in their characterization or properties. For example, cellular functions like growth, adhesion, motility, morbidity, etc. are influenced by the presence of nanoparticles. Also, the potential risks of employing nanoparticles are evaluated by researchers before entering into a daily life or clinical application. In this regard, nanoparticles engineered from the metal, metal oxides, and metal sulfides played a key role in the field of oncology. In the case of metal nanoparticles, gold and silver are considered to be noble NPs. Gold nanoparticles (Au nanoparticles) are biocompatible and nontoxic and so applied for several medical purposes from the ancient period (nearly 5000 years ago).

Several synthesis methods are available for Au nanoparticles which are easy, safe, and consistent producing various shapes like nanosphere, nanorods, nanocages, nanostars, etc., Due to surface plasmon resonance, Au nanoparticles have unique optical and electronic characteristics which were responsible for cancer diagnosis and treatments. Recent research works have shown the importance and improvement in the cancer diagnosis and treatment of cancer with these Au nanoparticles. Next to Au nanoparticles, silver nanoparticles (Ag nanoparticles) occupy their place in cancer diagnosis and therapy. Ag nanoparticles have similar advantages as Au nanoparticles and are synthesized by chemical and biological methods. In metal oxide nanoparticles, several nanoparticles exist. Here, iron oxide and zinc oxide were taken for diagnosis and treatment discussion, respectively. As iron oxide produced a major effect in producing imaging of cancer cells with magnetic resonance technique (MRI), zinc oxide was used in apoptosis (programmed cell death) of cancer cells, due to cytotoxicity effect. Next, recently metal sulfides are also considered in cancer diagnosis and treatment. From research reports zinc sulfide, copper sulfide, and rhenium sulfides were involved in targeting the cancer cells. In this chapter, we are covering the research works on metals, metal oxides, and metal sulfide nanoparticles and their major role in cancer diagnosis and treatment.

6.2   Metal Nanoparticles for Cancer Diagnosis and Treatment

Amid metal nanoparticles, gold (Au) and silver (Ag) nanoparticles are considered to be the noble metal nanoparticles due to their inimitable properties like small size, stable nature, simplistic preparation (green and chemical methods), biocompatibility, non-cytotoxicity, tunable optical properties, surface plasmon resonance, easy surface chemistry, and high surface to volume ratio. These properties of Au nanoparticles and Ag nanoparticles simultaneously facilitate both cancer diagnostic and therapeutic functions yielding a new term "theranostics."

These metal nanoparticles have been synthesized with different shapes (sphere, urchin, rod, shell, cage, etc.) and sizes (10–200 nm) by using different chemical and biological methods. In chemical method by utilizing chemicals and solvents, metal nanoparticles were prepared, while in biological method, several medicinal plants and microorganisms were employed in obtaining required nanoparticles. The biologically synthesized metal nanoparticles were found to be eco-friendly, while chemically synthesized nanoparticles possess several issues on human health and the environment.

6.2.1   Gold Nanoparticle in Cancer Diagnosis and Treatment

In 1857 Michael Faraday identified metallic nanoparticles in the solution, and he was the pioneer to prepare the colloidal Au nanoparticles of the size 100 nms in diameter by reducing the gold chloride solution using phosphorus. In 1908 Mie had reported on the color of nanoparticles and its sized dependency. Based on his report many researchers have synthesised Au nanoparticles of different size and shape. In this regard, research works were proposed with Au nanoparticles which showed the promising results for the diagnosis (in vitro and in vivo imaging) and treatment of cancer (Guo et al. 2017).

Photo Imaging: Cancer Diagnostic Process

In the field of oncology, the surgeons face the difficulties in deciding the boundary of cancer cells/tumor. Hence, during the surgery the possibility of removing healthy tissues or leaving behind the cancer cells might occur. Imaging techniques such as computed tomography (CT), positron emission tomography (PET), magnetic resonance, etc. could be utilized to detect the tumor only when its size is in the order of millimeter. In this context, photo diagnosis imaging is the unique process which guides the surgeons in fixing the lesions/tumors at early stage and assuring the removal of the entire cancer tissues.

Photo diagnostic imaging was performed by coupling the existing imaging methods such as PET, computed tomography, NIR fluorescence imaging, Raman spectroscopy, and MRI with that of Au nanoparticles to provide the imaging of the malignant cells. In the photo diagnostic imaging process near-infrared wavelength regions 650–800 nm and 950–1350 nm were found to be best in exciting the tissue. Further, it was noted that the several studies employed functionalized Au nanocages and Au nanorods possessing maximum absorption around at ~800 nm and injected in to the tumors. These gold nanoparticles binded with cancer cells shine upon irradiation with the suitable NIR laser and heat up that binded cancer cell causing irreversible damage to that particular cell leading to apoptosis. Thus, the Au nanoparticles were used simultaneously in both photo diagnosis imaging and phototherapy process (Ai et al. 2014; Bagheri et al. 2018).

Initially, Pitsillides et al. (2003) had applied the Au nanoparticles of 30 nm size and sphere shape combined with IgG antibodies to target cluster of differentiation eight receptors on lymphocytes; CD8 (cluster of differentiation 8) receptors on lymphocytes were detected and killed. In the detection of breast cancer cells, SK-BR-3 gold nanoparticles of 40 nm size conjugated with monoclonal antibody Herceptin were employed as it binds with cell surface receptor HER2 released by those cancer cells. By using an optical acoustic tomography, one of the medical imaging techniques, those breast cancer cells were found effectively at a depth of 6 cm even with a low concentration of Au nanoparticles (Copland et al. 2004). El-Sayed et al. (2005) have reported on the diagnosis of oral epithelial cancer cells using Au nanoparticles. In this study, Au nanoparticles was conjugated with an antibody (anti-EGFR) which acted as a biosensor. These particles have produced appreciable surface plasmon resonance (SPR) absorption spectra and surface plasmon resonance imaging used in the delineation between the oral cancer cells and normal cells. The anti-EGFR after combining with the Au nanoparticles was found to possess more affinity (600%) towards the cancerous cells than the normal cells which was observed with red shift of SPR absorption band for cancer cells when compared to that of normal cells.

Computed tomography imaging system was used to identify the prostate cancer cells which express the prostate-specific membrane antigen (PSMA) protein in its cell membrane with a bioconjugate of functionalized Au nanoparticles and peptide molecules (aptamer). Au nanoparticles binded aptamers have shown the high-intensity computed tomography signal. These particles were found to be more effective when loaded with doxorubicin drug in the detection of prostate cancer cell LNCap followed by PC3 cells (Kim et al. 2010).

Wang et al. (2016b) have proposed the imaging with Au nanostar with hyaluronic acid which binds with the CD44 antigen responsible for cell-cell interaction/cell adhesion and migration released by cancer cells and viewed using dark-field optical microscope. Following these many have reported on photoimaging techniques in the diagnosis of cancer cells. Recently, an in vivo study of the optical coherence tomography technique for the detection of oral cancer was reported by Kim et al. (2018). In which they have developed Au nanoclusters from seed Au nanoparticles through acid-cleavable linkers. The Au nanoclusters were injected to a hamster

cheek pouch model which contained early-stage squamous carcinoma tissue, and the imaging was carried with the optical coherence tomography (OCT) technique. This study had shown that Au nanoclusters have the capability to play an effective role as a contrast agent and produced diagnostic signals based on the presence of early-stage cancer cells. Thus, both at a in vitro and in vivo scenario, suitable Au nanoparticles due to its unique physiochemical and biological properties were proved to possess capability in diagnosing/imaging the cancer cells and therapy. Tables 6.1 and 6.2 provide in detail about the proposed in vivo work carried out with Au nanoparticles in diagnosing (imaging) of cancer cell and treatment techniques (photodynamic therapy – PDT and photothermal therapy – PTT).

Cancer Therapy

In this method Au nanoparticles of various shapes and sizes conjugated with antibodies are absorbed only by tumors (cancer cells) forming simple gold-thiol bioconjugation (Riley and Day 2017). Cancer cells produce epidermal growth factors at cell membranes of it. Then, the cells are irradiated using red laser light (NIR region) which produces selective hyperthermia leading to protein denaturation and cell membrane destruction of cancer cells, while normal cells are not affected and remain same. Figure 6.1 shows the different shapes and sizes of Au nanoparticles used for PTT. During PTT to have stabilization of nanoparticles, they were coated with agents like polymers (polyethylene glycol-PEG), serum protein, silica gel, etc., which promises entire destruction of cancer cells without causing any damage to normal cells.

Zharov et al. (2005) proposed an in vitro approach in which they have applied a synergistic method of using gold nanoclusters which improved photothermolysis of cancer cells through near-infrared (NIR) laser (1064 nm) activation. Gold nanoparticles of 40 nm size conjugated with antibodies targeted the MDA-MB-231 breast cancer cells by producing increased absorption representing red shift as compared to normal cells that did not possess nanoclusters. Thus, this group has demonstrated the potential technique for cancer therapy.

Similarly, Au nanoparticles conjugated with anti-epidermal growth factor (anti-EGFR) were used a photothermal agent in cancer cell targeting. It was found that the oral squamous epithelial carcinoma cells require half less laser energy to be killed than the benign cells which were incubated with Au nanoparticles combined with anti-EGFR. Further, in the absence of Au nanoparticles, photothermal damage was not observed in any cells (El-Sayed et al. 2006). The same research group also discussed the Au nanorods with anti-EGFR efficiency in cancer cell diagnosis and photothermal therapy. In this study, the Au nanorods combined with anti-EGFR were incubated in cell culture comprising of two cancer oral epithelial cell lines (HOC 313 clone 8 and HSC 3) and normal epithelial cell line (HaCaT) and found that the malignant cells binded to the Au nanorods anti-EGFR as it produced more EGFR readily available on its cytoplasmic membrane. The gold nanorods strongly dispersed the near-infrared laser light (800 nm) which helped to visualize the cancer

Table 6.1 Different gold nanocomplexes used in "in vivo imaging" of various types of cancer (Originally published by Guo et al. 2017 and reprinted with permission from Dove Medical Press Ltd.)

Type of cancer	Imaging technique	In vivo model	Functional ligand	Reference
Gold nanocages				
Breast cancer (EMT-6 cells)	PET/CT	S.C. xeno-graft mouse	Stabilizing ligand: PEG emitter: ^{64}Cu	Wang et al. (2012)
Gold nanotripods				
Glioblastoma (U87 MG cells)	PAI	S.C. xeno-graft mouse	Stabilizing ligand: PEG Targeting ligand: RGD	Cheng et al. (2014)
Gold nanoclusters				
Glioma (U87MG cells)	MRI and SERS imaging	Orthotopic xenograft mouse	pH-sensitive ligand: azide and alkyne functionalities	Gao et al. (2017)
Glioblastoma (U87 MG cells)	PET IVIS® imaging system	S.C. xeno-graft mouse	Emitter: ^{64}Cu	Hu et al. (2014)
Melanoma (M14 cells)	NIR fluores-cence imaging	S.C. xeno-graft mouse	Stabilizing ligand: hair-pin DNA	Han et al. (2017)
Pancreatic tumor (MiaPaca-2 cells)	Maestro™ 2 in vivo imaging system	S.C. xeno-graft mouse	Stabilizing ligand: BSA Nuclear imaging moi-ety: Hoechst	Croissant et al. (2016)
Liver cancer (HepG2 cells) Adenocarci-noma (A549 cells)	NIR fluores-cence imaging	S.C. xeno-graft mouse	Stabilizing ligand: BSA Targeting ligand: FA and HA	Zhang et al. (2014a)
Prostate cancer (PC3 cells)	PET/CT	S.C. xeno-graft mouse	Stabilizing ligand: PEG emitter: ^{64}Cu	Zhao et al. (2014b)
Breast cancer (MCF-7 cells)	CT NIR fluo-rescence imaging MRI	S.C. xeno-graft mouse	Stabilizing ligand: BSA emitter: Gd^{3+}	Hu et al. (2013b)
Breast cancer (MDA-MB-231 cells)	NIR fluores-cence imaging	S.C. xeno-graft mouse	Stabilizing ligand: BSA Targeting ligand: methi-onine NIR dye: hydro-philic ICG	Chen et al. (2012)
Gold nanospheres				
Melanoma (SKMeL23 cells)	CT	S.C. xeno-graft mouse	Stabilizing ligands: PEG and glucose Targeting ligand: glucose	Meir et al. (2015)
Papilloma (KB cells)	CT	S.C. xeno-graft mouse	Gold nanospheres Sta-bilizing ligand: PEG and PEI targeting ligand: FA	Zhou et al. (2016)
Lung cancer (SPC-AI cells)	CT	S.C. xeno-graft mouse	Stabilizing ligand: PEG	Peng et al. (2012)
Glioblastoma (U87 cells)	MRI	Orthotopic xenograft mouse	Stabilizing ligand: PEG Targeting ligand: TAT Emitter: Gd^{3+}	Kim et al. (2011a)

(continued)

Table 6.1 (continued)

Type of cancer	Imaging technique	In vivo model	Functional ligand	Reference
Lung cancer	PET	Urethane-induced lung cancer mouse	Hybrid formulation: mesoporous silica Nanoparticles emitter: ^{64}Cu	Cheng et al. (2016)
Colorectal cancer (HT-29 cells)	CT NIR fluorescence imaging	S.C. xenograft mouse	Stabilizing ligand: GC MMP sensitive linker: MMP peptide NIR dye: Cy5.5	Sun et al. (2011)
Glioblastoma (U87 MG cells)	SPECT/CT	S.C. xenograft mouse	Stabilizing ligand: PEG Targeting ligand: RGD Emitter: ^{125}I	Kim et al. (2011b)
Colon adenocarcinoma (HT-29 cells)	PAI CT	S.C. xenograft mouse	Photostability enhancer: PB	Jing et al. (2014)
Squamous carcinoma (SCC7 cells)	PAI NIR fluorescence imaging	S.C. allograft mouse	Stabilizing ligand: PEG NIR dye: Cy5.5	Gao et al. (2016)
TNBC (4TI cells)	SPECT/CT	Orthotopic allograft mouse	Stabilizing ligand: PEG Targeting ligand: DAPTA	Zhao et al. (2016)
Colon carcinoma (CT26 cells)	CT	S.C. allograft mouse	Stabilizing ligand: PEG fluorescent dye	Zhang et al. (2015a)
Gold nanoshells				
Colorectal cancer (SW620 cells)	MRI CT	S.C. xenograft mouse	Targeting ligand: lectin MRI contrast agents: Fe_3O_4 nanoparticles	He et al. (2014)
Hepatoma (H22 cells)	CT and PAT imaging and MRI	S.C. allograft mouse	MMP-triggering ligand: gelatin MRI contrast agent: Fe_3O_4	Li et al. (2016)
Epithelial carcinoma (A431 cells)	PET	S.C. xenograft mouse	Stabilizing ligand: PPAA shell targeting ligand: CET emitter: ^{89}Zr	Karmani et al. (2013)
Head and neck squamous cell carcinoma (SCC4 cells)	PET/CT	S.C. xenograft rat	Stabilizing ligand: PEG emitter: ^{64}Cu	Xie et al. (2010)
Melanoma (B16- F10 cells)	MRI X-ray imaging optical imaging	S.C. xenograft mouse	Stabilizing ligand: PEG emitter: Gd^{3+}	Coughlin et al. (2014)
Pancreatic cancer (AsPC-1 cells)	MRI NIR fluorescence imaging	S.C. xenograft mouse	Targeting ligand: antibody (anti-NGAL) MRI contrast agents: Fe_3O_4 nanoparticles	Chen et al. (2014b)
Hollow gold nanoparticles				
Glioblastoma (U87 cells)	PET/CT PAI	Orthotopic xenograft mouse	Stabilizing ligand: PEG Targeting ligand: RGD emitter: ^{64}Cu	Lu et al. (2011)
Liver carcinoma (VX2 tumor)	PET/CT	Orthotopic allograft rabbit	Stabilizing ligand: PEG Targeting ligand: RGD emitter: ^{64}Cu	Tian et al. (2013)

(continued)

Table 6.1 (continued)

Type of cancer	Imaging technique	In vivo model	Functional ligand	Reference
Adenocarcinoma (A549 cells)	CT	S.C. xeno-graft mouse	Stabilizing ligand: PEG	Park et al. (2015)
Gold nanoprisms				
Colorectal cancer (HT-29 cells)	PAI	S.C. xeno-graft mouse	Stabilizing ligand: PEG	Bao et al. (2013)
Gold nanorods				
Ovarian cancer (MDA-435S, HEY, SKOV3 cells)	PAI SERS imaging	S.C. xeno-graft mouse	Stabilizing ligand: PEG SERS reporters	Jokerst et al. (2012)
Squamous carcinoma (SCC7 cells)	PAI	S.C. allo-graft mouse	Stabilizing ligand: PEG Targeting ligand: biotin	Chen et al. (2015)
Epithelial carcinoma (A431 cells)	NIR fluores-cence imaging	S.C. xeno-graft mouse	Stabilizing ligand: PEG Targeting ligand: CET	Choi et al. (2012)
Squamous carcinoma (SCC7 cells)	NIR fluores-cence imaging	S.C. xeno-graft mouse	Stabilizing ligand: PEG NIR dye and photosen-sitizer: $AlPcS_4$	Jang et al. (2011)
Glioblastoma (U87 MG cells)	PAI	S.C. xeno-graft mouse	Amphiphilic ligands: PEG and PLGA	Song et al. (2015)
Liver cancer (HepG2, Huh-7)	PAI NIR fluorescence imaging	Orthotopic xenograft mouse	Stabilizing ligand: liposome	Guan et al. (2017)
Stabilizing ligand: PNIPAAmMA MRI contrast agents: Fe_3O_4 nanoparticles	PET PAI	S.C. xeno-graft mouse	Glioma (C6 cells)	Yang et al. (2013)
Gold nanostars				
Ovarian cancer (SKOV3)	Raman spectroscopy	S.C. xeno-graft mouse	SERS labeling ligand: DTNB	D'hollander et al. (2016)
Primary soft-tissue sarcomas	CT Two-photon luminescence imaging	Transgenic mouse	Stabilizing ligand: PEG Raman reporter: p-mercaptobenzoic acid	Liu et al. (2015b)
Adenocarcinoma (A549 cells)	MRI, CT, and NIR fluores-cence imaging	S.C. xeno-graft mouse	Emitter: Gd^{3+}	Hou et al. (2017b)
Breast cancer (4T1 cells)	PAI	S.C. allo-graft mouse	Stabilizing ligand: PEG	Huang et al. (2015)

Abbreviations: *AIe* aggregation-induced emission, *Au nanoparticles* gold nanoparticles, *BSA* bovine serum albumin, *CeT* cetuximab, *CT* computed tomography, *DAPTA* d-Ala1-peptide T-amide, *DTNB* 5,5-dithio-bis-(2-nitrobenzoic acid), *FA* folic acid, *GC* glycol chitosan, *GNRs* gold nanorods, *HA* hyaluronic acid, *ICG* indocyanine green, *i.v.* intravenous, *LbL* layer-by-layer, *MMP* matrix metalloproteinase, *MPNA* magnetoplasmonic nanoassembly, *MRI* magnetic resonance imaging, *NGAL* neutrophil gelatinase-associated lipocalin, *NIR* near-infrared, *PAI* photoacoustic imaging, *PB* Prussian blue, *PEG* polyethylene glycol, *PEI* polyethylenimine, *PET* positron emission tomography, *PLGA* poly(lactic-*co*-glycolic acid), *PPAA* plasma-polymerized allylamine shell, *PTT* photothermal therapy, *SPECT* single-photon emission CT, *S.C.* subcutaneous, *SERS* surface-enhanced Raman spectroscopy, *TAT* transactivator of transcription, *TNBC* triple-negative breast cancer

Table 6.2 Different gold nanocomplexes used to carry out PTT and PDT for various types of cancer (Originally published by Guo et al. 2017 and reprinted with permission from Dove Medical Press Ltd.)

Type of cancer	Gold NP type	In vivo model	Functional ligand	Reference
PDT				
Adenocarcinoma (HeLa cells)	Au nanorods	S.C. xenograft mouse	Endosome disruptive ligand: Tat/HA2 Photosensitizer: AlPcS$_4$	Ye et al. (2015)
Melanoma (MDA-MB-435 cells)	Au nanoclusters	S.C. xenograft mouse	Au nanoparticles encapsulated in silica Photosensitizer: Ce6	Huang et al. (2013)
Melanoma (B16F0 cells)	Au nanorods	S.C. allograft mouse	Stabilizing ligand: PEG Targeting ligand: FA	Vankayala et al. (2014)
Glioma (C6 cells)	Au quantum clusters	S.C. xenograft mouse	Stabilizing ligand: lipoic acid targeting ligand: FA Photosensitizer: PPIX	Nair et al. (2015)
Colon cancer (Colon-26 cells)	Au nanocages	S.C. allograft mouse	Stabilizing ligand: PEG Photosensitizer: HPPH	Srivatsan et al. (2014)
Liver cancer (H22 cells)	Au nanorods	S.C. allograft mouse	Stabilizing ligand: CHI Photosensitizer: ICG	Chen et al. (2013)
Squamous carcinoma (SCC7 cells)	Au nanorods	S.C. allograft mouse	Au nanoparticles encapsulated in Pluronic nanogel Photosensitizer: Ce6	Kim et al. (2013)
Oral squamous carcinoma	Au nanorods	A carcinogen was topically injected into the left cheek pouch mucosa	Stabilizing ligand: poly (allylamine hydrochloride) Photosensitizer: RB	Wang et al. (2014a)
Adenocarcinoma (A549 cells)	Au nanospheres	S.C. xenograft mouse	Coating materials: heparin Photosensitizer: PhA	Li et al. (2013)
Adenocarcinoma (HeLa cells)	Au nanorods	S.C. xenograft mouse	Coating materials: silica and PEG photosensitizer: PPIX	Zhang et al. (2013)
PTT				
Breast cancer (MDA-MB-231 cells)	Au nanostars	S.C. xenograft mouse	Surface coating: organosilica	Gao et al. (2015)
Non-small-cell lung cancer (PC-9 cells)	Au nanorods	S.C. xenograft mouse	Stabilizing ligand: dendrimer	Wang et al. (2016c)
Breast cancer (4T1 cells)	Au nanocages	S.C. allograft mouse	Gold surface was coated with PVP and RBC membranes	Piao et al. (2014)

Table 6.2 (continued)

Type of cancer	Gold NP type	In vivo model	Functional ligand	Reference
Colon carcinoma (26 cells)	Au nanorods	S.C. allograft mouse	Stabilizing ligand: PEG and dendrimers	Li et al. (2014b)
Fibrosarcoma (HT-1080 cells)	Au nanoclusters	S.C. xenograft mouse	A pH-sensitive ligand inducing Au nanoclusters in mild acidic environments	Kang et al. (2015)
Breast cancer (MDA-MB-231 cells)	Au nanoshells	Orthotopic xeno-graft mouse	Multilayered Au nanoparticles with silica and gold, also termed Au nanomatryoshkas	Ayala-Orozco et al. (2014)
Breast cancer (4T1 cells)	Au nanoplates	S.C. allograft mouse	Stabilizing ligand: PEG	Chen et al. (2014a)
Adenocarcinoma (A549 cells)	Au nanorods	S.C. xenograft mouse	Stabilizing ligand: PEG Targeting ligand: anti-body for anaerobic bac-teria (*C. difficile*)	Luo et al. (2016)
Breast cancer (4T1 cells)	Au nanoshells	S.C. allograft mouse	Stabilizing coating: MPCMs Inner core: silica	Xuan et al. (2016)
Gastric cancer (MGC803 cells)	Au nanorods	S.C. xenograft mouse	Coating material: silica Targeting ligand: anti-body for CXCR4	Liu et al. (2016)
Breast cancer (MDA-MB-231 cells)	Au nanocages	S.C. xenograft mouse	Targeting ligand: HA	Wang et al. (2014b)
Breast cancer (4T1 cells)	Au nanorods	S.C. allograft mouse	Au nanorods encapsu-lated in CHI/sodium ALG microcapsules	Shao et al. (2015)
Ovarian carci-noma (SKOV3 cells)	Hollow Au nanospheres	S.C. xenograft mouse	Stabilizing ligand: PEG Targeting ligand: a pep-tide (TNYL)	Wang et al. (2015b)
Melanoma (MDA-MB-435 cells)	Au nanorods	S.C. xenograft mouse	Stabilizing ligand: PEG	Von Maltzahn et al. (2009)
Liver cancer Bel-7402 cells	Au nanoshells	S.C. xenograft mouse	Stabilizing ligand: PEG Inner core: PeI-PAsp (DIP/MeA) nanoparticles	Wang et al. (2016a)
Glioblastoma (U87 MG cells)	Au nanorods	S.C. xenograft mouse	Stabilizing ligand: PEG Targeting ligand: RGD	Sun et al. (2014)
Glioblastoma (U87 MG cells)	Au nanoshells	S.C. xenograft mouse	Stabilizing ligand: PEG Inner core: PLGA nanoparticles	Hao et al. (2015)

(continued)

Table 6.2 (continued)

Type of cancer	Gold NP type	In vivo model	Functional ligand	Reference
Glioblastoma (U87 MG cells)	Au nanostars	S.C. xenograft mouse	Stabilizing ligand: PEG Targeting ligand: RGD	Nie et al. (2014)
Breast cancer (4T1 cells)	Au nanorods	S.C. allograft mouse	Coating material: silica	Zhang et al. (2014b)
Adenocarcinoma (A549 cells)	Au nanorods	S.C. xenograft mouse	Coating materials: PvP and $AgNO_3$ Targeting ligand: aptamer	Shi et al. (2014)
Breast cancer (4T1 cells)	Au nanoshells	S.C. allograft mouse	Stabilizing ligand: PEG	Li et al. (2014a)
Ovarian carcinoma (SKOv3 cells)	Hollow Au nanospheres	S.C. xenograft mouse	Stabilizing ligand: PvP and citrate	Zhou et al. (2015)

Abbreviations: *ALG* alginate, *Au nanoparticles* gold nanoparticles, *C. difficile Clostridium difficile*, *Ce6* chlorin e6, *CHI* chitosan, *DOX* doxorubicin, *FA* folic acid, *GNRs* gold nanorods, *HA* hyaluronic acid, *HPPH* 3-devinyl-3-(1′-hexyloxyethyl)pyropheophorbide, *ICG* indocyanine green, *iPS* Induced pluripotent stem, *i.v.* intravenous, *LeD* light-emitting diode, *MPCMs* macrophage cell membranes, *MSCs* mesenchymal stem cells, *NIR* near-infrared, *PDT* photodynamic therapy, *PEG* polyethylene glycol, *PeI* polyethylenimine, *PeI-PAsp (DIP/MeA)* polyethylenimine-b-poly (2-diisopropylamino/2-mercaptoethylamine) ethyl aspartate, *PhA* pheophorbide a, *PLGA* poly(lactic-*co*-glycolic acid), *PPIX* protoporphyrin IX, *PTT* photothermal therapy, *PvP* polyvinylpyrrolidone, *RB* Rose Bengal, *RBC* red blood cell, *ROS* reactive oxygen species, *S.C.* subcutaneous, *SERS* surface-enhanced Raman spectroscopy, *SPR* surface plasmon resonance

cells from normal cells using a laboratory optical microscope. After exposure to red laser light, the photothermal destruction process was carried out to destroy cancer cells as it acquires only lesser half energy compared to that of normal cells (Huang et al. 2006).

Based on the above idea of photothermal therapy with contrast agent, Au nanoparticles for cancer treatment were proposed by research groups. The liposome Au nanoparticles were tested in mouse tumor using NIR laser (750 nm) which confirmed the demolition of tumor mass and prolonged survival of mouse without any reoccurrence of cancer cells (Rengan et al. 2015). Photodynamic therapy (PDT) is one of the very old techniques in which a suitable wavelength of light activates the photosensitiser such as porphyrin injected to the target that produces singlet oxygen and reactive oxygen species producing damage to the cancer cell by apoptosis. The photosensitisers were not readily soluble to load them to tumor cells.

Hence, PDT and PTT simultaneously coupled with the photosensitizers conjugated to Au nanoparticles were delivered to the targeted cancer cells (Fig. 6.2). Gao et al. (2012) have performed the in vitro PDT and PTT therapy with hypocrellin-loaded Au nanocages which were proven to be the best quenchers of a photosensitizer from the result of fluorescence and electron spin resonance methods, a best

Fig. 6.1 Different possible shapes and sizes of gold nanoparticles which was employed in photothermal therapy (PTT)

Nanocage (~40-60 nm)
Drug Loading

Nanorods (~10x40 nm)
Diffusion of Particles

Nanostars (~120 nm)
Biomolecule Binding

Nanoshells (~50 nm)
Bioimaging & Drug Delivery
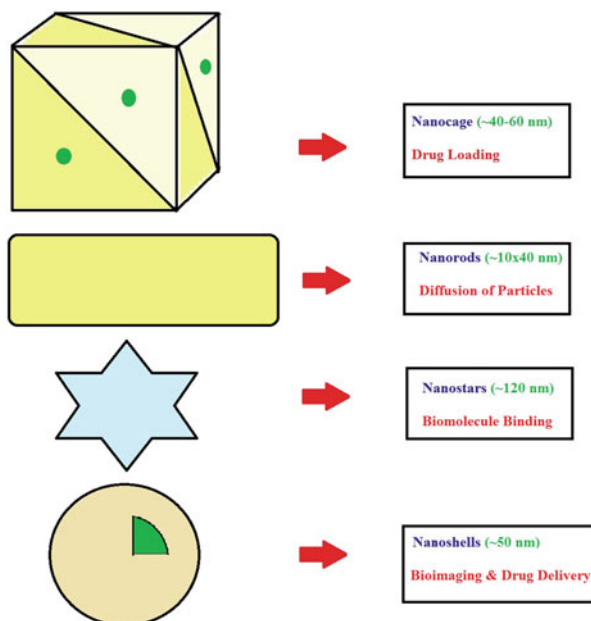
combination of anticancer therapy. Another work reports the appreciable result in destroying cancer cells with the PTT and PDT coupled when compared with its solo performance, and silicon 2,3-naphthalocyanine dihydroxide-binded Au nanorods exhibit superior efficacy in cancer cell destruction as compared to photodynamic therapy and photothermal therapy alone.

6.2.2 Silver Nanoparticle in Cancer Diagnosis and Treatment

One of the noble metal nanoparticle silver (Ag) nanoparticles like Au nanoparticles possesses better light absorption, affinity, and resolution to various functionalization characters. Silver nanoparticles were synthesized by using chemical and biological methods and have been used for diagnostic and therapeutic purposes in the oncology field. In this context, it was worth to note that Ag nanoparticles might not be used for long term due to its potential toxicity (Ong et al. 2013). Silver nanoparticles used as a third-harmonic generation (THG) strong contrast agent in the molecule-specific third-harmonic generation (THG) microscopy in the detection of cancer cells. These Ag nanoparticles combined with anti-HER2 antibodies produced matchable surface plasmon resonance wavelength to that of THG wavelength, and the cancer cell membranes with high expression of HER2/neu oncogene representing breast cancer were imaged successfully (Tai et al. 2007).

Gopinath et al. (2008) have performed the in vitro study on apoptosis of cancer cell and noncancerous cell and optimized the concentration of Ag nanoparticles to
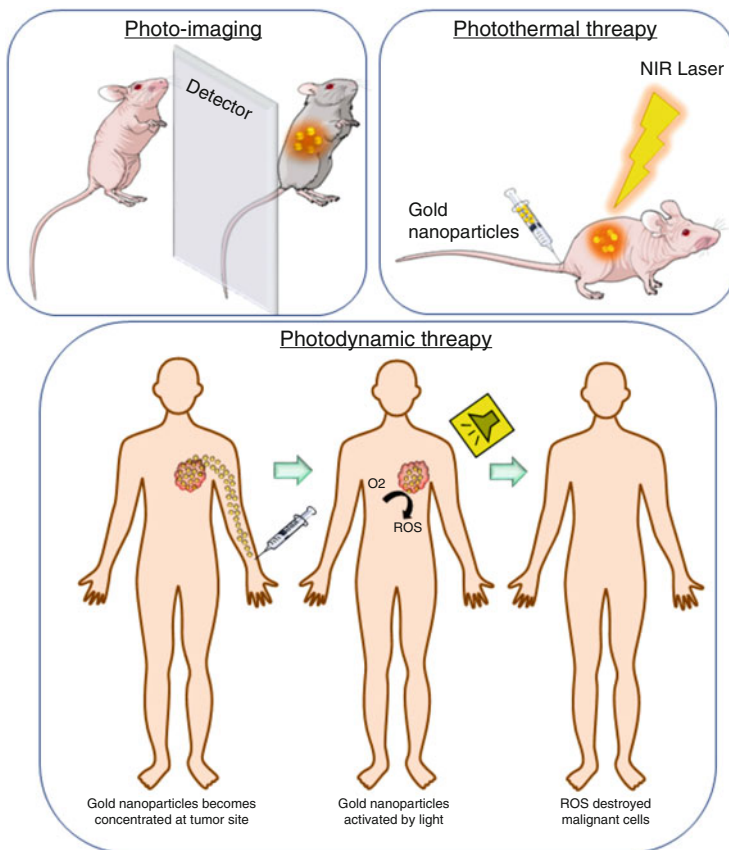
Fig. 6.2 Gold nanoparticles in cancer diagnosis and treatment (Reprinted with permission of "Gold Nanoparticles in Diagnostics and Therapeutics for Human Cancer," Int. J. Mol. Sci., Copyright 2018, MDPI, from (Singh et al. 2018))

act as cytotoxic agent. The cytotoxic effect of Ag nanoparticles made them available as a chemosensitizer in cancer therapy along with conventional gene therapy. Another in vitro work was demonstrated to show the cytotoxicity nature of Ag nanoparticles. In this study, Ag nanoparticles which were protected with cucurbituril (CB) [7] were developed to destruct the MCF7 and NCI-H358 breast and lung cancer cell lines, respectively (Premkumar et al. 2010). In 2010, Ostad et al. have performed the cytotoxic activity of Ag nanoparticles against the breast cancer cell lines (T47D) which was tamoxifen-resistant. In these Ag nanoparticles, Ag ions, tamoxifen, Ag nanoparticles with tamoxifen, and Ag ions with tamoxifen were found to be cytotoxic against cancer cells. The results obtained from this study show that the even less dose of tamoxifen produces similar cytotoxic effects on cancer cells. Sanpui et al. (2011) have reported on the cytotoxic effect of the Ag nanoparticles using chitosan nanocarrier on targeting human colon cancer cells

(HT 29). Depolarization of mitochondrial membrane potential provides the Ag nanoparticles chitosan nanocarrier influence on the pathway of mitochondria to induce programmed cell death. An in vitro study of Ag nanoparticles in the mechanism of cytotoxicity using HeLa-cervical cancer cell line and HaCaT human dermal cell lines was demonstrated by Mukherjee et al. (2012). It was found that Ag nanoparticles enhanced the levels of oxidative stress, decrease in antioxidant glutathione, and damage to the cell membrane that leads to the apoptosis of the cancer cell.

Further, the sensitivity of the cervical and human dermal cell lines was differentiated from one another by using their original antioxidant levels. Ag nanoparticles coated with PVP and Ag ions were used to study the cellular toxicity over the alveolar cell line. The cytotoxicity of Ag nanoparticles and Ag ions was reduced by treating with an antioxidant and N-acetyl-cysteine. Reactive oxygen species (ROS) and mitochondrial damage were calculated to know the programmed cell death or apoptosis rate caused by Ag nanoparticles. In turn DNA level was increased depending upon ROS showing Ag nanoparticles as a mediator of ROS-induced cytotoxicity/genotoxicity. Renugadevi et al. (2012) have reported on the Ag nanoparticles' cytotoxicity effect to differentiate cancer and normal cells. They have used an MTT assay by treating cancer and normal cells at different concentrations of Ag nanoparticles (20 μg, 40 μg, 60 μg, 80 μg, 100 μg, 120 μg, 140 μg, and 160 μg). It was found that the normal cells at 20 μg possessed toxicity 10% with IC50 value 90 μg, whereas cancer cells at 20 μg possessed toxicity 12% with IC50 value 64 μg and confirmed that less amount of Ag nanoparticles was enough to kill the cancer cell compared to that of normal cell. Similarly, Ag nanoparticles' cytotoxicity effect on MDA-MB-231 human breast cancer cells and prostate cancer cells (PC3) was reported (Gurunathan et al. 2013a, b, c; Firdhouse and Lalitha 2013).

Mishra et al. (2012) have reported that cytotoxicity of Ag nanoparticles depends on total protein concentration of the cervix cancer cells (SiHa) under investigation. The IC50 of neem-extracted Ag nanoparticles was found to be ≤4.25 μg/ml, and α-amylase-mediated Ag nanoparticles were ≤32.5 μg/ml. Satapathy et al. (2013) have studied the Ag nanoparticles treatment in a p53-knockout HCT116 colon cancer cells. Ag nanoparticles' exposure to cancer cells increased the level of 4′,6-diamidino-2-phenylindole-stained apoptotic nuclei and cleaved poly(ADP-ribose) polymerase; BAX/BCL-XL ratio; caspases 3, 8, and 9; p53; and p21, by a decrease in the levels of AKT and NF-κB. After the exposure of the cancer cell with Ag nanoparticles, G1 phase population was found to be reduced, whereas S-phase population increased in their level. In this study, it was proved that Ag nanoparticles act as a good anticancer agent that depends upon a protein p53 released by colon cancer cells. These research discoveries prove the cytotoxic properties of Ag nanoparticles and suggest that they may be a cost-effective and an alternative measure in the field of cancer therapeutics.

A continuous wave near-infrared study of Ag nanotriangles was conjugated with chitosan targeting the NIH: OVCAR-3 of folate receptor of human ovary cancer cell line was performed by Boca-Farcau et al. (2013), i.e., dark-field microscopy used to detect the ovarian cancer cells. Hu et al. (2013a) have demonstrated the in vitro study

on reduced graphene oxide (RGO) combined with Ag nanoparticles with folic acid (FA) molecules which were used to detect the cancer cells using folate receptors. The binding of nanoparticles inside the cell was confirmed with a transmission electron microscope and confocal Raman laser scanning (Visible wavelength of 514 nm). This method proved that the RGO-Ag nanoparticles with FA were very much capable in diagnosing the cancer cells. Parveen and Rao (2015) have reported on the cytotoxicity and genotoxicity of green synthesized gold and silver nanoparticles on human cancer cell lines by employing MTT assay. It was once again proved that Ag nanoparticles were more toxic towards the cancer cell lines. Poon et al. (2014) have reported on the diagnosis of prostate cancer. They have utilized Ag nanoparticles binded with antibody to identify the prostate-specific antigen (PSA). This study have employed the immunoassay process in which detection of cancer cells was carried out in a glass flow cell with detection limit at 9 pM.

Ag nanoparticles were used to induce p53-mediated apoptotic pathway to perform programmed cell death of cancer cell. The chemotherapeutic drugs present in this apoptotic pathway were triggered more in the presence of Ag nanoparticles than in ordinary conditions which confirm that the Ag nanoparticles act as a best therapeutic agent (Gopinath et al. 2010). In the detection of nasopharyngeal and cervix cancer, surface-enhanced Raman spectroscopic analysis was performed with the blood plasma samples of cancer patients and normal subjects. This was done by adding Ag nanoparticles as the SERS-active component to enhance the vibrational signal of the Raman bands that arise from the different biomolecules such as protein, nucleic acids, amino acids, amide groups, lipids, etc. present in the blood plasma. The addition of Ag nanoparticles ensures the enhancement of entire Raman peaks/bands present in the selected wavenumber regions (Feng et al. 2010, 2013). Similarly, Lin et al. 2011 have explored the SERS technique using Ag nanoparticles in the detection of gastric cancer using serum protein acquired from blood plasma. Similarly, Lin et al. (2014) reported on the detection of esophageal cancer using blood plasma samples under surface-enhanced Raman spectroscopy. Yang et al. 2012 have performed the above SERS technique in the detection of breast cancer cells by recognizing the epidermal growth factor receptor 2 (HER2).

In this they have made a SERS optical probe which uses the combination of anti-HER2 and Ag nanoparticles and which specifically targets a gene HER2 from breast cancer cells. The Raman signals of SKBR3 (HER2 positive) and MCF7 (HER2 negative) cells were employed in differentiating breast cancer cells from normal cells. The SERS signal shows that SKBR3 cells possessed much stronger signals than MCF7 cells. Thus, this Raman study shows that SERS with Ag nanoparticles has the capability in diagnosing the breast cancer cell. Magnetic nanoparticles (MNanoparticles) were used in destroying the cancer cells. Mostly, high concentrations of MNanoparticles were applied in destroying the tumor. In this scenario, to decrease the dosage level of MNanoparticles and to increase the sensitivity of therapy, Ag nanoparticles were introduced along with MNanoparticles. It was found that Ag nanoparticles along with MNanoparticles enhanced the Bax expression of cancer cells of rats with gliomas and act as a very good thermosensitizer at particle size 20.6 ± 2.7 nm (Liu et al. 2011).

Austin et al. (2011a, b) have carried out the detection and treatment of oral cancer. They have employed the plasmonic scattering and nuclear-targeting nature of Ag nanoparticles to identify the oral cancer cells and to induce apoptosis. They have recorded the real-time imaging of oral squamous carcinoma cell (HSC-3) which showed the self-destruction of cancer cells. The same group have reported on the detection of cancer (HSC-3) and healthy (HaCaT) cell lines with Ag nanoparticles with size of ~35 nm. The real-time dark-field imaging of the cancer cells targeted with Ag nanoparticles underwent programmed cell death without any delay. Lai et al. (2011) have utilized the Ag nanoparticle-enriched carbon nanotube to detect the tumor markers. The process comprises of sandwich-type immune complexes to which Ag nanoparticles are deposited on every single array. Based on surface plasmon resonance of Ag nanoparticles, a biosensor was employed in the detection of blood serum squamous cell carcinoma antigen present in cervical cancer patients (Zhao et al. 2014a). Mittal et al. (2014) synthesized Ag nanoparticles from *Syzygium cumini* fruit extract of size 10–15 nm, and the antioxidant properties of these Ag nanoparticles were determined using various assays. These Ag nanoparticles targeted towards Dalton lymphoma cell lines under in vitro condition. As with the discussed ideas, functionalization of noble metal nanoparticles, imaging technique, therapeutic drugs, and optical probe became a lethal combination in the diagnosis and treatment of cancer. Zhang et al. (2015b) have proposed Ag nanoparticle mesoporous silica-coated gold nanorods in the cancer detection followed by cyto-toxicity of nanoparticles towards cancer cells. These nanoparticle combinations were irradiated with NIR laser light to rise the local temperature which in turn increases the cytotoxicity of cell.

Au nanoparticles and Ag nanoparticles were prepared from *Butea monosperma* (*BM*) leaf extract. These nanoparticles are found to possess cancer cell proliferation (B16F10, MCF-7) using doxorubicin (DOX) [b-Au-500-DOX and b-Ag-750-DOX] compared to pristine drug (Patra et al. 2015). Swanner et al. (2015) have reported on the cytotoxic effect of Ag nanoparticles on triple and non-triple-negative breast cancer cells. Benyettou et al. (2015) have employed Ag nanoparticles coated with bisphosphonate to deliver the drugs to cancer cells by delivering the anticancer drugs doxorubicin (Dox) and alendronate (Ald). They concluded that anticancer activity of anticancer drugs doxorubicin or alendronate was found to be less when used alone, whereas when they are treated with Ag nanoparticles, they have produced enhanced anticancer effect. Also, they mentioned the Ag nanoparticles could be attached with other anticancer drugs and targets, thereby offering basic ideas for drug delivery. Ag nanoparticles prepared from *Bacillus tequilensis* and *Calocybe indica* were used in targeting MDA-MB-231 human breast cancer cells. Both the Ag nanoparticles showed appreciable cytotoxicity against breast cancer cells. Dose-dependent assay indicates that Ag nanoparticles from *Calocybe indica* possess more potential than *Bacillus tequilensis* Ag nanoparticles. Further, this study concluded that bioderived Ag nanoparticles also have therapeutic response towards cancer (Gurunathan et al. 2015).

6.3 Metal Oxide Nanoparticles for Cancer Diagnosis and Treatment

Metal oxide nanoparticles were designed in such a way to face the challenges and requirements in the field of oncology. The metal oxide nanoparticles were considered because of its unique physiochemical properties. Metal oxide nanoparticles are synthesized using significant techniques such as co-precipitation method, thermal decomposition, sonochemical, microemulsion, and hydrothermal synthesis. Several studies have reported on the essential role of metal oxide nanoparticles such as iron oxides (magnetite-Fe_3O_4; maghemite-Fe_2O_3), zinc oxide, titanium oxide (TiO_2), copper oxide (CuO), cerium oxide CeO_2, silicon dioxide or silica (SiO), etc., in cancer diagnosis, drug delivery, destruction of cancer cells, and treatment monitoring process. Such reports with various metal oxides nanoparticles as anticancer agents are discussed here.

6.3.1 Iron Oxide

Iron oxide nanoparticle is the only magnetic nanoparticle approved by the US Food and Drug Administration for clinical purpose, as it contains less toxicity when compared to that of other magnetic nanoparticles (Tartaj et al. 2003). In this regard, the size, surface charge, and attraction towards the water molecule of nanoparticles decide the distribution of it inside the human body and toxicity level. Mostly, the iron oxide nanoparticles were directly introduced to the body through injection, as it goes with the bloodstream and reaches the organs with cancer cells (Fig. 6.3). These iron oxide nanoparticles possess their own life cycle and so are eliminated from the body (Kolosnjaj-Tabi et al. 2015).

Weissleder et al. (1989) have reported first on the superparamagnetic iron oxide (SPIO) nanoparticle's (AMI-25) distribution, metabolism, biocompatibility, excretion, and toxicity. They have characterized AMI-25 on rats with several studies. First, with 59Fe radiotracer measurement, they traced iron oxide nanoparticles' settlement in the organs after 1 hour of injection to rat; majorly in the liver, – 82.6 +/− 0.3% was found and in the spleen 6.2 +/− 7.6%. Relaxation time was 2 h for liver and 4 h for spleen. 59Fe slowly cleared from the liver (half-life, 3 days) and spleen (half-life, 4 days). Further, cleared on reverse iron deficiency anemia, histologic examination and various laboratory parameters found that iron oxide NP (AMI-25) was a biocompatible, suitable contrast agent for magnetic resonance imaging (MRI) and had no toxic effects. In the same year, liver metastasis diagnosis was carried out clinically by superparamagnetic iron oxide nanoparticles as a tissue-specific contrast agent for MRI at high fields of 1.5 T to evaluate IO nanoparticles for clinical setup (Marchal et al. 1989).

Kvistad et al. (2000) have reported on the contrast MRI of axillary lymph nodes in the case of breast cancer. MRI imaging of axillary lymph nodes was taken and
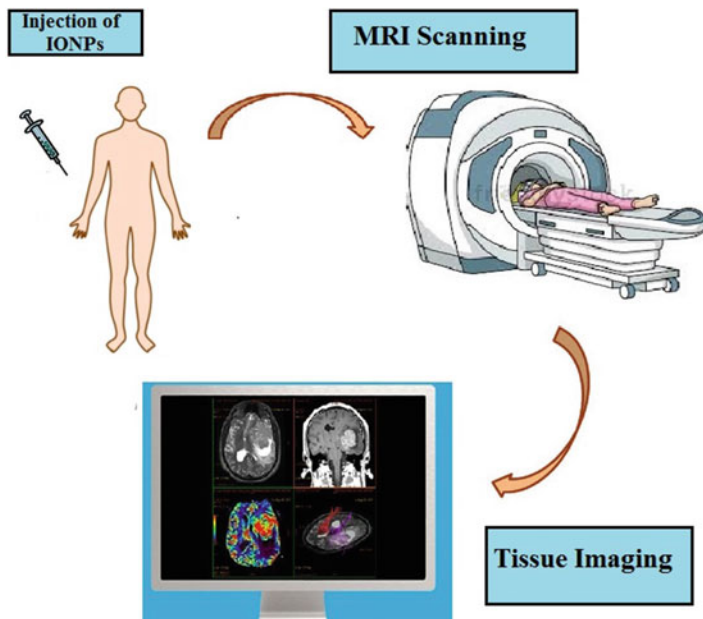
Fig. 6.3 Cancer diagnosis by MRI using iron oxide nanoparticles as a contrast agent

compared with that of the histopathological report of the same patients with the sensitivity of 83%, specificity 90%, and accuracy of 88%. This study suggests the surgeon could have an idea on the localization of metastasis on lymph nodes when they deal with the breast cancer patients. Many experiments and clinical trial studies were carried out using IO nanoparticles as a contrast agent for MRI in the diagnosis of liver, spleen, and lymph node metastasis. Baghi et al. (2005) have used the ultrasmall superparamagnetic iron oxide (USPIO) to have enhanced magnetic resonance imaging (MRI) and compared with that of plain MRI of head and neck cancer. They have taken enhanced and plain MRI with T1 and T2 sequences in axial and sagittal slice orientation of the suspected region. Conventional histopathological report showed 34 metastases from 363 lymph nodes, USPIO MRI provided 28 metastases yielding sensitivity of 82.3%, whereas 329 nonmetastatic lymph nodes were identified as normal providing specificity of 100%. This study confirmed the usage of USPIO nanoparticles as an effective contrast agent which could be employed in cancer diagnosis to identify the borderline of lymph nodes with metastasis and could be used by the surgeon as reference to make the effective treatment plan.

The visualization of cancer cells with large core IO nanoparticles was prepared by coating with a protein/cell-resistant polymer like polyvinylpyrrolidone (PVP); peptide – chlorotoxin and PSPIONs were checked for its size stability and life cycle in the system (Sun et al. 2008; Huang et al. 2010). Polymer-coated SPIO nanoparticles were checked for various pH levels undergoing incubation in serum

and were observed that its size remains the same after 24 h. Also, a macrophage study was carried out in which polymer SPIO nanoparticles' uptake by macrophage cell was less compared to the ordinary contrast agent, proving that it escapes from the reticular endothelial system (RES) long living in the plasma. The physiochemical properties of the IO nanoparticles determine their pharmacokinetic properties such as distribution, metabolism, biocompatibility, excretion, and toxicity which in turn determine their ability to accumulate in the target organ. Tumor metabolism visualization was also done using IO nanoparticles. Feng et al. (2011) has reported on the macrophage metabolism by employing nuclear magnetic resonance with the effect of USPIO nanoparticles. Both the cells and culture medium of murine RAW264.7 macrophages were studied using USPIO nanoparticles.

These macrophage cells have shown variations in their biomolecules level upon treating with USPIO nanoparticles. Some amino acids like triglycerides, essential amino acids such as valine and isoleucine, and choline metabolites were decreased in their level, whereas glycerophospholipids, glutamate, and aminoacids – tyrosine, phenylalanine, lysine, and glycine were found to be increased. Also, from the remaining products available in cell media after the completion of incubation was helpful in understanding the metabolism. This study shows that USPIO nanoparticles were phagocytosed and released by macrophages; the information on the metabolism, for example, changes in choline level used to achieve an information regarding cell membrane.

Another interesting study on "visualization of tumor metabolism" was carried out with one of the riboflavin protein carriers – flavin adenine dinucleotide binded ultrasmall superparamagnetic iron oxide nanoparticles (FAD USPIO) by Jayapaul et al. (2012). These carrier protein-targeted magnetic resonance agents were accepted only by cancer cells and accepted to be valuable nanoparticles in viewing the changes in metabolism. Many more reports are available on the IO nanoparticles which entirely put up to exhibit its efficiency in the diagnosis of cancer using magnetic resonance imaging. In addition to diagnosis of cancer cells, IO nanoparticles are also applied in the cancer treatment/therapy. The cancer cells were destroyed due to hyperthermia or production of reactive oxygen species (ROS) caused by near-infrared rays or magnetic fields which were absorbed by the iron oxide nanoparticles which were injected in the sample and got heated up. Since IO nanoparticles are absorbed only by the tumors and not by normal cells, the selective destruction of cancer cells alone takes place, such that radiant energy absorbed by IO nanoparticles causes ROS only in cancer cells and healthy tissues not damaged at any cause.

Based on this process, many research works were given out on IO nanoparticles' anticancer effect which was combined with drug/aptamer/dye loaded for performing both magnetic resonance imaging and targeted cancer treatment (Fig. 6.4). Orel et al. (2015) have expressed a method in which magneto-sensitive iron oxide nanoparticles combined with anticancer drug doxorubicin (DOXO) to produce antitumor effect. This treatment involving magneto-sensitive material was found to be more effective and significant than classical doxorubicin therapy. The reason due to the more anticancer activity was that the external magnetic field induces electron
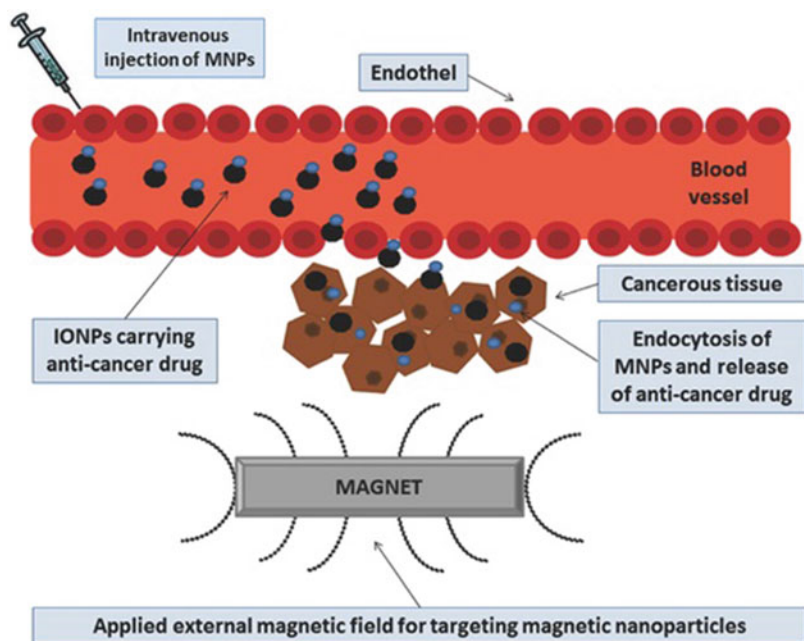
Fig. 6.4 Anticancer drug binded IO nanoparticles for cancer therapy (Reprinted with permission of "Iron oxide nanoparticles: innovative tool in cancer diagnosis and therapy," Adv. Healthcare Mat., Copyright 2018, Wiley-VCH Verlag GmbH from (Pavla Martinkova et al. 2018))

transitions in the iron oxide nanoparticles injected to the system which in turn activate the hydroxyl radicals. These radicals are responsible to produce programmed cell death by breaking down the biomolecules such as proteins, lipids, DNA, amides, mitochondria, etc., thus giving away the potential way of treatment of cancers. In another study, polyethylene glycol-coated iron oxide nanoparticles cubical shaped and 19 nm sized was utilized to induce hyperthermia in the cancer cell environment.

The IO nanoparticles were injected into mice followed by heating produced with external magnetic field. Then the IO nanoparticles were monitored for its interaction with cells. It was found that majority of the nanoparticles were settled down at the collagen-rich matrix (cancer environment possesses more structural protein than the normal tissue) and drug penetrate in to the cell with nanoparticle driven by hyperthermia, causing destruction of cancer cells. While considering the in vivo hyperthermia applications, iron oxide nanoparticles should possess 30–40 nm because after the removal of external fields there was a possibility of nanoparticle aggregation which leads to severe health issues. So in many biomedical applications, nanoparticles of small size are required to handle the tumor regions without disturbing the normal cells (Bañobre-López et al. 2013).

6.3.2   Zinc oxide

Zinc oxide nanoparticles are synthesized in both ways chemical and physical methods. Green synthesis as a biological way which used different reducing agents such as plant extracts, bacteria, other microorganisms, enzymes, etc. is a natural and best eco-friendly way when compared with chemical and physical methods (Agarwal et al. 2017). The ZnO nanoparticle shows the unique variation in its properties like structure, magnetic, electronic, etc., when compared to the bulk form and responsible for its application in the biomedical field. ZnO nanoparticles possess relatively high biocompatibility and biodegradability. Due to these properties, anticancer activities were evaluated for it.

In oncology, ZnO nanoparticles were mainly employed in cancer therapy and drug delivery. Various ZnO nanostructures (nanorods, nanowires, nanobelts, nanotubes, and other complex morphologies) were developed using suitable synthesis process. These ZnO nanoparticles produce reactive oxygen species (ROS) under irradiation of light, and phototoxicity was initiated in cells helping in anticancer activity (Akhtar et al. 2012) (Fig. 6.5). This ROS generation was increased by modifying ZnO nanoparticles with metal doping and hybriding, polymer doping, etc. (Sivakumar et al. 2018). Considering cancer, zinc oxide nanoparticles (ZnO nanoparticles) were mainly used to induce the apoptosis and autophagy of cancer cell by activation of p53 and LC3 proteins. The protein p53 or TP53 is a very important tumor protein; it regulates the cell activity and helps in tumor suppression. Similarly, LC3 is a central protein that occurs in the autophagosome pathway. It
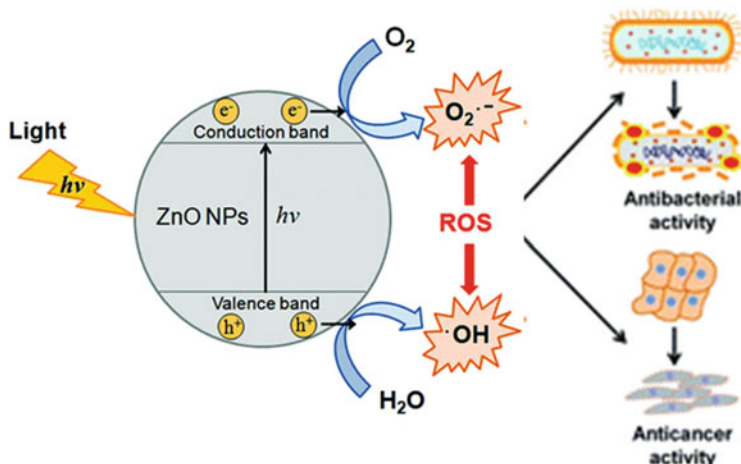
Fig. 6.5 ZnO nanoparticles – ROS generation on light irradiation and anticancer activity (Reprinted with permission of "Photo-triggered antibacterial and anticancer activities of zinc oxide nanoparticles," J. Mater. Chem. B, Copyright 2018, Royal Society of Chemistry from (Sivakumar et al. 2018))
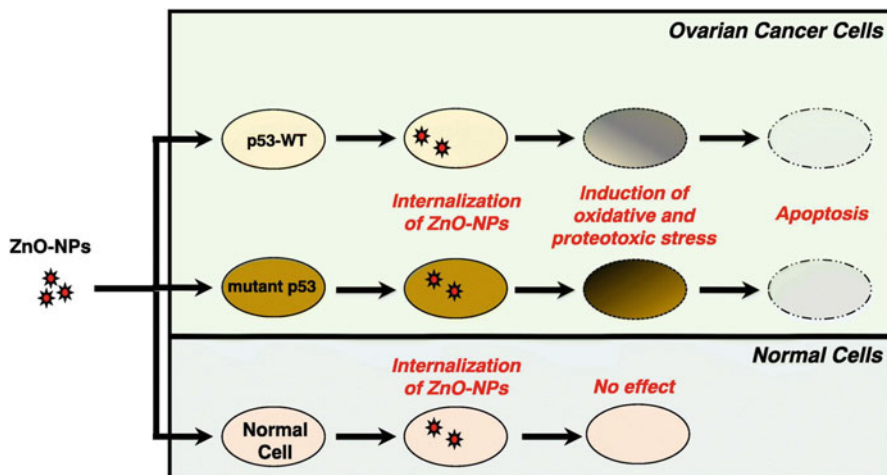
Fig. 6.6 ZnO Nanoparticles intiating apoptosis process – Independent of p53 mutation. (Reprinted with permission of "Zinc oxide nanoparticles induce oxidative and proteotoxic stress in ovarian cancer cells and trigger apoptosis independent of p53-mutation status," Appl. Surf. Sci., Copyright 2019, Elsevier, from (Padmanabhan et al. 2019))

helps to regulate the orderliness in degradation and recycling effect of cellular components, thus removing the unnecessary components if available in the cell.

Roy et al. (2014) have reported on the ZnO nanoparticle-induced programmed cell death by improving the autophagy mechanism. They proposed that ZnO nanoparticles produce reactive oxygen species (ROS) by reducing the antioxidant enzymes, lipid peroxidation, and increase of p53 protein. Phosphorylated Akt, PI3K, and mTOR were reduced remarkably on ZnO nanoparticles' exposure. This study demonstrates that zinc oxide nanoparticles support the autophagy mechanism and support apoptosis of cancer cell. Another work reported on the ZnO nanoparticles produce apoptosis of cancer cells. This cytotoxic effect of ZnO nanoparticles on cancer cells was observed. Human bronchial epithelial (BEAS-2B), human lung adenocarcinoma (A549), human hepatocellular carcinoma (HepG2), and primary rat cells (astrocytes and hepatocytes) were chosen for the study. ZnO nanoparticles destroyed cancer cells, whereas no effect was observed on primary rat cells astrocytes and hepatocytes.

The cytotoxicity process of ZnO nanoparticles was further viewed with hepatocellular carcinoma HepG2 cells. It was observed that tumor suppressor gene p53 and apoptotic gene were upregulated. The antiapoptotic gene bcl-2 was found to be downregulated. It was also found that in HepG2 cells, ZnO nanoparticles activated oxidative stress, ROS generation, and caspase-3 enzyme. The study concluded that ZnO nanoparticles induce cancer cell apoptosis by ROS generation through p53 tumor suppressor protein along with the trigger of anticancer drug. Recently, Padmanabhan et al. (2019) have reported on ZnO nanoparticles' relation with apoptosis of ovarian cancer cells depending upon oxidative and proteotoxic stress and independent of p53-mutation (Fig. 6.6).
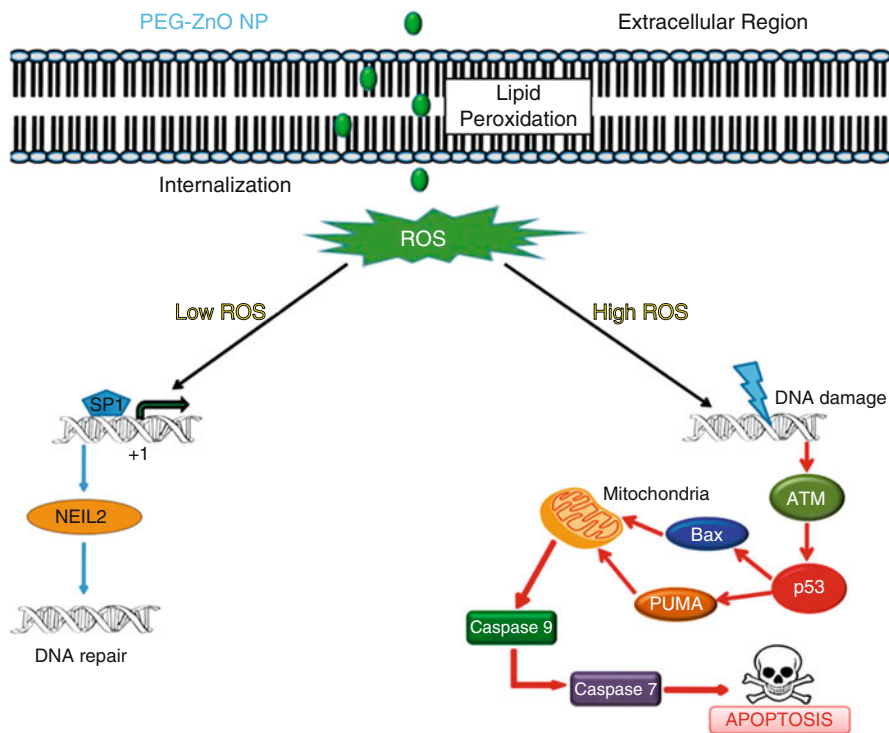
Fig. 6.7 ZnO nanoparticles – ROS – cell apoptosis. (Reprinted with permission of "PEG-functionalized zinc oxide nanoparticles induce apoptosis in breast cancer cells through reactive oxygen species-dependent impairment of DNA damage repair enzyme NEIL2," Free Radic. Biol. Med., Copyright 2017, Elsevier, from (Chakraborti et al. 2017))

When the size of ZnO nanoparticles was decreased, the cytotoxicity effect was found to increase. The mutant p53 protein present in ovarian cancer cells was found not responsible for apoptosis, i.e., ZnO nanoparticles reduced wild-type and gain-of-function mutant p53 protein. Thus, ZnO nanoparticles were observed as good anticancer therapeutic agents which were independent of the p53 mutants of the cancer cells. Chakraborti et al. (2017) have done the breast cancer cells apoptosis using polyethylene glycol-coated ZnO nanoparticles through ROS time-dependent of DNA repair with enzyme NEIL2. While the early hours of treatment with ZnO nanoparticles induce low-level ROS, but at late hours, the high level of ROS activity happens making the DNA repair process slow and making the cancer cells undergo apoptosis (Fig. 6.7).

6.4 Metal Sulfide Nanoparticles for Cancer Diagnosis and Treatment

6.4.1 Zinc Sulfide

Mathew et al. (2010) have demonstrated the dual usage of folate-combined carboxymethyl chitosan with manganese-doped zinc sulfide quantum dot nanoparticles (FA-CMC-ZnS-Mn) in drug delivery and fluorescence imaging of cancer cells. The 5-Fluorouracil (5 FU) was used as the anticancer drug in the treatment of breast cancer, which used to cover the FA-CMC-ZnS-Mn nanoparticle like a nutshell with a ratio of 1:2, respectively, with drug coating efficiency of 92.8%. The in vitro analysis of release of drug 5 FU from FA-CMC-ZnS-Mn was found to be in a consistent manner, supporting cancer treatment. Fluorescence imaging of breast cancer cell line (MCF-7) was obtained with this 5 FU-coated FA-CMC-ZnS-Mn nanoparticle and found to be toxic to the same cell lines. Nanoparticle (FA-CMC-ZnS-Mn) without 5F U produced nontoxicity towards the L929 fibroblast cells of mouse showing the capability of in vivo probe. This study provided the possibility of diagnosis and drug delivery at the same time utilizing ZnS nanoparticle.

Similarly, another work was carried out on folic acid-binded ZnS with Mn-doped ZnS quantum dot nanoparticles utilized as a probe to view the breast cancer cell (T47D) employing two-photon confocal fluorescence imaging of cancer cells. It was observed that the ZnS shell covered quantum dot nanoparticles with and without folic acid exposed the lower toxicity towards T47D and MCF-7 breast cancer cell lines by knowing the IC50 values (Geszke et al. 2011).

Fluorescent cell imaging bioprobe with mannosylated chitosan ZnS nanocrystals was doped with Mn used in detection of oral cancer cells. The chitosan was employed to target the mannose one type of protein/lipid by delivering the suitable functional groups. These ZnS nanocrystals were found to be highly cytocompatible and enhanced attachment to mannose receptor from cancer cells, thus segregating cancer cells and its colonies from normal cells. Furthermore, metabolic activity and morphology of the cell were also appreciable that these fluorescent bioprobes do not alter the surface morphology and metabolism of cancer cells (Jayasree et al. 2011).

Bwatanglang et al. (2016) have employed the encapsulation of Mn:ZnS quantum dots over folic acid – chitosan for simultaneous targeting drug delivery and cancer therapy, theranostic application. In this study, they have utilized the idea of over release of folic acid from the cancer cells as a target. These cancer cells showed high binding affinity towards nanocomposites. Studies on in vitro cytotoxicity have shown that these ZnS-based nanocomposites were nontoxic towards breast cell lines and found to emit at ~600 nm (orange-red fluorescence) by confocal laser scanning microscope, demonstrating specific cellular consumption of nanocomposites by folic acid expressing cancer cells. This work proved that the potential of aqueous synthesized Mn:ZnS quantum dots with biodegradable polymer chitosan is effective in targeted drug delivery and imaging of cancer cells using folic acid a high binding ligand as a target for these folate receptors (Fig. 6.8).
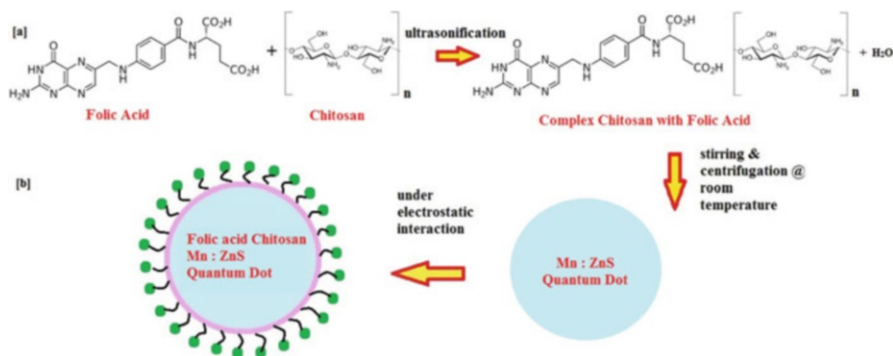
Fig. 6.8 Preparation of Folic Acid Chitosan – Mn:ZnS quantum dot for theranostic application (**a**) Step 1: Synthesis of complex chitosan with folic acid. (**b**) Step 2: Binding of complex chitosan – folic acid with Mn:ZnS quantum dots

Similarly, Bujňáková et al. (2017) have reported on the bioimaging of the human cancer cell lines HCT116 (human colorectal carcinoma), HeLa (human cervical adenocarcinoma), MCF-7 (human breast adenocarcinoma), and CaCo-2 (human colorectal adenocarcinoma), which were more fluorescent upon treating with ZnS-coated chitosan nanocomposites. The cytotoxic effects of the green synthesized zinc nanoparticles were studied against the MCF-7 breast cancer cell line, and IC50 values IC50 were 400 and 2000 μg/ml for ZnS nanoparticles and Stevia extract against MCF-7 cell line (Alijani et al. 2019).

6.4.2 Copper Sulfide

Copper sulfide nanoparticles (CuS nanoparticles) have several advantages over gold nanoparticles. It is prepared at low cost when compared to that of gold nanoparticles. While considering absorption characteristics, copper sulfide nanoparticles' NIR absorption depends upon the d-d transition of Cu^{2+} ions whereas surface plasmon resonance in Au nanoparticles. Then, the CuS nanoparticles have a size less than 40 nm which could support the target delivery than Au nanoparticles. Through renal discharge these nanoparticles were easily removed from the system after laser irradiation process. Due to these notable merits, CuS nanoparticles have found various opportunities in the biomedical field, especially in cancer diagnosis, drug delivery, and therapeutic applications (Fig. 6.9).

Li et al. (2010) dynamically reported on CuS nanoparticles as a novel agent to carry out photothermal ablation of cancer cells. Cells were treated with CuS nanoparticles and exposed to NIR laser light of 808 nm with a power of approximately 16 W/cm^2. NIR absorption of CuS occurred at ~900 nm. Photothermal destruction of HeLa cancer cells was observed which depends upon the
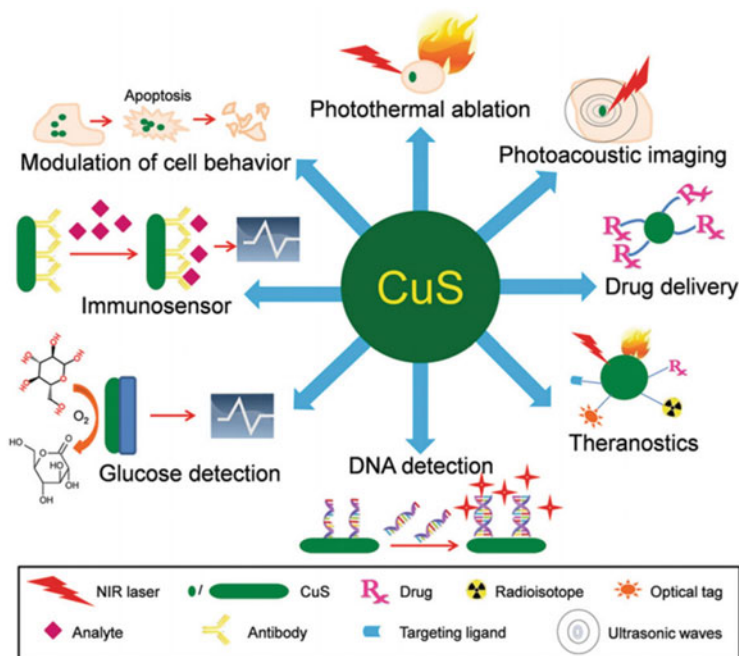
Fig. 6.9 Role of CuS in biomedical applications. (Reprinted with permission of "Synthesis and biomedical applications of copper sulfide nanoparticles: from sensors to theranostics," Small, Copyright 2014, Wiley-VCH Verlag GmbH & Co, from (Goel et al. 2014))

concentration of CuS nanoparticles and power of NIR laser. To get apoptosis of cells with 808 nm laser, the power applied has to be ~ 48 and 72 times higher than that of the safety limit ~0.33 W/cm^2. This condition makes a great constraint to use CuS nanoparticles with NIR laser. Following this work, Tian et al. (2011) reported on CuS nanoparticles superstructures for photothermal therapy with 980 nm laser. They addressed that even the safety limit of laser power of 0.51 W/cm^2 can destroy the cancer cells completely. To prove the efficiency of this photothermal therapy, they had no quantitative data showing the percentage of cell viability.

Guo et al. (2014) have reported that instead of solo performance of immunotherapy and photothermal abalation therapy, combined effect of photothermal immunotherapy on tumor destruction was very effective. In this study they have used the chitosan-coated hollow CuS nanoparticles in bringing together the adjuvants of oligodeoxynucleotides containing the cytosine guanine (CpG) pattern. These immunoadjuvant structures got split up after the laser irradiation. Combined approach of photothermal abalation immunotherapy have improved the destruction of tumor and avoids the further tumor growth by antitumor effects with the release of appropriate tumor antigens.

Another work explores the photoacoustic molecular imaging of breast cancer cell by using CuS nanoparticles. As a contrasting agent, CuS nanoparticles allowed to

Fig. 6.10 CuS inducing ROS generation by converting light into heat. (Reprinted with permission of "Plasmonic copper sulfide nanocrystals exhibiting near-infrared photothermal and photodynamic therapeutic effects," ACS Nano, Copyright 2015, American Chemical Society, from (Wang et al. 2015a, b))
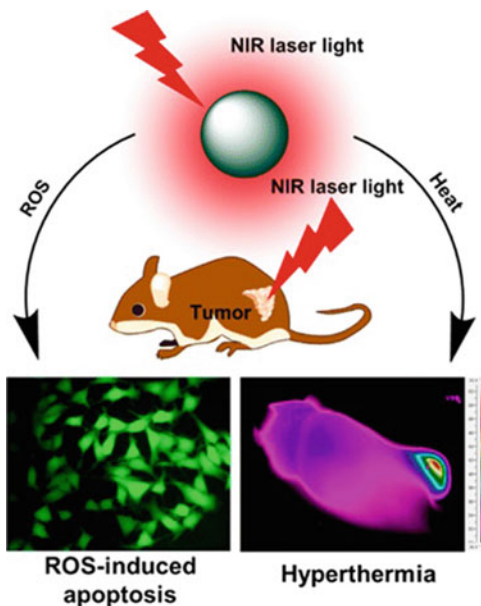
view the mouse brain (intracranial injection of nanoparticles), rat lymph nodes, and chicken breast muscle (CuS nanoparticles with agarose gel at a 5 cm depth). Photoacoustic excitation of samples was done with Nd:YAG laser of 1064 nm. The chicken breast muscle has been imaged with resolution of ∼800 μm and a sensitivity of ∼0.7 nmol per imaging voxel, leading to the conclusion that human breast lesions could be done at a depth of 40 mm of imaging resolution and same sensitivity as CuS nanoparticles in chicken breast muscles (Ku et al. 2012).

Liu et al. (2015a) have demonstrated the Mn (II) chelate-functionalized CuS nanoparticles in the cancer diagnosis and therapy with magnetic resonance imaging followed by photoacoustic therapy. The in vivo image by MRI shows that nanoparticles settle down in the tumor region very effectively within 24 h after intravenous injection, and tumors were destroyed by PTT effect. Since Mn(II)CuS nanoparticles possess a small size and low in vitro cytotoxicity, the rate of photothermal conversion was high and had no side effects; it could be employed in he theranostic application of cancer. Wang et al. (2015a) described the mechanism of photodynamic property of PEG-coated CuS nanoparticles in tumor treatment along with photothermal effect. They carried out a study on melanoma cells and murine melanoma with NIR irradiation. They report that along with photothermal therapy activity, CuS nanoparticles also exhibit the NIR-induced photodynamic effect producing enhanced ROS in the tumor site (Fig. 6.10).

Wang et al. (2016d) prepared a copper sulfide ferritin (CuS FN nanoparticles) by employing a biomimetic synthesis technique. Ferritin is a biomolecule with a sphere shape of 12 nm in size consisting of 24 subunits of protein forming and 8 nm hollow inner sphere. This feature was used as a cage to hold the CuS within it, thus forming
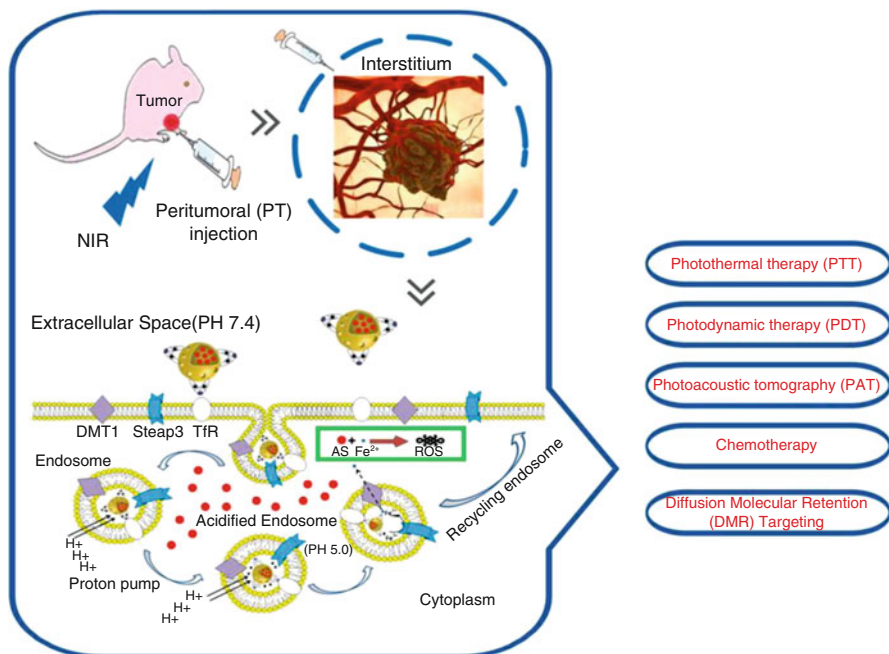
Fig. 6.11 Localized delivery for synergistic tumor treatment with metal sulfide nanoparticles. (Reprinted with permission of "Copper sulfide nanoparticle-based localized drug delivery system as an effective cancer synergistic treatment and theranostic platform," Acta Biomaterialia, Copyright 2017, Elsevier, from (Hou et al. 2017a, b))

the CuS FN nanoparticles exhibiting high binding between FN and Cu. These nanoparticles have shown the biocompatibility, homogeneous nature (control over size and shape), NIR absorption, high stability, and mainly tumor uptake. The pharmacokinetics behavior of CuS FN nanoparticles was determined with photoacoustic imaging and positron emission tomography for both in vivo and in vitro conditions. Destruction of entire cancer cells was obtained by intravenous injecting CuS FN nanoparticles with NIR laser irradiation of wavelength 808 nm of power 0.8 for the exposure time of 5 min.

Similarly, Hou et al. (2017a) proposed a multifunctional iron-dependent artesunate coupled transferrin-hollow mesoporous CuS nanoparticles (AS Tf-HMCuS nanoparticles) for identifying the cancer cells using photoacoustic imaging (PAI) followed by photothermal therapy and photodynamic therapy characteristics in treatment of cancer (Fig. 6.11). From the observation it was found that MCF-7 cells acquired AS Tf-HMCuS nanoparticles and converted NIR laser light into heat leading to PTT which in turn generated an enhanced level of ROS supporting PDT. An in vivo study was carried on mice with cancer cell, after injection of these AS Tf-HMCuS nanoparticles through peritumoral injection; NIR irradiation has shown the 74.8% inhibition rate. To understand the diffusion molecular retention (DMR), so as to track the nature of AS Tf-HMCuS nanoparticles, was

done with PAT and immunofluorescence properties and found to be a significant method in cancer treatment.

Zhou et al. (2018) reported on the multimodal technique for imaging and treatment of cancer by employing ultrasmall CuS nanoparticles (nanodots) of size less than 6 nm. They have synthesized by doping of manganese (Mn2+) and gallium3+ (Ga3+) into CuS to produce the final nanodots in the presence of bovine serum albumin. With these nanoparticles, SKOV-3 tumor (ovarian cancer) imaging was carried out with combination of imaging methods MR, PET, and PAT providing highly resolved images of cells. These nanoparticles are nontoxic to the cell under the absence of laser irradiation, whereas when laser light was exposed on SKOV-3 tumor cells, they were destroyed completely through necrosis and apoptosis process. It was worth to note that all the nanoparticles are excreted out by the renal system. Shi et al. (2019) reported dynamically on the real-time noninvasive in vivo method of multispectral optoacoustic tomography. This was done by observing the capacity of CuS-coupled PEG in their excellent tumor imaging (here SKOV3 ovarian cancer) capacity with MOS. Further, nude mice were utilized to understand the biodegradability of CuS PEG nanoparticles by noting down the alteration in hematological and hepatological factors under different laser irradiations.

Xiong et al. (2019) have synthesized CuS nanoparticles with polydopamine (PDA) then chelated with iron ions resulting the final nanoparticles mentioned as CuPDF nanoparticles. PDA had provided both biocompatibility and active under MRI method. CuPDF nanoparticles have increased photothermal efficacy when compared with that of raw PDA nanoparticles. To check the biocompatibility, in vitro analysis was performed with histology evaluation and cytotoxicity effect. The CuPDF nanoparticles were settled down in the tumor region through IV injection, and irradiation was done with NIR laser with appropriate power. In vivo application was carried out with mice bearing 4T1 tumor, and damage to normal tissues was less. All results demonstrated that CuS nanoparticles have a great potential to play a role as a better theranostic agent in oncology.

6.4.3 Rhenium Sulfide

Rhenium sulfide was used in sentinel lymph nodes (SLN) mapping with gamma detector in cancer diagnosis. Kato et al. (2003) proposed the work in the detection of esophageal squamous cell carcinoma by employing SLNs mapping coupled with cytokeratin immunohistochemistry. Out of 25 patients, 23 patient's sentinel lymph nodes were detected with lymphoscintigraphy yielding 92% efficiency. The significant value or probability value P was found to be less than 0.01 ($P < 0.01$) for lymph node status and $P < 0.05$ for pathologic stage and metastatic lymph node stage. Thus, it proved that CK immunohistochemistry with SLN mapping enhances the diagnostic accuracy of sentinel lymph node staging in esophageal cancer, to make up suitable treatment plan (Fig. 6.12). Similarly, Mochiki et al. (2006) reported on the SLN mapping with technetium-99m colloidal rhenium sulfide to detect gastric
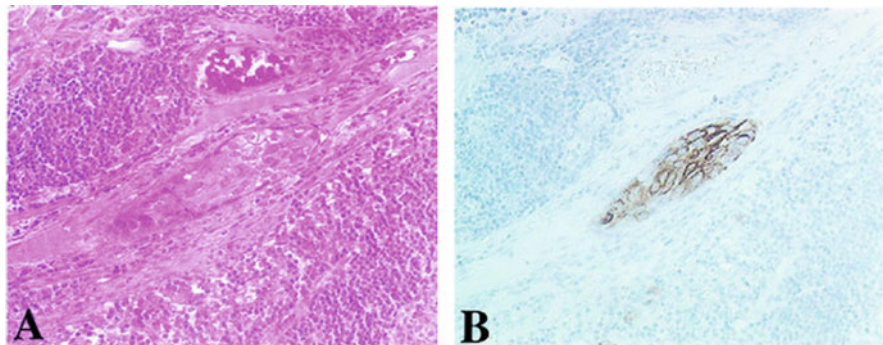
Fig. 6.12 Sentinel lymph node on (**a**) conventional hematoxylin-eosin staining. (**b**) Cytokeratin immunohistochemical staining (Reprinted with permission of "Sentinel lymph nodes with technetium-99m colloidal rhenium sulphide in patients with esophageal carcinoma," Cancer, Copyright 2003, American Cancer Society, from (Kato et al. 2003))

carcinoma. Out of 59 patients, SLNs were detectable at the lymphatic basin in 57 patients yielding 96%. The sensitivity for T1, T2 and T3 groups were found to be 100%, 91.6% and 62.5%, respectively. Rhenium sulfide for SLN mapping in the diagnosis of gastric cancer have produced the diagnostic accuracy of 92.9%.

Watanabe et al. (2001) reported on breast cancer detection with rhenium sulfide. Technetium-99 rhenium sulfide was injected at four sites surrounding the tumor in the breast tissue 24 h before operation. The study was carried out for 87 patients possessing breast cancer. Lymphoscintigraphy was carried out for each patient after 2 h of injection; axillary hot spots and SLN were observed in all patients during operation, yielding 100% accuracy. Similar work was carried out by Koizumi et al. (2003) with dose determination of colloidal rhenium sulfide in 1 day and 2 days protocol. The patients with large BMI and postmenopausal patients have shown the less uptake of colloid by SLN. Also, it is worth to note that size of the colloidal particles plays a major role in the absorption by tumor cell. If the particle size is larger than 200 nm, only one node is involved, whereas small size colloids (<50 nm) were absorbed by several nodes. To get significant sensitivity, the recommended dosages of colloid for 1 day protocol and 2 days protocol were 7.4 MBq and 37 MBq, respectively.

6.5 Summary and Conclusion

In summary, the metals, metal oxides, and metal sulfide nanoparticles due to their merits such as tunable/flexible optical behavior, biocompatibility, nontoxicity, renal clearance, chemical and biological simple synthesis, etc. made them a unique and unavoidable tool in diagnosis and treatment of cancer. Noble metals, gold and silver derived, gold (Au) and silver (Ag) nanoparticles, are considered to be the best metal

nanoparticles because of their biocompatibility nature in the diagnosis and treatment of cancer. In metal oxide nanoparticles, iron oxide nanoparticles were utilized as a contrasting agent in magnetic resonance imaging method to image the cancer cells, whereas the zinc oxide nanoparticles due to its cytotoxicity were employed in destruction of cancer cells. Zinc sulfide and copper sulfides were also used in theranostic application because of their cytotoxic effect. Rhenium sulfide was probed to map the sentinel lymph nodes (SLN) in various types of cancer in the breast, esophagus, gastric, etc., with the gamma detector. Further, deep research in these nanomaterials will reveal the entire potential, thereby enabling them to couple with the classical tools available in the hospitals.

References

Agarwal H, Kumar SV, Rajeshkumar S (2017) A review on green synthesis of zinc oxide nanoparticles–an eco-friendly approach. Res-Effic Technol 3(4):406–413. https://doi.org/10.1016/j.reffit.2017.03.002

Ai J, Xu Y, Lou B, Li D, Wang E (2014) Multifunctional AS1411-functionalized fluorescent gold nanoparticles for targeted cancer cell imaging and efficient photodynamic therapy. Talanta 118:54–60. https://doi.org/10.1016/j.talanta.2013.09.062

Akhtar MJ, Ahamed M, Kumar S, Khan MM, Ahmad J, Alrokayan SA (2012) Zinc oxide nanoparticles selectively induce apoptosis in human cancer cells through reactive oxygen species. Int J Nanomedicine 7:845–847. https://doi.org/10.2147/IJN.S29129

Alijani HQ, Pourseyedi S, Mahani MT, Khatami M (2019) Green synthesis of zinc sulphide (ZnS) nanoparticles using Stevia rebaudiana Bertoni and evaluation of its cytotoxic properties. J Mol Struct 1175:214–218. https://doi.org/10.1016/j.molstruc.2018.07.103

Austin LA, Kang B, Yen CW, El-Sayed MA (2011a) Plasmonic imaging of human oral cancer cell communities during programmed cell death by nuclear-targeting silver nanoparticles. J Am Chem Soc 133(44):17594–17597. https://doi.org/10.1021/ja207807t

Austin LA, Kang B, Yen CW, El-Sayed MA (2011b) Nuclear targeted silver nanospheres perturb the cancer cell cycle differently than those of nanogold. Bioconjug Chem 22(11):2324–2331. https://doi.org/10.1021/bc200386m

Ayala-Orozco C, Urban C, Knight MW, Urban AS, Neumann O, Bishnoi SW, Mukherjee S, Goodman AM, Charron H, Mitchell T, Shea M (2014) Au nanomatryoshkas as efficient near-infrared photothermal transducers for cancer treatment: benchmarking against nanoshells. ACS Nano 8(6):6372–6381. https://doi.org/10.1021/nn501871d

Bagheri S, Yasemi M, Safaie-Qamsari E, Rashidiani J, Abkar M, Hassani M, Mirhosseini SA, Kooshki H (2018) Using gold nanoparticles in diagnosis and treatment of melanoma cancer. Artif Cells Nanomed Biotechnol 46(sup1):462–471. https://doi.org/10.1080/21691401.2018.1430585

Baghi M, Mack MG, Hambek M, Rieger J, Vogl T, Gstoettner W, Knecht R (2005) The efficacy of MRI with ultrasmall superparamagnetic iron oxide particles (USPIO) in head and neck cancers. Anticancer Res 25(5):3665–3670

Bañobre-López M, Teijeiro A, Rivas J (2013) Magnetic nanoparticle-based hyperthermia for cancer treatment. Rep Prac Oncol Radiother 18(6):397–400. https://doi.org/10.1016/j.rpor.2013.09.011

Bao C, Beziere N, del Pino P, Pelaz B, Estrada G, Tian F, Ntziachristos V, de la Fuente JM, Cui D (2013) Gold nanoprisms as optoacoustic signal nanoamplifiers for in vivo bioimaging of gastrointestinal cancers. Small 9(1):68–74. https://doi.org/10.1002/smll.201201779

Benyettou F, Rezgui R, Ravaux F, Jaber T, Blumer K, Jouiad M, Motte L, Olsen JC, Platas-Iglesias C, Magzoub M, Trabolsi A (2015) Synthesis of silver nanoparticles for the dual delivery of doxorubicin and alendronate to cancer cells. J Mater Chem B 3(36):7237–7245. https://doi.org/10.1039/c5tb00994d

Boca-Farcau S, Potara M, Simon T, Juhem A, Baldeck P, Astilean S (2013) Folic acid-conjugated, SERS-labeled silver nanotriangles for multimodal detection and targeted photothermal treatment on human ovarian cancer cells. Mol Pharm 11(2):391–399. https://doi.org/10.1021/mp400300m

Bujňáková Z, Dutková E, Kello M, Mojžiš J, Baláž M, Baláž P, Shpotyuk O (2017) Mechanochemistry of chitosan-coated zinc sulfide (ZnS) nanocrystals for bio-imaging applications. Nanoscale Res Lett 12(1):328. https://doi.org/10.1186/s11671-017-2103-z

Bwatanglang IB, Mohammad F, Yusof NA, Abdullah J, Hussein MZ, Alitheen NB, Abu N (2016) Folic acid targeted Mn: ZnS quantum dots for theranostic applications of cancer cell imaging and therapy. Int J Nanomedicine 11:413–428. https://doi.org/10.2147/IJN.S90198

Chakraborti S, Chakraborty S, Saha S, Manna A, Banerjee S, Adhikary A, Sarwar S, Hazra TK, Das T, Chakrabarti P (2017) PEG-functionalized zinc oxide nanoparticles induce apoptosis in breast cancer cells through reactive oxygen species-dependent impairment of DNA damage repair enzyme NEIL2. Free Radic Biol Med 103:35–47. https://doi.org/10.1016/j.freeradbiomed.2016.11.048

Chen H, Li B, Ren X, Li S, Ma Y, Cui S, Gu Y (2012) Multifunctional near-infrared-emitting nanoconjugates based on gold clusters for tumor imaging and therapy. Biomaterials 33(33):8461–8476. https://doi.org/10.1016/j.biomaterials.2012.08.034

Chen R, Wang X, Yao X, Zheng X, Wang J, Jiang X (2013) Near-IR-triggered photothermal/photodynamic dual-modality therapy system via chitosan hybrid nanospheres. Biomaterials 34(33):8314–8322. https://doi.org/10.1016/j.biomaterials.2013.07.034

Chen M, Tang S, Guo Z, Wang X, Mo S, Huang X, Liu G, Zheng N (2014a) Core–Shell Pd@ Au nanoplates as theranostic agents for in-vivo photoacoustic imaging, CT imaging, and photothermal therapy. Adv Mater 26(48):8210–8216. https://doi.org/10.1002/adma.201404013

Chen W, Ayala-Orozco C, Biswal NC, Perez-Torres C, Bartels M, Bardhan R, Stinnet G, Liu XD, Ji B, Deorukhkar A, Brown LV (2014b) Targeting pancreatic cancer with magneto-fluorescent theranostic gold nanoshells. Nanomedicine 9(8):1209–1222. https://doi.org/10.2217/nnm.13.84

Chen WH, Yang CX, Qiu WX, Luo GF, Jia HZ, Lei Q, Wang XY, Liu G, Zhuo RX, Zhang XZ (2015) Multifunctional theranostic nanoplatform for cancer combined therapy based on gold nanorods. Adv Healthc Mater 4(15):2247–2259. https://doi.org/10.1002/adhm.201500453

Cheng K, Kothapalli SR, Liu H, Koh AL, Jokerst JV, Jiang H, Yang M, Li J, Levi J, Wu JC, Gambhir SS (2014) Construction and validation of nano gold tripods for molecular imaging of living subjects. J Am Chem Soc 136(9):3560–3571. https://doi.org/10.1021/ja412001e

Cheng B, He H, Huang T, Berr SS, He J, Fan D, Zhang J, Xu P (2016) Gold nanosphere gated mesoporous silica nanoparticle responsive to near-infrared light and redox potential as a theranostic platform for cancer therapy. J Biomed Nanotechnol 12(3):435–449. https://doi.org/10.1166/jbn.2016.2195

Choi J, Yang J, Bang D, Park J, Suh JS, Huh YM, Haam S (2012) Targetable gold nanorods for epithelial cancer therapy guided by near-IR absorption imaging. Small 8(5):746–753. https://doi.org/10.1002/smll.201101789

Copland JA, Eghtedari M, Popov VL, Kotov N, Mamedova N, Motamedi M, Oraevsky AA (2004) Bioconjugated gold nanoparticles as a molecular based contrast agent: implications for imaging of deep tumors using optoacoustic tomography. Mol Imaging Biol 6(5):341–349. https://doi.org/10.1016/j.mibio.2004.06.002

Coughlin AJ, Ananta JS, Deng N, Larina IV, Decuzzi P, West JL (2014) Gadolinium-conjugated gold nanoshells for multimodal diagnostic imaging and photothermal cancer therapy. Small 10 (3):556–565. https://doi.org/10.1002/smll.201302217

Croissant JG, Zhang D, Alsaiari S, Lu J, Deng L, Tamanoi F, AlMalik AM, Zink JI, Khashab NM (2016) Protein-gold clusters-capped mesoporous silica nanoparticles for high drug loading, autonomous gemcitabine/doxorubicin co-delivery, and in-vivo tumor imaging. J Control Release 229:183–191. https://doi.org/10.1016/j.jconrel.2016.03.030

D'Hollander A, Mathieu E, Jans H, Velde GV, Stakenborg T, Van Dorpe P, Himmelreich U, Lagae L (2016) Development of nanostars as a biocompatible tumor contrast agent: toward in vivo SERS imaging. Int J Nanomedicine 11:3703. https://doi.org/10.2147/IJN.S91340

El-Sayed IH, Huang X, El-Sayed MA (2005) Surface plasmon resonance scattering and absorption of anti-EGFR antibody conjugated gold nanoparticles in cancer diagnostics: applications in oral cancer. Nano Lett 5(5):829–834. https://doi.org/10.1021/nl050074e

El-Sayed IH, Huang X, El-Sayed MA (2006) Selective laser photo-thermal therapy of epithelial carcinoma using anti-EGFR antibody conjugated gold nanoparticles. Cancer Lett 239 (1):129–135. https://doi.org/10.1016/j.canlet.2005.07.035

Feng S, Chen R, Lin J, Pan J, Chen G, Li Y, Cheng M, Huang Z, Chen J, Zeng H (2010) Nasopharyngeal cancer detection based on blood plasma surface-enhanced Raman spectroscopy and multivariate analysis. Biosens Bioelectron 25(11):2414–2419. https://doi.org/10.1016/j.bios.2010.03.033

Feng J, Zhao J, Hao F, Chen C, Bhakoo K, Tang H (2011) NMR-based metabonomic analyses of the effects of ultrasmall superparamagnetic particles of iron oxide (USPIO) on macrophage metabolism. J Nanopart Res 13(5):2049–2062. https://doi.org/10.1007/s11051-010-9959-5

Feng S, Lin D, Lin J, Li B, Huang Z, Chen G, Zhang W, Wang L, Pan J, Chen R, Zeng H (2013) Blood plasma surface-enhanced Raman spectroscopy for non-invasive optical detection of cervical cancer. Analyst 138(14):3967–3974. https://doi.org/10.1039/c3an36890d

Firdhouse MJ, Lalitha P (2013) Biosynthesis of silver nanoparticles using the extract of Alternanthera sessilis—antiproliferative effect against prostate cancer cells. Cancer Nanotechnol 4(6):137–143. https://doi.org/10.1007/s12645-013-0045-4

Gao L, Fei J, Zhao J, Li H, Cui Y, Li J (2012) Hypocrellin-loaded gold nanocages with high two-photon efficiency for photothermal/photodynamic cancer therapy in vitro. ACS Nano 6 (9):8030–8040. https://doi.org/10.1021/nn302634m

Gao Y, Li Y, Chen J, Zhu S, Liu X, Zhou L, Shi P, Niu D, Gu J, Shi J (2015) Multifunctional gold nanostar-based nanocomposite: synthesis and application for noninvasive MR-SERS imaging-guided photothermal ablation. Biomaterials 60:31–41. https://doi.org/10.1016/j.biomaterials.2015.05.004

Gao S, Zhang L, Wang G, Yang K, Chen M, Tian R, Ma Q, Zhu L (2016) Hybrid graphene/Au activatable theranostic agent for multimodalities imaging guided enhanced photothermal therapy. Biomaterials 79:36–45. https://doi.org/10.1016/j.biomaterials.2015.11.041

Gao X, Yue Q, Liu Z, Ke M, Zhou X, Li S, Zhang J, Zhang R, Chen L, Mao Y, Li C (2017) Guiding brain-tumor surgery via blood–brain-barrier-permeable gold nanoprobes with acid-triggered MRI/SERRS signals. Adv Mater 29(21):1603917. https://doi.org/10.1002/adma.201603917

Geszke M, Murias M, Balan L, Medjahdi G, Korczynski J, Moritz M, Lulek J, Schneider R (2011) Folic acid-conjugated core/shell ZnS: Mn/ZnS quantum dots as targeted probes for two photon fluorescence imaging of cancer cells. Acta Biomater 7(3):1327–1338. https://doi.org/10.1016/j.actbio.2010.10.012

Goel S, Chen F, Cai W (2014) Synthesis and biomedical applications of copper sulphide nanoparticles: from sensors to theranostics. Small 10(4):631–645. https://doi.org/10.1002/smll.201301174

Gopinath P, Gogoi SK, Chattopadhyay A, Ghosh SS (2008) Implications of silver nanoparticle induced cell apoptosis for in vitro gene therapy. Nanotechnology 19(7):075104. https://doi.org/10.1088/0957-4484/19/7/075104

Gopinath P, Gogoi SK, Sanpui P, Paul A, Chattopadhyay A, Ghosh SS (2010) Signaling gene cascade in silver nanoparticle induced apoptosis. Colloids Surf B: Biointerfaces 77(2):240–245. https://doi.org/10.1016/j.colsurfb.2010.01.033

Guan T, Shang W, Li H, Yang X, Fang C, Tian J, Wang K (2017) From detection to resection: photoacoustic tomography and surgery Guidance with indocyanine green loaded gold Nanorod@ liposome core–shell nanoparticles in liver Cancer. Bioconjug Chem 28 (4):1221–1228. https://doi.org/10.1021/acs.bioconjchem.7b00065

Guo L, Yan DD, Yang D, Li Y, Wang X, Zalewski O, Yan B, Lu W (2014) Combinatorial photothermal and immuno cancer therapy using chitosan-coated hollow copper sulphide nanoparticles. ACS Nano 8(6):5670–5681. https://doi.org/10.1021/nn5002112

Guo J, Rahme K, He Y, Li L-L, Holmes JD, O'Driscoll CM (2017) Gold nanoparticles enlighten the future of cancer theranostics. Int J Nanomedicine 12:6131–6152. https://doi.org/10.2147/IJN.S140772

Gurunathan S, Han JW, Eppakayala V, Jeyaraj M, Kim JH (2013a) Cytotoxicity of biologically synthesized silver nanoparticles in MDA-MB-231 human breast cancer cells. Biomed Res Int 2013. https://doi.org/10.1155/2013/535796

Gurunathan S, Raman J, Malek SNA, John PA, Vikineswary S (2013b) Green synthesis of silver nanoparticles using Ganoderma neo-japonicum Imazeki: a potential cytotoxic agent against breast cancer cells. Int J Nanomedicine 8:4399–4413. https://doi.org/10.2147/IJN.S51881

Gurunathan S, Han JW, Dayem AA, Eppakayala V, Park JH, Cho SG, Lee KJ, Kim JH (2013c) Green synthesis of anisotropic silver nanoparticles and its potential cytotoxicity in human breast cancer cells (MCF-7). J Ind Eng Chem 19(5):1600–1605. https://doi.org/10.1016/j.jiec.2013.01.029

Gurunathan S, Park JH, Han JW, Kim JH (2015) Comparative assessment of the apoptotic potential of silver nanoparticles synthesized by Bacillus tequilensis and Calocybe indica in MDA-MB-231 human breast cancer cells: targeting p53 for anticancer therapy. Int J Nanomedicine 10:4203–4223. https://doi.org/10.2147/IJN.S83953

Han S, Samanta A, Xie X, Huang L, Peng J, Park SJ, Teh DBL, Choi Y, Chang YT, All AH, Yang Y (2017) Gold and hairpin DNA functionalization of upconversion nanocrystals for imaging and in vivo drug delivery. Adv Mater 29(18):1700244. https://doi.org/10.1002/adma.201700244

Hao Y, Zhang B, Zheng C, Ji R, Ren X, Guo F, Sun S, Shi J, Zhang H, Zhang Z, Wang L (2015) The tumor-targeting core–shell structured DTX-loaded PLGA@ Au nanoparticles for chemo-photothermal therapy and X-ray imaging. J Control Release 220:545–555. https://doi.org/10.1016/j.jconrel.2015.11.016

He X, Liu F, Liu L, Duan T, Zhang H, Wang Z (2014) Lectin-conjugated Fe2O3@ Au core@ shell nanoparticles as dual mode contrast agents for in vivo detection of tumor. Mol Pharm 11 (3):738–745. https://doi.org/10.1021/mp400456j

Hou L, Shan X, Hao L, Feng Q, Zhang Z (2017a) Copper sulphide nanoparticle-based localized drug delivery system as an effective cancer synergistic treatment and theranostic platform. Acta Biomater 54:307–320. https://doi.org/10.1016/j.actbio.2017.03.005

Hou W, Xia F, Alfranca G, Yan H, Zhi X, Liu Y, Peng C, Zhang C, de la Fuente JM, Cui D (2017b) Nanoparticles for multi-modality cancer diagnosis: simple protocol for self-assembly of gold nanoclusters mediated by gadolinium ions. Biomaterials 120:103–114. https://doi.org/10.1016/j.biomaterials.2016.12.027

Hu C, Liu Y, Qin J, Nie G, Lei B, Xiao Y, Zheng M, Rong J (2013a) Fabrication of reduced graphene oxide and sliver nanoparticle hybrids for Raman detection of absorbed folic acid: a potential cancer diagnostic probe. ACS Appl Mater Interfaces 5(11):4760–4768. https://doi.org/10.1021/am4000485

Hu DH, Sheng ZH, Zhang PF, Yang DZ, Liu SH, Gong P, Gao DY, Fang ST, Ma YF, Cai LT (2013b) Hybrid gold–gadolinium nanoclusters for tumor-targeted NIRF/CT/MRI triple-modal imaging in vivo. Nanoscale 5(4):1624–1628. https://doi.org/10.1039/C2NR33543C

Hu H, Huang P, Weiss OJ, Yan X, Yue X, Zhang MG, Tang Y, Nie L, Ma Y, Niu G, Wu K (2014) PET and NIR optical imaging using self-illuminating 64Cu-doped chelator-free gold nanoclusters. Biomaterials 35(37):9868–9876. https://doi.org/10.1016/j.biomaterials.2014.08.038

Huang X, El-Sayed IH, Qian W, El-Sayed MA (2006) Cancer cell imaging and photothermal therapy in the near-infrared region by using gold nanorods. J Am Chem Soc 128(6):2115–2120. https://doi.org/10.1021/ja057254a

Huang J, Bu L, Xie J, Chen K, Cheng Z, Li X, Chen X (2010) Effects of nanoparticle size on cellular uptake and liver MRI with polyvinylpyrrolidone-coated iron oxide nanoparticles. ACS Nano 4(12):7151–7160. https://doi.org/10.1021/nn101643u

Huang P, Lin J, Wang S, Zhou Z, Li Z, Wang Z, Zhang C, Yue X, Niu G, Yang M, Cui D (2013) Photosensitizer-conjugated silica-coated gold nanoclusters for fluorescence imaging-guided photodynamic therapy. Biomaterials 34(19):4643–4654. https://doi.org/10.1016/j.biomaterials.2013.02.063

Huang J, Guo M, Ke H, Zong C, Ren B, Liu G, Shen H, Ma Y, Wang X, Zhang H, Deng Z (2015) Rational design and synthesis of γFe2O3@ Au magnetic gold nanoflowers for efficient cancer theranostics. Adv Mater 27(34):5049–5056. https://doi.org/10.1002/adma.201501942

Jang B, Park JY, Tung CH, Kim IH, Choi Y (2011) Gold nanorod− photosensitizer complex for near-infrared fluorescence imaging and photodynamic/photothermal therapy in vivo. ACS Nano 5(2):1086–1094. https://doi.org/10.1021/nn102722z

Jayapaul J, Arns S, Lederle W, Lammers T, Comba P, Gätjens J, Kiessling F (2012) Riboflavin carrier protein-targeted fluorescent USPIO for the assessment of vascular metabolism in tumors. Biomaterials 33(34):8822–8829. https://doi.org/10.1016/j.biomaterials.2012.08.036

Jayasree A, Sasidharan S, Koyakutty M, Nair S, Menon D (2011) Mannosylated chitosan-zinc sulphide nanocrystals as fluorescent bioprobes for targeted cancer imaging. Carbohydr Polym 85(1):37–43. https://doi.org/10.1016/j.carbpol.2011.01.034

Jing L, Liang X, Deng Z, Feng S, Li X, Huang M, Li C, Dai Z (2014) Prussian blue coated gold nanoparticles for simultaneous photoacoustic/CT bimodal imaging and photothermal ablation of cancer. Biomaterials 35(22):5814–5821. https://doi.org/10.1016/j.biomaterials.2014.04.005

Jokerst JV, Cole AJ, Van de Sompel D, Gambhir SS (2012) Gold nanorods for ovarian cancer detection with photoacoustic imaging and resection guidance via Raman imaging in living mice. ACS Nano 6(11):10366–10377. https://doi.org/10.1021/nn304347g

Kang S, Bhang SH, Hwang S, Yoon JK, Song J, Jang HK, Kim S, Kim BS (2015) Mesenchymal stem cells aggregate and deliver gold nanoparticles to tumors for photothermal therapy. ACS Nano 9(10):9678–9690. https://doi.org/10.1021/acsnano.5b02207

Karmani L, Labar D, Valembois V, Bouchat V, Nagaswaran PG, Bol A, Gillart J, Levêque P, Bouzin C, Bonifazi D, Michiels C (2013) Antibody-functionalized nanoparticles for imaging cancer: influence of conjugation to gold nanoparticles on the biodistribution of 89Zr-labeled cetuximab in mice. Contrast Media Mol Imaging 8(5):402–408. https://doi.org/10.1002/cmmi.1539

Kato H, Miyazaki T, Nakajima M, Takita J, Sohda M, Fukai Y, Masuda N, Fukuchi M, Manda R, Ojima H, Tsukada K (2003) Sentinel lymph nodes with technetium-99m colloidal rhenium sulphide in patients with esophageal carcinoma. Cancer Interdiscipl Int J Am Cancer Soc 98(5):932–939. https://doi.org/10.1002/cncr.11559

Kim D, Jeong YY, Jon S (2010) A drug-loaded aptamer- gold nanoparticle bioconjugate for combined CT imaging and therapy of prostate cancer. ACS Nano 4(7):3689–3696. https://doi.org/10.1021/nn901877h

Kim S, Chen YS, Luke GP, Emelianov SY (2011a) In vivo three-dimensional spectroscopic photoacoustic imaging for monitoring nanoparticle delivery. Biomed Opt Express 2(9):2540–2550. https://doi.org/10.1364/BOE.2.002540

Kim YH, Jeon J, Hong SH, Rhim WK, Lee YS, Youn H, Chung JK, Lee MC, Lee DS, Kang KW, Nam JM (2011b) Tumor targeting and imaging using cyclic RGD-PEGylated gold nanoparticle probes with directly conjugated iodine-125. Small 7(14):2052–2060. https://doi.org/10.1002/smll.201100927

Kim JY, Choi WI, Kim M, Tae G (2013) Tumor-targeting nanogel that can function independently for both photodynamic and photothermal therapy and its synergy from the procedure of PDT followed by PTT. J Control Release 171(2):113–121. https://doi.org/10.1016/j.jconrel.2013.07.006

Kim CS, Ingato D, Wilder-Smith P, Chen Z, Kwon YJ (2018) Stimuli-disassembling gold nanoclusters for diagnosis of early stage oral cancer by optical coherence tomography. Nano Convergence 5(1):1–1. https://doi.org/10.1186/s40580-018-0134-5

Koizumi M, Nomura E, Yamada Y, Takiguchi T, Tanaka K, Yoshimoto M, Makita M, Sakamoto G, Kasumi F, Ogata E (2003) Sentinel node detection using 99mTc-rhenium sulphide colloid in breast cancer patients: evaluation of 1 day and 2 day protocols, and a dose-finding study. Nucl Med Commun 24(6):663–670. https://doi.org/10.1097/00006231-200306000-00008

Kolosnjaj-Tabi J, Javed Y, Lartigue L, Volatron J, Elgrabli D, Marangon I, Pugliese G, Caron B, Figuerola A, Luciani N, Pellegrino T (2015) The one-year fate of iron oxide coated gold nanoparticles in mice. ACS Nano 9(8):7925–7939. https://doi.org/10.1021/acsnano.5b00042

Ku G, Zhou M, Song S, Huang Q, Hazle J, Li C (2012) Copper sulphide nanoparticles as a new class of photoacoustic contrast agent for deep tissue imaging at 1064 nm. ACS Nano 6 (8):7489–7496. https://doi.org/10.1021/nn302782y

Kvistad KA, Rydland J, Smethurst HB, Lundgren S, Fjøsne HE, Haraldseth O (2000) Axillary lymph node metastases in breast cancer: preoperative detection with dynamic contrast-enhanced MRI. Eur Radiol 10(9):1464–1471. https://doi.org/10.1007/s003300000370

Lai G, Wu J, Ju H, Yan F (2011) Streptavidin-functionalized silver-nanoparticle-enriched carbon nanotube tag for ultrasensitive multiplexed detection of tumor markers. Adv Funct Mater 21 (15):2938–2943. https://doi.org/10.1002/adfm.201100396

Li Y, Lu W, Huang Q, Li C, Chen W (2010) Copper sulphide nanoparticles for photothermal ablation of tumor cells. Nanomedicine 5(8):1161–1171. https://doi.org/10.2217/nnm.10.85

Li L, Nurunnabi M, Nafiujjaman M, Lee YK, Huh KM (2013) GSH-mediated photoactivity of pheophorbide a-conjugated heparin/gold nanoparticle for photodynamic therapy. J Control Release 171(2):241–250. https://doi.org/10.1016/j.jconrel.2013.07.002

Li W, Zhang X, Zhou M, Tian B, Yu C, Jie J, Hao X, Zhang X (2014a) Functional core/shell drug nanoparticles for highly effective synergistic cancer therapy. Adv Healthc Mater 3 (9):1475–1485. https://doi.org/10.1002/adhm.201300577

Li X, Takashima M, Yuba E, Harada A, Kono K (2014b) PEGylated PAMAM dendrimer–doxorubicin conjugate-hybridized gold nanorod for combined photothermal-chemotherapy. Biomaterials 35(24):6576–6584. https://doi.org/10.1016/j.biomaterials.2014.04.043

Li L, Fu S, Chen C, Wang X, Fu C, Wang S, Guo W, Yu X, Zhang X, Liu Z, Qiu J (2016) Microenvironment-driven bioelimination of magnetoplasmonic nanoassemblies and their multimodal imaging-guided tumor photothermal therapy. ACS Nano 10(7):7094–7105. https://doi.org/10.1021/acsnano.6b03238

Lin J, Chen R, Feng S, Pan J, Li Y, Chen G, Cheng M, Huang Z, Yu Y, Zeng H (2011) A novel blood plasma analysis technique combining membrane electrophoresis with silver nanoparticle-based SERS spectroscopy for potential applications in noninvasive cancer detection. Nanomedicine 7(5):655–663. https://doi.org/10.1016/j.nano.2011.01.012

Lin D, Feng S, Huang H, Chen W, Shi H, Liu N, Chen L, Chen W, Yu Y, Chen R (2014) Label-free detection of blood plasma using silver nanoparticle based surface-enhanced Raman spectroscopy for esophageal cancer screening. J Biomed Nanotechnol 10(3):478–484. https://doi.org/10.1166/jbn.2014.1750

Liu L, Ni F, Zhang J, Jiang X, Lu X, Guo Z, Xu R (2011) Silver nanocrystals sensitize magnetic-nanoparticle-mediated thermo-induced killing of cancer cells. Acta Biochim Biophys Sin 43 (4):316–323. https://doi.org/10.1093/abbs/gmr015

Liu R, Jing L, Peng D, Li Y, Tian J, Dai Z (2015a) Manganese (II) chelate functionalized copper sulphide nanoparticles for efficient magnetic resonance/photoacoustic dual-modal imaging guided photothermal therapy. Theranostics 5(10):1144–1153. https://doi.org/10.7150/thno.11754

Liu Y, Ashton JR, Moding EJ, Yuan H, Register JK, Fales AM, Choi J, Whitley MJ, Zhao X, Qi Y, Ma Y (2015b) A plasmonic gold nanostar theranostic probe for in vivo tumor imaging and photothermal therapy. Theranostics 5(9):946–960

Liu Y, Yang M, Zhang J, Zhi X, Li C, Zhang C, Pan F, Wang K, Yang Y, Martinez de la Fuentea J, Cui D (2016) Human induced pluripotent stem cells for tumor targeted delivery of gold nanorods and enhanced photothermal therapy. ACS Nano 10(2):2375–2385. https://doi.org/10.1021/acsnano.5b07172

Lu W, Melancon MP, Xiong C, Huang Q, Elliott A, Song S, Zhang R, Flores LG, Gelovani JG, Wang LV, Ku G (2011) Effects of photoacoustic imaging and photothermal ablation therapy mediated by targeted hollow gold nanospheres in an orthotopic mouse xenograft model of glioma. Cancer Res 71(19):6116–6121. https://doi.org/10.1158/0008-5472.CAN-10-4557

Luo CH, Huang CT, Su CH, Yeh CS (2016) Bacteria-mediated hypoxia-specific delivery of nanoparticles for tumors imaging and therapy. Nano Lett 16(6):3493–3499. https://doi.org/10.1021/acs.nanolett.6b00262

Marchal G, Van Hecke P, Demaerel P, Decrop E, Kennis C, Baert AL, Van der Schueren E (1989) Detection of liver metastases with superparamagnetic iron oxide in 15 patients: results of MR imaging at 1.5 T. Am J Roentgenol 152(4):771–775. https://doi.org/10.2214/ajr.152.4.771

Martinkova P, Brtnicky M, Kynicky J, Pohanka M (2018) Iron oxide nanoparticles: innovative tool in cancer diagnosis and therapy. Adv Healthc Mater 7(5):1700932. https://doi.org/10.1002/adhm.201700932

Mathew ME, Mohan JC, Manzoor K, Nair SV, Tamura H, Jayakumar R (2010) Folate conjugated carboxymethyl chitosan–manganese doped zinc sulphide nanoparticles for targeted drug delivery and imaging of cancer cells. Carbohydr Polym 80(2):442–448. https://doi.org/10.1016/j.carbpol.2009.11.047

Mehlen P, Puisieux A (2006) Metastasis: a question of life or death. Nat Rev Cancer 6:449–458. https://doi.org/10.1038/nrc1886

Meir R, Shamalov K, Betzer O, Motiei M, Horovitz-Fried M, Yehuda R, Popovtzer A, Popovtzer R, Cohen CJ (2015) Nanomedicine for cancer immunotherapy: tracking cancer-specific T-cells in vivo with gold nanoparticles and CT imaging. ACS Nano 9(6):6363–6372. https://doi.org/10.1021/acsnano.5b01939

Mishra A, Mehdi SJ, Irshad M, Ali A, Sardar M, Moshahid M, Rizvi A (2012) Effect of biologically synthesized silver nanoparticles on human cancer cells. Sci Adv Mater 4(12):1200–1206. https://doi.org/10.1166/sam.2012.1414

Mittal AK, Bhaumik J, Kumar S, Banerjee UC (2014) Biosynthesis of silver nanoparticles: elucidation of prospective mechanism and therapeutic potential. J Colloid Interface Sci 415:39–47. https://doi.org/10.1016/j.jcis.2013.10.018

Mochiki E, Kuwano H, Kamiyama Y, Aihara R, Nakabayashi T, Katoh H, Asao T, Oriuchi N, Endo K (2006) Sentinel lymph node mapping with technetium-99m colloidal rhenium sulphide in patients with gastric carcinoma. Am J Surg 191(4):465–469. https://doi.org/10.1016/j.amjsurg.2005.09.002

Mukherjee SG, O'Claonadh N, Casey A, Chambers G (2012) Comparative in vitro cytotoxicity study of silver nanoparticle on two mammalian cell lines. Toxicol in Vitro 26(2):238–251. https://doi.org/10.1016/j.tiv.2011.12.004

Nair LV, Nazeer SS, Jayasree RS, Ajayaghosh A (2015) Fluorescence imaging assisted photodynamic therapy using photosensitizer-linked gold quantum clusters. ACS Nano 9(6):5825–5832. https://doi.org/10.1021/acsnano.5b00406

Nie L, Wang S, Wang X, Rong P, Ma Y, Liu G, Huang P, Lu G, Chen X (2014) In vivo volumetric photoacoustic molecular angiography and therapeutic monitoring with targeted plasmonic nanostars. Small 10(8):1585–1593. https://doi.org/10.1002/smll.201302924

Ong C, Lim JZZ, Ng CT, Li JJ, Yung LY, Bay BH (2013) Silver nanoparticles in cancer: therapeutic efficacy and toxicity. Curr Med Chem 20(6):772–781. https://doi.org/10.2174/0929867311320060003

Orel V, Shevchenko A, Romanov A, Tselepi M, Mitrelias T, Barnes CH, Burlaka A, Lukin S, Shchepotin I (2015) Magnetic properties and antitumor effect of nanocomplexes of iron oxide and doxorubicin. Nanomedicine 11:47–55. https://doi.org/10.1016/j.nano.2014.07.007

Padmanabhan A, Kaushik M, Niranjan R, Richards JS, Ebright B, Venkatasubbu GD (2019) Zinc oxide nanoparticles induce oxidative and proteotoxic stress in ovarian cancer cells and trigger apoptosis independent of p53-mutation status. Appl Surf Sci 487:807–818. https://doi.org/10.1016/j.apsusc.2019.05.099

Park J, Park J, Ju EJ, Park SS, Choi J, Lee JH, Lee KJ, Shin SH, Ko EJ, Park I, Kim C (2015) Multifunctional hollow gold nanoparticles designed for triple combination therapy and CT imaging. J Control Release 207:77–85. https://doi.org/10.1016/j.jconrel.2015.04.007

Parveen A, Rao S (2015) Cytotoxicity and genotoxicity of biosynthesized gold and silver nanoparticles on human cancer cell lines. J Clust Sci 26(3):775–788. https://doi.org/10.1007/s10876-014-0744-y

Patra S, Mukherjee S, Barui AK, Ganguly A, Sreedhar B, Patra CR (2015) Green synthesis, characterization of gold and silver nanoparticles and their potential application for cancer therapeutics. Mater Sci Eng C 53:298–309. https://doi.org/10.1016/j.msec.2015.04.048

Peng C, Zheng L, Chen Q, Shen M, Guo R, Wang H, Cao X, Zhang G, Shi X (2012) PEGylated dendrimer-entrapped gold nanoparticles for in vivo blood pool and tumor imaging by computed tomography. Biomaterials 33(4):1107–1119. https://doi.org/10.1016/j.biomaterials.2011.10.052

Piao JG, Wang L, Gao F, You YZ, Xiong Y, Yang L (2014) Erythrocyte membrane is an alternative coating to polyethylene glycol for prolonging the circulation lifetime of gold nanocages for photothermal therapy. ACS Nano 8(10):10414–10425. https://doi.org/10.1021/nn503779d

Pitsillides CM, Joe EK, Wei X, Anderson RR, Lin CP (2003) Selective cell targeting with light-absorbing microparticles and nanoparticles. Biophys J 84(6):4023–4032. https://doi.org/10.1016/S0006-3495(03)75128-5

Poon CY, Chan HM, Li HW (2014) Direct detection of prostate specific antigen by darkfield microscopy using single immunotargeting silver nanoparticle. Sensors Actuators B Chem 190:737–744. https://doi.org/10.1016/j.snb.2013.09.057

Premkumar T, Lee Y, Geckeler KE (2010) Macrocycles as a tool: a facile and one pot synthesis of silver nanoparticles using cucurbituril designed for cancer therapeutics. Chem Eur J 16(38):11563–11566. https://doi.org/10.1002/chem.201001325

Rengan AK, Bukhari AB, Pradhan A, Malhotra R, Banerjee R, Srivastava R, De A (2015) In vivo analysis of biodegradable liposome gold nanoparticles as efficient agents for photothermal therapy of cancer. Nano Lett 15(2):842–848. https://doi.org/10.1021/nl5045378

Renugadevi K, Inbakandan D, Bavanilatha M, Poornima V (2012) Cissus quadrangularis assisted biosynthesis of silver nanoparticles with antimicrobial and anticancer potentials. Int J Pharm Bio Sci 3(3):437–445

Riley RS, Day ES (2017) Gold nanoparticle-mediated photothermal therapy: applications and opportunities for multimodal cancer treatment. Wiley Interdiscipl Rev Nanomed Nanobiotechnol 9(4):e1449. https://doi.org/10.1002/wnan.1449

Roy R, Singh SK, Chauhan LKS, Das M, Tripathi A, Dwivedi PD (2014) Zinc oxide nanoparticles induce apoptosis by enhancement of autophagy via PI3K/Akt/mTOR inhibition. Toxicol Lett 227(1):29–40. https://doi.org/10.1016/j.toxlet.2014.02.024

Sanpui P, Chattopadhyay A, Ghosh SS (2011) Induction of apoptosis in cancer cells at low silver nanoparticle concentrations using chitosan nanocarrier. ACS Appl Mater Interfaces 3(2):218–228. https://doi.org/10.1021/am100840c

Satapathy SR, Mohapatra P, Preet R, Das D, Sarkar B, Choudhuri T, Wyatt MD, Kundu CN (2013) Silver-based nanoparticles induce apoptosis in human colon cancer cells mediated through p53. Nanomedicine 8(8):1307–1322. https://doi.org/10.2217/nnm.12.176

Shao J, Xuan M, Dai L, Si T, Li J, He Q (2015) Near-infrared-activated nanocalorifiers in microcapsules: vapor bubble generation for in vivo enhanced cancer therapy. Angew Chem Int Ed 54(43):12782–12787. https://doi.org/10.1002/anie.201506115

Shi H, Ye X, He X, Wang K, Cui W, He D, Li D, Jia X (2014) Au@ Ag/Au nanoparticles assembled with activatable aptamer probes as smart "nano-doctors" for image-guided cancer thermotherapy. Nanoscale 6(15):8754–8761. https://doi.org/10.1039/C4NR01927J

Shi S, Wen X, Li T, Wen X, Cao Q, Liu X, Liu Y, Pagel MD, Li C (2019) Thermosensitive biodegradable copper sulphide nanoparticles for real-time multispectral optoacoustic tomography. ACS Appl BioMater. https://doi.org/10.1021/acsabm.9b00133

Singh P, Pandit S, Mokkapati VRSS, Garg A, Ravikumar V, Mijakovic I (2018) Gold nanoparticles in diagnostics and therapeutics for human cancer. Int J Mol Sci 19(7):1979. https://doi.org/10.3390/ijms19071979

Sivakumar P, Lee M, Kim YS, Shim MS (2018) Photo-triggered antibacterial and anticancer activities of zinc oxide nanoparticles. J Mater Chem B 6(30):4852–4871. https://doi.org/10.1039/C8TB00948A

Song J, Yang X, Jacobson O, Huang P, Sun X, Lin L, Yan X, Niu G, Ma Q, Chen X (2015) Ultrasmall gold nanorod vesicles with enhanced tumor accumulation and fast excretion from the body for cancer therapy. Adv Mater 27(33):4910–4917. https://doi.org/10.1002/adma.201502486

Srivatsan A, Jenkins SV, Jeon M, Wu Z, Kim C, Chen J, Pandey RK (2014) Gold nanocage-photosensitizer conjugates for dual-modal image-guided enhanced photodynamic therapy. Theranostics 4(2):163. https://doi.org/10.7150/thno.7064

Sun C, Fang C, Stephen Z, Veiseh O, Hansen S, Lee D, Ellenbogen RG, Olson J, Zhang M (2008) Tumor-targeted drug delivery and MRI contrast enhancement by chlorotoxin-conjugated iron oxide nanoparticles. Nanomedicine (London) 3(4):495–505. https://doi.org/10.2217/17435889.3.4.495

Sun IC, Eun DK, Koo H, Ko CY, Kim HS, Yi DK, Choi K, Kwon IC, Kim K, Ahn CH (2011) Tumor-targeting gold particles for dual computed tomography/optical cancer imaging. Angew Chem Int Ed 50(40):9348–9351. https://doi.org/10.1002/anie.201102892

Sun X, Huang X, Yan X, Wang Y, Guo J, Jacobson O, Liu D, Szajek LP, Zhu W, Niu G, Kiesewetter DO (2014) Chelator-free 64Cu-integrated gold nanomaterials for positron emission tomography imaging guided photothermal cancer therapy. ACS Nano 8(8):8438–8446. https://doi.org/10.1021/nn502950t

Swanner J, Mims J, Carroll DL, Akman SA, Furdui CM, Torti SV, Singh RN (2015) Differential cytotoxic and radiosensitizing effects of silver nanoparticles on triple-negative breast cancer and non-triple-negative breast cells. Int J Nanomedicine 10:3937. https://doi.org/10.2147/IJN.S80349

Tai SP, Wu Y, Shieh DB, Chen LJ, Lin KJ, Yu CH, Chu SW, Chang CH, Shi XY, Wen YC, Lin KH (2007) Molecular imaging of cancer cells using plasmon-resonant-enhanced third-harmonic-generation in silver nanoparticles. Adv Mater 19(24):4520–4523. https://doi.org/10.1002/adma.200602213

Tartaj P, del Puerto Morales M, Veintemillas-Verdaguer S, González-Carreño T, Serna CJ (2003) The preparation of magnetic nanoparticles for applications in biomedicine. J Phys D Appl Phys 36(13):R182. https://doi.org/10.1088/0022-3727/36/13/202

Tian Q, Tang M, Sun Y, Zou R, Chen Z, Zhu M, Yang S, Wang J, Wang J, Hu J (2011) Hydrophilic flower-like CuS superstructures as an efficient 980 nm laser-driven photothermal agent for ablation of cancer cells. Adv Mater 23(31):3542–3547. https://doi.org/10.1002/adma.201101295

Tian M, Lu W, Zhang R, Xiong C, Ensor J, Nazario J, Jackson J, Shaw C, Dixon KA, Miller J, Wright K (2013) Tumor uptake of hollow gold nanospheres after intravenous and intra-arterial injection: PET/CT study in a rabbit VX2 liver cancer model. Mol Imaging Biol 15(5):614–624. https://doi.org/10.1007/s11307-013-0635-x

Vankayala R, Huang YK, Kalluru P, Chiang CS, Hwang KC (2014) First demonstration of gold nanorods-mediated photodynamic therapeutic destruction of tumors via near infra-red light activation. Small 10(8):1612–1622. https://doi.org/10.1002/smll.201302719

Von Maltzahn G, Park JH, Agrawal A, Bandaru NK, Das SK, Sailor MJ, Bhatia SN (2009) Computationally guided photothermal tumor therapy using long-circulating gold nanorod antennas. Cancer Res 69(9):3892–3900. https://doi.org/10.1158/0008-5472.CAN-08-4242

Wang Y, Liu Y, Luehmann H, Xia X, Brown P, Jarreau C, Welch M, Xia Y (2012) Evaluating the pharmacokinetics and in vivo cancer targeting capability of Au nanocages by positron emission tomography imaging. ACS Nano 6(7):5880–5888. https://doi.org/10.1021/nn300464r

Wang B, Wang JH, Liu Q, Huang H, Chen M, Li K, Li C, Yu XF, Chu PK (2014a) Rose-bengal-conjugated gold nanorods for in vivo photodynamic and photothermal oral cancer therapies. Biomaterials 35(6):1954–1966. https://doi.org/10.1016/j.biomaterials.2013.11.066

Wang Z, Chen Z, Liu Z, Shi P, Dong K, Ju E, Ren J, Qu X (2014b) A multi-stimuli responsive gold nanocage–hyaluronic platform for targeted photothermal and chemotherapy. Biomaterials 35(36):9678–9688. https://doi.org/10.1016/j.biomaterials.2014.08.013

Wang S, Riedinger A, Li H, Fu C, Liu H, Li L, Liu T, Tan L, Barthel MJ, Pugliese G, De Donato F (2015a) Plasmonic copper sulphide nanocrystals exhibiting near-infrared photothermal and photodynamic therapeutic effects. ACS Nano 9(2):1788–1800. https://doi.org/10.1021/nn506687t

Wang Z, Sun J, Qiu Y, Li W, Guo X, Li Q, Zhang H, Zhou J, Du Y, Yuan H, Hu F (2015b) Specific photothermal therapy to the tumors with high EphB4 receptor expression. Biomaterials 68:32–41. https://doi.org/10.1016/j.biomaterials.2015.07.058

Wang L, Yuan Y, Lin S, Huang J, Dai J, Jiang Q, Cheng D, Shuai X (2016a) Photothermo-chemotherapy of cancer employing drug leakage-free gold nanoshells. Biomaterials 78:40–49. https://doi.org/10.1016/j.biomaterials.2015.11.024

Wang S, Tian Y, Tian W, Sun J, Zhao S, Liu Y, Wang C, Tang Y, Ma X, Teng Z, Lu G (2016b) Selectively sensitizing malignant cells to photothermal therapy using a CD44-targeting heat shock protein 72 depletion nanosystem. ACS Nano 10(9):8578–8590. https://doi.org/10.1021/acsnano.6b03874

Wang X, Wang H, Wang Y, Yu X, Zhang S, Zhang Q, Cheng Y (2016c) A facile strategy to prepare dendrimer-stabilized gold nanorods with sub-10-nm size for efficient photothermal cancer therapy. Sci Rep 6:22764. https://doi.org/10.1038/srep22764

Wang Z, Huang P, Jacobson O, Wang Z, Liu Y, Lin L, Lin J, Lu N, Zhang H, Tian R, Niu G (2016d) Biomineralization-inspired synthesis of copper sulphide–ferritin nanocages as cancer theranostics. ACS Nano 10(3):3453–3460. https://doi.org/10.1021/acsnano.5b07521

Watanabe T, Kimijima I, Ohtake T, Tsuchiya A, Shishido F, Takenoshita S (2001) Sentinel node biopsy with technetium-99m colloidal rhenium sulphide in patients with breast cancer. Br J Surg 88:704–707. https://doi.org/10.1046/j.1365-2168.2001.01767.x

Weissleder RA, Stark DD, Engelstad BL, Bacon BR, Compton CC, White DL, Jacobs P, Lewis J (1989) Superparamagnetic iron oxide: pharmacokinetics and toxicity. Am J Roentgenol 152(1):167–173. https://doi.org/10.2214/ajr.152.1.167

Xie H, Wang ZJ, Bao A, Goins B, Phillips WT (2010) In vivo PET imaging and biodistribution of radiolabeled gold nanoshells in rats with tumor xenografts. Int J Pharm 395(1–2):324–330. https://doi.org/10.1016/j.ijpharm.2010.06.005

Xiong Y, Sun F, Zhang Y, Yang Z, Liu P, Zou Y, Yu Y, Tong F, Yi C, Yang S, Xu Z (2019) Polydopamine-mediated bio-inspired synthesis of copper sulphide nanoparticles for T1-weighted magnetic resonance imaging guided photothermal cancer therapy. Colloids Surf B: Biointerfaces 173:607–615. https://doi.org/10.1016/j.colsurfb.2018.10.023

Xuan M, Shao J, Dai L, Li J, He Q (2016) Macrophage cell membrane camouflaged Au nanoshells for in vivo prolonged circulation life and enhanced cancer photothermal therapy. ACS Appl Mater Interfaces 8(15):9610–9618. https://doi.org/10.1021/acsami.6b00853

Yang J, Wang Z, Zong S, Song C, Zhang R, Cui Y (2012) Distinguishing breast cancer cells using surface-enhanced Raman scattering. Anal Bioanal Chem 402(3):1093–1100. https://doi.org/10.1007/s00216-011-5577-z

Yang HW, Liu HL, Li ML, Hsi IW, Fan CT, Huang CY, Lu YJ, Hua MY, Chou HY, Liaw JW, Ma CCM (2013) Magnetic gold-nanorod/PNIPAAmMA nanoparticles for dual magnetic resonance and photoacoustic imaging and targeted photothermal therapy. Biomaterials 34(22):5651–5660. https://doi.org/10.1016/j.biomaterials.2013.03.085

Ye S, Kang N, Chen M, Wang C, Wang T, Wang Y, Liu Y, Li D, Ren L (2015) Tat/HA2 peptides conjugated AuNR@ pNIPAAm as a photosensitizer carrier for near infrared triggered photo-dynamic therapy. Mol Pharm 12(7):2444–2458. https://doi.org/10.1021/acs.molpharmaceut.5b00161

Zhang Y, Qian J, Wang D, Wang Y, He S (2013) Multifunctional gold nanorods with ultrahigh stability and tunability for in vivo fluorescence imaging, SERS detection, and photodynamic therapy. Angew Chem Int Ed 52(4):1148–1151. https://doi.org/10.1002/anie.201207909

Zhang P, Yang XX, Wang Y, Zhao NW, Huang CZ (2014a) Rapid synthesis of highly luminescent and stable Au 20 nanoclusters for active tumor-targeted imaging in vitro and in vivo. Nanoscale 6(4):2261–2269. https://doi.org/10.1039/C3NR05269A

Zhang Z, Wang J, Nie X, Wen T, Ji Y, Wu X, Zhao Y, Chen C (2014b) Near infrared laser-induced targeted cancer therapy using thermoresponsive polymer encapsulated gold nanorods. J Am Chem Soc 136(20):7317–7326. https://doi.org/10.1021/ja412735p

Zhang J, Li C, Zhang X, Huo S, Jin S, An FF, Wang X, Xue X, Okeke CI, Duan G, Guo F (2015a) In vivo tumor-targeted dual-modal fluorescence/CT imaging using a nanoprobe co-loaded with an aggregation-induced emission dye and gold nanoparticles. Biomaterials 42:103–111. https://doi.org/10.1016/j.biomaterials.2014.11.053

Zhang Z, Liu C, Bai J, Wu C, Xiao Y, Li Y, Zheng J, Yang R, Tan W (2015b) Silver nanoparticle gated, mesoporous silica coated gold nanorods (AuNR@ MS@ AgNanoparticles): low prema-ture release and multifunctional cancer theranostic platform. ACS Appl Mater Interfaces 7 (11):6211–6219. https://doi.org/10.1021/acsami.5b00368

Zhao Q, Duan R, Yuan J, Quan Y, Yang H, Xi M (2014a) A reusable localized surface plasmon resonance biosensor for quantitative detection of serum squamous cell carcinoma antigen in cervical cancer patients based on silver nanoparticles array. Int J Nanomedicine 9:1097. https://doi.org/10.2147/IJN.S58499

Zhao Y, Sultan D, Detering L, Luehmann H, Liu Y (2014b) Facile synthesis, pharmacokinetic and systemic clearance evaluation, and positron emission tomography cancer imaging of 64 Cu–Au alloy nanoclusters. Nanoscale 6(22):13501–13509. https://doi.org/10.1039/C4NR04569F

Zhao Y, Pang B, Luehmann H, Detering L, Yang X, Sultan D, Harpstrite S, Sharma V, Cutler CS, Xia Y, Liu Y (2016) Gold nanoparticles doped with 199Au atoms and their use for targeted cancer imaging by SPECT. Adv Healthc Mater 5(8):928–935. https://doi.org/10.1002/adhm.201500992

Zharov VP, Galitovskaya EN, Johnson C, Kelly T (2005) Synergistic enhancement of selective nanophotothermolysis with gold nanoclusters: potential for cancer therapy. Lasers Surg Med Off J Am Soc Laser Med Surg 37(3):219–226. https://doi.org/10.1002/lsm.20223

Zhou J, Wang Z, Li Q, Liu F, Du Y, Yuan H, Hu F, Wei Y, You J (2015) Hybridized doxorubicin-Au nanospheres exhibit enhanced near-infrared surface plasmon absorption for photothermal therapy applications. Nanoscale 7(13):5869–5883. https://doi.org/10.1039/C4NR07279K

Zhou B, Yang J, Peng C, Zhu J, Tang Y, Zhu X, Shen M, Zhang G, Shi X (2016) PEGylated polyethylenimine-entrapped gold nanoparticles modified with folic acid for targeted tumor CT imaging. Colloids Surf B: Biointerfaces 140:489–496. https://doi.org/10.1016/j.colsurfb.2016.01.019

Zhou B, Zhao J, Qiao Y, Wei Q, He J, Li W, Zhong D, Ma F, Li Y, Zhou M (2018) Simultaneous multimodal imaging and photothermal therapy via renal-clearable manganese-doped copper sulphide nanodots. Appl Mater Today 13:285–297. https://doi.org/10.1016/j.apmt.2018.09.011

Chapter 7
Nanomaterials-Based Electrochemical Sensors and Biosensors for Early Identification and Monitoring of Diseases

Pramod K. Kalambate and Yunhui Huang

Contents

Abstract Early detection of disease is important to avoid future risk and increase survival time. The conventional detection methods seriously suffered from various factors such as multistep sample treatment, sophisticated instrumentation, accuracy and sensitivity, and long analysis time. To address these issues, several attempts have been made in recent times. This chapter discusses the recent advancement in electrochemical (bio) sensors for the quantification of disease biomarkers and drug molecules. These sensing devices are highly sensitive and selective and can be used even in picomolar to nanomolar detection range. Additionally, the electrochemical response is unaffected by possible interferents in biological matrices. In this chapter, the detection of several drug molecules and biomarkers has been discussed by several electrochemical methods, including voltammetric, impedimetric, and potentiometric. Furthermore, limitations, present challenges, and future scope in this area are highlighted in the end.

P. K. Kalambate · Y. Huang (✉)
State Key Laboratory of Materials Processing and Die & Mould Technology, School of Materials Science and Engineering, Huazhong University of Science and Technology, Wuhan, Hubei, P. R. China
e-mail: pramod@hust.edu.cn; huangyh@hust.edu.cn

Keywords Biosensors · Electrochemical sensors · Biomarkers · Drug analysis · Nanomaterials

Abbreviations

AgNPs	Silver nanoparticles
AuNPs	Gold nanoparticles
AuSPE	Gold screen-printed electrode
CV	Cyclic voltammetry
DPV	Differential pulse voltammetry
EIS	Electrochemical impedance spectroscopy
GCE	Glassy carbon electrode
GO	Graphene oxide
GOx	Glucose oxidase
LOD	Limit of detection
MIP	Molecularly imprinted polymers
PBS	Phosphate-buffered saline
PdNPs	Palladium nanoparticles
PGE	Pencil graphite electrode
PSA	Prostate-specific antigen
PtNPs	Platinum nanoparticles
rGO	Reduced graphene oxide
SDS	Sodium dodecyl sulfate
SPE	Screen-printed electrode
XPS	X-ray photoelectron spectroscopy
SEM	Scanning electron spectroscopy
AFM	Atomic force microscopy
TEM	Transmission electron spectroscopy
RSD	Relative standard deviation

7.1 Introduction

Early identification of disease is an essential step in the clinical field to increase the possibility of successful treatment and prolong survival time. There are a variety of techniques available to detect or identify a particular disease. For instance, imaging (magnetic resonance imaging, computed tomography (CT), etc.), ultrasound, and tissue sampling have been frequently used for cancer detection. Apart from this, conventional detection methods such as chromatography, spectroscopy, and immunoassay have been utilized immensely for detection purpose. However, most of these techniques are quite complex and required extensive sample pretreatment steps and expensive setup. With the rapidly increasing health concerns in society, the development of sensitive, accurate, and reliable diagnostic tools is of utmost

important. An electrochemical sensor is a subdivision of a chemical sensor that operates by reaction (oxidation and reduction) with a target analyte and produces an electrochemical signal proportional to the concentration (Wang et al. 2018). However, for disease diagnosis, the concentration of biomarkers present in body fluids is very low; therefore, conventional electrochemical sensors are not suitable for such precise measurements.

Recent advancements in nanoscience and nanotechnology have made it possible to conquer the downsides of conventional electrochemical sensors leading to stable devices exhibiting low detection limits and high sensitivity and selectivity (Zhu et al. 2015; Wongkaew et al. 2019). In the past, nanomaterials-based electrochemical sensors as diagnostic tools were employed for the quantification of biomarkers, drugs, environmental monitoring, and other important biomedical applications (Chen and Chatterjee 2013; Kalambate et al. 2017, 2019a; Dhanjai et al. 2019). For instance, Wei et al. (2018) developed an aptasensor for PSA that can be used for the identification of prostate cancer employing gold nanoparticles (AuNPs) and reduced graphene oxide (rGO) nanocomposite. The sensor could detect PSA in serum samples with the lowest limit of detection (LOD) 10 pg mL^{-1} in the linearity range from 0.05 to 200 ng mL^{-1}. On the other hand, such electrochemical sensors have potential applications in monitoring disease by regularly analyzing the concentration of particular drugs in body fluids, which can help to optimize the treatment. Because of the advancements in materials science, the variety of nanomaterials can be synthesized precisely with controllable size, shape, and composition. These sensors possess numerous advantages, viz., simple operation, facile to fabricate at low cost, and portability, and require a small sample volume. To date, numerous materials have been investigated for the construction of sensitive platforms including carbonaceous materials (graphene, carbon nanotubes, etc.), metal organic frameworks (MOFs), metal nanoparticles (AuNPs, AgNPs, PdNPs, etc.), synthetic molecularly imprinted polymers (MIPs), and different metal oxides (ZnO, MnO$_2$, etc.) (Zhu et al. 2015; Wongkaew et al. 2019). These nanomaterials with high active surface area and superior catalytic activities promote the fast electron transfer between the analyte and the electrode that causes amplification of the electrochemical signal.

This chapter discusses the recent advancements in the field of advanced functional nanomaterials-based electrochemical (bio)sensor systems for the analysis of various disease biomarkers and the analysis of various drug molecules for monitoring of disease. The unique synthetic strategies, properties of the nanomaterials, constructions of the sensing platform, and future perspectives for the design of high-performance sensing platforms have been discussed. Several electrochemical techniques, including amperometric, impedimetric, and potentiometric, have been discussed for the detection of important species.

7.2 Basic Concept of Electrochemical Sensors

The electrochemical sensor consists of a receptor or bioreceptor as a sensing element and a transducer to transform receptor signal to the measurable signal based on electrical, optical, and mass techniques (Fig. 7.1). Additionally, the signal processor is also essential to amplify the signal. The bioreceptor and analyte are linked together, which causes specific interaction to produce a signal proportional to the concentration of the analyte (Sharifi et al. 2019). In electrochemical sensors, an electric current generated by the electrochemical reaction taking place on the sensing electrode is measured. Several bioreceptors such as DNA, RNA, enzymes, and antibodies with high affinities and specificities for target analytes have been explored (Fracchiolla et al. 2013; Xie et al. 2017). A typical electrochemical sensor is composed of three-electrode setup, such as a working electrode (WE) or indicator electrode, a reference electrode (RE), and the counter electrode (CE). Each electrode has a specific role to play in the sensing device. For example, the electrochemical reaction (oxidation or reduction) always occurs on the WE. These reactions are catalyzed by the specific electrode materials designed for the target analyte. The potential of the working electrode is not constant due to continuous electrochemical reactions taking place on its surface that cause a decrease in performance. Hence, the RE is incorporated in close proximity to the working electrode to apply fix potential to the working electrode. After the electrochemical reaction, the current flowing between the WE and the CE is reported, and it is proportional to the concentration of the target analyte. Another important component of the sensor is an electrolyte, which eases the cell reaction and carries the ionic charge across the electrodes.
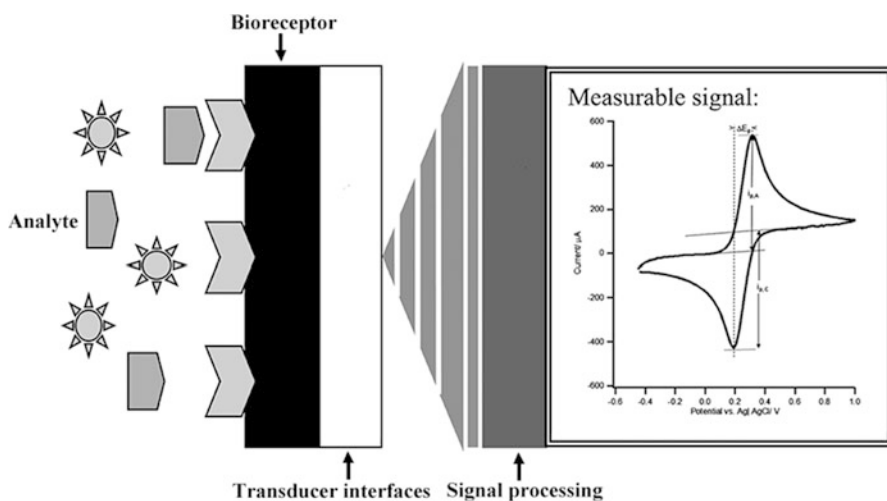
Fig. 7.1 Schematic illustration of the working of the electrochemical (bio) sensor (Sharifi et al. 2019)

Additionally, it must be compatible with the materials used in the sensors and should not evaporate too quickly.

A critical challenge in the development of these sensors is to identify an appropriate electrode modifier that can improve the detection limit and enhance the signal-to-noise ratio. Other challenges in this field are homogeneity issues, complex matrices, and multicomponent analysis. The modification of the working electrode with a suitable modifier is the first step in the electrochemical sensing. Several conductive electrodes such as GCE, SPE, noble metal electrodes (Au, Pt), boron-doped diamond electrodes, and PGE are used as bare conductive substrates. The modification of the electrodes is performed by a specific approach based on the nature of the material to be deposited, such as electrochemical polymerization, covalent bond formation, electrochemical deposition, self-assembled layers, etc. Carbon nanostructures are frequently employed in electrochemical sensing due to their cheapness, natural abundance, high chemical stability, high surface area, great mechanical strength, and resistance to fouling. Furthermore, sensing platforms prepared from them exhibit low background current, wide potential window, and renewability and easily integrate with other materials (Kalambate et al. 2019b; Dhanjai et al. 2018). Noble metal NPs have contributed immensely to the development of these sensors due to their high catalytic activities, high conductivities, high surface area, and ease of synthesis and surface functionalization (Prakash et al. 2013; Guo and Wang 2011).

Electrochemical sensors are classified based on the nature of the receptor, i.e., bioreceptor or non-bioreceptor type. In many cases, bioreceptors are chosen over non-bioreceptor type because of the strong affinity and specific interaction to analyte leading to an accurate determination. Now, based on bioreceptor, they are classified into three categories, such as aptasensor (DNA/RNA), immunosensor (antibodies), and enzyme-based electrochemical sensors. A popular glucose biosensor containing enzyme glucose oxidase was discovered by Clark and Lyons in 1962 (Clark and Lyons 1962). Since then, enormous efforts have gone towards the development of glucose biosensor leading to a commercial device. Bioreceptor-based sensors are a promising candidate for the detection of biomarkers. On the contrary, non-bioreceptor-based sensors are important for the analysis of specific drug molecules. For instance, certain drugs exhibit serious side effects on patients. In such a case, it is possible to optimize the treatment by detecting the concentration of drug in the body fluids by a regular interval of time (Sanghavi et al. 2014). The stability of the non-bioreceptor-type sensor is better than the bioreceptor type.

7.3 Electrochemical Sensors for Detection of Biomarkers

This section describes the application of electrochemical sensors for glucose, hydrogen peroxide, cancer biomarkers, and drug molecule detection. The electrochemical properties of the sensors, such as detection limit, detection range, sensitivity, and storage stability, are discussed.

7.3.1 Glucose Sensors

Glucose is an important human biomarker because a large number of diseases are co-related to the alteration of glucose concentration in the blood. For instance, in diabetes mellitus, hyperglycemia (high blood sugar) is linked to a deficiency of insulin. Additionally, pituitary, pancreatitis, and thyroid dysfunctions, renal failure, and liver disease are also responsible for high blood glucose concentration. On the contrary, hypoglycemia (low blood sugar) may arise due to hypopituitarism, insulinemia, and neoplasms. In recent years, extensive research has been done for the development of glucose sensors using a variety of nanomaterials (Sabu et al. 2019). Both enzymatic and nonenzymatic sensing strategies have been developed for glucose with low LOD, high sensitivity, and selectivity.

Parlak et al. (2017) fabricated MoS_2/AuNPs/GOx electrode for sensitive analysis of glucose. For the construction of the biosensor, AuNPs were self-assembled onto two-dimensional MoS_2 nanosheets, and finally, GOx was assembled on MoS_2/AuNPs hybrid structure. MoS_2/AuNPs hybrid structure was characterized by SEM, AFM, zeta potential, TEM, and contact angle measurements. The working electrode was fabricated by drop casting MoS_2 hybrid composite on a gold electrode. A schematic illustration of the fabrication of glucose sensor is shown in Fig. 7.2 using ferrocene carboxylic acid mediator.

The active surface area of the MoS_2/AuNPs was 0.65 cm^2, which is found to be 1.5 times more than MoS_2 (0.42 cm^2). Furthermore, the electrochemical impedance

Fig. 7.2 Schematic illustration of the preparation of MoS_2/AuNPs/GOx on the gold electrode for the detection of glucose (Parlak et al. 2017)
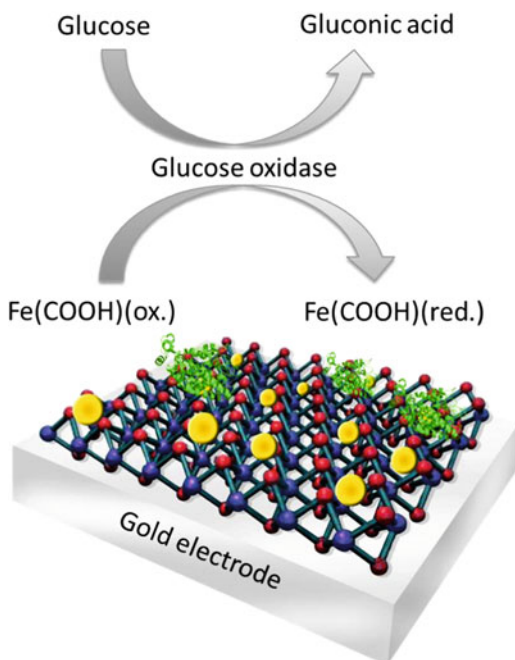
Fig. 7.3 (**a**) Amperometric responses and (**b**) the corresponding calibration curves of glucose on MoS$_2$/GOx and MoS$_2$/Au NPs/GOx electrodes in 0.1 M PBS at +0.35 V vs. Ag/AgCl (Parlak et al. 2017)
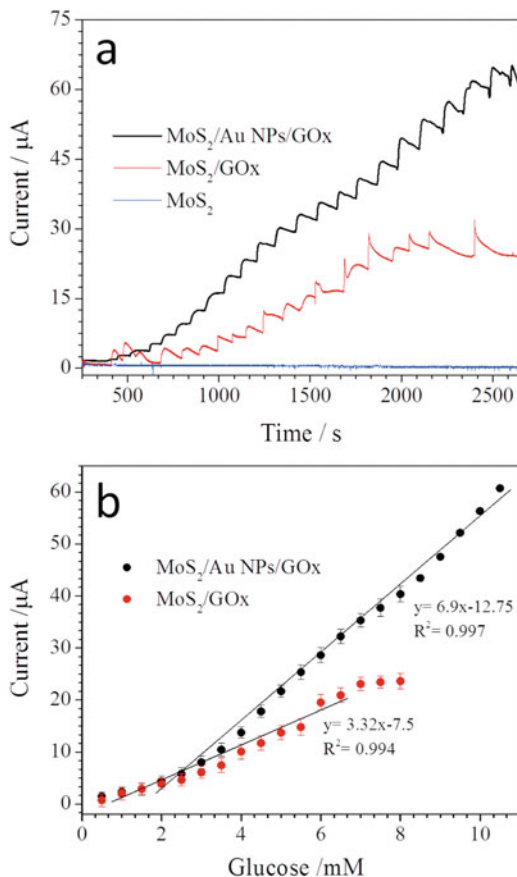
spectroscopy (EIS) study of MoS$_2$, MoS$_2$/AuNPs, and MoS$_2$/AuNPs/GOx showed R$_{ct}$ values of 0.66, 0.46, and 0.89 kΩ, respectively. The high R$_{ct}$ value of MoS$_2$/AuNPs/GOx is due to the insulating nature of biolayers, which caused slight inhibition of electron transfer of the redox couple. The electrocatalytic oxidation of glucose was investigated by employing amperometry at +350 mV (vs. SCE) in 0.1 M PBS (7.4) and 1 mM ferrocene carboxylic acid. The representative amperogram and calibration curve are shown in Fig. 7.3. The MoS$_2$/AuNPs/GOx exhibited LOD of 0.042 μM (S/N = 3) over the linear detection range from 0.25 to 13.2 mM and sensitivity of 13.80 μA/μM/cm^2. The MoS$_2$/AuNPs/GO$_x$ displayed a great catalytic activity for the detection of glucose in broad linearity ranges with high sensitivity. The high catalytic activity of the enzyme electrode is ascribed to several factors such as the larger surface area of MoS$_2$ for immobilization of enzyme, synergistic effect of MoS$_2$/AuNPs, biocompatibility of MoS$_2$, and fast mass transport.

Enzyme-based sensors possess excellent selectivity; however, it has some downsides, like the possibility of enzyme inactivation, high cost, and reproducibility of
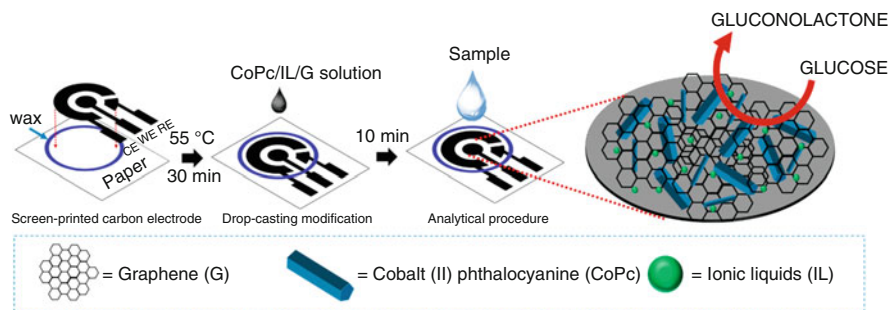
Fig. 7.4 Schematic showing the construction and working of the glucose sensor (Chaiyo et al. 2018)

enzyme immobilization. Hence, recent trends are to develop nonenzymatic sensing platforms. For instance, a nonenzymatic detection of glucose was performed on paper-based sensor utilizing a cobalt phthalocyanine, graphene, and ionic liquid composite (Chaiyo et al. 2018). The disposable device was prepared by modifying an SPE with CoPc/G/IL. The fabrication process of the CoPc/G/IL/SPCE is shown in Fig. 7.4. The surface and structural characterization of the composite was done by SEM, TEM, EDX, and UV–Vis spectroscopy. This disposable device shows excellent conductivity and catalytic activity for oxidation of glucose in 0.1 M NaOH. The performance of the sensor was studied by CV and EIS; however, quantitative detection was performed by chronoamperometry. The sensing platform displayed a linear response towards oxidation of glucose in the two detection ranges from 0.01 to 1.3 mM and from 1.3 to 5.0 mM with an LOD of 0.67 μM (S/N = 3). The sensor could detect glucose in honey, human serum, and white wine samples with acceptable recoveries from 95.2 to 104.9% and RSDs from 2.6 to 5.2%. Additionally, the obtained results are comparable to the commercial glucometer, confirming the potential application of this paper-based sensor for point-of-care analysis of glucose. Such low-cost, disposable, and sample-saving devices can be used for the analysis of a large number of samples with reliable results.

7.3.2 Cancer Biomarkers

Cancer is the life-threatening disease caused by abnormal cells that grow beyond their boundaries, which then invade and spread to different parts of the body. As reported by the WHO, there were about nine million deaths occurred in 2009 due to different cancers, and the rate is increasing sharply (Forouzanfar et al. 2016). To find a suitable method for the early identification of cancer is a major challenge faced by science and industries. Due to its widespread occurrence and mortality rate, intense research has been carried out for early identification as well as monitoring over the past decade. Electrochemical biosensors, as a sensitive tool, find a promising
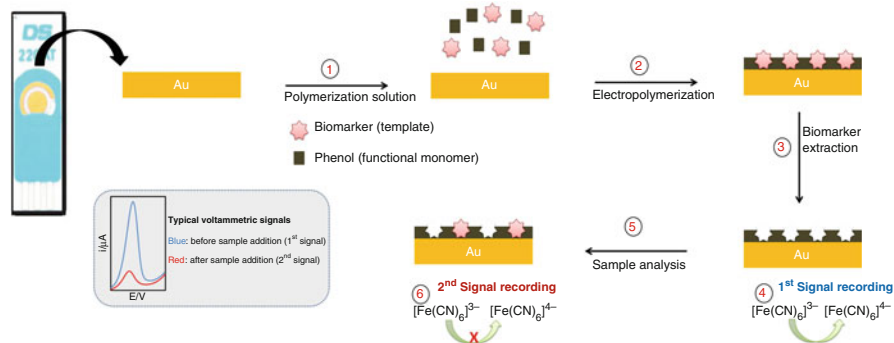
Fig. 7.5 Schematic representation showing the fabrication and working principle of the MIP/AuSPE sensor (Pacheco et al. 2018)

application in the detection of several cancer biomarkers. Hence, nanomaterials-based sensors have been constructed for numerous cancer biomarkers, including breast cancer, lung cancer, prostate cancer, etc. (Sharifi et al. 2019).

A sensitive sensor was constructed for breast cancer biomarker (HER2-ECD) utilizing MIP (Pacheco et al. 2018). Its detection in peripheral blood could provide an important contribution to diagnosis and patient follow-ups. The detection of HER2-ECD in serum is performed by ELISA, and the approved cut-off concentration is 15 ng/mL. Additionally, ELISA tests are not highly sensitive in prognosis detection. Therefore, the fabrication of low-cost, sensitive, and selective method is highly recommended to conquer the flaws of ELISA. In this study, the sensor was prepared by CV through electro-polymerization in a solution of phenol and HER2-ECD on AuSPE. The HER2-ECD was analyzed in $[Fe(CN_6)]^{3-4-}$ by DPV. The fabrication and working principle of the sensor are shown in Fig. 7.5. The MIP–AuSPE showed a linear response towards HER2-ECD in the range of 10–70 ng/mL with LOD and LOQ of 1.6 ng/mL and 5.2 ng/mL, respectively. The LOD of the sensor is below cut-off value in clinical practice (15 ng/mL), showing the suitability of the sensor. The sensor is very selective towards HER2-ECD in the presence of the other two biomarkers, including CA 15-3 and cystatin C. Additionally, the recoveries obtained in serum samples were between 80% and 90% with RSD less than 10.2%. The developed methodology provides a disposable, low-cost, and selective sensor for early identification of breast cancer. MIP-based sensors are extremely selective and can be employed effectively, even in the presence of components of similar properties without any interference.

In another example, Heydari-Bafrooei and co-workers developed ultrasensitive aptasensor for a PSA by employing densely packed AuNPs on rGO–MWCNT surface (Heydari-Bafrooei and Shamszadeh 2017). The synthesis process consists of the preparation of GO by a modified Hummers method and then mixing it with MWCNT. Then, the dispersion was drop casted on GCE followed by reduction of GO to rGO at −0.9 V (vs. Ag/AgCl) for 1000 s in PBS (0.1 M, pH 4.2). AuNPs were uniformly deposited on the rGO–MWCNT surface at −0.2 V in the electrochemical

cell containing 1.0 mM HAuCl$_4$ in 0.1 M KNO$_3$ for 180 s. Finally, the electrode was immersed in 0.1 M PBS containing DNA aptamer (200 nM) (5′-HS-(CH2)6-TTT TTA ATT AAA GCT CGC CAT CAA ATA GCT TT-3′) to get aptamer-modified sensor. The detection was based on the variation of the electron transfer resistance (R$_{ct}$), and DPV current was relevant to the formation of aptamer–PSA complex. The sensor could detect PSA with a low detection limit of 1.0 pg mL^{-1} in the linearity range from 0.005 to 20 ng mL^{-1} and from 0.005 to100 ng mL^{-1} for DPV and EIS, respectively. For real sample analysis, serum samples were tested, and outcomes were compared with the standard immunoradiometric assay. The performance shows that the developed sensor could be a favorable tool for the analysis of PSA in clinical samples.

DNA biosensor has been designed by Chen and co-workers utilizing 3D graphene–AgNPs for ultrasensitive determination of CYFRA21-1 in non-small lung cancer (Chen et al. 2018). In this study, the probe as DNA was immobilized on 3D graphene–AgNPs through the strong Ag–S bond. The peak currents showed linear relation with the logarithmic concentration of CYFRA21-1 in the range from 10 fM to 0.1 μM, and the sensor could detect CYFRA21-1 down to 10 fM. Furthermore, analysis of real lung cancer samples showed promising results. This biosensor has several advantages over conventional DNA detection technologies in terms of short assay time, low-cost, fast response, and high sensitivity and can be adopted for routine analysis. Thus, the sensor could serve as a reliable tool for the early identification of non-small lung cancer. Similarly, several electrochemical (bio) sensors were developed for a variety of cancer biomarkers in recent times based on nanostructured material incorporating biological material (Sharifi et al. 2019).

7.3.3   H$_2$O$_2$ Sensors

Hydrogen peroxide (H$_2$O$_2$) is an essential compound extensively used in pharmaceutical, environmental, clinical, chemical industries, and food manufacturing, due to its outstanding oxidizing and reducing properties (Chen et al. 2012). In living organisms, it is a side product of a biochemical reaction involving different oxidases. H$_2$O$_2$ acts as a signaling molecule in regulating various biological transduction processes, viz., immune cell activation, stomatal closure, vascular remodeling, root growth, and apoptosis (Giorgio et al. 2007). Additionally, it acts as an oxidative stress marker in aging and disease and the defense agent for the invasion of pathogens (Lippert et al. 2011). H$_2$O$_2$ burst can lead to several disorders such as diabetes, Alzheimer's and Parkinson's diseases, cancer, and neurodegenerative disorders (Miller et al. 2010; Winterbourn 2008). Thus, monitoring concentration of H$_2$O$_2$ is of prime importance in clinical, academic, and industrial purposes. Similar to the glucose sensor, H$_2$O$_2$ sensing has been performed by the enzymatic and nonenzymatic approach. To date, numerous attempts have gone towards the construction of a sensitive platform employing a variety of nanomaterials.
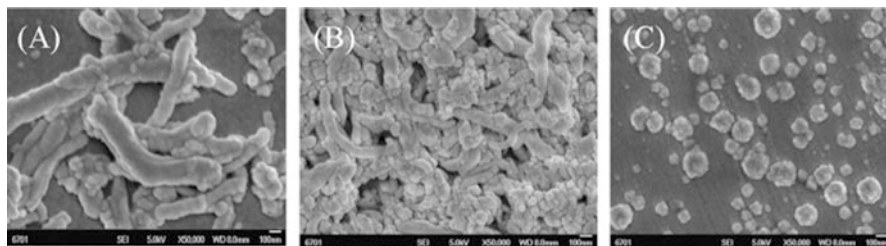
Fig. 7.6 SEM images of (**a**) MWCNTs–SDS/GCE, (**b**) PtNPs/MWCNTs–SDS/GCE, and (**c**) PtNPs/GCE (Li et al. 2014)

Nandini and her co-workers constructed an enzymatic H_2O_2 sensor by co-deposition of palladium and horseradish peroxidase (HRP) on functionalized graphene (Nandini et al. 2013). The electrochemical response of the enzyme electrode was tested by CV and DPV, while conductivity and capacitance were studied by EIS. The effects of pH, temperature dependence, and scan rate on the electrochemical performance were investigated in order to obtain a sensitive response. The sensor exhibited fast amperometric response <2 s, broad linear range 25 μM– 3.5 mM, high sensitivity 92.82 μA mM^{-1} cm^{-2}, and Michaelis–Menten constant (K_M) of 0.11 mM. The remarkable performance of the biosensor is because of high affinity, the bioactivity of HRP towards H_2O_2, and the synergist effect of all components in the electrode system. The developed biosensor exhibits low overpotential for determination of H_2O_2 that minimizes interference from the interfering species and enhanced selectivity.

A nonenzymatic amperometric sensor was developed for H_2O_2 by loading Pt nanoparticles on the surface of MWCNTs (Li et al. 2014). The MWCNTs were modified with anionic surfactant SDS; then, PtNPs were deposited on MWCNTs– SDS surface by electrodeposition. SEM images revealed that a large number of PtNPs were coated on MWCNTs–SDS (Fig. 7.6). Chronoamperometry response of the sensor at different concentrations of H_2O_2 with calibration curves is shown in Fig. 7.7. The results indicated the fabricated sensor displayed excellence catalytic activity towards H_2O_2 with a linear response in the broad range of 5.8 nM–1.1 mM with a limit of detection of 1.9 nM. The superior performance of the sensor is due to MWCNTs–SDS that acts as an effective load matrix for high loading of PtNPs and synergistic amplification effect between PtNPs and MWCNTs. When serum samples are analyzed by the developed sensor, the results are found to be encouraging, suggesting real-time applications. The fabricated sensor showed a linear response in a broad working range, suggesting its potential applications in numerous fields from very low concentration (nM) in biological systems to the high concentration (mM) level in industrial processes.
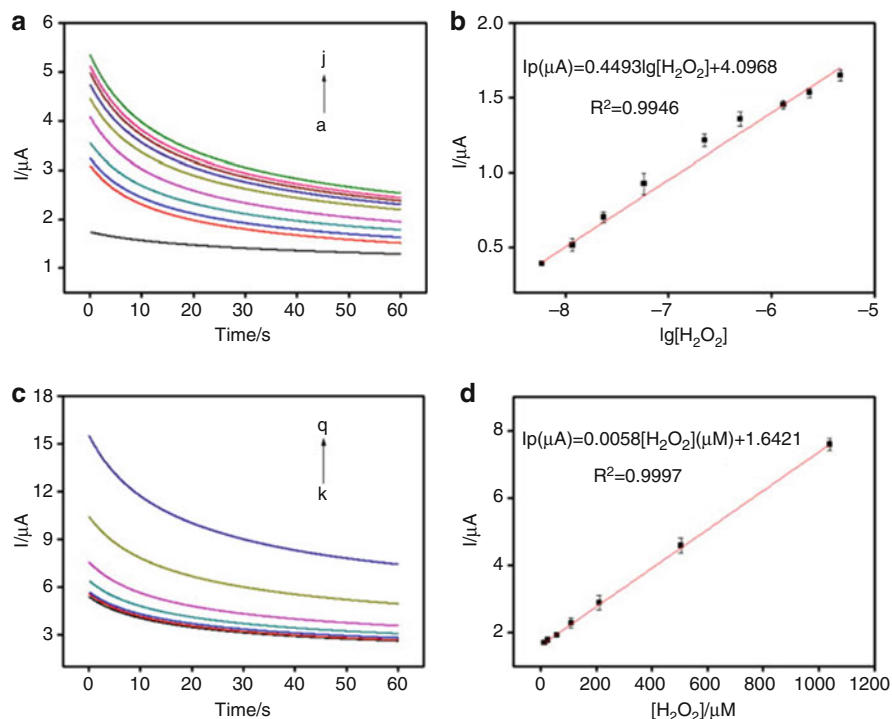
Fig. 7.7 (**a**) The chronoamperometry i–t curve of PtNPs/MWCNTs–SDS/GCE in N_2- saturated 0.2 M PBS (pH 7.0) to different concentrations of H_2O_2 (from a to j: 0, 0.0058, 0.012, 0.023, 0.058, 0.22, 0.51, 1.3, 2.4, 5 μM at −0.1 V). (**b**) The corresponding calibration curve between current and lg[H_2O_2]. (**c**) The i–t curve of the sensor to different concentrations of H_2O_2 (from k to q: 13, 25, 57, 110, 220, 510, 1100 μM). (**d**) The corresponding calibration plot showing the linear electrode response to H_2O_2 addition (Li et al. 2014)

7.4 Analysis of Drug Molecules

Drug testing is an important step for the monitoring of disease treatment. For instance, our group (Kalambate et al. 2019c) has developed a voltammetric method for the simultaneous and individual quantification of doxorubicin and dasatinib using mesoporous Pd@Pt/MWCNT composite electrode. Doxorubicin and dasatinib are used extensively to treat different cancers such as breast cancer, bladder cancer, cervical cancers, prostate cancer, lung cancer, leukemia, etc. However, effective treatment is always restricted by drug resistance and cardiotoxicity. Additionally, it exhibits several side effects, including marrow suppression and gastrointestinal and dermatological disorders. The combination therapy is used to reduce the resistance and undesirable side effects. The Pd@Pt/MWCNT-based composite was prepared by an easy one-pot method in which Pd@Pd core shell nanoparticles were co-reduced simultaneously and deposited on the surface of MWCNT employing

ascorbic acid and F127 as reducing agent and structure-directing agent, respectively. In this structure, MWCNT provides a larger surface area for the deposition of Pd@Pt nanoparticles and prevents aggregation of nanoparticles. The formation of Pd@Pt on the MWCNT surface was confirmed by TEM, HR-TEM, EDX, XPS, and XRD. The BET area of the sensor was 142.87 m^2 g^{-1}. The Pd@Pt/MWCNT composite was drop cast onto GCE, and measurements were performed in 0.1 M PBS of pH 6.0. The electrochemical performance of the sensor was access through CV, DPV, and adsorptive stripping SWV. The effective surface area of the Pd@Pt/MWCNT (0.038 cm^2) was two times more than GCE (0.018 cm^2). Pd@Pt/MWCNT platform exhibits several characteristic features such as high conductivities, a unique mesoporous structure that facilitates mass/electron transfer, and larger surface area, and synergistic effect of all components leads to the sensitive determination. Adsorptive stripping SWV response was linear for simultaneous determination of doxorubicin and dasatinib over the detection ranges from 4.4 to 8580 nm and 38 to 9880 nm with LOD of 0.86 and 6.72 nm, respectively. At the same time, sensor was employed for individual quantification of doxorubicin and dasatinib with LODs of 0.73 and 8.53 nm, respectively. The sensor was utilized for analysis of blood plasma and urine samples with acceptable recoveries in the range from 98.39 to 100.57%, suggesting a potential application of sensor in quality control of pharmaceuticals, optimization of chemotherapeutic treatment, and clinical analysis. The repeatability of the sensor for determinations of these drugs was good with RSD of 2.2% for peak current measurements (n = 6). Additionally, the sensor is unaffected by most of the potential interfering species in a biological matrix, viz., AA, BSA, glucose, sucrose, aspartic acid, sodium chloride, and potassium chloride. The storage stability of the sensor is also satisfying, as it retained 95.5% of the initial response after 30 days.

In another example, Singh and group reported a biomimetic polymer-based sensor for ultratrace sensing of cyanocobalamin (Cbl) on MB-rGO/MWCNTs (Singh et al. 2018). Cbl is an important B-complex vitamin required for the functioning of the brain, red blood cell formation, coenzymatic activity in DNA synthesis, and cell/fatty acid metabolism. Deficiency of Cbl causes several health issues related to hematological and neurological disorders. It is widely used in pharmaceutical products and food supplements. Thus, its detection in real-world samples is highly essential. In this study, MIP was synthesized by mimicking the template in the polymer matrix and creating channels for selective sensing of cyanocobalamin. The typical synthesis process consists of the preparation of MB-rGO/MWCNTs composite followed by vinylation via acryloylurea (AU) through a series of reactions to produce a multifunctional monomer for MIP. The schematic illustration of the synthesis of MB-rGO/MWCNTs/AU-MIP is shown in Fig. 7.8. MB is a water-soluble compound containing sulfo groups that were adsorbed on the surface of the rGO surface through π–π interaction. Thus, this interaction facilitates water dispersion and enhances conductivity. The sensor was developed by spin coating of a mixture solution containing template (Cbl), initiator (APS), co-initiator (N, N, N′, N′ tetramethylethylenediamine), and monomer on a pencil graphite electrode. Next, the Cbl was extracted from the electrode surface by immersing the electrode in methanol–water solution for 30 min in order to get cavities in MIP. Employing
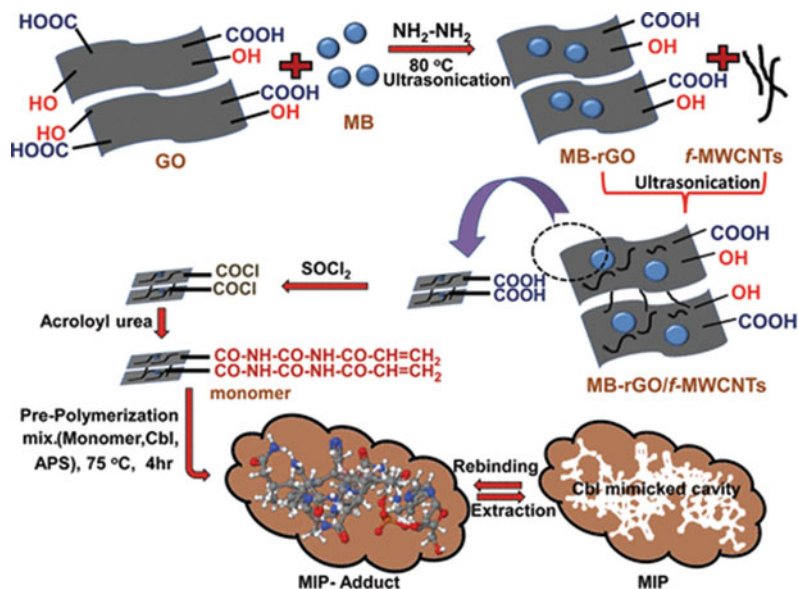
Fig. 7.8 Schematic diagram displaying the synthesis of MB-rGO/f-MWCNTs/AU-MIP composite (Singh et al. 2018)

differential pulse anodic voltammetry, the electrode possessed the linear response to Cbl over the range of 0.021–1.440 ng mL^{-1} with an LOD of 0.0056 ng mL^{-1}. The sensor was tested for the analysis of pharmaceutics, cerebrospinal fluid, blood serum, and urine samples with promising results. The fabricated sensor displayed high selectivity in several real samples without interference from a complicated matrix with an imprinting factor of 34.73.

Recently, a disposable SPE sensor was reported for hemoglobin (Hb) using ferrocenoyl cysteine conjugates (Han et al. 2019). Most organisms need molecular oxygen (O_2) to live, and O_2 binds to Fe (II) in Hb. Malfunctioning level of Hb in human leads to various complications, including heart disease, anemia, leukemia, and thalassemia. Hence, the reliable method for quantification of Hb is of immense interest in the clinical field. In the first step, SPE was modified with AuNPs by potentiostatic deposition. Fc[CO-Cys(Trt)-OMe]$_2$ (denoted as Fc(Cys)$_2$) and Fc [CO-Glu-CysGly-OH] (denoted as Fc-ECG) were then self-assembled on AuNPs by covalent bonds Au–S to obtain two electrodes, Fc(Cys)$_2$/AuNPs/SPE and Fc-ECG/AuNPs/SPE, respectively. The electrochemical performance of the sensing platform was assessed through CV, EIS, and DPV in which Fc–ECG/AuNPs/SPE showed high sensitivity and selectivity for Hb.

Under optimized conditions, the Fc–ECG/AuNPs/SPE showed a linear response to Hb in the broad detection range from 0.1 to 1000 µg/mL and with an LOD of 0.03 µg/mL. Figure 7.9 represents DPV responses at various concentrations of Hb, interference study, repeatability, and reproducibility studies of the developed sensor, which confirmed a reliable selectivity, repeatability, and reproducibility of the
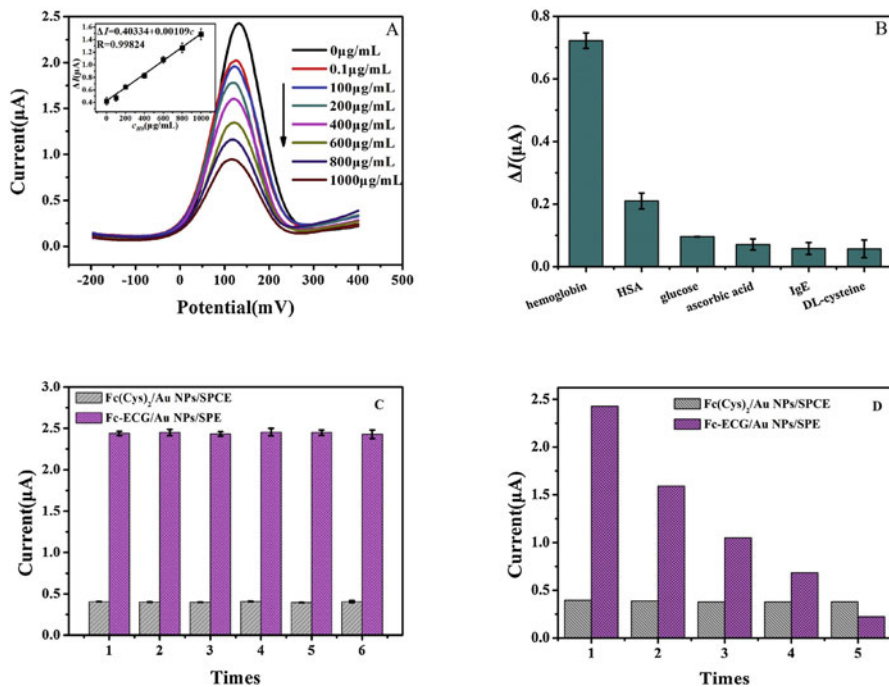
Fig. 7.9 (**a**) DPVs for increasing concentrations of Hb. Inset is the calibration plot obtained for increasing concentrations of Hb. (**b**) Selectivity of Fc-ECG/AuNPs/SPE in the presence of various species (300 μg/mL each). (**c**) Repeatability and (**d**) reproducibility of the sensors (Han et al. 2019)

sensor. The sensor could detect Hb in serum samples in which the contents obtained by the sensor and typical clinical analysis were 101.22 and 100 μg/mL, respectively, confirming the accuracy of the sensor. Additionally, the recoveries obtained in real samples were in the range from 95.5 to 103.2% with RSD of 4.7%. A major benefit of using such a disposable sensor is that the analysis is quick and results are reproducible. Additionally, the cost of fabrication of such screen-printed electrodes is quite low; hence, a large number of samples can be analyzed in a short time with promising results. Similarly, several electrochemical sensors were fabricated recently for a variety of drug molecules (Kalambate et al. 2015a, Kalambate et al. 2015b, Kalambate and Srivastava 2016, Kalambate et al. 2016).

7.5 Conclusion and Perspectives

In summary, we have discussed the state-of-the-art development and applications of nanomaterials-enabled electrochemical (bio) sensors for detection and quantification of several biomarkers and drugs for the early identification and monitoring of diseases, respectively. Over the past decade, nanomaterials-based sensors have

achieved huge success due to remarkable chemical, electrical, and mechanical properties of the nanomaterials. With advancements in materials science, the materials of a specific shape, size, and composition could be prepared for the development of a specific sensing platform. Hence, materials synthesis is the most important step in sensing applications. Additionally, biomaterials could be used in combination with several nanomaterials for sensitive detection. The unique features and properties of carbon-based materials, metal nanoparticles, polymers, and several hybrid nanostructures were discussed in the construction of the sensor. The fascinating properties of these materials result in a sensitive sensing platform with improved electrochemical performance, excellent stability, selectivity, and rapid response. The LOD values obtained by several sensors are in the range of picomolar to nanomolar range confirming its advantage over conventional detection methods. Both enzymatic and nonenzymatic approaches have been discussed for glucose and H_2O_2; each approach has its own benefits and downsides. The use of ultrasensitive electrochemical sensing platforms is found to be an effective solution to overcome the limitations of conventional detection methods, which possess high cost of analysis, low sensitivity, lengthy sample pretreatment steps, and low selectivity.

Despite achieving huge popularity in recent years, there still exist a lot of challenges for further development. Firstly, noble metal nanoparticles are expensive and still need to search for financially accessible and abundant materials. Additionally, new synthesis methods to produce uniform and stable nanomaterials are highly essential. Secondly, during electrochemical measurements, the carbon-based materials tend to detach (fouling issues) from the surface of the electrode that severally degrade the response of the sensor. Hence, suitable immobilization methods need to be searched for effective attachment. We believe that further advancements in this field will lead to a stable sensing platform for diagnosis and monitoring of disease.

References

Chaiyo S, Mehmeti E, Siangproh W, Hoang TL, Nguyen HP, Chailapakul O, Kalcher K (2018) Non-enzymatic electrochemical detection of glucose with a disposable paper-based sensor using a cobalt phthalocyanine-ionic liquid-graphene composite. Biosens Bioelectron 102:113–120. https://doi.org/10.1016/j.bios.2017.11.015

Chen A, Chatterjee S (2013) Nanomaterials based electrochemical sensors for biomedical applications. Chem Soc Rev 42:5425–5438. https://doi.org/10.1039/C3CS35518G

Chen W, Cai S, Ren QQ, Wen W, Zhao YD (2012) Recent advances in electrochemical sensing for hydrogen peroxide: a review. Analyst 137(1):49–58. https://doi.org/10.1039/C1AN15738H

Chen M, Wang Y, Su H, Mao L, Jiang X, Zhang T, Dai X (2018) Three-dimensional electrochemical DNA biosensor based on 3D graphene-Ag nanoparticles for sensitive detection of CYFRA21-1 in non-small cell lung cancer. Sens Actuators B 255:2910–2918. https://doi.org/10.1016/j.snb.2017.09.111

Clark LC, Lyons C (1962) Electrode system for continuous monitoring in cardiovascular surgery. Ann N Y Acad Sci 102:29–45. https://doi.org/10.1111/j.1749-6632.1962.tb13623.x

Dhanjai SA, Lu X, Wu L, Tan D, Li Y, Chen J, Jain R (2018) Voltammetric sensing of bio-molecules at carbon based electrode interfaces: a review. Trends Anal Chem 98:174–189. https://doi.org/10.1016/j.trac.2017.11.010

Dhanjai SA, Kalambate PK, Mugo SM, Kamau P, Chen J, Jain R (2019) Polymer hydrogel interfaces in electrochemical sensing strategies: a review. Trends Anal Chem 118:488–501. https://doi.org/10.1016/j.trac.2019.06.014

Forouzanfar MH, Afshin A, Alexander LT, Anderson HR, Bhutta ZA, Biryukov S et al (2016) Global, regional, and national comparative risk assessment of 79 behavioural, environmental and occupational, and metabolic risks or clusters of risks, 1990–2015: a systematic analysis for the global burden of disease study 2015. Lancet 388:1659. https://doi.org/10.1016/S0140-6736 (16)31679-8

Fracchiolla NS, Artuso S, Cortelezzi A (2013) Biosensors in clinical practice: focus on oncohematology. Sensors 13(5):6423–6447. https://doi.org/10.3390/s130506423

Giorgio M, Trinei M, Migliaccio E, Pelicci PG (2007) Hydrogen peroxide: a metabolic by-product or a common mediator of ageing signals? Nat Rev Mol Cell Biol 8(9):722–728. https://doi.org/10.1038/nrm2240

Guo S, Wang E (2011) Noble metal nanomaterials: controllable synthesis and application in fuel cells and analytical sensors. Nano Today 6:240–264. https://doi.org/10.1016/j.nantod.2011.04.007

Han GC, Su X, Hou J, Ferranco A, Feng XZ, Zeng R, Chen Z, Kraatz HB (2019) Disposable electrochemical sensors for hemoglobin detection based on ferrocenoyl cysteine conjugates modified electrode. Sens Actuators B 282:130–136. https://doi.org/10.1016/j.snb.2018.11.042

Heydari-Bafrooei E, Shamszadeh NS (2017) Electrochemical bioassay development for ultrasensitive aptasensing of prostate specific antigen. Biosens Bioelectron 91:284–292. https://doi.org/10.1016/j.bios.2016.12.048

Kalambate PK, Srivastava AK (2016) Simultaneous voltammetric determination of paracetamol, cetirizine and phenylephrine using a multiwalled carbon nanotube-platinum nanoparticles nanocomposite modified carbon paste electrode. Sens Actuators B 233:237–248. https://doi.org/10.1016/j.snb.2016.04.063

Kalambate PK, Sanghavi BJ, Karna SP, Srivastava AK (2015a) Simultaneous voltammetric determination of paracetamol and domperidone based on a graphene/platinum nanoparticles/nafion composite modified glassy carbon electrode. Sens Actuators B 213:285–294. https://doi.org/10.1016/j.snb.2015.02.090

Kalambate PK, Biradar MR, Karna SP, Srivastava AK (2015b) Adsorptive stripping differential pulse voltammetry determination of rivastigmine at graphene nanosheet-gold nanoparticle/carbon paste electrode. J Electroanal Chem 757:150–158. https://doi.org/10.1016/j.jelechem.2015.09.027

Kalambate PK, Rawool CR, Srivastava AK (2016) Voltammetric determination of pyrazinamide at graphene-zinc oxide nanocomposite modified carbon paste electrode employing differential pulse voltammetry. Sens Actuators B 237:196–205. https://doi.org/10.1016/j.snb.2016.06.019

Kalambate PK, Rawool CR, Srivastava AK (2017) Fabrication of graphene nanosheet-multiwalled carbon nanotube-polyaniline modified carbon paste electrode for the simultaneous electrochemical determination of terbutaline sulphate and guaifenesin. New J Chem 41:7061–7072. https://doi.org/10.1039/C7NJ00101K

Kalambate PK, Dhanjai HZ, Li Y, Shen Y, Xie M, Huang Y, Srivastava AK (2019a) Core@shell nanomaterials based sensing devices: a review. Trends Anal Chem 115:147–161. https://doi.org/10.1016/j.trac.2019.04.002

Kalambate PK, Gadhari NS, Li X, Navale S, Shen Y, Patil VR, Huang Y (2019b) Recent advances in MXene based electrochemical sensors and biosensors. Trends Anal Chem 120:115643. https://doi.org/10.1016/j.trac.2019.115643

Kalambate PK, Li Y, Shen Y, Huang Y (2019c) Mesoporous Pd@Pt core-shell nanoparticles supported on multi-walled carbon nanotubes as a sensing platform: application in simultaneous

electrochemical detection of anticancer drugs doxorubicin and dasatinib. Anal Methods 11:443–453. https://doi.org/10.1039/C8AY02381F

Li X, Liu X, Wang W, Li L, Lu X (2014) High loading Pt nanoparticles on functionalization of carbon nanotubes for fabricating nonenzyme hydrogen peroxide sensor. Biosens Bioelectron 59:221–226. https://doi.org/10.1016/j.bios.2014.03.046

Lippert AR, DeBittner GCV, Chang CJ (2011) Boronate oxidation as a bioorthogonal reaction approach for studying the chemistry of hydrogen peroxide in living systems. Acc Chem Res 44 (9):793–804. https://doi.org/10.1021/ar200126t

Miller EW, Dickinson BC, Chang CJ (2010) Aquaporin-3 mediates hydrogen peroxide uptake to regulate downstream intracellular signaling. Proc Natl Acad Sci 107(36):15681–15686. https://doi.org/10.1073/pnas.1005776107

Nandini S, Nalini S, Manjunatha R, Shanmugam S, Melo JS, Suresh GS (2013) Electrochemical biosensor for the selective determination of hydrogen peroxide based on the co-deposition of palladium, horseradish peroxidase on functionalized-graphene modified graphite electrode as composite. J Electroanal Chem 689:233–242. https://doi.org/10.1016/j.jelechem.2012.11.004

Pacheco JG, Rebelo P, Freitas M, Nouws HPA, Delerue-Matos C (2018) Breast cancer biomarker (HER2-ECD) detection using a molecularly imprinted electrochemical sensor. Sens Actuators B 273:1008–1014. https://doi.org/10.1016/j.snb.2018.06.113

Parlak O, İncel A, Uzun L, Turner APF, Tiwari A (2017) Structuring Au nanoparticles on two-dimensional MoS_2 nanosheets for electrochemical glucose biosensors. Biosens Bioelectron 89:545–550. https://doi.org/10.1016/j.bios.2016.03.024

Prakash S, Chakrabarty T, Singh AK, Shahi VK (2013) Polymer thin films embedded with metal nanoparticles for electrochemical biosensors applications. Biosens Bioelectron 41:43–53. https://doi.org/10.1016/j.bios.2012.09.031

Sabu C, Henna TK, Raphey VR, Nivitha KP, Pramod K (2019) Advanced biosensors for glucose and insulin. Biosens Bioelectron 141:111201. https://doi.org/10.1016/j.bios.2019.03.034

Sanghavi BJ, Kalambate PK, Karna SP, Srivastava AK (2014) Voltammetric determination of sumatriptan based on a graphene/gold nanoparticles/Nafion composite modified glassy carbon electrode. Talanta 120:1–9. https://doi.org/10.1016/j.talanta.2013.11.077

Sharifi M, Avadi MR, Attar F, Dashtestani F, Ghorchian H, Rezayat SM, Saboury AA, Falahati M (2019) Cancer diagnosis using nanomaterials based electrochemical nanobiosensors. Biosens Bioelectron 126:773–784. https://doi.org/10.1016/j.bios.2018.11.026

Singh R, Jaiswal S, Singh K, Fatma S, Prasad BB (2018) Biomimetic polymer-based electrochemical sensor using methyl blue-adsorbed reduced graphene oxide and functionalized multiwalled carbon nanotubes for trace sensing of cyanocobalamin. ACS Appl Nano Mater 1:4652–4660. https://doi.org/10.1021/acsanm.8b00902

Wang G, Morrin A, Li M, Liu N, Luo X (2018) Nanomaterial-doped conducting polymers for electrochemical sensors and biosensors. J Mater Chem B 6:4173–4190. https://doi.org/10.1039/C8TB00817E

Wei B, Mao K, Liu N, Zhang M, Yang Z (2018) Graphene nanocomposites modified electrochemical aptamer sensor for rapid and highly sensitive detection of prostate specific antigen. Biosens Bioelectron 121:41–46. https://doi.org/10.1016/j.bios.2018.08.067

Winterbourn CC (2008) Reconciling the chemistry and biology of reactive oxygen species. Nat Chem Biol 4(5):278–286. https://doi.org/10.1038/nchembio.85

Wongkaew N, Simsek M, Griesche C, Baeumner AJ (2019) Functional nanomaterials and nanostructures enhancing electrochemical biosensors and lab-on-a-chip performances: recent progress, applications, and future perspective. Chem Rev 119(1):120–194. https://doi.org/10.1021/acs.chemrev.8b00172

Xie Y, Chen D, Lin S (2017) Microfluidic electrochemical detection techniques of cancer biomarkers. Nano Biomed Eng 9(1):57–71. https://doi.org/10.5101/nbe.v9i1.p57-71

Zhu C, Yang G, Li H, Du D, Lin Y (2015) Electrochemical sensors and biosensors based on nanomaterials and nanostructures. Anal Chem 87:230–249. https://doi.org/10.1021/ac5039863

Chapter 8
Inorganic Nanoparticles for Bioimaging Applications

S. Prabha, D. Durgalakshmi, P. Aruna, and S. Ganesan

Contents

Abstract Nanomaterials for biomedical applications are a more welcoming and positively developing field of research. Based on the material aspects, nanoparticles can be differentiated into organic, inorganic, and polymeric for biomedical applications. Of the various biomedical applications research, nanomaterials designed for bioimaging need more understanding on physics, material science, and biological concepts. Noteworthy, organic fluorescence dyes are widely in use for therapy and bioimaging applications due to its higher quantum efficiency. However during imaging, due to its photobleaching at shorter time of exposure, opens the research possibilities of inorganic nanoparticles with low toxicity and stable used as a sensitive probe for the bioimaging applications. In this chapter we discuss on some of the inorganic nanoparticles such as iron oxide, gold, mesoporous, and quantum dots for bioimaging applications.

Keywords Inorganic nanoparticle · Flouoroscence · Bioimaging · Quantum dots · MRI

S. Prabha · D. Durgalakshmi (✉) · P. Aruna · S. Ganesan
Department of Medical Physics, Anna University, Chennai, Tamil Nadu, India

227

8.1   Introduction

Nanoparticles (NPs) and nanostructured materials are an energetic area of research by the reason of adjustable physicochemical characteristics such as electrical, melting point, light absorption, scattering, wettability, and thermal conductivity. In the last 20 years, it has seen large number applications in the field of biomedical. Nanoparticles can be prepared with organic polymers/inorganic elements (Pal et al. 2011; Jeevanandam et al. 2018). Liposomes, carbon nanomaterials, and polymeric micelles are examples of the organic nanoparticle. Liposomes have the bilayer membrane structure similar to the biological membrane. As a result of amphiphilic nature, these transport hydrophilic drugs within their aqueous interior and hydrophobic drugs are dissolved in the membrane. It also has good penetration and diffusion property. Carbon nanotubes are used as biosensor, drug carriers, and tissue repair scaffolds. Quantum dots and magnetic, metallic, and ceramic nanoparticles are the core of inorganic nanoparticles. When the sizes of inorganic materials are reduced to the nanoscale range, they exhibit unexpected chemical, electrical, magnetic, optical, and mechanical properties compared to bulk structures. Quantum dots, i.e., semiconductor nanocrystals, reveal size dependence optical properties when their size is smaller than the Bohr exciton radius. Highly fluorescent quantum dots are used as a fluorescent label due to the unusual optical properties compared to the fluorescent dyes. By varying the composition and size, the emission spectrum shifts from visible to NIR region. Magnetic iron oxide nanoparticles turn to superparamagnetic when their sizes decreased below the critical size where they behave as individual magnetic domains. Graphene exhibits incredible electron mobility, and carbon nanotubes show extraordinary tensile strength. The ultrasmall nanoparticles also play a role in biomedical application because of the majority of their atoms located on their surface. Hence, this increase in surface-to-volume ratio gives some of the enhance properties like iron oxide become paramagnetic and gold as fluorescent (Kim et al. 2013).

Nanoparticles of organic molecules have been widely studied for thermal therapy and imaging. While organic dye molecules with low tissue absorbance exhibit photothermal effects, photobleaching remains one of their major drawbacks. Some common organic dyes used for biological labeling and staining are DAPI Hoechst, MitoTracker, Alexa Fluor, and Allophycocyanin, whereas inorganic nanoparticles have interested attention in the fields of heat-induced cancer therapy and imaging. Hence, they are an attractive alternative for imaging and therapies. In most of the cases, organic dyes were used as a probe because of its high quantum efficiency. However, optically stable sensitive dyes are in need for real-time analysis and detection of biomolecules. However, when using powerful excitation, the dyes undergo photobleaching, which causes drawback in the transport requirement. Hence, the research turns towards the development of inorganic nanomaterial with low toxicity and highly stable and sensitive probes (Liang et al. 2014; Zhang and Ferenz 2018; Le Trequesser et al. 2013).

In the structure of lattice, atoms may be arranged in different ways depending on the outward conditions such as pressure and temperature. Therefore, the same elements have different crystal structures. In the case of nanomaterial, the crystal structure difference causes the physicochemical properties, which also affects toxicity. For example, TiO_2 nanomaterial in the form of rutile crystal structure is used in paint and sunscreen, whereas the anatase form is used in photocatalytic application. Not only TiO_2 nanomaterial but also iron oxide, silicon dioxide, and carbon have different crystal structures. Graphite is used in concrete cutting and lubricant due to its hardness and deformability of crystal lattice respectively. Thus, altering the property of crystal structure is an alternative material approach to a broad spectrum of applications.

The metallic semiconductor has covalent bonds between their constituting atoms. The organic semiconductors in the form of molecules are having van der Waals bonding between them. This bond is weaker than the covalent bond. According to the molecular nature of the organic material, the energy level splitting of the molecular orbitals is small so the bands are narrow. In the case of organic material, the valence band is termed as HOMO and the conduction band as LUMO. However, in metal, splitting of energy level is larger, and it causes wide energy bands. In most of the cases, energy band structure must be discussed before the material introduction, because the energy band structure affects the electrical and optical implementation of the material. It is shown in below scheme diagram.

Bioimaging is a diagnostics tool for modern medicine. Nano-assisted bioimaging is used for early detection of cancer. Even very small tumor entities can be detected using these nanoparticle-based targets. There are many techniques available for bioimaging studies, such as in vivo stem cell tracking, in vivo fluorescent imaging, and magnetic resonance imaging. Nanoparticle used as a contrast agent in imaging is chosen by the reason of enhancement of the image. These are offering more advantages compared to conventional chemical agents. The combinations help to the guidance of stem cell therapies, image-guided surgery, pathogen detection, and gene therapy. The detection limit is also improved by these combinations. Even though the inorganic nanoparticle-based imaging techniques give lot of advantages compared to organic fluorophores, there is only limited works available in the former topic. The comparison between inorganic quantum dots, which can be used as fluorophores for bioimaging application with organic fluorophores, is given in Table 8.1.

8.2 Functionalization

There are two methods of synthesizing inorganic quantum dots for bioimaging applications: (i) hydrophobic condition and (ii) direct synthesis in an aqueous medium, resulting in hydrophobic and hydrophilic nanoparticle, respectively. Notably, water-soluble functionalized nanomaterial is essential for biomedical application. The coating can aid to convert hydrophobic into hydrophilic water-soluble

Table 8.1 Comparison between inorganic and organic fluorophores for bioimaging applications

Properties	Quantum dots (inorganic nanomaterials)	Organic fluorophores
Photoluminescence (PL) occurrence	Present	Present
Photostability	Superior	Low
Lifetime	10–100 ns	1–10 ns
Quantum yield	High (10–90%)	Lower
Excitation–emission range	Wide (UV–Vis–IR)	Visible
Excitation and emission band	Broad and narrow band	Narrow and broad band
Emission spectra	Size-dependent	Fixed emission wavelength
Size	6–60 nm (hydrodynamic diameter); colloid	~0.5 nm; molecule
Thermal stability	High; depends on shell or ligands	Dependent on dye class; can be critical for NIR-wavelength dyes
Photobleaching	High resistance to photobleaching	Poor resistance to photobleaching

Wojnarowska-Nowak et al. (2017)
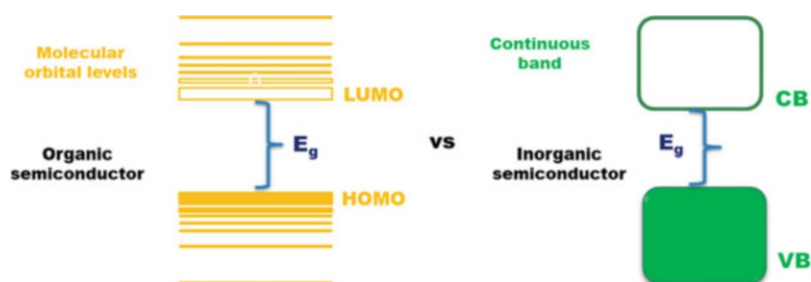
Scheme: Band structure of organic/polymeric and inorganic semiconductors. *VB* valence band; *CB* conduction band

particles. Chemical functionalization onto the particle surface can be done by covalent bonding with water molecules. Another way to change from hydrophobic into hydrophilic surfaces involves (i) ligand exchange by hydrophilic ligands like thiols or another functional groups, (ii) direct encapsulation of the hydrophobic nanoparticles by hydrophilic polymers, and (iii) formation of interdigitated bilayer between the amphiphilic polymer and passivating layer on the surface of the nanoparticle. Water-soluble quantum dots utilize a coating of thiols, polymers, micelles, and silica. Table 8.2 shows the different functionalization and coating material. In the synthesis process of nanoparticles, ligand-bound is used not only to control growth but also to stop aggregation. The ligand chosen is very important because it plays a major role in enhancing the stability of the nanoparticles. The

Table 8.2 Nanoparticles surface functionalization with respective coating materials

Function of modification	Coating material	Description
Increase of suspension molecules stability	Molecules, polymers, charged polymers	One layer mostly applied during production or during processing
Improvement of wettability	Molecules, polymers, inorganic layers	For an easier production of nanoparticle mixtures with water (hydrophilic) or organic solvents and polymers (hydrophobic)
Decreased solubility	Inorganic layers, mostly silica	Smaller particles have an increased solubility. Layer shall retain the chemical properties (ZnO/SiO_2; Ag, Au/ SiO_2)
Improvement of physical and chemical function, improved efficiency	Inorganic layers, mostly silica or ZnO, in combination with SiO_2	Strong increase in fluorescence of quantum dots, if free surface bonds are saturated
Reduction of costs and material	Noble metals, e.g., palladium	Thin, incomplete layers of noble metal as a catalyst on a cheap carrier material
Protection	Organic layers	Protection of particle functionality, e.g., from catalyst poisoning
Biocompatibility and functionality	Biocompatible polymers and inorganic layers, antibodies, and peptides	Biocompatible SiO_2 or polyethylene glycol (PEG) can decrease the corona effect Antibodies used for targeting cells

Gubala et al. (2018)

ligand bound to the nanoparticle can be obtained by electrostatic attraction or hydrophobic interaction at the head of the ligand. However, biomolecules like protein, DNA/RNA, oligonucleotides, fluorescent dyes, antibodies, polymers, and tumor markers can also be functionalized for biological application. In this point of view, polyethylene glycol (PEG) is used as a nanocarrier in the broad area. It has excellent stabilization and biodistribution in vivo and in vitro. Any other molecules bound to the nanoparticle by non-bonding interaction, i.e., steric effect, are prevented by PEG. Thus PEG act more stable in the biological domain in avoiding nonspecific binding to cells and proteins, which is important for in vivo application. For functionalization, the fluorophores are also used to observe the biologically relevant targets. For example, a green fluorescent protein (GFP) detects the protein such as fibrinogen, immunoglobulin G, and human serum albumin in biological elements (serum). Functionalization of nanoparticle with biomolecule faces various obstacles. Even after conjugate with a biomolecule, the stability of the nanoparticle is considered to be an important factor of functionalization process. The standard protocol for functionalization is not yet to be reported. It only depends on the stability, functionalized biomolecule, and environmental factors such as temperature, pH, and solvent. The efficient biomolecule conjugation with the nanoparticle is acheived through optimizing these parameters. Some of the relevant techniques for this can be obtained by functionalization like electrostatic binding, covalent

coupling, and physical adsorption (Erathodiyil and Ying 2011; Selvan et al. 2009; Sperling and Parak 2010; Conde et al. 2014).

8.3 Inorganic Nanoparticles for Bioimaging

8.3.1 Gold nanoparticles

The properties of gold nanoparticles (Au NPs) are different from its bulk form. There is notable advantageous shift in their physicochemical properties like surface plasmon resonance, redox behavior, conductivity, and high surface area. The colour of the Au NPs in the solution is depend on the size of the particles; for example the bulk form of Au NPs is yellow in colour, and thus the colours vary depending on the particle size. The sizes are ranging from 1 nm to 8 μm. The shape of the Au NPs will also enhance the property, resulting in various applications. Au nanoparticles can also be synthesized in different shapes such as in spherical, nanotriangle, nanorod, decahedral, octahedral, nanoprism, multiple twined, and irregular. Among all shapes, triangle shape has comparatively amplified the optical properties compared to rest of the shapes. The fluorescent Au NPs possess highly biocompatible property and hence been used in cell labeling, imaging, and therapy. This particle also has better enhancement and tunable emission in both visible and NIR regions and opens its application possibilities in biosensor and photothermal therapy for cancer. The biosynthesis of Au NPs, i.e., synthesized from plant extracts, is also suggested for various biomedical applications. Due to their versatile shape and size, biocompatibility and ease to functionalized with biomolecules, they are travel very easily to target the cell for drug delivery applications. Due to its low toxicity, it binds with various organic molecules as a biomarker in biomedical application. They can also be readily integrated with antibodies or oligonucleotides for the detection of biomolecules. As a result of its optical properties, it has been used in cell imaging in different techniques (Yeh et al. 2012; Khan et al. 2014).

There are various methods for prepared gold nanoparticle such as physical method, chemical method, and green method (Guo et al. 2017). Colloidal gold nanoparticles were first prepared by Faraday et al. in 1857 (Faraday 1857). In this work, the gold chloride was reduced by phosphorous and stabilized by carbon disulfide. In 1951, Turkevich et al. (1951) synthesized the colloidal gold nanoparticle using trisodium citrate as a reducing agent and tetrachloroauric acid as precursor. Later Frens et al. modified the same procedure for improved formation of particles. In the resent years, different shapes and sizes of gold nanoparticles were synthesized by numerous chemical methods. Depending on the properties, the applications were also well progressed. Sandhya Clement et al. synthesized gold nanoparticle conjugated with verteporfin (VP) and compared the photodynamic therapy effectivity of the photosensitizer by using deeply penetrating X-rays administered in standard radiotherapy doses using red light. The results show that the Au NPs enhance the interaction of ionizing radiation with a photosensitizer. Both VP

and gold nanoparticle conjugated with VP were tested in pancreatic cancer cells and the nuclei stained with Hoechst 33345 (blue) using laser scanning confocal microscopy. Both show bright fluorescence in 690 nm. Hence, they conclude that this material can be used as a dual-mode PDT treatment for deep tissue tumors and also for bioimaging. Alexander Nazirov et al. (2016) prepared gold nanoparticles and water-soluble luminescent with an average size of 2.3 nm by green method. In this method, chitosan derivative nontoxic N-(4-imidazolyl) methyl chitosan acts as both reducing and stabilizing agent. By this method, catalytic activity was high compared to other Au nanoparticle with the luminescence at 375 nm. The imidazoyl shows good binding capability with both the proteins and drug results in enhanced biological activity, and it suggested for bioimaging, drug delivery, and catalysis. Sang Bong Lee et al. (2016) reported the radionuclide embedded gold nanoparticle as an optical imaging agent for dendritic cell (DC)-based immunotherapy and tracking of DC migration to lymph nodes. It was prepared by the simple strategy of DNA-based radiolabeling chemistry in addition to gold shell formation. It has longtime monitoring of DC migration and also can image through PET owing to strong and stable radio sensitivity. Further, it is also applicable for CLI-based optical imaging due to their sensitivity and penetration depth. Hence, it poses the possibility in new work for multimodal imaging for optical and nuclear imaging applications. Shengnan Huang et al. (2017) designed the gold nanocage with hollow and porous structure. Doxorubicin was loaded into the system consists of hyaluronic acid grafted and A54 peptide targeted PEGylated gold nanocage for liver cancer drug delivery. The cell uptake was demonstrated by the BEL-7402 cells incubated with HA-grafted PEGylated gold nanocage (HPAuNCs) and HA-grafted A54 peptide-targeted PEGylated gold nanocage (HTPAuNCs) for different time period and investigated by the fluorescence microscopy. The cells treated with HTPAuNCs show strong fluorescence intensity than the HPAuNCs. Hence the smart delivery system could increase the cellular uptake of AuNCs. Thus, they conclude, this system enhanced the therapeutic effect with limited toxicity. Yong Wang et al. (2013) proposed the nanocomposite of transferrin functionalized gold nanoclusters with graphene oxide as NIR fluorescent probe for bioimaging. These composites have good water solubility and biocompatibility with negligible cytotoxicity. The fluorescence bioimaging of cancer cell in mice at varied time period is shown in Fig. 8.1.

8.3.2 *Iron Oxide Nanoparticles*

In the last decades, magnetic nanoparticle shows potential interest in the research field, and these applications are in the broad area due to their unique properties of low Curie temperature, high magnetic susceptibility, low toxicity, and higher surface-to-volume ratio. The applications of iron oxide nanoparticles in the biomedical field include detection and bioseparation of a cell, enzyme, protein, bacteria, etc. and further applications in magnetic resonance imaging and in magnetic-targeted drug delivery process (Ali et al. 2016).
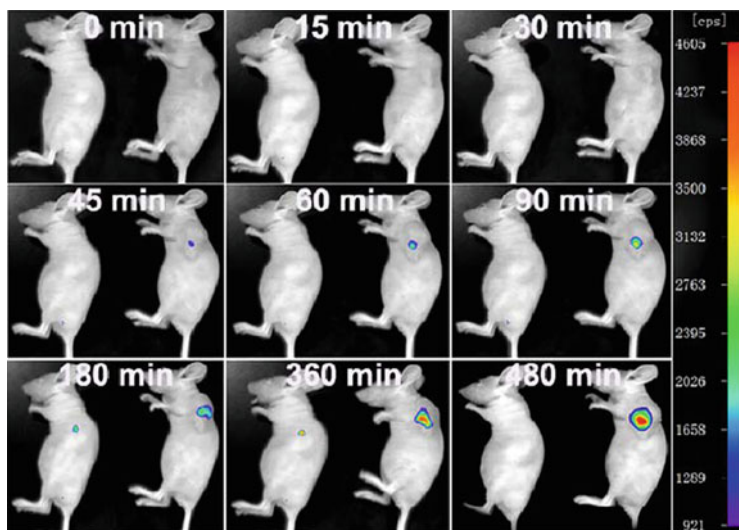
Fig. 8.1 Time-dependent fluorescence imaging of HeLa tumor-bearing mice and normal nude mice. The fluorescent probe was intratumorally injected into the tumor-bearing mice (right) and subcutaneously injected into the left forelimb region of the normal nude mice (left) (Wang et al. 2013)

These nanoparticles do not only apply in the biomedical field but also extend its application in commercial and technological applications such as data storage, magnetic fluids, and catalysis. Iron oxide is magnetically soft with high magnetic moment density, and they are inexpensive. However, when the size is less than 20 nm, these materials acquire superparamagnetic properties. They are widely used in biomedical field by the reason of innocuous toxicity. Functionalization of these nanoparticles is also possible with small molecules, nanostructures, and coating agents such as fatty acids, PVA, and PEG. As of now, eight types of iron oxides were found; among them, magnetite (Fe_3O_4), maghemite (γ-Fe_2O_3), and hematite (α-Fe_2O_3) are admirable for various applications, and their crystal structure is shown in Fig. 8.2 (Wu et al. 2015).

Hematite (α-Fe_2O_3) is an n-type semiconductor with higher stability compared to other iron oxides. Hematite is used in gas sensors and pigments due to its high resistance to corrosion and bandgap of 2.3 eV. The energy diagram of this compound consists of empty d orbitals of Fe^{3+} in the conduction band and occupied 3d orbitals of Fe^{3+} with the addition of 2p nonbonding orbitals of O (Zhang et al. 1993). Another iron oxide crystal, magnetite (Fe_3O_4), has FCC spinel structure. It is unique among all other iron oxides, as it consists of both divalent and trivalent irons. Hence it can act as both n and p-type semiconductor with a bandgap of 0.1 eV. Maghemite (γ-Fe_2O_3) is a cubic structure and considered as fully oxidized magnetite. It is an n-type semiconductor with the bandgap of 2 eV (Boxall et al. 1996). Till this date, there are several methods for the synthesis of iron oxide nanoparticle which include
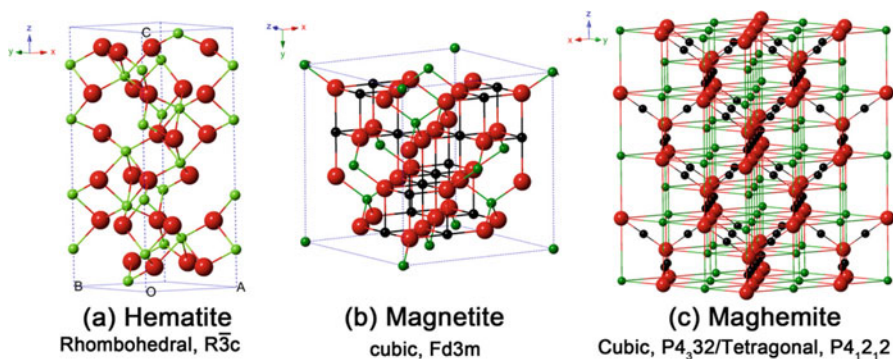
Fig. 8.2 Crystal structure and crystallographic data of the hematite, magnetite, and maghemite (the black ball is Fe^{2+}, the green ball is Fe^{3+}, and the red ball is O^{2-}) (Wu et al. 2015)

both chemical and physical methods, viz., electrochemical method, aerosol/vapor method, sol–gel method, microemulsion, hydrothermal, co-precipitation, biological synthesis, and thermal decomposition

Seda Demirel Topel et al. (2015) reported uniform PEG-coated magnetic Fe_3O_4 by a co-precipitation method, and Bodipy-5 was conjugated by DCC/DMAP coupling reaction. The imaging ability of this sample was found in the presence of A549 cancer cells. From the in vitro experiment, the fluorescence images show that the nanoparticles could be easily penetrated into the cytoplasm. Hence, it is suitable for MRI contrast agent. Kamil R. Wierzbinski et al. (2018) reported DMSA-coated superparamagnetic iron oxide by the thermal decomposition and ligand exchange reaction as an agent for direct cell labeling for stem cell imaging. Heng Li Chee et al. (2018) reported on the ultrasmall superparamagnetic iron oxide nanoparticles (of USPIONs) and the short peptides and ligands on the surface of USPIONs. The bisphosphorylated peptide has enhanced magnetic resonance property compared with the commercially MRI contrast agents. The peptide-coated USPIONs were functionalized with a biomarker for tracking the breast cancer tumors. Hence it is used as a cancer diagnosis with a high-resolution contrast-enhanced MRI. Yuran Huang et al. (2014) were the first to report on the rattle-type metal nanostructure for theranostics application. In this work, multifunctional metal nanocarrier was designed by choosing porous gold shell to carry superparamagnetic iron oxide nanoparticle. The intermediate layer of porous silica was coated by condensation of TEOS. And also functionalized was done with an amino group of APTES. This multifunctional material was used as MRI contrast agent-guided therapy for cancer. Carbon quantum dots doped with SPIONS (FeCD) by hydrothermal method was reported by Bodhisatwa Das et al. (2019). The results show that it has well cytocompatible and also hemocompatible property. It is used for fluorescence as well as MR imaging. It was extended for tissue engineering as a 3D printed composite. To understand the histological study, MR imaging of the kidney and liver of animals treated with the functionalized nanoparticles was examined and shown in Fig. 8.3.

Fig. 8.3 In vivo rodent model MR imaging at the T2 mode: (**a**) before injection; (**b**) immediately after injection; (**c**) 15 min after injection (Das et al. 2019)

T2/FeC

Before Injection   Immediate after Injection   after 15 min
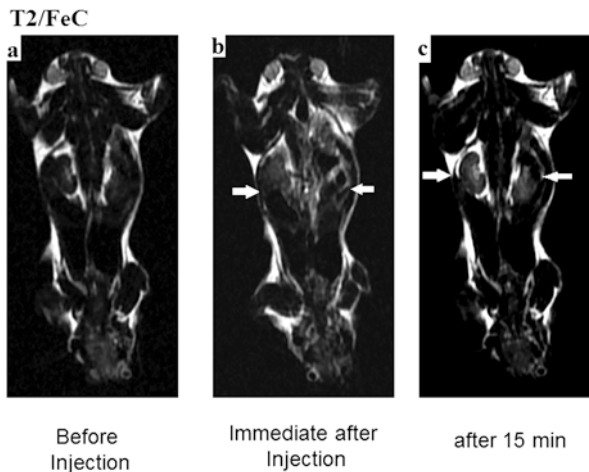
8.3.3   Mesoporous Silica Nanoparticles

Mesoporous silica material discovered in 1992 in the labs of the Mobil Oil Corporation was in the M41S phase having pore diameters from approximately 2 to 10 nm (Hoffmann et al. 2006). As per IUPAC (International Union of Pure and Applied Chemistry), the porous materials classified according to their pore size were tabulated (Barrabino 2011). (Table 8.3).

Mobil silica crystalline materials were developed as an inorganic drug delivery agent. The materials are often referred to MCM materials, which stands for Mobil Composition of Matter (Caras 2011), and most popular MCM materials are MCM-41 (Mobile Crystalline Material) and MCM-48 in which MCM-41 material is a 2D hexagonal arrangement of pores, whereas MCM-48 is a 3D cubic pore system. Others are SBA 15 (Santa Barbara Amorphous), TUD, MCM 50, HMS, TMS, etc. It has received considerable attention due to their superior textual properties such as high surface area and large pore volume, tunable particle size (10–1000 nm) and pore diameter (2–30 nm), flexible morphology, effortless surface functionalization and uniform mesoporosity, tunable and narrow pore size distribution, and excellent biocompatibility and biodegradation. MSNs were developed as an inorganic drug delivery agent. The application of MSNPs has controlled drug delivery system, bioimaging and biotherapeutic agent delivery, and tissue regeneration owing to its surface functionalization and drug loading capacity. In imaging, it gives high spatial resolution with enhancing tissue penetration and imaging accuracy with sensitivity. Moreover, fluorescent MSNPs also play a role in multi-labeling in theranostics applications due to its targeting ligands with surface modification and photostability (Wang et al. 2015; Pratiwi et al. 2018).

Tatsuya Nakamura et al. (2015) developed the ^{19}F MRI contrast agent inside the mesoporous silica nanoparticles. For cellular imaging and drug delivery, it was conjugated with folic acid, and also the anticancer drug doxorubicin was loaded into the pores of folate conjugates mesoporous silica. Because of the integrated

Table 8.3 Classification of porous material

Types of porous material	The diameter of pores (nm)
Microporous	Diameter < 2
Mesoporous	2 < diameter < 50
Macroporous	Diameter > 50

Hoffmann et al. (2006)
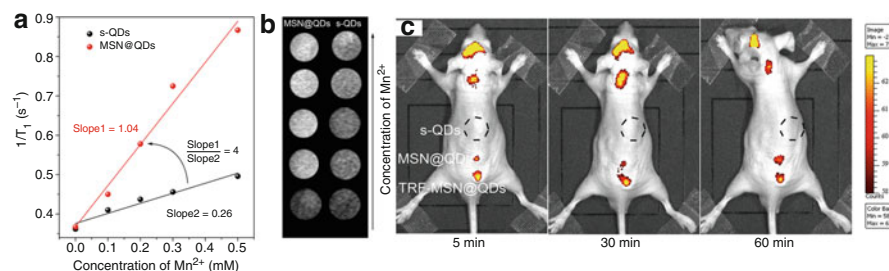
Fig. 8.4 MRI enhancement performance of the MSN@QDs NPs over s-QDs: (**a**) T1 relaxivity curves and (**b**) T1-weighted MR images. (**c**) In vivo fluorescence images of nude mouse after injection with s-QDs, MSN@QDs, and TRF-MSN@QDs (Zhou et al. 2018)

system, it was used as a fluorescence imaging with the drug delivery vehicle tested in tumor-bearing mice. Ronghui Zhou et al. (2018) studied Mn-doped ZnS quantum dots with mesoporous silica for dual model imaging. Mn^{2+} itself maximizes the fluorescence and at the same time shows possibility for MR imaging. Thus, synthesized Mn-doped ZnSe quantum dots were loaded into the large pores of mesoporous silica. Before loading the mesoporous silica functionalized with amine group, it shows enhanced fluorescence brightness and also magnetic signal with higher biocompatibility. For increasing the cell affinity, transferrin is used as tumor-targeting ligand. It has high luminescent and also shows paramagnetism property, so it was used for optical and MRI dual model imaging depicted in Fig. 8.4.

Elisabete Oliveira et al. (2019) reported quantum dots coated with mesoporous silica CdTe@MNs. The luminescent of CdTe helps in imaging of cell internalization and visualized doxorubicin drug release. The ability of the nanocarrier was examined in HeLa cells by laser scanning microscopy, where the nanocarrier acts as a protein scavenger. The protein identification was not found in a sample in the absence of nanoparticle. Qinfu Zhao et al. (2017) presented carbon dots capped with hollow mesoporous silica nanoparticles (HMSN) for bioimaging as well as drug delivery. The carbon dots act as a gatekeeper and imaging agent, grafted on the HMSN opening pores via disulfide bonds. The hyaluronic acid was graft onto the HMSN for drug delivery application. This sample has good biocompatibility with fluorescent properties. The cellular uptake was examined using A549 cells and NIH-3 T3 by laser scanning microscopy. The doxorubicin-loaded material has higher anticancer activity. Thus, this material is used for real-time imaging and drug delivery. Min Sil Kang et al. (2017) prepared carbon dot with mesoporous hollow organosilica nanoparticle for imaging and therapy. In vivo, it showed the

strong optical signal and the stability over a week. In case of drug influence, doxorubicin significantly suppressed the tumor growth with apoptotic function.

8.3.4 Quantum Dots (CdSe, CdTe, and ZnS)

The bandgap of semiconductor (II–VI) has a significant role in most of the electrical and optical applications of materials. It is one of the most attracted areas of all experimental and theoretical researchers. Among all those semiconductor, cadmium telluride (CdTe) has tunable emission possibilities. However, cytotoxicity is the major challenge of this material. Until now, a lot of research is happening to minimize the toxicity of cadmium-based quantum dots, which is a big challenge. The toxic can be reduced by coating silica and zinc-based biocompatible shell with core cadmium nanoparticle. Compared to organic dyes for fluorescence imaging, by using these kinds of inorganic nanoparticles, photobleaching can be greatly reduced. However, cytotoxicity and instability of these materials limit its application in bioimaging. Shaohuazhang et al. (2016) reported watermelon-like structure mesoporous silica core and CdTe quantum dots which was protected by silica for improving the stability. The resultant particle analyzed with A549 cells by confocal laser scanning microscopy and in vivo fluorescence imaging shows high fluorescent image in mice at different times with the injection of material. Sander F. Wuister et al. (2003) reported on colloidal water-soluble CdTe quantum dots. The quantum yields of this material are up to 60% at room temperature. D. Saikia et al. (2017) studied highly stable CdTe@ZnScore@shell quantum dots capped with mercaptosuccinic acid. The stability was excellent after 100 days of synthesis. The quantum yield is four times higher than that of CdTe alone, and in the presence of *E. coli* cells, it provides enhanced fluorescence emission properties, in which the shell of ZnS controls the stability of the core CdTe nanoparticle. Ganjin et al. synthesized CdTe-PVA, CdTe-PSS, and CdTe-PDDA towards bioimaging. The MTT, PVA, and PSS analysis shows the material has less toxicity and suggested for bioimaging in Ca127 and HeLa cells with the quantum yield about 65%. Zdenka Bujňáková et al. (2017) synthesized InAs/ZnS nanocrystal mixture by high-energy milling in chitosan to get the stable suspension. The bioimaging was done on cancer cell lines such as CaCo-2, HCT116, MCF7, and HeLa. From this study, the materials entered into the cytoplasm and surrounded the nuclei.

In general, zinc sulfide-based quantum dots are nontoxic materials, but the major drawback is the excitation in the UV region bandgap, which limits its beneficial for bioimaging. Whereas when it is combined with cadmium-based quantum dots, the bandgap shifts towards visible region, but it is not desirable for bioimaging due to its cytotoxicity. In the earlier work, the glutathione (GSH)-capped Mn-ZnS was studied for RTP sensing of Pb^{2+}. It showed GSH capping had good sensitivity and selectivity. Hence it was extended to bioimaging by the reason of fluorescence by Manju Singhal et al. (2019). In that work GSH was acted as a functionalization agent for $ZnS:Mn^{2+}$ quantum dots. From the multiphoton-excited time-resolved photoluminescence study, it was very stable, and lifetime is in millisecond; thus it
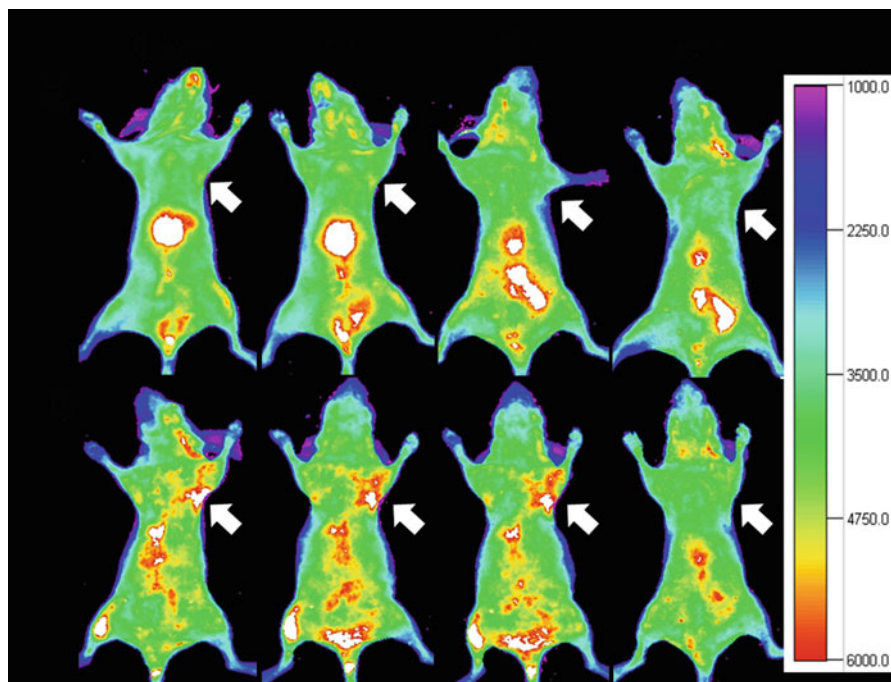
Fig. 8.5 In vivo NIR fluorescence imaging of U87MG tumor-bearing mice (arrows) injected with (**a**) ZCIS/ZnS QDs and (**b**) ZCIS/ZnS-RGD QDs (Guo 2013)

avoided autofluorescence. Hence, this is a promising material for bioimaging. The core@shell of Zn-Cu-In-S (ZCIS)@ ZnS conjugated with cRGD peptide were also examined for in vivo NIR fluorescence imaging. The cytotoxicity and biocompatibility test with 3T3 cells shows the results of lesser toxicity, and hence it was injected into U87MG tumor of nude mice through the tail vein. The MR images (Fig. 8.5) showed signal from the tumor region injected with ZCIS@ZnS.

8.4 The Advanced Technique of FRET in Present and Future

Forster resonance energy transfer (FRET) is a powerful technique used to study nano-bio combination for bioimaging applications. In 1922, the FRET concept was discovered by Cario and Franck using mercury to thallium atomic vapor. In 1927, it was theoretically explained by Jean Perrin as the molecular transfer of energy, and Perrin reported dipole interaction was responsible for energy transfer when the intermolecular distance was 1000 Å. After that, the influence of spectral overlap between donor emission and acceptor absorption on energy efficiency was reported by Perrin's son Francis using quantum mechanical theory; and he calculated that the

average distance between the intermolecular was 250 Å. However, it was larger than the experimental result. Then Forster with Jean and Francis developed the equation depending on the spectral overlap and intermolecular distance, and he calculated the distance to be 10–100 Å. Thus, FRET is a more sensitive distance-dependent fluorescence signal to monitor the molecular interaction in vitro and in vivo (Shi et al. 2015; Cario and Franck 1922; Förster 1948).

FRET based on organic dye has simple preparation and low cost. But short lifetime and low chemical stability are the challenges of FRET in organic dyes. FRET involves the energy transfer between donor and acceptor, i.e., one fluorophore to another, by the fluorescence emission shift. It also provides the spatial and kinetic information about the interaction between the fluorescent nanoparticle and cells or protein labeled by the fluorescent. It is a growing area in imaging application by using materials such as luminescent semiconductor quantum dots, upconversion material, inorganic material, and dye-doped nanoparticles. This technique provides more advantages compared with the conventional fluorescent labeling technique. The mechanism involves the non-radiative energy transfer from an excited donor to a ground-state acceptor. Excitation of the donor results in emission by the acceptor and at the same time quenching of donor fluorescence. The emission of the donor must be able to excite the acceptor. Thus, the donor fluorescence overlaps with the acceptor excitation spectrum. The FRET efficiency is higher, when donor and acceptor molecules are within 10 nm from each other and their dipoles are parallel (Fig. 8.6). To increase the FRET efficiency, the traditional organic dyes were replaced by nanoparticles such as quantum dots, graphene quantum dots, and upconversion nanoparticle. The table shows different biological targets with nanoparticle in FRET. In the future, the nanoparticle with FRET assay will govern a predominant role in bioimaging applications owing to low cost, high sensitivity, specificity, and stability for both in vivo and in vitro applications (Charron and Zheng 2018). (Table 8.4)

Normalized excitation and emission spectra of four different FRET pairs with spectral overlaps are shown in Fig. 8.7. The four FRET pairs are protein–protein,

Fig. 8.6 Requirements for FRET (Broussard and Green 2017)
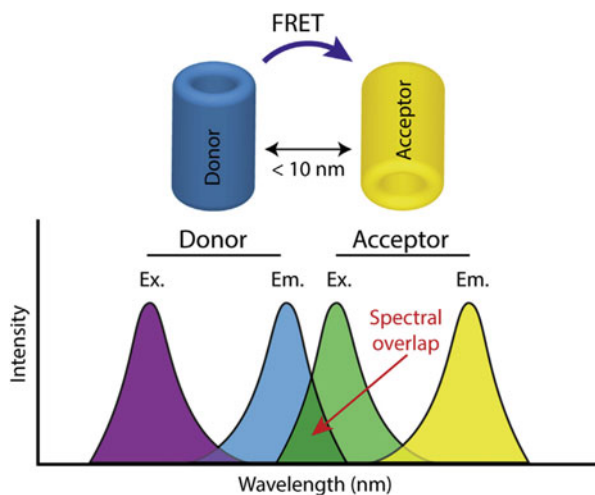
Table 8.4 Some of the FRET molecules discovered

Biological targets	Donor/acceptor
DNA hybridization	QD/Cy5
DNA hybridization	QD/Cy3 on optical fiber
Estrogen receptor b (ER-b) antigen	QD/Alexa Fluor
Thrombin	QD/aptamer-dye
Cancer marker type IV collagenase	QD/AuNP
Cancer marker MUC1	QD/mCherry
Caspase-3 activity	QD/AuNP
Bacteria DNA	GQD/AuNP
DNA hybridization	GQD/CNT
Glucose	UCNP/GO
Virus gene	UCNP/AuNP
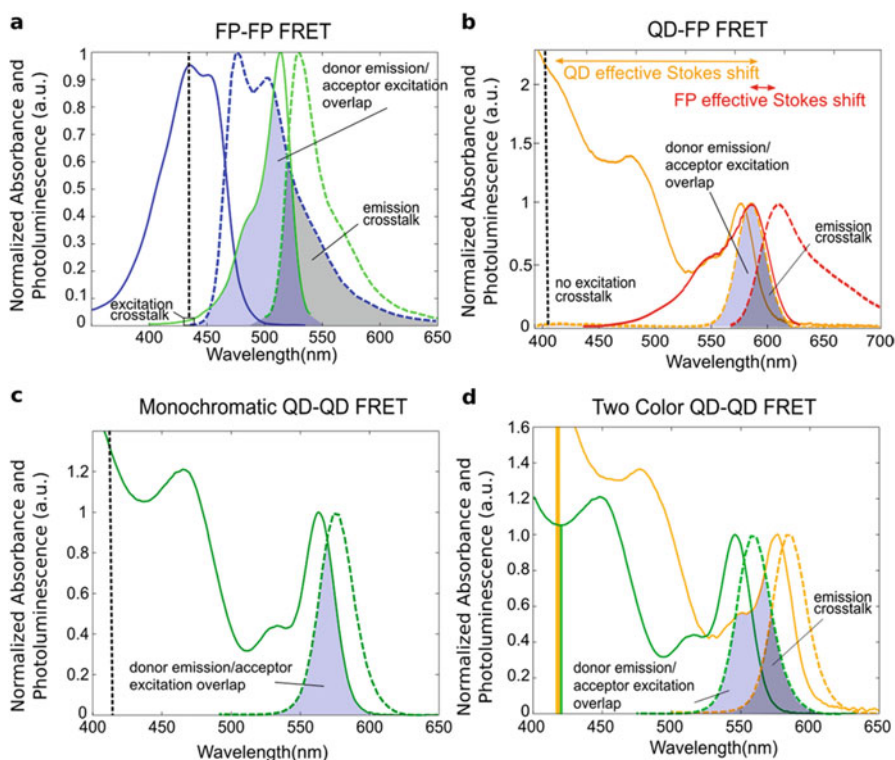
Fig. 8.7 (**a**) Enhanced cyan fluorescent protein (ECFP, blue, donor) and enhanced yellow fluorescent protein (EYFP, green, acceptor); (**b**) A 3.7 nm CdSe/ZnS QD (orange, donor) and the fluorescent protein mCherry (red, acceptor); (**c**) A 3.3 nm diameter CdSe/ZnS QD acting as both donor and acceptor; (**d**) A 2.9 nm diameter CdSe/ZnS QD (green, donor) and 3.7 nm diameter CdSe/ZnS QD (yellow, acceptor)

quantum dot–protein, monochromatic quantum dot that acts as both donor and acceptor, and two color quantum dots.

8.5 Summary

Nanostructuring material is a well-established field of research, which spreads its applications in wider field. Especially, the biocompatible inorganic nanoparticle with different functionalities marks an important role for biomedical applications and requires lot of innovation. In this field, shift is moving towards inorganic nanoparticle as it is more stable than organic nanoparticle. Inorganic nanoparticles not only involved in therapy but also involved in cell tracking, signaling, and interaction at the molecular and cellular levels.

Fluorescence is one of the techniques used in bioimaging. There are numerous fluorophores of organic dyes and also inorganic nanoparticles used for imaging. Inorganic nanoparticles portraying the enhanced light property than organic are highlighted in this chapter. In future, inorganic nanoparticle will play a prominent role as a diagnostic tool of bioimaging due to its advance technology of Forster resonance energy transfer (FRET).

References

Ali A, Hira Zafar MZ, ul Haq I, Phull AR, Ali JS, Hussain A (2016) Synthesis, characterization, applications, and challenges of iron oxide nanoparticles. Nanotechnol Sci Appl 9:49

Barrabino A (2011) Synthesis of mesoporous silica particles with control of both pore diameter and particle size.

Boxall C, Kelsall G, Zhang Z (1996) Photoelectrophoresis of colloidal iron oxides. Part 2.—Magnetite ($Fe_3 O_4$). J Chem Soc Faraday Trans 92(5):791–802

Broussard JA, Green KJ (2017) Research techniques made simple: methodology and applications of Förster Resonance Energy Transfer (FRET) microscopy. J Investig Dermatol 137(11):e185–e191

Bujňáková Z, Dutková E, Zorkovská A, Baláž M, Kováč J, Kello M, Mojžiš J, Briančin J, Baláž P (2017) Mechanochemical synthesis and in vitro studies of chitosan-coated InAs/ZnS mixed nanocrystals. J Mater Sci 52(2):721–735

Caras A (2011) Glucan particle delivery of mesoporous silica-drug nanoparticles. UMASS Medical School

Cario G, Franck J (1922) Über zerlegung von wasserstoffmolekülen durch angeregte quecksilberatome. Zeitschrift für Physik A Hadrons and Nuclei 11(1):161–166

Charron DM, Zheng G (2018) Nanomedicine development guided by FRET imaging. Nano Today 18:124–136

Chee HL, Gan CRR, Ng M, Low L, Fernig DG, Bhakoo KK, Paramelle D (2018) Biocompatible peptide-coated ultrasmall superparamagnetic iron oxide nanoparticles for in vivo contrast-enhanced magnetic resonance imaging. ACS Nano 12(7):6480–6491

Conde J, Dias JT, Grazú V, Moros M, Baptista PV, de la Fuente JM (2014) Revisiting 30 years of biofunctionalization and surface chemistry of inorganic nanoparticles for nanomedicine. Front Chem 2:48

Das B, Girigoswami A, Dutta A, Pal P, Dutta J, Dadhich P, Srivas PK, Dhara S (2019) Carbon nanodots doped super paramagnetic iron oxide nanoparticles for multimodal bioimaging and osteochondral tissue regeneration via external magnetic actuation. ACS Biomaterial Sci & Eng 5:3549–3560

Erathodiyil N, Ying JY (2011) Functionalization of inorganic nanoparticles for bioimaging applications. Acc Chem Res 44(10):925–935

Faraday M (1857) The Bakerian lecture—experimental relations of gold (and other metals) to light. Philos T R Soc London 147:145–181

Förster T (1948) Energy transfer and fluorescence between molecules. Ann Phys 437(1–2):55–75

Gubala V, Johnston LJ, Liu Z, Krug H, Moore CJ, Ober CK, Schwenk M, Vert M (2018) Engineered nanomaterials and human health: Part 1. Preparation, functionalization and characterization (IUPAC Technical Report). Pure Appl Chem 90(8):1283–1324

Guo W (2013) Synthesis of Zn-Cu-In-S/ZnS core/shell quantum dots with inhibited blue-shift photoluminescence and applications for tumor targeted bioimaging. Theranostics 3(2):99

Guo J, Rahme K, He Y, Li L-L, Holmes JD, O'Driscoll CM (2017) Gold nanoparticles enlighten the future of cancer theranostics. Int J Nanomedicine 12:6131

Hoffmann F, Cornelius M, Morell J, Fröba M (2006) Silica-based mesoporous organic–inorganic hybrid materials. Angew Chem Int Ed 45(20):3216–3251

Huang Y, Wei T, Yu J, Hou Y, Cai K, Liang X-J (2014) Multifunctional metal rattle-type nanocarriers for MRI-guided photothermal cancer therapy. Mol Pharm 11(10):3386–3394

Huang S, Li C, Wang W, Li H, Sun Z, Song C, Li B, Duan S, Hu Y (2017) A54 peptide-mediated functionalized gold nanocages for targeted delivery of DOX as a combinational photothermal-chemotherapy for liver cancer. Int J Nanomedicine 12:5163

Jeevanandam J, Barhoum A, Chan YS, Dufresne A, Danquah MK (2018) Review on nanoparticles and nanostructured materials: history, sources, toxicity and regulations. Beilstein J Nanotechnol 9(1):1050–1074

Kang MS, Singh RK, Kim T-H, Kim J-H, Patel KD, Kim H-W (2017) Optical imaging and anticancer chemotherapy through carbon dot created hollow mesoporous silica nanoparticles. Acta Biomater 55:466–480

Khan A, Rashid R, Murtaza G, Zahra A (2014) Gold nanoparticles: synthesis and applications in drug delivery. Trop J Pharm Res 13(7):1169–1177

Kim BH, Hackett MJ, Park J, Hyeon T (2013) Synthesis, characterization, and application of ultrasmall nanoparticles. Chem Mater 26(1):59–71

Le Trequesser Q, Seznec H, Delville M-H (2013) Functionalized nanomaterials: their use as contrast agents in bioimaging: mono-and multimodal approaches. Nanotechnol Rev 2 (2):125–169

Lee SB, Ahn SB, Lee S-W, Jeong SY, Ghilsuk Y, Ahn B-C, Kim E-M, Jeong H-J, Lee J, Lim D-K (2016) Radionuclide-embedded gold nanoparticles for enhanced dendritic cell-based cancer immunotherapy, sensitive and quantitative tracking of dendritic cells with PET and Cerenkov luminescence. NPG Asia Material 8(6):e281

Liang R, Wei M, Evans DG, Duan X (2014) Inorganic nanomaterials for bioimaging, targeted drug delivery and therapeutics. Chem Commun 50(91):14071–14081

Nakamura T, Sugihara F, Matsushita H, Yoshioka Y, Mizukami S, Kikuchi K (2015) Mesoporous silica nanoparticles for 19 F magnetic resonance imaging, fluorescence imaging, and drug delivery. Chem Sci 6(3):1986–1990

Nazirov A, Pestov A, Privar Y, Ustinov A, Modin E, Bratskaya S (2016) One-pot green synthesis of luminescent gold nanoparticles using imidazole derivative of chitosan. Carbohydr Polym 151:649–655

Oliveira E, Santos HM, Jorge S, Rodríguez-González B, Novio F, Lorenzo J, Ruiz-Molina D, Capelo JL, Lodeiro C (2019) Sustainable synthesis of luminescent CdTe quantum dots coated with modified silica mesoporous nanoparticles: Towards new protein scavengers and smart drug delivery carriers. Dyes Pigment 161:360–369

Pal SL, Jana U, Manna PK, Mohanta GP, Manavalan R (2011) Nanoparticle: An overview of preparation and characterization. J Appl Pharm Sci 1(6):228–234

Pratiwi FW, Kuo CW, Wu S-H, Chen Y-P, Mou CY, Chen P (2018) The bioimaging applications of mesoporous silica nanoparticles. The Enzymes 43:123–153

Saikia D, Chakravarty S, Sarma N, Bhattacharjee S, Datta P, Adhikary N (2017) Aqueous synthesis of highly stable CdTe/ZnS Core/Shell quantum dots for bioimaging. Luminescence 32 (3):401–408

Selvan ST, Tan TTY, Yi DK, Jana NR (2009) Functional and multifunctional nanoparticles for bioimaging and biosensing. Langmuir 26(14):11631–11641

Shi J, Tian F, Lyu J, Yang M (2015) Nanoparticle based fluorescence resonance energy transfer (FRET) for biosensing applications. J Mater Chem B 3(35):6989–7005

Singhal M, Sharma J, Jeon H, Kang T, Kumar S (2019) Synthesis and characterisation of functional manganese doped ZnS quantum dots for bio-imaging application. Adv Appl Ceram 118 (6):321–328

Sperling RA, Parak WJ (2010) Surface modification, functionalization and bioconjugation of colloidal inorganic nanoparticles. Philos Trans R Soc A Math Phys Eng Sci 368 (1915):1333–1383

Topel SD, Topel Ö, Bostancıoğlu RB, Koparal AT (2015) Synthesis and characterization of Bodipy functionalized magnetic iron oxide nanoparticles for potential bioimaging applications. Colloids Surf B Biointerfaces 128:245–253

Turkevich J, Stevenson PC, Hillier J (1951) A study of the nucleation and growth processes in the synthesis of colloidal gold. Discuss Faraday Soc 11:55–75

Wang Y, Chen J-T, Yan X-P (2013) Fabrication of transferrin functionalized gold nanoclusters/ graphene oxide nanocomposite for turn-on near-infrared fluorescent bioimaging of cancer cells and small animals. Anal Chem 85(4):2529–2535

Wang Y, Zhao Q, Han N, Bai L, Li J, Liu J, Che E, Hu L, Zhang Q, Jiang T (2015) Mesoporous silica nanoparticles in drug delivery and biomedical applications. Nanomedicine 11(2):313–327

Wierzbinski KR, Szymanski T, Rozwadowska N, Rybka JD, Zimna A, Zalewski T, Nowicka-Bauer K, Malcher A, Nowaczyk M, Krupinski M (2018) Potential use of superparamagnetic iron oxide nanoparticles for in vitro and in vivo bioimaging of human myoblasts. Sci Rep 8 (1):3682

Wojnarowska-Nowak R, Polit J, Zięba A, Stolyarchuk I, Nowak S, Romerowicz-Misielak M, Sheregii E (2017) Colloidal quantum dots conjugated with human serum albumin–interactions and bioimaging properties. Opto-Electronic Rev 25(2):137–147

Wu W, Wu Z, Yu T, Jiang C, Kim W-S (2015) Recent progress on magnetic iron oxide nanoparticles: synthesis, surface functional strategies and biomedical applications. Sci Technol Adv Mater 16(2):023501

Wuister SF, Swart I, van Driel F, Hickey SG, de Mello DC (2003) Highly luminescent water-soluble CdTe quantum dots. Nano Lett 3(4):503–507

Yeh Y-C, Creran B, Rotello VM (2012) Gold nanoparticles: preparation, properties, and applications in bionanotechnology. Nanoscale 4(6):1871–1880

Zhang C, Ferenz K (2018) Nano-bio-imaging and therapeutic nanoparticles. J Nanosci Nanomed 2 (1):19

Zhang Z, Boxall C, Kelsall G (1993) Photoelectrophoresis of colloidal iron oxides 1. Hematite (α-Fe$_2$O$_3$). In: Colloids in the aquatic environment. Elsevier, pp 145–163

Zhang S, Wen L, Yang J, Zeng J, Sun Q, Li Z, Zhao D, Dou S (2016) Facile fabrication of dendritic mesoporous SiO$_2$@ CdTe@ SiO$_2$ fluorescent nanoparticles for bioimaging. Part Part Syst Charact 33(5):261–270

Zhao Q, Wang S, Yang Y, Li X, Di D, Zhang C, Jiang T, Wang S (2017) Hyaluronic acid and carbon dots-gated hollow mesoporous silica for redox and enzyme-triggered targeted drug delivery and bioimaging. Mater Sci Eng C 78:475–484

Zhou R, Sun S, Li C, Wu L, Hou X, Wu P (2018) Enriching Mn-doped ZnSe quantum dots onto mesoporous silica nanoparticles for enhanced fluorescence/magnetic resonance imaging dual-modal bio-imaging. ACS Appl Mater Interfaces 10(40):34060–34067

Chapter 9
Application of Metal and Metal Oxides in Sustainable Synthesis and Biology

Siva Prasad Y., Lalitha Krishnamoorthy, Tamizhanban Ayyapillai, Atul Sharma, Muskan Bhatnagar, and Nagarajan Subbiah

Contents

Siva Prasad Y. · L. Krishnamoorthy · T. Ayyapillai
Department of Chemistry, School of Chemical and Biotechnology, SASTRA Deemed
University, Thanjavur, Tamil Nadu, India

A. Sharma · M. Bhatnagar
Department of Chemistry, National Institute of Technology Warangal (Institute of National
Importance), Warangal, Telangana, India

N. Subbiah (✉)
Department of Chemistry, School of Chemical and Biotechnology, SASTRA Deemed
University, Thanjavur, Tamil Nadu, India

Department of Chemistry, National Institute of Technology Warangal (Institute of National
Importance), Warangal, Telangana, India
e-mail: snagarajan@nitw.ac.in

Abstract Modern technologies such as nanotechnology, biotechnology, and material science are combined together to develop a vast number of potential molecules for various biological applications. In many new reactions, transition metal complexes such as alkenylidene and allenylidenes are reported as key intermediates producing a wide range of products. Hence here, we discuss the synthetic applicability of transition metal complexes. Metal oxide nanoparticles have been paid special attention in the field of biomedical therapeutics, bioimaging, and biosensing due to their unique nature, good catalytic behavior, high surface area, biocompatibility, and excellent mechanical stability. As these materials are nontoxic and eco-friendly, they are used in many medical applications like medical implants, cancer therapy, wound dressings, contrast agents for magnetic resonance imaging (MRI), and as a vehicle to deliver the drug. In this chapter, we also discuss the significance of various metal oxides and their role in delivering the drug and other biomedical applications.

9.1   Introduction

The use of metals in synthetic organic chemistry has seen tremendous strides in achieving selective C–H bond functionalization since the organometallic chemistry has come into the light (Goldman and Goldberg 2004). Many new bonds like C-heteroatom and C–C formation occur via catalytic C–H bond activation. Fritea and co-workers have highlighted the significant advances carried out in organic and inorganic chemistry towards the synthesis of coordination complexes of pharmaceutically important substances like nicotinic acid, captopril, and guanfacine (Jurca et al. 2017). Here, we focus on the metal and their complexes' usage in the synthesis of organic compounds mainly drug and drug-like molecules. In addition, we also discuss the medical applications of metals and metal oxides. The usage of metals and their complexes in synthetic organic chemistry can be broadly divided into two main topics – organometallic complexes as catalysts and transition metal alkenylidenes and allenylidenes as catalysts. In the first topic, C–C bond formation with reactions such as transmetalation, reactions occurring at terminal alkynes, reactions involving other carbon nucleophiles, and the C–H bond activation reactions has been discussed. In the next topic, transition metals alkenylidenes and allenylidenes usage in the formation of C–C and C-heteroatom bond has been discussed. These are basically unsaturated carbenes complexed with transition metals. Earlier, it was believed that the metal–carbon double bond was highly stable to undergo chemical reactions, but in the past three decades, extensive work has been carried out on these

metal-complexed carbenes that illustrate their catalytic activity. Easy access to these metal vinylidene complexes from alkynes has made them quite attractive as intermediates for new reaction targets.

9.2   Transition Metal Complexes in Organic Synthesis

Although there are several well-known methods to synthesize organic molecules, the carbon–carbon bond formation is certainly an important reaction in synthetic organic chemistry (Dyker 2008). In particular, there may be hundreds of methods available with the usage of metals or transition metals. In this chapter, we talk about some of the recent advancements in the C–C bond-forming techniques.

9.2.1   Transmetalation

It is the process in which ligands attached to the metal get exchanged with other metal species present. The key step that drives the reaction further in the case of cross-coupling reactions is transmetalation. Suzuki cross-coupling, Stille cross-coupling, and Sonogashira and Negishi cross-coupling reactions are some of the famous transmetalation reactions. The majority of cross-coupling reactions employ Pd-based catalysts to catalyze the reactions. For instance, Cho et al. reported the enantiopure p-bromophenyl methyl sulfoximine synthesis that serves as a key intermediate to synthesize functionalized aryl sulfoximines from p-bromophenyl methyl sulfinate by tuning the reaction condition via Buchwald/Hartwig, Suzuki, and Stille coupling reactions, which are catalyzed by Pd (Gae et al. 2005). Suzuki coupling reaction is the cross-coupling reaction of organic halides with organoboranes, organoboronic acids, and esters (Norio Miyaura 2008; Norio Miyaura and Suzuki 1995). In addition to the most frequently used catalyst Pd $(PPh_3)_4$, the utility of in situ catalysts like $PdCl_2(PPh_3)_2$, $Pd(OAc)_2$, and PPh_3 in the Suzuki coupling reactions was reported recently in good yields (Miyaura 1998). Similarly, the usage of tris(dibenzylideneacetone)dipalladium, $Pd_2(dba)_3$, to produce catalytically active palladium species (Zalesskiy and Ananikov 2012) and polymer-bound palladium catalyst under mild conditions that permit easy separation and reusability more than ten times without the loss of activity was also reported (Jang 1997). Although we can use the bases like $NaHCO_3$, Na_2CO_3, NaOH, or NaOEt–EtOH for coupling, weak bases are used to couple the less sterically hindered aryl boronic acids, whereas the strong bases are used for aryl boronic acids that experience more steric hindrance as the reactivity of sterically hindered boronic acids depends upon the strength of the base (Xiaohong et al. 1999; H. Zhang, Kwong, Tian, & Chan, 1998). The functionalized dienes can be produced by carrying out the cross-coupling reactions with palladium catalyst and organic bases like amines in water with high yield (Dienes et al. 1995). Coleman and Walczak have demonstrated
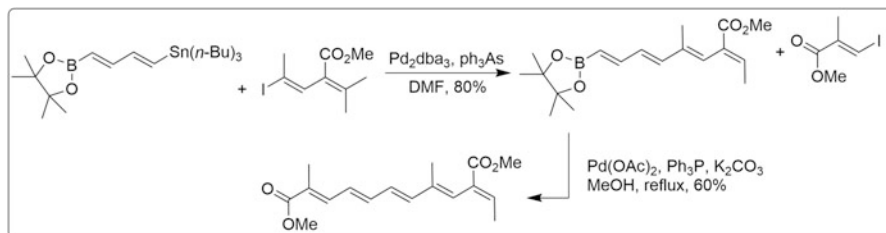
Scheme 9.1 Assembly of lucilactaene pentane side chain (Coleman and Walczak 2005)
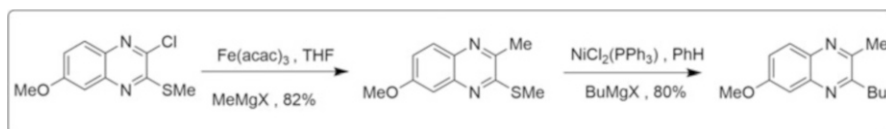
Scheme 9.2 Regioselective synthesis of unsymmetrical quinoxalines (Venkatesh et al. 2005)
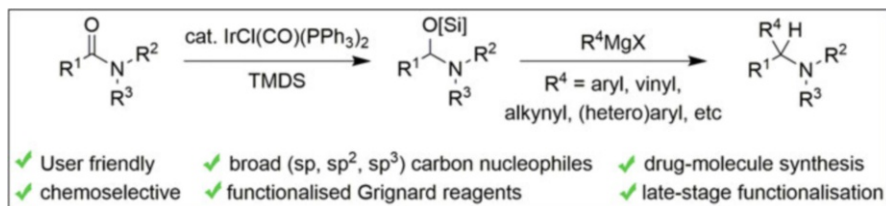
Scheme 9.3 Reductive functionalization of amides (Xie and Dixon 2017)

the one-pot sequential Stille/Suzuki–Miyaura coupling and the application of this method to construct the side chain, pentane chain in the *Fusarium* metabolite lucilactaene (Scheme 9.1) (Coleman and Walczak 2005).

Though Grignard reagents play a vital role in organic synthesis, their application in coupling reactions is not easy on account of their high reactivity towards various functional groups. Like palladium (Pd), nickel (Ni) is often employed as a catalyst in the coupling of Grignard reagents. 3-Chloro-2-thiomethylquinoxalines undergo sequential coupling reaction with Grignard reagent catalyzed by iron and nickel (Scheme 9.2) (Venkatesh et al. 2005).

Xie and Dixon reported the iridium-catalyzed reductive coupling of tertiary amides and Grignard reagents affording tertiary amine (Scheme 9.3) (Xie and Dixon 2017). They have also reported the utility of this reductive coupling for the functionalization of piperine, the psychoactive drug fipexide, and pargyline, a permanent selective monoamine oxidase inhibitor (Fig. 9.1) (Xie and Dixon 2017).

The first enantioselective nickel-catalyzed cross-coupling of α-bromoamides in the presence of organozinc reagents was reported by Fischer and Fu (Scheme 9.4) (Fischer and Fu 2005).
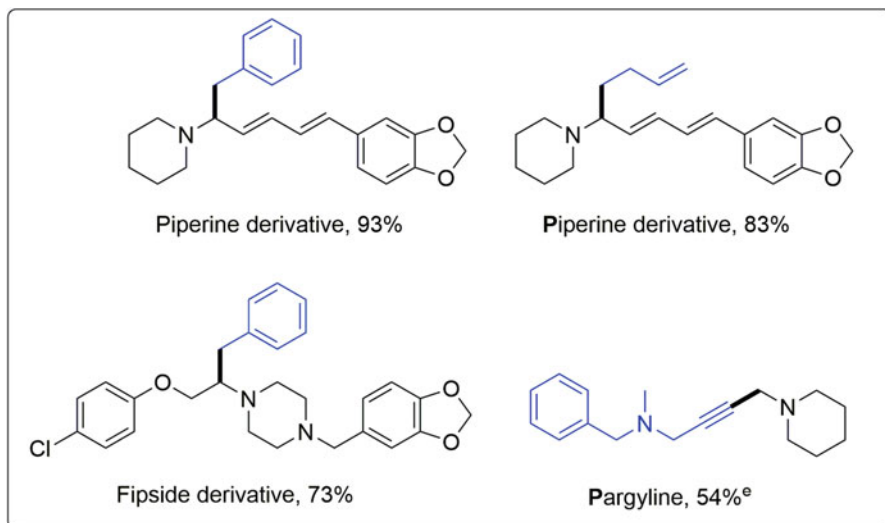
Fig. 9.1 Representative examples of bioactive molecules undergoing reductive functionalization of amides (Xie and Dixon 2017)
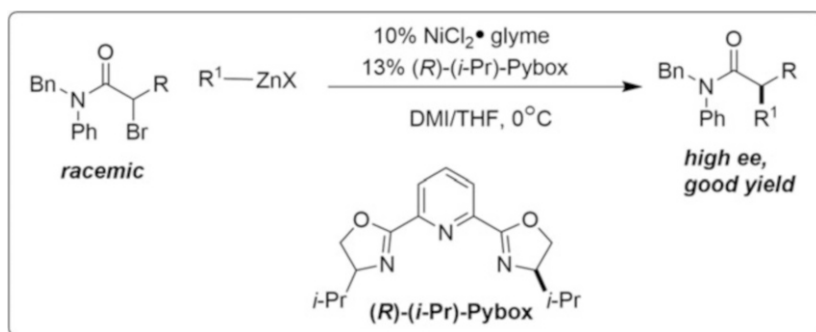
Scheme 9.4 Nickel-catalyzed cross-coupling of α-bromoamides in the presence of organozinc reagents (Fischer and Fu 2005)

Negishi coupling is another transmetalation method to prepare C–C bond with palladium (Pd(0)) as catalyst and zinc (Zn)-based organometal compounds. Although nickel can be used as a catalyst for this coupling, palladium is the most preferred catalyst. The practical applicability of Negishi reactions at an industrial scale is difficult because of the air and moisture sensitivities of organozinc compounds. Scheme 9.5 depicts methodology to produce 1,1-diarylpropadienes and 1,3-diarylpropynes in which the sequential lithiation of arylpropynes, transmetalation, and Pd-catalyzed coupling with aryl iodide by altering the reaction conditions (Ma et al. 2005).
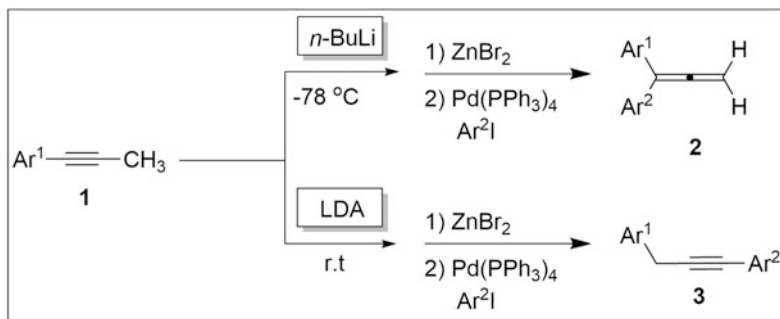
Scheme 9.5 Synthesis of 1,1-diarylpropadienes and 1,3-diarylpropynes (Ma et al. 2005)

Scheme 9.6 Organosilicon-based cross-coupling of aryl and alkenyl iodides (Nakao et al. 2005)

Organosilicon reagents are gaining popularity for cross-coupling reactions because of their stability, nontoxicity, chemoselectivity, and ease of generation and handling. Earlier fluoride activators were used to initiate the reaction, but they are generally expensive and unsuited for numerous functional groups. Highly stable and easily accessible organosilicon reagents like alkenyl- and aryl [2-(hydroxymethyl)phenyl]dimethylsilanes capable of coupling several aryl and alkenyl iodides in the absence of any fluoride activators under mild conditions were reported (Scheme 9.6) (Nakao et al. 2005).

9.2.2 Terminal Alkynes

Sonogashira coupling is the best example of C–C bond formation with terminal alkynes by employing palladium as the catalyst and copper(I) iodide as a co-catalyst with an amine base as solvent (Scheme 9.7) (Schaub and Kivala 2013; Sonogashira et al. 1975).

Figure 9.2 depicts the traditionally accepted mechanism of Sonogashira reaction in which the C–C bond is formed by using the terminal alkynes (Schaub and Kivala 2013). The overall efficiency of this coupling reaction depends on amine base, solvents, copper salt, ligands, and the steric and electronic characteristics of the organohalides and alkyne. Generally, the reactivity of the electron-deficient

Scheme 9.7 Schematic representation of Sonogashira coupling (Schaub and Kivala 2013)

R-X + H $\equiv$ R' $\xrightarrow[\text{Amine base}]{\text{Pd cat., CuI}}$ R $\equiv$ R'

R = aryl, vinyl
R = aryl, alkenyl, SiR$_3$
X = Br, I, OTf
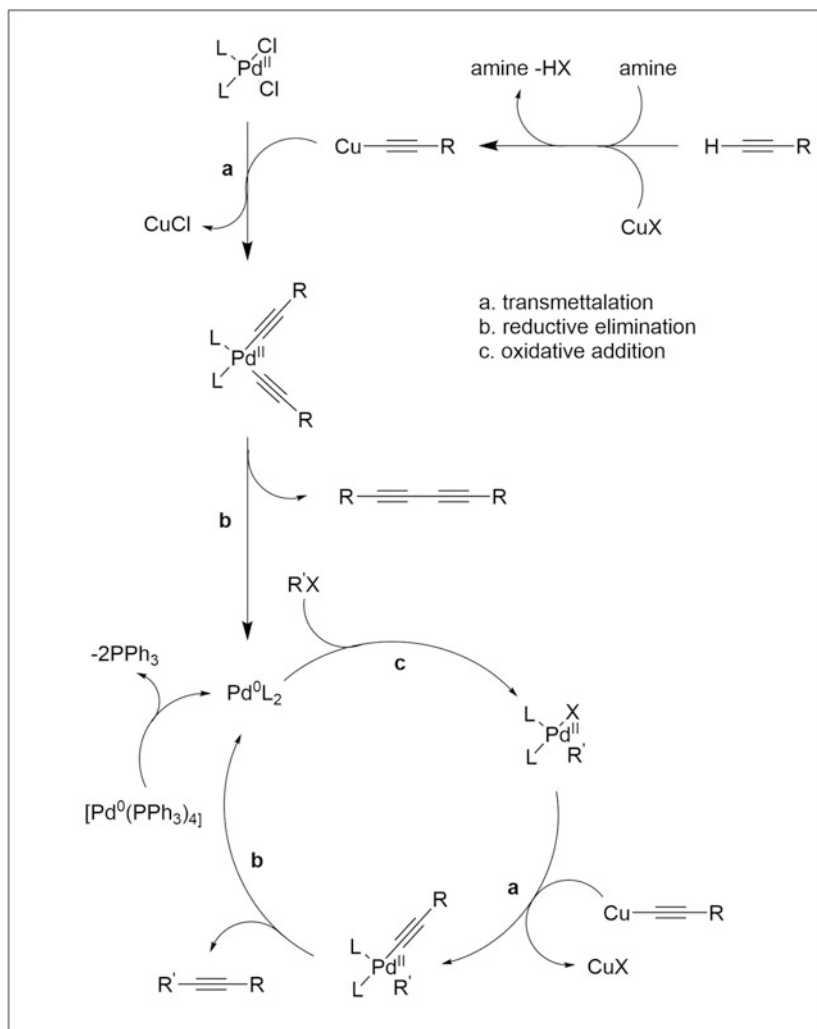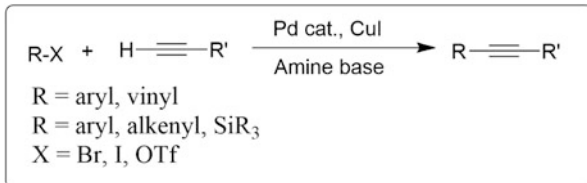
Fig. 9.2 Mechanism of Sonogashira reaction (Schaub and Kivala 2013)
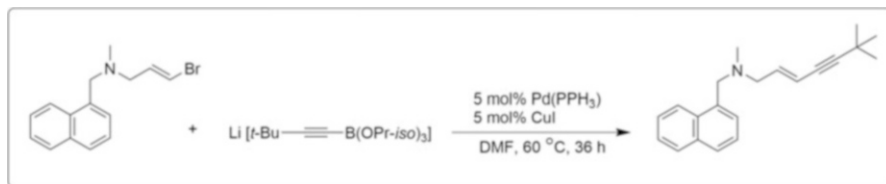
Scheme 9.8 Synthesis of terbinafine, an antifungal agent (Chang Ho Oh and Seung Hyun Jung 2000)
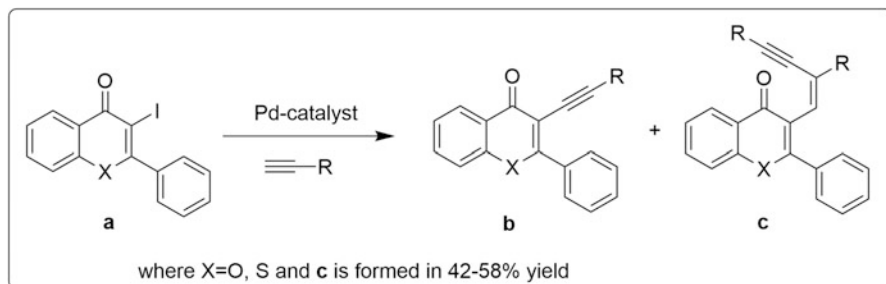
Scheme 9.9 Synthesis of 3-enynyl substituted flavones/thioflavones (Pal et al. 2005)

organohalides is greater than electron-rich organohalides, whereas electron-rich alkynes are more reactive than the electron-deficient alkynes (Schaub and Kivala 2013). Bases like piperidine, pyrrolidine, Et_3N, Et_2NH, and $^{i}Pr_2NH$ are widely used, and the literature survey reveals that the reactivity order for the base is n-$BuNH_2$ > Et_3N > i-Pr_2-NH > Et_2NH > K_2CO_3 and piperidine, pyrrolidine > i-Pr_2-NH (Schaub and Kivala 2013). The literature survey also shows the enhancement of yield with the addition of silver salts like AgI, Ag_2CO_3, $AgNO_3$, AgTf, tetrabutylammonium hydroxide (TBAOH) (room temperature cross-coupling), and tetrabutylammonium iodide (TBAI) (low-temperature cross-coupling) (Schaub and Kivala 2013). We can use $PdCl_2(PPh_3)_2$, $Pd(PPh_3)_4$, $Pd(OAc)_2$, or $PdCl_2$ as palladium catalyst. Initially, in Sonogashira reaction, amine base alone served both as the solvent and base but, but later it was reported that the yield was increased by using a mixture of amine and co-solvents like THF (widely used cosolvent), DMF, NMP, benzene, and toluene (Schaub and Kivala 2013).

The synthesis of terbinafine, an antifungal agent used to treat skin mycoses, was reported by Oh and Jung with a 98% yield. The vinyl bromide was treated with t-butylethynyl(triisopropoxy)borate using $Pd(PH_3)_4$ catalyst and CuI as co-catalyst (Scheme 9.8) (Chang Ho Oh and Seung Hyun Jung 2000).

Copper-free cross-coupling reaction of terminal alkyne with 3-iodo(thio)flavones catalyzed by $Pd(PPh_3)_2Cl_2$ yielded the stereo- and regioselective 3-enynyl substituted flavones/thioflavones (42–58%) which are of biological interest (Scheme 9.9) (Pal et al. 2005). This methodology suited well to introduce enynyl moiety at the C-3 position in flavones/thioflavones irrespective of the ring substituent and terminal

alkynes except for aryl alkynes (Pal et al. 2005). Moreover, syn orientation was observed for the acetylenic and (thio)flavonyl moieties across the double bond (Pal et al. 2005).

9.2.3 Other Carbon Nucleophiles

Recent discoveries have revealed the Pd-catalyzed arylation of the C–H bond in the ortho position of the pyridine and pyrazoles with aryl iodides (Scheme 9.10) (Shabashov and Daugulis 2005).

Similarly, Zaitsev et al. detailed the palladium-catalyzed C–H activation-based arylation process that facilitates β-arylation of the carboxylic acid derivatives and in the case of amine derivatives, γ-arylation method (Scheme 9.11) (Zaitsev et al. 2005).

Owing to the importance of the functionalized azirines in designing the pharmaceuticals, functional synthetics, and bioactive compounds, Sames and co-workers have developed a protocol for site-specific arylation of pyridine. Cross-coupling of iodobenzene with pyridine using phosphido-bridged binuclear ruthenium complexes was reported (Scheme 9.12) (Godula et al. 2005).

Currently, Heck reaction is also very popular for C–C coupling of aryl/vinyl halides with the activated alkenes catalyzed by palladium in the presence of a base.
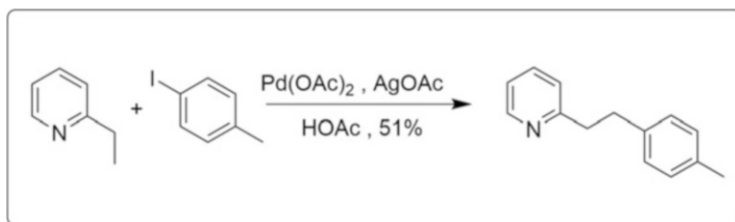
Scheme 9.10 Palladium-catalyzed arylation of pyridines (Shabashov and Daugulis 2005)
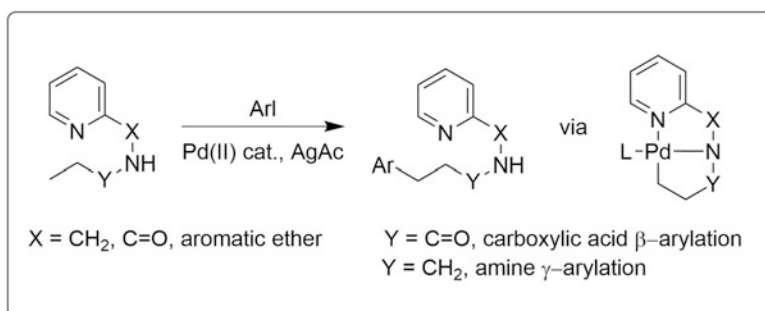
Scheme 9.11 Palladium-catalyzed C–H activation-based arylation process (Zaitsev et al. 2005)
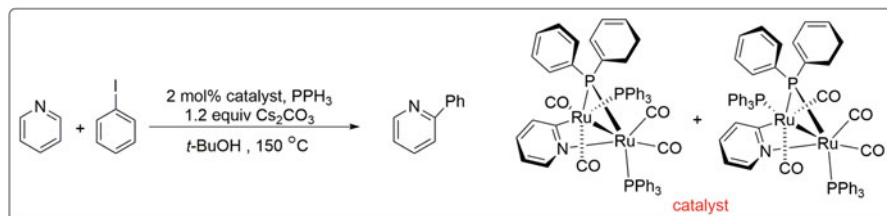
Scheme 9.12 Ruthenium complex-catalyzed cross-coupling (Godula et al. 2005)

R = Me, CH$_2$OR, OMe, CF$_3$, Cl, pyrrolidine

R" = Cl, NHAc, F, OMe

Y = esters, amides, cyano

n = 1, 2

R = Me, CH$_2$OR, OMe

R' = Cl, NHAc, F

R" = H, Me

Y = esters
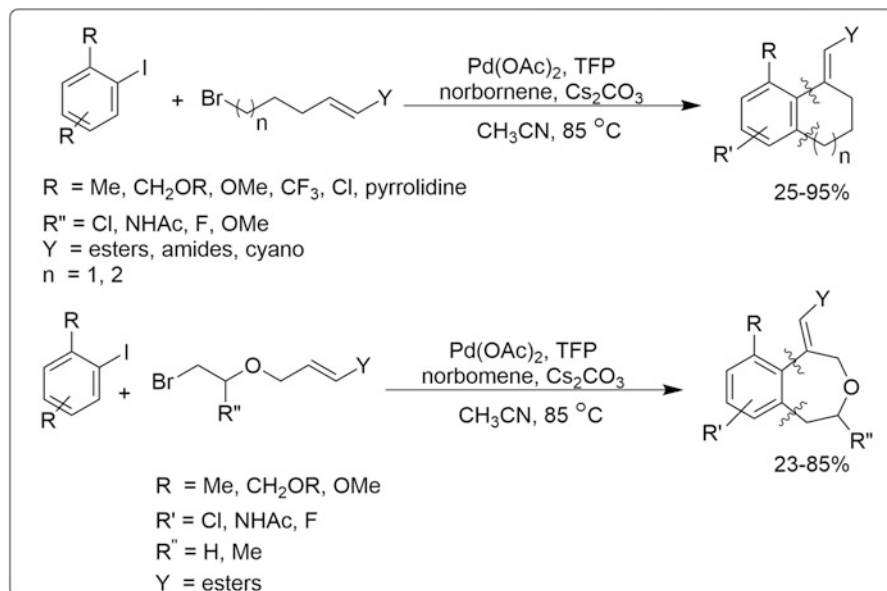
Scheme 9.13 Synthesis of fused aromatic carbocycles and 2,5-disubstituted-4-benzoxepines using Heck reaction (Alberico et al. 2005)

Polycyclic and highly substituted six- and seven-membered fused aromatic and heterocycles were synthesized from aryl iodides and substituted bromoenoates using the Pd(OAc)$_2$ and tri-2-furylphosphine (TFP) in the presence of Cs$_2$CO$_3$ and norbornene (Scheme 9.13) (Alberico et al. 2005).

Some representative examples for natural products synthesized by involving various Heck transformations like intermolecular asymmetric induction, multiple component reactions and domino coupling reaction, palladium-catalyzed heteroannulations, and intramolecular Heck reactions are given in Fig. 9.3 (Jagtap 2017).

Shen has discussed the current applications of C–C cross-coupling in the pharmaceutical industries, various catalysts and coupling reagents employed, and the efficient synthetic methods which can help the medicinal chemist to design and produce a drug moiety in a large scale (Crawley and Trost 2012).
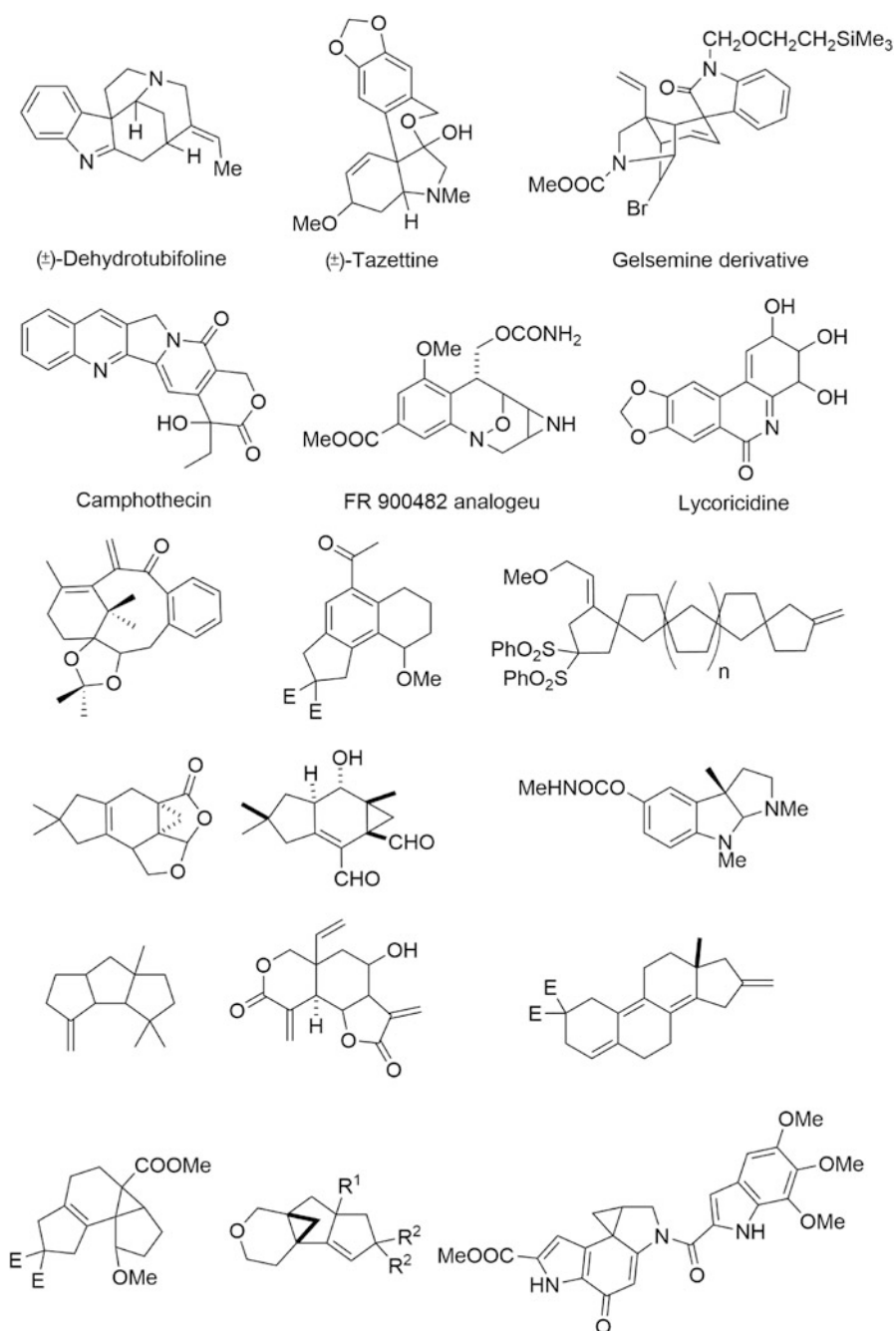
Fig. 9.3 Representative examples of natural products that were synthesized by involving various Heck transformations (Jagtap 2017)

9.2.4 C–H Bond Activation

Generally, the selective C–H bond cleavage accompanied by C–C bond formation plays a vital role during the synthesis of potentially useful compounds from the hydrocarbons. Such a C–H bond cleavage occurs easily in case of acidic C–H bond, but in other cases, it is practically not easy. In 1993, Murai et al. reported ruthenium-catalyzed selective insertion of olefins into specific C-H bond of arene. They reported regiospecific addition of trimethylvinylsilane to the ortho position of phenylmethyl ketone in the presence of ruthenium-based complex as catalyst, $RuH_2(CO)(PPh_3)_3$ (Scheme 9.14) (Murai et al. 1993; Murai et al. 1994; Sonoda et al. 1995).

The applications are not only limited to aromatic compounds but also to α,-β-unsaturated ketones and esters (Scheme 9.15) (Kakiuchi et al. 1995; Trost et al. 1995).

Palladium metal-catalyzed C–H activation has also been reported. Rice and Cai synthesized isomeric benzofluoroanthenes via bis(triphenylphosphine)palladium-
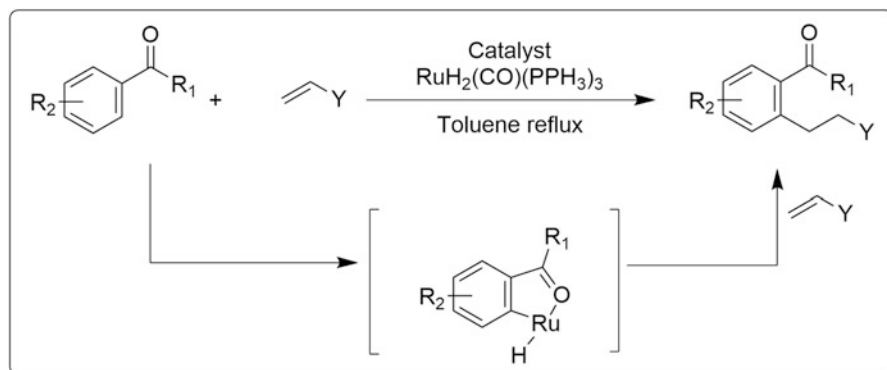
Scheme 9.14 Ru-catalyzed reaction of aromatic ketone with olefins via cyclometallated intermediate (Murai et al. 1993, 1994; Sonoda et al. 1995)
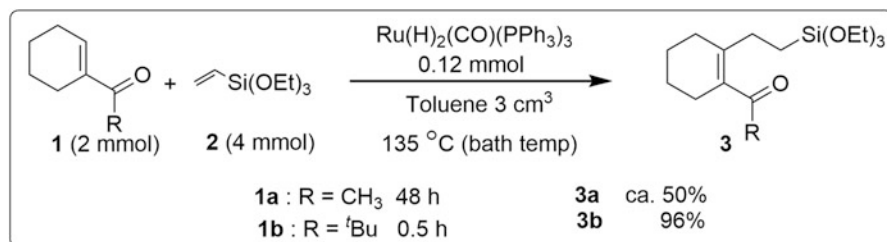
Scheme 9.15 Schematic representation of the catalytic addition of olefinic C–H bonds to olefins (Kakiuchi et al. 1995)

(II) chloride-catalyzed intramolecular triflate–arene coupling reaction (Rice and Cai 1993).

9.3   Transition Metal Alkenylidenes and Allenylidenes as Catalysts in Organic Synthesis

9.3.1   Metal Alkenylidenes (or Vinylidenes)

In the past few years, metal alkenylidene-mediated catalysis has reached tremendous growth in organic synthesis and forms the key step in a number of complex organic syntheses. Generally, the metal alkenylidene can be prepared from the alkynes, and three different pathways have been proposed based on the metal employed (Fig. 9.4) (Roh et al. 2019).

Fenske and Kostić have shown that the ligands in the organometallic complexes undergo nucleophilic addition at the α-carbon atom, whereas with the β-carbon atom, the electrophilic addition occurs (Kostić and Fenske 1982).

Carbon–Heteroatom Bond Formation

Dixneuf and Sasaki reported the ruthenium-catalyzed addition of carbamic acids to terminal alkynes (Roh et al. 2019). The reaction exhibited the anti-Markovnikov selectivity. Metal vinylidene complex generated alkenyl carbamate from terminal alkyne, amine, and carbon dioxide as shown in Scheme 9.16 (Roh et al. 2019). Ruthenium vinylidene formed in the first step from 1-hexyne subsequently undergoes nucleophilic addition at the α-carbon of *N,N*-diethylcarbamate. The alkenyl ruthenium gets protonated to form the carbamate product and the ruthenium
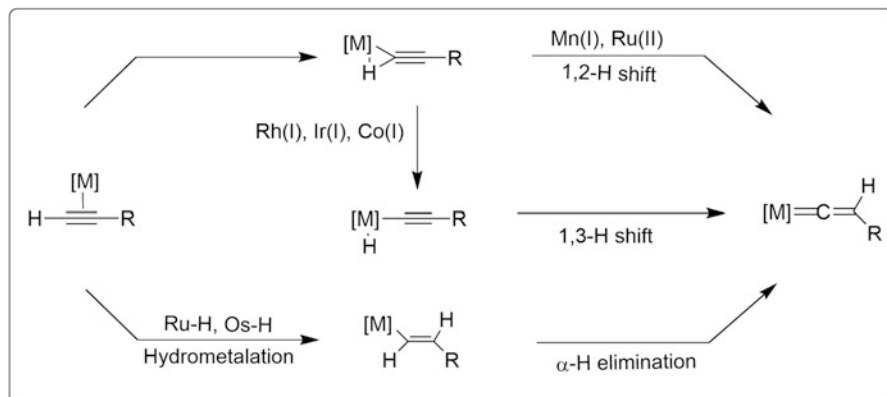
Fig. 9.4 Schematic representation of metal alkenylidene-mediated catalysis (Roh et al. 2019)
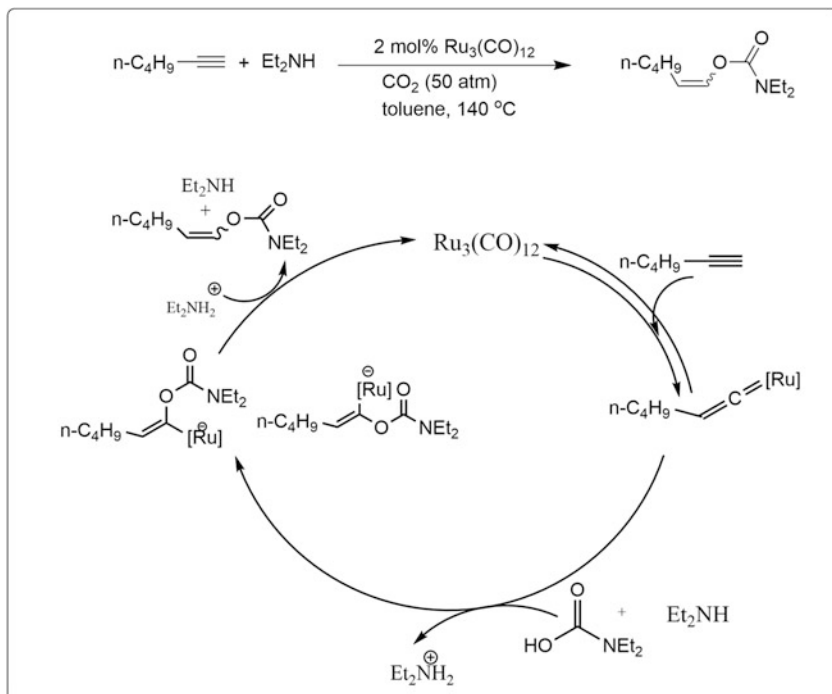
Scheme 9.16 Generation of alkenyl carbamate from terminal alkyne and its mechanism via metal vinylidene intermediate (Roh et al. 2019)

catalyst gets regenerated (Roh et al. 2019). Despite the low yield and E/Z selectivity, this reaction has significance as it revealed that a metal vinylidene can be used as a catalytic intermediate (Roh et al. 2019).

Dixneuf and his group investigated a number of ruthenium complexes such as $RuCl_3\cdot3H_2O$, $RuCl_2(CH_3CN)$(p-cymene), $RuCl_2(pyr)_2(nbd)$, [RuCl $(CH_3CN)_2$(p-cymene)]BF_4, $RuCl_2(PMe_3)$(p-cymene), and $RuCl_2(PMe_3)(C_6Me_6)$ for their effectiveness and observed that $RuCl_2(PMe_3)(C_6Me_6)$ was the most effective (Roh et al. 2019). Just like carbamate addition, metal vinylidene complexes' catalyzed reactions of terminal alkynes with carboxylic acids are also known. Ru (dppb)-catalyzed regio- and stereoselective coupling of carboxylic acids with terminal alkynes yielded Z-alkenyl carboxylates as the predominant product (Scheme 9.17) (Roh et al. 2019; Doucet et al. 1993, 1995).

Similar to ruthenium complexes, rhodium can also be used as a catalyst for the hydro-carboxylation of terminal alkynes. Breit and co-workers reported the efficient and selective anti-Markovnikov coupling carboxylic acids with terminal alkynes using rhodium complexed with P,N-ligand as the catalyst to produce Z-enol in good yields. The catalyst was found to display tolerance to various functional groups and exhibited a broad substrate scope (Scheme 9.18) (Lumbroso et al. 2010; Roh et al. 2019).
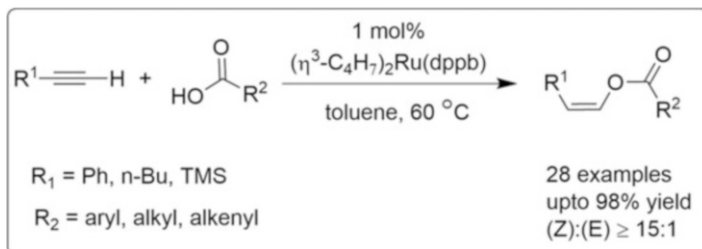
Scheme 9.17 Ruthenium-catalyzed regio- and stereoselective coupling of carboxylic acids with terminal alkynes (Roh et al. 2019; Doucet et al. 1993, 1995)
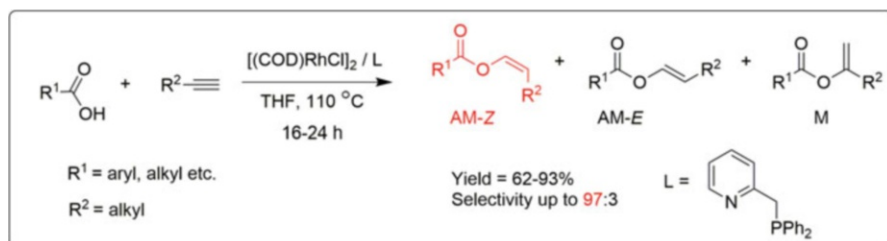
Scheme 9.18 Rhodium complex-catalyzed stereoselective anti-Markovnikov addition of carboxylic acids to terminal alkynes (Markovnikov (M) and/or *anti*-Markovnikov (AM-*Z*, AM*E*) enol esters with high levels of regio- and stereocontrol) (Lumbroso et al. 2010; Roh et al. 2019)

Organic synthesis employing water as a reagent has received much significance because of its cheapness, safety, and eco-friendliness. Wakatsuki and Tokunaga reported first the ruthenium(II) complex-catalyzed selective anti-Markovnikov hydration of terminal alkyne to yield aldehydes as the major product and ketones as the minor product (Tokunaga and Wakatsuki 1998). It was later revealed that the ruthenium complex, RuCpCl(dppm) (2–10 mol%), excellently catalyzes this hydration reaction performed at 100 °C in 2-propanol and yielded regioselectively 95% aldehyde product (Scheme 9.19) (Suzuki et al. 2001). The anti-Markovnikov hydration pathway was identified from the formation of ruthenium vinylidene which is in equilibrium with π-complex (Roh et al. 2019; Suzuki et al. 2001).

Carbon–Carbon Bond Formation

A nucleophilic carbon atom can also add to the electrophilic center of the metal vinylidene like the nucleophilic heteroatom. In 1997, McDonald and Olson synthesized 1.1-disubstituted-2-cyclopentenes via the molybdenum complex-catalyzed coupling of terminal alkyne with β-dicarbonyls (Scheme 9.20) (McDonald and Olson 1997).

Takai and co-workers reported the rhenium complex-catalyzed intermolecular anti-Markovnikov coupling of nucleophilic carbon with unactivated terminal
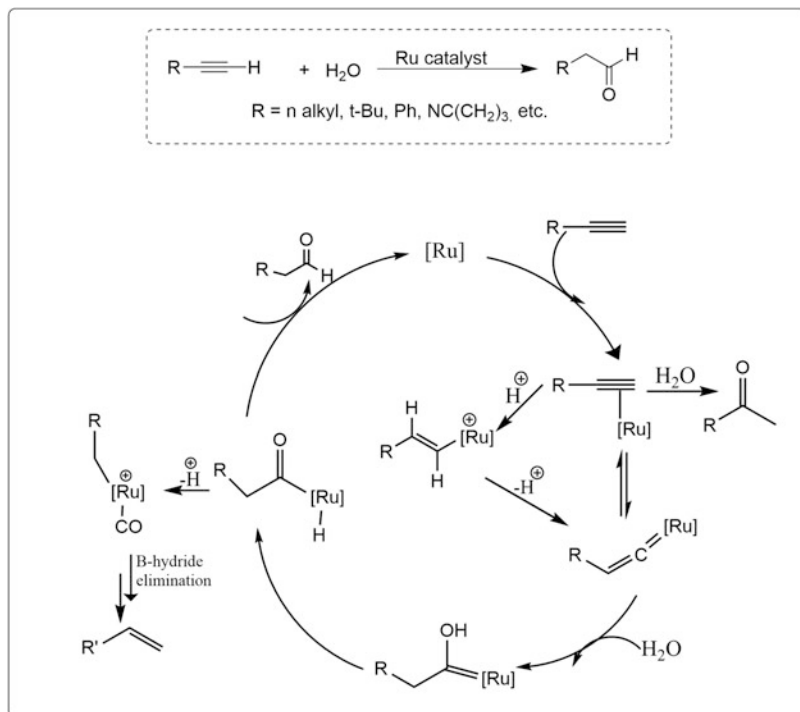
Scheme 9.19 Ruthenium complex-catalyzed anti-Markovnikov hydration of terminal alkyne (Roh et al. 2019; Suzuki et al. 2001)

alkynes under neutral condition via the metal vinylidene intermediate (Scheme 9.21) (Hori et al. 2015).

Trimethyl methanetricarboxylate and 2-phenylmalonate gave good yields with 1-dodecyne, 92% and 52% (Hori et al. 2015). Terminal alkynes undergo rhodium-catalyzed hydrocyanation with acetone cyanohydrins when used as an alternative to HCN and yielded anti-Markovnikov acrylonitriles with *E*-configuration for both aromatic and aliphatic substrates (Ye et al. 2017). Anti-Markovnikov to Markovnikov product (a-M:M where M = Markovnikov; a-M = anti-Markovnikov) was found to increase from 9:1 to 20:1 on changing the alkyl substituent in terminal alkyne from cyclohexane to cyclohexyl and was observed to increase further (a-M: M > 20:1) for *t*-butyl substituent in terminal alkyne (Scheme 9.22) (Ye et al. 2017).

As the electrocyclization of less reactive metal vinylidene intermediates followed by subsequent reductive elimination can be used to synthesize substituted arenes, Merlic group reported the ruthenium-catalyzed 6π-electrocyclization of metal vinylidene that is suitable for the synthesis of biologically relevant molecules (Scheme 9.23) (Merlic and Pauly 1996).

Ruthenium-catalyzed cycloisomerization of 2,2′-ethynylbiphenyls to 9-ethynylphenanthrenes at room temperature occurs via the [2 + 2] cycloaddition
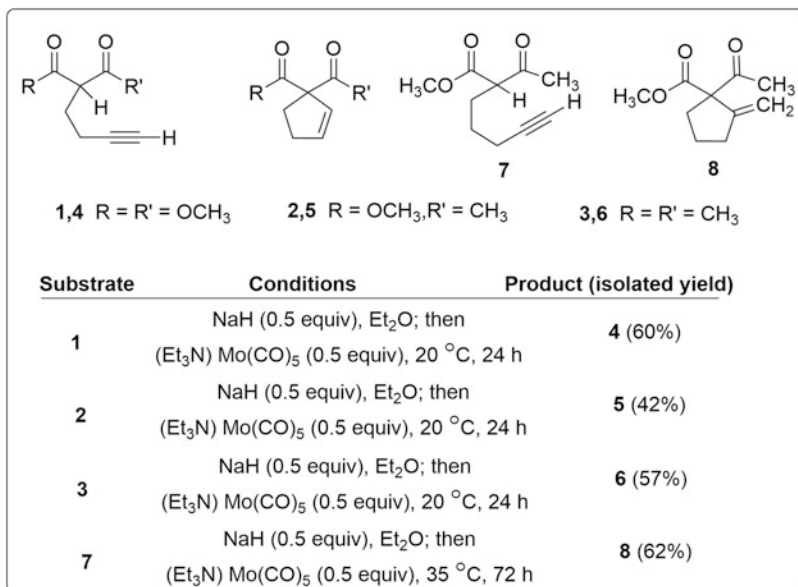
Scheme 9.20 Molybdenum promoted *Endo*-carbocyclization (McDonald and Olson 1997)
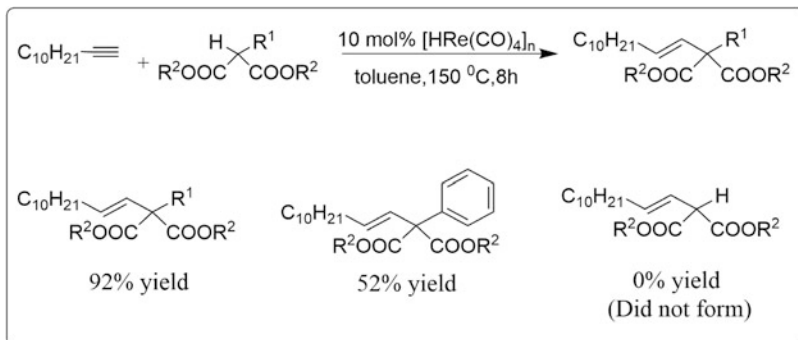
Scheme 9.21 Re-catalyzed ant-Markovnikov addition (Hori et al. 2015)

of the $C_\alpha = C_\beta$ bond of the ruthenium vinylidene intermediate with the pendent alkyne affording cyclobutene that subsequently undergoes cycloreversion and decomplexation to produce a new ethynyl group at the 9-position of the phenanthrene (Scheme 9.24) (Matsuda et al. 2016).

Ohe and co-workers have established chromium- or tungsten-triggered valence isomerization of the pi bonds of the cyclopropane-tethered ketoalkyne via [3,3]-sigmatropic rearrangement to give phenol in good yield (Ohe et al. 2002) (Scheme 9.25).
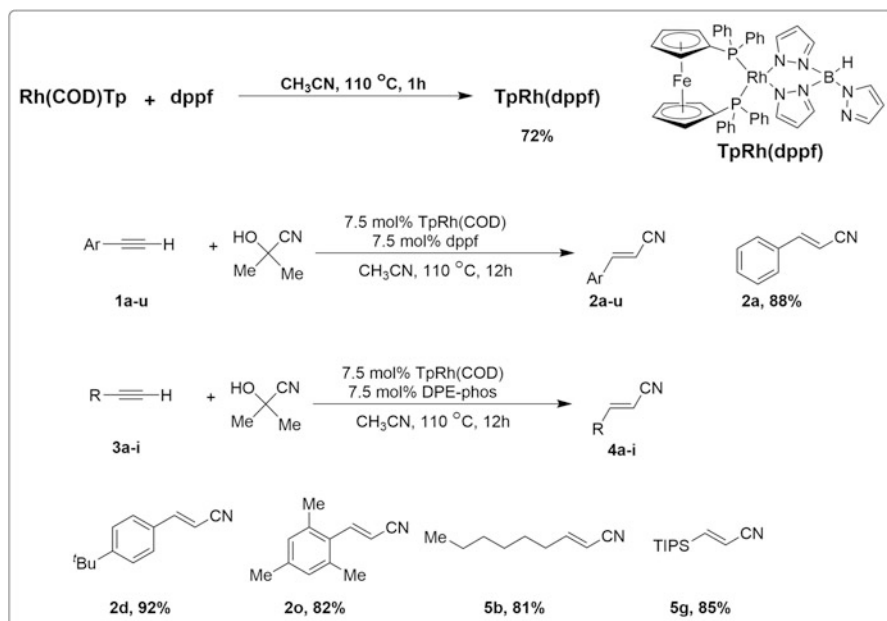
Scheme 9.22 Rhodium-catalyzed anti-Markovnikov hydrocyanation of terminal alkynes (Ye et al. 2017)
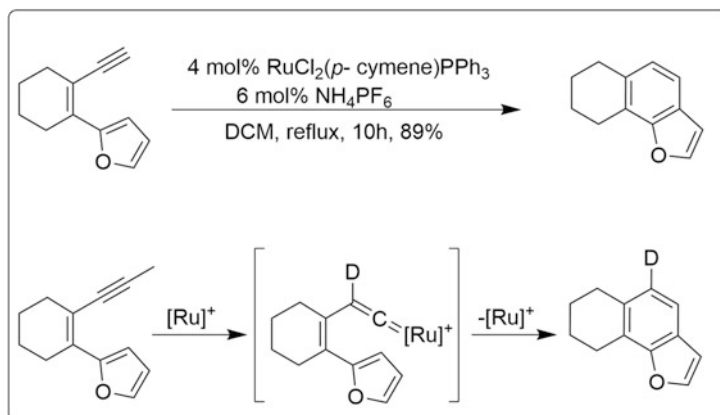
Scheme 9.23 Ruthenium-catalyzed 6π-electrocyclization of metal vinylidene intermediates (Merlic and Pauly 1996)
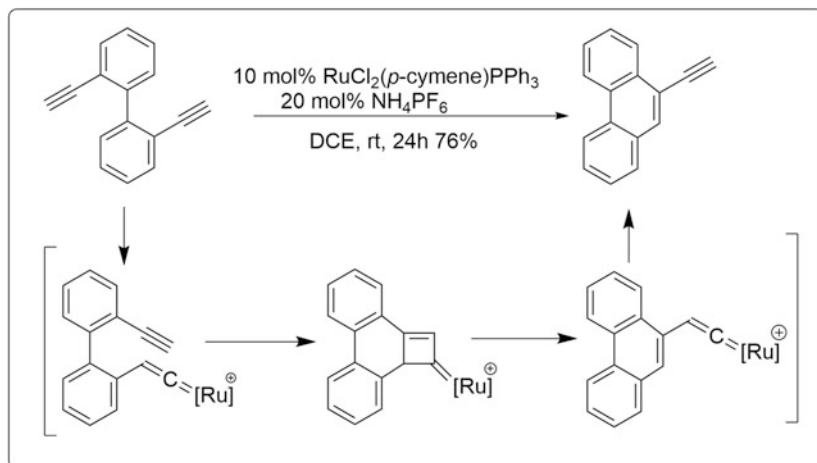
Scheme 9.24 [2 + 2] cycloaddition and cycloreversion (Matsuda et al. 2016)
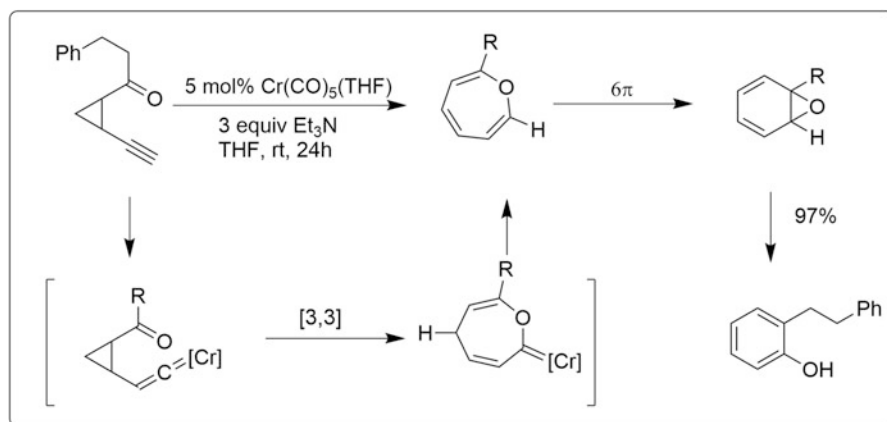
Scheme 9.25 [3,3]-Sigmatropic rearrangement from alkynyl ketones (Ohe et al. 2002)

9.3.2   Metal Allenylidene Complexes

Allenylidene is a class of unsaturated carbenes consisting of two cumulated double bonds, as opposed to a single double bond in alkenylidenes. They can be prepared from metal vinylidene intermediates (Scheme 9.26). Esteruelas and co-workers showed that the reaction of cyclopentadienyl ruthenium-based complex, [Ru $(\eta^5C_5H_5)\{\eta^1\text{-}OC(CH_3)_2\}(CO)(PPr^i{}_3)]BF_4$, with alkyn-1-ols yielded α,β-unsaturated hydroxy carbenes via the formation of ruthenium allenylidene complex intermediate (Esteruelas et al. 1996).
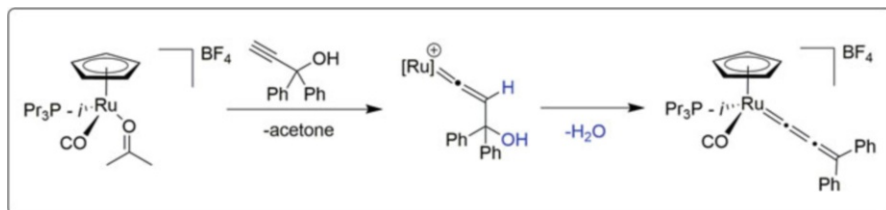
Scheme 9.26 Allenylidene complex preparation from propargyl alcohol (Roh et al. 2019; Esteruelas et al. 1996)
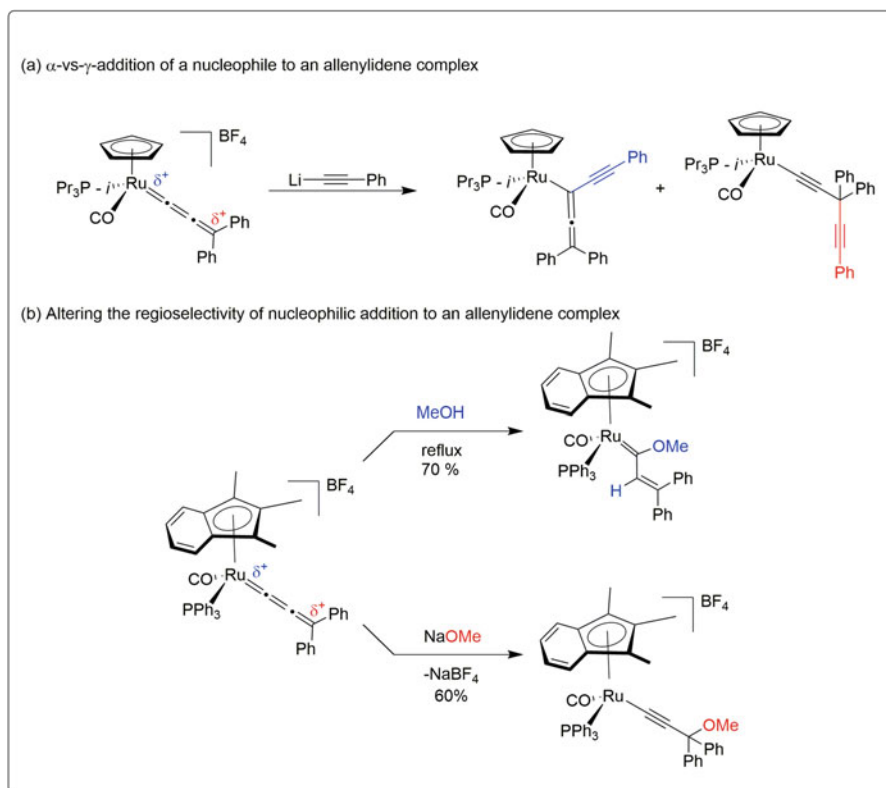
Scheme 9.27 Nucleophilic addition can take place at both the α- and the γ-positions of allenylidene complexes (Roh et al. 2019; Esteruelas et al. 1997; Pilar Gamasa et al. 1997)

The reactivity of allenylidene complexes is quite analogous to alkenylidene complexes. As the α- and γ-positions of allenylidene complexes are electrophilic, the nucleophilic addition can take place at both the α- and the γ-positions of allenylidene complexes, whereas electrophile can add to the nucleophilic β-position (Roh et al. 2019; Esteruelas et al. 1997; Pilar Gamasa et al. 1997). As shown in Scheme 9.27, the reaction of ruthenium allenylidene with a lithium
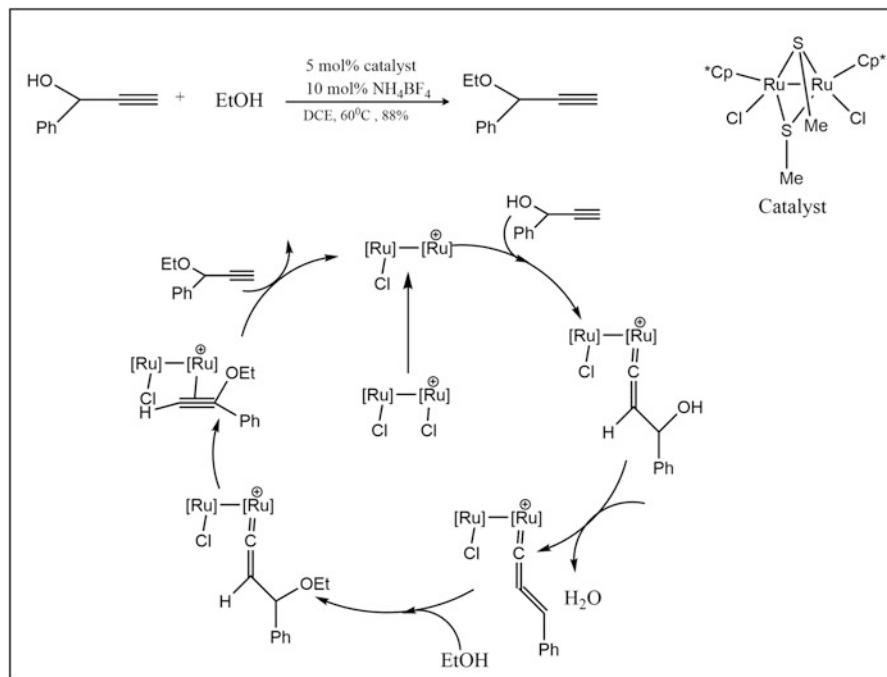
Scheme 9.28 Propargylic substitution using alcohol nucleophiles (Roh et al. 2019; Ammal et al. 2005)

acetylide gave a mixture of α- and γ-adduct, whereas different products (α- or γ-product) are obtained in the reaction of trimethylindenylruthenium allenylidene with methanol/sodium methoxide. Methanol gave an α-addition, while γ-product was formed with methoxide (Roh et al. 2019; Esteruelas et al. 1997; Pilar Gamasa et al. 1997).

Owing to the enhanced activation of substrates by the polynuclear metal complexes compared to mononuclear metal complexes, Hidai and co-workers reported the synthesis of a series of thiolate-bridged diruthenium complexes suitable for catalytic transformations of terminal alkynes (Nishibayashi et al. 2000). The applicability of thiolate-bridged diruthenium catalyst [Cp*RuCl(μ$_2$-SMe)]$_2$ to afford propargylic derivatives by regioselective nucleophilic substitution of the propargylic alcohols was explored (Nishibayashi et al. 2000, 2005). They have explored the bimetallic effect, scope of diruthenium complex in catalyzing the heteroatom-centered nucleophilic substitution of propargylic alcohols, and their limitations (Nishibayashi et al. 2005; Ammal et al. 2005). The proposed mechanism in the diruthenium complex reaction with propargylic alcohol involves the vinylidene complex formation which then gets dehydrated to form allenylidene complexes that are attacked by the nucleophile like alcohol, amine, and thiol on C$_\gamma$ atom to form vinylidene complex which is shown in Scheme 9.28 (Ammal et al. 2005). This complex isomerizes to form a π-complex from which the product formation and catalyst regeneration occur (Ammal et al. 2005). It has been showed using in silico
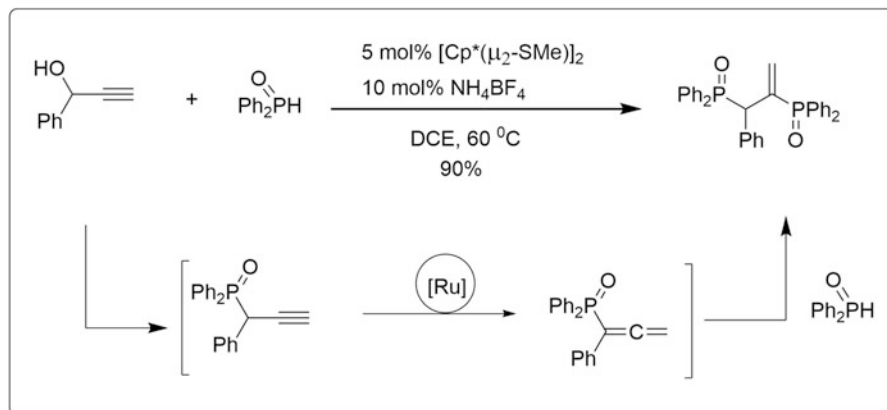
Scheme 9.29 Phosphinylation of propargylic alcohols with diphenylphosphine oxide (Roh et al. 2019; Nishibayashi et al. 2005)
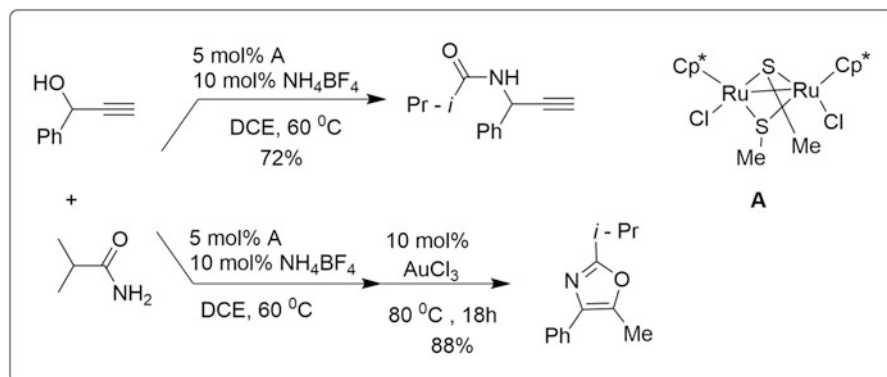
Scheme 9.30 Propargylic amidation of propargyl alcohol (Roh et al. 2019; Nishibayashi et al. 2005)

experiments that Ru–Ru bond of the catalyst greatly decreases the activation energy barrier of the catalytic steps (Ammal et al. 2005).

Phosphorous- and nitrogen-centered nucleophilic substitution of various propargylic alcohols using the same thiolate-bridged diruthenium catalyst, [Cp*RuCl(μ₂-SMe)]₂, has also been reported (Scheme 9.29) (Roh et al. 2019; Nishibayashi et al. 2005). A good yield of bisphosphinylated product is obtained when the dinuclear ruthenium-catalyzed phosphinylation of propargyl alcohol was carried out at 60 °C, whereas at 25 °C this reaction afforded monophosphinylated product in good yield (Roh et al. 2019; Nishibayashi et al. 2005).

Similarly, the ruthenium-catalyzed amidation/amination of propargyl alcohol with the nitrogen-centered nucleophiles such as carboxamides, sulfonamide, and arylamines was also reported. Scheme 9.30 shows the representative example of the amidation of propargylic alcohol (Roh et al. 2019; Nishibayashi et al. 2005).
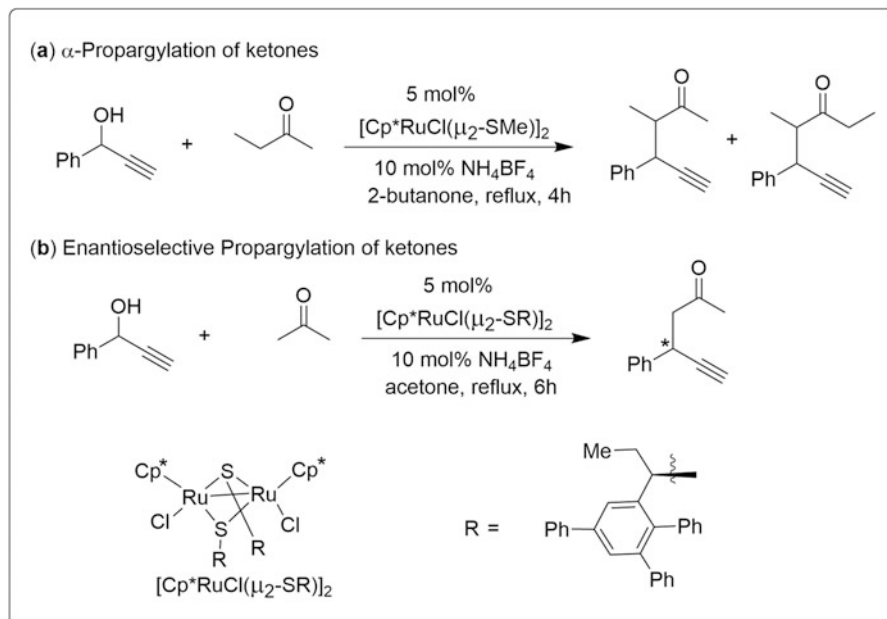
Scheme 9.31 Thiolate-bridged diruthenium-catalyzed regioselective propargylation of ketone (Nishibayashi et al. 2001)

The use of metal allenylidene as catalyst in carbon–carbon bond formation was first reported by Hidai group (Scheme 9.31) (Nishibayashi et al. 2001). They have shown that simple dialkyl ketone such as acetone and 2-butanone can also be used to form regioselective alkynylketones upon refluxing propargylic alcohol by employing diruthenium complex, $[Cp*Ru(\mu_2\text{-}SMe)Cl]_2$, catalysts to afford the product in good yield (Nishibayashi et al. 2001).

Excellent amount of highly diastereoselective oxypropargylation of alkenes using the propargylic/simple alcohols and ruthenium complex as catalyst is found to occur via ruthenium allenylidene as intermediate (Yamauchi et al. 2009). Nishibayashi and co-workers have shown the oxypropargylation of ethyl vinyl ether with 1-Phenyl-2-propyn-1-ol in the presence of ethanol using the ruthenium complex, $[Cp*Ru(\mu_2\text{-}SMe)Cl]_2$, via the ruthenium allenylidene intermediate (Scheme 9.32) (Yamauchi et al. 2009).

Propargylic alcohols undergo reductive coupling reaction in the presence of diruthenium catalyst leading to an excellent yield of 1,5-hexadiynes via the ruthenium allenylidene intermediates (Scheme 9.33). In this reaction, initially the hydroboration occurs at the $C_\beta = C_\gamma$ bond-generated ruthenium allenylidene intermediate that initiates successive radical reactions leading to the formation of homocoupled product (Onodera et al. 2006).
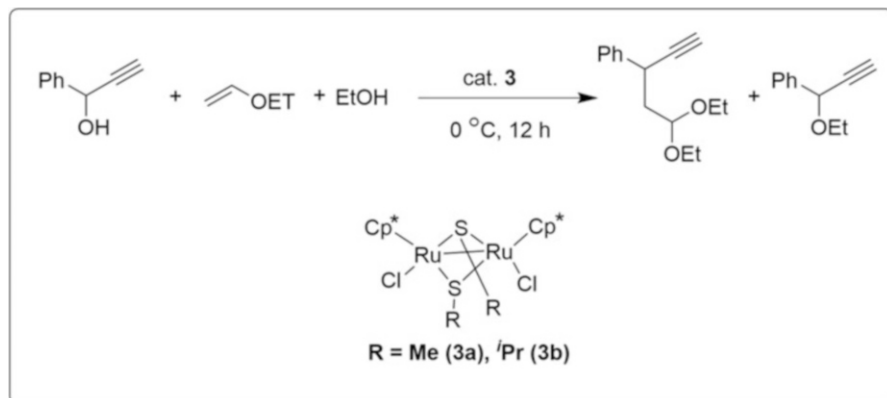
Scheme 9.32 Oxypropargylation of ethyl vinyl ether with 1-Phenyl-2-propyn-1-ol (Yamauchi et al. 2009)
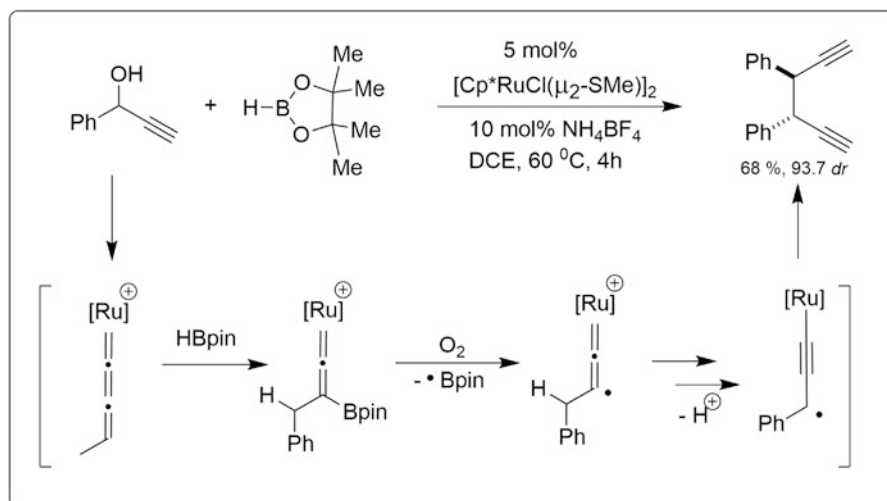
Scheme 9.33 Dimerization of propargyl alcohol (Onodera et al. 2006)

9.4 Applications of Metal Oxides

The interest towards the design and synthesis of metal oxides of suitable size and morphology has increased significantly because of the increased thermal conductivity, improved catalytic activity, nontoxicity, excellent antibacterial activity, and versatility of metal and metal oxide nanomaterials. In recent years, the use of metal and metal oxide nanoparticles in the detection and drug delivery application has increased tremendously as the size and hence the properties of the nanoparticles can be tuned (Yadavalli and Shukla 2017). Hence, various metal and metal oxide

nanoparticles have been designed and implemented as antimicrobial coatings, for wound healing, and to treat various diseases like cancers and antibacterial infection. Here we discuss the applications of few metal oxides in the field of medicine.

9.4.1 Iron Oxide

Iron is a transition metal whose oxide is widely used in biomedical applications. Generally, the efficiency of the drug is limited by factors such as systemic toxicities, poor availability of the drug at the target area, and the random distribution of drug molecules in healthy cells leading to the side effects. These drawbacks necessitate the need for nanocarrier for target-specific delivery. Superparamagnetic iron oxide nanoparticles (SPIONs) are extensively used as drug carriers, biosensors, imaging, and targeted therapeutic agent because of their unique properties like inertness, less toxicity, biocompatibility, and potent catalytic and magnetic behavior (Yadavalli and Shukla 2017; Zhang et al. 2013). As these nanoparticles can be guided magnetically to the desired place, it is suitable for magnetic resonance imaging (MRI) and magnetic hyperthermia (Janko et al. 2019). Figure 9.5 depicts the various applications of iron oxide nanoparticles.

- *Use of iron oxide nanoparticles for pancreatic cancer*

Pancreatic ductal adenocarcinoma (PDAC) is a cancer with unmet medical needs. Abundant expressions of the anti-phagocytosis signal CD47 have also been observed in pancreatic cancer cells, in particular, a subset of cancer stem cells (CSCs) responsible for resistance to standard therapy and metastatic potential (Hoskins 2014). The CD47 receptor is found on pancreatic cancer and highly expressed on cancer stem cells, but not on the normal pancreas. Inhibiting CD47 using monoclonal antibodies has been shown as an effective strategy to treat
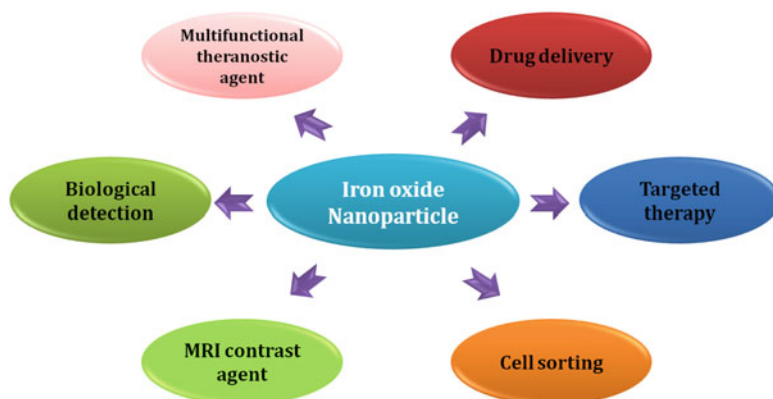
Fig. 9.5 Potential applications of iron oxide nanoparticle in various fields (Hoskins 2014)

pancreatic ductal adenocarcinoma in vivo (Hoskins 2014). Thus, CD47 inhibition effectively slowed tumor growth only in combination with gemcitabine or Abraxane. Chauhan and co-workers have developed superparamagnetic iron oxide nanoparticle formulation of curcumin and demonstrated efficiency of superparamagnetic iron oxide nanoparticles formulation of curcumin in delivering the bioactive, nontoxic curcumin to pancreatic cancer cells (Hoskins 2014; Khan et al. 2019).

- *Iron oxide usage for magnetic hyperthermia*

The external magnetic field enables the magnetic nanoparticles to serve as thermal seeds that are suitable for targeted magnetic hyperthermia treatment of cancers (Chang et al. 2018). Generally, hyperthermia is referred to as the mild elevation of body temperature (40–43 $^\circ$C) inducing the death of cancer cells and enhances the effect of radiotherapy and chemotherapy (Chang et al. 2018). The practical difficulty occurring in this method of treatment is its difficulties to heat preferentially the tumor cells. As the iron oxide nanoparticles can produce heat by absorbing magnetic energy, the generated heat can be used effectively to elevate the temperature in tumors and combat them. This kind of targeted approach helps in heating the malignant cells without affecting healthy cells. Iron oxides like magnetite (Fe_3O_4) and maghemite (γ-Fe_2O_3) are commonly used as materials for magnetic hyperthermia. A combination of magnetite (Fe_3O_4) and maghemite (γ-Fe_2O_3) forms the magnetic iron oxide nanoparticles (MIONs), and the existence of crystal structure comprising multivalency for the ions contributes significantly for their magnetic properties (Chang et al. 2018).

- *Usage of iron oxide as a delivery agent in chemotherapy*

Chen and co-workers have developed doxorubicin-loaded human serum albumin-coated iron oxide nanoparticle (D-HINPs) to deliver doxorubicin in a sustained fashion. They have also shown that doxorubicin-loaded human serum albumin-coated iron oxide nanoparticle can suppress the tumor significantly. Moreover, they have shown that human serum albumin-coated iron oxide nanoparticle can be used as theranostic nanoplatform by delivering small molecules (Quan et al. 2011). Tietze et al. have discussed the use of superparamagnetic iron oxide nanoparticles for conjugating drugs and their subsequent release with the application of an external magnetic field (Tietze et al. 2015). El-Boubbou has emphasized the significance of past and present magnetic formulations that were used as medical theranostics (El-Boubbou 2018).

Owing to the importance of self-healability and stimuli-responsive character in designing and constructing the smart materials, Nagarajan and co-workers have synthesized simple fluorescent self-assembled molecular gelators using the renewable resource as cashew nut shell liquid (CNSL) (Scheme 9.34) to construct a self-healing magnetic stimuli-responsive gel by encapsulating Fe_3O_4 nanoparticle in situ into the organogel by a simple process.

They have investigated the self-assembly mechanism based on the molecular structure of the gelator. Rheological investigations confirmed the stability, mechanical strength, and self-healing behavior of the magnetic gels. This magnetic stimuli-
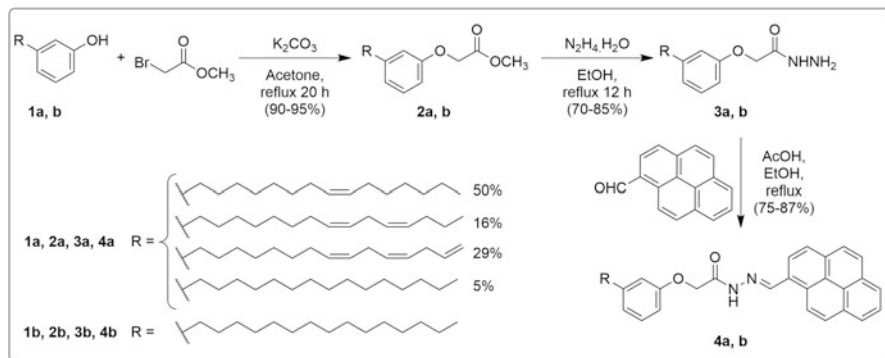
Scheme 9.34 Synthesis of π-gelators

responsive self-healing gel might potentially suitable for environmental, electronic, biological, and medical applications.

9.4.2 Titanium Oxide

Though titania (TiO_2) ranks second among the most abundantly consumed nanoparticle with potential applications like food additive, sunscreens, photovoltaic, and environmental scavenger because of its less toxic nature, the usage of titania for medical application is not explored completely (Rehman et al. 2016). Literature reveals that the usage of titania begins with investigation of photodynamic therapeutic properties of titania in killing cancer cells and the nano-titania coating over medical implants (Cai et al. 1991; Fujishima et al. 1993; Ellingsen 1991). As titania is a very good photo-redox catalyst, photo-irradiation of TiO_2 particles initiates various chemical reactions leading to the formation of radicals such as hydroxy and per hydroxy radicals and kills the cancer cells (Cai et al. 1991; Fujishima et al. 1993). On comparing the adsorption of human serum protein on titania surface and hydroxyapatite surface (Ellingsen 1991), Ellingsen revealed that titania surface exhibited a similar calcium-binding mechanism that is exhibited by hydroxyapatite (Ellingsen 1991). Figure 9.6 shows the various applications of nano-titania (Rehman et al. 2016).

Photodynamic therapy is a treatment that utilizes photosensitizing agents that are nontoxic and get activated or "turned on," on exposure to certain light to kill cancer cells. Excitation of the photosensitizer occurs by the absorption of photons from the visible light source and produces singlet oxygen and reactive oxygen species by transferring energy to oxygen molecules. Owing to the advantages of photodynamic therapy such as nontoxicity, cost-effectiveness, higher safety, and zero complications compared to conventional cancer treatment, the photodynamic therapy is most

Fig. 9.6 Pictorial representation of the applications of nano-titania, TiO$_2$, in various fields (Rehman et al. 2016)

efficient for the vital organs like the brain, head, and neck, pulmonary tissues, pancreas, and bladder (Rehman et al. 2016).

9.4.3 Zinc Oxide

Zinc (symbol, Zn) is a silvery-white transition metal with many beneficial applications. Zinc oxide topical (for the skin) is used to treat severely chapped skin, diaper rashes, and other minor skin irritations. Zinc is most commonly used to galvanize, coating molten zinc over the surface of other metals such as iron or steel in order to create a protective coating that prevents rusting. Some of the important applications of zinc oxide (ZnO) are depicted in Fig. 9.7 (Barui et al. 2018).

As nanocomposite can afford cost-effective thin layers suitable for drug delivery, antimicrobial, and microelectronic applications, Jacob and co-workers reported the eco-friendly zinc oxide/polymer nanocomposite thin film formation by co-depositing the polymer derived from geranium oil with zinc nanoparticles that are produced by decomposing zinc acetylacetonate thermally (Al-Jumaili et al. 2019). This eco-friendly zinc oxide/polymer nanocomposite thin film can be used as the encapsulation coating for medical devices because of its capability to release zinc oxide that inhibits the adhesion and colonization of microbes (Al-Jumaili et al. 2019). In recent years, the development of multidrug-resistant bacterial strain has
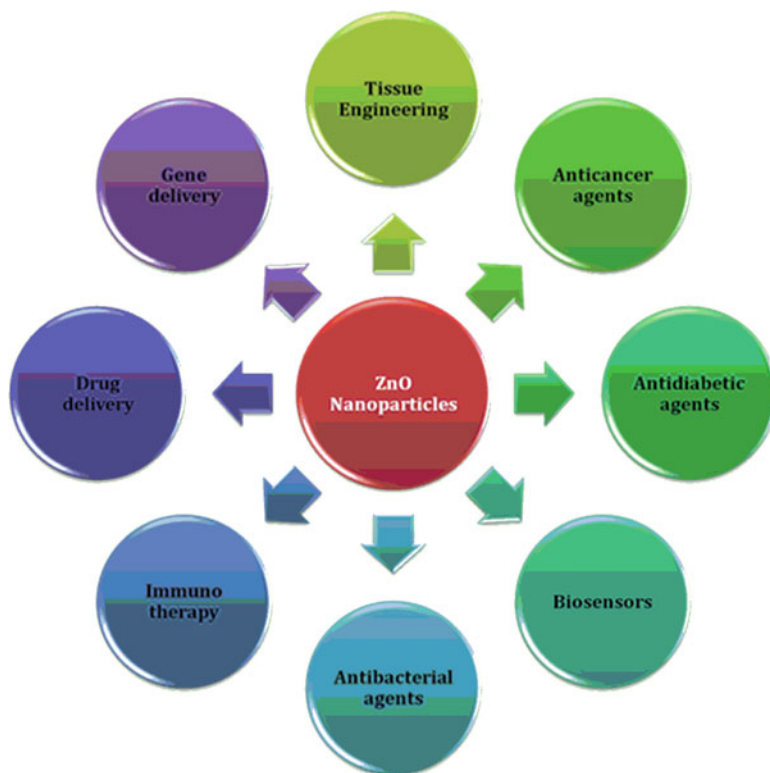
Fig. 9.7 Pictorial representation of the applications of zinc oxide nanoparticles in the field of medicine, sensing, and biology (Barui et al. 2018)

created an enormous demand for alternative antimicrobial treatments. Nitric oxide (NO) is a gaseous molecule with potent antimicrobial activity, and *S*-nitrosoglutathione serves as the natural nitric oxide carrier possessing long storage stability upon mixing with Vaseline at 24 °C (Doverspike et al. 2019). Nitric oxide release from *S*-nitrosoglutathione/Vaseline mixture can be triggered by using zinc oxide particles (Fig. 9.8) (Doverspike et al. 2019).

9.4.4 Copper Oxide

Copper oxide (CuO) is one among the smart transition metal oxides with high surface area, excellent electrochemical activity, redox potential, and high stability in solutions. Like other transition metal oxides, copper oxide nanoparticles such as CuO, Cu_2O nanoparticles, and their nanocomposites have gained much attention because of their wide usage as antibacterial agent, gas sensor, solar cells, catalysis, biocides, antifouling paints, magnetic storage media, and semiconductors in electronics (Grigore et al. 2016). Verma and Kumar have discussed the various synthetic
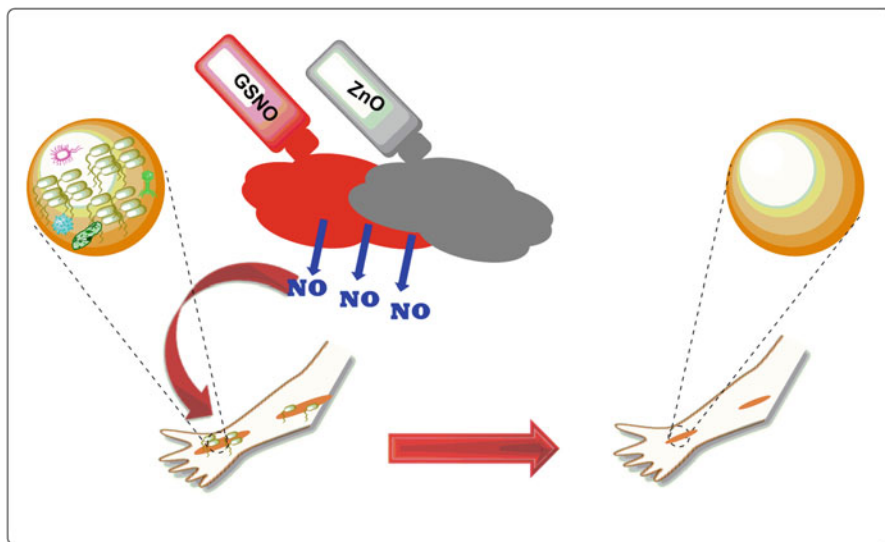
Fig. 9.8 Schematic representation of zinc oxide (ZnO) triggered nitric oxide (NO) release from *S*-nitrosoglutathione (GSNO)/Vaseline mixture modified after (Doverspike et al. 2019)

approaches to produce copper oxide nanoparticles of tunable size and investigated the physicochemical properties and their role in biomedical applications (Fig. 9.9).

9.4.5 Other Oxides

Aluminum oxide (alumina) (Al_2O_3) occurs in nature as bauxite or corundum. Alumina is used as an adsorbent, a desiccant, a catalyst, an ingredient of dental cement, and an abrasive in toothpaste and as dispersing agent food additive and in hemodialysis. Exposure to aluminum-containing dust or particles will cause severe pulmonary reactions including emphysema and pneumothorax, fibrosis, and eye and upper respiratory tract irritation. Long-term inhalational effects due to continuous exposure may affect the central nervous system.

Manganese oxide nanoparticles are used as magnetic resonance imaging contrast agents to visualize the brain tumors though their antiproliferative properties are poorly studied. Diverse therapeutic and surgical approaches are developed to prevent and treat neuropathology.

Analogous to transition metal oxides, graphene oxide nanomaterials have created much interest due to their unique physicochemical properties, biocompatibility, and 2D allotropic structure which make themselves suitable for biological applications. The biomedical application of graphene and its composites is as the antimicrobial agent for medical implant, anticancer therapy, and drug and gene delivery (Fig. 9.10).

Fig. 9.9 Application of CuO nanoparticles in the field of medicine and biology
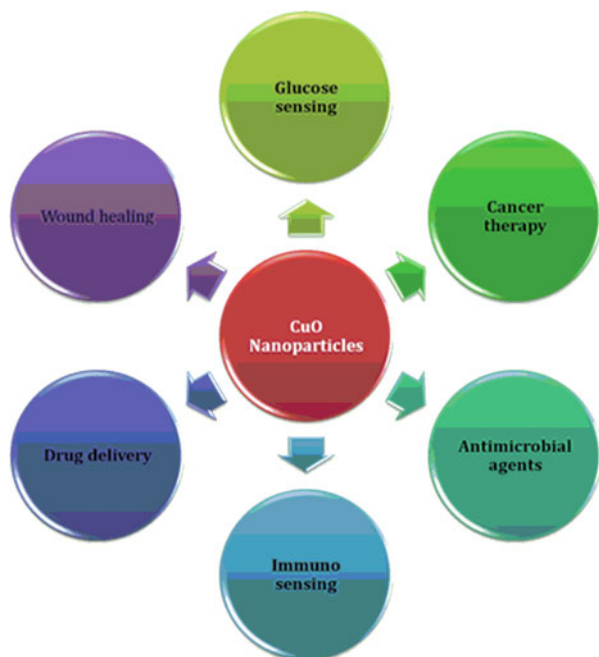
Fig. 9.10 Pictorial representation of the applications of graphene oxide nanoparticles
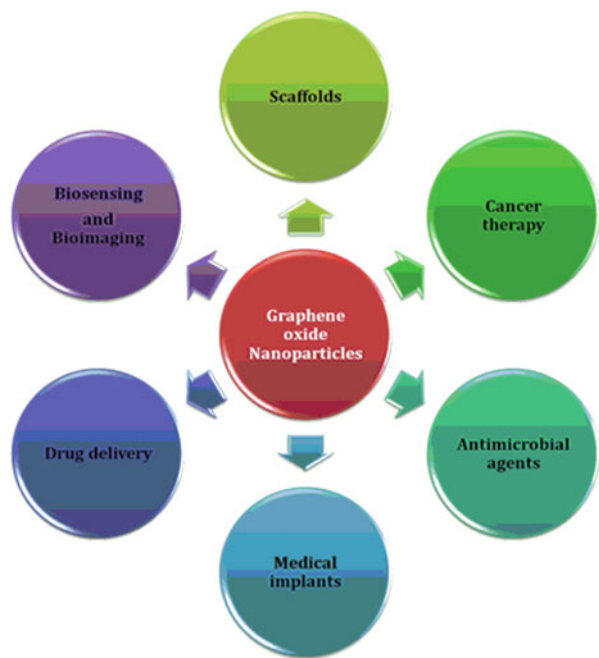
9.5 Conclusion

The functionalization of C–H bond selectively is crucial in synthetic organic chemistry to achieve the desired biologically active molecules. In this chapter, we have discussed the catalytic activity of organometallic complexes and usage of transition metals alkenylidenes and allenylidenes for the C–C bond formation via transmetalation. Terminal alkynes use other carbon nucleophiles, and the reactions occur via the activation of C–H bond. In addition to the synthetic applications, metals and metal oxides can be widely used in the field of medicine, biology, and electronics. Hence, in this chapter, we have discussed the applications of various metals and metal oxide nanoparticles as antimicrobial coatings, for wound healing, and to treat various diseases like cancers and antibacterial and infection.

References

Alberico D, Paquin JF, Lautens M (2005) Palladium-catalyzed sequential alkylation-alkenylation reactions: application towards the synthesis of polyfunctionalized fused aromatic rings. Tetrahedron 61(26):6283–6297. https://doi.org/10.1016/j.tet.2005.03.128

Al-Jumaili A, Mulvey P, Kumar A, Prasad K, Bazaka K, Warner J, Jacob MV (2019) Eco-friendly nanocomposites derived from geranium oil and zinc oxide in one step approach. Sci Rep 9 (1):1–16. https://doi.org/10.1038/s41598-019-42211-z

Ammal SC, Yoshikai N, Inada Y, Nishibayashi Y, Nakamura E (2005) Synergistic dimetallic effects in propargylic substitution reaction catalyzed by thiolate-bridged diruthenium complex. J Am Chem Soc 127(26):9428–9438. https://doi.org/10.1021/ja050298z

Barui AK, Kotcherlakota R, Patra CR (2018) Biomedical applications of zinc oxide nanoparticles. In: Inorganic frameworks as smart nanomedicines. Elsevier. https://doi.org/10.1016/B978-0-12-813661-4.00006-7

Cai R, Hashimoto K, Itoh K, Kubota Y, Fujishima A (1991) Photokilling of malignant cells with ultrafine TiO2 powder. Bull Chem Soc Jpn. https://doi.org/10.1246/bcsj.64.1268

Chang Ho Oh, Seung Hyun Jung (2000) Efficient coupling reactions of lithium alkynyl (triisopropoxy)borates with aryl halides: application to the antifungal terbinafine synthesis. Tetrahedron Lett 41(44):8513–8516

Chang D, Lim M, Goos JACM, Qiao R, Ng YY, Mansfeld FM et al (2018) Biologically targeted magnetic hyperthermia: potential and limitations. Front Pharmacol 9(Aug). https://doi.org/10.3389/fphar.2018.00831

Coleman RS, Walczak MC (2005) Tandem Stille/Suzuki-Miyaura coupling of a hetero-bis-metalated diene. Rapid, one-pot assembly of polyene systems. Org Lett 7(11):2289–2291. https://doi.org/10.1021/ol050768u

Crawley ML, Trost BM (2012) Applications of transition metal catalysis in drug discovery and development: an industrial perspective. Applications of transition metal catalysis in drug discovery and development: an industrial perspective. https://doi.org/10.1002/9781118309872

Dienes F, Pierre J, Linquist A, Blart E, Mouri V, Savignac M et al (1995) Suzuki-type cross coupling reactions using palladium-water soluble catalyst. Synthesis of functionalized dienes. Tetrahedron Lett 36(9):1443–1446

Doucet H, Höfer J, Bruneau C, Dixneuf PH (1993) Stereoselective synthesis of Z-enol esters catalysed by [bis(diphenylphosphino)alkane]bis(2-methylpropenyl)ruthenium complexes. J Chem Soc Chem Commun 10:850–851. https://doi.org/10.1039/C39930000850

Doucet H, Martin-Vaca B, Bruneau C, Dixneuf PH (1995) General synthesis of (2)-Alk-1-en-1-yl esters via ruthenium-catalyzed anti-1Markovnikov trans-addition of carboxylic acids to terminal alkynes. J Org Chem 60(2):7247–7255

Doverspike JC, Zhou Y, Wu J, Tan X, Xi C, Meyerhoff ME (2019) Nitric oxide releasing two-part creams containing S-nitrosoglutathione and zinc oxide for potential topical antimicrobial applications. Nitric Oxide 90(March):1–9. https://doi.org/10.1016/j.niox.2019.05.009

Dyker G (2008) Handbook of C-H transformations: applications in organic synthesis, vol 1–2. https://doi.org/10.1002/9783527619450

El-Boubbou K (2018) Magnetic iron oxide nanoparticles as drug carriers: clinical relevance. Nanomedicine. https://doi.org/10.2217/nnm-2017-0336

Ellingsen JE (1991) A study on the mechanism of protein adsorption to TiO2. Biomaterials 12 (6):593–596. https://doi.org/10.1016/0142-9612(91)90057-H

Esteruelas MA, Gómez AV, Lahoz FJ, López AM, Oñate E, Oro LA (1996) Five-coordinate complex [RuHCl(CO)(PPri3)2] as a precursor for the preparation of new cyclopentadienylruthenium compounds containing unsaturated η1-carbon ligands. Organometallics 15(15):3423–3435

Esteruelas MA, Go AV, Lo AM, Modrego J (1997) Addition of carbon nucleophiles to the allenylidene ligand of [Ru(η5-C 5H 5)(C dC dCPh 2)(CO)(P iPr3)]BF 4: synthesis of new organic ligands by formal C–C coupling between mutually inert fragments. Organometallics 16 (2):5826–5835

Fischer C, Fu GC (2005) Asymmetric nickel-catalyzed Negishi cross-couplings of secondary α-bromo amides with organozinc reagents. J Am Chem Soc 127(13):4594–4595. https://doi.org/10.1021/ja0506509

Fujishima A, Cai RX, Otsuki J, Hashimoto K, Itoh K, Yamashita T, Kubota Y (1993) Biochemical application of photoelectrochemistry: photokilling of malignant cells with TiO2 powder. Electrochim Acta. https://doi.org/10.1016/0013-4686(93)80022-R

Gae YC, Okamura H, Bolm C (2005) Synthesis and palladium-catalyzed coupling reactions of enantiopure p-bromophenyl methyl sulfoximine. J Org Chem 70(6):2346–2349. https://doi.org/10.1021/jo047940c

Godula K, Sezen B, Sames D (2005) Site-specific phenylation of pyridine catalyzed by phosphido-bridged ruthenium dimer complexes: a prototype for C–H arylation of electron-deficient heteroarenes. J Am Chem Soc 127(11):3648–3649. https://doi.org/10.1021/ja042510p

Goldman AS, Goldberg KI (2004) Organometallic C–H bond activation: an introduction, pp 1–43. https://doi.org/10.1021/bk-2004-0885.ch001

Grigore ME, Biscu ER, Holban AM, Gestal MC, Grumezescu AM (2016) Methods of synthesis, properties and biomedical applications of CuO nanoparticles. Pharmaceuticals 9(4):1–14. https://doi.org/10.3390/ph9040075

Hori S, Murai M, Takai K (2015) Rhenium-catalyzed anti-Markovnikov addition reaction of methanetricarboxylates to unactivated terminal acetylenes. J Am Chem Soc 137 (4):1452–1457. https://doi.org/10.1021/ja5090755

Hoskins C (2014) The use of iron oxide nanoparticles for pancreatic cancer therapy. J Nanomed Res. https://doi.org/10.15406/jnmr.2014.01.00004

Jagtap S (2017) Heck reaction – state of the art. Catalysts. https://doi.org/10.3390/catal7090267

Jang SB (1997) Polymer-bound palladium-catalyzed cross-coupling of organoboron compounds with organic halides and organic triflates. Tetrahedron Lett. https://doi.org/10.1016/S0040-4039(97)00171-8

Janko C, Ratschker T, Nguyen K, Zschiesche L, Tietze R, Lyer S, Alexiou C (2019) Functionalized superparamagnetic iron oxide nanoparticles (SPIONs) as platform for the targeted multimodal tumor therapy. Front Oncol 9(Feb):1–9. https://doi.org/10.3389/fonc.2019.00059

Jurca T, Marian E, Vicaş LG, Mureşan ME, Fritea L (2017) Metal complexes of pharmaceutical substances. In: Spectroscopic analyses – developments and applications. https://doi.org/10.5772/65390

Kakiuchi F, Tanaka Y, Sato T, Chatani N, Murai S (1995) Catalytic addition of olefinic C–H bonds to olefins. Chem Lett. https://doi.org/10.1246/cl.1995.679

Khan S, Setua S, Kumari S, Dan N, Massey A, Hafeez BB et al (2019) Superparamagnetic iron oxide nanoparticles of curcumin enhance gemcitabine therapeutic response in pancreatic cancer. Biomaterials. https://doi.org/10.1016/j.biomaterials.2019.04.005

Kostić NM, Fenske RF (1982) Molecular orbital study of bonding, conformations, and reactivity of transition-metal complexes containing unsaturated organic ligands. Electrophilic and nucleophilic additions to acetylide, vinylidene, vinyl, and carbene ligands. Organometallics 1 (7):974–982. https://doi.org/10.1021/om00067a015

Lumbroso A, Vautravers NR, Breit B (2010) Rhodium-catalyzed selective anti-markovnikov addition of carboxylic acids to alkynes. Org Lett 12(23):5498–5501. https://doi.org/10.1021/ol102365e

Ma S, He Q, Zhang X (2005) Pd(0)-catalyzed highly selective synthesis of 1,1-diarylpropadienes and 1,3-diarylpropynes from 1-aryl-1-propynes and aryl halides. J Org Chem 70(8):3336–3338. https://doi.org/10.1021/jo050183d

Matsuda T, Kato K, Goya T, Shimada S, Murakami M (2016) Ruthenium-catalyzed cycloisomerization of 2,2′-diethynyl- biphenyls involving cleavage of a carbon-carbon triple bond. Chem Eur J 22(6):1941–1943. https://doi.org/10.1002/chem.201504937

McDonald FE, Olson TC (1997) Group VI metal-promoted endo-carbocyclizations via alkyne-derived metal vinylidene carbenes. Tetrahedron Lett 38(44):7691–7692. https://doi.org/10.1016/S0040-4039(97)10007-7

Merlic CA, Pauly ME (1996) Ruthenium-catalyzed cyclizations of dienylalkynes via vinylidene intermediates. J Am Chem Soc 118(45):11319–11320. https://doi.org/10.1021/ja962684+

Miyaura N (1998) Synthesis of biaryls via the cross-coupling reaction of arylboronic acids. Adv Metal-Organ Chem 6:187–243

Miyaura N (2008) Metal-catalyzed cross-coupling reactions of organoboron compounds with organic halides. In: Metal-catalyzed cross-coupling reactions. https://doi.org/10.1002/9783527619535.ch2

Miyaura N, Suzuki A (1995) Palladium-catalyzed cross-coupling reactions of organoboron compounds. Chem Rev. https://doi.org/10.1021/cr00039a007

Murai S, Kakiuchi F, Sekine S, Tanaka Y, Kamatani A, Sonoda M, Chatani N (1993) Efficient catalytic addition of aromatic carbon-hydrogen bonds to olefins. Nature 366(6455):529–531. https://doi.org/10.1038/366529a0

Murai S, Tanaka Y, Kamatani A, Sonoda M, Chatani N (1994) Catalytic C-H/olefin coupling. Pure Appl Chem 66(7):1527–1534

Nakao Y, Imanaka H, Sahoo AK, Yada A, Hiyama T (2005) Alkenyl- and aryl[2-(hydroxymethyl)-phenyl]dimethylsilanes: an entry to tetraorganosilicon reagents for the silicon-based cross-coupling reaction. J Am Chem Soc 127(19):6952–6953. https://doi.org/10.1021/ja051281j

Nishibayashi Y, Wakiji I, Hidai M (2000) Novel propargylic substitution reactions catalyzed by thiolate-bridged diruthenium complexes via allenylidene intermediates. J Am Chem Soc 122 (44):11019–11020. https://doi.org/10.1021/ja0021161

Nishibayashi Y, Wakiji I, Ishii Y, Uemura S, Hidai M (2001) Ruthenium-catalyzed propargylic alkylation of propargylic alcohols with ketones: straightforward synthesis of γ-keto acetylenes [2]. J Am Chem Soc 123(14):3393–3394. https://doi.org/10.1021/ja015670z

Nishibayashi Y, Milton MD, Inada Y, Yoshikawa M, Wakiji I, Hidai M, Uemura S (2005) Ruthenium-catalyzed propargylic substitution reactions of propargylic alcohols with oxygen-, nitrogen-, and phosphorus-centered nucleophiles. Chem Eur J 11(5):1433–1451. https://doi.org/10.1002/chem.200400833

Ohe K, Yokoi T, Miki K, Nishino F, Uemura S (2002) Chromium- and tungsten-triggered valence isomerism of (2-acylcyclopropyl) vinylidene – metal intermediates. J Am Chem Soc 124(entry 10):13–14. https://doi.org/10.1021/ja017037

Onodera G, Nishibayashi Y, Uemura S (2006) Ruthenium-catalyzed reductive coupling reaction of propargylic alcohols via hydroboration of allenylidene intermediates. Organometallics 25 (1):35–37. https://doi.org/10.1021/om0509241

Pal M, Dakarapu R, Parasuraman K, Subramanian V, Yeleswarapu KR (2005) Regio- and stereo-specific synthesis of novel 3-enynyl-substituted thioflavones/flavones using a copper-free palladium-catalyzed reaction. J Org Chem 70(18):7179–7187. https://doi.org/10.1021/jo050828+

Pilar Gamasa M, Gimeno J, González-Bernardo C, Borge J, García-Granda S (1997) Synthesis of ruthenium(II) 1,2,3-trimethylindenyl complexes: x-ray crystal structure of [Ru(dCdCdCPh2) (η5-1,2,3-Me3C9H4)(CO)(PPh3)][BF4]. Organometallics 16(12):2483–2485

Quan Q, Xie J, Gao H, Yang M, Zhang F, Liu G et al (2011) HSA coated iron oxide nanoparticles as drug delivery vehicles for cancer therapy. Mol Pharm. https://doi.org/10.1021/mp200006f

Rehman FU, Zhao C, Jiang H, Wang X (2016) Biomedical applications of nano-titania in theranostics and photodynamic therapy. Biomater Sci 4(1):40–54. https://doi.org/10.1039/c5bm00332f

Rice JE, Cai ZW (1993) An intramolecular arene-triflate coupling reaction for the regiospecific synthesis of substituted benzofluoranthenes. J Org Chem 58(6):1415–1424. https://doi.org/10.1021/jo00058a023

Roh SW, Choi K, Lee C (2019) Transition metal vinylidene- and allenylidene-mediated catalysis in organic synthesis. Chem Rev 119(6):4293–4356. https://doi.org/10.1021/acs.chemrev.8b00568

Schaub TA, Kivala M (2013) Cross-coupling reactions to sp carbon atoms. In: Metal catalyzed cross-coupling reactions and more, vol 3, pp 665–762. https://doi.org/10.1002/9783527655588.ch9

Shabashov D, Daugulis O (2005) Catalytic coupling of C-H and C-I bonds using pyridine as a directing group. Org Lett 7(17):3657–3659. https://doi.org/10.1021/ol051255q

Sonoda M, Kakiuchi F, Chatani N, Murai S (1995) Directing effect of functional groups in ruthenium-catalyzed addition of substituted acetophonones to an olefin. J Organomet Chem 504(1–2):151–152. https://doi.org/10.1016/0022-328X(95)05607-Q

Sonogashira K, Tohda Y, Hagihara N (1975) A convenient synthesis of acetylenes: catalytic substitutions of acetylenic hydrogen with bromoalkenes, iodoarenes and bromopyridines. Tetrahedron Lett. https://doi.org/10.1016/S0040-4039(00)91094-3

Suzuki T, Tokunaga M, Wakatsuki Y (2001) Ruthenium complex-catalyzed anti-Markovnikov hydration of terminal alkynes. Org Lett 3(5):735–736. https://doi.org/10.1021/ol0003937

Tietze R, Zaloga J, Unterweger H, Lyer S, Friedrich RP, Janko C et al (2015) Magnetic nanoparticle-based drug delivery for cancer therapy. Biochem Biophys Res Commun. https://doi.org/10.1016/j.bbrc.2015.08.022

Tokunaga M, Wakatsuki Y (1998) The first anti-Markovnikov hydration of terminal alkynes: formation of aldehydes catalyzed by a ruthenium(ii)/phosphane mixture. Angew Chem Int Ed 37:2867–2869

Trost BM, Imi K, Davies IW (1995) Elaboration of conjugated alkenes initiated by insertion into a vinylic C-H bond. J Am Chem Soc 117(19):5371–5372. https://doi.org/10.1021/ja00124a025

Venkatesh C, Singh B, Mahata PK, Ila H, Junjappa H (2005) Heteroannulation of nitroketene N, S-arylaminoacetals with POCL3: a novel highly regioselective synthesis of unsymmetrical 2,3-substituted quinoxalines. Org Lett 7(11):2169–2172. https://doi.org/10.1021/ol0505095

Xiaohong B, Crevier T, Guram AS, Jandeleit B, Powers TS, Turner HW et al (1999) A convenient palladium/ligand catalyst for Suzuki cross-coupling reactions of arylboronic acids and aryl chlorides. Tetrahedron Lett 40(20):3855–3858. https://doi.org/10.1016/S0040-4039(99)00642-5

Xie LG, Dixon DJ (2017) Tertiary amine synthesis: via reductive coupling of amides with Grignard reagents. Chem Sci 8(11):7492–7497. https://doi.org/10.1039/c7sc03613b

Yadavalli T, Shukla D (2017) Role of metal and metal oxide nanoparticles as diagnostic and therapeutic tools for highly prevalent viral infections. Nanomedicine 13(1):219–230. https://doi.org/10.1016/j.nano.2016.08.016

Yamauchi Y, Miyake Y, Nishibayashi Y (2009) Ruthenium-catalyzed oxypropargylation of alkenes. Organometallics 28(1):48–50. https://doi.org/10.1021/om801092a

Ye F, Chen J, Ritter T (2017) Rh-catalyzed anti-Markovnikov hydrocyanation of terminal alkynes. J Am Chem Soc 139(21):7184–7187. https://doi.org/10.1021/jacs.7b03749

Zaitsev VG, Shabashov D, Daugulis O (2005) Highly regioselective arylation of sp3 C-H bonds catalyzed by palladium acetate. J Am Chem Soc 127(38):13154–13155. https://doi.org/10.1021/ja054549f

Zalesskiy SS, Ananikov VP (2012) Pd 2(dba) 3 as a precursor of soluble metal complexes and nanoparticles: determination of palladium active species for catalysis and synthesis. Organometallics 31(6):2302–2309. https://doi.org/10.1021/om201217r

Zhang H, Kwong FY, Tian Y, Chan KS (1998) Base and cation effects on the suzuki cross-coupling of bulky arylboronic acid with halopyridines: synthesis of pyridylphenols. J Org Chem. https://doi.org/10.1021/jo980646y

Zhang L, Dong WF, Sun HB (2013) Multifunctional superparamagnetic iron oxide nanoparticles: design, synthesis and biomedical photonic applications. Nanoscale. https://doi.org/10.1039/c3nr01616a

Chapter 10
Metal Oxides as Anticancer Agents

Sankar Jagadeeshan and Rajesh Parsanathan

Contents

Abstract Cancer, the fractious growth of cells, is a significant cause of death throughout the world. Although intense efforts have been made in the treatment of cancer over the past years, cancer continues to be a significant health issue, and, therefore, extensive studies are being made in searching for new therapeutic approaches. Metal and metal oxide have emerged as innovative tools to address the development of new therapeutic anticancer agents alone or in combination with standard treatments such as surgery, chemotherapy, and radiotherapy. The potential use of metal oxide against cancer is based on their pro-apoptotic activity, induction of autophagy, inhibition of cell growth and metastasis, and generation of reactive oxygen species as well as radiosensitizing properties. Most of the metal oxide-based anticancer studies known in literature use their nano-formulation for better

S. Jagadeeshan (✉)
The Shraga Segal Department of Microbiology, Immunology, and Genetics, Faculty of Health Sciences, Ben-Gurion University of the Negev, Beer-Sheva, Israel

R. Parsanathan
Department of Pediatrics and Centre for Cardiovascular Diseases and Sciences, Louisiana State University Health Sciences Center, Shreveport, LA, USA

bioavailability either as a single agent or in combination with conventional drugs. In this book chapter, we give a comprehensive detailing of various metal oxide nanoparticles and their mode of activity in the ever-growing metal-based cancer therapy field.

Keywords Cancer · Metal oxides · Nanoparticles · Reactive oxygen species · Anticancer agents

Abbreviations

DNA   Deoxyribonucleic acid
NIR   Near infrared
PDT   Photodynamic therapy
ROS   Reactive oxygen species
SDT   Sonodynamic therapy
UV   Ultraviolet

10.1 Introduction

Cancer accounts for the vast majority of mortality worldwide and represents a severe health concern. The treatment of cancer involves different therapies including radiotherapy and chemotherapy, which are based on antimetabolites, biological agents, alkylating agents, etc. Limited efficiency and significant side effects delimit these major therapeutic modules. Thus, the search for new therapies is essential. Therapeutic potentials of metal-based compounds for the treatment of various disease conditions date back to ancient times. History of Egyptian, Chinese, and Indian civilization had provided ambient evidence that they had used metals such as gold and copper for treatment of many disease conditions (Pricker 1996).

Metals play an essential role in biological systems by functioning as catalytic or structural cofactors for many enzymes. Additionally, metals play diverse roles in biology – by operating in critical biosynthetic pathways generating metabolic products, as well as functioning as environmental toxins. Elucidating the crucial roles of metals in biological systems requires a multidisciplinary approach at the interface of chemistry and biology. It is increasingly recognized that metals are involved in many cellular and subcellular functions. For instance, divalent cations Zn^{2+}, Ca^{2+}, and Mg^{2+} play essential regulatory roles in cells. Iron deficiency is common in cancer patients, and it is associated with complications in surgery. Copper is another metal recognized as an essential metalloelement because of its influence on various copper-dependent cellular enzymes. Most of the metal ions are transported by the blood plasma which is achieved through the formation of protein complexes such as enzyme–ion complexes. Metals are also used as inorganic drugs for many diseases. The ability of metals to form oxides with a wide range of

structural geometries has enabled them to exhibit metallic, semiconductor, or insulating properties. Therapeutic potential of metal oxides in cancer therapy has attracted much interest mainly because metals exhibit unique characteristics, such as redox activity, variable coordination modes, and reactivity towards the organic substrate (Frezza et al. 2010). These properties become an attractive probe that selectively binds to the biomolecular target with a resultant alteration in the cellular mechanism of proliferation (Frezza et al. 2010). The appropriate manipulation of these materials at the nanoscale and the production of metal oxide nanoparticles enabled the study of their interaction with biological systems (e.g., cells) (Vinardell and Mitjans 2018). Platinum drugs remain the backbone of the metal-based compounds in the treatment of cancer, but the recent upsurge of activities relying on the structural information aimed at improving and developing other forms of metal-based compounds, which include metal oxide nanoparticles. One new mode of cancer therapy is based on the use and synthesis of metal oxide nanoparticles, which, due to their small size, can be used to target the cancer tissue more accurately. Since then, these metal oxide nanoparticles are increasingly being studied for clinical applications as anticancer therapy drugs. Although a wide range of metal oxides is available, their use in therapeutics is limited to those of less toxic metals. For instance, metal oxide nanoparticles of cadmium, arsenic, lead, and mercury are highly toxic to mammals (Tchounwou et al. 2012). Conversely, other derivatives such as titanium dioxide (TiO_2), zinc oxide (ZnO), copper(II) oxide (CuO), ferrous oxide (Fe_3O_4), and ferric oxide (Fe_2O_3) appear as relatively safe agents (Ren et al. 2009; von Wilmowsky et al. 2009; Augustine et al. 2016; Chhabra et al. 2016; Augustine et al. 2017). The most therapeutically relevant metal oxides, their anticancer activity, and currently available literature evidence for mechanism of action will be briefly described in this chapter.

10.2 Applications of Metal Oxide Nanoparticles in Biomedical Research

Unique optical, magnetic, and electrical activity exhibited by the metal oxide nanoparticles has reiterated their application in biomedical research. For instance, iron, nickel, and cobalt nanoparticles are applied in medical biotechnology because of their magnetic properties. The anticancer activity of metal oxide nanoparticles is either due to the intrinsic features such as their antioxidant action or due to application of external stimuli, such as hyperthermia, in response to the administration of infrared rays or magnetic fields, which can generate reactive oxygen species that can kill cancer cells (Fig. 10.1). Interaction of metal oxide nanoparticles with tumor environments, especially with blood vessels or stroma, could interfere with the development of tumor mass and thus delay tumor progression. Thus, inductions of DNA damage, oxidative stress, genotoxic effects, and anti-inflammatory responses
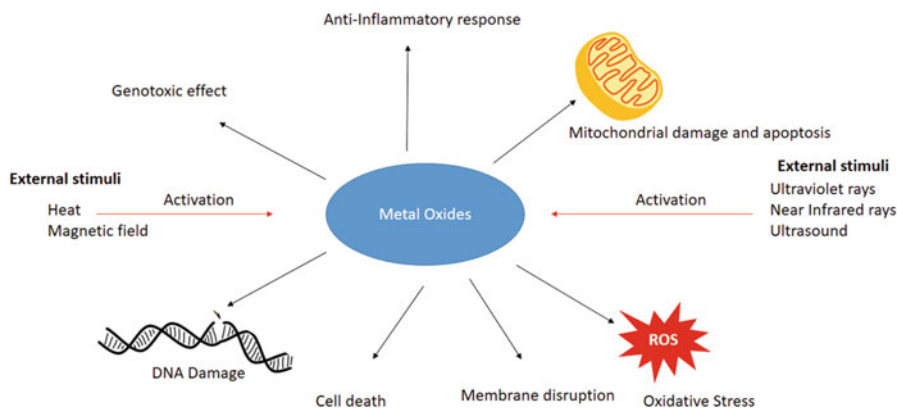
Fig. 10.1 Activation of metal oxide by external stimulus and induction of multiple anticancer mechanisms triggered by activated metal oxides in the cell

are among the joint effects of metal oxide nanoparticles that can contribute to their potential application for therapeutic anticancer use (Tuli et al. 2015).

Recently, metal oxide nanoparticles have gained attention as carriers of anticancer drugs, allowing more accessibility of the drug into the cancer cells (Javed et al. 2015; Vinardell and Mitjans 2015). In addition to that, synergistic effects of metal oxide nanoparticles with traditional cancer treatments have also been reported (Sack et al. 2014; Zhang et al. 2015). Thus, metal oxide nanoparticles are finding an increased application in the biomedical field. Particularly in cancer biology, metal oxide nanoparticles are being designed for both diagnostics and therapeutic applications. Current research in this field has paved the way for new technologies where metal oxide nanoparticles are synthesized as required and further modified with various chemical functional groups. This functionalization enhances their ability to conjugate with other biological molecules such as antibodies, nucleic acids, peptides, ligands, and anticancer drugs.

10.2.1 Arsenic Trioxide Nanoparticles

Arsenic compounds are natural substances with therapeutic potential. They were used for medical treatment in China for more than 25 centuries. Previous literature have shown that arsenic trioxide (As_2O_3) has been used in patients with acute promyelocytic leukemia. Arsenic trioxide is found to be safe and useful not only in patients with leukemia but also in patients with many other malignancies (Feng et al. 2002). Mechanism of action of arsenic trioxide in combating cancer has been postulated by several means – by induction of a p53-dependent cell cycle arrest at G1 or G2/M, through an activation of caspase-8 or caspase-9 (Liu et al. 2003), by the upregulation of p53 and Bax, and simultaneous downregulation of Bcl-2 (Shi et al.

2002) or apoptosis (Li et al. 2002; Hyun Park et al. 2003; Shen et al. 2003). The induction of apoptosis by arsenic trioxide could also be related to an increase in the production of reactive oxygen species and a decrease in anti-oxidation capacity (Shen et al. 2003). Toxic lipid peroxidation products such as the polyunsaturated fatty acid docosahexaenoic acid (DHA), formed due to reactive oxygen species-inducing anticancer agents' activity, sensitize tumor cells (Sturlan et al. 2003). Evidence have shown that arsenic trioxide induces an upsurge in GSH content as a response to oxidative stress (Yeh et al. 2002). Many studies have shown several cancer cell lines are sensitive to arsenic trioxide: esophageal carcinoma cells (Shen et al. 2003), renal carcinoma cells (Hyun Park et al. 2003), and small cell lung cancer cells (NeI-H cells) (Shi et al. 2002). It has also been evident that arsenic trioxide is shown to be active against nasopharyngeal carcinoma xenografts in Balb/c nude mice (Mayorga et al. 2002; Du et al. 2003).

10.2.2   Iron Oxide Nanoparticles

The ions of iron control physiological processes such as DNA synthesis, oxygen transport, mitochondrial respiration, and heme synthesis and also metabolic functions at the central nervous system by regulating nitric oxide metabolism, oxidative phosphorylation, and myelin and neurotransmitter synthesis. In this way, iron plays a prominent role in various biological processes, and its dysregulation or improper transport leads to disturbed physiological functions and cytotoxic reactions. In cells, the free intracellular Fe^{2+} ions react with hydrogen peroxide (H_2O_2) to generate reactive oxygen species which activates a cascade of deleterious events that includes the release of iron ions into the cytosol – from the mitochondria by inducing an increased permeability of its outer membrane and damaging effects on lysosomal membrane, enhancing lipid peroxidation, damaging proteins, breaking DNA chains and degrading bases, inducing mutations, and deletions or translocations at the nuclear level ultimately leading to cell death (Moacă et al. 2018).

Iron oxide nanoparticle has unique properties especially superparamagnetism, making it the most biocompatible material for biomedical research. Iron oxide nanoparticles are known in three forms, including hematite (α-Fe_2O_3), magnetite (Fe_3O_4), and maghemite (γ-Fe_2O_3), but only magnetite and maghemite are biocompatible, and so they are the only ones used in biomedicine (Li et al. 2011). The smaller size of iron oxide nanoparticles (10–100 nm) exerts prolonged circulation in the bloodstream and penetration to the tissues. Spherical iron oxide nanoparticles were approved as a medical device for magnetic tumor hyperthermia in the brain in many countries (van Landeghem et al. 2009; Gamarra et al. 2011) and prostate cancer (Johannsen et al. 2010), in combination with radiotherapy or chemotherapy (Maier-Hauff et al. 2011). Magneto-sensitive iron oxide nanoparticle complexes with the anticancer drug doxorubicin have been shown to increase the antitumor effect compared to conventional doxorubicin therapy. This exemplified antitumor effect is probably due to the fact that an external magnetic field can induce electron

transitions in the nanocomplexes and also produce additional free radicals; and the antitumor drug by the activation of the hydroxyl radicals breaks mitochondria, lipids, proteins, DNA, and other structures in tumor cells, leading to apoptosis or necrosis of the tumor cell. Thus, the synergy of magnetic fields and an anticancer magneto-sensitive nanocomplex provides a new strategy for future effective treatments against cancer (Orel et al. 2015).

The core–shell structure of nanoparticles using iron oxides as core is recently emerging as a new type of carrier with the potential of controlled drug release. Szerekes et al. (2013) prepared iron oxide core covered by different types of shells including citric acid, gallic acid, poly(acrylic acid), and poly(acrylic acid-co-maleic acid). These thermoresponsive iron core–shell nanoparticles combine magnetic drug targeting with hyperthermia and subsequent drug release. This procedure enables anticancer drug delivery directly into tumors with minimizing side effects and maximizing drug concentration specifically in tumor tissue for maximal therapeutic effect (Martinkova et al. 2018).

Anticancer hyperthermia therapy is one of the anticancer treatment modes with the application of heat at a temperature above 40 °C to induce tumor cell death (Bhattacharyya et al. 2011). Different nanostructures have been used extensively in hyperthermia applications, including magnetic iron oxide nanoparticles with promising results both in vitro and in vivo cell models (as previously reviewed by Danhier et al. 2010). When iron oxide nanoparticles are exposed to radiofrequency oscillating magnetic fields, they produce heat due to the reorientation of the magnetization process. This unique property of the iron oxide nanoparticles is harnessed in hyperthermia therapy.

Recent studies have shown that iron oxide nanoparticles could be used as radiosensitizing agents in combination with X-ray sources. In vitro studies showed that citrate- and malate-coated superparamagnetic iron oxide nanoparticles sensitized tumor cells to X-rays by catalyzing reactive oxygen species formation (Klein et al. 2014). These promising results deserve additional investigation for delineating the biological mechanisms following reactive oxygen species production.

10.2.3 Titanium Dioxide Nanoparticles

TiO_2 is a white, odorless, and noncombustible powder. Titanium dioxide has been known in different names, such as titanium(IV) oxide, titania, titanic acid anhydride, and Ti white. It has been evident that the activity of titanium dioxide nanoparticles varies with the alterations that are done on the surface of these nanoparticles (Abid et al. 2013). According to the study of Kongseng et al. (2016), pro-inflammatory cytokine levels got elevated on TiO_2 nanoparticle treatment (Kongseng et al. 2016). Also, many studies proved that TiO_2 nanoparticles induce the formation of reactive oxygen species which causes cell death in multiple ways. In a few studies, TiO_2 nanoparticles have been shown to induce significant genotoxicity and to adversely

affect both major DNA repair mechanisms: base excision repair and nucleotide excision repair (Biola-Clier et al. 2017; Bogdan et al. 2017).

In the study of Youkhana et al., TiO_2 nanoparticles are used as radiosensitizers. According to their study, TiO_2 nanoparticles were found nontoxic up to 4 mM, and with concentrations of more than 4 mM, the viability of cells stayed constant. In conclusion, they have found that TiO_2 nanoparticles positively affect dose delivery. This research shows that TiO_2 nanoparticles have implications for future radiotherapy treatments. Recent literature have shown that Ti_2O_3 nanoparticles have been found proper for imaging and could be used as theranostic agents (Youkhana et al. 2017).

Photodynamic therapy (PDT) is based on the principle that a photosensitizer consisting of a hydrophobic organic molecule is excited with electromagnetic radiation in the range of visible or UV light to produce cytotoxic reactive oxygen species that promotes apoptosis. TiO_2 is known to act as a photocatalyst that produces oxidizing radicals by reacting with water during UV exposure and can damage nearby cells (Jańczyk et al. 2008; Liu et al. 2010). Many PDT studies have used TiO_2 nanoparticles as direct photosensitizing agents in place of photosensitizer molecules (Zhang and Sun 2004; Seo et al. 2007; Thevenot et al. 2008). TiO_2 particles usually get incorporated into the cell membrane and the cytoplasm and are found to induce cytotoxicity in multiple cancerous cell lines (Thevenot et al. 2008). Photocatalyzed titanium dioxide (TiO_2) nanoparticles also have been shown to eradicate cancer cells.

Considering the deeper tissue penetration of near-infrared (NIR) light than UV light, TiO_2 nanoparticle-based NIR light-mediated PDT exhibited more efficient tumor inhibition in comparison to UV light-irradiated TiO_2 nanoparticles. Similar results were observed in HeLa cells in vitro and in vivo in a tumor model using female Balb/c nude mice on treating with TiO_2 nanoparticle-based NIR light-mediated PDT (Hou et al. 2015).

Many authors have reported the synthesis of core–shell upconversion nanoparticles (UCNs) with a thin and continuous layer of TiO_2. In these UCNs, TiO_2 acts as nanotransducers to convert low-energy NIR light to high energy, thus enabling better deeper tissue penetration (Idris et al. 2014). Lucky et al. reported the capacity of these synthesized UCNs to suppress the growth of oral squamous cell carcinoma in vivo (Lucky et al. 2015).

Limitations of the PDT have encouraged researchers to search for alternative methods such as SDT (sonodynamic therapy). In SDT, sonosensitizers are used along with ultrasound. Ultrasound is less invasive and more effective than UV radiation to reach deeper in tumor cells by stimulating sonosensitizer particles. As a result, activated sonosensitizers such as TiO_2 generate ROS in target cells. TiO_2 nanoparticle-based sonosensitizers are usually conjugated with metals or antibodies. Recent data proved that TiO_2 nanoparticle-impregnated glioma cells are shown to be killed after ultrasonic stimulation (Yamaguchi et al. 2011). In another study, cytotoxicity of pre-S1/S2 (an antibody that is recognized by hepatocytes) conjugated with TiO_2 nanoparticles to HepG2 cells was tested (Ogino et al. 2010). It was seen

that this conjugation increased the cytotoxic effect of nanoparticles (Ogino et al. 2010).

Investigation on the long-circulating hydrophilized titanium dioxide nanoparticles in sonodynamic therapy demonstrated hydrophilized TiO_2 nanoparticles are more resistant to degradation than conventional sonosensitizers because titanium dioxide is not degraded by reactive oxygen species. In vivo mapping of O_2 in tumor in ultrasonically treated cells with hydrophilized TiO_2 nanoparticles indicated that reactive oxygen species level had increased more in blood vessels than in the deeper sites (You et al. 2016). Ninomiya et al. claimed that using avidin-modified TiO_2 nanoparticles preferentially discriminated cancerous cells from healthy cells, and these cancer cells undergo death on ultrasound treatment due to the generation of hydroxyl radicals (Ninomiya et al. 2014).

10.2.4   Cerium Oxide Nanoparticles

Cerium, a metal from the lanthanide series, is one of the abundant rare earth elements, possessing stable cerium(IV) oxidation state that coexists with cerium (III). In the nanoparticle form, cerium oxide atoms form a cubic crystalline fluorite lattice structure where Ce^{3+} and the compensating oxygen vacancies localize at the nanoparticle surface (Trovarelli and Fornasiero 2013). The medicinal application of cerium oxide nanoparticles is mainly due to their exceptional auto-regenerative antioxidant activity, which can scavenge noxious reactive oxygen/nitrogen species (ROS/RNS) generated by exogenous or endogenous sources (Schieber and Chandel 2014). This could be accomplished by combining either by a superoxide dismutase mimetic activity, responsible for reducing superoxide or peroxynitrite to peroxide and nitrate (respectively) undergoing oxidation from Ce^{3+} to Ce^{4+} (Heckert et al. 2008; Dowding et al. 2013), or with a catalase mimetic activity, where Ce^{4+} is reduced back to Ce^{3+} by oxidizing hydrogen peroxide to molecular oxygen and water (Pirmohamed et al. 2010). Thus, cerium oxide nanoparticles undergo a complete, energy-free redox cycle, eliminating the most toxic reactive oxygen species while regenerating the original redox status (Celardo et al. 2011). The absence of genotoxicity effect is another advantage of using cerium oxide nanoparticles for various medical applications apart from their antioxidant activity (De Marzi et al. 2013).

Cerium oxide nanoparticles provide a novel and very interesting material for radiation therapy as they possess a unique capability to selectively induce cell death of irradiated cancer cells (Wason et al. 2013) while protecting the healthy surrounding tissue from radiation-induced oxidative stress and damage (Tarnuzzer et al. 2005; Colon et al. 2010). Therefore, cerium oxide nanoparticles have the dual feature of simultaneously acting as radio-protecting and radiosensitizing agents. The selective toxicity of cerium oxide nanoparticles against cancer cells is hypothesized to be due to the inhibition of the catalase-like activity of cerium oxide nanoparticles that occurs in acidic (pH 4.3) environments (Wason et al. 2013). Another mechanism for

the differential toxicity of cerium oxide nanoparticles on cancer cells is possibly due to their superoxide dismutase-like activity. Superoxide dismutase enzyme acts as a radiosensitizing agent, by potentiating the DNA damage response and delaying the G2/M transition, thus favoring G2 phase cell accumulation and modulating DNA repair. Therefore, cerium nanoparticles may act as radiosensitizing agents by a biological mechanism that controls the response to DNA damage (Ali et al. 2015).

Recent results using pancreatic cell lines L3.6pl demonstrated that cerium oxide nanoparticles are cytotoxic to cancer cells but showed minimal or no inhibitory effect on the healthy cells hTERT-HPNE. This finding highlights the use of these nanoparticles as stand-alone therapy for pancreatic cancer treatment (Wason et al. 2013). A recent study using cancer and healthy human cells showed the effect of cerium oxide nanoparticles and concluded that these nanoparticles are specifically toxic to the cancer cells. The low cytotoxic activity of cerium oxide on normal human cell lines implicates their potential to be safer for human usage in medicine (Pešić et al. 2015)

Redox-active cerium oxide nanoparticles are known to exhibit significant antitumor activity in cells derived from human skin tumors in vitro and in vivo. The pro-apoptotic and anti-invasive effects of these cerium oxide nanoparticles are in a reactive oxygen species-dependent manner (Sack et al. 2014). Cerium oxide nanoparticle treatment increases the reactive oxygen species level in tumor cells, resulting in apoptosis, whereas they exhibited antioxidant and protective properties in healthy cells (Alili et al. 2011). In vivo xenograft studies with redox-active cerium oxide nanoparticles using immunodeficient nude mice showed a decrease in tumor weight and volume after treatment with cerium oxide nanoparticles. This observed tumor regression might be attributed due to the particular pro-oxidative and antioxidant properties of cerium oxide nanoparticles (Alili et al. 2013). The combination of conventional chemotherapies with cerium oxide nanoparticles may offer an ingenious way to treat cancer, with more significant benefit for patients, by augmenting antitumor activity and minimizing the damaging side effects (De Marzi et al. 2013).

10.2.5   Zinc Oxide Nanoparticles

Zinc oxide is a white powder nearly insoluble in water. Their unique optical, electrical, and thermal performance made them one of the critical ingredients widely used in the field of catalysis, cosmetics, food packaging, and paint materials. Zinc oxide nanoparticles' relative ease of production, ability to modify their physico-chemical characteristics, inherent antibacterial and anticancerous activity, and ability to conjugate with chemotherapeutic drugs and cancer-targeting molecules make them an attractive candidate for biomedical applications (Moosavi et al. 2010; Goharshadi et al. 2011).

Zinc oxide nanoparticles' exposure in target cells induces reactive oxygen species generation and activation of multiple downstream signaling pathways leading to disruption of cellular homeostasis. The disparity in the reactive oxygen species

production and antioxidant defense system of cells induced by zinc oxide nanoparticles results in varied outcomes ultimately leading to cell death (Sharma et al. 2009). The oxidative stress mechanism of zinc oxide nanoparticles could be attributed by the generation of reactive oxygen species on the surface of particles (Park et al. 2011), dissolution and release of Zn^{2+} ions, and physical interaction of zinc oxide nanoparticles with the membranes leading to the deformation and rupture of membranes (Li et al. 2008).

Application of zinc oxide nanoparticles has shown that they sensitize cells by increasing both mitotic (linked to cytogenetic damage) and interphase (apoptosis) deaths. These results could help design more potent anticancer agents for therapeutic uses (Wahab et al. 2013a, b). Studies have shown that zinc oxide nanoparticles' preincubation followed by UVA-1 irradiation induced a significant reduction in viability of head and neck squamous cell carcinoma cell lines in vitro (Hackenberg et al. 2010). Zinc oxide nanoparticles were used at a very low concentration against HepG2 (liver cancer) and MCF-7 (breast cancer) cancer cells and were found to exhibit activity in a dose-dependent manner by modulating the expression of p53, Bax, Bcl-2, and caspase-3 (Wahab et al. 2014).

Zinc oxide nanoparticles also have a photodynamic property: illumination leads to the production of large amounts of reactive oxygen species and can result in cell apoptosis (Ryter et al. 2007). The combination of zinc oxide nanoparticles with conventional chemotherapeutics such as paclitaxel and cisplatin (Hackenberg et al. 2012) or daunorubicin (Guo et al. 2008) increases the anticancer effect of these chemotherapeutics in cell lines in vitro. It is evident that differently sized zinc oxide nanoparticles could significantly enable the accumulation of daunorubicin in leukemia cells and could thus act as an active agent to enhance drug delivery (Guo et al. 2008). Thus, the supplementation of nanoparticles with conventional cancer drugs reduces side effects by minimizing drug dosage for the treatment.

10.2.6 Copper Oxide Nanoparticles

Copper is an essential trace element known to modulate many vital biological pathways in the human body (O'Dell 1976; Gregoriadis et al. 1983). Biologically essential enzymes, such as Cu–Zn superoxide dismutase, tyrosinase, ceruloplasmin, and cytochrome oxidase, are activated by copper (Tapiero et al. 2003). Cellular imbalance in copper could lead to many disease conditions (Wang et al. 2010). Copper oxide nanoparticles have many industrial applications (Zhang et al. 2008), but recent studies have also reported the antimicrobial properties of copper nanoparticles/polymer composites (Cioffi et al. 2005). The green synthesis of these nanoparticles has been proposed as a reliable, simple, nontoxic, and eco-friendly method (Narayanan and Sakthivel 2010). Biosynthesis of copper oxide nanoparticles from biological sources, such as that of *Ficus religiosa* (Sankar et al. 2014) or

Acalypha indica (Sivaraj et al. 2014) plant extracts, has been reported. These copper oxide nanoparticles exhibited cytotoxic effects mechanistically through the induction of apoptosis with enhanced reactive oxygen species generation.

Cuprous oxide nanoparticles have been demonstrated to selectively induce the apoptosis of tumor cells in vitro (Hu et al. 2012). Using HeLa cells, mitochondrial targeting of copper oxide nanoparticles resulted in the release of cytochrome C with subsequent activation of caspase-3 and caspase-9, causing apoptosis of cells. Thus, it was postulated that copper oxide nanoparticles could induce mitochondrion-mediated apoptosis pathway, which raises the possibility that copper oxide nanoparticles could be used as a therapeutic agent against cancer. Copper oxide nanoparticles were also found to induce cytotoxicity in a human liver carcinoma cell line (HepG2) in a dose-dependent manner, which was probably mediated through reactive oxygen species generation and oxidative stress (Siddiqui et al. 2013). C6 glioma cells rapidly accumulate copper after exposure to cuprous oxide nanoparticles in a time-, concentration-, and temperature-dependent manner, and the increased copper content is accompanied by severe toxicity to C6 glioma cells (Joshi et al. 2016).

Copper oxide nanoparticles significantly reduced the growth of B16-F10 melanoma in vivo, inhibited their metastasis, and elevated the survival rate of tumor-bearing mice. In another study, copper oxide nanoparticles inhibit the growth and metastasis of melanoma in a tumor-bearing mice model and are rapidly cleared by mice with low toxicity (Wang et al. 2013). Cuprous oxide nanoparticles also suppressed the growth of human melanoma in tumor-bearing nonobese diabetic–severe combined immunodeficiency mice, which was accompanied by structural necrosis and fibrosis of the tumor. Importantly, in vivo data showed reduced systemic toxicity with rapid clearance of copper oxide nanoparticles from the organs.

10.2.7 Silicon Dioxide Nanoparticles

Targeted drug delivery and controlled release to tumor sites are of great importance for minimized side effects and enhanced therapeutic efficiency. A wide range of nanomaterials has been developed and explored for drug delivery. Among the different types of nanocarriers, silica-based nanoparticles, particularly mesoporous silica nanoparticles, have been highlighted as promising candidates for tumor-targeted drug delivery due to their vast advantages. The size- and shape-controllable pores of mesoporous silica nanoparticles enable them to store pharmaceutical drugs and prevent their premature release and degradation before reaching their target site. Chemotherapeutic drugs thus could be loaded into mesoporous silica nanoparticles, replacing the need to use solvents that are often toxic for healthy tissues. In contrast to other metal oxide nanoparticles with antitumor effects per se, silica is a good

carrier for different anticancer drugs, such as gemcitabine and paclitaxel, in the treatment of pancreas cancer in mice (Meng et al. 2015).

It has been well-known that silica nanoparticles have an innate ability to aggregate, due to their hydrogen bond interactions between external silanol groups. In order to use this type of nanomaterial in biological applications for improved biodistribution and cellular uptake, the reduction of their natural tendency to form aggregates is required. This could be achieved by providing chemical modifications.

Cell internalization and in vitro efficacy assays demonstrated that silica nanoparticles entered cells via endocytosis, and the intracellular release of the cargo induced cell death. In a study using silica nanoparticles with camptothecin (CPT) in vivo, it showed that the silica nanoparticles boost CPT concentration in tumor compared to administration of the free drug, although the silica nanoparticles-CPT tended to accumulate in organs of the reticuloendothelial system. Silica nanoparticles-CPT treatment delayed subcutaneous tumors growth while significantly reducing the systemic toxicity associated with CPT administration. These results indicate that silica nanoparticles-CPT could be used as a robust drug delivery system for antitumor treatments based on CPT (Botella et al. 2011). In another study, Yu and co-workers synthesized hyaluronic acid (HA)-modified silica nanoparticles targeting CD44 over-expressed HCT-116 (human colon cancer cells).Compared to bare SNanoparticles, HA-modified silica nanoparticles exhibited a higher cellular uptake via HA receptor-mediated endocytosis, leading to more significant cytotoxicity to HCT-116 cells than free drug and drug-loaded bare silica nanoparticles (Yu et al. 2013).

10.3 Conclusions

Cancer is getting a more significant problem every day all over the world, and no cure extinguishes cancer completely. Therefore, it was considered that in addition to radiotherapy, chemotherapy, and other methods, metal oxide nanoparticles could be ingenious tools in cancer treatment studies. Several studies demonstrated the anticancer activity of different metal oxide nanomaterials in vitro and in vivo (Tables 10.1 and 10.2). More research in this area is needed for the better understanding of efficient use and mechanism of action of metal oxides as prospective anticancer agents. Studies related to the distribution, biocompatibility, and low toxicity for healthy tissues are necessary before clinical trials of these metal-based therapeutics are warranted. Future research in this field will reveal the full spectrum of advantages of these materials and, hopefully, will enable their integration into standard clinical tools.

Table 10.1 In vitro anticancer activity of metal oxide nanoparticles against different types of tumor

Metal oxide	Tumor	References
Arsenic trioxide	Leukemia	Feng et al. (2002)
	Esophageal	Shen et al. (2003)
	Renal	Hyun Park et al. (2003)
Iron oxide	Glioma	Richard et al. (2016)
	Lung	Khan et al. (2012) and Pandey et al. (2016)
	Myeloma	Yang et al. (2016)
	Colon	Klein et al. (2014)
	Breast	Klein et al. (2014)
Titanium oxide	Colorectal	Zijno et al. (2015)
	Bladder	Thevenot et al. (2008)
	Blood	Thevenot et al. (2008)
Cerium oxide	Melanoma	Sack et al. (2014) and Ali et al. (2015)
	Gastric	Xiao et al. (2016)
	Pancreatic	Wason et al. (2013)
	Ovarian	Hijaz et al. (2016)
	Breast	Chen et al. (2015)
	Lung	Pešić et al. (2015)
Zinc oxide	Breast	Biplab et al. (2016)
	Cervical	Pandurangan et al. (2016)
	Colorectal	Zijno et al. (2015) and Condello et al. (2016)
	Lung	Wang et al. (2015)
	Brain	An et al. (2014)
	Head and neck	Hackenberg et al. (2010)
Copper oxide	Brain	Joshi et al. (2016)
	Melanoma	Yu et al. (2017)
	Lung	Sankar et al. (2014) and Pandey et al. (2016)
	Colorectal	Khan et al. (2017)
	Leukemia	Shafagh et al. (2015)
	Cervical	Xia et al. (2017)
Silicon dioxide	Liver	Siddiqui et al. (2013)
	Lung	Wang et al. (2017)
	Brain	An et al. (2014)

Table 10.2 In vivo anticancer activity of metal oxide nanoparticles

Metal oxide	Tumor	References
Cerium oxide	Pancreatic	Wason et al. (2013)
	Melanoma	Alili et al. (2011)
Titanium dioxide	Head and neck	Lucky et al. (2015)
Copper oxide	Melanoma	Wang et al. (2013)

References

Abid AD et al (2013) Novel lanthanide-labeled metal oxide nanoparticles improve the measurement of in vivo clearance and translocation. Particle Fibre Toxicol 10(1):1. https://doi.org/10.1186/1743-8977-10-1

Ali D et al (2015) Cerium oxide nanoparticles induce oxidative stress and genotoxicity in human skin melanoma cells. Cell Biochem Biophys 71(3):1643–1651. https://doi.org/10.1007/s12013-014-0386-6

Alili L et al (2011) Combined cytotoxic and anti-invasive properties of redox-active nanoparticles in tumor–stroma interactions. Biomaterials 32(11):2918–2929. https://doi.org/10.1016/j.biomaterials.2010.12.056

Alili L et al (2013) Downregulation of tumor growth and invasion by redox-active nanoparticles. Antioxid Redox Signal 19(8):765–778. https://doi.org/10.1089/ars.2012.4831

An SSA et al (2014) In vitro cytotoxicity of SiO2 or ZnO nanoparticles with different sizes and surface charges on U373MG human glioblastoma cells. Int J Nanomed 9(Suppl 2):235. https://doi.org/10.2147/IJN.S57936

Augustine R et al (2016) Monitoring and separation of food-borne pathogens using magnetic nanoparticles. In: Novel approaches of nanotechnology in food. Elsevier, pp 271–312. https://doi.org/10.1016/B978-0-12-804308-0.00009-1

Augustine R, Mathew AP, Sosnik A (2017) Metal oxide nanoparticles as versatile therapeutic agents modulating cell signaling pathways: linking nanotechnology with molecular medicine. Appl Mater Today. Elsevier 7:91–103. https://doi.org/10.1016/J.APMT.2017.01.010

Bhattacharyya S et al (2011) Inorganic nanoparticles in cancer therapy. Pharm Res 28(2):237–259. https://doi.org/10.1007/s11095-010-0318-0

Biola-Clier M et al (2017) Comparison of the DNA damage response in BEAS-2B and A549 cells exposed to titanium dioxide nanoparticles. Mutagenesis 32(1):161–172. https://doi.org/10.1093/mutage/gew055

Biplab KC et al (2016) Enhanced preferential cytotoxicity through surface modification: synthesis, characterization and comparative in vitro evaluation of TritonX-100 modified and unmodified zinc oxide nanoparticles in human breast cancer cell (MDA-MB-231). Chem Central J. BioMed Central 10(1):16. https://doi.org/10.1186/s13065-016-0162-3

Bogdan J, Pławińska-Czarnak J, Zarzyńska J (2017) Nanoparticles of titanium and zinc oxides as novel agents in tumor treatment: a review. Nanoscale Res Lett 12(1):225. https://doi.org/10.1186/s11671-017-2007-y

Botella P et al (2011) Surface-modified silica nanoparticles for tumor-targeted delivery of camptothecin and its biological evaluation. J Control Release 156(2):246–257. https://doi.org/10.1016/j.jconrel.2011.06.039

Celardo I et al (2011) Ce^{3}+ ions determine redox-dependent anti-apoptotic effect of cerium oxide nanoparticles. ACS Nano 5(6):4537–4549. https://doi.org/10.1021/nn200126a

Chen F et al (2015) Enhancement of radiotherapy by ceria nanoparticles modified with neogambogic acid in breast cancer cells. Int J Nanomed. Dove Press 10:4957–4969. https://doi.org/10.2147/IJN.S82980

Chhabra H et al (2016) A nano zinc oxide doped electrospun scaffold improves wound healing in a rodent model. RSC Adv. The Royal Society of Chemistry 6(2):1428–1439. https://doi.org/10.1039/C5RA21821G

Cioffi N et al (2005) Copper nanoparticle/polymer composites with antifungal and bacteriostatic properties. Am Chem Soc. https://doi.org/10.1021/CM0505244

Colon J et al (2010) Cerium oxide nanoparticles protect gastrointestinal epithelium from radiation-induced damage by reduction of reactive oxygen species and upregulation of superoxide dismutase 2. Nanomed Nanotechnol Biol Med 6(5):698–705. https://doi.org/10.1016/j.nano.2010.01.010

Condello M et al (2016) ZnO nanoparticle tracking from uptake to genotoxic damage in human colon carcinoma cells. Toxicol In Vitro 35:169–179. https://doi.org/10.1016/j.tiv.2016.06.005

Danhier F, Feron O, Préat V (2010) To exploit the tumor microenvironment: passive and active tumor targeting of nanocarriers for anti-cancer drug delivery. J Control Release 148 (2):135–146. https://doi.org/10.1016/j.jconrel.2010.08.027

De Marzi L et al (2013) Cytotoxicity and genotoxicity of ceria nanoparticles on different cell lines in vitro. Int J Mol Sci 14(2):3065–3077. https://doi.org/10.3390/ijms14023065

Dowding JM, Seal S, Self WT (2013) Cerium oxide nanoparticles accelerate the decay of peroxynitrite (ONOO−). Drug Deliv Transl Res 3(4):375–379. https://doi.org/10.1007/s13346-013-0136-0

Du C-W et al (2003) Arsenic trioxide induces differentiation of human nasopharyngeal carcinoma in BALB/C nude mice xenograft model. Ai zheng = Aizheng = Chin J Cancer 22(1):21–25. Available at: http://www.ncbi.nlm.nih.gov/pubmed/12561430. Accessed 20 Aug 2019

Feng C, Ma W, Zheng W (2002) Research advances on effect of arsenic trioxide on tumor. Ai zheng = Aizheng = Chin J Cancer 21(12):1386–1389. Available at: http://www.ncbi.nlm.nih.gov/pubmed/12520754. Accessed 20 Aug 2019

Frezza M et al (2010) Novel metals and metal complexes as platforms for cancer therapy. Curr Pharma Des. NIH Public Access 16(16):1813–1825. Available at: http://www.ncbi.nlm.nih.gov/pubmed/20337575. Accessed 13 July 2019

Gamarra L et al (2011) Application of hyperthermia induced by superparamagnetic iron oxide nanoparticles in glioma treatment. Int J Nanomedicine 6:591. https://doi.org/10.2147/IJN.S14737

Goharshadi EK et al (2011) Preparation, structural characterization, semiconductor and photoluminescent properties of zinc oxide nanoparticles in a phosphonium-based ionic liquid. Mater Sci Semiconduct Process. Elsevier 14(1):69–72. https://doi.org/10.1016/j.mssp.2011.01.011

Gregoriadis GC et al (1983) A comparative study of trace elements in normal and cancerous colorectal tissues. Cancer 52(3):508–519. https://doi.org/10.1002/1097-0142(19830801)52:3<508::aid-cncr2820520322>3.0.co;2-8

Guo D et al (2008) Synergistic cytotoxic effect of different sized ZnO nanoparticles and daunorubicin against leukemia cancer cells under UV irradiation. J Photochem Photobiol B Biol 93 (3):119–126. https://doi.org/10.1016/j.jphotobiol.2008.07.009

Hackenberg S, Scherzed A, Kessler M, Froelich K, Ginzkey C, Koehler C, Burghartz M, Hagen R, K. N. (2010) Zinc oxide nanoparticles induce photocatalytic cell death in human head and neck squamous cell carcinoma cell lines in vitro. Int J Oncol 37(6):1583–1590. https://doi.org/10.3892/ijo_00000812

Hackenberg S et al (2012) Antitumor activity of photo-stimulated zinc oxide nanoparticles combined with paclitaxel or cisplatin in HNSCC cell lines. J Photochem Photobiol B Biol 114:87–93. https://doi.org/10.1016/j.jphotobiol.2012.05.014

Heckert EG et al (2008) The role of cerium redox state in the SOD mimetic activity of nanoceria. Biomaterials 29(18):2705–2709. https://doi.org/10.1016/j.biomaterials.2008.03.014

Hijaz M et al (2016) Folic acid tagged nanoceria as a novel therapeutic agent in ovarian cancer. BMC Cancer 16(1):220. https://doi.org/10.1186/s12885-016-2206-4

Hou Z et al (2015) UV-emitting upconversion-based TiO2 photosensitizing nanoplatform: near-infrared light mediated in vivo photodynamic therapy via mitochondria-involved apoptosis pathway. ACS Nano 9(3):2584–2599. https://doi.org/10.1021/nn506107c

Hu Y et al (2012) Cuprous oxide nanoparticles selectively induce apoptosis of tumor cells. Int J Nanomedicine 7:2641. https://doi.org/10.2147/IJN.S31133

Hyun Park W et al (2003) Arsenic trioxide inhibits the growth of A498 renal cell carcinoma cells via cell cycle arrest or apoptosis. Biochem Biophys Res Commun 300(1):230–235. https://doi.org/10.1016/s0006-291x(02)02831-0

Idris NM et al (2014) Photoactivation of core–shell titania coated upconversion nanoparticles and their effect on cell death. J Mater Chem B. The Royal Society of Chemistry 2(40):7017–7026. https://doi.org/10.1039/C4TB01169D

Jańczyk A et al (2008) Photodynamic activity of platinum(IV) chloride surface-modified TiO2 irradiated with visible light. Free Radic Biol Med 44(6):1120–1130. https://doi.org/10.1016/j. freeradbiomed.2007.12.019

Javed KR et al (2015) Comparison of doxorubicin anticancer drug loading on different metal oxide nanoparticles. Medicine 94(11):e617. https://doi.org/10.1097/MD.0000000000000617

Johannsen M et al (2010) Magnetic nanoparticle hyperthermia for prostate cancer. Int J Hyperth 26 (8):790–795. https://doi.org/10.3109/02656731003745740

Joshi A et al (2016) Uptake and toxicity of copper oxide nanoparticles in C6 glioma cells. Neurochem Res. Springer US 41(11):3004–3019. https://doi.org/10.1007/s11064-016-2020-z

Khan MI et al (2012) Induction of ROS, mitochondrial damage and autophagy in lung epithelial cancer cells by iron oxide nanoparticles. Biomaterials 33(5):1477–1488. https://doi.org/10. 1016/j.biomaterials.2011.10.080

Khan S et al (2017) In vitro evaluation of cytotoxicity, possible alteration of apoptotic regulatory proteins, and antibacterial activity of synthesized copper oxide nanoparticles. Colloids Surf B Biointerfaces 153:320–326. https://doi.org/10.1016/j.colsurfb.2017.03.005

Klein S et al (2014) Superparamagnetic iron oxide nanoparticles as novel x-ray enhancer for low-dose radiation therapy. J Phys Chem B 118(23):6159–6166. https://doi.org/10.1021/ jp5026224

Kongseng S et al (2016) Cytotoxic and inflammatory responses of TiO2 nanoparticles on human peripheral blood mononuclear cells. J Appl Toxicol 36(10):1364–1373. https://doi.org/10.1002/ jat.3342

Li D et al (2002) Inhibition of growth of human nasopharyngeal cancer xenografts in SCID mice by arsenic trioxide. Tumori 88(6):522–526. Available at: http://www.ncbi.nlm.nih.gov/pubmed/ 12597150. Accessed 20 Aug 2019

Li N, Xia T, Nel AE (2008) The role of oxidative stress in ambient particulate matter-induced lung diseases and its implications in the toxicity of engineered nanoparticles. Free Radic Biol Med 44 (9):1689–1699. https://doi.org/10.1016/j.freeradbiomed.2008.01.028

Li X et al (2011) Biosynthesis of nanoparticles by microorganisms and their applications. J Nanomater. Hindawi 2011:1–16. https://doi.org/10.1155/2011/270974

Liu Q, Hilsenbeck S, Gazitt Y (2003) Arsenic trioxide-induced apoptosis in myeloma cells: p53-dependent G1 or G2/M cell cycle arrest, activation of caspase-8 or caspase-9, and synergy with APO2/TRAIL. Blood 101(10):4078–4087. https://doi.org/10.1182/blood-2002-10-3231

Liu L et al (2010) Study of Pt/TiO2 nanocomposite for cancer-cell treatment. J Photochem Photobiol B Biol 98(3):207–210. https://doi.org/10.1016/j.jphotobiol.2010.01.005

Lucky SS et al (2015) Titania coated upconversion nanoparticles for near-infrared light triggered photodynamic therapy. ACS Nano 9(1):191–205. https://doi.org/10.1021/nn503450t

Maier-Hauff K et al (2011) Efficacy and safety of intratumoral thermotherapy using magnetic iron-oxide nanoparticles combined with external beam radiotherapy on patients with recurrent glioblastoma multiforme. J Neuro-Oncol 103(2):317–324. https://doi.org/10.1007/s11060-010-0389-0

Martinkova P et al (2018) Iron oxide nanoparticles: innovative tool in cancer diagnosis and therapy. Adv Healthcare Mater. Wiley 7(5):1700932. https://doi.org/10.1002/adhm.201700932

Mayorga J, Richardson-Hardin C, Dicke KA (2002) Arsenic trioxide as effective therapy for relapsed acute promyelocytic leukemia. Clin J Oncol Nurs 6(6):341–346. https://doi.org/10. 1188/02.CJON.341-346

Meng H et al (2015) Use of a lipid-coated mesoporous silica nanoparticle platform for synergistic gemcitabine and paclitaxel delivery to human pancreatic cancer in mice. ACS Nano 9 (4):3540–3557. https://doi.org/10.1021/acsnano.5b00510

Moacă E-A, Coricovac ED, Soica CM, Pinzaru IA, Păcurariu CS, Dehelean CA (2018) Preclinical aspects on magnetic iron oxide nanoparticles and their interventions as anticancer agents: enucleation, apoptosis and other mechanism. In: Iron ores and iron oxide materials, pp 229–254. https://doi.org/10.5772/intechopen.74176

Moosavi M, Goharshadi EK, Youssefi A (2010) Fabrication, characterization, and measurement of some physicochemical properties of ZnO nanofluids. Int J Heat Fluid Flow. Elsevier Inc 31 (4):599–605. https://doi.org/10.1016/j.ijheatfluidflow.2010.01.011

Narayanan KB, Sakthivel N (2010) Biological synthesis of metal nanoparticles by microbes. Adv Colloid Interf Sci 156(1–2):1–13. https://doi.org/10.1016/j.cis.2010.02.001

Ninomiya K et al (2014) Targeted sonocatalytic cancer cell injury using avidin-conjugated titanium dioxide nanoparticles. Ultrason Sonochem 21(5):1624–1628. https://doi.org/10.1016/j.ultsonch.2014.03.010

O'Dell BL (1976) Biochemistry of copper. Med Clin North Am 60(4):687–703. https://doi.org/10.1016/s0025-7125(16)31853-3

Ogino C et al (2010) Construction of protein-modified TiO2 nanoparticles for use with ultrasound irradiation in a novel cell injuring method. Bioorg Med Chem Lett 20(17):5320–5325. https://doi.org/10.1016/j.bmcl.2010.06.124

Orel V et al (2015) Magnetic properties and antitumor effect of nanocomplexes of iron oxide and doxorubicin. Nanomed Nanotechnol Biol Med 11(1):47–55. https://doi.org/10.1016/j.nano.2014.07.007

Pandey N et al (2016) Transition metal oxide nanoparticles are effective in inhibiting lung cancer cell survival in the hypoxic tumor microenvironment. Chem Biol Interact 254:221–230. https://doi.org/10.1016/j.cbi.2016.06.006

Pandurangan M et al (2016) Anti-proliferative effect of copper oxide nanorods against human cervical carcinoma cells. Biol Trace Elem Res 173(1):62–70. https://doi.org/10.1007/s12011-016-0628-0

Park SJ et al (2011) Comparing the toxic mechanism of synthesized zinc oxide nanomaterials by physicochemical characterization and reactive oxygen species properties. Toxicol Lett 207 (3):197–203. https://doi.org/10.1016/j.toxlet.2011.09.011

Pešić M et al (2015) Anti-cancer effects of cerium oxide nanoparticles and its intracellular redox activity. Chem Biol Interact 232:85–93. https://doi.org/10.1016/j.cbi.2015.03.013

Pirmohamed T et al (2010) Nanoceria exhibit redox state-dependent catalase mimetic activity. Chem Commun 46(16):2736. https://doi.org/10.1039/b922024k

Pricker SP (1996) Medical uses of gold compounds: past, present and future. Gold Bull. Springer 29 (2):53–60. https://doi.org/10.1007/BF03215464

Ren G et al (2009) Characterisation of copper oxide nanoparticles for antimicrobial applications. Int J Antimicrob Agents 33(6):587–590. https://doi.org/10.1016/j.ijantimicag.2008.12.004

Richard S et al (2016) Antioxidative theranostic Iron oxide nanoparticles toward brain tumors imaging and ROS production. ACS Chem Biol 11(10):2812–2819. https://doi.org/10.1021/acschembio.6b00558

Ryter SW et al (2007) Mechanisms of cell death in oxidative stress. Antioxid Redox Signal 9 (1):49–89. https://doi.org/10.1089/ars.2007.9.49

Sack M et al (2014) Combination of conventional chemotherapeutics with redox-active cerium oxide nanoparticles – a novel aspect in cancer therapy. Mol Cancer Ther 13(7):1740–1749. https://doi.org/10.1158/1535-7163.MCT-13-0950

Sankar R et al (2014) Anticancer activity of Ficus religiosa engineered copper oxide nanoparticles. Mater Sci Eng C 44:234–239. https://doi.org/10.1016/j.msec.2014.08.030

Schieber M, Chandel NS (2014) ROS function in redox signaling and oxidative stress. Curr Biol 24 (10):R453–R462. https://doi.org/10.1016/j.cub.2014.03.034

Seo J et al (2007) Development of water-soluble single-crystalline TiO2 nanoparticles for photocatalytic cancer-cell treatment. Small 3(5):850–853. https://doi.org/10.1002/smll.200600488

Shafagh M, Rahmani F, Delirezh N (2015) CuO nanoparticles induce cytotoxicity and apoptosis in human K562 cancer cell line via mitochondrial pathway, through reactive oxygen species and P53. Iran J Basic Med Sci 18(10):993–1000. Mashhad University of Medical Sciences. Available at: http://www.ncbi.nlm.nih.gov/pubmed/26730334. Accessed 21 Aug 2019

Sharma V et al (2009) DNA damaging potential of zinc oxide nanoparticles in human epidermal cells. Toxicol Lett 185(3):211–218. https://doi.org/10.1016/j.toxlet.2009.01.008

Shen Z-Y et al (2003) Reactive oxygen species and antioxidants in apoptosis of esophageal cancer cells induced by As2O3. Int J Mol Med 11(4):479–484. Available at: http://www.ncbi.nlm.nih.gov/pubmed/12632101. Accessed 20 Aug 2019

Shi Y et al (2002) Arsenic trioxide induced apoptosis and expression of p53 and bcl-2 genes in human small cell lung cancer cells. Zhonghua jie he he hu xi za zhi = Zhonghua jiehe he huxi zazhi = Chin J Tuberculosis Respiratory Dis 25(11):665–666. Available at: http://www.ncbi.nlm.nih.gov/pubmed/12490120. Accessed 20 Aug 2019

Siddiqui MA et al (2013) Copper oxide nanoparticles induced mitochondria mediated apoptosis in human hepatocarcinoma cells. PLoS One 8(8):e69534. Edited by AB Pant. https://doi.org/10.1371/journal.pone.0069534

Sivaraj R et al (2014) Biosynthesis and characterization of Acalypha indica mediated copper oxide nanoparticles and evaluation of its antimicrobial and anticancer activity. Spectrochim Acta A Mol Biomol Spectrosc 129:255–258. https://doi.org/10.1016/j.saa.2014.03.027

Sturlan S et al (2003) Docosahexaenoic acid enhances arsenic trioxide-mediated apoptosis in arsenic trioxide-resistant HL-60 cells. Blood 101(12):4990–4997. https://doi.org/10.1182/blood-2002-08-2391

Szekeres M et al (2013) Chemical and colloidal stability of carboxylated core-shell magnetite nanoparticles designed for biomedical applications. Int J Mol Sci 14(7):14550–14574. https://doi.org/10.3390/ijms140714550

Tapiero H, Townsend DM, Tew KD (2003) Trace elements in human physiology and pathology. Copper. Biomed Pharmacother 57(9):386–398. Available at: http://www.ncbi.nlm.nih.gov/pubmed/14652164. Accessed 20 Aug 2019

Tarnuzzer RW et al (2005) Vacancy engineered ceria nanostructures for protection from radiation-induced cellular damage. Nano Lett 5(12):2573–2577. https://doi.org/10.1021/nl052024f

Tchounwou PB et al (2012) Heavy metal toxicity and the environment. Springer, Basel, pp 133–164. https://doi.org/10.1007/978-3-7643-8340-4_6

Thevenot P et al (2008) Surface chemistry influences cancer killing effect of TiO2 nanoparticles. Nanomed Nanotechnol Biol Med 4(3):226–236. https://doi.org/10.1016/j.nano.2008.04.001

Trovarelli A, Fornasiero P (2013) Catalysis by ceria and related materials, Catalytic science series. Imperial College Press. https://doi.org/10.1142/p870

Tuli HS et al (2015) Molecular aspects of metal oxide nanoparticle (MO-nanoparticles) mediated pharmacological effects. Life Sci 143:71–79. https://doi.org/10.1016/j.lfs.2015.10.021

van Landeghem FKH et al (2009) Post-mortem studies in glioblastoma patients treated with thermotherapy using magnetic nanoparticles. Biomaterials 30(1):52–57. https://doi.org/10.1016/j.biomaterials.2008.09.044

Vinardell MP, Mitjans M (2015) Antitumor activities of metal oxide nanoparticles. Nanomaterials (Basel, Switzerland). Multidisciplinary Digital Publishing Institute (MDPI) 5(2):1004–1021. https://doi.org/10.3390/nano5021004

Vinardell MP, Mitjans M (2018) Metal/metal oxide nanoparticles for cancer therapy. Springer, Cham, pp 341–364. https://doi.org/10.1007/978-3-319-89878-0_10

von Wilmowsky C et al (2009) In vivo evaluation of anodic TiO 2 nanotubes: an experimental study in the pig. J Biomed Mater Res Part B Appl Biomater. Wiley 89B(1):165–171. https://doi.org/10.1002/jbm.b.31201

Wahab R, Dwivedi S et al (2013a) ZnO nanoparticles induce oxidative stress in Cloudman S91 melanoma cancer cells. J Biomed Nanotechnol, Available at: http://www.ncbi.nlm.nih.gov/pubmed/23621000. Accessed 20 Aug 2019 9(3):441–449

Wahab R, Kaushik NK et al (2013b) ZnO nanoparticles induces cell death in malignant human T98G gliomas, KB and non-malignant HEK cells. J Biomed Nanotechnol 9(7):1181–1189. Available at: http://www.ncbi.nlm.nih.gov/pubmed/23909132. Accessed 20 Aug 2019

Wahab R et al (2014) ZnO nanoparticles induced oxidative stress and apoptosis in HepG2 and MCF-7 cancer cells and their antibacterial activity. Colloids Surf B: Biointerfaces 117:267–276. https://doi.org/10.1016/j.colsurfb.2014.02.038

Wang F et al (2010) Turning tumor-promoting copper into an anti-cancer weapon via high-throughput chemistry. Curr Med Chem 17(25):2685–2698. NIH Public Access. Available at: http://www.ncbi.nlm.nih.gov/pubmed/20586723. Accessed 20 Aug 2019

Wang Y et al (2013) Cuprous oxide nanoparticles inhibit the growth and metastasis of melanoma by targeting mitochondria. Cell Death Dis 4(8):e783–e783. https://doi.org/10.1038/cddis.2013.314

Wang C et al (2015) ZnO nanoparticles treatment induces apoptosis by increasing intracellular ROS levels in LTEP-a-2 cells. BioMed Res Int. Hindawi 2015:1–9. https://doi.org/10.1155/2015/423287

Wang T, Liu Y, Wu C (2017) Effect of paclitaxel-mesoporous silica nanoparticles with a core-shell structure on the human lung cancer cell line A549. Nanoscale Res Lett. Springer 12(1):66. https://doi.org/10.1186/s11671-017-1826-1

Wason MS et al (2013) 'Sensitization of pancreatic cancer cells to radiation by cerium oxide nanoparticle-induced ROS production. Nanomed Nanotechnol Biol Med 9(4):558–569. https://doi.org/10.1016/j.nano.2012.10.010

Xia L et al (2017) Cuprous oxide nanoparticles inhibit the growth of cervical carcinoma by inducing autophagy. Oncotarget 8(37):61083–61092. https://doi.org/10.18632/oncotarget.17854

Xiao Y-F et al (2016) Cerium oxide nanoparticles inhibit the migration and proliferation of gastric cancer by increasing DHX15 expression. Int J Nanomedicine 11:3023–3034. https://doi.org/10.2147/IJN.S103648

Yamaguchi S et al (2011) Sonodynamic therapy using water-dispersed TiO2-polyethylene glycol compound on glioma cells: comparison of cytotoxic mechanism with photodynamic therapy. Ultrason Sonochem 18(5):1197–1204. https://doi.org/10.1016/j.ultsonch.2010.12.017

Yang S-M et al (2016) Cerium oxide nanoparticles inhibit the migration and proliferation of gastric cancer by increasing DHX15 expression. Int J Nanomedicine 11:3023–3034. https://doi.org/10.2147/IJN.S103648

Yeh JY et al (2002) Differential influences of various arsenic compounds on glutathione redox status and antioxidative enzymes in porcine endothelial cells. Cell Mol Life Sci 59 (11):1972–1982. Available at: http://www.ncbi.nlm.nih.gov/pubmed/12530527. Accessed 20 Aug 2019

You DG et al (2016) 'ROS-generating TiO2 nanoparticles for non-invasive sonodynamic therapy of cancer', Scientific Reports, 6(1), p. 23200. https://doi.org/10.1038/srep23200

Youkhana EQ et al (2017) Titanium dioxide nanoparticles as radiosensitisers: an in vitro and phantom-based study. Int J Med Sci 14(6):602–614. https://doi.org/10.7150/ijms.19058

Yu M et al (2013) Hyaluronic acid modified mesoporous silica nanoparticles for targeted drug delivery to CD44-overexpressing cancer cells. Nanoscale 5(1):178–183. https://doi.org/10.1039/C2NR32145A

Yu B et al (2017) Cuprous oxide nanoparticle-inhibited melanoma progress by targeting melanoma stem cells. Int J Nanomedicine 12:2553–2567. https://doi.org/10.2147/IJN.S130753

Zhang A-P, Sun Y-P (2004) Photocatalytic killing effect of TiO2 nanoparticles on Ls-174-t human colon carcinoma cells. World J Gastroenterol 10(21):3191. https://doi.org/10.3748/wjg.v10.i21.3191

Zhang X et al (2008) Different CuO nanostructures: synthesis, characterization, and applications for glucose sensors. J Phys Chem C. American Chemical Society 112(43):16845–16849. https://doi.org/10.1021/jp806985k

Zhang W et al (2015) Inducing cell cycle arrest and apoptosis by dimercaptosuccinic acid modified Fe3O4 magnetic nanoparticles combined with nontoxic concentration of bortezomib and gambogic acid in RPMI-8226 cells. Int J Nanomedicine 10:3275–3289. https://doi.org/10.2147/IJN.S80795

Zijno A et al (2015) Different mechanisms are involved in oxidative DNA damage and genotoxicity induction by ZnO and TiO2 nanoparticles in human colon carcinoma cells. Toxicol In Vitro 29 (7):1503–1512. https://doi.org/10.1016/j.tiv.2015.06.009

Chapter 11
Metal induced Neurotoxicity and Neurodegeneration

Krishnapriya Madhu Varier, Arpita Salkade, Babu Gajendran, Yanmei Li, Yang Xiaosheng, Arulvasu Chinnasamy, and Sumathi Thangarajan

Contents

Abstract Metals are abundantly present in the earth's crust and have many occupational uses. They are also vital for living organisms as they are required in small quantities to carry out physiological functions. However, increased exposure leads to accumulation of metals leading to toxic effects. Metals are distributed in

Krishnapriya Madhu Varier and Arpita Salkade contributed equally to this chapter.

K. M. Varier · S. Thangarajan
Department of Medical Biochemistry, Dr. ALM PGIBMS, University of Madras, Chennai, Tamil Nadu, India

A. Salkade
Living Systems Institute, College of Medicine and Health, University of Exeter, Exeter, UK

B. Gajendran (✉) · Y. Li · Y. Xiaosheng
Department of Biology and Chemistry, The Key Laboratory of Chemistry for Natural Products of Guizhou Province and Chinese Academy of Sciences, Guiyang, Guizhou Province, China

State Key Laboratory of Functions and Applications of Medicinal Plants, Guizhou Medical University, Guiyang, Guizhou Province, China

A. Chinnasamy
Department of Zoology, University of Madras, Chennai, Tamil Nadu, India

environment due to pollution and industrial effluents thus increasing the human exposure to toxic metals. Elevated levels of metals in the body facilitate their transportation to various organs including the brain resulting in physiological disturbances. Neurotoxic effects of metals lead to dementia and cognitive defects resulting in neurodegenerative disorders. The highly toxic metals include mercury, lead, aluminum, iron, cadmium, and arsenic. Although iron is essential for cellular homeostasis, yet when present in excess leads to wide variety of neurodegenerative disease. In this chapter, we have focused on these six metals and their neurotoxic complications.

Keywords Toxicity · Metal · Mercury · Aluminium · Lead · Iron · Cadmium · Arsenic · Reactive oxygen species · Oxidative stress · Apoptosis · Neuroinflammation · Neurodegeneration

11.1   Introduction

Metals are opaque, hard, lustrous, sonorous substances found in the earth'scrust. They are also found in water bodies, plants, and variousecosystems (Chen et al. 2016). On the basis of periodic table, the metals are categorized as alkali metals, alkaline earth metals, and transition metals. There are certain other substances called metalloids which possess characteristics of both metals and non-metals. Among these, some are essential metals, whereas some are non-essentials metals for human body. Essential alkali and alkaline earth metals are sodium and potassium and calcium, respectively. Dietary importance of essential transition metals, namely, copper, cobalt, manganese, magnesium, zinc, iron, nickel, selenium, and chromium in micro quantities, has been recognized by humans. Metals are crucial for the normal functioning of human body as they function as cofactors or prosthetic groups for enzymes in various metabolic processes. The very important component of the human body, the blood, also requires iron for the formation of hemoglobin. They are responsible for a host of physiological processes like immune responses, electron transport chain, protein modifications, and metabolism of proteins, fats, and carbohydrates (Chen et al. 2016).

Metals are also imperative for the nervous system. Fundamental neural processes like generation of action potentials and membrane polarization are under tight regulation of Na^+, K^+, and Ca^{2+}. Zinc is bound to metalloproteins in glia and neurons. Similarly, iron and copper are responsible for neurotransmitter synthesis. Neurotransmitter L-3,4-dihydroxyphenylalanine (L-DOPA) is synthesized from tyrosine catalyzed by tyrosine hydroxylase, which requires Fe^{2+} as cofactor. Likewise, noradrenaline is formed from dopamine requiring β-dopamine hydroxylase, a Cu-containing enzyme (Chen et al. 2016).
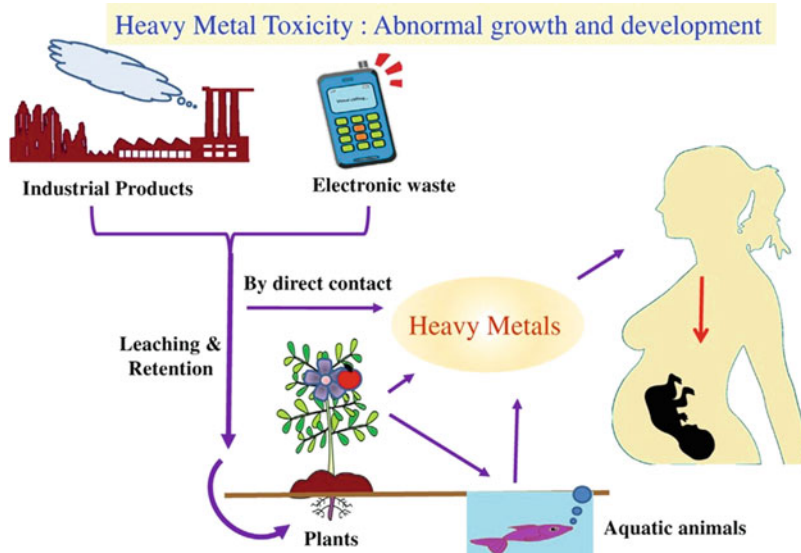
Fig. 11.1 Routes of entry of heavy metals into the environment and ecosystem (Vimalraj et al. 2017; copyright received)

Despite the significance of metals for plants and animals, their requirement is in trace quantities. Augmented levels of metals lead to agglomeration of metals in various organs including the brain causing neurotoxicity leading to neurodegeneration. In spite of the multifactorial etiology of the neurodegenerative diseases, there are potential evidences indicating that exposure to chemicals and environmental pollutions containing heavy and toxic metals makes an individual susceptible to neurodegenerative disease later in life. Heavy metals are hazardous environmental pollutants posing a threat to mankind. These enter ecological systems through natural and human activities (Fig. 11.1). The most commonly found heavy metals in wastewater cause risks for human health and the environment. Earlier studies have pointed out that oxidation of biomolecules is a major consequence of the binding of heavy metals to DNA and nuclear proteins (Lambert et al. 2000). Tables 11.1 and 11.2 depicts the common molecules involved in toxicity and transport proteins involved in major metal toxicities, respectively.

In the recent years with technological developments, metals are omnipresent in currencies, jewelries, batteries, wires, automobiles, microchips enclosed in plastic-covered electronic devices, dyes, and pigments (Fig. 11.2). Metals have a widespread use owing to their malleability and ductility (Caito and Aschner 2015). Several heavy metals cause many havocs (Morais et al. 2012). According to estimates of World Health Organization (WHO), over 25% of the total disease burden is related to environmental factors including exposure to noxious chemicals (Mamtani et al. 2011).

Table 11.1 Molecules involved in blocking teratogenic effects of toxic metals (Vimalraj et al. 2017; copyright received)

Molecules	Function
NO	NO rescued Cd-induced abnormalities in chick embryos by normalizing NO-cGMP signaling and peroxynitrite-induced apoptosis
Glutathione	Glutathione reduces metaltoxicity by chelating metal ions by its antioxidant property and prevents activation of c-Jun N-terminal kinase
Mercaptoacrylic acid (MFA)	MFA chelates Cd ions and protects against Cd-induced malformations and embryonic death
DNA methylation	Cd has cardiac depressant effects which are rescued by inhibition of DNA methylation
Grapefruit juice	Antioxidant activity of grapefruit juice protects against teratogenic and genotoxic effects of Cd
Spirulina	Antioxidant activity of spirulina potentially decreases teratogenic effects of Cd
Glycine	Antioxidant activity of glycine protects against teratogenic effects of Cd
Caffeine	Antioxidant activity of caffeine protects against Cd-induced deformities in the eye, abdomen, and skeleton of mouse embryos
Zn	Cd toxic disrupts peridermal cell adhesion and induces cell death in the mesoderm. Zn pretreatment prevents these teratogenic effects
Dithiothreitol	Arsenite-induced expressions of heat shock protein 27 (hsp27), alpha B crystallin, and hsp70 are downregulated by dithiothreitol in glioma cells
Ergothioneine	Antioxidant activity of ergothioneine may have preventive role on Cd-induced teratogenic effects
Selenium	Selenium antagonizes the induction of heme oxygenase by Cd and As toxicity. Heme oxygenase-1 drives metaflammation and insulin resistance
Verapamil	Verapamil, a Ca-channel blocker, could protect against Cd-induced teratogenicity

Consequently, we are exposed to metals to an extent uncommon in the pre-industrial era. This has resulted in a surge in cases of neurodegenerative diseases like HD, AD, and PD worldwide. In the current chapter, we have made an attempt to emphasize on the neurotoxic effects of key metals involved in neurodegeneration, namely, mercury, aluminum, lead, and iron.

11.2 Metals Involved in Neurotoxicity and Neurodegeneration

11.2.1 Mercury

Mercury is a highly poisonous element occurring in various forms as elemental Hg (Hg^0), inorganic Hg compounds (mercurous Hg_2^{2+} and mercuric Hg^{2+}), and organic Hg compounds (e.g., MeHg, ethylmercury, etc.). Hg is found in the earth's crust and

Table 11.2 Metal transport proteins and their functions (Vimalraj et al. 2017; copyright received)

Metal transporter	Function
Human serum albumin	Binds to Cu, Zn, Ni, Co, and Cd ions in the circulation which helps in transportation of these ions
	Cysteine-rich proteins which can bind mono and divalent metal ions and play a vital role in homeostasis of essential zinc and copper ions. Evidence indicates that certain
Metallothioneins (MTs)	MTs bind metals like zinc and copper. Increased levels of these MTs correlated with accumulation of these ions
8 zinc-like iron-like protein (ZIP8)	Transport of Cd ion from the extracellular and/or intracellular space into cytosols of vascular endothelial cells
14 zinc-like iron-like protein (ZIP14)	ZIP14 and ZIP8 regulate transport, subcellular localization, and tissue distribution Cd. Oral treatment with Cd alters ZIP14 expression. ZIP14 knockout mice accumulate Cd ion
Transient receptor potential vanilloid type	These receptors are involved in Cd ion transportation and homeostasis. Cd can cause decreased expression of TRPV5/6, if Cd levels decrease
5/6 (TRPV5/6) transporter-1 (DMT1)	DMT1 is a member of the hydrogen-coupled metal ion transporter family and is involved in transport of eight metal ions (Cd, Pb, Ni, Co, Zn, Mn, Cu). DMT1 levels are associated with increased concentrations of Cd ion in blood
Voltage-dependent calcium channels (VDCC)	A family of calcium channels involved in membrane permeation of Cd and Pb ions
Divalent metal ion	
Organic cation transporters 1/2 (OCT1/2)	OCT1/2 transporters facilitate active/passive transport of Cd ion from basolateral membranes of cells to renal proximal tubular cells
Glutathione (GSH)	A major intracellular antioxidant which plays a role in detoxification of heavy metals such as cadmium. GSH and MTs have a cooperative role against Cd ion toxicity
L-cysteine (L-Cys)	L-Cys forms a complex ($[Ca(CysS)_4]^{-2}$) with Cd and contributes to detoxification of Cd ion
L-homocysteine (L-Hcy)	L-Hcy can transport Cd ion from lumen of glands or ducts. This leads to intracellular accumulation of Cd ion
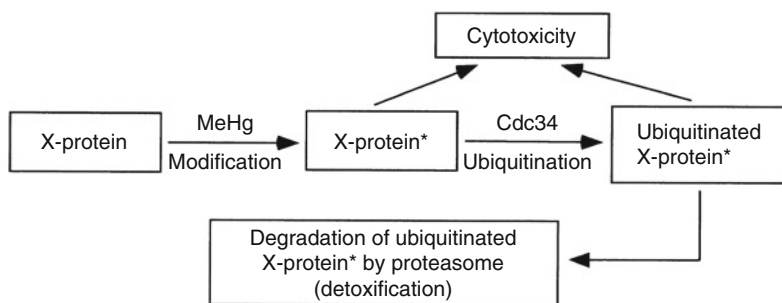
Fig. 11.2 The mechanism of methylmercury causing cytotoxicity (Hwang et al. 2002; copyright received)

in minute quantities in air (Clarson and Magos 2006). Mercury is deposited in the environment as gaseous mercury which can be inhaled or as methylmercury (MeHg), a highly toxic compound, through natural processes like volcanic eruptions or forest fires and anthropogenic sources like municipal waste, industrial effluents, smelting, cement production, incineration, agriculture, mining, and coal combustion (Caito and Aschner 2015). Dispersal of mercury into water bodies accounts for the conversion of Hg into MeHg by anaerobic and sulfate-reducing bacteria (Parks et al. 2013). Eventually, MeHg undergoes biomagnification and entering food chain. Consumption of aquatic animals contaminated by MeHg is the major source of human exposure to MeHg (Sheehan et al. 2014). Additionally, Hg is widely used in paper industry, barometers, thermometers, fluorescent lamps, mercury arc lamps, antiseptics, skin-lightening agents, teething powders, and dental amalgams (Jaishankar et al. 2014; Caito and Aschner 2015).

Mercury is considered among the top ten chemicals of "major public health concern" by the WHO (WHO 2013). Chronic exposure to MeHg results in Minamata disease affecting particularly children, characterized by hearing impairment, depression, blurred vision, neurological problems, and gustatory and olfactory disturbances. Sizable studies have proven that in utero exposure to MeHg is associated with developmental neurotoxicity (Sheehan et al. 2014). A study conducted by Yuan et al. shows that in utero exposure to MeHg affects neuronal differentiation resulting in long-term neurological effects in adulthood (Yuan et al. 2018). Chronic exposure to mercury vapors causes tremors, memory loss, cognitive disturbance, anxiety, and erythrism. Occupational exposure to mercury declines visuomotor coordination and visual scanning along with reduction in verbal and visual memory (Ekino et al. 2007; Bernhoft 2012).

Mechanism of Mercury Neurotoxicity

The brain is the primary target organ for mercury. Several mechanisms are proposed to be responsible for mercury neurotoxicity. Accumulation of MeHg is seen in central nervous system (CNS) predominantly in astrocytes. Absorption of elemental HG occurs from the lungs from where it is diffused to blood–brain barrier (BBB). MeHg is absorbed from the gastrointestinal tract and lungs and via the percutaneous route from where it is easily transported to BBB (Unoki et al. 2018). MeHg traverses blood–brain barrier (BBB) with the assistance of amino acid transport system 1, which amicably complexes with L-cysteine and enhances increasing Hg accumulation in the brain by threefold (Unoki et al. 2018). Mercury acts as an electrophile and reacts with selenol (SeH) and thiol (-SH) groups resulting in denaturation of tertiary and quaternary structure of proteins and thus altering cellular functions (Ballatori and Clarkson 1985; Bernhoft 2012). MeHg reacts with GSH and forms glutamine synthetase (GS)–HgCH$_3$ complex, elevating the GSSG: GSH ratio resulting in reduced antioxidant activity in microglia and astrocytes. MeHg also hampers the activity of glutathione peroxidase (GPx) and electron transport chain which causes enhanced ROS production ultimately leading to protein oxidation,

lipid peroxidation, and DNA oxidation (Ni et al. 2010; Caito and Aschner 2015). Mercury also interferes with the transcription and translation processes leading to elimination of ribosomes and endoplasmic reticulum and also causes loss of activity of natural killer cells (Jaishankar et al. 2014).

Methyl mercury inhibits the activity of proteins required for calcium homeostasis, glutamate transportation, and GABA signaling. Accumulation of MeHg in astrocytes increases the concentration of excitatory neurotransmitter, glutamate, resulting in excitotoxicity. MeHg spikes mercuric chloride levels in astrocytes, thus decreasing glutamine transport due to reduction of glutamine synthetase activity. It also decreases GABA signaling, playing a key role in MeHg neurotoxicity (Ballatori and Clarkson 1985). Various studies have indicated the activation of heat shock factor protein 1 (Hsf1), proteasome-ubiquitination system, and autophagic processes as cellular defense mechanisms in response to MeHg-induced cytotoxicity (Hwang et al. 2002; Yoshida et al. 2011). The mechanism of its toxicity is mentioned in Fig. 11.2.

11.2.2 Aluminium

Aluminum (Al) is one of the most abundant elements in the earth's crust occurring in air, water, and soil. The high reactivity of Al to carbon and oxygen makes it highly toxic for living organisms. Al is widely used in food preservatives, cookwares, vaccines, cars, and cans (Shaw and Tomljenovic 2013). Al and its alloys are used in wiring, electronics, food packaging, fireworks and explosives, rocket propellants, vehicles, building materials, and fire-resistant abrasives (Riihimaki and Aitio 2012; Krewski et al. 2007). Nevertheless, the total consumption of Al differs significantly according to nation and dietary composition. Daily dietary Al intake of humans is almost 10 mg; 9.6 mg of this quantity is drawn from food, 0.1–0.4 mg from cooking utensils and packaging, and 5 µg is taken from air (Vargel 2004).

Mechanism of Aluminum Neurotoxicity

Although Al gaining entry into the human biological system by dietary intake and environmental exposure is rapidly eliminated by the kidneys, yet Al salts as adjuvants are biologically available and are accrued in the nervous system (Shaw and Tomljenovic 2013). Presence of citrate in the gastrointestinal tract has also been implicated for enhanced absorption of Al by completing with other binding ligands for Al (Glynn et al. 2001). However, increased intake of silicone compounds reduces the absorption of Al by expediting its excretion (Krewski et al. 2007). Absorption of Al is greatly affected by iron and calcium intake. Iron competes with Al for binding to transferrin, thus reduced dietary intake of iron facilitates increased Al absorption. Similarly, calcium deficiency promotes Al absorption (Provan and Yokel

1998–1990). Symptoms of chronic aluminum exposure include mild depression, fatigue, memory loss, and concentration problems (Caito and Aschner 2015).

Aluminum is found in only one oxidation state, Al^{3+}. It exhibits greater affinity for negatively charged oxygen ligands. This facilitates the strong between Al and phosphates moieties of DNA and RNA perturbing the topology of DNA and eventually resulting in altered gene expressions. Al^{3+} is also able to interact with the phosphate groups of ADP and ATP, thereby affecting energy metabolism. Strong binding of Al to phosphorylated amino acids encourages the aggregation of phosphorylated cytoskeletal proteins like neurofilaments and microtubule-associated proteins (Kawahara and Kato-Negishi 2011, Walton 2010).

Al also promotes lipid peroxidation leading to production of oxidative end products like malondialdehyde, peroxynitrites, and carbonyl which create an imbalance in oxidant and antioxidant enzymes, thereby altering the cellular redox potential leading to oxidative stress (Markewberry 1994).

Aluminum and Alzheimer's Disease

Alzheimer's disease is one of the predominant neurodegenerative diseases affecting human population. The pathological hallmarks of AD include deposition of extracellular senile plaques, formation of intracellular neurofibrillary tangles (NFTs), and the selective loss of synapses and neurons in the cerebral, cortical, and hippocampal regions (Kawahara and Kato-Negishi 2011). NFTs comprise mainly of phosphorylated tau protein, and senile plaques contain β-amyloid protein. Over the years, several studies have implicated that exposure to Al contributes to the development of Alzheimer's disease (Selkoe 1991). Most instances of AD are not hereditary, but rather sporadic, supporting the involvement of environmental exposures in neurodegenerative diseases. Excessive levels of Al in brain cause disturbances in cholinergic transmission by decreasing the activity of cholineacetyl transferase and acetylcholinesterase enzymes (Yellamma et al. 2010). A study conducted by Shen et al. in China reported a relation between levels of Al in soil and the mortality caused by AD (Shen et al. 2014).

Abundant research has indicated a potential link between inductions of NF-kB-sensitive pro-inflammatory miRNAs by aluminum sulfates. Aluminum significantly upregulates the transcription factor NF-kB which increases expression of NF-kB-sensitive miRNAs which eventually downregulates the expression of complement factor H (CFH) and neurotropic signaling compromised in AD (Pogue et al. 2009). The deleterious effects of Al are mentioned in Fig. 11.3.

Long-term intoxication of rats by Al at a dose of 20 g/day in the food/twice weekly from 6 months of age to the end of their lives upsurges the synthesis of amyloid-β (Aβ) by elevating the amount of amyloid precursor protein (APP) in the hippocampus and cortex (Walton and Wang 2009). Degradation of APP by β- and γ-secretase complexes produces Aβ (Thinakaran and Koo 2008).

Al also promotes the formation of aggregation of tau and neurofilament monomers from their soluble form to non-fibrillary material. Al induces

Fig. 11.3 Summary of the effects of aluminum in the brain (Morris et al. 2017; copyright received)
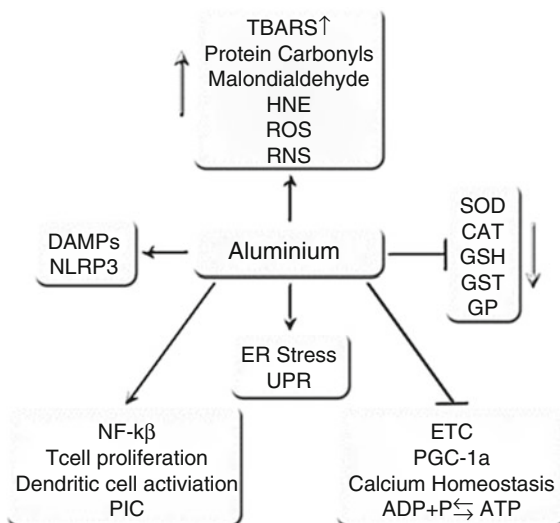
hyperphosphorylation of tau by impeding protein phosphatase 2A (PP2A) activity in pyramidal cells (Walton 2010).

11.2.3 Lead (Pb)

Lead is a bright silvery and slightly bluish metal found in dry atmosphere (Caito and Aschner 2015). It is classified as non-essential heavy metal with no potential beneficial effects for humans and is found abundantly in the ecosystem (Mason et al. 2014). Anthropogenic activities like manufacturing, mining, and combustion of fossil fuels have led to multiplication of Pb to obnoxious levels. Lead exists naturally in the environment as ores, namely, galena, cerussite, and anglesite (Needleman 2004). The non-biodegradable nature and continual usage of Pb have led to its accretion in the environment posing serious health hazards. Individuals employed in industries pertaining to gasoline, smelting, and combustion of lead, armaments, and paint are constantly exposed to lead. Batteries, pigments, plumbing pipes, toys, pottery, lead bullets, and cosmetics also contain lead. Vehicle exhausts and industrial emissions release large amounts of lead into the atmosphere (Thurmer et al. 2002; Wani et al. 2015; Martin and Griswold 2009) (Fig. 11.4). Thus, lead enters the food chain via soil and water bodies ultimately exposing humans to lead through food and drinking water (Wani et al. 2015).

Red blood cells transport Pb to the liver and kidney from where it is distributed to bone, teeth, and hair in the form of phosphate salt. It is excreted through urine and bile (Mason et al. 2014).
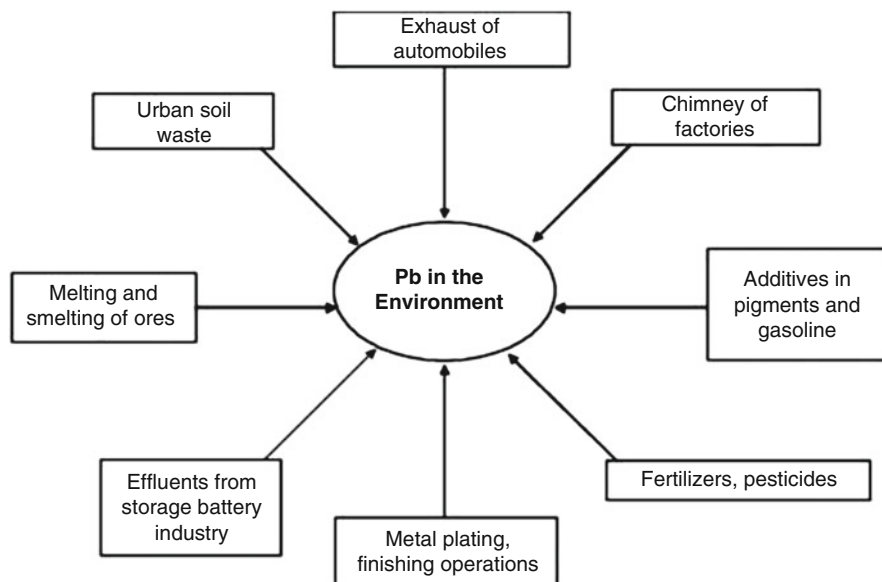
Fig. 11.4 Sources of lead entry into the environment (Sharma and Dubey 2005; copyright received)

Mechanism of Lead-Induced Neurotoxicity

Symptoms of lead-induced neurodegeneration include headache, hallucinations, hyperactivity, sleeplessness, memory deficits, disturbance in visuospatial and motor skills, irritability, muscle pain, and weakness (Martin and Griswold 2009; Caito and Aschner 2015; Mason et al. 2014). The primary target of Pb is the hippocampus in the brain (Nava-Ruiz et al. 2012). Lead poisoning causes depletion of myelin sheath and diminished neuronal count (Pearson and Schonfeld 2003). It can easily traverse through endothelial cells of the BBB (Brunton et al. 2007). Lead vitiates learning and memory by inhibiting N-methyl-D-aspartate receptor (NMDAR), blocking the release of neurotransmission thereby inhibiting neurotransmission, impeding the neuronal voltage-gated calcium (Ca^{2+}) channels (VGCCs), and reducing the expression of brain-derived neurotrophic factor (BDNF) (Engwa et al. 2018). It has been confirmed in various studies that exposure of pregnant rats to Pb leads to developmental learning deficits in pups comparable to absence of NMDAR (Morris et al. 1982). A study demonstrated that rats chronically exposed to rats exhibit reduction in the release of Ca^{2+}-dependent glutamate and γ-aminobutyric acid (GABA) in the hippocampus. Lead inhibits neurotransmission by blocking voltage-gated calcium channels. Furthermore, Pb also downregulates the expression of synaptophysin and synaptobrevin, presynaptic proteins involved in vesicular neurotransmission release (Xiao et al. 2006; Braga et al. 1999). Several other molecular mechanisms such as oxidative stress, mitochondrial dysfunction,

and inhibition of nitric oxide synthase are also implicated in Pb-induced neurodegeneration (Struzyñska et al. 2001).

11.2.4   Iron (Fe)

Iron is a very important element required for growth and survival of living beings. It acts as a vital cofactor for enzymes like catalase and cytochromes and is constituent of important biological molecules like hemoglobin and myoglobin as it can easily oscillate between Fe^{2+} and Fe^{3+} ionic state. Humans are primarily exposed to Fe through food (Arber et al. 2016). The main sources of iron are mining activities and the oxidation of iron pyrites (FeS_2) in coal seams releasing Fe^{2+} and dispensing sulfuric acid (Valko et al. 2005). It is required in small amounts for maintaining physiological functions; however, accumulation of Fe to toxic levels is primarily due to deranged Fe homeostasis and metabolism in the brain (Salvador et al. 2010).

Mechanism of Iron Neurotoxicity

Non-binding of free absorbed iron to proteins leads to formation of free radicals. Iron in its free state generates hydroxyl radicals ($OH^{\cdot}$) by Fenton reaction which is as follows:

$$Fe^{3+} + O^{2-} \rightarrow Fe^{2+} + O_2$$

$$Fe^{3+} + O_2{}^- \rightarrow Fe^{2+} + O_2$$

$$Fe^{2+} + H_2O_2 \rightarrow Fe^{3+} + OH^{\cdot} + OH^- \, (Fenton\ reaction)$$
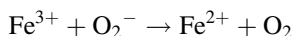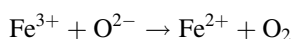
The hydroxyl radical generated reacts with biomolecules and leads to oxidation of proteins, lipids, and DNA (Valko et al. 2004).

Accumulation of iron and disturbances in iron homeostasis are linked with a number of neurodegenerative diseases like Alzheimer's disease, Parkinson's disease, Huntington's disease, and neurodegeneration with brain iron accumulation (NBIA). Increased accumulation of Fe has been observed in the brains of patients suffering from HD, AD, and PD. In AD Fe accumulation promotes aggregation of β-amyloid, whereas in PD, same is observed with α-synuclein (Chen et al. 2016).

Iron, as Fe^{2+}, is transported across BBB by DMT1 transporter (Moos and Morgan 2004), and Fe^{3+} ions are transported by transferrin receptor-mediated endocytosis (TfR-ME) (Huebers et al. 1983). Different research studies have indicated that upregulation of DMT1 takes place in mice and rats intoxicated with 1-methyl-4-phenyl-1,2,3,6-tetrahydropyridine (MPTP) and 6-hydroxydopamine (6-OHDA), respectively (Salazar et al. 2008; Jiang et al. 2010). Iron is taken up into the brain
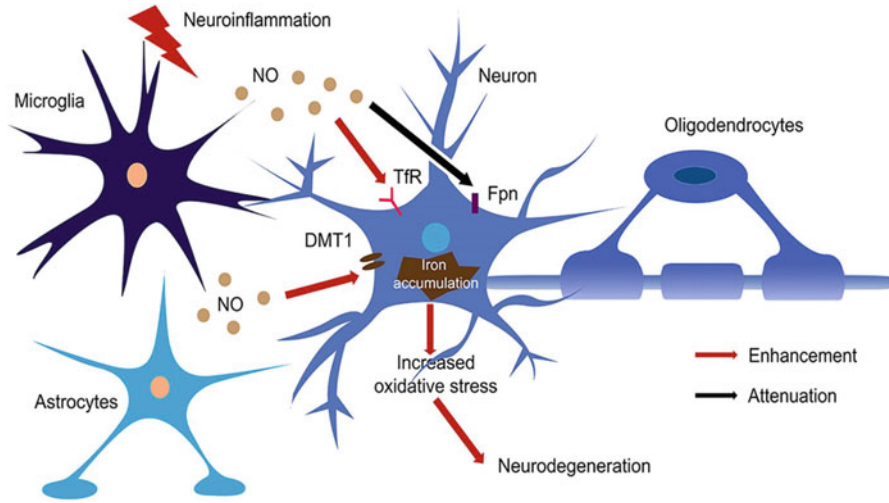
Fig. 11.5 Description on Fe-induced neurodegeneration. Nitric oxide (NO), which regulates iron homeostasis, is released during neuroinflammation due to activation of iNOS**.** NO upregulated Tfr and DMT1 and downregulated Fpn leading to accumulation of iron in neurons. This results in oxidative stress and ultimately neurodegeneration (Courtesy to Liu et al. 2019; copyright received)

by the capillary endothelial cells of the blood–brain barrier through TfR in the form of transferrin- Fe^{3+}. Transferrin is crucial for myelin sheath formation where oligodendrocytes also play an important role. Therefore, there is always a high demand of iron for oligodendrocytes. The efflux of iron takes place through ferroportin (Fpn) (Zecca et al. 2004). Iron is exported from astrocytes with ceruloplasmins playing a major role in conversion of Fe^{2+} to Fe^{3+} (Moos et al. 2006). During inflammatory conditions, iron accumulation occurs in microglia instead of iron being transported to astrocytes (Zarruk et al. 2015). This results in activation of inducible nitric oxide synthase (iNOS) in neuroinflammatory conditions. Immune response molecules like interleukin-4 (IL-4), transforming growth factor-beta (TGF-β), or IL-10 (Green et al. 1994) feebly inhibit iNOS resulting in production of nitric oxide (NO). This NO facilitates increased iron uptake through DMT1 due to enhanced S-nitrosylation leading to Fe accumulation over time (Liu et al. 2019; Fig. 11.5).

Synapses are highly vulnerable to iron-induced oxidative stress as evident from lipid peroxidation of membranes, mitochondrial dysfunction, and impairment of ion-motive ATPases resulting in activation of PI3K, Akt, and GSK-3β in the synaptic endings of nerves undergoing iron-induced oxidative stress (20). Additionally, iron activates apoptotic pathway in intact neurons by activation of caspase-3, mitochondrial calcium uptake, and ROS accumulation (Uranga et al. 2009).

11.2.5 Cadmium

Cadmium from either industrial or natural means could affect the human life very deleteriously (Rafati et al. 2013). Cadmium is a soft element silvery off-white blue colored and odorless (Adriano 2001). Cadmium also forms complexes with amines, sulfur, and chlorides (Cobb 2008).

Mode of Neurotoxicity of Cadmium (cd)

The cadmium (Cd) is a metal which is highly prone to cause a wide range of neurotoxicity. According to Kumar et al. (1996), Cd can disrupt the cellular membrane potentials, majorly in the hippocampus (Fig. 11.6). The Cd^{+2} ion could enter the neuronal cytosol which mimics the Ca^{+2} altering the voltage of its channel. This, in turn, results in the downregulated expression of brain-derived neurotrophic factor (BDNF) and upregulation of intracellular Ca^{+2}, thus forming free radicals which results in neuronal apoptosis (Wong and Klaassen 1982). However, the experimentation in mice pups revealed that the utero acquaintance to Cd can instinctively impede the acetylcholine esterase (AchE) and sodium potassium ATPase pump, thus
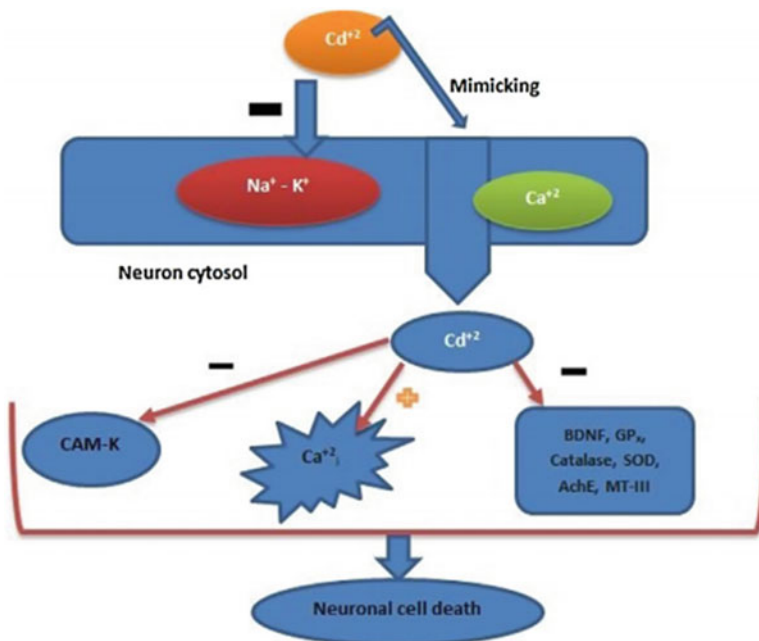
Fig. 11.6 Mechanism of cadmium causing neuronal death (Karri et al. 2016)

reducing the neuronal activity (Chandra 1991). This Ca^{+2}-mimicking property of Cd^{+2} results in various processor like cell proliferation, differentiation (Xu et al. 2011), and neurotransmitters release (Huguenard 1996). The Cd mode of action is represented in Fig. 11.6. Some study revealed that Cd could even affect the Ca^{+2}-binding molecules like calmodulin K (CAM-K) (Hayat et al. 2003). The experimental dose-dependent studies explored the fact that the intracellular Ca^{+2} concentration was elevated in neurons under higher Cd exposure and other deleterious effects (Orrenius and Nicotera 1994; Alshuaib and Byerly 1996). Mainly, this results in elevated reactive oxygen species (ROS) production and consequent reduction of intracellular antioxidants and impeded activity of MT-III (Lopez et al. 2006).This was derived by Mendez-Armenta and Rios (2007) by a study in cerebral cortical neurons, which they claimed as the major target of Cd-induced neuronal apoptosis.

11.2.6   Arsenic (As)

For the past century onwards, arsenic (As) is used as a pesticide and component of variety of manmade products (Hughes et al. 2011); thus globally the rate of As exposure was increased drastically (Singh et al. 2015). According to statistics, around 145 million people are exposed to As through drinking water in various corners of the world (Ravenscroft et al. 2009). However, many reports are there to establish the deleterious toxicities of As; its neurotoxic effects are less comprehended (Guha and Dasgupta 2011; Ishii et al. 2018; Mochizuki et al. 2019). Despite these levels, As accumulation in animals sheds light on the significance of the bioaccumulation in the food chain (Onishi 1969). As a metabolic product, As always accumulates in the body as arsenobetaine (C5H11AsO2), which is toxic to the biodiversity (Newcombe et al. 2010). Figure 11.7 depicts the various sources of As toxicity in the biosphere.

Fig. 11.7 Sources of arsenic causing neurotoxicity (Sahoo and Kim 2013; copyright received)
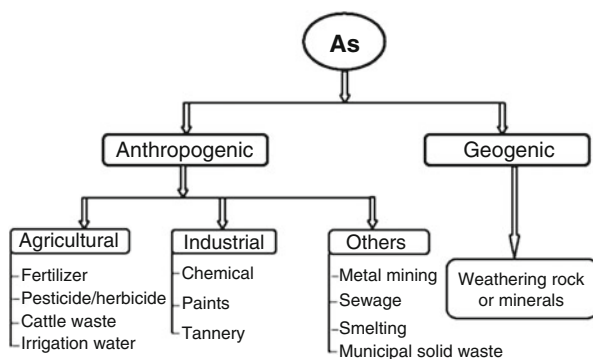
Mode of Neurotoxicity of Arsenic

The minor exposure to As result usually in cognitive impairments (Naujokas et al. 2013), while its higher intoxications causes delayed neuronal development via neuronal tube imperfections (Ahmed et al. 2011). Wasserman and team have established that neonatal As exposure could reduce the performance scores (Wasserman et al. 2004). This was correlated in the experimental models as the potent alteration in the hippocampus causes dysfunctional cognitive behavior (Cronican et al. 2013) and primarily controls the synaptic plasticity of neurons in this region (Kruger et al. 2006). Moreover, the ex vivo cell culture study substantiated that the As intoxication in cells increased the amyloid protein, which resulted in hyperphosphorylation of tau protein causing neurodegeneration (Gaisson et al. 2002).

In vivo study in rat from prenatal to early life stage has found that As exposure produces imbalance in defensive antioxidative mechanism and neurotransmitter metabolism in the hippocampus region of the brain (Xi et al. 2010), where As reduces GSH, glutathione peroxide (GPx), and glutathione synthase (GS) activity and elevates the lipid peroxidation at postnatal day 0, 28, and 42, respectively (Rigon et al. 2008). In As-related oxidative stress, the released ROS and lipid peroxidation elements increase the activity of SOD and decrease the hyperphosphorylation of tau protein resulting in neurodegeneration (Gaisson et al. 2002). Cellular level experiments reported that As has property to alter the metabolism of assorted neurotransmitters like monoamines, acetylcholine, gamma amino butyric acid (GABA), and glutamate (Rodriguez et al. 2002). In the past decade, in many As-intoxicated cellular models, there was a heavy drop in monoamines like dopamine, adrenaline, serotonin, as well as noradrenaline (Yadav et al. 2010). The metal even subdues the NMDA receptors of the hippocampus, by altering the synaptic plasticity and memory (Luo et al. 2009). According to Patlolla and Tchounwou (2005), As affects the neurotransmitter metabolism causing increased AChE action and glutamate decarboxylase (GAD) mRNA expression, directly acting on the antioxidant status (Fig. 11.8). The toxicity even causes the imbalances in the glutathione-related enzymes, leading to variations in propositions in the cellular redox status (Rao and Avani 2004). Mechanistically, this metal-mediated toxicity causes activation of apoptotic factors in the brain by triggering p38 mitogen-activated protein kinase (P38 MAPK) and c-Jun N-terminal kinase 3 (JNK3)(Namgung and Xia 2001), which subsequently enhances the DNA damage and death of the brain cells (Felix et al. 2005) causing alternations in the neurobehavioral function (Prakash et al. 2015).
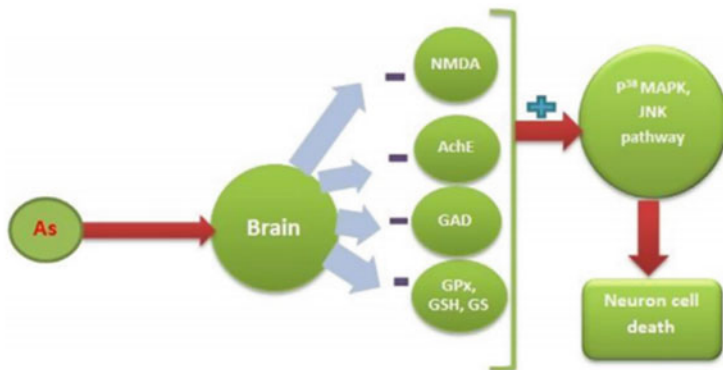
sign indicates inhibition of cellular elements and + sign shows rising apoptotic factors

Fig. 11.8 Mechanism of arsenic intoxication in the human brain (Karri et al. 2016)

11.3 Conclusion

Occupational exposure to metals has been increasing day by day in the modern era of industrialization. The neurotoxic effects of metals are varying depending on the type of metal and route of exposure. Metal-induced neurotoxicity is responsible for a variety of neurodegenerative diseases like HD, PD, and AD. It is highly important to develop biomarker test for diagnosis of metal-induced neurotoxicity to prevent further damages to healthy individual. It is also the need of the hour to emphasize on the development of therapeutic strategies to overcome the toxic effects of accumulation of metals.

References

Adriano DC (2001) Trace elements in terrestrial environments biogeochemistry, bioavailability and risks of metals, 2nd edn. Springer-Verlag, New York. https://doi.org/10.1007/978-0-387-21510-5, 264 pp

Ahmed S, Mahabbate KS, Rekha RS, Gardner RM, Ameer SS, Moore S et al (2011) Arsenic associated oxidative stress, inflammation, and immune disruption in human placenta and cord blood. Environ Health Perspect 119(2):258–264. https://doi.org/10.1289/ehp.1002086

Alshuaib WB, Byerly L (1996) Modulation of membrane currents by cyclic AMP in cleavage arrested drosophila neurons. J Exp Biol 199(3):537–548. https://jeb.biologists.org/content/jexbio/199/3/537.full.pdf

Arber CE, Li A, Houlden H, Wray S (2016) Review: insights into molecular mechanisms of disease in neurodegeneration with brain iron accumulation: unifying theories. Neuropathol Appl Neurobiol 42(3):220–241. https://doi.org/10.1111/nan.12242

Ballatori N, Clarkson TW (1985) Biliary secretion of glutathione and of glutathione-metal complexes. Fundam Appl Toxicol 5:816–831. PMID: 4065458

Bernhoft RA (2012) Mercury toxicity and treatment: a review of the literature. Int J Environ Res Public Health:1–10. https://doi.org/10.1155/2012/460508

Braga MF, Pereira EF, Albuquerque EX (1999) Nanomolar concentrations of lead inhibit glutamatergic and GABAergic transmission in hippocampal neurons. Brain Res 826:22–34. https://doi.org/10.1016/S0006-8993(99)01194-4

Brunton LL, Goodman LS, Blumenthal D, Buxton I, Parker KL (2007) Principles of toxicology. Goodman and Gilman's manual of pharmacology and therapeutics. McGraw-Hill Professional. ISBN 0-07-144343-6

Caito S, Aschner M (2015) Neurotoxicity of metals. Handbook of clinical neurology, vol 131 (3rd series) Occupational Neurology, p 528

Chandra V (1991) Gestational cadmium exposure development: a biochemical study. Ind Health 29 (2):65–71. https://doi.org/10.2486/indhealth.29.65

Chen P, Miah MP, Aschner M (2016) Metals and neurodegeneration. Version 1. F1000Res. 2016; 5: F1000 Faculty Rev-366. https://doi.org/10.12688/f1000research.7431.1

Clarkson TW, Magos L (2006) The toxicology of mercury and its chemical compounds. Crit Rev Toxicol 36:609–662. https://doi.org/10.1080/10408440600845619

Cobb AB (2008) The elements cadmium, vol 2008, 1st edn. Marshall Cavendish Corporation, New York, pp 8–10

Cronican AA, Fitz NF, Carter A, Saleem M, Shiva S, Barchowsky A et al (2013) Genome wide alteration of histone H3K9 acetylation pattern in mouse offspring prenatally exposed to arsenic. PLoS One 8(2):e53478. https://doi.org/10.1371/journal.pone.0053478

Ekino S, Susa M, Ninomiya T, Imamura K, Kitamura T (2007) Minamata disease revisited: an update on the acute and chronic manifestations of methyl mercury poisoning. J Neurol Sci 262:131–144. https://doi.org/10.1016/j.jns.2007.06.036

Engwa GA, Ferdinand PU, Nwalo FN, Marian N (2018) Mechanism and health effects of heavy metal toxicity in humans. https://doi.org/10.5772/intechopen.82511

Felix K, Manna SK, Wise K, Barr J, Ramesh GT (2005) Low levels of arsenite activates nuclear factor kappaB and activator protein-1 in immortalized mesencephalic cells. J Biochem Mol Toxicol 19(2):67–77. https://doi.org/10.1002/jbt.20062

Gaisson BI, Sampathu DM, Wilson CA, Vogelsberg-Ragaglia V, Mushynski WE, Lee VMY (2002) The environmental toxin arsenite induces tau hyperphosphorylation. Biochemistry 41 (51):15376–15387. https://doi.org/10.1021/bi026813c

Glynn AW, Sparén A, Danielsson LG, Sundström B, Jorhem L (2001) The influence of complexing agents on the solubility and absorption of aluminium in rats exposed to aluminium in water. Food Addit Contam 18(6):515–523. https://doi.org/10.1080/02652030118639

Green SJ, Scheller LF, Marletta MA, Seguin MC, Klotz FW, Slayter M et al (1994) Nitric oxide: cytokine-regulation of nitric oxide in host resistance to intracellular pathogens. Immunol Lett 43:87–94. https://doi.org/10.1016/0165-2478(94)00158-8

Guha MD, Dasgupta UB (2011) Chronic arsenic toxicity: studies in West Bengal, India. Kaohsiung. J Med Sci 27:360–370. https://doi.org/10.1016/j.kjms.2011.05.003

Hayat S, Wigley CB, Robbins J (2003) Intracellular calcium handling in rat olfactory ensheathing cells and its role in axonal regeneration. Mol Cell Neurosci 22(2):259–270. https://doi.org/10.1016/S1044-7431(03)00051-4

Huebers HA, Csiba E, Huebers E, Finch CA (1983) Competitive advantage of diferric transferrin in delivering iron to reticulocytes. Proc Natl Acad Sci U S A 80:300–304. https://doi.org/10.1073/pnas.80.1.300

Hughes MF, Beck BD, Chen Y, Lewis AS, Thomas DJ (2011) Arsenic exposure and toxicology: a historical perspective. Toxicol Sci 123:305–332. https://doi.org/10.1093/toxsci/kfr184

Huguenard JR (1996) Low threshold calcium currents in central nervous system neurons. Annu Rev Physiol 58:329–348. https://doi.org/10.1146/annurev.ph.58.030196.001553

Hwang GW, Furuchi T, Naganuma A (2002) A ubiquitin-proteasome system is responsible for the protection of yeast and human cells against methylmercury. FASEB J 16(7):709–711. https://doi.org/10.1096/fj.01-0899fje

Ishii N, Mochizuki H, Ebihara Y, Shiomi K, Nakazato M (2018) Clinical symptoms, neurological signs, and electrophysiological findings in surviving residents with probable arsenic exposure in Toroku, Japan. Arch Environ Contam Toxicol 75:521–529. https://doi.org/10.1007/s00244-018-0544-8

Jaishankar M, Tseten T, Anbalagan N, Mathew BB, Beeregowda KN (2014) Toxicity, mechanism and health effects of some heavy metals. Interdiscip Toxicol 7(2):60–72. https://doi.org/10.2478/intox-2014-0009

Jiang H, Song N, Xu H, Zhang S, Wang J, Xie J (2010) Up-regulation of divalent metal transporter 1 in 6-hydroxydopamine intoxication is IRE/IRP dependent. Cell Res 20(3):345–356. https://doi.org/10.1038/cr.2010.20

Karri V, Schuhmacher M, Kumar V (2016) Heavy metals (Pb, Cd, As and MeHg) as risk factors for cognitive dysfunction: a general review of metal mixture mechanism in brain. Environ Toxicol Pharm 48:203–213. https://doi.org/10.1016/j.etap.2016.09.016

Kawahara M, Kato-Negishi M (2011) Link between aluminum and the pathogenesis of Alzheimer's disease: the integration of the aluminum and amyloid cascade hypotheses. Int J Alzheimers Dis:1–17. https://doi.org/10.4061/2011/276393

Krewski D, Yokel RA, Nieboer E, Borchelt D, Cohen J, Harry J et al (2007) Human health risk assessment for aluminium, aluminium oxide, and aluminium hydroxide. J Toxicol Environ Health B Crit Rev 10(Suppl 1):1–269. https://doi.org/10.1080/10937400701597766

Kruger K, Binding N, Straub H, Mushoff U (2006) Effects of arsenite on long term potentiation in hippocampal slices from young and adult rats. Toxicol Lett 165(2):167–173. https://doi.org/10.1016/j.toxlet.2006.03.005

Kumar R, Agarwal AK, Seth PK (1996) Oxidative stress-mediated neurotoxicity of cadmium. Toxicol Lett 89(1):65–69. https://doi.org/10.1016/S0378-4274(96)03780-0

Lambert M, Leven BA, Green RM (2000) New methods of cleaning up heavy metal in soils and water; environmental science and technology briefs for citizens. Kansas State University, Manhattan, pp 1–3. https://cfpub.epa.gov/ncer_abstracts/index.cfm/fuseaction/display.files/fileID/14295

Liu C, Liang MC, Soong TW (2019) Nitric oxide, Iron and neurodegeneration. Front Neurosci 13:114. https://doi.org/10.3389/fnins.2019.00114

Lopez E, Arce C, Oset-Gasque MJ, Canadas S, Gonzalez MP (2006) Cadmium induces reactive oxygen species generation and lipid peroxidation in cortical neurons in culture. Free Radic Biol Med 40(6):940–951. https://doi.org/10.1016/j.freeradbiomed.2005.10.062

Luo J, Qiu Z, Shu W, Zhang Y, Zhang L, Chen J (2009) Effects of arsenic exposure from drinking water on spatial memory, ultra-structures and NMDAR gene expression of hippocampus in rats. Toxicol Lett 184(2):121–125. https://doi.org/10.1016/j.toxlet.2008.10.029

Mamtani R, Stern P, Dawood I, Cheema S (2011) Metals and disease: a global primary health care perspective. J Toxicol 2011., Article ID 319136, 11 pages. https://doi.org/10.1155/2011/319136

Markewberry WR (1994) Oxidative stress hypothesis in Alzheimer's disease. Free Radic Biol Med 23:134–147. https://doi.org/10.1016/S0891-5849(96)00629-6

Martin S, Griswold W (2009) Human health effects of heavy metals. Environ Sci Technol Briefs Citizens 15:1–6. www.engg.ksu.edu/CHSR

Mason LH, Harp JP, Han DY (2014) Pb neurotoxicity: neuropsychological effects of lead toxicity. Biomed Res Int:840547. https://doi.org/10.1155/2014/840547

Mendez-Armenta M, Rios C (2007) Cadmium neurotoxicity. Environ Toxicol Pharmacol 23(3):350–358. https://doi.org/10.1016/j.etap.2006.11.009

Mochizuki H, Phyu KP, Aung MN, Zin PW, Yano Y, Myint MZ et al (2019) Peripheral neuropathy induced by drinking water contaminated with low-dose arsenic in Myanmar. Environ Health Prev Med 24(1):23. https://doi.org/10.1186/s12199-019-0781-0

Moos T, Morgan EH (2004) The significance of the mutated divalent metal transporter (DMT1) on iron transport into the Belgrade rat brain. J Neurochem 88:233–245. https://doi.org/10.1046/j.1471-4159.2003.02142.x

Moos T, Skjoerringe T, Gosk S, Morgan EH (2006) Brain capillary endothelial cells mediate iron transport into the brain by segregating iron from transferrin without the involvement of divalent metal transporter 1. J Neurochem 98:1946–1958. https://doi.org/10.1111/j.1471-4159.2006.04023.x

Morais S, Costa FG, Pereira ML (2012) Heavy metals and human health. In: Oosthuizen J (ed) Environmental health – emerging issues and practice, pp 227–246. https://doi.org/10.5772/29869

Morris RG, Garrud P, Rawlins JN, O'Keefe J (1982) Place navigation impaired in rats with hippocampal lesions. Nature 297:681–683. https://doi.org/10.1038/297681a0

Morris G, Basant KP, Richard EF (2017) The putative role of environmental aluminium in the development of chronic neuropathology in adults and children. How strong is the evidence and what could be the mechanisms involved? Metab Brain Dis 32:1335–1355. https://doi.org/10.1007/s11011-017-0077-2

Namgung U, Xia Z (2001) Arsenic induces apoptosis in rat cerebellar neurons via activation of JNK3 and p38 MAP kinases. Toxicol Appl Pharmacol 174(2):130–138. https://doi.org/10.1006/taap.2001.9200

Naujokas MF, Anderson B, Ahsan H, Aposhian HV, Graziano JH, Thompson C et al (2013) The broad scope of health effects from chronic arsenic exposure: update on a worldwide public health problem. Environ Health Perspect 121(3):295–302. https://doi.org/10.1289/ehp.1205875

Nava-Ruiz C, Méndez-Armenta M, Ríos C (2012) Lead neurotoxicity: effects on brain nitric oxide synthase. J Mol Histol 43(5):553–563. https://doi.org/10.1007/s10735-012-9414-2

Needleman H (2004) Lead poisoning. Annu Rev Med 55:209–222. https://doi.org/10.1146/annurev.med.55.091902.103653

Newcombe C, Raab A, Williams PN, Deacon C, Haris PI, Meharg AA et al (2010) Accumulation or production of arsenobetaine in humans? J Environ Monit 12:832–837. https://doi.org/10.1039/B921588C

Ni M, Li X, Yin Z, Jiang H, Sidoryk-Wegrzynowicz M, Milatovic D et al (2010) Methylmercury induces acute oxidative stress, altering Nrf2 protein level in primary microglial cells. Toxicol Sci 116:590–603. https://doi.org/10.1093/toxsci/kfq126

Onishi H (1969) Arsenic. In handbook of geochemistry, Wedepohl KH (ed), vol II. Springer, New York

Orrenius S, Nicotera P (1994) The calcium ion and cell death. J Neural Transm Suppl 43:1–11. PMID: 7884392

Parks JM, Johs A, Podar M, Bridou R, Hurt RA Jr, Smith SD et al (2013) The genetic basis for bacterial mercury methylation. Science 339(6125):1332–1335. https://doi.org/10.1126/science.1230667

Patlolla AK, Tchounwou PB (2005) Serum acetyl cholinesterase as a biomarker of arsenic induced neurotoxicity in Sprague dawley rats. Int J Environ Res Public Health 2(1):80–83. PMCID: PMC3814700

Pearson HA, Schonfeld DJ (2003) Lead. In: Rudolph CD (ed) Rudolph's pediatrics, 21st edn. McGraw Hill professional

Pogue AI, Li YY, Cui JG, Zhao Y, Kruck TP, Percy ME et al (2009) Characterization of an NF-kappa B-regulated, miRNA-146a-mediated down-regulation of complement factor H (CFH) in metal-sulfate-stressed human brain cells. J Inorg Biochem 103(11):1591–1595. https://doi.org/10.1016/j.jinorgbio.2009.05.012

Prakash C, Soni M, Kumar V (2015) Mitochondrial oxidative stress and dysfunction in arsenic neurotoxicity: a review. J Appl Toxicol 36(2):179–188. https://doi.org/10.1002/jat.3256

Provan SD, Yokel RA (1998–1990) Reduced intestinal calcium and dietary calcium intake, increased aluminum absorption, and tissue concentration in the rat. Biol Trace Elem Res Winter 23:119–132. https://doi.org/10.1007/BF02917183

Rafati RM, Rafati RM, Moghadamnia AA (2013) Arsenic compounds toxicity. J Babol Univ Med Sci 15:51–68. https://www.sid.ir/en/journal/ViewPaper.aspx?id=288092

Rao MV, Avani G (2004) Arsenic induced free radical toxicity in brain of mice. Indian J Exp Biol 42(5):495–498. PMID:15233475

Ravenscroft P, Brammer H, Richards K (2009) Arsenic pollution—a global synthesis. Oxford, Wiley-Blackwell

Rigon AP, Cordova FM, Oliveira CS, Posser T, Costa AP, Silva IG et al (2008) Neurotoxicity of cadmium on immature hippocampus and a neuroprotective role for p38MAPK. Neurotox 29 (4):727–734. https://doi.org/10.1016/j.neuro.2008.04.017

Riihimaki V, Aitio A (2012) Occupational exposure to aluminum and its biomonitoring in perspective. Crit Rev Toxicol 42:827–853. https://doi.org/10.3109/10408444.2012.725027

Rodriguez VM, Carrizales L, Mendoza MS, Fajardo OR, Giordano M (2002) Effects of sodium arsenite exposure on development and behavior in the rat. Neurotoxicol Teratol 24(6):743–750. https://doi.org/10.1016/S0892-0362(02)00313-6

Sahoo PK, Kim K (2013) A review of the arsenic concentration in paddy rice from the perspective of geoscience. Geosci J 17(1):107–122. https://doi.org/10.1007/s12303-013-0004-4

Salazar J, Mena N, Hunot S, Prigent A, Alvarez-Fischer D, Arredondo M et al (2008) Divalent metal transporter 1 (DMT1) contributes to neurodegeneration in animal models of Parkinson's disease. Proc Natl Acad Sci U S A 105(47):18578–18583. https://doi.org/10.1073/pnas.0804373105

Salvador GA, Uranga RM, Giusto NM (2010) Iron and mechanisms of neurotoxicity. Int J Alzheimers Dis 27:720658. https://doi.org/10.4061/2011/720658

Selkoe DJ (1991) The molecular pathology of Alzheimer's disease. Neuron 6(4):487–498. https://doi.org/10.1016/0896-6273(91)90052-2

Sharma P, Dubey RS (2005) Lead toxicity in plants. Braz J of Plant Physio 17(1):35–52. https://www.scielo.br/pdf/%0D/bjpp/v17n1/a04v17n1.pdf

Shaw CA, Tomljenovic L (2013) Aluminum in the central nervous system (CNS): toxicity in humans and animals, vaccine adjuvants, and autoimmunity. Immunol Res 56(2–3):304–316. https://doi.org/10.1007/s12026-013-8403-1

Sheehan MC, Burke TA, Navas-Acien A, Breysse PN, McGready J, Fox MA (2014) Global methylmercury exposure from seafood consumption and risk of developmental neurotoxicity: a systematic review. Bull World Health Organ 92(4):254–269F. https://doi.org/10.2471/BLT.12.116152

Shen XL, Yu JH, Zhang DF, Xie JX, Jiang H (2014) Positive relationship between mortality from Alzheimer's disease and soil metal concentration in mainland China. J Alzheimers Dis 42:893–900. https://doi.org/10.3233/JAD-140153

Singh R, Singh S, Parihar P, Singh VP, Prasad SM (2015) Arsenic contamination, consequences and remediation techniques: a review. Ecotoxicol Environ Saf 112:247–270. https://doi.org/10.1016/j.ecoenv.2014.10.009

Struzyñska L, Bubko I, Walski M, Rafałowska U (2001) Astroglial reaction during the early phase of acute lead toxicity in the adult rat brain. Toxicology 165(2–3):121–131. https://doi.org/10.1016/S0300-483X(01)00415-2

Thinakaran G, Koo EH (2008) Amyloid precursor protein trafficking, processing, and function. J Biol Chem 283(44):29615–29619. https://doi.org/10.1074/jbc.R800019200

Thurmer K, Williams E, Reutt-Robey J (2002) Autocatalytic oxidation of lead crystallite surfaces. Science 297(5589):2033–2035. https://doi.org/10.1126/science.297.5589.2033

Unoki T, Akiyama M, Kumagai Y, Gonçalves FM, Farina M, Rocha JBT et al (2018) Molecular pathways associated with methylmercury-induced Nrf2 modulation. Front Genet 9:373. https://doi.org/10.3389/fgene.2018.00373

Uranga RM, Giusto NM, Salvador GA (2009) Iron-induced oxidative injury differentially regulates PI3K/Akt/GSK3beta pathway in synaptic endings from adult and aged rats. Toxicol Sci 111 (2):331–344. https://doi.org/10.1093/toxsci/kfp152

Valko M, Izakovic M, Mazur M, Rhodes CJ, Telser J (2004) Role of oxygen radicals in DNA damage and cancer incidence. Mol Cell Biochem 266:37–56. https://doi.org/10.1002/jnr.21406

Valko M, Morris H, Cronin MT (2005) Metals, toxicity and oxidative stress. Curr Med Chem 12 (10):1161–1208. https://doi.org/10.2174/0929867053764635

Vargel C (2004) 1st ed. Elseiver. Food Industry, Oxford

Vimalraj S, Sumantran VN, Chatterjee S (2017) MicroRNAs: impaired vasculogenesis in metal induced teratogenicity. Reprod Toxicol 70:30–48. https://doi.org/10.1016/j.reprotox.2017.02.014

Walton JR (2010) Evidence for participation of aluminum in neurofibrillary tangle formation and growth in Alzheimer's disease. J Alzheimers Dis 22:65–77. https://doi.org/10.3233/JAD-2010-100486

Walton JR, Wang MX (2009) APP expression, distribution and accumulation are altered by aluminum in a rodent model for Alzheimer's disease. J Inorg Biochem 103(11):1548–1554. https://doi.org/10.1016/j.jinorgbio.2009.07.027

Wani AL, Ara A, Usmani JA (2015) Lead toxicity: a review. Interdiscip Toxicol 8(2):55–64. https://doi.org/10.1515/intox-2015-0009

Wasserman GA, Liu X, Parvez F, Ahsan H, Factor-Litvak P, van Geen A et al (2004) Water arsenic exposure and children's intellectual function in araihazar, Bangladesh. Environ Health Perspect 112(13):1329–1333. https://doi.org/10.1289/ehp.6964

Wong KL, Klaassen CD (1982) Neurotoxic effects of cadmium in young rats. Toxicol Appl Pharmacol 63(3):330–337. https://doi.org/10.1016/0041-008X(82)90261-7

World Health Organization [Internet] (2013) Mercury and health, Fact sheet No. 361. WHO, Geneva. https://www.who.int/news-room/fact-sheets/detail/mercury-and-health

Xi S, Guo L, Qi R, Sun W, Jin Y, Sun G (2010) Prenatal and early life arsenic exposure induced oxidative damage and altered activities and mRNA expressions of neurotransmitter metabolic enzymes in offspring rat brain. J Biochem Mol Toxicol 24(6):368–378. https://doi.org/10.1002/jbt.20349

Xiao C, Gu Y, Zhou CY, Wang L, Zhang MM (2006) Pb2+ impairs GABAergic synaptic transmission in rat hippocampal slices: a possible involvement of presynaptic calcium channels. Brain Res 1088:93–100. https://doi.org/10.1016/j.brainres.2006.03.005

Xu B, Chen S, Luo Y, Chen Z, Liu L, Zhou H et al (2011) Calcium signaling is involved in cadmium induced neuronal apoptosis via induction of reactive oxygen species and activation of MAPK/mTOR network. PLoS One 6(4):e19052. https://doi.org/10.1371/journal.pone.0019052

Yadav RS, Shukla RK, Sankhwar ML, Patel DK, Ansari RW, Pant AB et al (2010) Neuroprotective effect of curcumin in arsenic induced neurotoxicity in rats. Neurotoxi 31(5):533–539. https://doi.org/10.1016/j.neuro.2010.05.001

Yellamma K, Saraswathamma S, Kumari BN (2010) Cholinergic system under aluminium toxicity in rat brain. Toxicol Int 17:106–112. https://doi.org/10.4103/0971-6580.72682

Yoshida E, Toyama T, Shinkai Y, Sawa T, Akaike T, Kumagai Y (2011) Detoxification of methylmercury by hydrogen sulfide-producing enzyme in mammalian cells. Chem Res Toxicol 24(10):1633–1635. https://doi.org/10.1021/tx200394g

Yuan X, Wang, Chan HM (2018) Sub-nanomolar methylmercury exposure promotes premature differentiation of murine embryonic neural precursor at the expense of their proliferation. Toxics 6(4):61. https://doi.org/10.3390/toxics6040061

Zarruk JG, Berard JL, Passos DSR, Kroner A, Lee J, Arosio P et al (2015) Expression of iron homeostasis proteins in the spinal cord in experimental autoimmune encephalomyelitis and their implications for iron accumulation. Neurobiol Dis 81:93–107. https://doi.org/10.1016/j.nbd.2015.02.001

Zecca L, Youdim MB, Riederer P, Connor JR, Crichton RR (2004) Iron, brain ageing and neurodegenerative disorders. Nat Rev Neurosci 5:863–873. https://doi.org/10.1038/nrn1537

Chapter 12
An Overview of Heavy Metal Toxicity

Dheepthi Jayamurali, Krishnapriya Madhu Varier, Wuling Liu, Jegadeesh Raman, Yaacov Ben-David, Xiangchun Shen, and Babu Gajendran

Contents

Dheepthi Jayamurali and Krishnapriya Madhu Varier contributed equally to the chapter.

D. Jayamurali
Department of Physiology, Dr. ALM PGIBMS, University of Madras, Chennai, Tamilnadu, India

K. M. Varier
Department of Medical Biochemistry, Dr. ALM PGIBMS, University of Madras, Chennai, Tamilnadu, India

W. Liu · Y. Ben-David · X. Shen · B. Gajendran (✉)
Department of Biology and Chemistry, The Key Laboratory of Chemistry for Natural Products of Guizhou Province and Chinese Academy of Sciences, Guiyang, Guizhou Province, China

State Key Laboratory of Functions and Applications of Medicinal Plants, Guizhou Medical University, Guiyang, Guizhou Province, China

J. Raman
Mushroom Research Division, National Institute of Horticultural and Herbal Science, Rural Development Administration, Eumsung, Republic of Korea

Abstract Metals are naturally occurring ingredients of Earth's crust, broadly classified as alkali metals, alkaline metals, basic metals, and transition metals, well-known for its exclusive properties – like electrical conductivity, malleability, ductility, and so on. The forte and the resilience capacity of these metals established their route in various fields of science and technology. Their repeated domestic, industrial, agricultural, medical, and technological applications have been widespread across the milieu, evolving into an environmental pollutant or contaminant. Above a certain limit, the living flora and fauna of the globe become exposed to these toxins resulting in several deleterious effects and risks. Toxicity, being a phenomenon of solubility of these metals, varies depending upon the dose, duration, solubility, route of exposure, etc. In response to the damages caused by the toxins, it is of extreme importance to understand the basis behind the mechanism of metal toxicity and to elicit remedial measures to treat the clinical conditions.

This chapter reviews heavy metal toxicity on in vitro and in vivo models. Mercury, lead, arsenic, cadmium, chromium, and aluminum – six ubiquitous heavy metals – were preferred on the basis of extent of their toxicity, their prevalence as an environmental contaminant/toxin and their potential hazards of human exposure. Several in vivo and in vitro models enable us to frame the effects of these metal toxins on all the possible ways. This chapter bestows a light upon the neurotoxicity, cardiotoxicity, hepatotoxicity, developmental and reproductive toxicity, etc. The phenomenon of toxicity mimicking is probable only through experimental models like rats, mouse, guinea pigs, hamsters, and fishes. The recent technical advancements visualize science in an entirely novel perspective, evolving for an exclusively innovative approach, which has been reviewed in this episode.

Keywords Toxicity · Metal · Arsenic · Cadmium · Chromium · Lead · Mercury · Aluminum · Rats · Zebrafish · Cell lines · In vitro · In vivo · ROS · Oxidative stress · Apoptosis · Inflammation

12.1 Introduction

12.1.1 Background of Metal Toxicity

Most elements of the periodic table constitute the metals. Around 25% of Earth's mass is composed of metals. A metal being abundant has varied applications. Their exponential usage has been amplified the risk of human exposure to these metals. A metal is reported to be highly toxic, based on the heaviness and harmfulness of the metal, which are mostly interrelated (Tchounwou et al. 2012). Although these heavy metals are present certainly in the background, human exposure to these toxins occur mainly because of industrial use, native use, as well as agricultural use of these metals (Goyer 2001). Metals being nondegradable and their persistent usage led to

the bioaccumulation in the human bodies, via food chain. The humans are forced to deal with these accumulated potential metals, the combo of which may modify the speciation of the metal, revolving it to have a toxic potential.

12.1.2   Mechanism of Toxicity

On reaction with biotic systems, a metal forms cations by losing its valent electrons (Goyer 2001), possessing oxidation property. Toxicity initially arises by the generation of reactive oxygen species (ROS) like superoxides, anions, hydrogen peroxides, hydroxyl ions, etc. (Ercal et al. 2001). The ROS are reported to produce oxidative stress, a potential hazard to the cells. The metals toxins are also known to deplete the antioxidant system of the body. Heavy metals like mercury, form stable compounds with molecules of the cell by nucleophilic attack (Farina et al. 2011). The complexes formed induce oxidative stress in the cells resulting in the depletion of enzymes, lipids, and nucleic acids – to the death ultimatum.

Arsenic compounds also form ROS, but the modes of action of these radicals take the path of DNA damage, inhibition of DNA repair mechanisms, and blockade in the signal transduction pathways (Hughes et al. 2011). Thus, the metal is reported to have genotoxic potential.

Hubaux et al. 2013 has reported that arsenic is capable of inducing cancer by epigenetic changes and posttranslational modifications. The mechanism includes alterations in the DNA methylation and in the modification of histones. The epigenetic alterations may be the mechanism underlying cancer, brought about by the toxic metal.

Heavy metals are reported to induce apoptosis in the cells. The mechanism by which the cell undergoes apoptosis is by arresting the cell cycle (Tchounwou et al. 2012). Also, apoptosis results when mitochondria are damaged by oxidative phosphorylation on exposure to the ROS (Sabath and Robles-Osorio 2012).

12.2   Metal Toxicity: In Vivo and In Vitro Studies

12.2.1   Arsenic Toxicity

Arsenic has been ranked as the first toxic, hazardous substance according to the US Agency for Toxic Substances and Disease Registry and the US Environmental Protection Agency Priority List of Hazardous Substances for the past 20 years, since 1997. Trivalent arsenite and pentavalent arsenate are the major inorganic forms of the element arsenic, well-known for its crystalline structure. Organic forms also exist as methylated metabolites – dimethylarsinic acid (DMA), trimethylarsine oxide, and monomethylarsonic acid (MMA). Trivalent compounds are reported to be more toxic than the pentavalent compounds depending upon the

chemical composition of the arsenic containing elements and the extent to which it is thiolated (Michael et al. 2018). Exposure to arsenic is usually by natural element present in the Earth's crust or by contamination of air, food, and water. Chronic arsenic exposure may lead to the development of various diseases like cardiovascular problems, kidney failure, neurotoxicity, diabetes, hepatotoxicity, hypertension, and various cancers (Singh et al. 2011; Guha 2008; Singh et al. 2013). Investigating the toxic effects of arsenic is complex, because it is highly influenced by its solubility, oxidative state, exposure dose, frequency, and duration in addition to many other intrinsic and extrinsic factors (Centeno et al. 2005). Inorganic and organic arsenic is reported to induce developmental and reproductive toxicity in various animal models like mice, rats, and rabbits. However, Golub et al. (1998) has reported a range of characteristic malformations during development that include intrauterine death, growth retardation, poor skeletal outgrowth, or exposure to inorganic arsenic injections (Table 12.1).

Exposure to inorganic arsenic orally for 45 days in rats has been documented to rise lipid peroxidation and reduce the antioxidant and anti-peroxidative enzymes in the cardiac tissue with myocardial fiber swelling, congestion of capillaries, and micro hemorrhages (Mathews et al. 2013).

Arsenic is a well-established carcinogen, and it has been extensively studied using mice model. When pregnant C3H mice (8–18 period of gestation only) were exposed to sodium arsenite at the dosage of – 0, 42.5 and 85 ppm in the drinking water, the offsprings revealed a dose-dependent stimulation of tumors in the liver, adrenal, lung, and ovary after they reached the adulthood. The corresponding genetic analysis of these tumors exhibited unusual expression of genes related with transplacental arsenic carcinogenesis (Waalkes 2004).

Sodium arsenite when exposed at the dosage of 10, 30, and 50 µg/L (ppb) for 60 days orally for rats showed microsomal degranulation in the liver and chromosomal aberrations like chromosomal fragments, chromatid breaks, gaps, and end-to-end associations in the bone marrow cells of female rats. So, it has been concluded

Table 12.1 Developmental and reproductive toxicity in various animal models (Golub et al. 1998; copyright received)

Species/agent/route of administration	Dose/effects
Mice	5, 50 mg As/L
Drinking water	Heavy deterioration of testicular germinal epithelium
Arsenic trioxide	
Rats	4.96 mg/m^3
Inhalation	Changes in sperm cells, preimplantation death, reduced life of progeny
Cesium arsenate	
Rabbits	Gavage
75% arsenic acid	Gd 6–18
	0,0.10,0.40, or 1.58 mg As/kg/d
	1.58 mg As/kg/d: maternal mortality, abortion, missing kidney, ureter
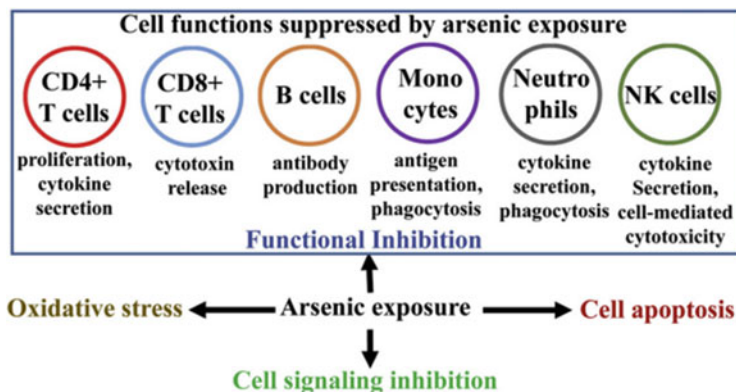
Fig. 12.1 Arsenic toxicity and potential mechanisms on immune cells (Xu et al. 2018; copyright received)

that arsenic has possible mutagenic and genotoxic potential (Hundal and Mehta 2014).

In accordance to the previous findings (Dreval et al. 2018), after 28 days of seeding of the human progenitor hepatic HepaRG cell line, HepaRG cells were exposed to sodium arsenite at a dosage of 0, 0.5, 1, 5, 20, 40, 80, or 200 μM. On exposure to the chemical, it repressed the differentiation of progenitor cells into hepatocyte like cells. Also the genes involving cell growth, proliferation, and survival were upregulated and the genes involving cell death were downregulated on exposure to sodium arsenite.

Low to high concentrations of arsenic is well-known to suppress the immune system via inhibiting the development of T-lymphocyte by inhibiting IL-7 pathway (Fig. 12.1; Xu et al. 2018).

12.2.2 Lead Toxicity

World Health Organization (2018) has reported lead as one of the ten chemicals to cause harmful, prominent effects and as of major health distress to the society. Since decades, lead has been widely used for its unique physicochemical properties and thus has evolved into an occupational contaminant and an environmental pollutant in the present scenario (Wani et al. 2015). Of all the potent heavy metal poisoning, lead is well documented to exert its hazardous effects on various physiological systems of the body. Lead toxicity has been extensively researched using in vivo and in vitro models to understand the mechanism of its action and to formulate the corresponding alternative treatment.

Lead has been reported to generate nephrotoxicity in male Wistar albino rats. This is underlined by the previous findings (Abdel et al. 2019), which reports rats on exposure to lead acetate (LA) at a dosage of 25, 50, and 100 mg/kg/day orally in 1%,

2%, and 4% saline solution for 1, 2, and 3 months each resulted in impaired renal structure and function. In addition, lead was found to get accumulated in the kidney leading to oxidative stress, apoptosis, and inflammation in the nephrons. Lead acetate toxicity was reported to significantly increase nitric oxide (NO) production and decrease heme oxygenase and hydrogen sulfide levels significantly. Also, the inflammatory proteins tumor necrosis factor-alpha (TNF-α) and interleukin-1β (IL-1β) and the apoptotic marker caspase-3 were found to be unregulated in the lead acetate induced group. The gasotransmitters L-arginine, trifluoro-DL-alanine, and zinc deuteroporphyrin modulated and aggravated the lead induced nephrotoxicity.

Juvenile largemouth bass (*Micropterus salmoides*) on exposure to lead at varying concentrations in water – 0, 10, 17.8, 31.6, 56.2, and 100 mg/L for 96 h revealed significant differential gene expressions associated with major pathways in the liver (Qian et al. 2019). Acute immune response including complement activation was observed on exposure to lead. Liver transcriptome analysis exposed differential gene expression in multiple pathways – the JAK-STAT pathway, p53 signaling pathway, and natural killer cell-mediated cytotoxicity pathway – and also concerned with cancer and systemic lupus erythematosus.

Lead acetate (50 mg/l) when administered to male albino rats in drinking water for 49 days showed marked testicular toxicity (Hassan et al. 2019) – with decreased spermatozoa count, testicular weight, seminal vesicle and epididymis, and low levels of reproductive hormones along with degenerative changes in the seminiferous tubules. Also the antioxidant levels like superoxide dismutase, glutathione peroxidase, and catalase were significantly reduced in the lead acetate exposed group revealing oxidative stress. The testicular damages were improved on exposure to epigallocatechin gallate (EGCG), green tea extract (Fig. 12.2; Hassan et al. 2019).

Neurons and glial cells are one of the vital targets of lead (Peng et al. 2018). It has been revealed that the glial cells like microglia and astrocyte cultures from rat cerebral cortices respond differentially to lead exposure. When the glial cells were exposed to escalating concentration of lead – (0, 5, 15, 30, 50, and 100 μmol/L) for 24 h, the viability of microglial cells were far more reduced than the astrocytes coupled with microglial oxidative stress and ROS. Primary cultures on treatment with lead acetate and subsequent inductively coupled plasma mass spectrometry (ICP-MS) revealed the primary astrocytes accumulated more lead than the microglial cells. The nuclear factor 2 (Nrf2) expressions were discovered to be the reason in the differential glial responses on exposure to lead (Forsythe et al. 2018).

12.2.3   Cadmium Toxicity

Cadmium is naturally present in the Earth's crust at very low concentrations of 0.1 part per million (Hans 1995). Although the metal exists in minimal quantity, it is highly poisonous exerting its acute and chronic effects on health and the environment. Cadmium usually occurs in complexes with other metals forming chelates.
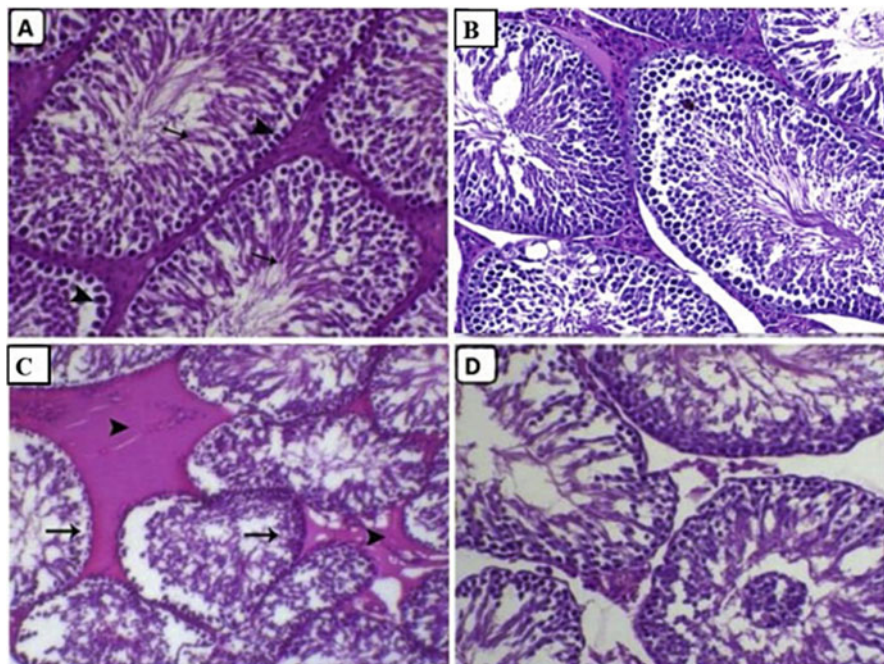
Fig. 12.2 Histological changes in the testis exposed to lead and epigallocatechin gallate. (**a**) Control testes exhibited normal spermatogenic cell layers with spermatogonia and normal free sperm (arrows). (**b**) EGCG-treated rat with normal spermatogenic cells with active spermiogenesis. (**c**) Testis of rat treated with PbAc showed degeneration of the lining spermatogenic layers of seminiferous tubules (arrows), with marked interstitial edema (arrowheads). (**d**) Testis of rat treated with PbAc + EGCG-exposed group showed mild to moderate testicular degeneration with desquamation of some spermatogenic cells. (Hassan et al. 2019; copyright received)

They also form salts like arsenates, phosphates, carbonates, and ferrocyanide compounds. Cadmium inhalation or ingestion has reported to cause deleterious effects on the human body (Hans 1995).

Cadmium has been reported as a potent carcinogen by the by the International Agency for Research on Cancer (IARC). Cadmium has known to induce cancer by one of the following mechanisms – oxidative stress induction, ROS production, inhibition of DNA repair mechanisms and the pathways involved, abnormal genetic expression, uncontrolled cell proliferation, and inhibition of apoptosis (Joseph 2009).

To associate the cadmium inhalation and lung cadmium accumulation, Sprague Dawley rats and C57B1/6J mice were smoke exposed – nose-only contact of cadmium of 1.13–0.16 pg Cd per cigarette on single or double exposure for 52 weeks (Gairola and Wagner 1991). This has led to highest cadmium accumulation in the lungs of the rats and mice when compared to the liver of the same. Moreover, rats exposed to air cadmium have been reported to possess higher lung

weight, decrease and later increase in the alveolar macrophages, and increase in the neutrophils and lymphocytes. It has also been documented the following alteration of clearance kinetics of test *Salmonella enteritidis* (rats) or *Pasteurella multocida* (mice) aerosols leading to increase in the death rate of the animals after inflammatory response (Bouley et al. 1979).

Zebrafish embryos on exposure to 1.5 mg/L cadmium chloride in water for 72 h exhibited renal damage with renal collagen deposition, oxidative stress, inflammation, and epithelial–mesenchymal transition and inhibited the nuclear-related factor-2 (Nrf-2), wherein the renal defects were reversed by resveratrol (Hu et al. 2017).

Cadmium has been reported to affect developmental, reproductive, renal, hepatic, hematological, and immunological functions in teleost fish. Zebrafish larvae when exposed to cadmium chloride at a dose of 10 mg/mL with dilutions in accordance to the embryo medium resulted in deformed opercular bone growth with obvious skeletal deformities. MTF-1 and cAMP/PKA signaling pathways have been reported to have a possible role in cadmium osteotoxicity by interfering with the genes involving osteoblast differentiation and bone matrix production (Tarasco et al. 2019).

Apoptosis has been reported to be the effect of many toxic elements, cadmium here, but the mechanism involved is not fully understood. A label-free digital holography in murine embryonic fibroblasts NIH 3T3 (Mugnano et al. 2018) evidenced that the exposure to cadmium chloride (CdCl2) at concentration of 10 μM for 24 h exhibited apoptosis and caused changes in the morphological parameters of the cells like cytoplasmic shrinkage, apoptotic blebbing of the cells, and cell membrane rupture with a consequential cell volume decrease (Fig. 12.3). This even evidenced that CdCl2-produced cytotoxicity was also confirmed by classical inverted microscope (Fig. 12.4).

12.2.4   Chromium Toxicity

Chromium in nature exists in three forms – chromium (0), chromium (III), and chromium (VI) – and also in association with various other compounds. Chromium exposure may occur via tanned leather, stainless steel cookware, wood processing and furniture, and metals that are used in hip replacements. Though chromium occurs at trace amounts in the environment, it is relatively very poisonous and causes severe toxicity issues. Hexavalent chromium is a powerful oxidizing agent when compared with trivalent chromium which is also reported to be toxic along with the former which has been reported to be absorbed mostly by the gastrointestinal tract, lungs, and to a certain extent by intact skin (Wilbur et al. 2012).

Evidence that chromium causes genotoxic damage has been reported (Fang et al. 2014). In vivo studies on yeast *S. cerevisiae* strain – SJR576 on exposure to – 300 mM CrO_3 for 24 hours and 150 mM CrCl3 for 24 h evaluated mutagenic potential of chromium by inactivating SUP4-o and exhibited DNA damage detected by comet assay (Fig. 12.5).
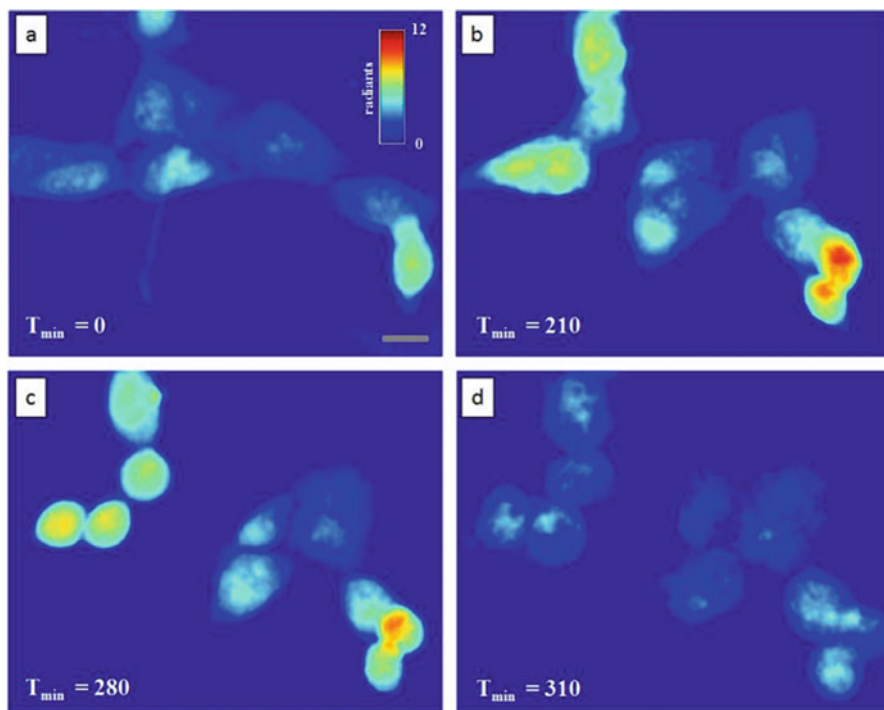
Fig. 12.3 Phase-contrast images of NIH-3T3 cells while cultured with cadmium chloride (Mugnano et al. 2018; copyright received). (**a**) 0 min, (**b**) 210 min, (**c**) 280 min, (**d**) 310 min. All cells died by apoptosis after 280 min
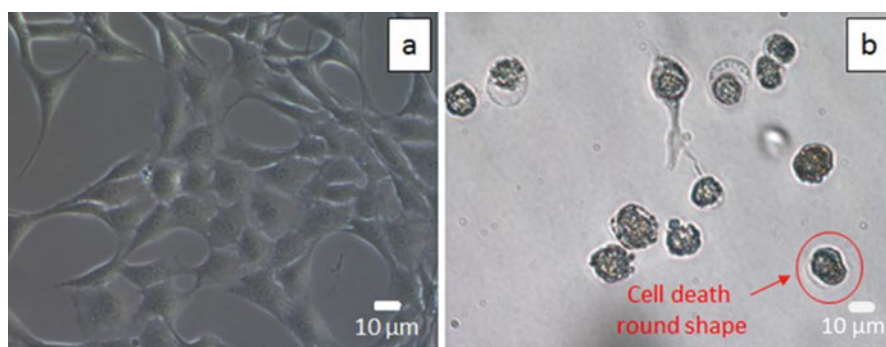
Fig. 12.4 Cells morphology changes when cells were exposed to CdCl2 (Mugnano et al. 2018; copyright received). Optical microscopy images of cells control (**a**) without CdCl2 and morphology changes upon exposure to 10 μM of CdCl2 (**b**), for 72 h. The microscopy observations suggested that CdCl2 induce cell death. (Mugnano et al. 2018; copyright received)
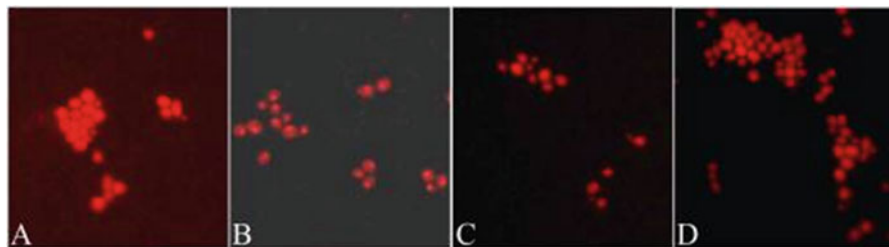
Fig. 12.5 (**a**) Control, (**b**) positive control, (**c**) 300 mM CrO$_3$ for 24 hours, (**d**) 150 mM CrCl3 for 24 h, fluorescent microscope imaging at magnification 200 X. (Fang et al. 2014; copyright received)
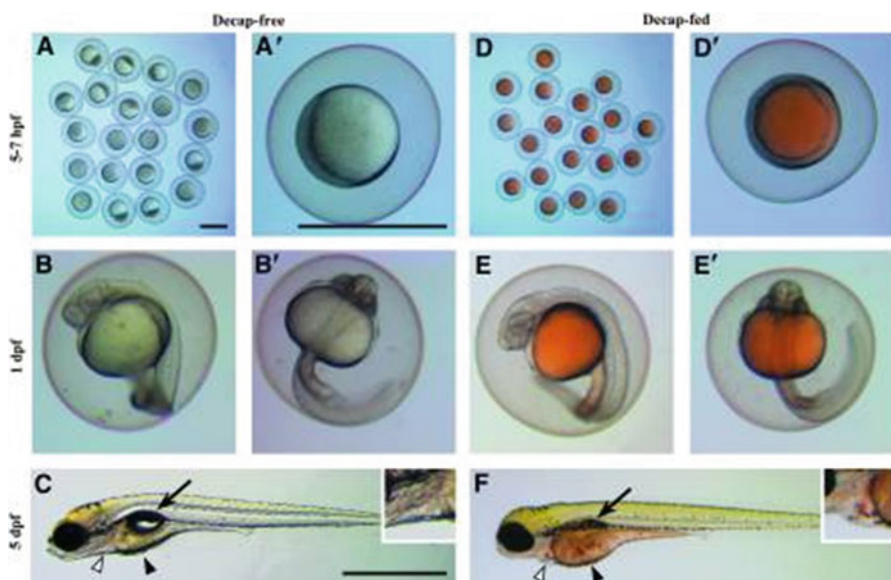
Fig. 12.6 Comparison of yolk color and morphological deformities between control and decaps group (Tye et al. 2018; copyright received)

In the same abovementioned research, the human T-cell leukemia Jurkat cells on exposure to 300 mM CrO$_3$ for 24 h and 150 mM CrCl$_3$ for 24 h exhibited genotoxicity confirmed by DNA damage and DNA degradation. But the mechanism of Cr (VI) and Cr (III) action on DNA is reported to be entirely different, with Cr(III) affected the phosphate backbone of DNA while Cr(VI) intercalated the DNA base pair planes and caused DNA structural changes and degradation (Fang et al. 2014).

Zebrafishes on being fed with nonhatching decapsulated brine shrimp cysts (decaps) were observed to exhibit orange color in the yolk and reduced the viability of the progeny (Fig. 12.7) (D–F) when compared with controls (A–C) not fed with decaps. These observations lead to the discovery that the decaps contained chromium as the major dietary component (69.6 mg/kg), 30-fold higher than other components of the diet (Fig. 12.6; Tye et al. 2018).
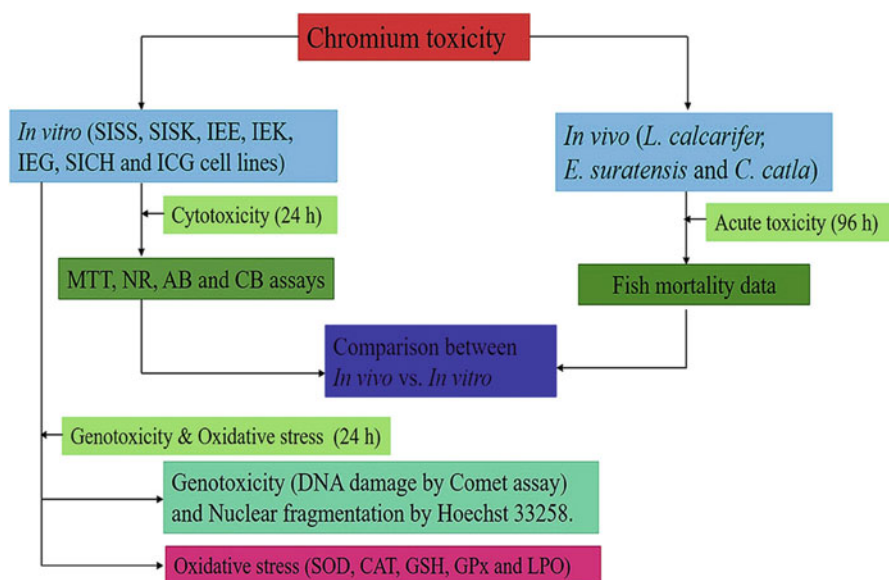
Fig. 12.7 Chromium toxicity on in vivo and in vitro models (Taju et al. 2017; copyright received)

On exposure of zebrafishes to chromium at a dosage 0.7 mg L^{-1} revealed behavioral alterations like significant changes in the swimming speed, swimming heights, and turning times (Nannan et al. 2017). Thus, the cumulative data from in vivo and in vitro models revealed that chromium at concentrations – 0, 10, 20, 30, 40, and 50 mg/L was able to induce cytotoxicity, genotoxicity, and oxidative stress (Fig. 12.7; Taju et al. 2017).

12.2.5   Mercury Toxicity

Mercury toxicity comes under heavy metal toxicity with well-established clinical presentations. Mercury exists in various forms like mercury vapor, metallic mercury, mercurous or mercuric salts, and organic mercury that contain carbon atoms. The type of clinical manifestation presented depends upon the different forms of mercury and their respective pharmacokinetic properties (Bernhoft 2012).

Mercury has been reported to provoke inflammatory responses and induce oxidative stress and apoptosis in Sprague Dawley rats (Caglayan et al. 2019). When mercuric chloride was administered at a dosage of 1.23 mg/kg b.w. to male rats, it possessed symptoms of nephrotoxicity. The mercury toxin elevated the levels of various interleukins and inflammatory markers. The toxin has been exposed to trigger the apoptotic pathway via caspase-3. The mercury-exposed groups had a significant decrease in the aquaporin-1 water channel protein resulting in
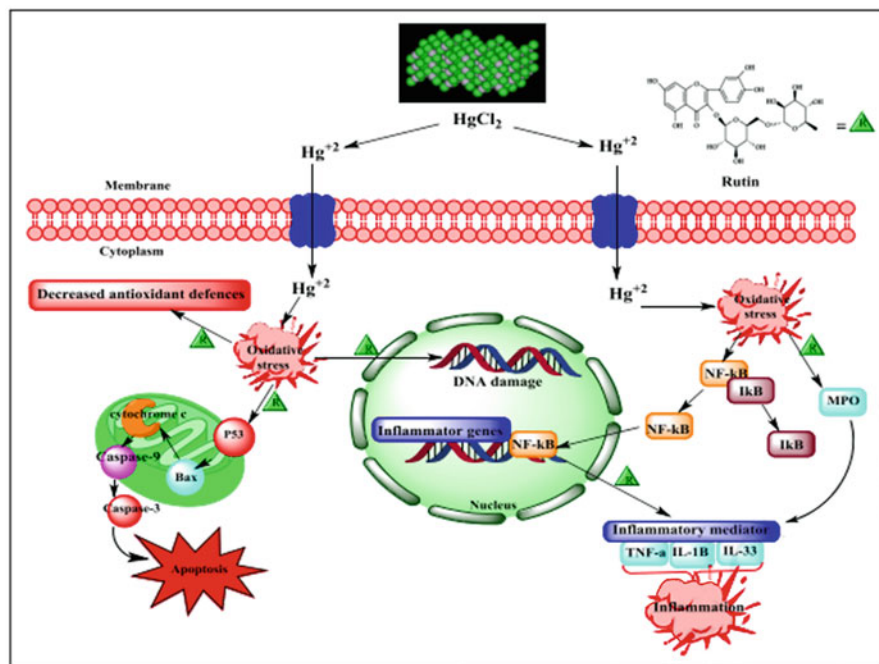
Fig. 12.8 Mercury induced nephrotoxicity and protective effect of rutin (Caglayan et al. 2019; copyright received)

disturbances of the renal architecture. However, rutin, a naturally occurring flavonoid has been documented to reverse the toxic effects of mercury (Fig. 12.8).

As reported above, mercury is well-known to produce nephrotoxicity. Additionally, Li et al. (2019) reported that Kunming mice on exposure to $HgCl_2$ (5 mg/kg b. w.) exhibited apoptosis; activation of Sirt1/Nrf2/OH-1 pathway; decrease in the levels of Mg, K, P, Mn, Fe, and Zn; increase in the levels of Na, Ca, Cu, and Se; and increase in the levels of various ATPases in the mice kidney. Mercury, in summary, affected the salt homeostasis, by dynamically altering the salt transporters in the kidneys of the mice, revealing the Sirt1/Nrf2/Na$^+$/Ca^{2+} pathway as vital checkpoint for the establishment of novel therapies (Fig. 12.9).

Zebrafish and its embryo has been evolved as a novel candidate for various fields – like neurology, pharmacology, toxicology, etc. The eye lens and the retina of the zebrafish are claimed to be the potential targets for mercury and its related compounds. There are reports that have documented the direct attack of methyl and ethyl mercury on the lens epithelial tissue on a maximal scale and to a lesser extent contributing the other neurological deficits. Localization and accumulation of the mercuric compounds on the lens epithelium and eyes of zebrafish were visualized using X-ray fluorescence mapping (Korbas et al. 2008). As per literature, mercury favorably occupied the periphery of the eye lens that possessed mitotically
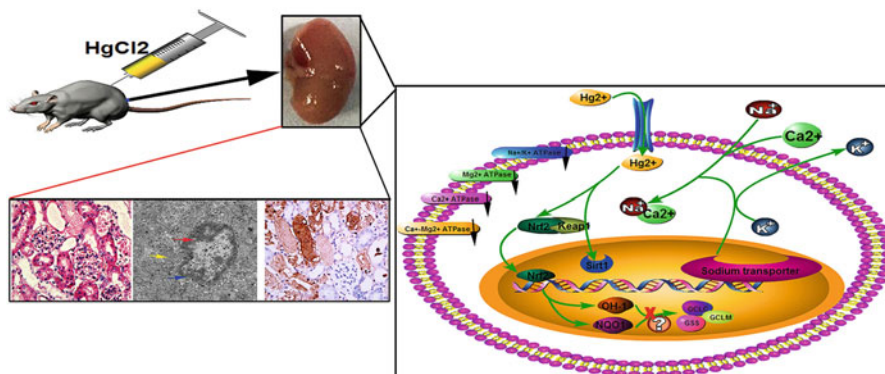
Fig. 12.9 Mercury toxicity activation of Sirt1/Nrf2/OH-1 pathway, regulation of salts and salt transporters (Li et al. 2019; copyright received)

active epithelial cells (Fig. 12.10a). Mercury also tends to occupy the outer portions of the retina; Fig. 12.10b and Fig. 12.10c revealed a tricolor map with mercury occupying the thin epithelial layer, enclosing the S-rich interior of lens and with Zn occupying the retinal portion of the eye. All these evidences suggested the direct negative effect of mercury on the optical system of the species.

The toxic effects also extend to affect the fertility and reproductive capacity. Sperm cells collected from *Cyprinus carpio* a tropical fish, on exposure to mercury chloride at different concentrations (0; 0.5; 1; 2.5; 5 ppm), altered the sperm parameters (Hayati et al. 2019). In vitro exposure of mercury significantly altered fish sperm's motility and viability, induced DNA fragmentation, disturbed the fertilization potential, and even transformed the architecture of the sperm head and impeded with the embryonic development (Table 12.2).

12.2.6 Aluminum Toxicity

Among the several types of metals causing human toxicity, aluminum (Al) is reported to be exceedingly toxic. Out of all the total mineral components reported, Al accounts about 8% of the total available metals. In nature, Al exists as trivalent cation (Al^{3+}), either associated with silicate or forming water-insoluble complexes, by reducing the bioavailability of the metal(Ganrot 1986).

Human exposure to Al is mainly caused by environmental factors, like soil contamination. Al can be mobilized as a consequence of soil acidification (Fig.12.11) due to the use of certain fertilizers or acid rain. The rainwater mixes with SO_x or NO_x complexes, which in turn makes hydroxyl aluminosilicates which when taken by plants are highly toxic (Guido et al. 2013). The major sites of the Al absorption are the gastrointestinal tracts (Ittel 1993), the skin (Exley 1998), as well as the olfactory or oral epithelia (Roberts 1986). Once absorbed, Al travels through
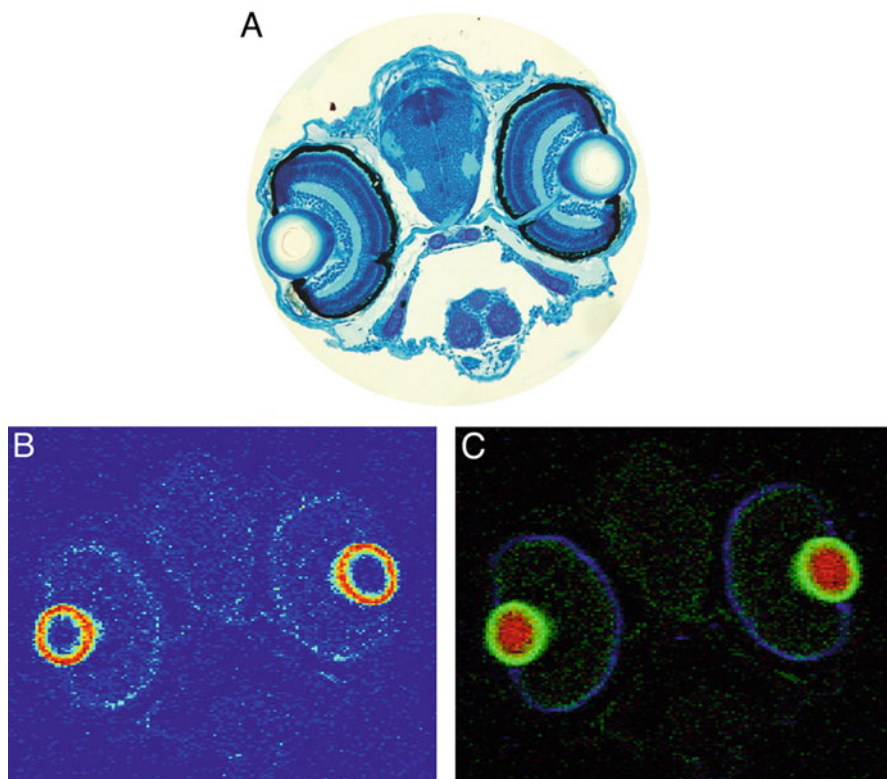
Fig. 12.10 Head section of zebrafish larva 4.5 dpf after treatment with methylmercury-L-cysteine at a concentration of 100 μM for 24 h. (**a**) Histology, (**b**) mercury distribution using X-ray fluorescence imaging at 2.5 μm resolution, (**c**) mercury (green) superimposed on S (red) and Zn (blue) (Korbas et al. 2008; copyright received)

the blood and circulates via binding to transferrin or citrate enzymes (Yokel 2002). The Al uptake in the organs occurs mainly by the affinity of it with the transferrin receptor, causing internalization pathway than of iron alone. As a consequence, Al crosses the blood–brain barrier as well (Yokel 2002) and gets accumulated in the glial as well as neuronal cells (Golub et al. 1999).

The Al intoxication even accounts for liver toxicity. However, in a study, post-intake of Al for 3 months, a clear Perl's positive iron deposition was observed in the pericentral parenchymal and Kupffer cells. An evident fibrosis was seen in the intoxicated liver sections, when compared to control group (Fig. 12.12). The heat shock protein 72 (a toxic stress protein) was unnoticeable in the control liver sections. However, in 3 months Al-treated liver, there were Al depositions in the pericentral hepatocytes, which got expressed in Kupffer cells after 6 months (Stacchiotti et al. 2006).

Table 12.2 Summary of 72 h of *Cyprinus carpio* embryonic development after in vitro mercury exposure with different concentrations (Hayati et al. 2019; copyright received)

Incubation (h)	Concentration of mercury (ppm)				
	0	0.5	1	2.5	5
12	Gastrula period. Early differentiation indicates development of the head and tail	Showed the mass of clustered eggs	The eggs were damaged	The eggs were damaged	The eggs were damaged
24	The segmentation period. Eggs turned whitish. The tail and head were slightly seen	The eggs were damaged	The eggs were damaged	Dead embryo	Dead embryo
36	The end of segmentation period. The tail and head were seen, eyes were clearly seen	Dead embryo	Dead embryo	Dead embryo	Dead embryo
48	The beginning of the pharyngula period. Head, eye, and tail regions were clearly seen	Dead embryo	Dead embryo	Dead embryo	Dead embryo
60	The end of pharyngula stage. The head, eye, and tail were more elongated than before	Dead embryo	Dead embryo	Dead embryo	Dead embryo
72	The larvae and pectoral fins were slightly seen	Dead embryo	Dead embryo	Dead embryo	Dead embryo
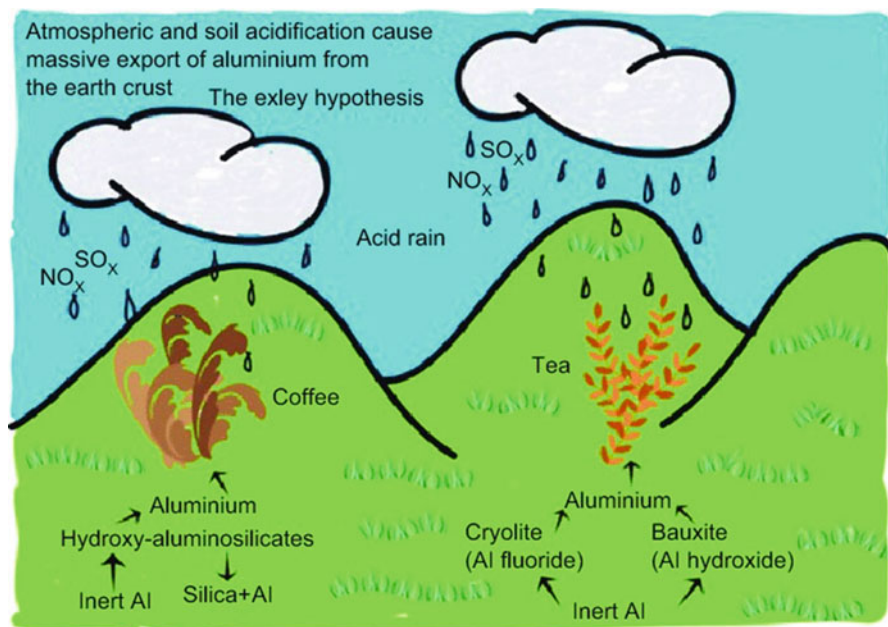
Fig. 12.11 Environmental sources of Al toxicity–acid train (Courtesy to Guido et al. 2013; copyright received)
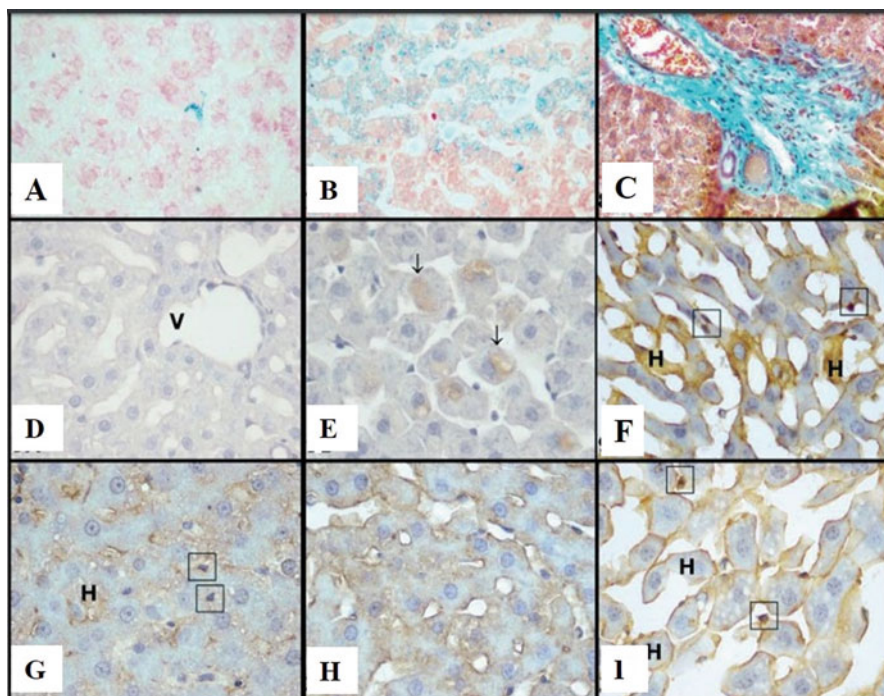
Fig. 12.12 Perl's staining in Control liver cells (**a**): Scarce signal; at 3 months Al (**b**) Perl's staining evident blue iron-deposition in the parenchyma. × 400. (**c**) Masson's staining in Al-treated liver. At 3 months periportal fibrosis. × 200. (**d**) HSP72 immunostaining in control rat liver with undetectable hepatocytes, (V) pericentral vein; at 3 months Al (**e**): HSP72 immunostaining with focal cytoplasmic signal in the hepatocytes (arrows); at 6 months Al (**f**): Extensive signals in hepatocytes (H) and in Kupffer cells (squares). (**g**) GRP75 immunostaining in rat liver. Controls with Faint hepatocytes (H) and Kupffer cells (squares); at 3 months Al (**h**): Moderate basolateral in the parenchyma; at 6 months Al (**i**): Enhanced in hepatocytes (H) and Kupffer cells (squares). × 400. (Stacchiotti et al. 2006; copyright received)

Al has no redox capacity in biological systems. However, extensive experimental evidence demonstrates both in vitro and in vivo that high Al concentrations cause oxidative stress. This condition causes an imbalance between antioxidants and oxidants, causing the disruption of redox signaling by molecular damage (Sies and Jones 2007). Moreover, in vitro, Al stimulates iron-initiated lipid oxidation (Gutteridge et al. 1985). The nervous system is particularly sensitive to oxidant-mediated damage because of:

- Its high oxygen demand
- Brain membranes having elevated levels of oxidizable polyunsaturated fatty acids (PUFA)
- Reduced brain antioxidant enzyme activities compared to other tissues
- High iron content in the brain (Youdim 1988)

In myelin fractions of Al-intoxicated mice, in addition to an elevation in the Al content, the cellular membranes became highly rigid with higher amounts of lipid oxidation products than those of controls (Verstraeten et al. 1997). The metal could even interact with the zwitterionic phospholipids, like phosphatidylcholine (PC) (Ohyashiki et al. 1998). Neuromelanin, brain pigment mainly found in substantia nigra and locus coeruleus, has a potent redox activity. The deposition of neuromelanin in these brain areas has been strongly associated with neurodegeneration, constituting a hallmark of PD (Fahn 2003). In addition to melanin deposits, both Al and iron are found in high amounts in brains from patients affected with this pathology. In vitro, Al can facilitate both iron- and copper-supported oxidation of dopamine to melanin (Di and Bi 2003a) and mediate the conversion of melanochrome to melanin (Di and Bi 2003b).

12.3   Conclusion and Future Prospects

This chapter reviewed the devastating effects of heavy metals like arsenic, lead, mercury, cadmium, chromium, and aluminum on in vitro and in vivo models. A complete exploration of all the reviewed articles had brought a light regarding the metals and their toxic elements. These toxicants are known to affect the humans with various toxicities – nephrotoxicity, neurotoxicity, hepatotoxicity, cytotoxicity, cardiotoxicity, pulmonary toxicity, developmental/reproductive toxicity, behavioral toxicity, and so on. The foremost human exposure occurs through inhalation, ingestion, or exposure of these metals on the skin. The toxicological kinetics and toxicological dynamics of the metals depend upon their relative solubility, chelating stability, particulate size, their valence shell electrons, their different forms of speciation, etc. These toxic metals gained an extra circle by even contaminating nutritionally vital metals like iron, calcium, copper, etc.

Clarifying toxic metals, their interactions with other metals, environment is essential for the management of health-related concerns. There are many reports suggesting metal toxicity, and there is an alarming rise on an exponential scale of metal toxicity-related health concerns that everyone should be alarmed about. Actual guidelines, surveys, rules, and standards for the usage of these metals are mandatory based on the prevalence of these heavy metals in the environment. Failure to address the health concern would lead to a major catastrophic issue in the near future. Advancement of techniques on biofilm production, engineering solutions, and bioremediation of heavy metals would be the future perspectives to eradicate these hazards.

References

Abdel-Zaher AO, Abd-ellatief Rasha B, Aboulhagag NA, Farghaly HSM, AL-Wasei FMM (2019) The interrelationship between gasotransmitters and lead-induced renal toxicity in rats. Toxicol Lett 310:39–50. https://doi.org/10.1016/j.toxlet.2019.04.012

Bernhoft RA (2012) Mercury toxicity and treatment: a review of the literature. J Environ Public Health 2012:1–10. https://doi.org/10.1155/2012/460508

Bouley G, Dubreuil A, Despaux N, Boudene C (1979) Toxic effects of cadmium microparticles on the respiratory system. An experimental study on rats and mice. Scand J Work Environ Health 3 (3):116–121. https://doi.org/10.5271/sjweh.2782

Caglayan C, Kandemir FM, Yildirim S, Kucukler S, Eser G (2019) Rutin protects mercuric chloride-induced nephrotoxicity via targeting of aquaporin 1 level, oxidative stress, apoptosis and inflammation in rats. J Trace Elem Med Biol 54:69–78. https://doi.org/10.1016/j.jtemb.2019.04.007

Centeno JA, Gray MA, Mullick FG, Tchounwou PB, Tseng C (2005) Arsenic in drinking water and health issues. In: Moore TA, Black A, Centeno JA, Harding JS, Trumm DA (eds) Metal contaminants in New Zealand. Resolutionz Press, Christchurch, pp 195–219

Di J, Bi S (2003a) Aluminum ions accelerated the oxidative stress of copper-mediated melanin formation. Spectrochim Acta A Mol Biomol Spectrosc 59:3075–3083. https://doi.org/10.1016/S1386-1425(03)00127-6

Di J, Bi S (2003b) Effect of aluminum (III) on the conversion of dopachrome in the melanin synthesis pathway. Spectrochim Acta A Mol Biomol Spectrosc 59:1689–1696. https://doi.org/10.1016/S1386-1425(02)00403-1

Dreval K, Tryndyak V, Kindrat I, Twaddle NC, Orisakwe OE, Mudalige TK, Pogribny IP (2018) Cellular and molecular effects of prolonged low-level sodium arsenite exposure on human hepatic HepaRG cells. Toxicol Sci 162(2):676–687. https://doi.org/10.1093/toxsci/kfx290

Ercal N, Gurer-Orhan H, Aykin-Burns N (2001) Toxic metals and oxidative stress Part I: Mechanisms involved in metal-induced oxidative damage. Curr Top Med Chem 1:529–539. https://doi.org/10.2174/1568026013394831

Exley C (1998) Does antiperspirant use increase the risk of aluminium-related disease, including Alzheimer's disease? Mol Med Today 4:107–109. https://doi.org/10.1016/S1357-4310(98)01209-X

Fahn S (2003) Description of Parkinson's disease as a clinical syndrome. Ann N Y Acad Sci 991:1–14. https://doi.org/10.1111/j.1749-6632.2003.tb07458.x

Fang Z, Zhao M, Zhen H, Chen L, Shi P, Huang Z (2014) Genotoxicity of tri- and Hexavalent chromium compounds *in vivo* and their modes of action on DNA damage *in vitro*. PLoS One 9 (8):e103194. https://doi.org/10.1371/journal.pone.0103194

Farina M, Rocha JB, Aschner M (2011) Mechanisms of methylmercury induced neurotoxicity: evidence from experimental studies. Life Sci 89:555–563. https://doi.org/10.1016/j.lfs.2011.05.019

Forsythe SD, Devarasetty M, Shupe T, Bishop C, Atala A, Soker S, Skardal A (2018) Environmental toxin screening using human-derived 3D bioengineered liver and cardiac organoids. Front Public Health 6. https://doi.org/10.3389/fpubh.2018.00103

Gairola CG, Wagner GJ (1991) Cadmium accumulation in the lung, liver and kidney of mice and rats chronically exposed to cigarette smoke. J Appl Toxicol 11(5):355–358. https://doi.org/10.1002/jat.2550110510

Ganrot PO (1986) Metabolism and possible health effects of aluminum. Environ Health Perspect 65:363–441. https://doi.org/10.1289/ehp.8665363

Golub MS, Macintosh MS, Baumrind N (1998) Developmental and reproductive toxicity of inorganic arsenic: animal studies and human concerns. J Toxicol Environ Health Part B 1 (3):199–237. https://doi.org/10.1080/10937409809524552

Golub MS, Han B, Keen CL (1999) Aluminum uptake and effects on transferrin mediated iron uptake in primary cultures of rat neurons, astrocytes and oligodendrocytes. Neurotoxicology 20:961–970

Goyer RA (2001) Toxic effects of metals. In: Klaassen CD (ed) Cassarett and Doull's toxicology: the basic science of poisons. McGraw-Hill Publisher, New York, pp 811–867

Guha MDN (2008) Chronic arsenic toxicity and human health. Indian J Med Res 128(4):436–447

Guido C, Daniela F, Clara G, Sonia N, Valeria MN, Miriam CA, Joanna IL, Gavino F (2013) The meaning of aluminium exposure on human health and aluminium-related diseases. Biomol Concepts 4(1):77–87. https://doi.org/10.1515/bmc-2012-0045

Gutteridge JM, Quinlan GJ, Clark I, Halliwell B (1985) Aluminium salts accelerate peroxidation of membrane lipids stimulated by iron salts. Biochim Biophys Acta 835:441–447. https://doi.org/10.1016/0005-2760(85)90113-4

Hans W (1995) The composition of the continental crust. Geochim Cosmochim Acta 59 (7):1217–1232. https://doi.org/10.1016/0016-7037(95)00038-2

Hassan E, Kahilo K, Kamal T, Hassan M, ELgawish M (2019) The protective effect of epigallocatechin-3-gallate on testicular oxidative stress in lead-induced toxicity mediated by Cyp19 gene/estradiol level. Toxicology 422:76–83. https://doi.org/10.1016/j.tox.2019.04.015

Hayati A, Wulansari E, Armando DS, Sofiyanti A, Amin MHF, Pramudya M (2019) Effects of in vitro exposure of mercury on sperm quality and fertility of tropical fish Cyprinus carpio L. Egyp J Aquat Res 45(2):189–195. https://doi.org/10.1016/j.ejar.2019.06.005

Hu J, Zhang B, Du L, Chen J, Lu Q (2017) Resveratrol ameliorates cadmium induced renal oxidative damage and inflammation. Int J Clin Exp Med 10(5):7563–7572. http://www.ijcem.com/files/ijcem0051065.pdf

Hubaux R, Becker-Santos DD, Enfield KS, Rowbotham D, Lam S, Lam WL, Martinez VD (2013) Molecular features in arsenic-induced lung tumors. Mol Cancer 12:20. https://doi.org/10.1186/1476-4598-12-20

Hughes MF, Beck BD, Chen Y, Lewis AS, Thomas DJ (2011) Arsenic exposure and toxicology: a historical perspective. Toxicol Sci 123:305–332. https://doi.org/10.1093/toxsci/kfr184

Hundal S, Mehta M (2014) Assessment of genotoxic potential of arsenic in female albino rats at permissible dose levels. Toxicol Int 21(1):24–28. https://doi.org/10.4103/0971-6580.128787

Ittel TH (1993) Determinants of gastrointestinal absorption and distribution of aluminium in health and uraemia. Nephrol Dial Transplant 8:17–24. https://doi.org/10.1093/ndt/8.suppl1.17

Joseph P (2009) Mechanisms of cadmium carcinogenesis. Toxicol Appl Pharmacol 238 (3):272–279. https://doi.org/10.1016/j.taap.2009.01.011

Korbas M, Blechinger SR, Krone PH, Pickering IJ, George GN (2008) Localizing organomercury uptake and accumulation in zebrafish larvae at the tissue and cellular level. PNAS 105 (34):12108–12112. https://doi.org/10.1073/pnas.0803147105

Li S, Jiang X, Luo Y, Zhou B, Shi M, Liu F, Sha A (2019) Sodium/calcium overload and Sirt1/Nrf2/OH-1 pathway are critical events in mercuric chloride-induced nephrotoxicity. Chemosphere 234:579–588. https://doi.org/10.1016/j.chemosphere.2019.06.095

Mathews VV, Paul MV, Abhilash M, Manju A, Abhilash S, Nair RH (2013) Myocardial toxicity of acute promyelocytic leukaemia drug-arsenic trioxide. Eur Rev Med Pharmacol Sci 17(Suppl 1):34–38

Michael C, Mark M, Nicholas VP, Timothy RM, Seth TW (2018) The gut microbiome is required for full protection against acute arsenic toxicity in mouse models. Nat Commun 9:5424. https://doi.org/10.1038/s41467-018-07803-9

Mugnano M, Memmolo P, Miccio L, Grilli S, Merola F, Calabuig A, Ferraro P (2018) In vitro cytotoxicity evaluation of cadmium by label-free holographic microscopy. J Biophotonics 11 (12). https://doi.org/10.1002/jbio.201800099

Nannan L, Shaohua S, Wuchang S, Ruibao J (2017) Behavioural toxicity in zebrafish (Danio rerio) exposed to waterborne zinc and chromium (VI). Chem Ecol 33(8):725–738. https://doi.org/10.1080/02757540.2017.1373767

Ohyashiki T, Suzuki S, Satoh E, Uemori Y (1998) A marked stimulation of Fe^{2+}−initiated lipid peroxidation in phospholipid liposomes by a lipophilic aluminum complex, aluminum acetylacetonate. Biochim Biophys Acta 1389:141–149. https://doi.org/10.1016/S0005-2760(97)00148-3

Peng J, Zhou F, Wang Y, Xu Y, Zhang H, Zou F, Meng X (2018) Differential response to lead toxicity in rat primary microglia and astrocytes. Toxicol Appl Pharmacol 363:64–71. https://doi.org/10.1016/j.taap.2018.11.010

Qian B, Xue L, Qi X, Bai Y, Wu Y (2019) Gene networks and toxicity/detoxification pathways in juvenile largemouth bass (Micropterus salmoides) liver induced by acute lead stress. Genomics. https://doi.org/10.1016/j.ygeno.2019.06.023

Roberts E (1986) Alzheimer's disease may begin in the nose and may be caused by aluminosilicates. Neurobiol Aging 7:561–567. https://doi.org/10.1016/0197-4580(86)90119-3

Sabath E, Robles-Osorio ML (2012) Medio ambiente y riñón: nefrotoxicidad por metales pesados [Renal health and the environment: heavy metal nephrotoxicity]. Nefrologia 32:279–286

Sies H, Jones D (2007) Oxidative stress. In: Fink G (ed) Encyclopedia of stress. Elsevier, San Diego, pp 45–48. https://books.google.co.in/books

Singh AP, Goel RK, Kaur T (2011) Mechanisms pertaining to arsenic toxicity. Toxicol Int 18(2):87–93. https://doi.org/10.4103/0971-6580.84258

Singh HP, Mahajan P, Kaur S, Daizy RB, Ravinder KK (2013) Chromium toxicity and tolerance in plants. Environ Chem Lett 11:229–254. https://doi.org/10.1007/s10311-013-0407-5

Stacchiotti A, Rodella LF, Ricci F, Rezzani R, Lavazza A, Bianchi R (2006) Stress proteins expression in rat kidney and liver chronically exposed to aluminium sulphate. Hist Histopath Cell Mol Biol 21:131–140. https://doi.org/10.14670/HH-21.131

Taju G, Abdul Majeed S, Nambi KSN, Sahul Hameed AS (2017) Application of fish cell lines for evaluating the chromium induced cytotoxicity, genotoxicity and oxidative stress. Chemosphere 184:1–12. https://doi.org/10.1016/j.chemosphere.2017.05.151

Tarasco M, Cardeira J, Viegas M, Caria J, Martins G, Gavaia P, Laizé V (2019) Anti-osteogenic activity of cadmium in zebrafish. Aust Fish 4(1):11. https://doi.org/10.3390/fishes4010011

Tchounwou PB, Yedjou CG, Patlolla AK, Sutton DJ (2012) Heavy metal toxicity and the environment. Mol Clin Environ Toxicol:133–164. https://doi.org/10.1007/978-3-7643-8340-4_6

Tye MT, Montgomery JE, Hobbs MR, Vanpelt KT, Masino MA (2018) An adult zebrafish diet contaminated with chromium reduces the viability of progeny. Zebrafish 15(2):179–187. https://doi.org/10.1089/zeb.2017.1514

Verstraeten SV, Golub MS, Keen CL, Oteiza PI (1997) Myelin is a preferential target of aluminum-mediated oxidative damage. Arch Biochem Biophys 344:289–294. https://doi.org/10.1006/abbi.1997.0146

Waalkes M (2004) Animal models for arsenic carcinogenesis: inorganic arsenic is a transplacental carcinogen in mice. Toxicol Appl Pharmacol 198(3):377–384. https://doi.org/10.1016/j.taap.2003.10.028

Wani AL, Ara A, Usmani JA (2015) Lead toxicity: a review. Interdiscip Toxicol 8(2):55–64. https://doi.org/10.1515/intox-2015-0009

Wilbur S, Abadin H, Fay M et al (2012) Toxicological profile for chromium. Agency for Toxic Substances and Disease Registry (US), Atlanta

Xu H, Wang X, Burchiel SW (2018) Toxicity of environmentally-relevant concentrations of arsenic on developing T lymphocyte. Environ Toxicol Pharmacol 62:107–113. https://doi.org/10.1016/j.etap.2018.07.003

Yokel RA (2002) Brain uptake, retention, and efflux of aluminum and manganese. Environ Health Perspect 110(5):699–704. https://doi.org/10.1289/ehp.02110s5699

Youdim MB (1988) Iron in the brain: implications for Parkinson's and Alzheimer's diseases. Mt Sinai J Med 55:97–101

Index